



# Preparation and characterization of supported metallacalix[4]arenes onto mesoporous silica for the conversion of olefins

Jeff Espinas

## ► To cite this version:

Jeff Espinas. Preparation and characterization of supported metallacalix[4]arenes onto mesoporous silica for the conversion of olefins. Other. Université Claude Bernard - Lyon I, 2010. English. NNT : 2010LYO10192 . tel-00837913

HAL Id: tel-00837913

<https://theses.hal.science/tel-00837913>

Submitted on 24 Jun 2013

**HAL** is a multi-disciplinary open access archive for the deposit and dissemination of scientific research documents, whether they are published or not. The documents may come from teaching and research institutions in France or abroad, or from public or private research centers.

L'archive ouverte pluridisciplinaire **HAL**, est destinée au dépôt et à la diffusion de documents scientifiques de niveau recherche, publiés ou non, émanant des établissements d'enseignement et de recherche français ou étrangers, des laboratoires publics ou privés.

# THESE

Présentée

devant L'UNIVERSITE CLAUDE BERNARD - LYON I  
et l'Ecole Doctorale de Chimie  
pour l'obtention  
du DIPLOME DE DOCTORAT  
(arrêté du 7 Août 2006)

soutenue publiquement  
le 27 Octobre 2010  
par

**Jeff ESPINAS**

Ingénieur CPE Lyon

---

## PREPARATION ET CARACTERISATION DE METALLACALIX[4]ARENES SUPPORTES SUR SILICE MESOPOREUSE POUR LA CONVERSION DES OLEFINES

---

Jury :

M. BASSET J.M.  
Mme. BONNAMOUR I.  
M. DARBOST U.  
M. GAUVIN R.  
M. MATT D.  
M. REGNOUF de VAINS J.B.  
M. TAOUIFIK M.

Rapporteurs :

M. GAUVIN R.  
M. MATT D.  
M. REGNOUF de VAINS J.B.







# THESE

Présentée

devant L'UNIVERSITE CLAUDE BERNARD - LYON I  
et l'Ecole Doctorale de Chimie  
pour l'obtention  
du **DIPLOME DE DOCTORAT**  
(arrêté du 7 Août 2006)

soutenue publiquement  
le 27 Octobre 2010  
par

**Jeff ESPINAS**

Ingénieur CPE Lyon

---

## PREPARATION ET CARACTERISATION DE METALLACALIX[4]ARENES SUPPORTES SUR SILICE MESOPOREUSE POUR LA CONVERSION DES OLEFINES

---

Jury :

M. BASSET J.M.  
Mme. BONNAMOUR I.  
M. DARBOST U.  
M. GAUVIN R.  
M. MATT D.  
M. REGNOUF de VAINS J.B.  
M. TAOUIFIK M.

Rapporteurs :

M. GAUVIN R.  
M. MATT D.  
M. REGNOUF de VAINS J.B.



## **UNIVERSITE CLAUDE BERNARD - LYON 1**

### **Président de l'Université**

Vice-président du Conseil Scientifique

Vice-président du Conseil d'Administration

Vice-président du Conseil des Etudes et de la Vie Universitaire

Secrétaire Général

### **M. le Professeur L. Collet**

M. le Professeur J-F. Mornex

M. le Professeur G. Annat

M. le Professeur D. Simon

M. G. Gay

### ***COMPOSANTES SANTE***

Faculté de Médecine Lyon Est – Claude Bernard

Faculté de Médecine Lyon Sud – Charles Mérieux

UFR d'Odontologie

Institut des Sciences Pharmaceutiques et Biologiques

Institut des Sciences et Techniques de Réadaptation

Département de Biologie Humaine

Directeur : M. le Professeur J. Etienne

Directeur : M. le Professeur F-N. Gilly

Directeur : M. le Professeur D. Bourgeois

Directeur : M. le Professeur F. Locher

Directeur : M. le Professeur Y. Matillon

Directeur : M. le Professeur P. Farge

### ***COMPOSANTES ET DEPARTEMENTS DE SCIENCES ET TECHNOLOGIE***

Faculté des Sciences et Technologies

Département Biologie

Département Chimie Biochimie

Département GEP

Département Informatique

Département Mathématiques

Département Mécanique

Département Physique

Département Sciences de la Terre

UFR Sciences et Techniques des Activités Physiques et Sportives

Observatoire de Lyon

Ecole Polytechnique Universitaire de Lyon 1

Institut Universitaire de Technologie de Lyon 1

Institut de Science Financière et d'Assurance

Institut Universitaire de Formation des Maîtres

Directeur : M. le Professeur F. Gieres

Directeur : M. le Professeur C. Gautier

Directeur : Mme le Professeur H. Parrot

Directeur : M. N. Siauve

Directeur : M. le Professeur S. Akkouche

Directeur : M. le Professeur A. Goldman

Directeur : M. le Professeur H. Ben Hadid

Directeur : Mme S. Fleck

Directeur : M. le Professeur P. Hantzpergue

Directeur : M. C. Collignon

Directeur : M. B. Guiderdoni

Directeur : M. le Professeur J. Lieto

Directeur : M. le Professeur C. Coulet

Directeur : M. le Professeur J-C. Augros

Directeur : M R. Bernard



*A mes parents, mon frère, ma petite sœur, ma grand-mère*

*A mon grand-père*



## **Remerciements**

*Les travaux rapportés dans ce mémoire ont été effectués à l'école de Chimie, Physique et Electronique de Lyon (CPE) dans le Laboratoire de Chimie Organométallique de Surface (LCOMS), en collaboration avec le Laboratoire de Chimie Supramoléculaire Appliquée (CSAp) à l'Université Claude Bernard Lyon 1. Je tiens à remercier Messieurs Gérard PIGNAULT, Directeur de CPE, et Lionel COLLET, Président de l'UCBL, de m'avoir accueilli dans leurs locaux.*

*Que Monsieur Jean-Marie BASSET, Directeur de Recherche au CNRS soit assuré de ma profonde gratitude pour m'avoir permis de réaliser cette thèse au sein de son équipe et donné de nombreux conseils, tant au niveau scientifique que dans l'élaboration de mon projet de carrière professionnelle.*

*Je remercie également Madame Bernadette CHARLEUX de m'avoir accueilli dans son laboratoire et pour ses conseils avisés dans l'élaboration de mon projet professionnel.*

*Je tiens tout particulièrement à remercier Monsieur Mostafa TAOUIFIK, Ingénieur de Recherche au CNRS, pour m'avoir encadré tout au long de ces trois années de thèse et dirigé ce travail avec compétence et sympathie. Sa créativité scientifique et son fort dynamisme m'auront permis de découvrir le monde de la recherche avec beaucoup d'enthousiasme. Enfin, je voudrais souligner la confiance et la liberté qu'il m'a accordées tout au long de ces travaux de recherche.*

*Je tiens également à remercier Madame Isabelle BONNAMOUR, Maître de Conférences à l'UCBL, pour m'avoir encadré, pour la confiance qu'elle m'a accordée et de l'intérêt constant qu'elle a porté à l'avancement de mes travaux.*

*Je tiens aussi à remercier Monsieur Ulrich DARBOST, Maître de Conférences à l'UCBL, qui a participé à l'encadrement de mes travaux tout au long de cette thèse.*

*Je suis reconnaissant à tous ceux qui ont contribué de près ou de loin à ce travail. Que Mesdames Christine LUCAS et Anne BAUDOIN soient remerciées pour leur aide précieuse lors de l'acquisition et l'interprétation des spectres RMN à l'état liquide et solide, respectivement. J'adresse également mes remerciements à Messieurs Denis BOUCHU et Christian DESCHAMPS pour leur collaboration en spectroscopie de masse, Messieurs Olivier BOYRON et Jean-Pierre BROYER pour la caractérisation des polymères, Monsieur Erwann JEANNEAU pour la détermination de structures par diffraction des rayons X, Messieurs Aimery DEMALLMANN et Kai SZETO pour l'acquisition de données EXAFS,*



*Sébastien NORSIC pour la préparation des réacteurs dynamiques, Monsieur Henry CHERMETTE pour les calculs théoriques et Docteur Erwan LEROUX, de l'Université de Bergen (Norvège) pour son assistance dans la synthèse et la caractérisation des supports mésoporeux.*

*Je voudrais aussi remercier Jérémie PELLETIER pour sa précieuse contribution dans la mise en place des expériences et la rédaction des articles scientifiques, ainsi que Nicolas MERLES pour m'avoir transmis ses nombreuses techniques expérimentales.*

*Je suis également reconnaissant envers tous les membres des équipes du LCOMS et du CSap pour leur accueil et leur soutien.*

*Que tous mes proches et amis reçoivent toute ma reconnaissance pour m'avoir soutenu dans les moments de désarroi, longues traversées du désert, et surtout accepté mon fort caractère.*

*Que Messieurs Régis Gauvin, Chargé de Recherches au CNRS, Dominique MATT, Directeur de Recherches au CNRS et Jean-Bernard REGNOUF DE VAINS, Professeur à l'Université Henri Poincaré à Nancy, soient remerciés d'avoir accepté de juger ce travail.*



---

## **RESUME en français**

Le présent manuscrit est consacré à l'élaboration de matériaux métallacalix[4]arènes pour la valorisation des hydrocarbures basée sur un nouveau concept de greffage par voie COMS. En effet, cette nouvelle méthode a été dans un premier temps mise au point par fonctionnalisation de supports silice en faisant réagir l'hydroquinone avec une espèce originale [ $(\equiv\text{SiO})_2\text{Al}(\text{Bu})(\text{Et}_2\text{O})$ ]. Cette dernière a été obtenue par greffage de  $\text{Al}(\text{Bu})(\text{Et}_2\text{O})$  avec une surface de silice déshydroxylée à 700°C. La réactivité du complexe  $\text{W}(\equiv\text{CtBu})(\text{CH}_2\text{tBu})_3$  avec l'hydroquinone supportée [ $(\equiv\text{SiO})_2\text{AlO-C}_6\text{H}_4\text{-OH}(\text{Et}_2\text{O})$ ] a permis de générer un nouveau système catalytique bien défini [ $(\equiv\text{SiO})_2\text{AlO-C}_6\text{H}_4\text{-OW}(\equiv\text{CtBu})(\text{CH}_2\text{tBu})_2(\text{Et}_2\text{O})$ ] entièrement caractérisé. Une fois prouvé, le concept d'insérer un « espaceur » de type phenoxy entre le support silice et l'espèce active a été appliquée aux espaceurs calixarènes. Ainsi, l'ancrage du calixarène [[4H]- $(\text{OH})_3(\text{H})$ ] sur le complexe de surface [ $(\equiv\text{SiO})_2\text{Al}(\text{Bu})(\text{Et}_2\text{O})$ ] supporté sur silice mésoporeuse SBA-15 larges pores<sub>(700)</sub> a conduit à l'espèce [ $(\equiv\text{SiO})_2\text{Al-O-[4H]-}(\text{OH})_2(\text{Et}_2\text{O})$ ], caractérisée par IR, RMN solide et microanalyse. L'incorporation de complexes organométalliques du groupe IV (Zr) et VI (W) mène à de nouveaux matériaux métallacalix[4]arènes bipodaux caractérisés par IR, RMN solide ( $^1\text{H}$ ,  $^{13}\text{C}$ , HETCOR), microanalyse et EXAFS. L'élucidation de leurs structures a été appuyée par comparaison avec les données spectroscopiques de leurs homologues solubles ou directement liés à la silice. Avant la préparation des matériaux métallacalix[4]arènes, une série de complexes titana-, zircona- et tantalacalix[4]arènes solubles bi- et tripodaux a été synthétisée et caractérisée à partir de plusieurs dérivés calix[4]arène présentant des modes de coordination différents pour le métal (podalité, ligands ancillaires, angle OMO). Parallèlement, une relation structure-réactivité dans la polymérisation des oléfines a été établie dans le cas des titanacalix[4]arènes, et pour les tantalacalix[4]arènes, des activations  $\text{Csp}^2\text{-H}$  et O-Me intramoléculaires ont été mises en évidence, pour donner des systèmes tétrapodaux caractérisés par RMN et RX. Ces modèles nous ont aussi orientés quant au choix des calixarènes à greffer. Les matériaux obtenus, présentant des espaceurs phenoxy (hydroquinone, calixarène), montrent des activités initiales supérieures à celles de leurs homologues supportés sur silice.

---

## **TITRE en anglais**

Preparation and characterization of supported metallacalix[4]arenes onto mesoporous silica for the conversion of olefins

---

## **RESUME en anglais**

This work deals with the generation of novel metallacalix[4]arenes materials applied to the valorization of hydrocarbons prepared using an unprecedented COMS method. It consists in the first functionalization of the silica support by reaction of hydroquinone with the unreported supported species [ $(\equiv\text{SiO})_2\text{Al}(\text{Bu})(\text{Et}_2\text{O})$ ]. This latter was obtained by grafting of  $\text{Al}(\text{Bu})(\text{Et}_2\text{O})$  onto a silica partially dehydroxylated at 700°C. The reactivity between the complex  $\text{W}(\equiv\text{CtBu})(\text{CH}_2\text{tBu})_3$  and the hydroquinone species [ $(\equiv\text{SiO})_2\text{AlO-C}_6\text{H}_4\text{-OH}(\text{Et}_2\text{O})$ ] allows the access to new well-defined catalytic systems [ $(\equiv\text{SiO})_2\text{AlO-C}_6\text{H}_4\text{-OW}(\equiv\text{CtBu})(\text{CH}_2\text{tBu})_2(\text{Et}_2\text{O})$ ]. The concept to insert a phenoxy type spacer between the silica support and the active metal center is then fully proved and can be further adapted to the calixarene spacers. In this way, the anchoring of the calixarene [[4H]- $(\text{OH})_3(\text{H})$ ] onto [ $(\equiv\text{SiO})_2\text{Al}(\text{Bu})(\text{Et}_2\text{O})$ ] supported on the mesoporous SBA-15 large pores<sub>(700)</sub> leads to the surface complex [ $(\equiv\text{SiO})_2\text{Al-O-[4H]-}(\text{OH})_2(\text{Et}_2\text{O})$ ], characterized by IR, solid state NMR and microanalysis. The subsequent incorporation of organometallic complexes from groups IV (Zr) and VI (W) provided novel bipodal metallacalix[4]arenes materials, characterized by IR, solid-state NMR ( $^1\text{H}$ ,  $^{13}\text{C}$ , HETCOR), microanalysis and EXAFS. The clarification of their structures was supported by comparison of the spectroscopic data collected from their soluble models or analogues directly bonded to silica. Before preparation of the materials, a set of bi- and tripodal titana-, zircona- and tantalacalix[4]arenes complexes were synthesized and characterized from different calix[4]arenes derivatives ligands, presenting different mode of coordination for the metal (podality, ancillary ligands, OMO bite angle). In parallel, a structure-reactivity relation in the polymerization of ethylene was established in the case of the titanacalix[4]arenes, while  $\text{Csp}^2\text{-H}$  and O-Me intramolecular activations were related for the tantalacalix[4]arenes, leading to tetrapodal systems, fully characterized by NMR and X-Ray structure determination. These models helped us to define the best calixarenes ligands to use as spacers for the preparation of the materials. All the new materials, presenting phenoxy linkers (hydroquinone, calix[4]arene), display higher initial conversion rates than their analogues directly grafted on silica.

---

**DISCIPLINE :** Chimie

---

**MOTS-CLES:** Calix[4]arènes / metallacalix[4]arènes / triisobutylaluminium / hydroquinone / SBA-15 / greffage / catalyse / chimie organométallique de surface / titane / zirconium / tantale / tungstène

---



## *Abréviations et acronymes*

Ar	Aromatic
bs	broad signal
BET	Brunauer, Emmett, Teller
BJH	Barret, Joyner and Halenda
Bn	benzyl
COMS	Chimie Organométallique de Surface
COSY	Correlated Spectroscopy
CP/MAS	Cross Polarization/ Magic Angle Spinning
d	doublet
DCM	DiChloroMethane
DEPT	Distortionless Enhancement by Polarization Transfer
DMF	N,N-dimethylformamide
DRIFT	Diffuse Reflectance Infra-red Fourier Transform
DSC	Differential Scanning Calorimetry
eq.	equivalent
ES	ElectroSpray
Et	Ethyl
EXAFS	Extended X-Ray Absorption Fine Structure
GC	Gas Chromatography
HDPE	High Density PolyEthylene
HTSEC	High Temperature Size Exclusion Chromatography
iBu	isobutyl
IR	Infra-Red
J	Coupling constant
KM	Kubelka Munk
m	multiplet
Me	Methyl
Mn	number average molecular weight
Mw	weight average molecular weight
NMR	Nuclear Magnetic Resonance
NOESY	Nuclear Overhauser Effect Spectroscopy
Np, Ns	Neopentyl (-CH <sub>2</sub> C(CH <sub>3</sub> ) <sub>3</sub> ), Neosilyl (-CH <sub>2</sub> Si(CH <sub>3</sub> ) <sub>3</sub> )
PE	PolyEthylene
Ph	Phenyl
PI (IP)	Polydispersity Index
Piv	Pivaloyl
POSS	PolySilSesquioxane
ppm	part per million



Pr	Propyl
q	quadruplet
RPE	Résonance Paramagnétique Electronique
s	singlet
SBA	Santa Barbara Amorphous
SOMC	Surface OrganoMetallic Chemistry
Support <sub>(T)</sub>	support partially dehydroxylated at T °C
t	triplet
TBAF	TetraButylAmmonium Fluoride
<i>t</i> Bu	<i>tert</i> butyl
TEM	Transmission Electronic Microscopy
TEOS	TetraOrthoSilicate
Tf	fusion temperature
THF	TetraHydroFuran
TMDS	TetraMethylDiSilazane
TMS	TetraMethylSilane
TOF	Turn Over Frequency
TON	Turn Over Number
UHMWPE	Ultra High Molecular Weight PolyEthylene
XANES	X-Ray Absorption Near Edge Structure
XRD	X-Ray Diffraction
xs	excess
δ	Chemical Shift



# **Sommaire**

<b>Introduction générale</b>	<b>29</b>
<b>Chapitre I : Etude bibliographique</b>	
<b>1. Introduction: les catalyses homogène et hétérogène, avantages et inconvénients</b>	<b>33</b>
1.1 La catalyse homogène	33
1.2 La catalyse hétérogène	34
<b>2. Concept de la Chimie Organométallique de Surface</b>	<b>35</b>
2.1 Les différents supports oxydes	36
2.1.1 <i>La silice</i>	36
• La silice amorphe	36
• Les silices mésoporeuses structurées	38
2.1.2 <i>L'alumine</i>	38
2.2 Hétérogénéité des supports oxydes dans la Chimie Organométallique de Surface	40
2.2.1 <i>Cas des espèces de zirconium supportées sur silice</i>	41
2.2.2 <i>Cas des espèces de titane supportées sur silice</i>	42
2.2.3 <i>Cas des espèces de tantale supportées sur silice</i>	43
2.2.4 <i>Cas des espèces de tungstène supportées sur silice</i>	44
2.3 Conclusion	45
<b>3. Les calixarènes</b>	<b>47</b>
3.1 Historique et nomenclature	47
3.2 La famille des calix[4]arènes, dérivés du <i>p-tertbutylcalix[4]arène</i>	49
<b>4. Préparation de matériaux inorganiques/organiques à base de calixarènes</b>	<b>51</b>
4.1 Greffage de calix[4]arènes sur un support oxyde par le petit col ou « lower-rim » fonctionnalisé	53
4.2 Greffage de calix[4]arènes sur un support oxyde par le grand col ou « upper-rim » fonctionnalisé	55
4.3 Greffage de calixarènes sur une silice fonctionnalisée	57
4.4 Conclusion	58
<b>5. Stratégie proposée pour le projet</b>	<b>59</b>
Notes et références	61

## **Chapitre II: Proof of the concept: Study of the reactivity between a phenolic function and supported triisobutylaluminum onto silica**

<b>1. Introduction</b>	<b>67</b>
<b>2. Bibliographic study</b>	<b>68</b>
2.1 Reactivity of trialkylaluminum with silica supports	68
2.2 Strategy	72
<b>3. Reactivity of <math>\text{Al}(\text{Bu}_3)_2\text{OEt}_2</math> with <math>\text{SiO}_{2-(700)}</math>. Generation of the material <math>[(\equiv\text{SiO})_2\text{Al}(\text{Bu}_3)(\text{Et}_2\text{O})]</math> (H1)</b>	<b>74</b>
3.1 Choice of the silica support $\text{SiO}_{2-(700)}$	74
3.2 Reactivity of $\text{Al}(\text{Bu}_3)_2\text{OEt}_2$ in diethylether with $\text{SiO}_{2-(700)}$	74
3.2.1 Preparation and characterization of $\text{Al}(\text{Bu}_3)_2\text{OEt}_2$	74
3.2.2 Preparation and characterization of $[(\equiv\text{SiO})_2\text{Al}(\text{Bu}_3)(\text{Et}_2\text{O})]$ (H1)	75
<b>4. Reactivity of hydroquinone with <math>[(\equiv\text{SiO})_2\text{Al}(\text{Bu}_3)(\text{Et}_2\text{O})]</math> (H1)</b>	<b>78</b>
<b>5. Grafting of <math>\text{Zr}(\text{CH}_2\text{Ph})_4</math> and <math>\text{W}(\equiv\text{CtBu}(\text{CH}_2\text{tBu})_3)</math> onto <math>\text{SiO}_{2-(700)}</math> and <math>[(\equiv\text{SiO})_2\text{AlO-C}_6\text{H}_4-\text{OH}(\text{Et}_2\text{O})]</math> (H2)</b>	<b>81</b>
5.1 Grafting of the zirconium complex $\text{Zr}(\text{CH}_2\text{Ph})_4$ onto $\text{SiO}_{2-(700)}$ and $[(\equiv\text{SiO})_2\text{AlO-C}_6\text{H}_4-\text{OH}(\text{Et}_2\text{O})]$ (H2)	82
5.1.1 Preparation and characterization of $[(\equiv\text{SiO})\text{Zr}(\text{CH}_2\text{Ph})_3]$ (H3)	82
5.1.2 Preparation and characterization of $[(\equiv\text{SiO})_2\text{AlO-C}_6\text{H}_4-\text{OZr}(\text{CH}_2\text{Ph})_3.\text{Et}_2\text{O}]$ (H4)	85
5.2 Grafting of the tungsten complex $[\text{W}(\equiv\text{CtBu}(\text{CH}_2\text{tBu})_3)]$ onto $[(\equiv\text{SiO})_2\text{AlO-C}_6\text{H}_4-\text{OH}(\text{Et}_2\text{O})]$ (H2)	88
5.2.1 Preparation and characterization of $[(\equiv\text{SiO})\text{W}(\equiv\text{CtBu}(\text{CH}_2\text{tBu})_2)]$ (H5)	88
5.2.2 Preparation and characterization of $[(\equiv\text{SiO})_2\text{AlO-C}_6\text{H}_4-\text{OW}(\equiv\text{CtBu}(\text{CH}_2\text{tBu})_2).\text{Et}_2\text{O}]$ (H6)	91
<b>6. Catalytic performance of <math>[(\equiv\text{SiO})\text{W}(\equiv\text{CtBu}(\text{CH}_2\text{tBu})_2)]</math> (H5) and <math>[(\equiv\text{SiO})_2\text{AlO-C}_6\text{H}_4-\text{OW}(\equiv\text{CtBu}(\text{CH}_2\text{tBu})_2).\text{Et}_2\text{O}]</math> (H6) in propylene metathesis</b>	<b>94</b>
6.1 Definitions of practical terms in catalysis	94
6.2 Catalytic tests	95
<b>7. General conclusion</b>	<b>99</b>
Experimental section	100
Notes and references	102

### **Chapter III: Synthesis of Titana- and Zirconacalix[4]arenes as soluble models of grafted species. (dichloro)metallacalix[4]arenes: application in homogeneous ethylene polymerization**

<b>1. Introduction</b>	<b>107</b>
<b>2. Bibliographic study: Polysilsesquioxane and calix[4]arene-based complexes as molecular models of silica-grafted species of titanium and zirconium</b>	<b>108</b>
2.1 Polyhedral Oligomeric Silsesquioxane-based complexes	109
2.1.1 <i>Polyhedral oligomeric silsesquioxane ligands</i>	109
2.1.2 <i>Titanium and zirconium POSS-based models</i>	110
2.2 Calix[4]arene-based complexes: the metallacalix[4]arene models	112
2.2.1 <i>Chlorine derivatives of the metallacalix[4]arenes</i>	112
2.2.2 <i>Alkyl derivatives of the metallacalix[4]arenes</i>	114
<b>3. Strategy</b>	<b>115</b>
<b>4. Preparation and conformational studies of the <i>p</i>-tertbutylcalix[4]arene derivatives ligands (L1-L10)</b>	<b>117</b>
4.1 Functionalized <i>p</i> -tertbutylcalix[4]arenes on distal positions (L1-L4)	117
4.2 Dehydroxylated <i>p</i> -tertbutylcalix[4]arene on distal positions (L5)	120
4.3 Functionalized <i>p</i> -tertbutylcalix[4]arenes on proximal positions (L6-L7)	123
4.4 Dehydroxylated <i>p</i> -tertbutylcalix[4]arene on proximal positions (L8)	125
4.5 Mono-dehydroxylated <i>p</i> -tertbutylcalix[4]arene (L9) and its mono-methoxy derivative (L10)	125
4.6 Conclusion	129
<b>5. Synthesis and characterization of bipodal (bis-chloro)titana- and (bis-chloro)zirconacalix[4]arenes. Application in ethylene polymerization</b>	<b>130</b>
5.1 Syntheses of the bipodal (bis-chloro)titanacalix[4]arenes (Ti1-Ti9) and (bis-chloro)zirconacalix[4]arene (Zr1)	130
5.1.1 <i>Preparation and conformational studies of the distal complexes presenting two alkoxy ligands (Ti1-Ti4 and Zr1):</i>	130
5.1.2 <i>Preparation and conformational studies of the distal complex presenting one methoxy ligand (Ti6)</i>	134
5.1.3 <i>Preparation and conformational studies of the distal complex free of alkoxy ligand (Ti5)</i>	135
5.1.4 <i>Preparation and conformational studies of the proximal complexes (Ti6-Ti8): study of the bite-angle effect</i>	136
5.1.5 <i>Conclusion</i>	140
5.2 Catalytic properties of the bipodal (bis-chloro)titanacalix[4]arene and (bis-chloro)zirconacalix[4]arene complexes (Ti1-Ti5, Ti7-Ti9, Zr1)	141

5.2.1	<i>Experimental conditions and results</i>	141
5.2.2	<i>Influence of the coordination mode on the catalytic performance of the metal center: effect of the electronic and geometric environment</i>	143
5.2.3	<i>Influence of the pressure and the temperature parameters. Optimization of the catalysis</i>	144
5.2.4	<i>Conclusion</i>	146
<b>6.</b>	<b>Synthesis and characterization of alkyl titana- and zirconacalix[4]arenes</b>	<b>146</b>
6.1	Syntheses of bipodal alkyl titana- and zirconacalix[4]arene models (T10-T13, Zr2)	147
6.2	Syntheses of the tripodal alkyl titana- and zirconacalix[4]arenes models	148
6.3	Conclusion	151
<b>7.</b>	<b>General conclusion</b>	<b>151</b>
	Experimental section	153
	Notes and references	165

## **Chapter IV: Synthesis of Tantalacalix[4]arenes as soluble models of grafted species**

<b>1.</b>	<b>Introduction</b>	<b>169</b>
<b>2.</b>	<b>Bibliographic study: bulky oxo donor ligands, polysilsesquioxanes, aryloxy and calix[4,6,8]arenes-based complexes as molecular models of silica-grafted species of tantalum</b>	<b>170</b>
2.1	Description of [Tritox], [Silox], 9-Oxytriptycene, as bulky oxo donor ligands, and POSS-based complexes of tantalum	170
2.2	Aryloxy and calix[4,6,8]arenes-based complexes of tantalum	173
<b>3.</b>	<b>Strategy</b>	<b>176</b>
<b>4.</b>	<b>Results and discussions</b>	<b>177</b>
4.1	Synthesis and characterization of the <i>p</i> - <i>tert</i> butylcalix[4]arene derivative ligands	177
4.1.1	<i>Synthesis of [[4+]-1,3-(OH)<sub>2</sub>(OBn)(H)] (L11)</i>	177
4.1.2	<i>Structural and conformational studies of [[4+]-1,3-(OH)<sub>2</sub>(OBn)(H)] (L11)</i>	178
4.2	Syntheses and characterization of bipodal and tripodal tantalacalix[4]arene complexes	179
4.2.1	<i>Synthesis and characterization of the bipodal tantalacalix[4]arenes</i>	179
4.2.2	<i>Synthesis and characterization of tripodal tantalacalix[4]arenes</i>	185
<b>5.</b>	<b>General conclusion</b>	<b>199</b>
	Experimental section	200
	Notes and references	204

## Chapter V: Preparation of supported metallacalix[4]arenes on SBA-15 LP<sub>-(700)</sub>

<b>1. Introduction</b>	<b>209</b>
<b>2. Choice of the support: SBA-15 LP</b>	<b>211</b>
2.1    Bibliographic studies	211
2.2    Preparation and characterization of SBA-15 LP <sub>-(700)</sub>	213
2.2.1 <i>Synthesis of SBA-15 LP<sub>-(700)</sub></i>	213
2.2.2 <i>Characterization and properties of SBA-15 LP<sub>-(700)</sub></i>	213
<b>3. Reactivity of Al<i>i</i>Bu<sub>3</sub>.Et<sub>2</sub>O with SBA-15 LP<sub>-(700)</sub></b>	<b>217</b>
<b>4. Preparation of supported metallacalix[4]arenes: reaction of calix[4]arene derivatives with [(≡SiO)<sub>2</sub>Al<i>i</i>Bu.(Et<sub>2</sub>O)]<sub>SBA-15 LP-(700)</sub> M1</b>	<b>223</b>
4.1    Preparation and characterization of bipodal metallacalix[4]arenes supported on mesoporous SBA-15 LP <sub>-(700)</sub>	223
4.1.1 <i>Grafting of the calixarene [[4H]-OH<sub>3</sub>(H)] onto [(≡SiO)<sub>2</sub>Al<i>i</i>Bu.(Et<sub>2</sub>O)]<sub>SBA-15 LP-(700)</sub> (M1)</i>	223
4.1.2 <i>Incorporation of Zr(<sup>13</sup>CH<sub>2</sub>Ph)<sub>4</sub> onto the material [(≡SiO)<sub>2</sub>Al-[O-[4H]-OH<sub>2</sub>(H)].(Et<sub>2</sub>O)]<sub>SBA-15 LP-(700)</sub> (M2)</i>	230
4.1.3 <i>Incorporation of W(≡CtBu(CH<sub>2</sub>tBu)<sub>3</sub>) onto the material [(≡SiO)<sub>2</sub>Al-[O-[4H]-OH<sub>2</sub>(H)].(Et<sub>2</sub>O)]<sub>SBA-15 LP-(700)</sub> (M2)</i>	236
4.2    Preparation of tripodal metallacalix[4]arenes supported on mesoporous SBA-15 LP <sub>-(700)</sub> by grafting of [[4H]-OH <sub>4</sub> ] onto [(≡SiO) <sub>2</sub> Al <i>i</i> Bu.(Et <sub>2</sub> O)] <sub>SBA-15 LP-(700)</sub> (M1) <sub>(700)</sub>	241
<b>5. Catalytic performance of [(≡SiO)<sub>2</sub>Al-[O-[4H]-H)(O)<sub>2</sub>W≡CHtBu(CH<sub>2</sub>tBu)].(Et<sub>2</sub>O)]<sub>SBA-15 LP-(700)</sub> (M4) in propylene metathesis</b>	<b>244</b>
<b>6. Conclusion</b>	<b>247</b>
Experimental section	248
Notes and references	251
 <b>Conclusion générale</b>	<b>255</b>
 <b>ANNEX I: Grafting techniques using the double Schlenk apparatus</b>	<b>267</b>
 <b>ANNEX II: Continuous flow reactor for the gas conversion</b>	<b>269</b>
 <b>ANNEX III: Crystallographic data</b>	<b>271</b>
 <b>ANNEX IV: Determination of specific surface by the BET method</b>	<b>273</b>
 <b>ANNEX V: Synthesis of [(≡SiO)<sub>2</sub>Zr(<sup>13</sup>CH<sub>2</sub>Ph)<sub>2</sub>] (M'3)</b>	<b>275</b>



## **Introduction générale**



Cette thèse sera consacrée au développement de nouveaux catalyseurs métallacalix[4]arènes supportés sur silice pour la valorisation des alcanes et des oléfines. Ce mémoire sera divisé en cinq chapitres.

Le premier chapitre dressera une étude bibliographique sur la Chimie Organométallique de Surface (COMS) et ses limites, ainsi que sur les techniques connues dans la préparation de matériaux calixarènes/support oxyde. A la suite de cette étude, les objectifs et l'approche pour aborder ce sujet seront présentés.

Le chapitre II sera consacré à l'élaboration d'une nouvelle méthode de greffage et de caractérisation de ligands du type phénoxy sur une surface silice, afin de prouver un nouveau concept d'ancre de bras espaceurs.

Les chapitres III et IV concerneront les synthèses de nouveaux complexes métallacalix[4]arènes solubles de métaux de transition des groupes IV et V, respectivement. Ces composés serviront, autant que possible, de modèles de leurs analogues greffés sur supports silice, synthétisés par la suite dans le chapitre V. Ils permettront aussi, par des études catalytiques en polymérisation de l'éthylène dans le cas du groupe IV, de comprendre l'influence des différents modes de coordination offerts par les calixarènes dans l'activité catalytique du centre métallique.

Enfin, le chapitre V présentera la préparation et la caractérisation de nouveaux matériaux métallacalix[4]arènes/silice mésoporeuse des métaux de transition des groupes IV-VI. Une étude comparative en métathèse des oléfines entre ces systèmes et leurs analogues directement liés à la surface de silice sera présentée.



# **Chapitre I**

## **Etude bibliographique**



## 1. Introduction: les catalyses homogène et hétérogène, avantages et inconvénients

La catalyse a une place primordiale en industrie pharmaceutique et pétrochimique, et de plus en plus dans la sauvegarde de l'environnement et la chimie verte. Plus de 60% des produits chimiques et 90% des procédés chimiques sont basés sur la catalyse, qui a connu un essor important depuis le début des années 1950, notamment avec le développement de la chimie organométallique et inorganique.

Suivant le type de catalyseur mis en jeu, on distingue différentes catalyses : homogène, hétérogène ou enzymatique, cette dernière ne sera pas développée dans cette étude. Le catalyseur, suivant son état liquide ou solide, va présenter à la fois des avantages et des inconvénients, plus particulièrement quant à son recyclage, la sélectivité des réactions, et pour des questions environnementales.

### 1.1 La catalyse homogène

En solution, la répartition homogène des différents sites actifs catalytiques, tout comme le contrôle de leur environnement et de leur structure, constituent les principaux avantages de la catalyse homogène par des complexes organométalliques dans des conditions idéales. Par conséquent, chacune des interactions entre lesdits sites actifs et le substrat sont uniformes du point de vue énergétique, présentant en général de grandes sélectivités (**Schéma 1**).

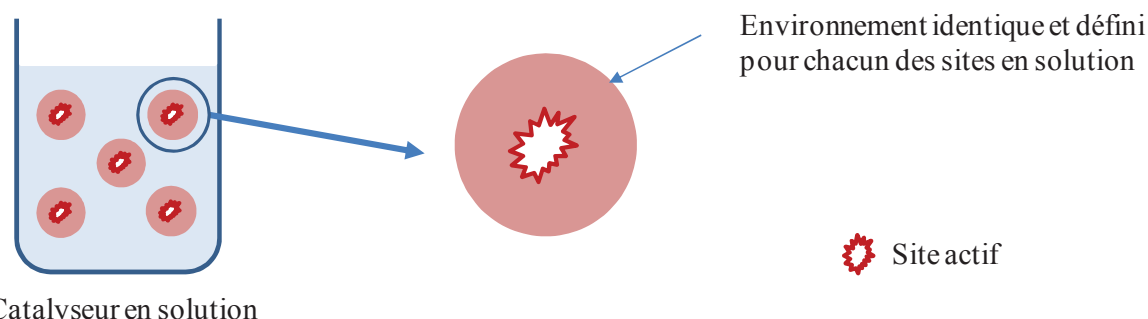


Schéma 1: Représentation schématique des sites actifs en catalyse homogène

Le catalyseur homogène est facilement caractérisable par les méthodes de routine (IR, RMN, spectroscopie de masse...) et il est donc aisément d'établir une relation structure-activité en fonction de l'environnement du site actif. Cependant, les inconvénients majeurs d'un tel

système catalytique sont : i) le non-recyclage du catalyseur, car difficilement séparable des produits obtenus, ii) l'utilisation de solvants polluants, contraire au concept de la chimie verte, et dans certain cas iii) la désactivation du catalyseur par des processus bimoléculaires.

## 1.2 La catalyse hétérogène

Les catalyseurs hétérogènes, quant à eux, ne présentent pas une telle distribution uniforme des sites actifs dans l'espace, car fixés de manière aléatoire sur le support. La plupart sont en forte interaction, ce qui leur donne un caractère moins sélectif lors des réactions (**Schéma 2**). Il en résulte ainsi une distribution hétérogène de l'activité et de la sélectivité de chaque site, et ceci de manière totalement incontrôlable. De plus, la relation structure-activité est difficile à établir car les techniques de caractérisation en phase solide ne sont pas forcement assez sensibles pour obtenir des informations précises sur chaque site actif. Par contre, la séparation du catalyseur des produits obtenus (ex : catalyse des gaz), donc son recyclage, et le fait de ne pas obligatoirement utiliser des solvants, constituent les points forts de la catalyse hétérogène, très prisée par l'industrie chimique.

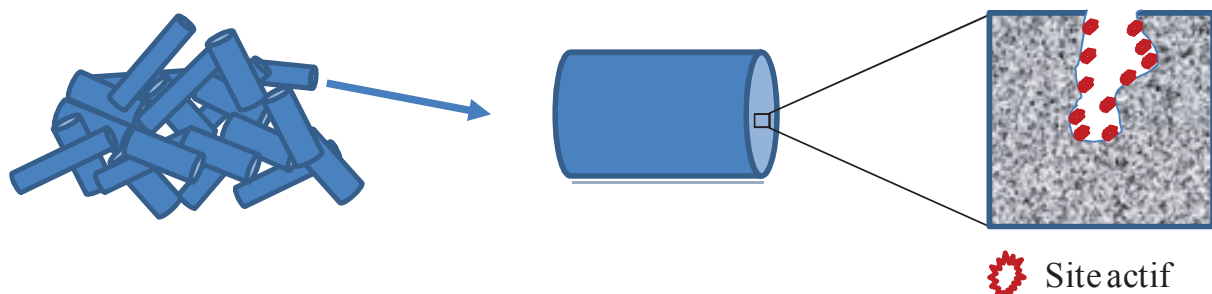
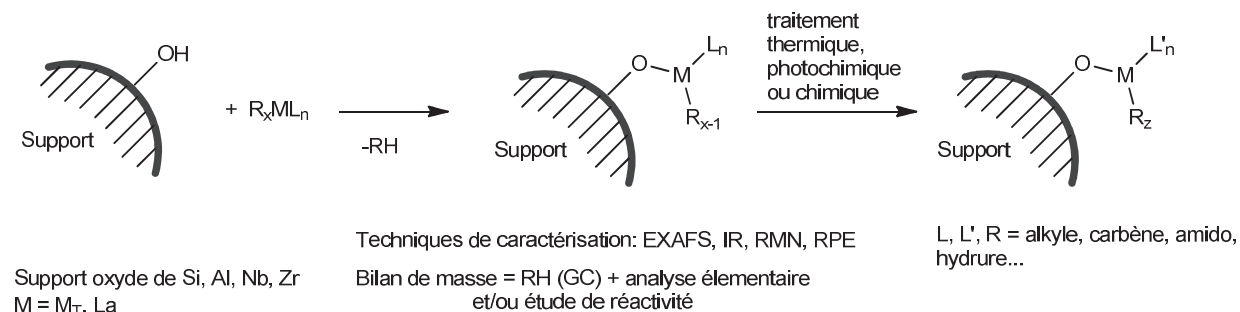


Schéma 2: Représentation schématique des sites actifs en catalyse hétérogène

Il convient donc de rassembler les avantages des catalyses homogène et hétérogène en créant des systèmes catalytiques en phase solide, recyclables, sélectifs, dont les sites actifs doivent être totalement caractérisés et bien définis, et pouvant amener à des réactions nouvelles. Le développement récent des techniques d'analyse de surface telle que la RMN à l'état solide peut faciliter les études mécanistiques menant à une meilleure compréhension des processus élémentaires de chimie organométallique, ainsi qu'à l'amélioration desdits catalyseurs.

## 2. Concept de la Chimie Organométallique de Surface

La chimie organométallique de surface (COMS ou SOMC en anglais) représente une nouvelle approche de la catalyse hétérogène<sup>1</sup>: elle consiste à greffer des complexes organométalliques sur une surface oxyde ou métallique. Les espèces de surface, liées par une ou plusieurs liaisons ioniques ou covalentes avec le support, présenteront ainsi une sphère de coordination bien définie autour d'un centre métallique (**Schéma 3**).<sup>1a,2</sup> Elles se caractérisent par le nombre de liaisons reliant le métal à la surface mais aussi par le type et la quantité de ligands coordinés. Ces ligands peuvent participer à la réaction catalytique mise en jeu ou encore être spectateurs tels que les ligands oxo, alkoxo, amido ou imido, et aussi influencer l'activité et la sélectivité de la réaction catalytique. Ainsi peuvent être obtenus des complexes mono-, bi- ou tripodaux suivant si le métal est greffé sur un, deux ou trois oxygènes dans le cas des supports oxyde. Le **Schéma 3** suivant illustre la stratégie de synthèse et de caractérisation des espèces supportées:



**Schéma 3: Synthèse et caractérisation à l'état solide des composés organométalliques de surface**

Les avantages qui découlent de cette approche sont nombreux. Elle rassemble ceux de la catalyse hétérogène, à savoir le recyclage du catalyseur, la séparation aisée des produits et doit, comme en catalyse homogène, permettre de préparer des catalyseurs à site unique, permettant de découvrir de nouvelles réactions chimiques plus sélectives. Aussi, en connaissant les caractéristiques du centre actif, il sera possible d'établir un mécanisme réactionnel. Enfin, l'isolation et la mobilité limitée des centres métalliques greffés permettent d'éviter, contrairement à la catalyse homogène, des réactions de décomposition (réactions bimoléculaires,<sup>3</sup> perte de ligands...) et d'accroître ainsi la stabilité de ces complexes.

Au laboratoire, il a été étudié la réactivité de nombreux complexes organométalliques utilisant un grand nombre de métaux de transition (Groupes IV-VIII), greffés sur des supports

variés (oxydes inorganiques amorphes<sup>4</sup>, zéolithes<sup>5</sup>, surfaces métalliques<sup>6</sup>). Ainsi, la chimie organométallique de surface a ouvert une voie sur des réactions parfois inédites en catalyse homogène ou hétérogène et ayant un très fort potentiel, notamment dans la pétrochimie. Les espèces phares du laboratoire sont:

- les ligands hydrures pour la métathèse des alcanes qui permet de transformer un alcane léger en ses homologues supérieurs ou inférieurs<sup>7</sup>, le couplage non-oxydant du méthane<sup>8</sup>, la métathèse croisée entre les aromatiques et les alcanes<sup>9</sup>, la dépolymérisation des polyoléfines<sup>10</sup> ou la conversion directe de l'éthylène en propylène<sup>11</sup>
- les ligands cyclopentadienyles pour la polymérisation des oléfines<sup>12</sup>
- les ligands oxo, alkoxo ou peroxo dans les réactions d'oxydation ou d'époxydation.<sup>1b,13</sup>
- les ligands carbènes ou carbynes pour la métathèse des oléfines ou des acétyléniques<sup>14</sup>

Les propriétés catalytiques de chacune de ces espèces préparées par voie COMS dépendent de la sphère de coordination du métal, du nombre de liaisons avec le support mais aussi de la nature de ces supports oxyde (silice, alumine, silice-alumine....). Dans le paragraphe suivant seront décrits les différents supports utilisés en COMS pour le greffage de complexes organométalliques.

## 2.1 Les différents supports oxydes

### 2.1.1 La silice

#### • La silice amorphe

La silice amorphe est un matériau construit à partir du bloc élémentaire  $\text{SiO}_4$ . Au laboratoire, la silice amorphe généralement utilisée est du type pyrogénique Degussa Aerosil 200. Il s'agit d'un support neutre et non poreux constitué de sphères régulières d'un diamètre de 150 Å. Elle se présente comme un réseau complexe de ces blocs  $\text{SiO}_4$  avec une distribution aléatoire des angles Si-O-Si, dont la valeur est centrée autour de 140°. Des groupements silanols Si-OH sont localisés sur la surface externe des groupes  $\text{SiO}_4$  présents à la périphérie des particules de silice et distribués de manière hétérogène. Plusieurs types de silanols ont été identifiés par le nombre de fonctions hydroxyle par atome de silice et par leur proximité dans l'espace. Ainsi on retrouve des silanols libres : isolés ( $\equiv\text{SiOH}$ ), géminaux ( $=\text{Si}(\text{OH})_2$ ),

vicinaux (ou pontés) et les silanols liés, c'est-à-dire interagissant par des liaisons hydrogènes avec des oxygènes de la surface (**Schéma 4**).

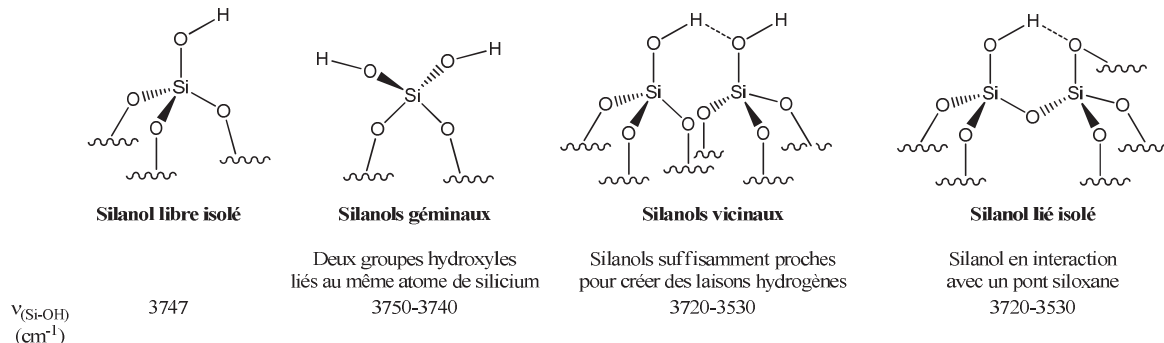


**Schéma 4:** Les différents types de silanols de surface du support silice et leur bande caractéristique en IR

L'IR d'une telle silice traitée à basse température montre une bande large dans la région 3600-3100 cm<sup>-1</sup>. Lorsqu'elle est traitée à des températures plus élevées (200, 300, 500 ou 700°C), les silanols interagissant par liaison hydrogène réagissent et sont éliminés sous forme d'une molécule d'eau, formant de nouveaux ponts siloxanes et abaissant la densité des silanols (**Schéma 5**). Ainsi la concentration des silanols de surface peut chuter de 3.5 OH.nm<sup>-2</sup> pour une silice traitée à 200°C, notée SiO<sub>2-(200)</sub>, à environ 0.8 OH.nm<sup>-2</sup> pour la silice SiO<sub>2-(700)</sub>.<sup>15</sup> Les IR de ces silices traitées montrent désormais une bande fine vers 3747 cm<sup>-1</sup>, caractéristique de l'elongation des silanols de surface isolés. La surface de la silice présente aussi des ponts siloxanes,  $\equiv\text{Si}-\text{O}-\text{Si}\equiv$ , qui forment des cycles à 2 ou 3 membres et dont la concentration augmente avec la température pour atteindre 1.5 puis 2.3 (SiO)<sub>2</sub> nm<sup>-2</sup> à 600 et 1200 °C respectivement (**Schéma 5**).<sup>16</sup>

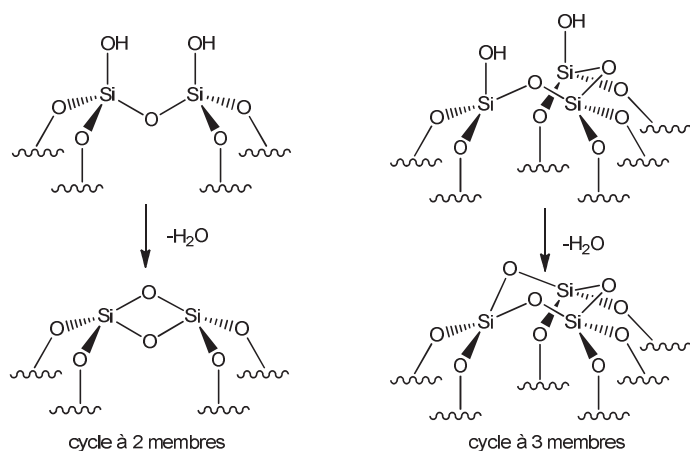


**Schéma 5:** Les différents types de cycles et ponts siloxanes de surface du support silice

La présence de ces cycles siloxanes très tendus doit être prise en compte lors de la réaction avec le complexe moléculaire. En effet, lors des réactions avec des complexes organométalliques de métaux très oxophiles (*e.g.* zirconium), les ponts siloxanes peuvent être ouverts avec formation concomitante d'une liaison  $\equiv \text{Si}-\text{R}$  (**Schéma 6**).<sup>17</sup>

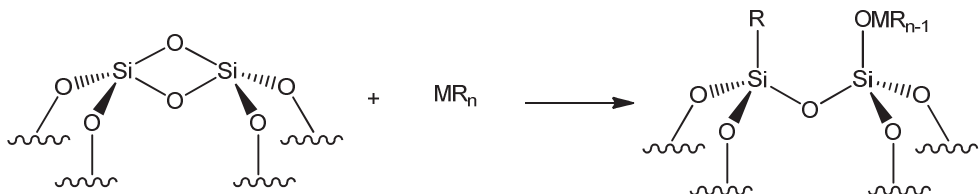


**Schéma 6:** Ouverture des ponts siloxanes en présence de complexes organométalliques de métaux oxophiles

- **Les silices mésoporeuses structurées**

Les silices mésoporeuses structurées, synthétisées pour la première fois en 1992 par la firme Mobil sous le nom de MCM (ou Mobile Composition of Matter) connaissent depuis une vingtaine d'années un vif succès car leurs applications dans la catalyse, les sciences de la séparation, la délivrance ciblée de médicaments ou encore dans les appareillages optiques sont de plus en plus prisées. Contrairement à la silice amorphe, elles constituent une famille particulière des tamis moléculaires dont le diamètre des pores est supérieur à 20 Å mais limité à 80 Å. En 1998, apparaît de nouvelles silices mésoporeuses à structure hexagonale, plus grands pores (de 20 à 300 Å), haut niveau d'ordre et plus stables thermiquement, du type SBA ou Santa-Barbara Amorphous, découvertes par l'équipe de Stucky à l'Université de Californie à Santa-Barbara.<sup>18</sup> Nous développerons au cours du chapitre V la synthèse, les caractérisations et les propriétés des SBA-15 larges pores, qui sera le support privilégié au cours de ce projet.

### 2.1.2 *L'alumine*

L'alumine, de formule  $\text{Al}_2\text{O}_3$ , est un oxyde très complexe, dont la structure fait l'objet de nombreuses études dans la littérature.<sup>19</sup> Contrairement à la silice ou à la silice-alumine, l'alumine est un solide ionique où les atomes d'aluminium ont des coordinations différentes. En fonction de la nature de la face cristallographique et de la température de déshydroxylation du solide, la structure de la surface varie. Plusieurs groupes de recherche ont essayé de modéliser la surface de différentes faces cristallographiques de l'alumine (en particulier les alumines de phases de transition  $\gamma$  ou  $\eta$ ). Le modèle de Knözinger est largement accepté.<sup>19e</sup>

Le modèle de Sautet<sup>19i</sup> établi grâce à une approche théorique, est très proche de celui de Busca et explique la plupart des données expérimentales.<sup>19f,g</sup>

L’alumine calcinée avant utilisation à 500 °C sous flux d’air sec puis déshydroxylée à la même température sous vide dynamique ( $10^{-5}$  torr) présente des fréquences d’absorption des vibrations en spectroscopie IR des différents groupes hydroxyles Al-OH, qui sont attribués en fonction du modèle choisi (**Table 1, Figure 1**) :

- OH terminal coordonné à un seul atome d’aluminium dans un environnement tétraédrique ( $\text{Al}_{\text{IV}}$ ) :  $\text{OH}-\mu_1-\text{Al}_{\text{IV}}$ , à un aluminium pentaédrique ( $\text{Al}_{\text{V}}$ ) :  $\text{OH}-\mu_1-\text{Al}_{\text{V}}$ , ou encore à un aluminium dans un environnement octaédrique ( $\text{Al}_{\text{VI}}$ ) :  $\text{OH}-\mu_1-\text{Al}_{\text{VI}}$
- OH pontant lié à :
  - deux atomes d’aluminium dans un environnement octaédrique  $\text{OH}-\mu_2-\text{Al}_{\text{VI}}$
  - trois atomes d’aluminium dans une coordination octaédrique  $\text{OH}-\mu_3-\text{Al}_{\text{VI}}$

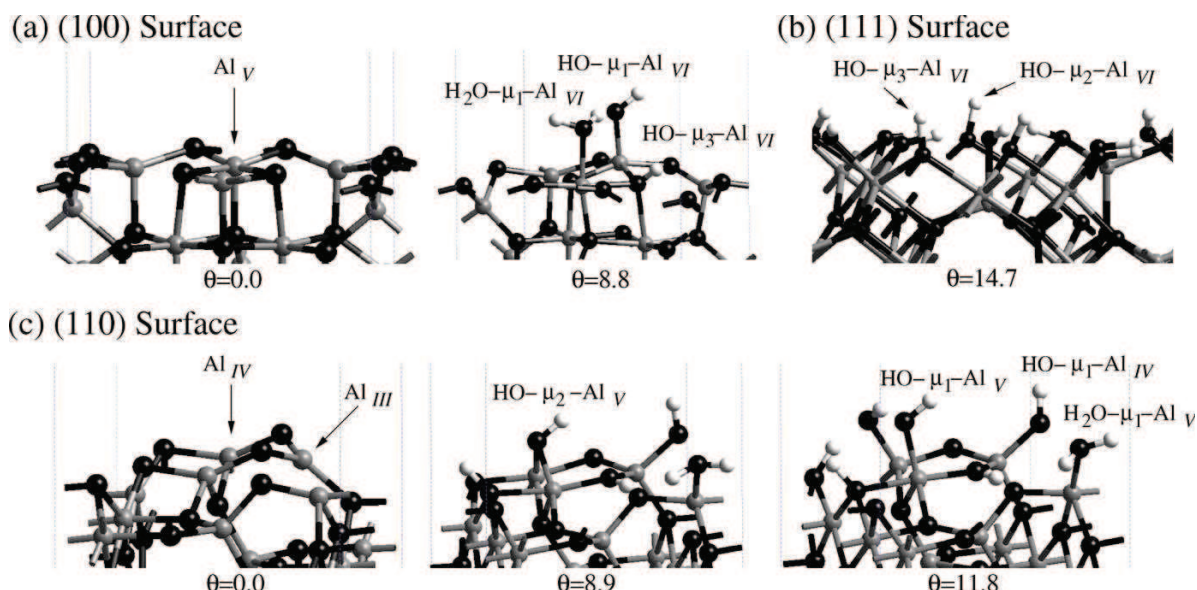


**Figure 1:** Configurations des hydroxyles des faces (a)  $\gamma\text{-Al}_2\text{O}_3(100)$ , (b)  $\gamma\text{-Al}_2\text{O}_3(111)$ , and (c)  $\gamma\text{-Al}_2\text{O}_3(110)$  pour différentes densités d’hydroxyles ( $\theta = \text{in OH}.\text{nm}^{-2}$ ), proposées d’après le modèle de Sautet.<sup>19i</sup>

**Table 1:** Attribution des vibrations IR des groupes hydroxyles en fonction du modèle choisi.

$\nu_{(\text{Al-OH})} (\text{cm}^{-1})$	Knözinger	Busca	Sautet
3785-3800	$\text{OH}-\mu_1-\text{Al}_{\text{VI}}$	$\text{OH}-\mu_1-\text{Al}_{\text{IV}}$	$\text{OH}-\mu_1-\text{Al}_{\text{IV}} (110)$
3760-3780	$\text{OH}-\mu_1-\text{Al}_{\text{IV}}$	$\text{OH}-\mu_1-\text{Al}_{\text{IV}} (+ \text{lacune})$	$\text{OH}-\mu_1-\text{Al}_{\text{VI}} (100)$
3740-3745	$\text{OH}-\mu_2-(\text{Al}_{\text{VI}}-\text{Al}_{\text{VI}})$	$\text{OH}-\mu_1-\text{Al}_{\text{VI}}$	$\text{OH}-\mu_3-\text{Al}_{\text{VI}} (111)$
3730-3735	$\text{OH}-\mu_2-(\text{Al}_{\text{IV}}-\text{Al}_{\text{VI}})$	$\text{OH}-\mu_1-\text{Al}_{\text{VI}} (+ \text{lacune})$	$\text{OH}-\mu_1-\text{Al}_{\text{V}} (110)$
3710-3690	$\text{OH } \mu_3$	$\text{OH } \mu_2$	$\text{OH}-\mu_2-\text{Al}_{\text{VI}} (110)$
3590-3650	H lié	$\text{OH } \mu_3$	$\text{OH}-\mu_3-\text{Al}_{\text{VI}} (100)$

Le spectre RMN  $^1\text{H}$  présente deux pics à 1.9 et 0.11 ppm attribués aux fonctions hydroxyles tandis que le spectre MAS-RMN  $^{27}\text{Al}$  montre deux pics à 62 ( $\text{Al}_{\text{IV}}$ ) et 4.2 ppm ( $\text{Al}_{\text{VI}}$ ). La présence de tous ces aluminiums tétraédriques et octaédriques montre la complexité de la surface d'alumine, et donc, comme les supports silice, leur influence dans la formation de différentes espèces organométalliques lors du greffage.

## 2.2 Hétérogénéité des supports oxydes dans la Chimie Organométallique de Surface

Comme décrit précédemment, la COMS permet, dans des conditions idéales, de palier les problèmes des catalyses homogène et hétérogène en greffant des espèces organométalliques sur des surfaces-ligands (oxydes...). Le challenge consiste donc à développer des catalyseurs hétérogènes à site unique, sans interactions site-site et qui présentent les avantages de cinétique et de sélectivité de la catalyse homogène. Mais la synthèse de tels composés sur les différents supports oxydes conduisent souvent à un mélange d'espèces, cependant définies, du à l'hétérogénéité de la surface, et notamment à la distribution des ponts M-O-M, de la nature des fonctions hydroxyles et leur densité de surface. Plusieurs études de greffage de divers composés organométalliques (Zr, Ti, Ta, W...) ont montré que seule une faible quantité de ces espèces constitue le centre actif pour la réaction envisagée. Les exemples des espèces supportées obtenues par chimie organométallique de surface du zirconium, titane, tantale, et tungstène seront développés, métaux étudiés par la suite dans le projet. Deux types majeurs d'espèces de surface de métaux de transition ont été développés au laboratoire :

- Les complexes alkyles supportés obtenus par réaction de surface entre un complexe organométallique et une silice déshydroxylée à différentes températures
- Les hydrures de ces métaux obtenus par traitement sous hydrogène des complexes alkyles correspondants.

Ces hydrures de métaux de transition supportés présentent un grand intérêt dans la polymérisation des olefines<sup>20</sup>, l'hydrogénolyse des polyoléfines<sup>10,21</sup> et des alcanes<sup>22</sup> ou encore la métathèse des alcanes<sup>23</sup>. Une étude bibliographique sur ces systèmes catalytiques sera développée ci-dessous.

### 2.2.1 Cas des espèces de zirconium supportées sur silice

La structure du complexe de surface obtenu par réaction entre le complexe moléculaire tétranéopentyle de zirconium  $\text{Zr}(\text{CH}_2t\text{Bu})_4$ , noté  $\text{ZrNp}_4$ , avec la silice dépend de la température de déshydroxylation de cette dernière ( $\text{SiO}_{2-(200)}$ ,  $\text{SiO}_{2-(500)}$ ,  $\text{SiO}_{2-(700)}$ ). Si avec  $\text{SiO}_{2-(500)}$  ou  $\text{SiO}_{2-(700)}$  le complexe de surface  $[(\equiv\text{SiO})\text{ZrNp}_3]$  monopodal est obtenu sélectivement (**Schéma 7**),<sup>24</sup> l'espèce bipodale  $[(\equiv\text{SiO})_2\text{ZrNp}_2]$  a été isolée et caractérisée sur  $\text{SiO}_{2-(200)}$ , du à la proximité des fonctions silanols.

L'hydrogénolyse de l'espèce monopodale  $[(\equiv\text{SiO})\text{ZrNp}_3]$  à 150°C conduit à la formation de deux espèces hydrures de zirconium supportés  $[(\equiv\text{SiO})_3\text{ZrH}]$  et  $[(\equiv\text{SiO})_2\text{ZrH}_2]$  (**Schéma 7**).<sup>25</sup> Les différentes espèces de surfaces ont été caractérisées par EXAFS, dosage des silanes, RMN  $^1\text{H}$  et  $^{29}\text{Si}$  à l'état solide.

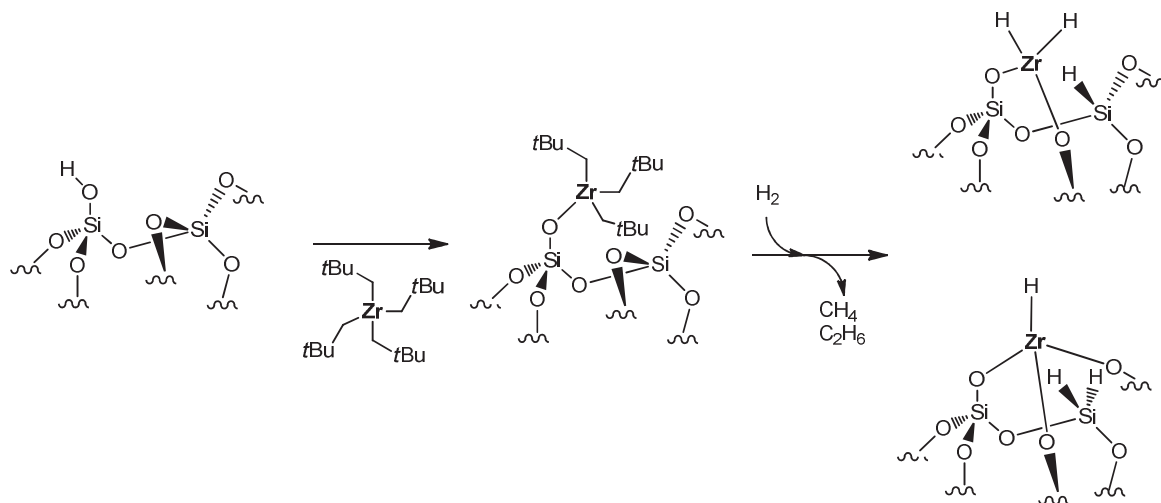


**Schéma 7:** Synthèse des espèces alkyles et hydrures de zirconium greffées sur silice

Le zirconium étant oxophile, il y a ouverture de ponts siloxane avec formation d'une nouvelle liaison Zr-O et d'un silane de surface lorsque la distance entre le pont et le centre métallique est assez courte. Par conséquent, un dihydrure de zirconium bipodal est obtenu à hauteur de 30% grâce à la proximité entre un seul pont siloxane et le centre métallique de surface. Le composé monohydrure tripodale est obtenu majoritairement à 70% par ouverture de deux ponts siloxane. Sauer *et al.* a pu déterminer par des études analytiques (RMN  $^1\text{H}$  à l'état solide, IR, GPC) lors de l'activation du méthane que l'espèce dihydrure en minorité réagit rapidement à température ambiante pour former  $[(\equiv\text{SiO})_2\text{ZrMe}_2]$  via l'intermédiaire  $[(\equiv\text{SiO})_2\text{ZrHMe}]$ , tandis que son analogue monohydrure donne plus lentement et partiellement  $[(\equiv\text{SiO})_3\text{ZrMe}]$  à 150°C (**Schéma 8**).<sup>25</sup>

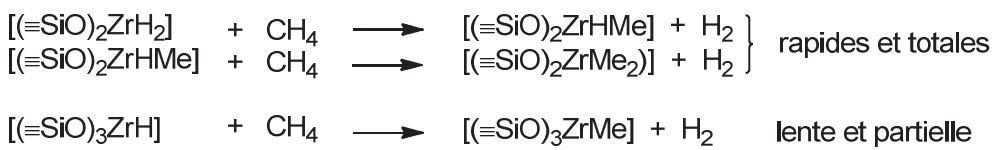


Schéma 8: Activation du méthane par les espèces hydrure de zirconium supportées sur silice

Ce cas illustre bien l'influence du nombre de ponts siloxanes, plus ou moins proches du centre métallique, sur la formation des différentes espèces de surface, ainsi que sur leur réactivité.

### 2.2.2 Cas des espèces de titane supportées sur silice

Le greffage de  $\text{Ti}(\text{CH}_2t\text{Bu})_4$ , noté  $\text{TiNp}_4$ , sur la MCM-41<sub>(500)</sub> conduit aux deux espèces monopodale  $[(\equiv \text{SiO})\text{TiNp}_3]$  et bipodale  $[(\equiv \text{SiO})_2\text{TiNp}_2]$ , majoritaire à 65%, tandis qu'avec  $\text{SiO}_2$ <sub>(500)</sub>, seule l'espèce monopodale est obtenue (Schéma 9).<sup>4</sup> La différente répartition des silanols sur les deux supports, plus proches dans le cas de la silice mésoporeuse, mais aussi à cause de la concavité des canaux de la MCM-41, sont à l'origine de cette distribution. Avec la MCM-41<sub>(200)</sub>, l'espèce bipodale est obtenue exclusivement, étant donné la densité des silanols, et donc leur proximité, plus élevée. Les analyses par EXAFS, informant sur la nature et la distance des atomes au voisinage direct du métal, pour la MCM-41<sub>(500)</sub>, montrent qu'environ 1.7 oxygènes sont à 1.81 Å et 2.3 carbones à 2.01 Å du centre métallique, d'où le ratio 35/65 pour les espèces  $[(\equiv \text{SiO})\text{TiNp}_3]/[(\equiv \text{SiO})_2\text{TiNp}_2]$ .

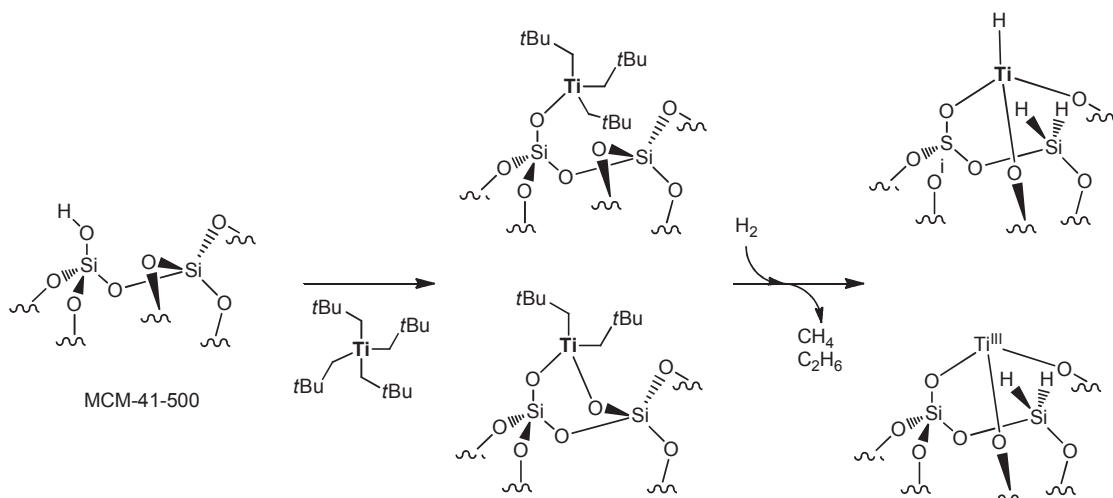


Schéma 9: Synthèse des espèces alkyles et hydrure de titane greffées sur MCM-41<sub>(500)</sub>

Traitées sous  $\text{H}_2$  à 150°C, un mélange de deux espèces tripodales  $[(\equiv \text{SiO})_3\text{TiH}]$  et  $[(\equiv \text{SiO})_3\text{Ti}^{\text{III}}]$  sont obtenues.<sup>26,27</sup> En  $^1\text{H}$ -RMN à l'état solide, l'hydrure de titane donne un pic à 8.5 ppm. Une étude RMN 2D double-quanta montre qu'il y a seulement des monohydrures de

titane, contrairement aux bis-hydrides observés dans le cas du zirconium. Les études EXAFS et RPE confirment les espèces tripodales  $[(\equiv \text{SiO})_3 \text{TiH}]$  et  $[(\equiv \text{SiO})_3 \text{Ti}^{\text{III}}]$  en ratio 80/20, avec environ 3 oxygènes équidistants à 1.83 Å du titane et 3 siliciums formant un angle Si-O-Ti d'environ 160°.

### 2.2.3 Cas des espèces de tantale supportées sur silice

Dans le cas de la chimie de surface du groupe V, la réaction entre le carbène de tantale  $\text{Ta}(=\text{CH}t\text{Bu})(\text{CH}_2t\text{Bu})_3$  (noté  $\text{TaNp}'\text{Np}_3$ , Np' représentant le ligand neopentylidène) et  $\text{SiO}_{2-(500)}$ , donne deux complexes alkyle de surface bipodal  $[(\equiv \text{SiO})_2 \text{TaNp}'\text{Np}]$  et monopodal  $[(\equiv \text{SiO}) \text{TaNp}'\text{Np}_2]$  (**Schéma 10**).<sup>28</sup> Seule l'espèce bipodale  $[(\equiv \text{SiO})_2 \text{TaNp}'\text{Np}]$  est obtenue dans le cas de  $\text{SiO}_{2-(300)}$  renfermant en majorité des silanols vicinaux. Inversement, seule l'espèce monopodale  $[(\equiv \text{SiO}) \text{TaNp}'\text{Np}_2]$  est observée avec  $\text{SiO}_{2-(700)}$  qui présente des silanols isolés.<sup>29</sup> L'hydrogénolyse de ces complexes de surface conduit à des espèces polyhydrures intermédiaires bis-siloxy  $[(\equiv \text{SiO})_2 \text{TaH}_x]$  ( $x = 1,3$ ) qui, comme dans le cas du zirconium, vont mener, par à un réarrangement du support silice, à la formation concomitante de silanes de surface et de nouvelles liaisons Ta-O.

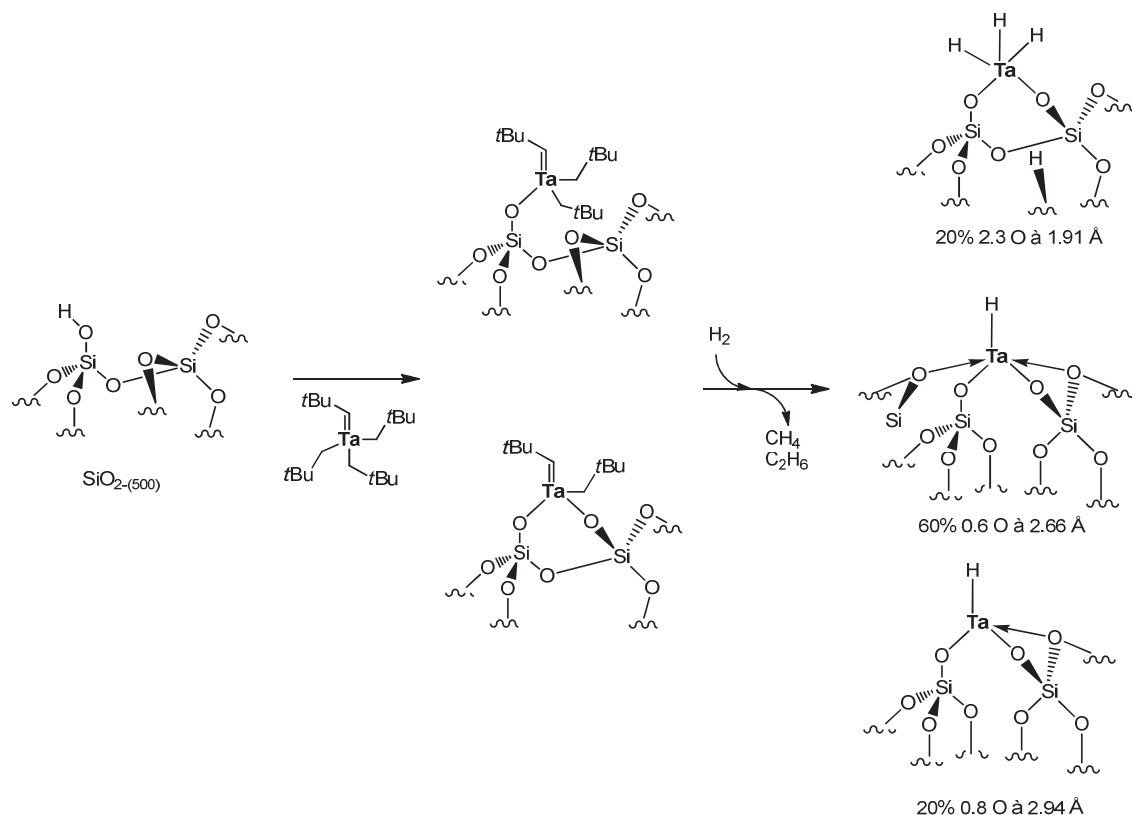


**Schéma 10:** Synthèse des espèces alkyles et hydrures de tantale greffées sur silice

Les trois espèces finales obtenues, actives dans la métathèse des alcanes, ont été mises en évidence par étude EXAFS. Les hydrures de tantale sont tous bipodaux (2.3 O à 1.91 Å), quelque soit la température de déshydroxylation de la silice, mais 20% ont en plus un oxygène à 2.94 Å du centre métallique, distance caractéristique d'une liaison dative entre un oxygène d'un pont siloxane et le tantale, et 60% interagissent avec deux ponts siloxanes (0.8 O à 2.94 Å et 0.6 O à 2.66 Å). Diverses expériences, notamment l'étude de l'empoisonnement des sites catalytiques par du dioxygène dans la métathèse du propane, permet de mettre en évidence une hétérogénéité de sites.<sup>30</sup> Ainsi, l'activité catalytique obtenue après 70 heures de métathèse du propane en fonction du pourcentage d'hydrures restants après empoisonnement à l'oxygène est représenté sur la **Figure 2**. Le caractère sélectif de l'oxygène envers les espèces inactives apparaît plus clairement. En effet, jusqu'à environ 50% d'empoisonnement des sites catalytiques, le TON reste quasiment constant autour de 50. Lorsque l'empoisonnement dépasse les 50%, le TON chute brutalement, mettant en évidence que la moitié des espèces de surface sont inactives dans la métathèse du propane.

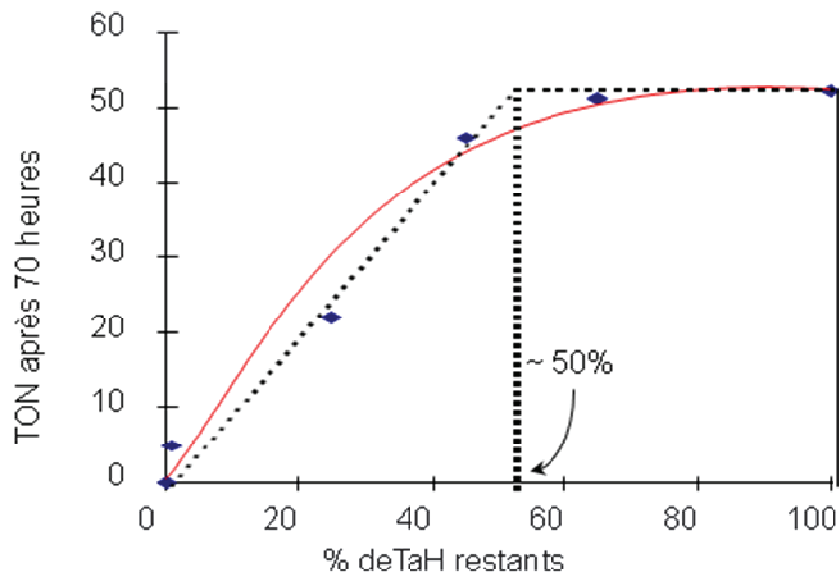


Figure 2: Activité catalytique (obtenue après 70 h) des espèces hydrures de tantale de surface dans la métathèse du propane en fonction du pourcentage d'hydrures restant après empoisonnement à l'oxygène

#### 2.2.4 Cas des espèces de tungstène supportées sur silice

Dans le cas du tungstène, métal du groupe VI, le greffage des complexes  $\text{W}(\equiv\text{C}t\text{Bu})(\text{CH}_2t\text{Bu})_3$ , ou  $\text{W}(=\text{NAr})(=\text{CH}t\text{Bu})(\text{CH}_2t\text{Bu})_2$ , sur les silices  $\text{SiO}_{2-(200)}$  et  $\text{SiO}_{2-(700)}$  donne respectivement et sélectivement les espèces de surface bis-siloxy et mono-siloxy (**Schéma 11**).<sup>31</sup>

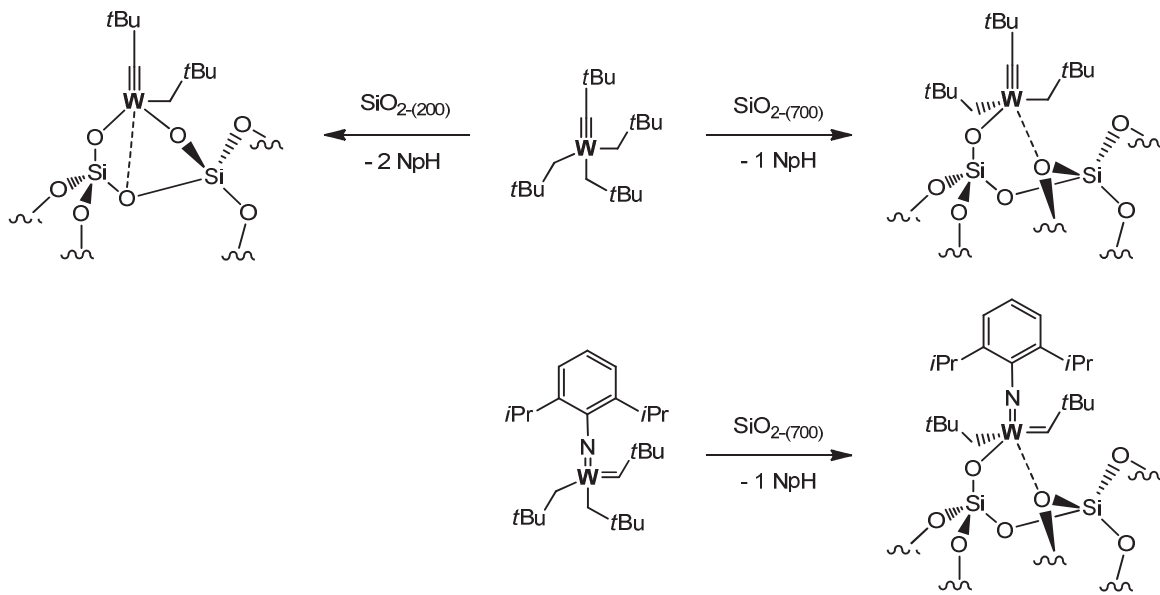


Schéma 11: Greffage des complexes  $\text{W}(\equiv\text{CtBu})(\text{CH}_2\text{tBu})_3$  et  $\text{W}(=\text{NAr})(=\text{CHtBu})(\text{CH}_2\text{tBu})_2$  sur  $\text{SiO}_2-(200)$  et  $\text{SiO}_2-(700)$

Ces complexes supportés ont été caractérisés par spectroscopie infra-rouge, RMN à l'état solide ( $^1\text{H}$ ,  $^{13}\text{C}$ , HETCOR) et bilan de matière (analyses élémentaires et quantification par GC du néopentane dégagé). En particulier, l'EXAFS montre la présence d'un atome d'oxygène à 2.43 Å du tungstène, caractéristique d'un pont siloxane coordonné diminuant ainsi le caractère électrophile du métal.

### 2.3 Conclusion

Les différents exemples précédents confirment que la réaction entre un complexe organométallique et une surface oxyde conduit inévitablement à un mélange d'espèces de surface, néanmoins connues et définies. La structure monopodale ou bipodale de ces espèces de surfaces dépendent de la nature du support et de la température de déshydroxylation. La caractérisation par spectroscopie EXAFS montre que des ponts siloxane peuvent être présents dans la sphère de coordination du métal oxophile. Ces derniers interviennent dans la transformation des espèces organométalliques supportées en leurs espèces hydrures correspondantes par une restructuration de la surface et par ouverture de ces ponts avec formation d'hydrure de silicium. Ce phénomène conduit à la formation d'un mélange de sites actifs dans de nombreuses réactions. Notre objectif est de palier ces problèmes, à savoir éviter ces interactions métal-support et favoriser la formation de sites uniques en faisant intervenir un bras espaceur. Le prochain paragraphe présente une étude bibliographique dans

l'utilisation d'espaces organiques pour le greffage de complexes organométalliques sur support oxyde, qui pourra constituer une solution à ce challenge.

L'immobilisation de complexes organométalliques sur des surfaces oxydes au travers d'espaces organiques est l'approche la plus utilisée pour générer des catalyseurs hétérogènes stables à site unique. Dans le cas du support silice, la stratégie générale consiste en la réaction de ce dernier, préalablement activé, avec un ligand fonctionnalisé portant un groupe alkoxysilane -Si(OR)<sub>3</sub> (R = Me, Et).<sup>4</sup> La protonolyse du groupe alkoxysilane par les silanols de surface permet de former de nouvelles liaisons Si-O entre la surface et le ligand. Deux différentes approches peuvent cependant être envisagées. La première méthode consiste à greffer une espèce organométallique connue de Rh<sup>32</sup>, Cu(II)<sup>33</sup>, Mn<sup>34</sup>, Cr<sup>35</sup> ou Au(I)<sup>36</sup> portant le ligand espaceur alkoxysilane servant de point d'ancrage sur le support oxyde, tandis que la deuxième, la plus utilisée, propose de faire d'abord réagir le ligand espaceur alkoxysilane avec la surface de silice, suivi de l'incorporation *in situ* du fragment organométallique de Ru<sup>37</sup>, Cr<sup>38</sup>, Fe-Pd<sup>39</sup>, Au(III)<sup>40</sup>, Pd(II)<sup>40</sup>, Rh<sup>41</sup> voire Ti.<sup>42</sup> Bien que la première méthode soit préférée dans le greffage de composés organométalliques des groupes VII-VIII, moins réactifs envers les silanols de surface, elle reste toutefois peu applicable dans le cas des métaux oxophiles des groupes IV-VI, car une compétition entre les fragments organométalliques et alkoxysilane avec les silanols de surface peut entrer en jeu. C'est pour cela que notre choix a été porté sur la deuxième méthode.

Dans notre cas, il est indispensable de choisir un ligand qui présente des modes de coordination variés afin d'obtenir des sites uniques de structures similaires aux sites actifs obtenus sur la silice par voie COMS. Pour cela, le ligand espaceur doit avoir les propriétés suivantes :

- une rigidité relative lorsqu'il est greffé sur la surface
- une certaine stabilité thermique permettant de réaliser des études catalytiques à températures élevées (T < 300°C)
- la possibilité de contrôler précisément l'environnement du métal, à savoir le nombre, le type et la disposition des points d'ancrages et des ligands environnant (oxygènes, hétéroatomes...)

Les calixarènes, en particulier les dérivés du calix[4]arène, ont été choisis et seront utilisés pour préparer des matériaux mettant à disposition du centre métallique un nombre variable (de 1 à 4) et contrôlé de groupements hydroxyles suivant l'espèce mono-, bi-, tri- ou tétrapodale

souhaitée (**Schéma 12**). Cette nouvelle approche permettra d'apporter une réponse quant au problème de l'obtention de différents sites sur les surfaces oxydes et si on le souhaite, de disposer d'un large panel de fonctions (alcool, phosphine, imidazole, amine...) capables de complexer le métal dans un environnement pré-organisé, bien défini, et d'étendre cette méthodologie aux métaux de transition de droite. Ces différents matériaux pourront être utilisés dans de nombreuses réactions catalytiques telles que la métathèse des alcanes et des oléfines, hydrogénéation, oligomérisation ou encore hydroformylation des oléfines.

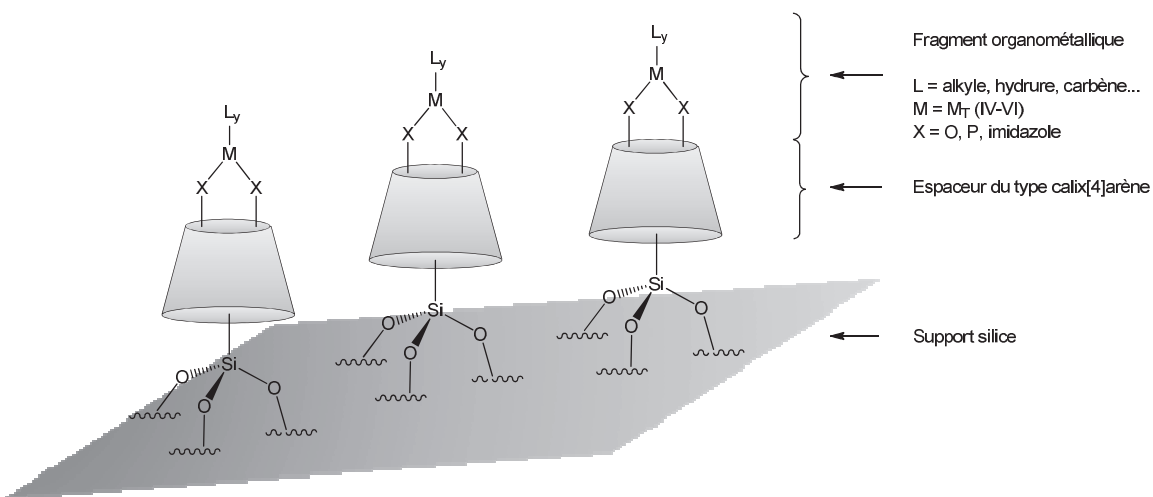


**Schéma 12:** Greffage de complexes organométalliques sur support silice *via* un espaceur du type calix[4]arène

Une étude bibliographique décrivant les dérivés calix[4]arènes et leur utilisation dans la préparation de matériaux sera l'objet du prochain paragraphe.

### 3. Les calixarènes

#### 3.1 Historique et nomenclature

L'origine des calixarènes remonte en 1872 lorsque Adolph von Baeyer obtint une résine noire en chauffant une solution de formaldéhyde avec du phénol.<sup>43</sup> Cependant, les techniques d'analyse de l'époque ne permettaient pas de caractériser ce nouveau composé et sa structure restera indéterminée jusqu'en 1905, où Leo Baekland s'inspira de cette même réaction pour produire le premier polymère synthétique commercial connu sous le nom de Bakelite<sup>44</sup>, de la famille des phenoplasts. C'est ainsi que dans les années 1940, Alois Zinke, de l'Université de Graz en Autriche,<sup>45</sup> s'intéressa dans la même perspective à la réaction entre différents *p*-alkylphénols et le formaldéhyde en présence d'hydroxyde de soude, pour obtenir

des composés solides et peu solubles que Zinke supposa cycliques et tétramériques. L'hypothèse de Zinke fut confirmée 30 ans plus tard par une étude cristallographique réalisée par G. D. Andretti.<sup>46</sup> A la fin des années 70, Gutsche étudia de manière systématique l'influence des conditions expérimentales sur la taille des oligomères cycliques formés par condensation de phénols et du formaldéhyde. Les oligomères les plus courants comportent de 4 à 8 unités phénoliques, mais des oligomères de plus de 10 unités phénoliques (jusqu'à 20) ont déjà été caractérisés.<sup>47</sup> Ces travaux fondamentaux permettent aujourd'hui de disposer de synthèses rationnelles permettant d'accéder, à l'échelle du laboratoire, à plusieurs centaines de grammes de ces oligomères cycliques. Pour décrire ces composés, Gutsche introduisit le terme de *p-R-calix[n]arène*. Le préfixe calix provient de la similitude entre la forme conique du tétramère à celle des vases grecs connus sous le même nom (en grec, *calix* = calice, **Figure 3**), et *arène* vient de l'incorporation des cycles aromatiques. [n] représente le nombre d'entités phénoliques formant le cycle, reliées par des ponts méthyléniques en position *ortho*, tandis que *R* qualifie le groupement présent en position *para* des fonctions phénols (**Schéma 13**).



**Figure 3:** Cratère en calice, Thèbes (début du IV<sup>eme</sup> siècle av. J.-C.) - Musée du Louvre.

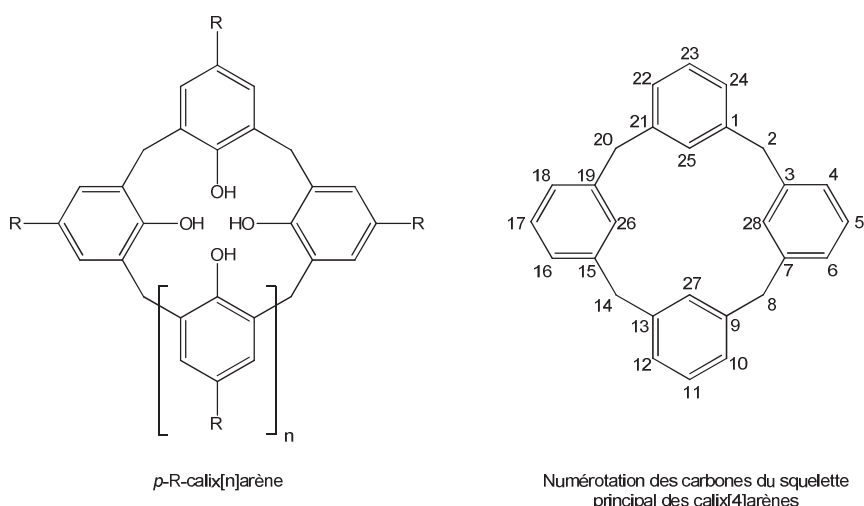


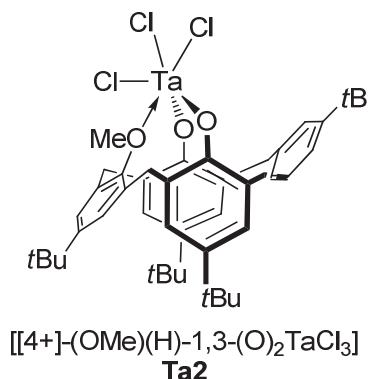
**Schéma 13: Représentation des *p-R-calix[n]arènes* et nomenclature générale des calix[4]arènes**

Nous nous sommes intéressés au cours de ce travail à la synthèse et au greffage des dérivés de calix[4]arène, dont la numérotation des atomes est présentée en **Schéma 13**. La nomenclature générique utilisée au cours de ce manuscrit est la suivante :



R :	Groupement en <i>para</i> des fonctions phénols, généralement <i>t</i> Bu (noté +) ou H
Positions :	1,2 pour les fonctions en position proximale (25 et 26) 1,3 pour les fonctions en position distale (25 et 27)
R1, R2, R3, R4 :	fonctions du lower-rim ( <i>vide infra</i> ) (OH, H, OR...)
M	métal éventuellement chélaté sur le calix[4]arène
L	ligands portés par le métal

*Exemple* : le composé **Ta2** étudié dans le chapitre III sera noté :



Les fonctions oxo portant le tantale sont en position 1,3, aussi nommée distale.

### 3.2 La famille des calix[4]arènes, dérivés du *p*-tertbutylcalix[4]arène

Le *p*-tertbutylcalix[4]arène, à l'origine de la plupart des dérivés calix[4]arènes, est synthétisé à l'échelle pouvant atteindre le kilogramme, à partir du *p*-tertbutylphénol et du formaldéhyde en présence de NaOH, composés extrêmement bon marché (**Schéma 14**).<sup>48</sup>

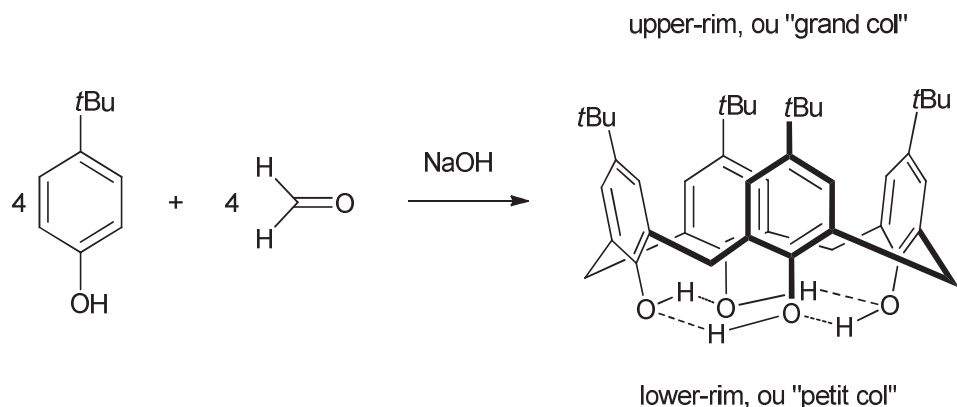


**Schéma 14:** Synthèse du *p*-tertbutylcalix[4]arène

Il se présente sous la forme d'une poudre cristalline blanche très peu soluble dans la plupart des solvants organiques et dont le point de fusion se situe vers 342-344°C sans dégradation. La partie supérieure du calixarène comportant les fonctions *t*Bu est appelée

« upper-rim » ou « grand col », tandis que la partie phénolique se nomme « lower-rim » ou encore « petit col ». La bande de vibration des O-H en IR présente dans la région 3150-3200 cm<sup>-1</sup>, et indépendante de la concentration, est caractéristique des fortes liaisons hydrogènes intramoléculaires entre les quatre fonctions hydroxyles. A l'état solide, ces dernières confèrent au calixarène une conformation dite « cône », où les entités phénoliques ont la même orientation. Cependant, Cornforth<sup>49</sup> révéla que les calix[4]arènes, selon leur fonctionnalisation en position *para* et sur les fonctions phénoliques, peuvent exister sous trois autres conformations, qualifiées par Gutsche<sup>50</sup> de : « cône partiel » ou « paco » pour « partial cone », « 1,2-alternée » et « 1,3-alternée » (**Schéma 15**).

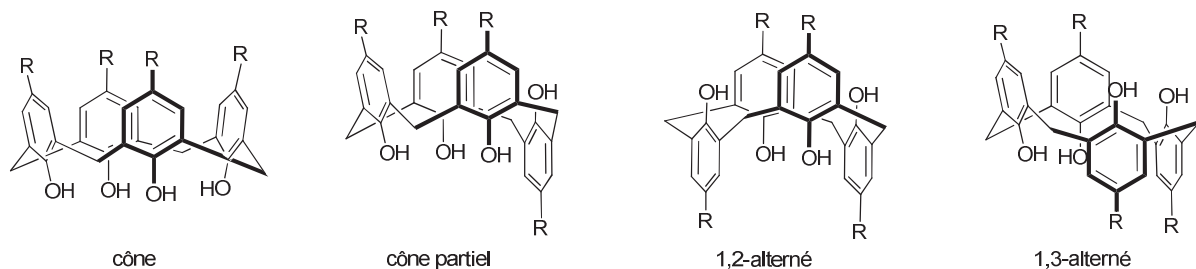


**Schéma 15:** Les quatre conformations possibles des calix[4]arènes

L'interconversion en solution de ces différentes conformations a été prouvée par Kämmerer<sup>51</sup> à l'aide d'études en <sup>1</sup>H-RMN dynamique du *p*-tertbutylcalix[4]arène. Les signaux des protons H<sub>A</sub> et H<sub>B</sub> de ses ponts méthyléniques (**Schéma 16**) se présentent sous la forme d'un singulets au-dessus de la température de coalescence (45°C) qui se transforme en une paire de doublets pour une température inférieure. La conformation cône s'interconvertissant rapidement à température élevée durant l'échelle de temps d'une acquisition RMN (100 s<sup>-1</sup> dans le cas du *p*-tertbutylcalix[4]arène), les protons méthyléniques axiaux H<sub>B</sub> (dirigés dans l'axe du calixarène) et équatoriaux H<sub>A</sub> (dirigés vers l'extérieur de la cavité) ne sont plus différentiables, d'où le signal singulet. Lorsque la température est abaissée en dessous de la température de coalescence, le taux d'interconversion s'affaiblit et chaque proton axial se couple avec le proton équatorial correspondant sous la forme d'un système AB.

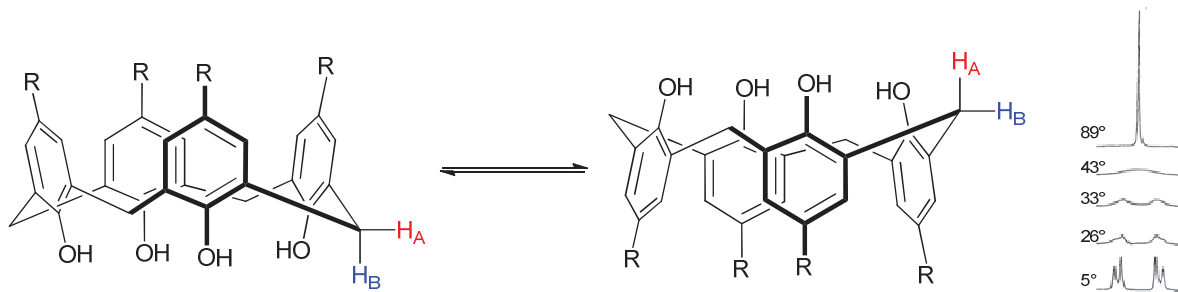


**Schéma 16:** Interconversion des calix[4]arènes en solution. Encart : RMN des protons méthyléniques  $H_A$  et  $H_B$  en fonctions de la température (5°C – 89°C)

L'introduction de groupes fonctionnels au niveau des oxygènes du petit col ou par substitution des fonctions *t*Bu sur le grand col conduisent à de nouveaux calixarènes dont la conformation dépendra aussi des conditions expérimentales choisies.<sup>50</sup> Lorsque les substituants du petit col sont relativement petits (par exemple OMe), on observe généralement, en solution, une interconversion entre divers conformères. Pour disposer d'un calixarène présentant une stabilité conformationnelle, seront préconisés des substituants suffisamment longs ou volumineux de manière à empêcher le basculement *trans*-annulaire des entités phénoliques à travers le macrocycle. L'identification des différentes conformations, en RMN, est basée non seulement sur les profils et la quantités des différents systèmes AB, signaux des groupes *t*Bu et des protons aromatiques, mais aussi sur une règle empirique, énoncée par de Mendoza<sup>52</sup>, concernant le déplacement chimique des atomes de carbone des ponts méthyléniques. Lorsqu'un groupe  $>CH_2$  ponte deux noyaux aromatiques orientés dans le même sens (*syn*), le déplacement de l'atome de carbone est situé entre 29 et 33 ppm. Pour deux unités phénoliques *anti*-orientées, le déplacement chimique du carbone est supérieur à 37 ppm.

#### 4. Préparation de matériaux inorganiques/organiques à base de calixarènes

Les matériaux organiques/inorganiques ont largement été étudiés en tant que phases stationnaires dans les sciences de la séparation et comme adsorbants sélectifs dans les sciences analytiques. Plus particulièrement, les matériaux silice/calixarène ont connu un essor depuis le début des années 2000 en tant que phases stationnaires dans les applications HPLC et GC<sup>53</sup>, mais aussi dans l'obtention de catalyseurs supportés, majoritairement développés par

Katz.<sup>54</sup> Grâce à leur grande flexibilité et fonctionnalisation potentielle, il est d'une part possible de greffer le calixarene soit par le lower-rim soit par l'upper-rim sur une silice activée ou fonctionnalisée, mais aussi de bloquer sa conformation (**Schéma 17**). Ainsi, ces matériaux totalement inédits présentent des propriétés uniques pour la séparation d'analytes en chromatographie, étant donné la capacité d'inclusion de petites molécules dans la cavité des calixarènes et dans la stabilisation de centres catalytiques supportés.<sup>54</sup> Le paragraphe ci-dessous sera consacré aux différentes méthodes de greffage de calixarènes, fonctionnalisés ou non, sur des supports oxydes (Silice, SBA, alumine). Parmi toutes les stratégies décrites dans la littérature, on distingue trois modes de greffage de calixarènes sur support oxyde (**Schéma 17**) :

- par le lower-rim (à partir d'un calixarene fonctionnalisé)
- par le upper-rim (à partir d'un calixarene fonctionnalisé)
- ou par réaction entre un support oxyde préalablement fonctionnalisé et un calixarene

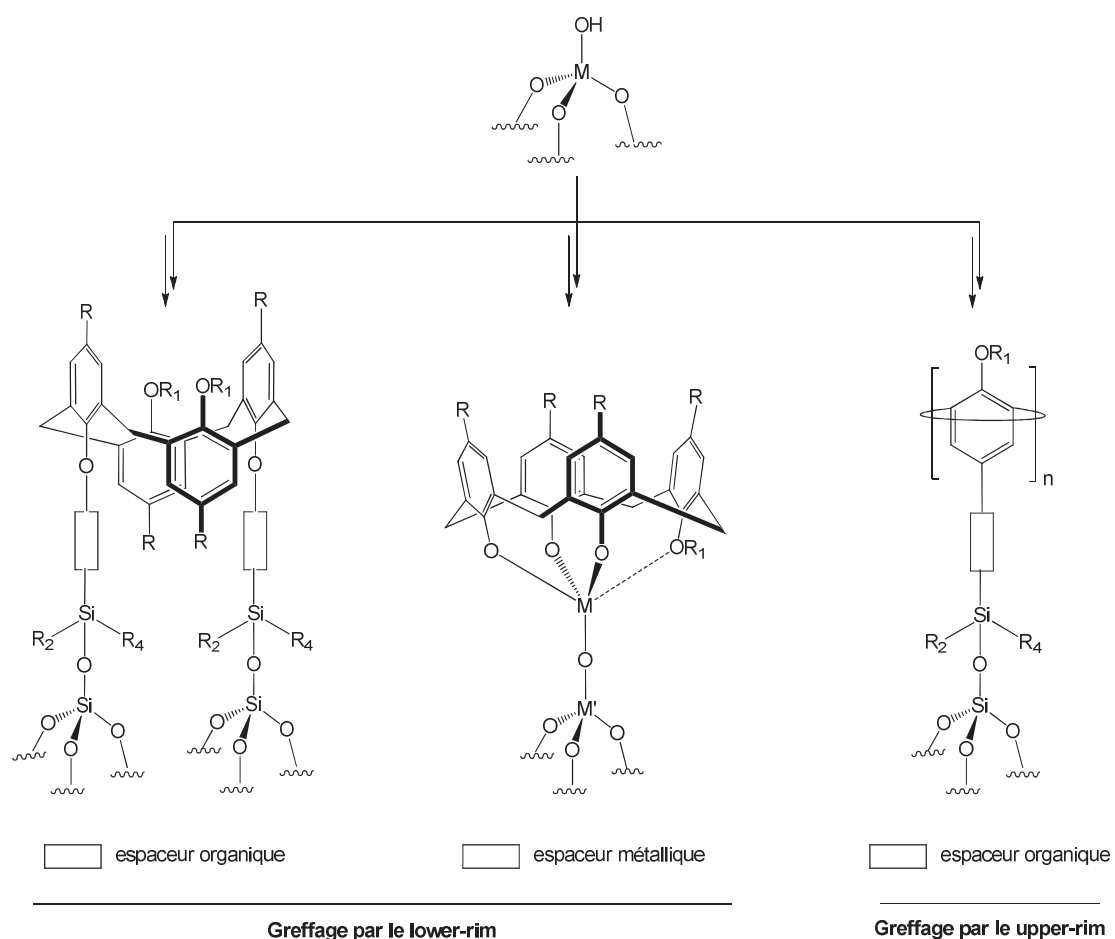


**Schéma 17:** Greffage de calix[4]arènes sur des supports oxydes *via* le lower-rim et l'upper-rim ( $R = H, tBu$  ;  $R_1 = \text{alkyl, ester, aromatique, amide}$  ;  $R_2, R_3, R_4 = \text{alkyl, Cl, alkoxy}$ )

#### 4.1 Greffage de calix[4]arènes sur un support oxyde par le petit col ou « lower-rim » fonctionnalisé

Plusieurs exemples sont décrits dans la littérature pour la préparation de matériaux silice/calixarènes covalents à partir de calixarènes fonctionnalisés sur le lower-rim. Le lower-rim du *p-tertbutylcalix[4]arène* est composé de quatre groupements phénoliques, tous potentiellement fonctionnalisables, de manière indépendante selon le processus et les conditions de fonctionnalisation mis au point. Ainsi, les calixarènes mis en jeu dans la préparation des matériaux présentent généralement des fragments alkoxysilane portés par leurs fonctions phénoxy, en vue de les faire réagir sur un support activé, notamment la silice. La synthèse de ces calixarènes fonctionnalisés nécessite plusieurs étapes qui consistent à introduire deux ou quatre chaînes alcènes terminales<sup>55</sup> qui, après un procédé d’hydrosilylation en présence d’un catalyseur, donnera des chaînes alkyle présentant une fonction alkoxysilane terminale (**Schéma 18**).<sup>56</sup> Afin de rendre le matériau plus original, les fonctions hydroxyles ne portant pas les bras espaceurs ont dans la plupart des cas été fonctionnalisés avec des groupements alkyl<sup>55a,55c</sup>, ester<sup>55c</sup>, aromatiques<sup>55c,57</sup> ou amide<sup>55b</sup>, avant l’étape d’insertion de l’alcène terminal. Ces groupements confèrent des propriétés uniques pour la complexation (ex : complexation d’ions mercurique<sup>55b</sup>  $Hg^{2+}$ ) et la séparation d’analytes en chromatographie (ex. : séparation d’alkylbenzènes<sup>55c</sup> ou d’isomères aromatiques<sup>57</sup>). A noter que ces groupements, majoritairement en position 1,3, peuvent forcer le calixarène en conformation 1,3-alternée, présentant des bras organiques pointant vers l’extérieur du matériau (**Schéma 18**). Par exemple, Kaszyńska *et al.* ont développé des matériaux calixarène/silice présentant des calix[4]arènes fonctionnalisés en conformation 1,3-alternée.<sup>55c,57</sup> Le calix[4]arène est dans un premier temps traité avec 2 eq. de bromure de *p*-nitrobenzyle en présence de  $K_2CO_3$  dans MeCN pour donner sélectivement le composé [[4H]-1,3-(OCH<sub>2</sub>(C<sub>6</sub>H<sub>4</sub>)-*p*-NO<sub>2</sub>)<sub>2</sub>(OH)<sub>2</sub>]. Les fonctions hydroxyles restantes sont éthérifiées avec un excès de iodure d’allyle en présence de Cs<sub>2</sub>CO<sub>3</sub> pour obtenir [[4H]-1,3-(OCH<sub>2</sub>(C<sub>6</sub>H<sub>4</sub>)-*p*-NO<sub>2</sub>)<sub>2</sub>(OCH<sub>2</sub>CHCH<sub>3</sub>)<sub>2</sub>] en conformation 1,3 alternée. L’hydrosilylation des bras allyle par Me<sub>2</sub>SiHCl en présence du catalyseur H<sub>2</sub>PtCl<sub>6</sub> donne finalement le dérivé chlorosilane [[4H]-1,3-(OCH<sub>2</sub>(C<sub>6</sub>H<sub>4</sub>)-*p*-NO<sub>2</sub>)<sub>2</sub>(O(CH<sub>2</sub>)<sub>3</sub>Si(CH<sub>3</sub>)<sub>2</sub>Cl)<sub>2</sub>] correspondant.

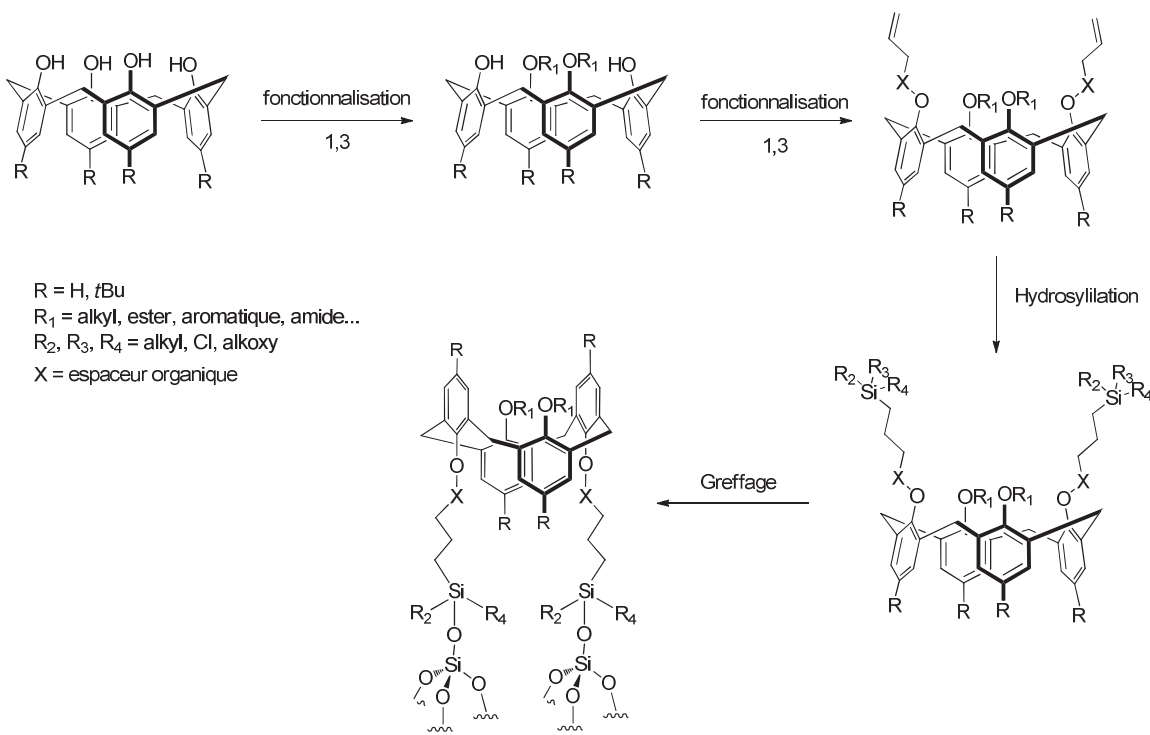


**Schéma 18:** Méthode de greffage de calix[4]arènes fonctionnalisés sur une silice activée *via* le lower-rim

Le dérivé calixarène est ensuite mis en contact avec une silice activée (ex : par déshydratation à une température donnée) pour générer le matériau calixarène/silice. L'analyse par spectroscopie infra-rouge de ces matériaux révèle la présence de silanols résiduels non modifiés par le fragment silane.<sup>57</sup> Les études structurale et conformationnelle en RMN à l'état solide de ces matériaux se révèlent parfois approximatives ou inexistantes.

Une autre méthode totalement inédite récemment développée par Katz *et al.* permet de greffer un calixarène sur une surface oxyde (silice<sup>54</sup>, alumine<sup>54a</sup>) par le lower-rim utilisant un espaceur métallique (**Schéma 19**). La rigidité et l'encombrement stérique des deux ligands (« ligand-support » silice et calixarène) assure l'isolation du centre métallique et sa stabilité durant des réactions catalytiques.<sup>54d</sup> Cela consiste à synthétiser dans un premier temps des métallacalix[4]arènes solubles bipodaux [[4+]-1,3-(OMe)<sub>2</sub>(O)<sub>2</sub>MR<sub>x</sub>] et tripodaux [[4+]- (OMe)(O)<sub>3</sub>MR<sub>x</sub>] (M = Si<sup>54c,54e</sup>, Ti ou V<sup>54b</sup>; R = Cl, alkoxy...) selon les stratégies établies par Floriani.<sup>58</sup> Le dérivé chloro ou alkoxy metallacalix[4]arène obtenu est ensuite mis à réagir avec une silice ou une alumine activée pour donner le matériau souhaité (**Schéma 19**), actif dans l'époxydation des oléfines pour M = Ti ou aux propriétés rédox intéressantes (M = V).

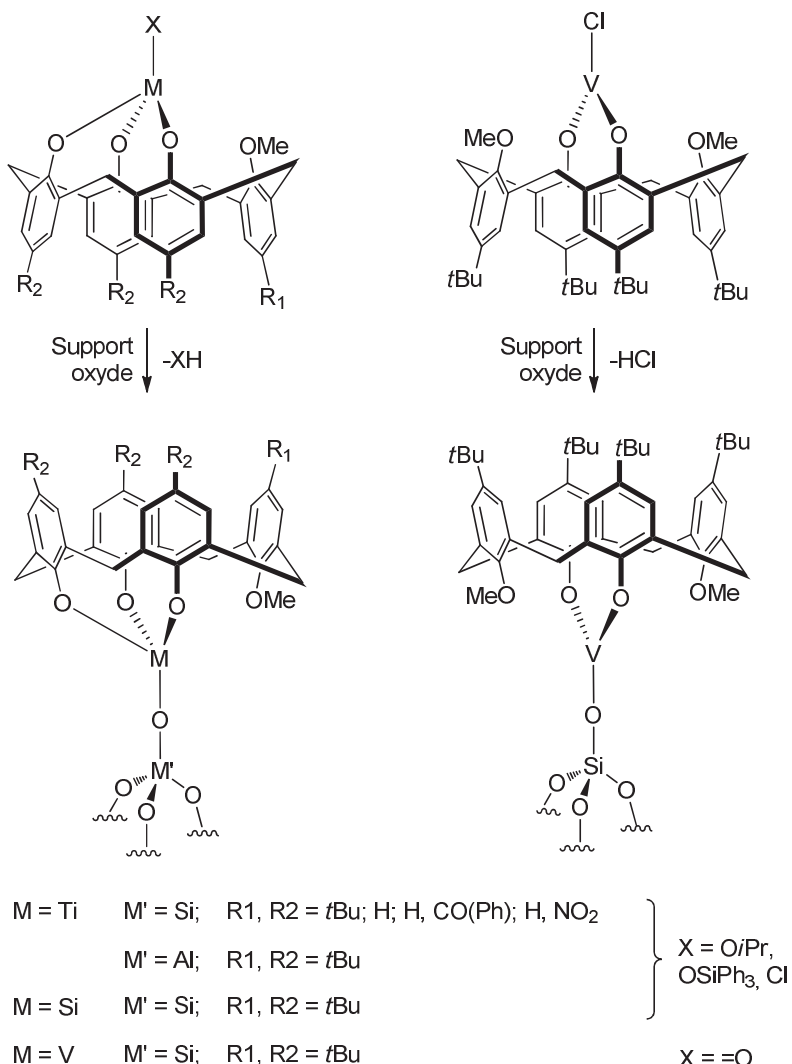


Schéma 19: Greffage de métallacalix[4]arènes sur supports oxydes (Silice, Alumine)

#### 4.2 Greffage de calix[4]arènes sur un support oxyde par le grand col ou « upper-rim » fonctionnalisé

Contrairement aux méthodes de greffage par le lower-rim, qui reste très facilement fonctionnalisable, celles utilisant l'upper-rim sont encore peu développées. Dans la plupart des cas répertoriés, la fonctionnalisation des calixarènes en *para* demande des étapes de synthèse supplémentaires faisant intervenir un réarrangement de Claisen.

D'une manière générale, le groupe *tert*butyl du *p*-*tert*butylphénol peut facilement être substitué par une réaction de *retro* Friedel-Craft laissant ainsi libre la position *para* pour la fonctionnalisation.<sup>59</sup> Cette réaction, catalysée par un acide de Lewis, a été adaptée aux calixarènes par Mainz *et al.*<sup>60</sup> Ainsi, les positions *para* détertbutylées du calix[4]arène permettent de nombreuses fonctionnalisations dont le réarrangement de type Claisen (**Schéma I**)

20). Cette méthode consiste à introduire un fragment allyle sur les fonctions hydroxyles par réaction d'éthérification suivie du réarrangement de Claisen pour obtenir des calixarènes portant de 1 à n chaînes allyle en position *para*.<sup>61</sup>

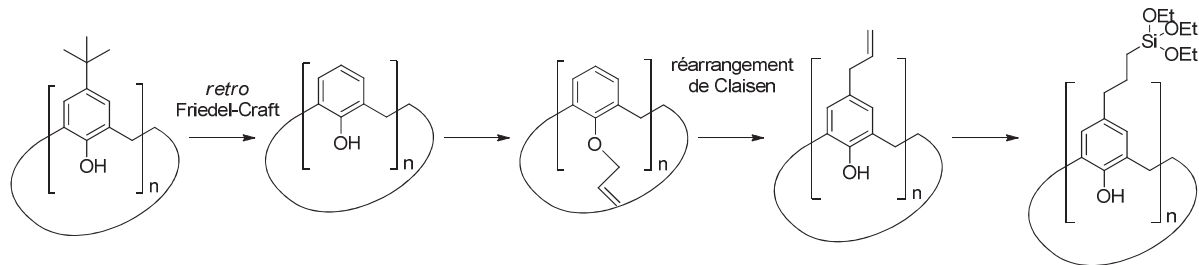


Schéma 20: Fonctionnalisation en upper-rim des calix[n]arènes via le réarrangement de Claisen

Le fragment allyle peut alors subir une réaction de thio- ou hydrosilylation avec, respectivement, des mercaptans silylés  $(EtO)_3Si(CH_2)_nSH$  ( $n = 3^{62}$ ;  $n = 6,10^{62a,b}$ ) ou des dérivés alkoxysilane  $(EtO)_3SiH^{63}$ , en présence de  $H_2PtCl_6$ , donnant les composés calixarènes portant des fragments tri(éthoxysilane). A noter que la fonctionnalisation subséquente des groupements phénols donne des propriétés uniques aux calixarènes greffés en matière de séparation d'entités par complexation sélective, notamment d'ions alcalins<sup>63-64</sup> et alcalino-terreux<sup>64</sup>, métaux de transition<sup>62c</sup>, métaux lourds<sup>65</sup> mais aussi de composés acides amino-ester.<sup>62a,63a</sup> Les matériaux silice/calixarène sont ensuite obtenus soit par réaction entre le calixarène fonctionnalisé en upper-rim et le support silice soit par procédé sol-gel pour obtenir des matériaux structurés.

Ainsi, Lambert *et al.* a récemment développé de nouveau matériaux hybrides organiques/inorganiques structurés par procédé sol-gel.<sup>66</sup> Les calixarenes présentant des fragments triéthoxysilane en position *para* sont polymérisés en présence de TEOS pour former de nouvelles matrices polysilsesquioxane. Les analyses XRD, TEM et BET révèlent que le polymère obtenu a une structure périodique avec une symétrie hexagonale, une surface spécifique allant de 210 à 650  $m^2 \cdot g^{-1}$  et des mésopores de diamètre 2.4-2.7 nm.

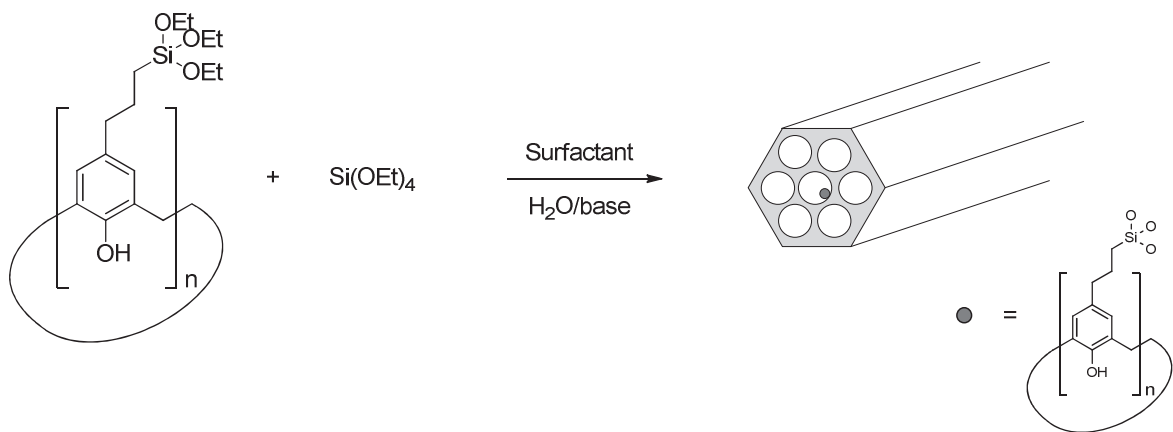


Schéma 21: Synthèse de matériaux calixarène/silice structurés *via* le procédé sol-gel

### 4.3 Greffage de calixarènes sur une silice fonctionnalisée

Une troisième stratégie a été développée pour la préparation de matériaux calixarène/silice à partir de supports oxydes fonctionnalisés. Par exemple, Glennon *et al.*<sup>62b</sup> ont étudié la réaction entre un organosilane du type (MeO)<sub>2</sub>MeSiH sur une silice activée pour donner un support organique/inorganique présentant des fragments avec une liaison Si-H. Ces derniers servent d'agents d'hydrosilylation lorsque mis en contact avec un calix[6]arène modifié portant des groupements allyle sur l'upper-rim en présence du catalyseur H<sub>2</sub>PtCl<sub>6</sub> (**Schéma 22**). Le matériau calix[6]arène/silice a été caractérisé par CP/MAS-NMR qui révèle que seule une partie des bras allyle réagissent avec la silice modifiée. Cette réaction partielle est due à l'encombrement stérique du calixarène ne permettant pas aux groupements allyle d'atteindre tous les sites silanes de la surface.<sup>62b</sup>

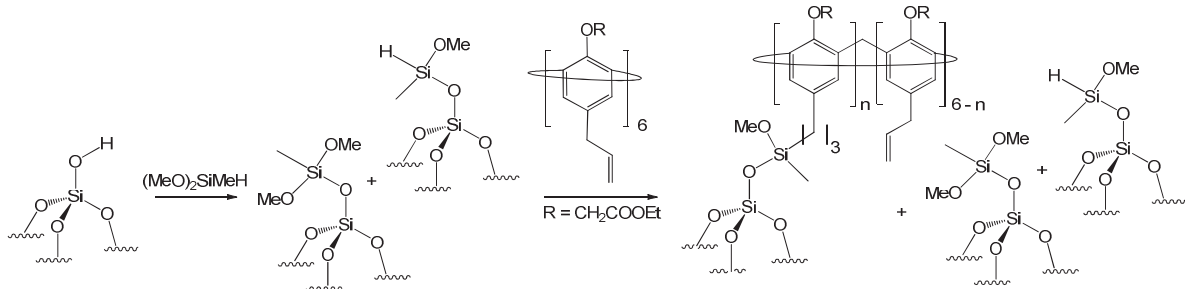
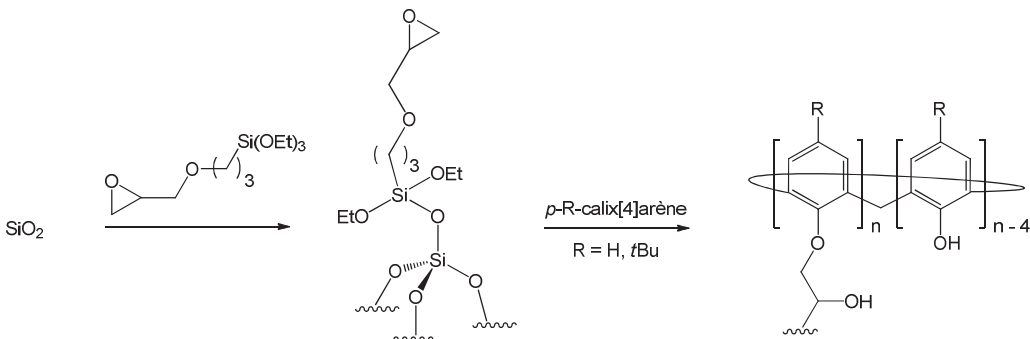


Schéma 22: Greffage de calix[6]arènes *via* le upper-rim sur une silice portant des silanes

Le greffage des *p*-R-calix[n]arène (R = H, *t*Bu ; n = 4, 6, 8) dont les groupements allyle sont portés par les fonctions phénoxy en présence du catalyseur de Wilkinson RhCl(Ph<sub>3</sub>)<sub>3</sub> constitue une alternative à cette méthode.<sup>67</sup> Enfin, Liu *et al.* ont développé une voie de fonctionnalisation préalable de la silice par des bras portant des fonctions

oxacyclopropane (**Schéma 23**). La réaction de surface par ouverture du fragment époxyde avec une fonction hydroxyle de divers *p*-R-calix[n]arènes ( $n = 4, 6$ ,  $R = H^{68}, tBu^{68}$ ;  $n = 8$ ,  $R = H^{68}, tBu^{68-69}$ ) permet d'obtenir le matériau silice/calixarène souhaité (**Schéma 23**).



**Schéma 23: Greffage de calixarènes sur une silice fonctionnalisée avec des bras oxacyclopropane**

Les analyses par spectroscopie infra-rouge de ces matériaux révèlent la présence de silanols résiduels dû à la fonctionnalisation partielle de la silice lors du greffage du bras espaceur.

#### 4.4 Conclusion

L'étude bibliographique a montré que différentes stratégies peuvent être mises en œuvre pour la génération de matériaux calixarène/silice, par greffage du calixarène soit par le lower-rim soit par l'upper-rim, sur une silice activée ou préalablement fonctionnalisée. Dans la majorité des cas, la fonctionnalisation des calixarènes requièrent plusieurs étapes de synthèse, et chacune des méthodes de greffage décrites recèle des limites pour l'incorporation subséquente de complexes organométalliques, à savoir :

- La présence de fonctions silanols résiduels : l'encombrement stérique du calixarène supporté peut créer un éloignement des macromolécules dans l'espace lors du greffage, laissant ainsi des silanols de surface libres. Ces derniers peuvent générer des sites actifs sur les phénoxys du calixarène supporté et sur les siloxys de la silice par réaction de ces matériaux avec les complexes organométalliques.
- Les techniques de greffage reportées nécessitent des alkoxy silanes qui produisent des alcools (éthanol, méthanol...), composés protiques pouvant réagir avec des ponts siloxanes pour générer des silanols.

## 5. Stratégie proposée pour le projet

La finalité du projet consiste à obtenir des catalyseurs greffés sur silice à sites uniques, en limitant les interactions support-métal, par éloignement du site actif à l'aide d'un espaceur organique du type calix[4]arène. La stratégie adoptée au cours de ce travail permettra de préparer des matériaux métallacalix[4]arènes supportés sur silice en utilisant une nouvelle méthode de fonctionnalisation totale de la silice par un complexe organométallique, suivie du greffage du calixarène. Pour cela, le choix du complexe et du calixarène est primordial pour l'élaboration de matériaux à sites uniques.

Une stratégie innovante permettant de fonctionnaliser totalement la surface de silice consiste à utiliser un complexe organométallique très réactif envers tous les silanols de surface. Le complexe organométallique de surface obtenu pourra présenter un point d'ancrage (liaison métal-alkyle ou métal-hydrure) pour le greffage des calixarènes par le lower-rim par réaction de protonolyse avec l'une des fonctions phénols. Le matériau calixarène/silice sera utilisé comme nouveau support pour le greffage de complexes organométalliques des groupes IV-VI.

La caractérisation des matériaux générés par ce nouveau concept nécessitera, en plus des techniques d'analyse chimiques et physiques habituelles (spectroscopies IR, Raman, Mössbauer et RMN à l'état solide, EXAFS), la synthèse de complexes métallacalix[4]arène modèles.

L'objectif de cette thèse est donc de préparer et de caractériser de nouveaux catalyseurs métallacalix[4]arènes supportés sur silice pour la conversion d'hydrocarbures. Ce travail sera divisé en trois grandes parties :

- La première partie consistera à prouver notre nouveau concept de greffage de dérivés phénoliques sur une surface exempte de fonctions silanols en utilisant l'hydroquinone comme modèle :
  - Préparation et caractérisation d'une espèce mono-alkyle d'aluminium supportée sur silice
  - Etude de la réactivité de l'hydroquinone sur ce matériau

- Greffage de complexes de zirconium et de tungstène sur la fonction phénol de l'hydroquinone supportée
  - Etude comparative des propriétés catalytiques de ces nouveaux systèmes avec leurs analogues liés directement à la silice
- Synthèse de modèles moléculaires solubles des groupes IV et V :
- Préparation et caractérisation de complexes titana- et zirconacalix[4]arènes.  
Application dans la polymérisation de l'éthylène
  - Préparation et caractérisation de complexes tantalacalix[4]arènes
- la dernière partie sera consacrée à la préparation et caractérisation de matériaux métallacalix[4]arènes de métaux de transition de groupes IV-VI supportés sur une silice mésoporeuse du type SBA-15 larges pores :
- Préparation et caractérisation d'une mono-alkyle aluminium supportée sur silice mésoporeuse du type SBA-15 larges pores
  - Etude de la réactivité des calixarènes  $[[4H]\text{-(OH)}_3\text{(H)}]$  et  $[[4H]\text{-(OH)}_4]$  avec le complexe supporté mono-alkyle aluminium.
  - Greffage de complexes de zirconium, tantale et tungstène sur les fonctions phénols du calixarène supporté
  - Etude comparative des propriétés catalytiques de ces nouveaux systèmes métallacalix[4]arènes/SBA-15 avec leurs analogues liés directement à la silice.

## Notes et références

- (1) (a) Lefebvre, F.; Candy, J.-P.; Mallmann, A. d.; Dufaud, V.; Niccolai, G.; Santini, C.; Thivolle-Cazat, J.; Basset, J.-M. *Actual. Chim.* **1996**, 47(b) Copéret, C.; Chabanas, M.; Petroff-Saint-Arroman, R.; Basset, J.-M. *Angew. Chem., Int. Ed.* **2003**, 42, 156.
- (2) (a) Scott, S. L.; Basset, J. M.; Niccolai, G. P.; Santini, C. C.; Candy, J. P.; Lecuyer, C.; Quignard, F.; Choplin, A. *New J. Chem.* **1994**, 18, 115(b) Lefebvre, F.; Candy, J.-P.; Santini, C. C.; Basset, J.-M. *Top. Catal.* **1998**, 4, 211(c) Basset, J. M.; Candy, J. P.; Choplin, A.; Didillon, B.; Quignard, F.; Theolier, A. **1992**, 125(d) Scott, S. L.; Basset, J.-M. *J. Mol. Catal.* **1994**, 86, 5(e) Lefebvre, F.; Thivolle-Cazat, J.; Dufaud, V.; Niccolai, G. P.; Basset, J.-M. *Appl. Catal., A* **1999**, 182, 1(f) Basset, J. M.; Candy, J. P.; Choplin, A.; Nédez, C.; Quignard, F.; Santini, C. C.; Théolier, A. *Mater. Chem. Phys.* **1991**, 29, 5(g) Lefebvre, F.; de Mallmann, A.; Basset, J.-M. *Eur. J. Inorg. Chem.* **1999**, 1999, 361.
- (3) Lopez, L. P. H.; Schrock, R. R.; Mueller, P. *Organometallics* **2006**, 25, 1978.
- (4) Basset, J.-M.; Psaro, R.; Roberto, D.; Ugo, R. *Modern Surface Organometallic Chemistry*; Wiley ed.: Weinheim, 2009.
- (5) Wang, X.; Zhao, H.; Lefebvre, F.; Basset, J.-M. *Chem. Lett.* **2000**, 1164.
- (6) Ryndin, Y. A.; Candy, J. P.; Didillon, B.; Savary, L.; Basset, J. M. *J. Catal.* **2001**, 198, 103.
- (7) (a) Le Roux, E.; Taoufik, M.; Copéret, C.; de Mallmann, A.; Thivolle-Cazat, J.; Basset, J.-M.; Maunders, B. M.; Sunley, G. J. *Angew. Chem., Int. Ed.* **2005**, 44, 6755(b) Taoufik, M.; Roux, E.; Thivolle-Cazat, J.; Copéret, C.; Basset, J.-M.; Maunders, B.; Sunley, G. *Top. Catal.* **2006**, 40, 65.
- (8) Szeto, K. C.; Norsic, S.; Hardou, L.; Le Roux, E.; Chakka, S.; Thivolle-Cazat, J.; Baudouin, A.; Papaioannou, C.; Basset, J. M.; Taoufik, M. *Chem. Commun.* **2010**, 46, 3985.
- (9) (a) Taoufik, M.; Schwab, E.; Schultz, M.; Vanoppen, D.; Walter, M.; Thivolle-Cazat, J.; Basset, J.-M. *Chem. Commun.* **2004**, 1434(b) Vanoppen, D.; Schwab, E.; Basset, J.-M.; Thivolle-Cazat, J.; Taoufik, M.; Schulz, M.; Hoehn, A.; (BASF Aktiengesellschaft, Germany). Application: WO, 2002.
- (10) Dufaud, V.; Basset, J.-M. *Angew. Chem., Int. Ed.* **1998**, 37, 806.
- (11) Taoufik, M.; Le Roux, E.; Thivolle-Cazat, J.; Basset, J.-M. *Angew. Chem., Int. Ed.* **2007**, 46, 7202.
- (12) Jezequel, M.; Dufaud, V.; Ruiz-Garcia, M. J.; Carrillo-Hermosilla, F.; Neugebauer, U.; Niccolai, G. P.; Lefebvre, F.; Bayard, F.; Corker, J.; Fiddy, S.; Evans, J.; Broyer, J.-P.; Malinge, J.; Basset, J.-M. *J. Am. Chem. Soc.* **2001**, 123, 3520.
- (13) Basset, J.-M.; Lefebvre, F.; Santini, C. *Coord. Chem. Rev.* **1998**, 178-180, 1703.
- (14) (a) Basset, J.-M.; Chabanas, M.; Coperet, C.; (BASF Aktiengesellschaft, Germany). Application: WO, 2002(b) Merle, N.; Taoufik, M.; Nayer, M.; Baudouin, A.; Roux, E. L.; Gauvin, R. M.; Lefebvre, F.; Thivolle-Cazat, J.; Basset, J.-M. *J. Organomet. Chem.* **2008**, 693, 1733.

- (15) Millot, N.; Santini, C. C.; Lefebvre, F.; Basset, J.-M. *C. R. Chim.* **2004**, *7*, 725.
- (16) Bartram, M. E.; Michalske, T. A.; Rogers, J. W. *J. Phys. Chem.* **1991**, *95*, 4453.
- (17) (a) Millot, N.; Soignier, S.; Santini, C. C.; Baudouin, A.; Basset, J.-M. *J. Am. Chem. Soc.* **2006**, *128*, 9361(b) Scott, S. L.; Basset, J.-M. *J. Am. Chem. Soc.* **1994**, *116*, 12069.
- (18) (a) Zhao, D.; Huo, Q.; Feng, J.; Chmelka, B. F.; Stucky, G. D. *J. Am. Chem. Soc.* **1998**, *120*, 6024(b) Zhao, D.; Feng, J.; Huo, Q.; Melosh, N.; Fredrickson, G. H.; Chmelka, B. F.; Stucky, G. D. *Science* **1998**, *279*, 548.
- (19) (a) Morrow, B. A.; McFarlan, A. *J. Non-Cryst. Solids* **1990**, *120*, 61(b) Peri, J. B. *J. Catal.* **1976**, *41*, 227(c) Peri, J. B.; Hannan, R. B. *J. Phys. Chem.* **1960**, *64*, 1526(d) Peri, J. B. *J. Phys. Chem.* **1965**, *69*, 220(e) Knoezinger, H.; Ratnasamy, P. *Catal. Rev.* **1978**, *17*, 31(f) Lavallee, J. C.; Bensitel, M.; Gallas, J. P.; Lamotte, J.; Busca, G.; Lorenzelli, V. *J. Mol. Struct.* **1988**, *175*, 453(g) Abbattista, F.; Delmastro, S.; Gozzelino, G.; Mazza, D.; Vallino, M.; Busca, G.; Lorenzelli, V.; Ramis, G. *J. Catal.* **1989**, *117*, 42(h) Morterra, C.; Magnacca, G. *Catal. Today* **1996**, *27*, 497(i) Digne, M.; Sautet, P.; Raybaud, P.; Euzeen, P.; Toulhoat, H. *J. Catal.* **2002**, *211*, 1(j) Digne, M.; Sautet, P.; Raybaud, P.; Euzeen, P.; Toulhoat, H. *J. Catal.* **2004**, *226*, 54(k) Joubert, J.; Fleurat-Lessard, P.; Delbecq, F.; Sautet, P. *J. Phys. Chem. B* **2006**, *110*, 7392(l) Corral Valero, M.; Raybaud, P.; Sautet, P. *J. Phys. Chem. B* **2006**, *110*, 1759.
- (20) Zakharov, V. A.; Dudchenko, V. K.; Paukshtis, E. A.; Karakchiev, L. G.; Yermakov, Y. I. *J. Mol. Catal.* **1977**, *2*, 421.
- (21) Mortensen, J. J.; Parrinello, M. *J. Phys. Chem. B* **2000**, *104*, 2901.
- (22) Chabanas, M.; Vidal, V.; Copéret, C.; Thivolle-Cazat, J.; Basset, J.-M. *Angew. Chem., Int. Ed.* **2000**, *39*, 1962.
- (23) (a) Basset, J. M.; Copéret, C.; Lefort, L.; Maunders, B. M.; Maury, O.; Le Roux, E.; Saggio, G.; Soignier, S.; Soulivong, D.; Sunley, G. J.; Taoufik, M.; Thivolle-Cazat, J. *J. Am. Chem. Soc.* **2005**, *127*, 8604(b) Schinzel, S.; Chermette, H.; Copéret, C.; Basset, J.-M. *J. Am. Chem. Soc.* **2008**, *130*, 7984(c) Vidal, V.; Theolier, A.; Thivolle-Cazat, J.; Basset, J.-M. *Science* **1997**, *276*, 99.
- (24) Quignard, F.; Lecuyer, C.; Bougault, C.; Lefebvre, F.; Choplin, A.; Olivier, D.; Basset, J. M. *Inorg. Chem.* **1992**, *31*, 928.
- (25) Thieuleux, C.; Quadrelli, E. A.; Basset, J.-M.; Doebler, J.; Sauer, J. *Chem. Commun.* **2004**, 1729.
- (26) Rosier, C.; Niccolai, G. P.; Basset, J.-M. *J. Am. Chem. Soc.* **1997**, *119*, 12408.
- (27) Rosier, C. (1999) Chimie organométallique de surface du titane. Application à l'époxydation des oléfines. PhD, Lyon 1
- (28) Dufaud, V.; Niccolai, G. P.; Thivolle-Cazat, J.; Basset, J.-M. *J. Am. Chem. Soc.* **1995**, *117*, 4288.
- (29) Lefort, L.; Chabanas, M.; Maury, O.; Meunier, D.; Copéret, C.; Thivolle-Cazat, J.; Basset, J.-M. *J. Organomet. Chem.* **2000**, *593-594*, 96.

- (30) Saggio, G. (2001) Etude de la réaction de métathèse des alcanes catalysée par l'hydrure de tantale supporté sur silice: compréhension des processus de désactivation de catalyseur. PhD, Lyon 1
- (31) (a) Le Roux, E.; Taoufik, M.; Chabanas, M.; Alcor, D.; Baudouin, A.; Copéret, C.; Thivolle-Cazat, J.; Basset, J.-M.; Lesage, A.; Hediger, S.; Emsley, L. *Organometallics* **2005**, *24*, 4274(b) Rhers, B.; Salameh, A.; Baudouin, A.; Quadrelli, E. A.; Taoufik, M.; Copéret, C.; Lefebvre, F.; Basset, J.-M.; Solans-Monfort, X.; Eisenstein, O.; Lukens, W. W.; Lopez, L. P. H.; Sinha, A.; Schrock, R. R. *Organometallics* **2006**, *25*, 3554(c) Rhers, B.; Quadrelli, E. A.; Baudouin, A.; Taoufik, M.; Coperet, C.; Lefebvre, F.; Basset, J.-M.; Fenet, B.; Sinha, A.; Schrock, R. R. *J. Organomet. Chem.* **2006**, *691*, 5448.
- (32) Gao, H.; Angelici, R. J. *J. Am. Chem. Soc.* **1997**, *119*, 6937.
- (33) Clarke, R. J.; Shannon, I. J. *Chem. Commun.* **2001**.
- (34) Bigi, F.; Moroni, L.; Maggi, R.; Sartori, G. *Chem. Commun.* **2002**.
- (35) Dioos, B. M. L.; Geurts, W. A.; Jacobs, P. A. *Catal. Lett.* **2004**, *97*, 125.
- (36) Corma, A.; Gutiérrez-Puebla, E.; Iglesias, M.; Monge, A.; Pérez-Ferreras, S.; Sánchez, F. *Adv. Synth. Catal.* **2006**, *348*, 1899.
- (37) Liu, C.-J.; Yu, W.-Y.; Li, S.-G.; Che, C.-M. *J. Org. Chem.* **1998**, *63*, 7364.
- (38) Zhou, X.-G.; Yu, X.-Q.; Huang, J.-S.; Che, C.-M.; Li, S.-G.; Li, L.-S. *Chem. Commun.* **1999**, *0*.
- (39) (a) Thomas, J. M.; Maschmeyer, T.; Johnson, B. F. G.; Shephard, D. S. *J. Mol. Catal. A: Chem.* **1999**, *141*, 139(b) F. G. Johnson, B.; A. Raynor, S.; S. Shephard, D.; Mashmeyer, T.; Meurig Thomas, J.; Sankar, G.; Bromley, S.; Oldroyd, R.; Gladden, L.; D. Mantle, M. *Chem. Commun.* **1999**, *0*.
- (40) Comas-Vives, A.; González-Arellano, C.; Corma, A.; Iglesias, M.; Sánchez, F.; Ujaque, G. *J. Am. Chem. Soc.* **2006**, *128*, 4756.
- (41) Pugin, B.; Blaser, H.-U. *Adv. Synth. Catal.* **2006**, *348*, 1743.
- (42) McKittrick, M. W.; Jones, C. W. *J. Am. Chem. Soc.* **2004**, *126*, 3052.
- (43) Baeyer, A. *Ber.* **1872**, *5*, 1094.
- (44) Baekeland, L. H. *Ind. Eng. Chem. Res.* **1913**, *5*, 506.
- (45) Zinke, E. *Z. Ber.* **1944**, *77*, 264.
- (46) Andreetti, G. D.; Ungaro, R.; Pochini, A. *J. Chem. Soc., Chem. Com.* **1979**, 1005.
- (47) Stewart, D. R.; Gutsche, C. D. *J. Am. Chem. Soc.* **1999**, *121*, 4136.
- (48) Gutsche, C. D.; Iqbal, M. *Org. Synth.* **1990**, *68*, 234.
- (49) Cornforth, J. W.; D'Arcy Hart, P.; Nicholls, G. A.; Rees, R. J. W.; Stock, J. A. *Br. J. Pharmacol.* **1955**, *10*, 73.
- (50) Gutsche, C. D.; Dhawan, B.; Levine, J. A.; Kwang, H. N.; Bauer, L. J. *Tetrahedron* **1983**, *39*, 409.
- (51) Happel, G.; Mathiasch, B.; Kaemmerer, H. *Makromol. Chem.* **1975**, *176*, 3317.

- (52) Jaime, C.; De Mendoza, J.; Prados, P.; Nieto, P. M.; Sanchez, C. *J. Org. Chem.* **1991**, *56*, 3372.
- (53) (a) Meyer, R.; Jira, T. *Curr. Anal. Chem.* **2007**, *3*, 161(b) Sliwka-Kaszynska, M. *Crit. Rev. Anal. Chem.* **2007**, *37*, 211
- (54) (a) Notestein, J. M.; Solovyov, A.; Andrini, L. R.; Requejo, F. G.; Katz, A.; Iglesia, E. *J. Am. Chem. Soc.* **2007**, *129*, 15585(b) de Silva, N.; Hwang, S.-J.; Durkin, K. A.; Katz, A. *Chem. Mater.* **2009**, *21*, 1852(c) Solovyov, A.; Amundsen, T. J.; Daniels, J. J.; Kim, Y.-G.; Katz, A. *Chem. Mater.* **2008**, *20*, 6316(d) Notestein, J. M.; Iglesia, E.; Katz, A. *J. Am. Chem. Soc.* **2004**, *126*, 16478(e) Notestein, J. M.; Katz, A.; Iglesia, E. *Langmuir* **2006**, *22*, 4004.
- (55) (a) Kang, Y.; Zyryanov, G. V.; Rudkevich, D. M. *Chem.--Eur. J.* **2005**, *11*, 1924(b) Metivier, R.; Leray, I.; Lebeau, B.; Valeur, B. *J. Mater. Chem.* **2005**, *15*, 2965(c) Sliwka-Kaszynska, M.; Jaszcolt, K.; Anusiewicz, I. *J. Sep. Sci.* **2009**, *32*, 3107(d) Zyryanov, G. V.; Kang, Y.; Rudkevich, D. M. *J. Am. Chem. Soc.* **2003**, *125*, 2997.
- (56) Sliwka-Kaszynska, M.; Gorczyca, G.; Sledioda, M. *J. Chromatogr., A* **1217**, 329.
- (57) Jaszcolt, K.; Sliwka-Kaszynska, M. *Chromatographia* **2007**, *66*, 837.
- (58) Zanotti-Gerosa, A.; Solari, E.; Giannini, L.; Floriani, C.; Re, N.; Chiesi-Villa, A.; Rizzoli, C. *Inorg. Chim. Acta* **1998**, *270*, 298.
- (59) Tashiro, M. *Synthesis* **1979**, *1979*, 921.
- (60) (a) Bohmer, V.; Rathay, D.; Kammerer, H. *Org. Prep. Proced. Int.* **1978**, *10*, 113(b) Kammerer, H.; Happel, G.; Bohmer, V.; Rathay, D. *Monatsh. Chem.* **1978**, *109*, 767.
- (61) Gutsche, C. D.; Lin, L.-G. *Tetrahedron* **1986**, *42*, 1633.
- (62) (a) Zhang, D.; Wang, J.; Lawson, T. R.; Bartsch, R. A. *Tetrahedron* **2007**, *63*, 5076(b) Brindle, R.; Albert, K.; Harris, S. J.; Troeltzsch, C.; Horne, E.; Glennon, J. D. *J. Chromatogr., A* **1996**, *731*, 41(c) Hutchinson, S.; Kearney, G. A.; Horne, E.; Lynch, B.; Glennon, J. D.; McKervey, M. A.; Harris, S. J. *Anal. Chim. Acta* **1994**, *291*, 269.
- (63) (a) Glennon, J. D.; Horne, E.; O'Connor, K.; Kearney, G.; Harris, S. J.; McKervey, M. A. *Anal. Proc.* **1994**, *31*, 33(b) Arena, G.; Contino, A.; Longo, E.; Sciotto, D.; Spoto, G.; Torrisi, A. *J. Supramol. Chem.* **2004**, *2*, 521.
- (64) Glennon, J. D.; Horne, E.; Hall, K.; Cocker, D.; Kuhn, A.; Harris, S. J.; McKervey, M. A. *J. Chromatogr., A* **1996**, *731*, 47.
- (65) Wang, J.; Zhang, D.; Lawson, T. R.; Bartsch, R. A. *Talanta* **2009**, *78*, 477.
- (66) Liu, C.; Lambert, J. B.; Fu, L. *J. Am. Chem. Soc.* **2003**, *125*, 6452.
- (67) (a) Menyes, U.; Roth, U.; Troeltzsch, C.; (Menyes, Ulf, Germany; Roth, Ulrich; Troeltzsch, Christof). Application: EP, 1997(b) Sokoliess, T.; Menyes, U.; Roth, U.; Jira, T. *J. Chromatogr., A* **2000**, *898*, 35(c) Sokoliess, T.; Menyes, U.; Roth, U.; Jira, T. *J. Chromatogr., A* **2002**, *948*, 309(d) Sokoliess, T.; Schonherr, J.; Menyes, U.; Roth, U.; Jira, T. *J. Chromatogr., A* **2003**, *1021*, 71.
- (68) Ding, C.; Qu, K.; Li, Y.; Hu, K.; Liu, H.; Ye, B.; Wu, Y.; Zhang, S. *J. Chromatogr., A* **2007**, *1170*, 73.
- (69) Li, L.-S.; Liu, M.; Da, S.-L.; Feng, Y.-Q. *Talanta* **2004**, *63*, 433.

## **Chapter II**

**Proof of the concept:**

**Study of the reactivity between a phenolic  
function and supported triisobutylaluminum  
onto silica**



## 1. Introduction

A promising approach to develop novel organometallic surface species can be envisaged by inserting a spacer moiety, such as an aromatic ring, between the organometallic fragment and the surface. One of the main interests of systems generated traditionally by SOMC is their remarkable catalytic activity for difficult chemical transformations.<sup>1</sup> However, the recurrent problem is the interactions occurring between the grafted species and the functions displayed by the surface. In this approach, the insertion of a spacer group can be proposed as a powerful solution. Indeed, the metal is moved away from the surface, thus preventing any unwanted interactions.

To emulate or even improve effectively their performance, several requirements have to be met when designing new species, namely the podality of the metal, the selectivity for grafting and the stability of the spacer. Taking this into account, a spacer moiety must be proposed that include the suitable number of hydroxyl groups available to coordinate the metal in way similar to a silanol. Furthermore, using an aromatic compound to connect the surface and the organometallic fragment can lead to its efficient isolation due to its large size, rigidity and relative inertness toward the metal.<sup>2</sup> Indeed, phenols and more specifically their calixarenic derivatives seem to be ideal candidates.

Secondly, the grafting strategy has to be highly selective so that only the hydroxyl group of the spacer is available. Otherwise, this could result in the presence of more than one type of hydroxyl group on the surface and finally different organometallic fragments. Typical synthetic methodology generally involves the reaction between alkoxy silane functions, borne by the compounds to be grafted, and the surface hydroxyls. Despite being well documented, this approach usually leaves residual surface silanols, thus providing different types of hydroxyl functions, in addition to the ligand ones. After grafting of an organometallic complex, a mixture of active sites could be obtained. One direction, hardly explored, is to treat the surface hydroxyl with a compound reactive enough to quantitatively consume them but also able to further react selectively with other chemicals. The reactivity of metal alkyl, as it has been documented using SOMC, makes them suitable candidates to meet these requirements. While SOMC studies has covered most of the transition metals<sup>3</sup>, aluminum alkyls have not received much attention. This is surprising in regard of their advantages: ready availability, high reactivity and low cost. It should be emphasized that the use of such species on inorganic supports such as silica had been well documented, particularly for generating

cocatalysts for the polymerization of olefins catalyzed by metal transition based complexes. However, these studies were more focused on the catalytic performances of these systems than on the characterization of the aluminum supported compounds.

Finally, the stability of the spacer moieties has to be sufficient to complete the reaction but also to allow the final products to be employed in any process of interest. In this chapter, we aim to define a new concept to prepare organometallic fragments supported on an oxide support (*i.e.* silica) *via* a phenolic spacer unit, consisting of an organometallic complex (*i.e.* aluminum alkyl) anchored to the surface and an aromatic compound to tether it to the organometallic fragment. Our study will examine separately the different parts: aluminum alkyl grafting, treatment with hydroquinone as phenolic model and then reaction with different metal alkyl. The catalytic activity of these new supports will be compared to their counterparts directly supported on silica in selected reaction. This is preliminary work to establish the grafting method before applying it to form calixarene-based tether (see Chapter V).

## 2. Bibliographic study

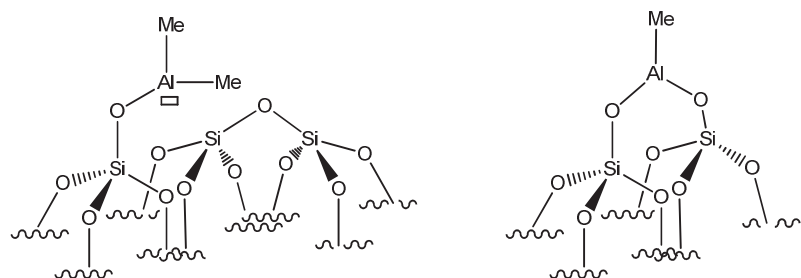
This section reviews the reactivity of aluminum alkyl species towards silica. Most of the reported aluminum alkyls supported on silica have been employed to generate cocatalyst and have been partially characterized (see **section 2.1**). Of particular relevance for this chapter is their incorporation into synthetic strategy to tether active catalytic species to the support.

### 2.1 Reactivity of trialkylaluminum with silica supports

Treatment of silica surfaces with trialkylaluminum compounds  $\text{AlR}_3$  have been largely employed to generate cocatalysts systems for the polymerization of olefins.<sup>4</sup> It can play two roles to generate the catalytically active species from the precatalyst: abstracting of a heteroatom and alkylation of the metal center M-X (Metal = Group IV, lanthanide...; X = halide, nitrogen...) and the extraction of a second heteroatom; hence generating a cationic metal alkyl propagation center for the polymerization of olefins. For instance, in the 1970's, many studies emerged on the grafting of  $\text{TiCl}_4/\text{AlMe}_3$  onto silica, thus forming active Ziegler-Natta catalysts for ethylene polymerization.<sup>4d,5</sup> Among all the existing trialkylaluminum compounds,  $\text{AlMe}_3$  is by far the best documented. Nonetheless, in spite of being examined

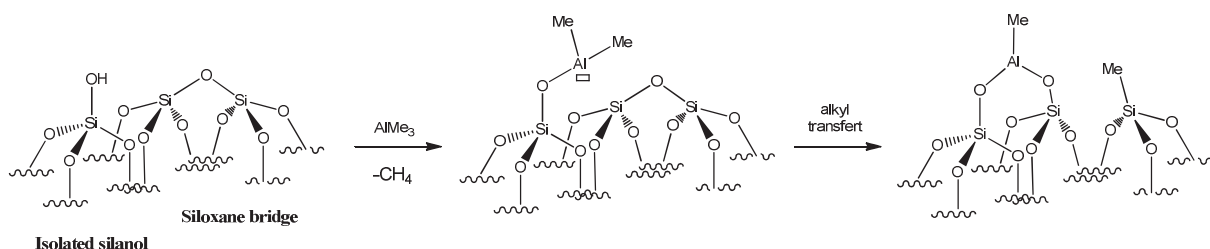
with different silica supports (fumed silica, porous glass<sup>6</sup>, silica gels<sup>7</sup> and MCM-41<sup>8</sup>) for numerous applications, its reactivity is still a subject of debate.

When considering all the functions displayed on the silica surface, (silanol vs siloxane), it seems reasonable to assume that the reactions involving the silanols are the fastest. It results in both the formation of Al-O-Si groups and the evolution of methane. In addition, scrutinizing spectroscopic and mass balance analysis data suggests the occurrence of side reactions. Regardless of the nature of the silica employed, the formation of isolated three-coordinate methylaluminum and dimethylaluminum sites was suggested by chemisorption on the surface (**Scheme 1**). Presumably the grafted aluminum compounds can further react with either another silanol, a siloxane or even another aluminum molecule.



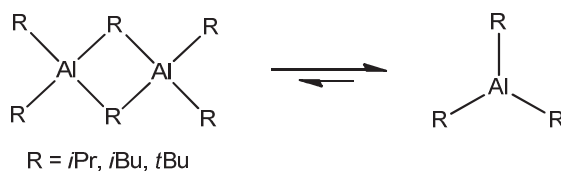
**Scheme 1: Suspected isolated three-coordinated dimethylaluminum and methylaluminum species on silica support**

The formation of grafted methylaluminum sites is accompanied by transfer of methyl groups from the aluminum to silicon atoms of the silica surface, although the extent of silicon methylation has not been resolved. In early studies, it was suggested that all the methyl groups on a trimethylaluminum-modified Aerosil surface were transferred to silicon atoms.<sup>6,9</sup> Due to its Lewis acidity, the grafted dimethylaluminum ( $\equiv\text{SiO})\text{AlMe}_2$ ) obtained first will provoke the opening of a neighboring siloxane bridge with the concomitant methyl transfer onto the silicon atom (**Scheme 2**).<sup>10</sup> However, recent studies involving  $\text{AlMe}_3$ -saturated MCM-41<sup>8a</sup> and silica gel<sup>7b</sup> reported that a substantial amount of ( $\equiv\text{SiO})\text{AlMe}_2$  persists in these materials. Finally, a recent solid state NMR study showed that  $\text{AlMe}_3$  causes little methylation of a silica surface.<sup>11</sup>



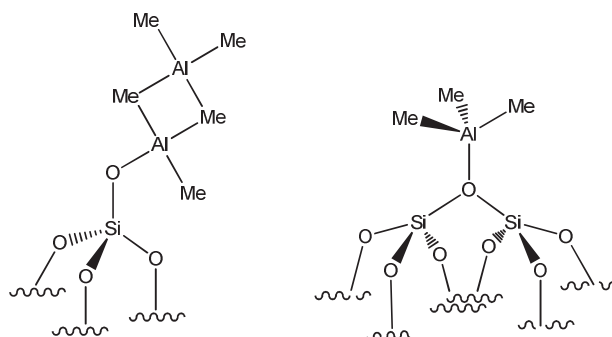
**Scheme 2:** Reaction of the surface silanols with  $\text{AlMe}_3$  and rearrangement of the silica support by siloxane bridges opening

In solution,  $\text{AlR}_3$  monomers tend to associate to form dimers;<sup>12</sup> both species are in equilibrium, the constant of which varies depending on the size of the alkyl group R and can be determined by spectroscopic measurements (**Scheme 3**). For example, the monomeric form prevails for  $\text{Al}t\text{Bu}_3$  but is less significant than for  $\text{Al}i\text{Pr}_3$  and  $\text{AlMe}_3$ .  $\text{Al}i\text{Bu}_3$  appears to be intermediate to its counterparts.<sup>13</sup>



**Scheme 3:** Equilibrium between the monomeric and the dimeric forms of  $\text{AlR}_3$

Although silica may inhibit the oligomerization of organometallic fragments on its surface, the presence of four-coordinate di-aluminum surface sites has been demonstrated, occurring on silica oversaturated with  $\text{AlMe}_3$  (**Scheme 4**).<sup>8a,10</sup> There is evidence that electron-deficient Al can associate with surface oxygens.

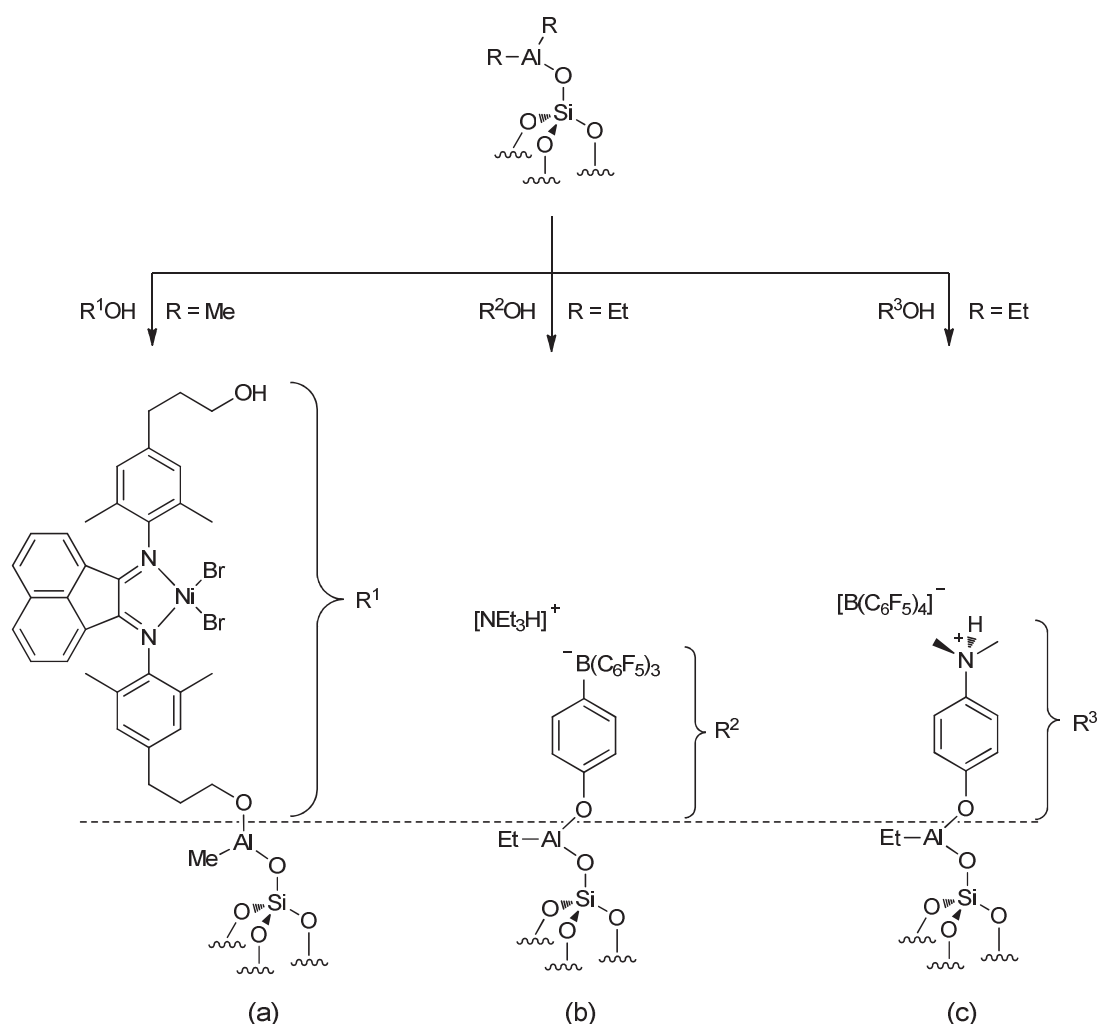


**Scheme 4:** Four-coordinate dialuminum surface species

The proposed mononuclear, three-coordinate Al structures shown in **Scheme 1** are highly unusual in organoaluminum chemistry, which strongly favors tetracoordination and oligomeric structures, except in the presence of particularly bulky ligands or extreme reaction conditions.<sup>14</sup> Furthermore, coordination of  $\text{AlR}_3$  to a nearby siloxane oxygen is likely to occur

in order to maintain the preferred tetracoordination of Al. The adsorption of a Lewis base such as Et<sub>2</sub>O may displace the coordinated siloxane oxygen atom and then limit the physisorption process.<sup>15</sup>

AlR<sub>3</sub> derivatives can also serve as passivators to provide a silica support inert towards reaction between organometallic complexes and surface silanols. The metal alkyl fragment can undergo a protolysis reaction by an alcoholic function.<sup>16</sup> In this approach, the remainder of the alcoholic compound can be considered as an organic linker. For instance, Brookhart *et al.* synthesized a variety of nickel  $\alpha$ -diimines containing amine or hydroxyl functional groups which were reacted with AlMe<sub>3</sub> passivated silica to form tethered precatalysts (Scheme 5, (a)).<sup>17</sup>



**Scheme 5:** Tethered co-catalysts through alkoxy (a) and aryloxy functions (b, c) on silica previously passivated with AlR<sub>3</sub>

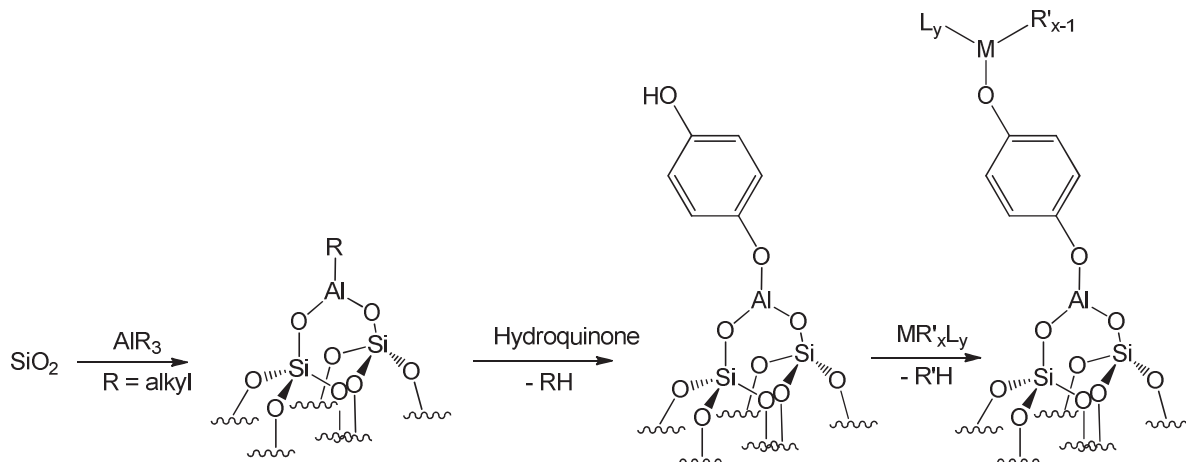
Other catalytic systems have been supported through aryloxy functions. For instance, Jacobsen *et al.* immobilized borate derivatives by contacting the ammonium borate

$[\text{HNEt}_3][\text{(C}_6\text{F}_5)_3\text{-BArOH}]$  with a silica surface passivated by treatment with  $\text{AlEt}_3$  (Scheme 5, **(b)**).<sup>18</sup> Triethylaluminum passivated supports have also been used by Holtcamp *et al.* in the immobilization of  $[\text{HOCH}_2\text{C}_6\text{H}_4\text{NMe}_2\text{H}][\text{B}(\text{C}_6\text{F}_5)_4]$  (Scheme 5, **(c)**).<sup>19</sup>

It should be noted that these resulting materials were not well-defined. Several phenomena such as dimerization and physisorption of trialkylaluminum, or alkyl transfer processes from the aluminum center to the surface, are obstacles in controlling the generation of single sites. In addition, the tethering of organic linkers through phenolic or hydroxyl functions onto a silica support previously treated with a trialkylaluminum is few documented and not fully characterized.

## 2.2 Strategy

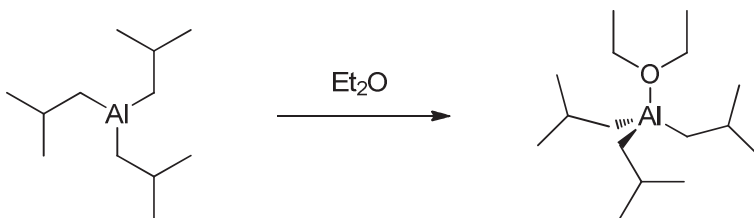
A synthetic methodology was conceived to allow the access to a novel silica-based support presenting single monografted monoaryloxy fragments. This multi-step preparation begins by the preliminary treatment of the silica with a selected trialkylaluminum. The aluminum species generated can then serve as an anchoring site for a phenol compounds displaying two hydroxyl functions, like hydroquinone (**Scheme 6**). The one remaining alcohol can then be reacted to immobilize a transition metal complex selected to provide a catalytically active centre.



**Scheme 6:** Multi-step preparation of supported complexes with a hydroquinone spacer ( $L = \text{oxo, imido...; R}' = \text{alkyl, carbene, carbone, hydride}$ )

Several parameters can be identified as essential for this approach to be successful: the choice of the support, the starting aluminum derivative and the selectivity of the grafting of the aryloxy ligand:

- A support presenting only isolated silanols will be employed to generate well-defined species. Aerosil Degussa type silica partially dehydroxylated at 700°C will be exclusively used.
- Monomeric trialkylaluminum compounds are preferable to dimeric ones (*vide supra*) for obtaining single well-defined surface species. In this way, triisobutylaluminum will be chosen because of its availability and its tendency to be monomeric. Furthermore, the utilization of a coordinating solvent is considered as a solution to circumvent the coordination processes. Due to its strong Lewis character, triisobutylaluminum associates easily with electron-donor species and forms, for instance, the monomeric neutral etherate adduct  $\text{Al}i\text{Bu}_3\cdot\text{OEt}_2$  when reacted with diethylether (Scheme 7).<sup>12-13</sup>



**Scheme 7: Formation of the monomeric etherate adduct of  $\text{Al}i\text{Bu}_3$**

Then, the grafting will be performed using the impregnation technique in diethylether, facilitating the elimination of the unreacted reagent and limiting the physisorption process, compared to the vapor deposition.

- Once fully characterized by solid-state NMR, DRIFT and mass balance analysis, the passivated silica presenting single alkyl aluminum anchoring sites will be reacted with the hydroquinone. The material obtained will serve as a novel support for the generation of new grafted catalysts by incorporation of organometallic complexes of zirconium and tungsten, for which the catalytic behavior in SOMC reactions will be directly compared to their silica grafted counterparts.

### 3. Reactivity of $\text{AliBu}_3\text{OEt}_2$ with $\text{SiO}_{2-(700)}$ . Generation of the material $[(\equiv\text{SiO})_2\text{AliBu}(\text{Et}_2\text{O})] (\text{H1})$

#### 3.1 Choice of the silica support $\text{SiO}_{2-(700)}$

Flame Degussa Aerosil 200  $\text{m}^2\cdot\text{g}^{-1}$  silica was selected as a support as it is well-known at LCOMS laboratory in the generation of well-defined supported metal alkyl complexes which will be compared to their supported aryloxy counterparts. Isolated surface silanols can be selectively obtained by dehydroxylation under high vacuum at 973K for 12 h. In the DRIFT spectrum of  $\text{SiO}_{2-(700)}$ , a narrow peak at  $3747 \text{ cm}^{-1}$  in the OH region reveals the one presence of isolated surface silanols (**Figure 1**). This support presents *ca.*  $0.8 \text{ OH}\cdot\text{nm}^{-2}$  corresponding to  $0.266 \text{ mmol}_{\text{OH}}\cdot\text{g}^{-1}$  of silica.<sup>20</sup>

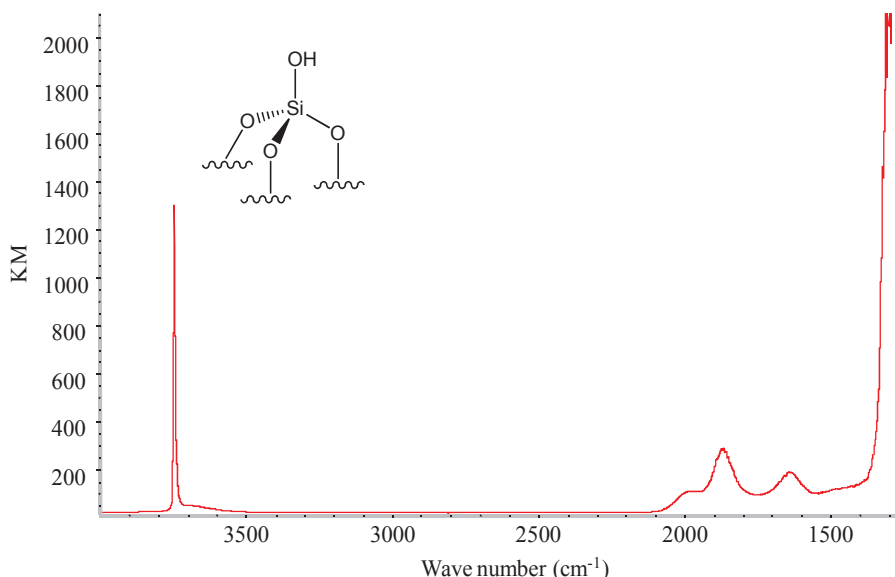
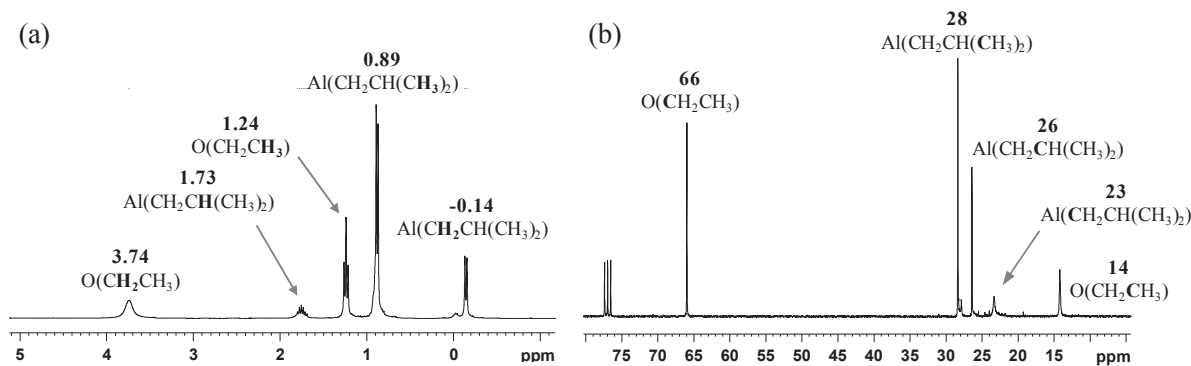


Figure 1: DRIFT spectrum of  $\text{SiO}_{2-(700)}$

#### 3.2 Reactivity of $\text{AliBu}_3\text{EtO}_2$ in diethylether with $\text{SiO}_{2-(700)}$

##### 3.2.1 Preparation and characterization of $\text{AliBu}_3\text{EtO}_2$

The starting material  $\text{AliBu}_3\text{EtO}_2$  is obtained by dilution of  $\text{AliBu}_3$  in diethylether. After evaporation of the excess solvent, the etherate is characterized by  $^1\text{H}$  and  $^{13}\text{C}$ -NMR. The  $^1\text{H}$ -NMR spectrum of  $\text{AliBu}_3\text{Et}_2\text{O}$  in  $\text{CDCl}_3$  reveals the signals of the coordinated diethylether molecule at 1.24 and 3.74 ppm that can be assigned to the methyl and the methylene fragments respectively (**Figure 2, (a)**).



**Figure 2:**  $^1\text{H}$  and  $^{13}\text{C}$ -NMR in  $\text{CDCl}_3$  of the triisobutylaluminum etherate  $\text{Al}(\text{iBu}_3)\cdot\text{Et}_2\text{O}$

The doublet from the  $\text{CH}_2$  of  $\text{Al}(\text{CH}_2\text{CH}(\text{CH}_3)_2)$  is displayed in the negative chemical shifts at -0.14 ppm while the doublet of  $\text{CH}_3$  of  $\text{Al}(\text{CH}_2\text{CH}(\text{CH}_3)_2)$  and the multiplet from the  $\text{CH}$  proton  $\text{Al}(\text{CH}_2\text{CH}(\text{CH}_3)_2)$  are observed at 0.89 and 1.73 ppm respectively. The  $^{13}\text{C}$ -NMR spectrum presents two peaks at 14 and 66 ppm corresponding to the diethylether carbons (**Figure 2, (b)**).  $\text{CH}_3$  and  $\text{CH}$  carbons of  $\text{Al}(\text{CH}_2\text{CH}(\text{CH}_3)_2)$  display respectively peaks at 28 and 26 even if  $\text{CH}_2$  gives a broad signal at 23 ppm due to the quadrupolar effect of the  $^{27}\text{Al}$  nucleus.

### 3.2.2 Preparation and characterization of $[(\equiv\text{SiO})_2\text{Al}(\text{iBu}_3)\cdot(\text{Et}_2\text{O})]$ (**H1**)

Using the double Schlenk technique (see Annex I),  $\text{SiO}_{2-(700)}$  was treated with 1.3 eq. of  $\text{Al}(\text{iBu}_3)$  (based on the number of surface silanols,  $0.266 \text{ mmol}_{\text{OH}\cdot\text{g}^{-1}}$ ) in diethylether (5 ml) for 2 h at room temperature. After repeated washings with diethylether (5 ml), followed by evacuation of the volatile, **H1** was afforded as a white powder and characterized by DRIFT, solid-state NMR and mass balance analysis.

- **Infra-red spectroscopy**

The DRIFT spectrum of **H1** revealed that the band at  $3747 \text{ cm}^{-1}$ , corresponding to the isolated silanols displayed on the surface, has been completely consumed (**Figure 3**). Simultaneously, the appearance of two series of bands at  $2800\text{-}3000$  and  $1300\text{-}1500 \text{ cm}^{-1}$  is consistent with the  $\nu_{(\text{C-H})}$  and  $\delta_{(\text{C-H})}$  vibrations of alkyl moieties, respectively.

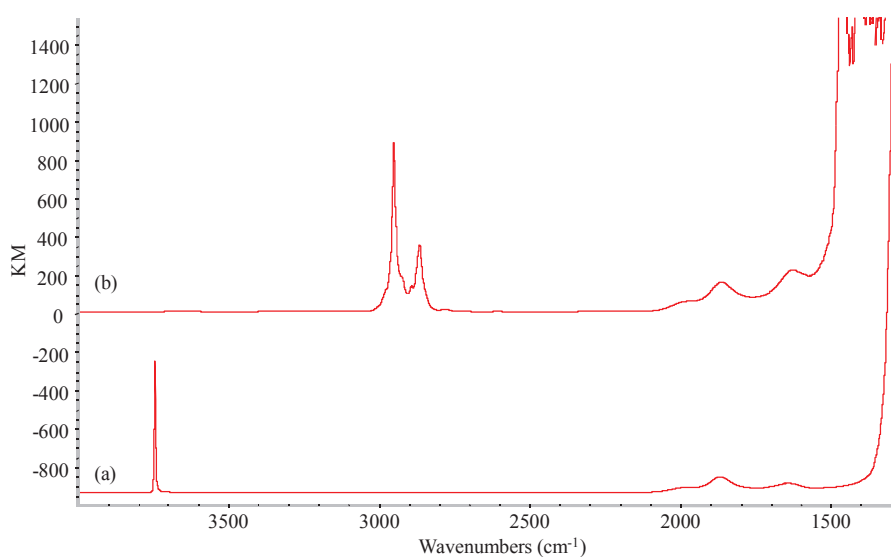


Figure 3: DRIFT spectra of  $\text{SiO}_{2-(700)}$  before (a) and after treatment with  $\text{Al}(\text{iBu})_3$  in  $\text{Et}_2\text{O}$ , H1 (b)

- **Mass-balance analysis**

The stoichiometry of the reaction between  $\text{SiO}_{2-(700)}$  and  $\text{Al}(\text{iBu})_3 \cdot \text{Et}_2\text{O}$  can be determined by comparing the gas evolved during the reaction and the aluminum and carbon content measured by elemental analysis. The aluminum content of 0.8%wt (corresponding to  $0.296 \text{ mmol.g}^{-1}$ ) is consistent with the total consumption of the surface silanols in accordance with the DRIFT spectrum. The gas evolved during the reaction between  $\text{SiO}_{2-(700)}$  and  $\text{Al}(\text{iBu})_3 \cdot \text{Et}_2\text{O}$  was identified as isobutane and quantified as  $0.270 \text{ mmol.g}^{-1}$  of silica by GC analysis. It accounts for 0.9  $i\text{BuH}/\text{Al}$ , hence suggesting a bisalkyl monografted aluminum species (**Table 1**). The carbon content is consistent with a C/Al ratio of 11 (th 12). The value of this ratio can be interpreted as the presence of one diethylether molecule chelated to the aluminum in addition to two supported isobutyl fragments.

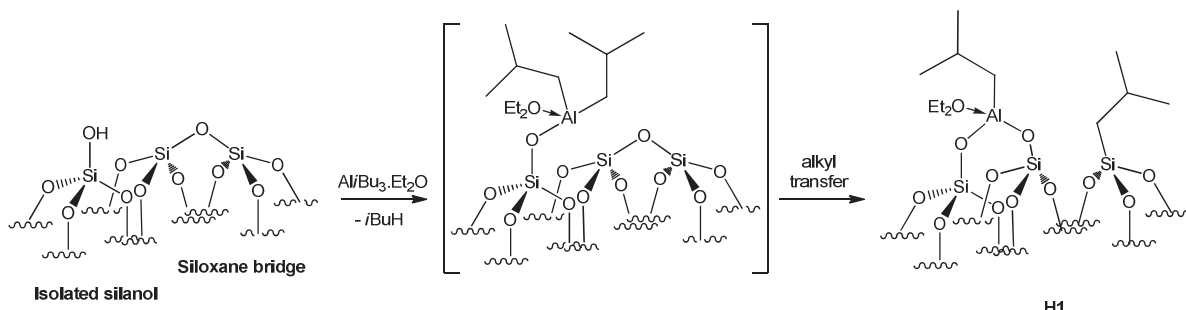
**Table 1: Mass balance analysis for H1**

	%wt Al <sup>[a]</sup>	$i\text{BuH}/\text{Al}$ <sup>[b]</sup>	%wt C <sup>[a]</sup>	C/Al
Grafting	0.80	0.9	3.90	11 (th 12)
Hydrolysis <sup>[c]</sup>	0.80	1.0	2.16	6

[a] Percentage determined by elemental analysis. [b] Isobutane released, quantified by GC. [c] Mass balance after water vapor treatment.

However, following the hydrolysis of **H1** by water vapor pressure, only 1 eq. of  $i\text{BuH}$  was collected instead of the expected 2 eq. for a bisalkyl aluminum species. Six carbon atoms was found instead of the four expected (considering the quasi-total elimination of the diethyl ether after hydrolysis). From these results, one isobutyl group remains anchored on the

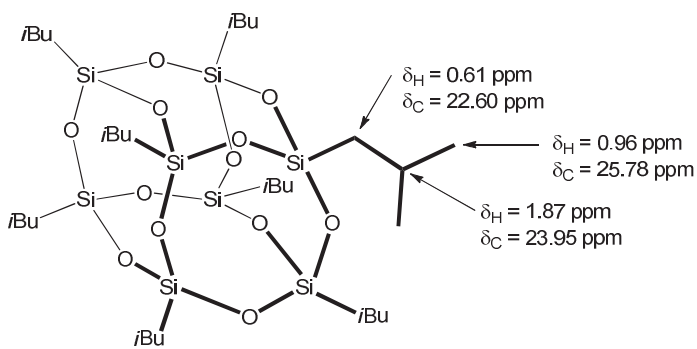
surface, plus a fraction of chemi- or physisorbed diethyl ether. This can be explained by the presence of the non hydrolysable Si-*i*Bu fragment generated by the cleavage of a neighboring siloxane bridge by the aluminum center with the concomitant isobutyl transfer onto the corresponding silicon (**Scheme 8**).



**Scheme 8:** Grafting of  $\text{Al}(\text{iBu})_3$  onto  $\text{SiO}_{2-(700)}$  in diethylether. Structure proposed for  $[(\equiv\text{SiO})_2\text{Al}(\text{iBu})(\text{Et}_2\text{O})]$  **H1**. Reagents and conditions: 1.3 eq.  $\text{Al}(\text{iBu})_3$ ,  $\text{Et}_2\text{O}$ , 2 h, RT.

- **Solid-state NMR spectroscopy**

The <sup>1</sup>H MAS and <sup>13</sup>C CP/MAS-NMR spectra contain a series of broad peaks that can be mostly assigned, for most of them, to the alkyl groups (**Figure 4**). The interpretation of the spectra of  $[(\equiv\text{SiO})_2\text{Al}(\text{iBu})(\text{Et}_2\text{O})]$  **H1** is supported by the <sup>1</sup>H-NMR spectrum of  $\text{Al}(\text{iBu}) \cdot \text{Et}_2\text{O}$  adduct in  $\text{CDCl}_3$  and octaisobutylsilsesquioxane POSS <sup>1</sup>H and <sup>13</sup>C NMR spectra in liquid state (**Scheme 9**),<sup>21</sup> which emulates the anchored isobutyl groups onto the silica. The following assignment can be proposed: the large signal centered at around 0.8 ppm is undoubtedly composed of several peaks from the CH<sub>3</sub> protons of M(CH<sub>2</sub>CH(CH<sub>3</sub>)<sub>2</sub>) (M = Si, Al) and the CH<sub>2</sub> protons of Si(CH<sub>2</sub>CH(CH<sub>3</sub>)<sub>2</sub>), whereas the peak at -0.14 ppm could be assigned to the CH<sub>2</sub> protons of Al(CH<sub>2</sub>CH(CH<sub>3</sub>)<sub>2</sub>). The shoulder observed at 1.73 ppm is attributed to the CH protons of M(CH<sub>2</sub>CH(CH<sub>3</sub>)<sub>2</sub>) (M = Si, Al). In addition, two broad peaks can be seen at 1.17 and 4.02 ppm, typically for CH<sub>3</sub> and CH<sub>2</sub> in diethylether. In the <sup>13</sup>C spectrum of **H1** (**Figure 4b**), one peak at 22 ppm corresponds to the CH<sub>2</sub> carbon of Al(CH<sub>2</sub>CH(CH<sub>3</sub>)<sub>2</sub>), whereas the peaks at 26 and 28 ppm are thought to encapsulate carbons from the isobutyl silicon fragment Si(CH<sub>2</sub>CH(CH<sub>3</sub>)<sub>2</sub>) and CH<sub>3</sub> and CH carbons of the fragment Al(CH<sub>2</sub>CH(CH<sub>3</sub>)<sub>2</sub>). Two additional signals at 13 and 67 ppm are characteristic of the CH<sub>3</sub> and the CH<sub>2</sub> carbons of diethylether. This structure was also confirmed by HETCOR 2D NMR and the reaction with O<sub>2</sub> in the case of the analogous SBA material  $[(\equiv\text{SiO})_2\text{Al}(\text{iBu})(\text{Et}_2\text{O})]_{\text{SBA LP-(700)}}$  **M1** (see Chapter V).



Scheme 9:  $^1\text{H}$  and  $^{13}\text{C}$  chemical shifts of the isobutyl groups from the octaisobutylsilsesquioxane POSS

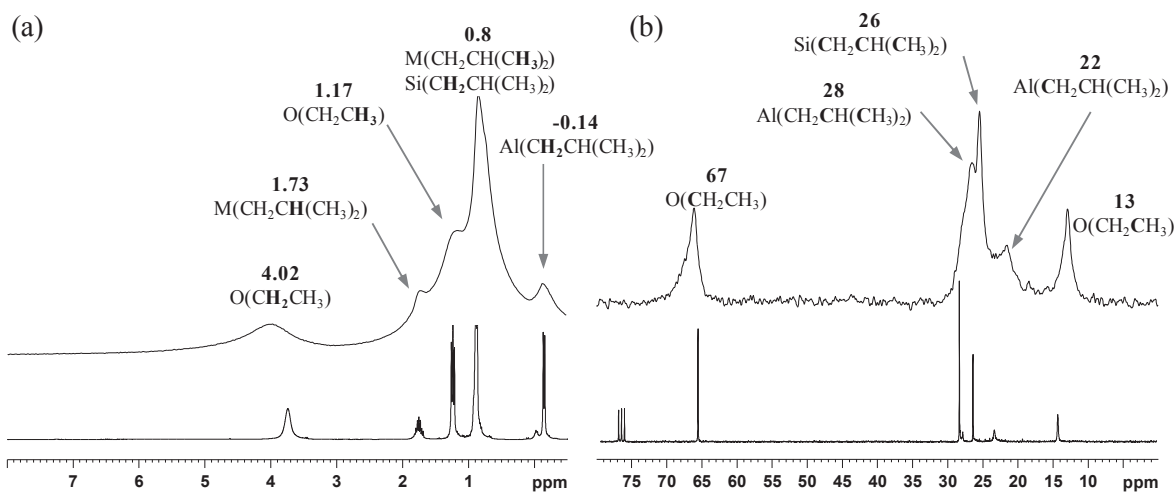


Figure 4:  $^1\text{H}$  MAS (a) and  $^{13}\text{C}$  CP/MAS-NMR (b) of  $[(\equiv\text{SiO})_2\text{Al}i\text{Bu}(\text{Et}_2\text{O})]$  H1 compared to the  $\text{Al}i\text{Bu}_3\text{-Et}_2\text{O}$   $^1\text{H}$  and  $^{13}\text{C}$ -NMR in liquid state

The unprecedented bis-grafted mono isobutyl aluminum etherate species  $[(\equiv\text{SiO})_2\text{Al}i\text{Bu}(\text{Et}_2\text{O})]$  **H1** was successfully prepared and fully characterized. The utilization of ether, to prevent aluminum alkyl dimerization, also serves as adsorption competitor. As a result, unreacted and physisorbed  $\text{Al}i\text{Bu}_3$  can be conveniently removed from the surface. Alkyl transfer from aluminum to silica has also been observed. This well-defined species will be employed in our synthetic method by undergoing treatment with hydroquinone in the following sections.

#### 4. Reactivity of hydroquinone with $[(\equiv\text{SiO})_2\text{Al}i\text{Bu}(\text{Et}_2\text{O})]$ (**H1**)

$[(\equiv\text{SiO})_2\text{Al}i\text{Bu}(\text{Et}_2\text{O})]$  **H1** was treated by 1.3 eq. of hydroquinone in diethylether (5 ml) over 16 h at room temperature using the double Schlenk technique. After repeated washings with diethylether (5 ml), followed by evacuation of the volatiles, **H2** was afforded

as a white powder and characterized using DRIFT, solid-state NMR spectroscopy and mass balance analysis.

- **Infra-red spectroscopy**

In comparison to the DRIFT spectrum of **H1**, new bands at 1500-1610 cm<sup>-1</sup> and 3000-3035 cm<sup>-1</sup> assigned to the aromatic ring stretchings  $\nu_{(\text{Csp}_2=\text{Csp}_2)}$  and  $\nu_{\text{Csp}_2-\text{H}}$ , respectively, appear (**Figure 5**), while the bands attributed to  $\nu_{\text{Csp}_3-\text{H}}$  at 2800-3000 cm<sup>-1</sup> from the isobutyl fragments and diethyl ether groups partially disappear. The residual alkyl come from the presence of unreacted Si-*i*Bu fragments toward hydroquinone. The examination of the OH stretching region reveals a large, weak band centered at 3300 cm<sup>-1</sup> coming from the phenol function. No signal from any free surface silanols is observed, proving the absence of protolysis from the reaction due to the stability of the Al-O-Si bond.

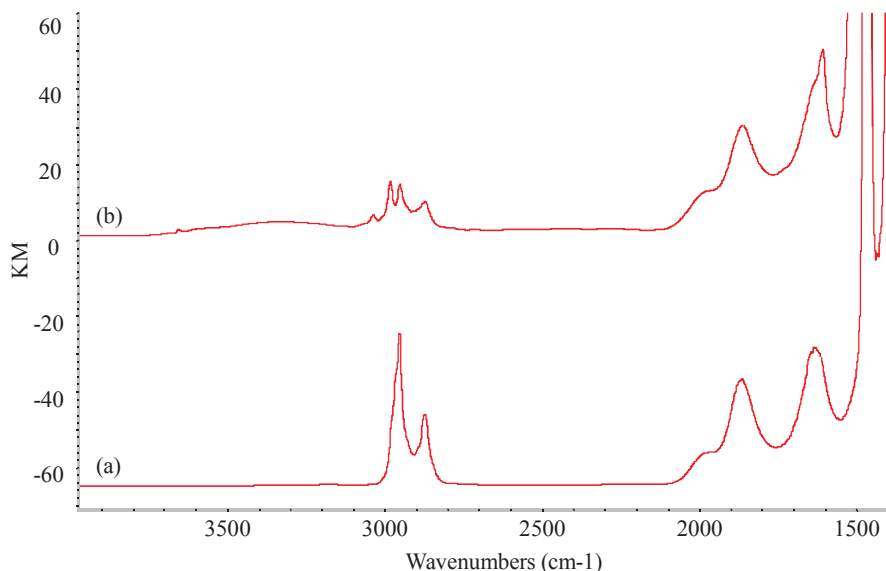


Figure 5: DRIFT spectra of [ $(\equiv\text{SiO})_2\text{Al}i\text{Bu}(\text{Et}_2\text{O})$ ] **H1** (a) and **H2** (b)

- **Mass-balance analysis**

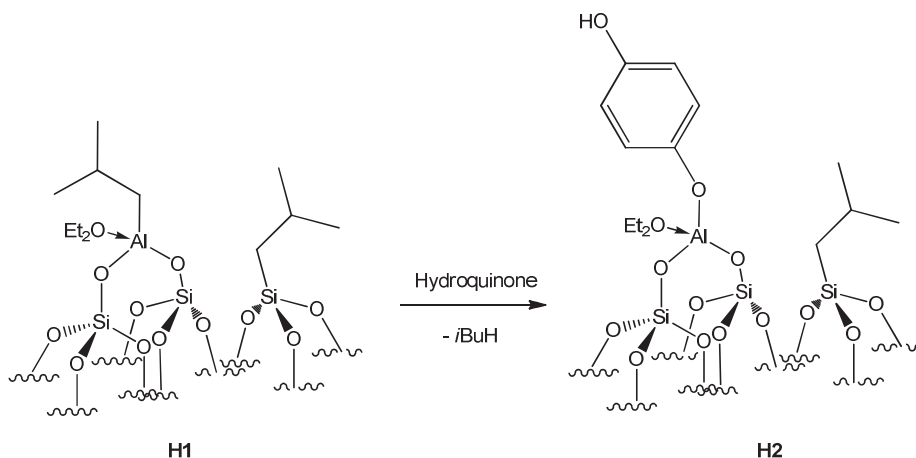
The percentage of aluminum after the grafting of the hydroquinone onto **H2** is of 0.84%wt whereas 0.9 eq. of isobutane was evolved per grafted aluminum, thus suggesting the anchoring of the hydroquinone on 90% of the isobutyl aluminum sites (**Table 2**).

**Table 2: Mass balance analysis for H2**

	Al %wt <sup>[a]</sup>	<i>i</i> BuH/Al <sup>[b]</sup>	C %wt <sup>[a]</sup>	C/Al
Grafting	0.84	0.9	4.11	11 (th 10 <sup>[c]</sup> )

[a] Percentage determined by elemental analysis. [b] Isobutane released, quantified by GC. [c] Considering partial diethyl ether release

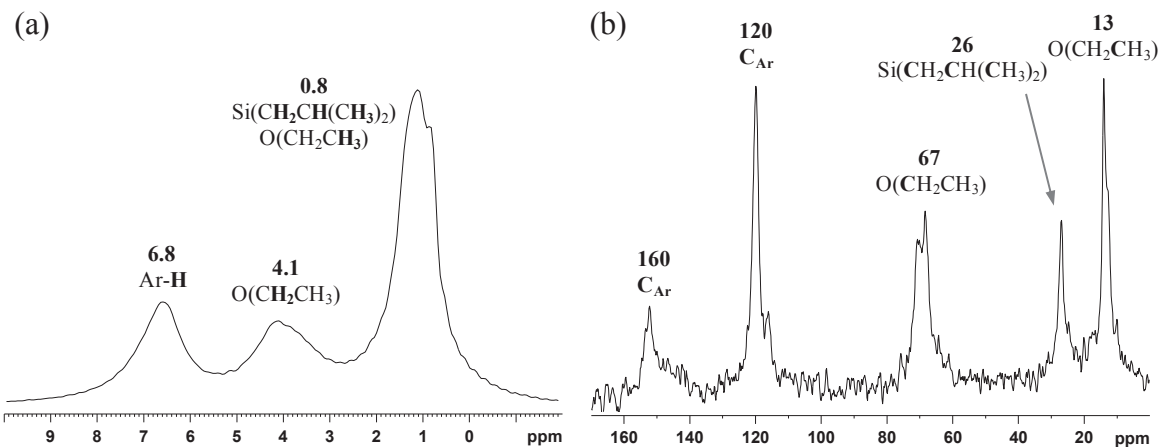
The experimental ratio of 11 C/Al is consistent with one molecule of hydroquinone grafted onto an aluminum atom alongside a Si-*i*Bu fragment (th 10, without diethyl ether). It is noteworthy that, during the elemental analysis procedure, molecules of diethylether molecule are released in some cases, especially when the aluminum atom is bonded to three oxygen atoms. However, NMR spectra confirm its presence in the generated material (*vide infra*), finally described as  $[(\equiv \text{SiO})_2\text{AlO-C}_6\text{H}_4\text{-OH}.\text{(Et}_2\text{O})]$  in **Scheme 10**.



**Scheme 10: Grafting of the hydroquinone onto  $[(\equiv \text{SiO})_2\text{Al-iBu}.\text{(Et}_2\text{O})]$  H1. Proposed structure for  $[(\equiv \text{SiO})_2\text{AlO-C}_6\text{H}_4\text{-OH}.\text{(Et}_2\text{O})]$  H2. Reagents and conditions: 1.3 eq. hydroquinone, Et<sub>2</sub>O, 16 h, RT.**

- **Solid-state NMR spectroscopy**

In comparison with  $[(\equiv \text{SiO})_2\text{Al-iBu}.\text{(Et}_2\text{O})]$  **H1**, the <sup>1</sup>H-NMR spectrum of  $[(\equiv \text{SiO})_2\text{AlO-C}_6\text{H}_4\text{-OH}.\text{(Et}_2\text{O})]$  **H2** shows new signals at 6.8 ppm, a typical shift for the aromatic protons and the disappearance of the peak at -0.14 ppm belonging to the CH<sub>2</sub> protons of the isobutyl aluminum fragment (**Scheme 11, (a)**). In the <sup>13</sup>C CP/MAS spectrum, both peaks at 22 and 28 ppm have disappeared proving the elimination of the isobutyl aluminum groups (**Scheme 11, (b)**). The remaining peak at 26 ppm corresponds to the isobutyl silicon carbons. Both peaks at 115-120 and 160 ppm corresponding of the C<sub>Ar-H</sub> and C<sub>Ar-O</sub> carbons are evidences for the hydroquinone grafting. The presence of diethylether molecule coordinated to the aluminum center is confirmed by the peaks at 13 and 67 ppm.



Scheme 11:  $^1\text{H}$  MAS (a) and  $^{13}\text{C}$  CP/MAS-NMR (b) of  $[(\equiv\text{SiO})_2\text{AlO-C}_6\text{H}_4\text{-OH}(\text{Et}_2\text{O})]$  H2

The reaction between the silica passivated by  $\text{AliBu}_3\text{-Et}_2\text{O}$  and the hydroquinone afforded selectively the monografted aryloxy  $[(\equiv\text{SiO})_2\text{AlO-C}_6\text{H}_4\text{-OH}(\text{Et}_2\text{O})]$  H2 species alongside the isobutyl silicon fragments. In regard of the next step, namely grafting alkyl metals on the prepared support, the spectroscopic data (*i.e.* DRIFT) suggest that the only hydroxyl groups available are those displayed by the grafted hydroquinone.

## 5. Grafting of $\text{Zr}(\text{CH}_2\text{Ph})_4$ and $\text{W}(\equiv\text{CtBu}(\text{CH}_2\text{tBu})_3)$ onto $\text{SiO}_{2-(700)}$ and $[(\equiv\text{SiO})_2\text{AlO-C}_6\text{H}_4\text{-OH}(\text{Et}_2\text{O})]$ (H2)

The aim of this chapter is also to study the influence of the phenoxy type spacer between the silica support and the organometallic fragment on the catalytic performances of usual SOMC catalysts. In this approach, a comparative study in catalytic reactions will be run between supported complexes directly bonded to the support and *via* the hydroquinone spacer. In SOMC, in order to control the grafting step, the molecular species which react with the surface are usually metal-alkyl complexes particularly those with ligands which do not have  $\beta$ -protons, *e.g.* neopentyl or benzyl fragments. Therefore our first goal was to find the right molecular complexes. Our choice was focused on the zirconium complex  $\text{Zr}(\text{CH}_2\text{Ph})_4$  in order to prove the concept of the grafting of an organometallic complex on a supported aryloxy linker. Our study will also be extended to the Schrock carbyne complex  $\text{W}(\equiv\text{CtBu})(\text{CH}_2\text{tBu})_3$ , due to its activity in olefin metathesis when grafted onto a silica support.<sup>22</sup> In this way, both complexes will be grafted onto  $\text{SiO}_{2-(700)}$  and the hydroquinone material  $[(\equiv\text{SiO})_2\text{AlO-C}_6\text{H}_4\text{-OH}(\text{Et}_2\text{O})]$  H2.

## 5.1 Grafting of the zirconium complex $\text{Zr}(\text{CH}_2\text{Ph})_4$ onto $\text{SiO}_{2-(700)}$ and $[(\equiv\text{SiO})_2\text{AlO-C}_6\text{H}_4-\text{OH}.(\text{Et}_2\text{O})]$ (**H2**)

### 5.1.1 Preparation and characterization of $[(\equiv\text{SiO})\text{Zr}(\text{CH}_2\text{Ph})_3]$ (**H3**)

The complex  $\text{Zr}(\text{CH}_2\text{Ph})_4$  was synthesized using an adaptation of a reported method (see experimental section).<sup>23</sup> Typically,  $\text{ZrCl}_4$  was alkylated with 4 eq. of  $\text{BnMgCl}$  at  $-33^\circ\text{C}$  in the dark to provide after purification  $\text{Zr}(\text{CH}_2\text{Ph})_4$  as orange crystals, in 80% yield. Using the double Schlenk technique, 1.3 eq. of  $\text{Zr}(\text{CH}_2\text{Ph})_4$  (based on the number of surface silanols:  $0.266 \text{ mmol}_{\text{OH}\cdot\text{g}^{-1}}$ ) in pentane (5 ml) were reacted with  $\text{SiO}_{2-(700)}$  over 3h at room temperature, also in the dark. After repeated washings with pentane (5 ml), followed by evacuation of the volatile, **H3** was afforded as a yellow powder and characterized by DRIFT, solid-state NMR spectroscopy and mass balance analysis.

- **Infra-red spectroscopy**

After reaction with  $\text{Zr}(\text{CH}_2\text{Ph})_4$ , the DRIFT spectrum of **H3** displays new bands at  $1592 \text{ cm}^{-1}$  and  $3020-3065 \text{ cm}^{-1}$  assigned to the aromatic ring stretching  $\nu_{(\text{Csp}2=\text{Csp}2)}$  and  $\nu_{(\text{Csp}2-\text{H})}$ , respectively (**Figure 6**). The  $\nu_{\text{Csp}3-\text{H}}$  bands from  $2870$  to  $2990 \text{ cm}^{-1}$  are the result of the  $\text{CH}_2$  bond vibration. No signal from any free surface silanols is observed.

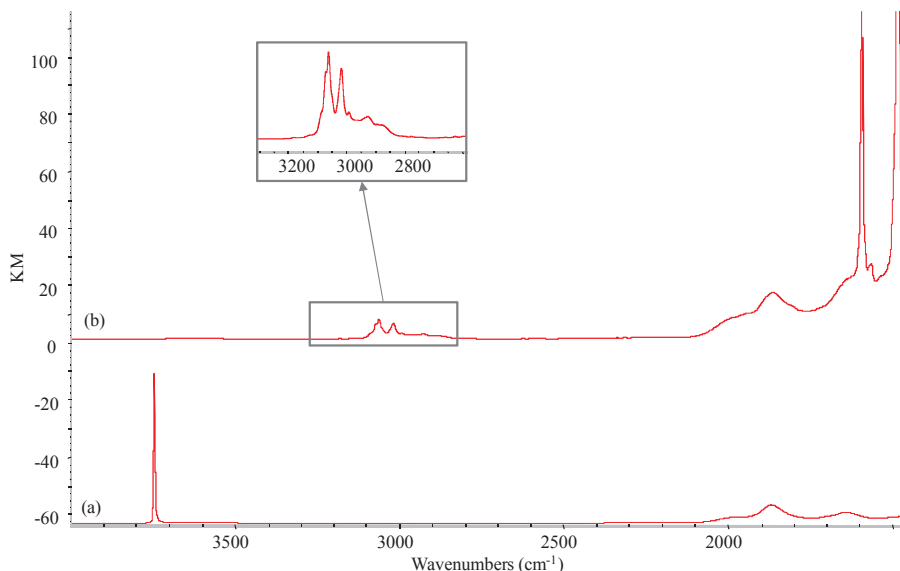


Figure 6: DRIFT spectra of  $\text{SiO}_{2-(700)}$  (a) and after grafting of  $\text{Zr}(\text{CH}_2\text{Ph})_4$ , **H3** (b)

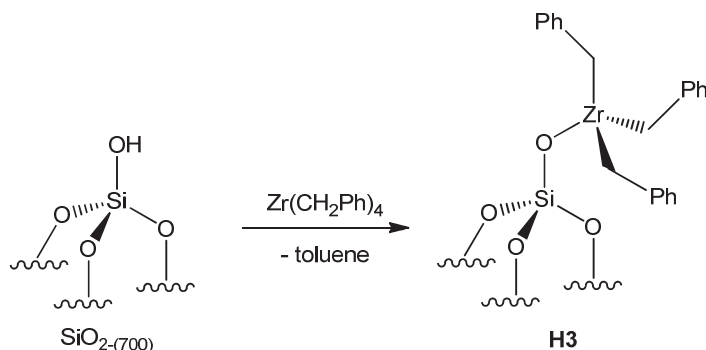
- **Mass-balance analysis**

It must be mentioned that the quantification by GC of the toluene released was not conclusive due its low vapor pressure and physisorption on the support. However, the percentages of zirconium and carbon after the grafting of  $\text{Zr}(\text{CH}_2\text{Ph})_4$  were found to 2.8%wt and 7.24%wt respectively, thus corresponding to 19.6 carbons per metal (**Table 3**). The monosiloxo trisbenzyl species  $[(\equiv\text{SiO})\text{Zr}(\text{CH}_2\text{Ph})_3]$  **H3** (accounting for 21 carbons) can rationally be proposed, as depicted in **Scheme 12**. In support of this, it is noteworthy that grafting of analogous tetraneopentyl complexes of group IV gives selectively monosiloxo species on  $\text{SiO}_{2-(700)}$ .<sup>24</sup>

**Table 3:** Mass balance analysis for **H3**

	%wt Zr <sup>[a]</sup>	%wt C <sup>[a]</sup>	C/Zr
Grafting	2.8	7.24	20 (th 21)

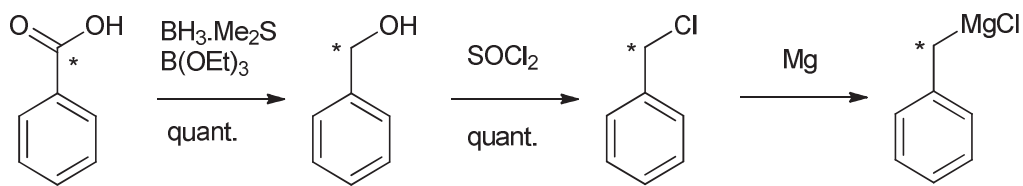
[a] Percentage determined by elemental analysis



**Scheme 12:** Grafting of  $\text{Zr}(\text{CH}_2\text{Ph})_4$  onto  $\text{SiO}_{2-(700)}$ . Synthesis of  $[(\equiv\text{SiO})\text{Zr}(\text{CH}_2\text{Ph})_3]$  **H3**. Reagents and conditions: 1.3 eq.  $\text{Zr}(\text{CH}_2\text{Ph})_4$ , pentane, 3 h, RT.

- **Solid-state NMR spectroscopy**

Generally,  $\alpha$ -carbons (such as methylene, carbene or carbyne carbons) are typically difficult to observe in the solid state  $^{13}\text{C}$  CP/MAS-NMR spectra. Their detection can be improved by employing  $\text{Zr}({}^{13}\text{CH}_2\text{Ph})_4$   $\alpha$ - $^{13}\text{C}$  randomly enriched at 20%. This complex can be prepared according the method for  $\text{Zr}(\text{CH}_2\text{Ph})_4$  but starting from  $\text{Ph}^{13}\text{CH}_2\text{MgCl}$   $\alpha$ - $^{13}\text{C}$  labeled at 20% (see experimental section).<sup>23</sup> The synthesis of  $\text{Ph}^{13}\text{CH}_2\text{MgCl}$   $\alpha$ - $^{13}\text{C}$  labeled involves a three-step sequence, starting with the available and relatively inexpensive benzoic acid  $\alpha$ - $^{13}\text{C}$  labeled at 100% (**Scheme 13**).



**Scheme 13:** Synthesis of  $\text{PhCH}_2\text{MgCl}$   $\alpha-^{13}\text{C}$  labeled from the benzoic acid  $\alpha-^{13}\text{C}$  labeled at 100%

In the first step, the reduction of the benzoic acid  $\alpha-^{13}\text{C}$  labeled at 100% into the benzylic alcohol was undertaken, followed by chlorination of the latter. The resulting benzyl chloride  $\alpha-^{13}\text{C}$  labeled at 100%, diluted five times with the non-labeled  $\text{PhCH}_2\text{Cl}$ , was reacted with magnesium turnings to finally provide the desired  $\text{Ph}^{13}\text{CH}_2\text{MgCl}$   $\alpha-^{13}\text{C}$  labeled at 20%.

$^1\text{H-NMR}$  of  $\text{Zr}(\text{PhCH}_2)_4$  in  $\text{C}_6\text{D}_6$  displays a singlet at 1.53 ppm corresponding to the  $\text{ZrCH}_2$  protons (**Figure 7, (a)**). A doublet appears clearly alongside this signal due to the  $^1\text{J}(\text{C}-\text{H})$  coupling of 135 Hz, thus confirming the isotopic enrichment of the methylenic carbon. The signal at 6.37 ppm is assigned to the *ortho* protons of the aromatic rings, whereas the multiplet at 6.96 ppm encapsulates the *ipso*, *meta* and *para* aromatic protons.  $^{13}\text{C-NMR}$  shows a significant peak at 72 ppm, belonging to the  $\text{Zr}^{13}\text{CH}_2$  labeled carbon (**Figure 7, (b)**). The chemical shifts of the aromatic carbons are at 125, 128, 130 and 139 ppm.

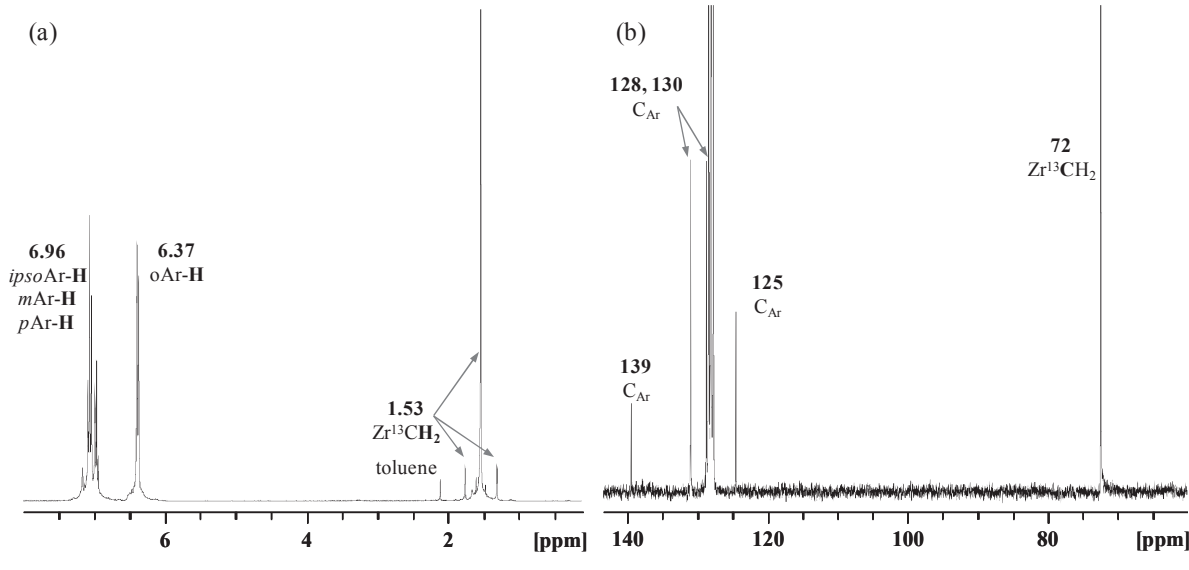
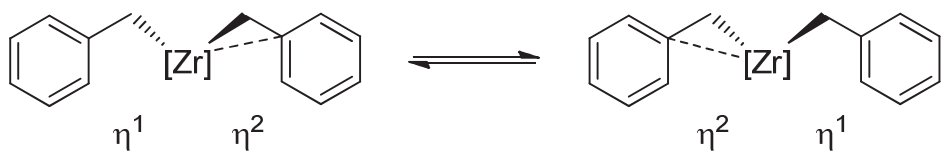


**Figure 7:**  $^1\text{H}$  (a) and  $^{13}\text{C-NMR}$  (b) of  $\text{Zr}(\text{PhCH}_2)_4$  in  $\text{C}_6\text{D}_6$

The molecular complex  $\text{Zr}(\text{PhCH}_2)_4$  was finally grafted on  $\text{SiO}_{2-(700)}$  as described above to yield **H3\***. The solid-state  $^1\text{H}$  MAS spectrum of **H3\*** exhibits a signal from 0.5 to 2.5 ppm assigned to  $\text{ZrCH}_2$  (**Figure 8**). Its broadness is probably due to the coordination

mode of the benzyl ligands  $\eta^1$  and  $\eta^2$  in equilibrium (**Scheme 14**). This phenomenon has already been described for such benzyl zirconium complexes.<sup>25</sup>



**Scheme 14:** Equilibrium between the two coordination modes of the benzyl ligands  $\eta^1$  and  $\eta^2$

Signals at 6.3 and 6.7 ppm are assigned to the aromatic protons. The thin peak at 1.8 ppm corresponds to the remaining surface silanols, thus confirming the large OH band in the DRIFT spectrum. The  $^{13}\text{C}$  CP/MAS-NMR displays a significant peak at 67 ppm, belonging to the Zr $^{13}\text{CH}_2$  carbons, and a series of peaks at 124, 128, 130 and 139 ppm for the aromatic fragments. In summary, reaction of  $\text{Zr}(\text{CH}_2\text{Ph})_4$  with  $\text{SiO}_{2-(700)}$  leads to the formation of the monosiloxo trisbenzylzirconium species whose general structure can be formulated as  $[(\equiv\text{SiO})\text{Zr}(\text{CH}_2\text{Ph})_3]$  (**H3\***) in which the zirconium atom is grafted to the surface *via* one covalent bond as evidenced by mass balance analysis and advanced solid-state NMR spectroscopy.

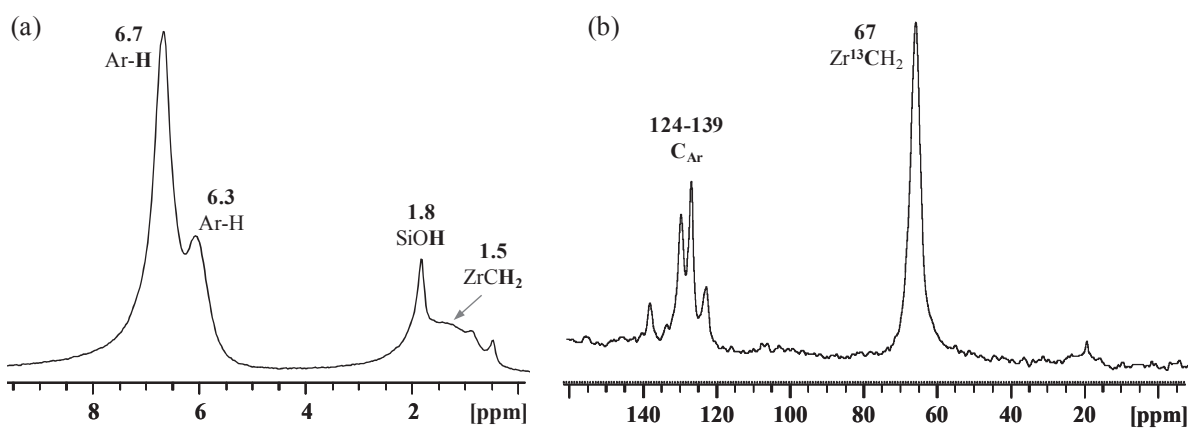


**Figure 8 :**  $^1\text{H}$  MAS (a) and  $^{13}\text{C}$  CP/MAS-NMR (b) of **H3\***

In summary, the reaction between  $\text{Zr}(\text{CH}_2\text{Ph})_4$  and  $\text{SiO}_{2-(700)}$  gives the well-defined mono-siloxo species  $[(\equiv\text{SiO})\text{Zr}(\text{CH}_2\text{Ph})_3]$  (**H3\***), fully characterized by DRIFT, solid-state NMR and mass balance analysis. EXAFS analysis is in progress. These species will be compared to its phenoxy counterpart.

### 5.1.2 Preparation and characterization of $[(\equiv SiO)_2AlO-C_6H_4-OZr(CH_2Ph)_3.Et_2O]$ (H4)

Using the double Schlenk technique, 1.3 eq. of  $Zr(^{13}CH_2Ph)_4$  in pentane (5 ml) were reacted with **H2** over 3h at room temperature in the dark. After repeated washings with pentane (5 ml), followed by evacuation of the volatiles, **H4** was afforded as a brown powder and characterized by DRIFT, solid-state NMR spectroscopy and mass balance analysis.

- **Infra-red spectroscopy**

After reaction with  $Zr(^{13}CH_2Ph)_4$ , the DRIFT spectrum of the generated material **H4** reveals an increase of the aromatic vibrations  $\nu_{Csp2=Csp2}$  at  $1608\text{ cm}^{-1}$  and  $\nu_{Csp2-H}$  at  $3026$  and  $3066\text{ cm}^{-1}$  from the benzyl zirconium groups (**Figure 9, (b)**). Note that the disappearance of the large band at  $3300\text{ cm}^{-1}$  proves the total consumption of the hydroxyl functions of the hydroquinone.

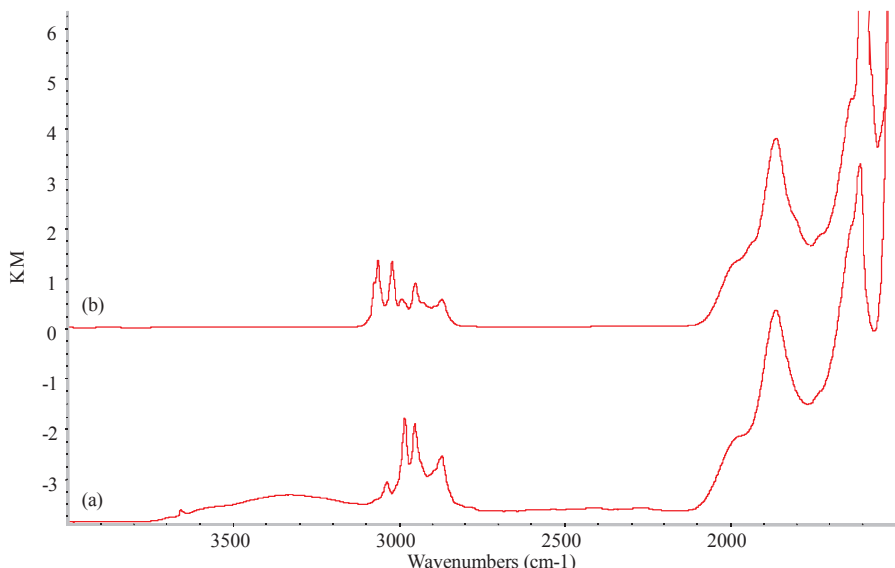


Figure 9: DRIFT spectra of H2 (a) and  $[(\equiv SiO)_2AlO-C_6H_4-OZr(CH_2Ph)_3]$  H4 (b)

- **Mass-balance analysis**

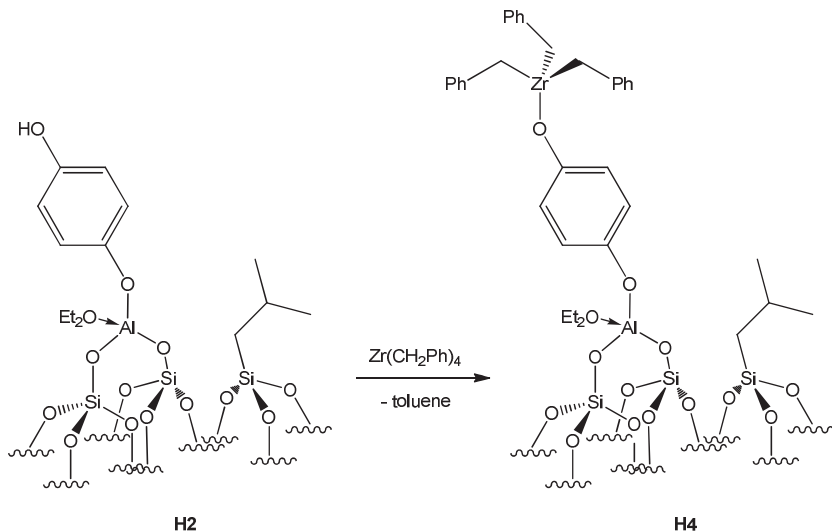
Elemental analysis shows the presence of the zirconium to the extent of 2.31%wt which corresponds to  $0.254\text{ mmol}_{Zr}\cdot g^{-1}$  of material **H4**, proving the total consumption of the phenol by  $Zr(CH_2Ph)_4$ , as already observed from DRIFT experiment (*vide supra*).

**Table 4: Mass balance analysis of H4**

	%wt Zr <sup>[a]</sup>	%wt C <sup>[a]</sup>	C/Zr
Grafting	2.31	9.18	30 (th 31 <sup>[b]</sup> )

[a] Percentage determined by elemental analysis. [b] Without diethyl ether

Considering the diethyl ether molecule released during the elemental analysis (*vide supra*), the charge in carbon of 9.18%wt gives 30 C/Zr (th 31, without diethyl ether) which supports the structure proposed displayed in **Scheme 15**.



**Scheme 15: Grafting of  $Zr(CH_2Ph)_4$  onto H2. Synthesis of  $[(\equiv SiO)_2AlO-C_6H_4-OZr(CH_2Ph)_3]$  H4. Reagents and conditions: 1.3 eq.  $Zr(CH_2Ph)_4$ , pentane, 3 h, RT.**

- **Solid-state NMR spectroscopy**

The solid-state  $^1H$  MAS-NMR spectrum of **H4** (**Figure 10, (a)**) exhibits signals at 0.9, 1.2, 3.5 and 6.9 ppm which can be assigned to the protons of the silicon isobutyl fragment, the methyl protons of the diethylether molecule, the methylene protons of the diethylether molecule and the aromatic protons from hydroquinone and benzyl groups respectively. Signal of  $ZrCH_2$  is probably underneath the peak between 0.9 and 1.2 ppm. In addition, the unexpected peak at 2.0 ppm can correspond to the methyl fragment of some toluene molecules, probably generated from the decomposition of surface species inside the rotor (increase of the temperature due to the high speed rotation of the rotor). Indeed, benzyl zirconium derivatives are known to be thermally unstable. From the  $^{13}C$  CP/MAS spectrum (**Figure 10, (b)**), the largest signal at 67 ppm is thought to encapsulate the  $^{13}C$  enriched  $ZrCH_2$  carbon and the methylene carbon of diethylether. Signals between 121 and 157 ppm

are assigned to the aromatic carbons belonging to the hydroquinone and the benzyl groups. Finally, the persistent signal at 26 ppm is undoubtedly attributed to the Si-*i*Bu fragments. The unexpected thin peak at 20 ppm could be assigned to the methyl of the toluene.

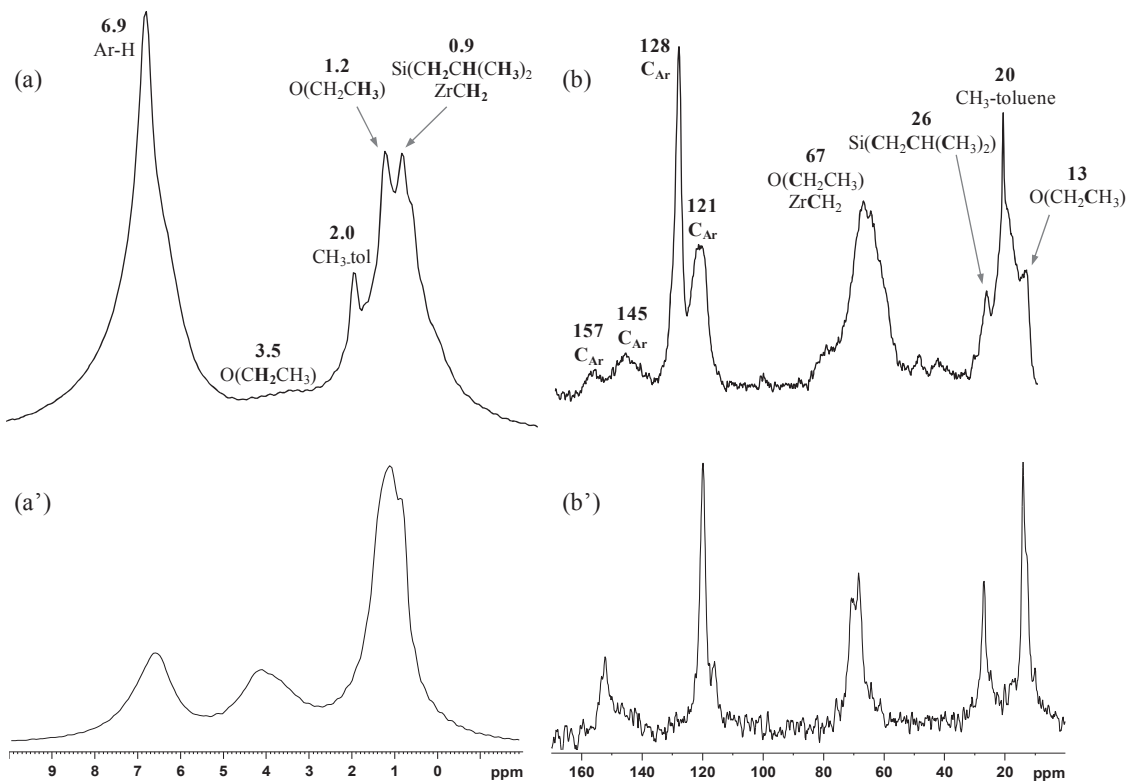


Figure 10:  $^1\text{H}$  MAS-NMR spectra of H2 (a') and H4 (a);  $^{13}\text{C}$  CP/MAS-NMR (b') of H2 and (b) of H4

## 5.2 Grafting of the tungsten complex $[\text{W}(\equiv\text{CtBu}(\text{CH}_2\text{tBu})_3)]$ onto $[(\equiv\text{SiO})_2\text{AlO-C}_6\text{H}_4\text{-OH}.(\text{Et}_2\text{O})]$ (H2)

### 5.2.1 Preparation and characterization of $[(\equiv\text{SiO})\text{W}(\equiv\text{CtBu})(\text{CH}_2\text{tBu})_2]$ (H5)

The grafting of  $\text{W}(\equiv\text{CtBu})(\text{CH}_2\text{tBu})_3$  onto  $\text{SiO}_{2-(700)}$  was realized as reported.<sup>22</sup> Using the double Schlenk technique, 1.3 eq. of  $\text{W}(\equiv\text{Ct-Bu})(\text{CH}_2\text{t-Bu})_3$  were stirred with  $\text{SiO}_{2-(700)}$  under argon at 66°C over 16 h (see Annex I for the mechanical stirring preparation). All the volatile compounds were expanded into a large flask of a known volume for the GC analysis and pentane (5 ml) was condensed over the solid. After three washing cycles and drying under high vacuum, the light brown solid **H5** was afforded

- **Infra-red spectroscopy**

DRIFT spectrum of **H5** revealed the total disappearance of the isolated silanol groups at  $3747\text{ cm}^{-1}$  and the concomitant apparition of the  $\nu_{(\text{Csp}^3-\text{H})}$  and  $\delta_{(\text{Csp}^3-\text{H})}$  vibrations at 3000-2800 and 1300-1500  $\text{cm}^{-1}$ , characteristic of the neopentyl ligands (**Figure 11**).

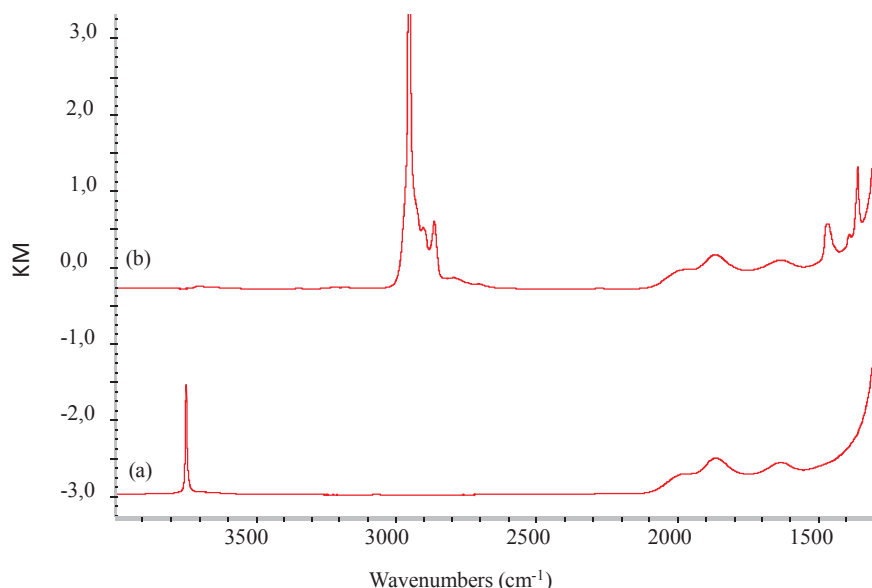


**Figure 11:** DRIFT spectra of  $\text{SiO}_{2-(700)}$  (a) and after grafting of  $\text{W}( \equiv \text{CtBu})(\text{CH}_2\text{tBu})_3$ , **H5** (b)

- **Mass-balance analysis**

Neopentane was the only gaseous product detected by GC amounting to 1 eq. formed per tungsten, present in 4.4%wt according to the elemental analysis (**Table 5**). The charge in carbon, 4.2%wt, nearly corresponds to 15 carbons per tungsten, thus suggesting a monopodal grafted tungsten.

**Table 5:** Mass balances analysis for **H5**

	%wt W <sup>[a]</sup>	NpH/W <sup>[b]</sup>	%wt C <sup>[a]</sup>	C/W
Grafting on $\text{SiO}_{2-(700)}$	4.4	1	4.2	14.5

[a] Percentage determined by elemental analysis. [b] Neopentane released, quantified by GC.

- **Solid-state NMR spectroscopy**

$^1\text{H}$  MAS-NMR spectrum of **H5** shows a large peak centered around 1 ppm attributed to the protons of the methyl groups of  $\text{W}( \equiv \text{Ct-Bu}(\text{CH}_2\text{t-Bu})_3)$  with two shoulders at 1.3 and 1.8 ppm for  $\text{W}( \equiv \text{CC}(\text{CH}_3)_3)$  and  $\text{W}(\text{CH}_2\text{C}(\text{CH}_3)_3)$  respectively (**Figure 12**). The solid state  $^{13}\text{C}$  CP/MAS-NMR spectrum of **H5** exhibits two different peaks at 32 and 90 ppm. The

former is assigned to the methyl groups of the neopentyl ligands  $\text{W}(\text{CH}_2\text{C}(\text{CH}_3)_3)$  while the latter corresponds to the methylenic carbon  $\text{W}(\text{CH}_2\text{C}(\text{CH}_3)_3)$ . It has been demonstrated<sup>22</sup> that the  $^{13}\text{C}$  labeling of  $\text{W}(\equiv^{13}\text{C}t\text{-Bu}(\text{CH}_2t\text{-Bu})_3)$  could help the interpretation, as a very intense signal at 90 ppm confirms these attributions, with apparition of the carbyne at 318 ppm.

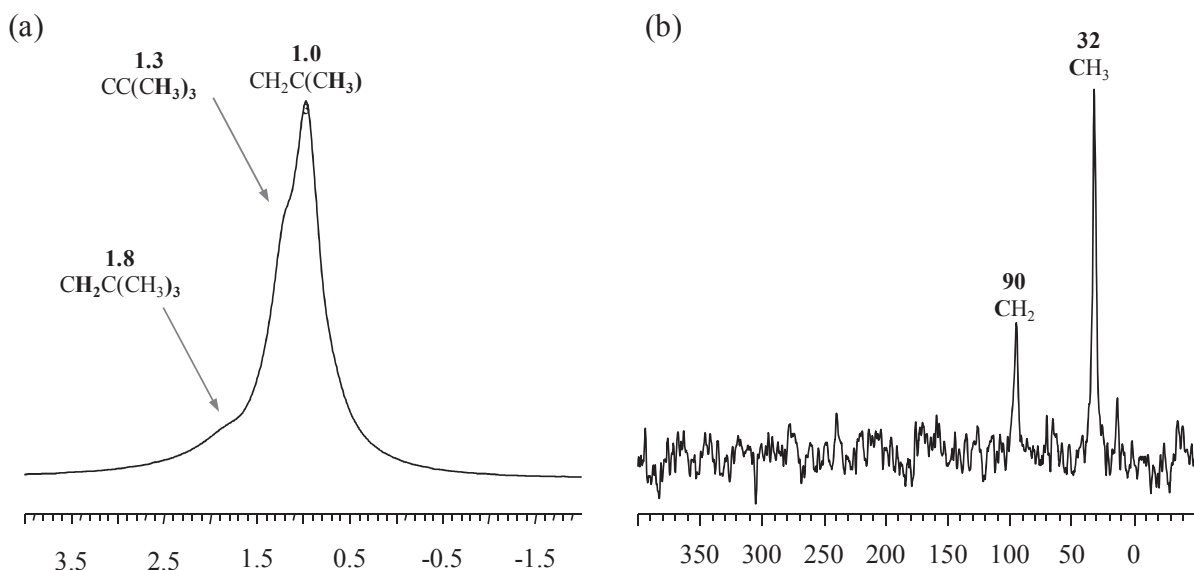
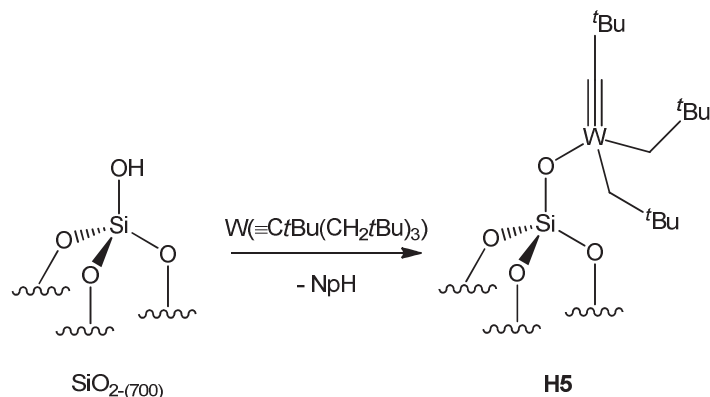


Figure 12:  $^1\text{H}$  MAS (a) and  $^{13}\text{C}$  CP/MAS-NMR (b) of H5

With regards to the analytical data, the well-defined monosiloxo  $[(\equiv\text{SiO})\text{W}(\equiv\text{C}t\text{Bu}(\text{CH}_2t\text{Bu})_2)]$  H5 can be proposed as the product of the grafting of  $[\text{W}(\equiv\text{C}t\text{Bu})(\text{CH}_2t\text{Bu})_3]$  onto  $\text{SiO}_{2-(700)}$  (**Scheme 16**).



**Scheme 16:** Structure of  $\text{W}(\equiv\text{C}t\text{Bu}(\text{CH}_2t\text{Bu})_3)/\text{SiO}_{2-(700)}$  H5. Reagents and conditions: 1.3 eq.  $\text{W}(\equiv\text{C}t\text{Bu}(\text{CH}_2t\text{Bu})_3)$ , 16 h, 66°.

### 5.2.2 Preparation and characterization of $[(\equiv SiO)_2AlO-C_6H_4-O-W\equiv CtBu(CH_2tBu)_2.(Et_2O)]$ (H6)

The grafting of 1.3 eq.  $W(\equiv CtBu(CH_2tBu)_3)$  onto the supported hydroquinone **H2** was realized by mechanical stirring at 66°C over 3h. The solid was then washed three times with freshly condensed pentane. After evacuation of the volatiles and drying under vacuum, the resulting light brown solid **H6** was characterized by DRIFT, solid-state NMR spectroscopy and mass balance analysis.

- **Infra-red spectroscopy**

In the DRIFT spectrum of **H6**, the weak band at 3658  $\text{cm}^{-1}$  corresponding to the hydroxyl function from the hydroquinone has disappeared. A weaker broad band appears at 3600-3700  $\text{cm}^{-1}$  in agreement with the presence of residual phenols which are probably in interaction with other surface functions. Concomitantly, two groups of bands appear in the 2800-3000  $\text{cm}^{-1}$  and 1300-1500  $\text{cm}^{-1}$  regions, which are assigned to  $\nu_{(Csp^3-H)}$  and  $\delta_{(Csp^3-H)}$  vibrations of neopentyl fragments bonded to tungsten. The persistent signals at 1500-1610  $\text{cm}^{-1}$  and 3035  $\text{cm}^{-1}$  are attributed to the aromatic ring stretchings of hydroquinone  $\nu_{(Csp^2=Csp^2)}$  and  $\nu_{(Csp^2-H)}$ , respectively.

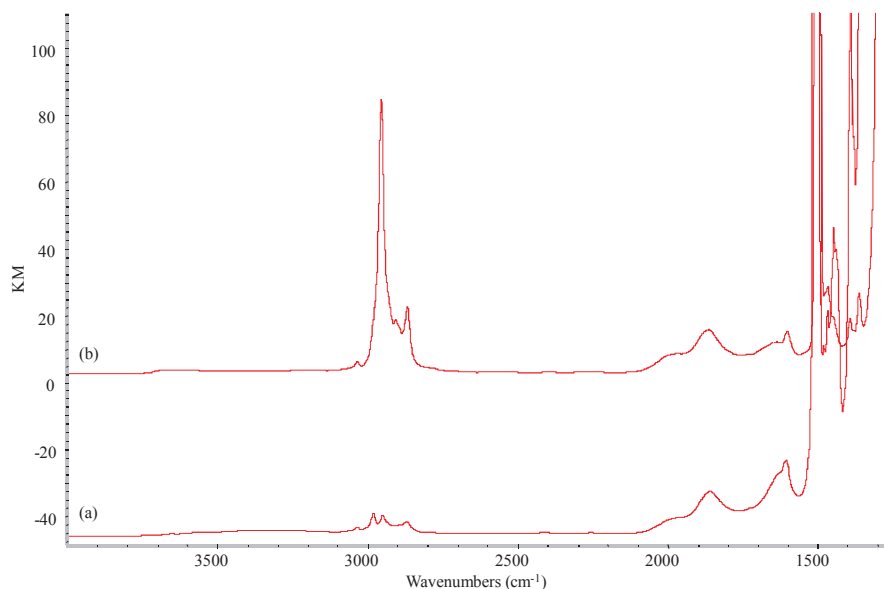


Figure 13: DRIFT spectra of **H2** (a) and after grafting of  $W(\equiv CtBu(CH_2tBu)_3)$ , **H6** (b)

- **Mass-balance analysis**

Regarding the elemental analysis of solid **H6**, 3.07%wt and 0.86%wt of tungsten and aluminum are grafted, respectively. The ratio of 0.53 W/Al informs us that the Schrock

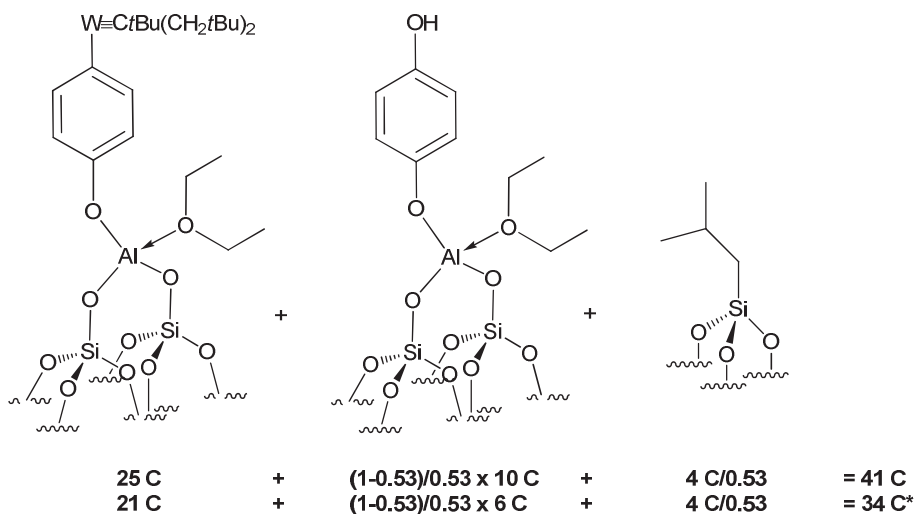
complex has reacted on 53% of the surface phenols. Moreover, during this process, 0.9 equiv of neopentane ( $0.151 \text{ mmol.g}^{-1}$ ) is evolved per grafted W. **H6** also shows the presence of 6.21%wt in carbon, which corresponds to 31 C/W.

**Table 6: Mass balance analysis for H6**

	%wt Al <sup>[a]</sup>	%wt W <sup>[a]</sup>	W/Al	%wt C <sup>[a]</sup>	C/W
Grafting	0.86	3.07	0.53	6.21	31

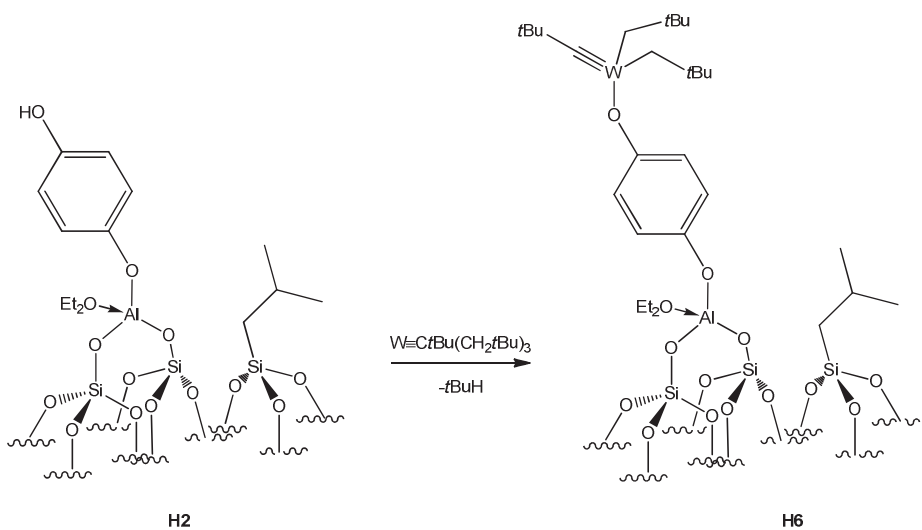
[a] Percentage determined by elemental analysis

If 53% of the surface phenoxy are considered to bear one  $\text{W}\equiv\text{C}t\text{Bu}(\text{CH}_2t\text{Bu})_2$  fragment, the correct expect count of carbon per tungsten atoms is 34 (without diethyl ether), thus confirming the experimental one of 31 (**Scheme 17**):



**Scheme 17: Carbon atom count of H6 reported to one tungsten atom. \* The second line is the corrected calculation by removing the two diethyl ether molecule from the two full oxidized aluminum centers**

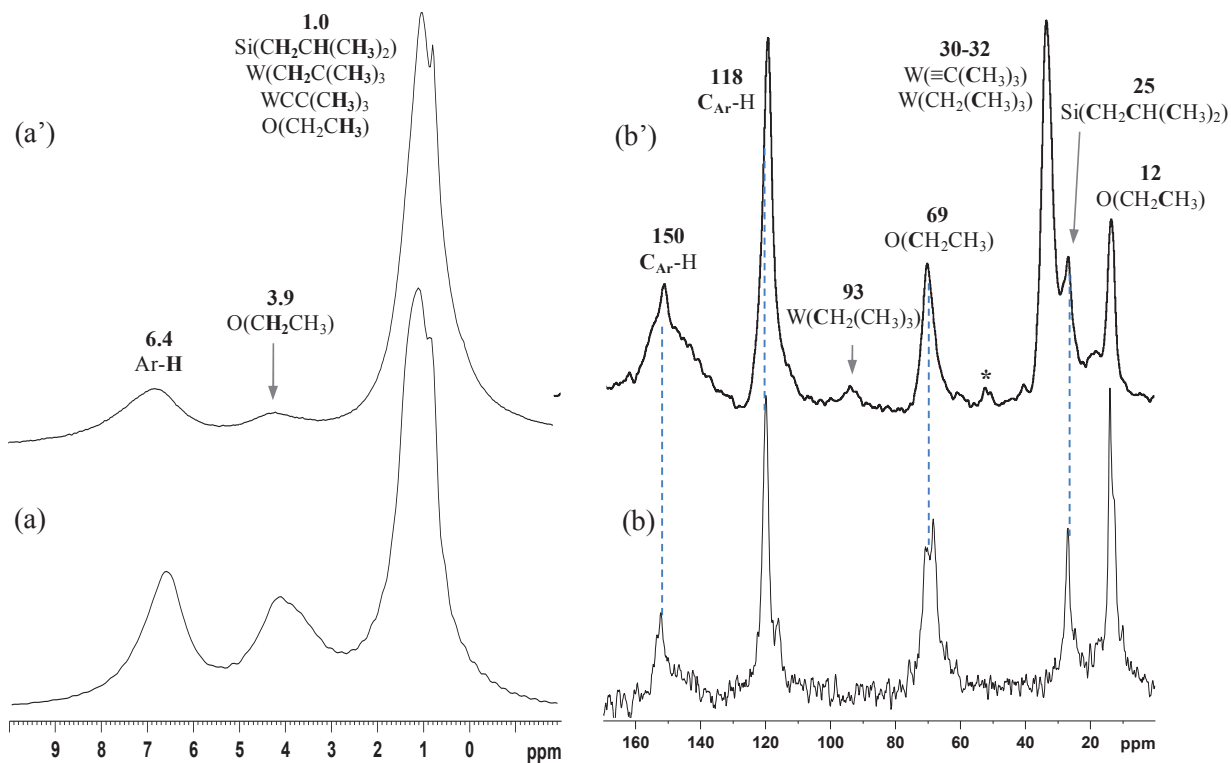
The mass balance analysis is in agreement with reaction of  $\text{W}\equiv\text{C}'\text{Bu}(\text{CH}_2'\text{Bu})_3$  with 53% of the surface phenols of the material **H2** to give about 1 eq. of neopentane per W, and a solid having monografted W atoms surrounded by 3 neopentyl-like ligands, leading to the structure proposed in **Scheme 18**, similar to its analogue directly bonded to silica.



**Scheme 18:** Synthesis of  $[(\equiv\text{SiO})_2\text{AlO-C}_6\text{H}_4-\text{OW}\equiv\text{CtBu}(\text{CH}_2\text{tBu})_2.\text{(Et}_2\text{O)}]$  **H6.** Reagents and conditions: 1.3 eq.  $\text{W}\equiv\text{CtBu}(\text{CH}_2\text{tBu})_3$ , 3 h,  $66^\circ\text{C}$ .

- **Solid-state NMR spectroscopy**

In comparison to **H2**,  $^1\text{H}$  MAS-NMR spectrum of **H6** shows a large peak centered around 1 ppm attributed to the protons of the  $\text{CH}_3$  and  $\text{CH}_2$  groups of  $\text{W}\equiv\text{CC}(\text{CH}_3)_3$  and  $\text{WCH}_2\text{C}(\text{CH}_3)_3$ , whereas both signals at 3.9 and 6.4 ppm corresponding to the diethylether and aromatic fragment, remain unchanged. The solid state  $^{13}\text{C}$  CP/MAS-NMR spectrum of **H6** exhibits peaks at 30-32 assigned to the  $\text{CH}_3$  carbon of the neopentylidyne  $\text{W}(\equiv\text{C}(\text{CH}_3)_3)$  and neopentyl  $\text{W}(\text{CH}_2\text{C}(\text{CH}_3)_3)$  moieties. A weak resonance for the  $\text{CH}_2$  carbon from  $\text{WCH}_2\text{C}(\text{CH}_3)_3$  appears at 93 ppm, similarly observed in the case of its counterpart mono-siloxo **H5** directly grafted on  $\text{SiO}_{2-(700)}$  (**Figure 12, (b)**). This signal could considerably be increased by using the  $^{13}\text{C}$  labeled starting complex  $\text{W}\equiv^{13}\text{C}'\text{Bu}(\text{CH}_2'\text{Bu})_3$ .<sup>22</sup> On the other hand, the signals of the aromatic carbons at 118 and 150 ppm, the isobutyl silicon at 25 ppm and the diethylether (12 and 69 ppm) remain unchanged.



Scheme 19: <sup>1</sup>H MAS and <sup>13</sup>C CP/MAS-NMR of H3 (a,b) and H6 (a', b') (\* Spinning side band)

## 6. Catalytic performance of $[(\equiv \text{SiO})\text{W}\equiv\text{C}t\text{Bu}(\text{CH}_2t\text{Bu})_2]$ (**H5**) and $[(\equiv \text{SiO})_2\text{AlO-C}_6\text{H}_4-\text{OW}\equiv\text{C}t\text{Bu}(\text{CH}_2t\text{Bu})_2.\text{(Et}_2\text{O})]$ (**H6**) in propylene metathesis

The tungsten-based surface complexes  $[(\equiv \text{SiO})\text{W}\equiv\text{C}t\text{Bu}(\text{CH}_2t\text{Bu})_2]$  **H5** and  $[(\equiv \text{SiO})_2\text{AlO-C}_6\text{H}_4-\text{OW}\equiv\text{C}t\text{Bu}(\text{CH}_2t\text{Bu})_2.\text{(Et}_2\text{O})]$  **H6** have been designed with a view to provide catalytically active components for olefin metathesis. Both **H5** and **H6** consist of monopodal complexes that differ by their tethering to the surfaces. Their screening will permit us to establish the effect of an aryloxy vs. a siloxy linker on their catalytic performances in propene metathesis.

### 6.1 Definitions of practical terms in catalysis

#### Conversion

The conversion X is the number of moles of reagent transformed divided by the number of moles of reagent introduced. If there is no accumulation of product in the reaction chamber, the conversion is equal to the total number of carbon atom equivalent of products formed divided by the number of carbon atom equivalent of reagent introduced; this latter

value is also equal to the total number of carbon atom equivalent of products plus the number of carbon atom equivalent of reagent which have not reacted.

$$X = \frac{nC_n \text{ transformed}}{nC_i \text{ introduced}}$$

$C_n$  is the reagent,  $C_i$  is the different products ( $i$  and  $n$  are respectively the number of carbons of the product and of the reagent considered).

### Turn over number and frequency

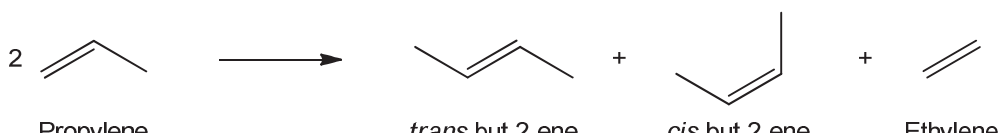
The turn over number (T.O.N) of the reaction is defined as the ratio of the number of moles of the reagent consumed to the number of surface metal.

$$T.O.N = \frac{\text{mol}_{\text{conv}}}{\text{mol}_{\text{cat}}} = R \cdot X \cdot t$$

$R$  is the number of moles of reactant which pass per unit of time and per metal, and  $t$  the duration of the reaction. The turn over frequency (T.O.F) corresponds to the ratio of the number of moles of the reagent consumed to the number of surface metal per unit of time.

## 6.2 Catalytic tests

Schrock tungsten compound  $W(\equiv C tBu(CH_2 tBu)_3)$  is known to be active in olefin metathesis when grafted onto silica support.<sup>22</sup> In this way, the catalytic behavior of the two systems **H5** and **H6** will be studied and compared in the self-metathesis of propylene (**Scheme 20**).



**Scheme 20: Propylene metathesis**

Catalytic tests were performed in a continuous flow reactor (see Annex II for the full description). The charge of catalyst of **H5** and **H6** were calculated based on their respective tungsten content in order to keep the quantity of active sites constant in both runs (**Table 7**). The propylene flow rate was maintained constant at  $25 \text{ ml} \cdot \text{min}^{-1}$  ( $61 \text{ mol}_{\text{C}_3\text{H}_6} \cdot \text{mol}_{\text{W}}^{-1} \cdot \text{min}^{-1}$ ) at  $60^\circ\text{C}$ . A gas chromatograph analyses the products generated at the outlet of the reactor.

**Table 7: Reaction conditions for the propylene metathesis catalyzed by H5 and H6**

	W %wt	Propylene flow rate (ml.min <sup>-1</sup> )	R <sup>[a]</sup> (mol <sub>C3=</sub> .mol <sub>W</sub> <sup>-1</sup> .min <sup>-1</sup> )	Temperature (°C)
Catalyst <b>H6</b>	3.1	25	61	60
Catalyst <b>H5</b>	4.4	25	61	60

[a] number of moles of propene which passes per tungsten atom per minute

The following graphs compare the conversions and the T.O.N of both catalysts **H6** and **H5** and were built from calculation of the accumulated data by the gas chromatograph (see experimental part for the full description).

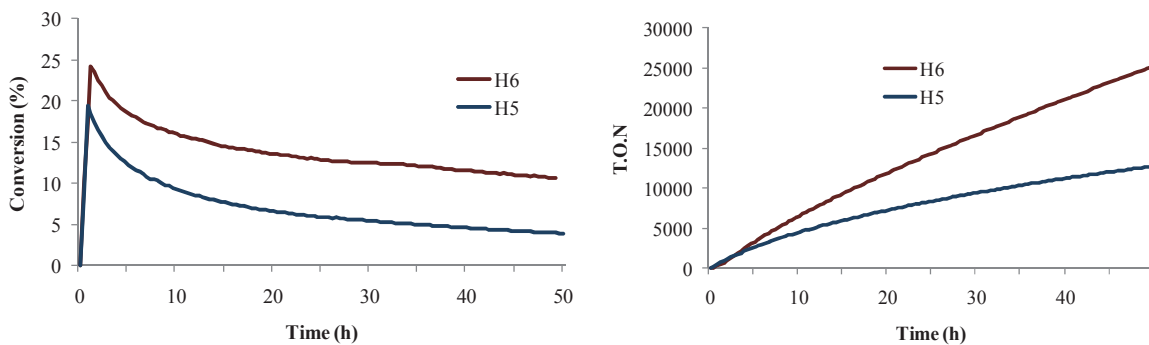


Figure 14: Comparison of the conversions and the TON of both catalysts H5 and H6

The catalyst **H6** reaches a higher initial conversion of 24% in comparison to 19% for the catalyst **H5**. The cumulated T.O.N achieved after 48 h of **H6** and **H5** are 24450 (T.O.F = 8.4 mol<sub>C3=</sub>.mol<sub>W</sub><sup>-1</sup>.min<sup>-1</sup>) and 12500 (T.O.F = 4.3 mol<sub>C3=</sub>.mol<sub>W</sub><sup>-1</sup>.min<sup>-1</sup>) respectively. There is evidence of a better catalytic activity displayed by the hydroquinone catalyst **H6** in addition to its slower deactivation along the experiment length. For both catalysts **H5** and **H6**, the selectivity remained constant with time on stream, with equimolar quantities of ethylene and but-2-enes, no other alkenes were detected (**Figure 15**).

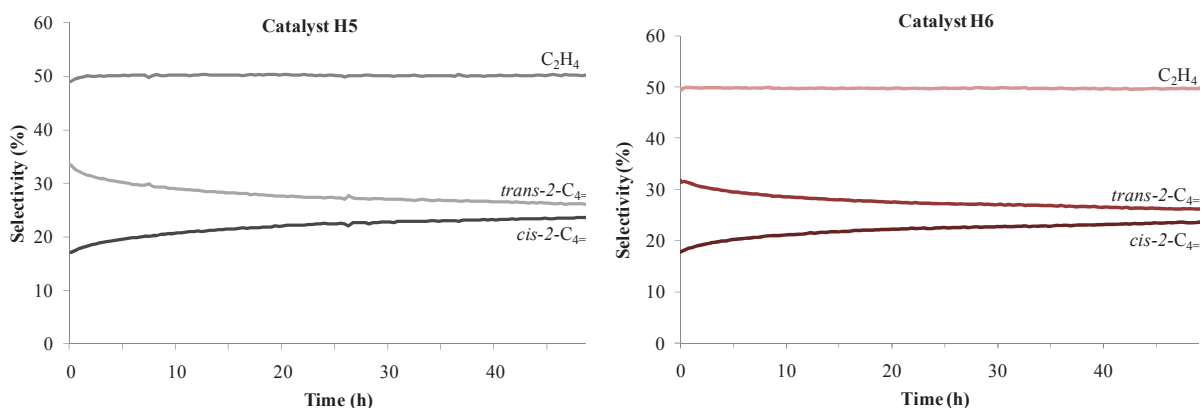
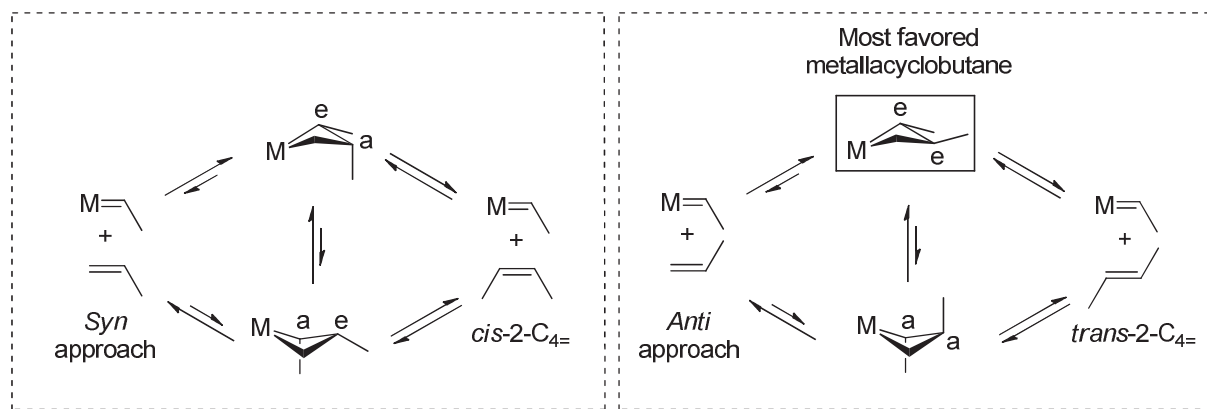


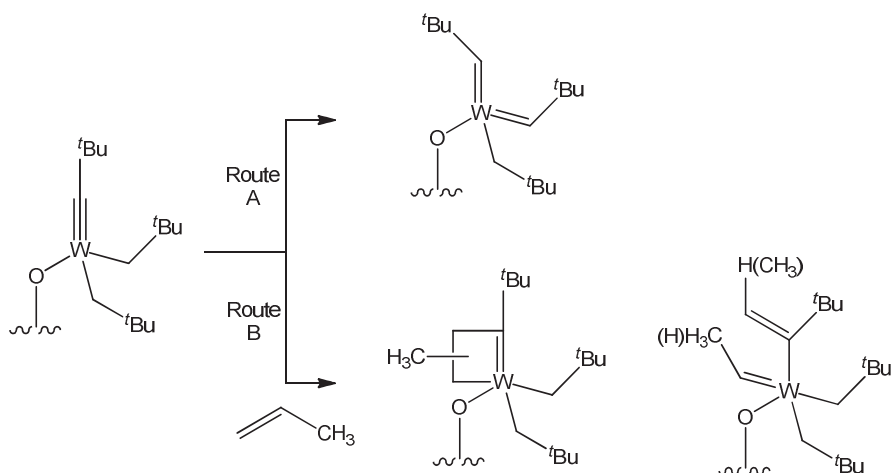
Figure 15: Selectivity in *trans*-but-2-ene (*trans*-2-C<sub>4</sub>=) and *cis*-but-2-ene (*cis*-2-C<sub>4</sub>=) for both catalysts H5 and H6

At 50 h, the *trans/cis* but-2-enes selectivity kept to a constant value of 1.1 in both cases (therm. eq. = 2.3),<sup>26</sup> in agreement with that observed in the literature for other d<sup>0</sup> systems; that is, terminal alkenes typically give the *trans*-alkene as the major kinetic product, due to the easier formation of the least sterically hindered metallacyclobutane by an *anti* approach (**Scheme 21**).<sup>27</sup>



**Scheme 21:** The stability of the intermediate metallacyclobutane dictates the selectivity of butenes

It must be mentioned that the systems **H5** and **H6** are precursors for olefin metathesis, for which the carbene ligand is probably generated *in situ*, either by  $\alpha$ -H transfer from an alkyl ligand to generate a bis-alkylidene (**Scheme 22**, Route A), or by direct metathesis of an olefin with an alkylidyne, which generates in turn a propagating ligand (**Scheme 22**, Route B).<sup>22</sup>



**Scheme 22:** Possible routes for the formation of the initiation carbene ligands from an alkylidyne (Route A) and H- transfer from an alkyl ligand to the alkylidyne (Route B), direct metathesis with the alkylidyne.

In summary, the insertion of an aryloxy linker between the surface and the tungsten center increases its catalytic activity in olefin metathesis. This phenomenon can be explained by limitation of the coordination between the organometallic fragment and siloxy group

displayed on the surface. The electron withdrawing character of the Al-Hydroquinone moiety can also participate to increase the electrophilicity of the tungsten and thus its activity.

## 7. General conclusion

In this chapter, a new synthetic methodology was conceived to allow access to a novel silica-based support presenting single monografted monoaryloxy fragments. This multi-step preparation consists of the preliminary treatment of the silica dehydroxylated at 700°C with triisobutylaluminum to form an unprecedented bis-grafted monoisobutyl aluminum etherate species  $[(\equiv\text{SiO})_2\text{Al}i\text{Bu}.(\text{Et}_2\text{O})]$  **H1**. This serves as an anchoring site for phenol compounds displaying two hydroxyl functions, such as hydroquinone, to generate selectively the monografted aryloxy  $[(\equiv\text{SiO})_2\text{AlO-C}_6\text{H}_4-\text{OH}.(\text{Et}_2\text{O})]$  **H2** species. The grafting of both zirconium  $\text{Zr}(\text{CH}_2\text{Ph})_4$  and tungsten  $\text{W}(\equiv\text{C}t\text{Bu}(\text{CH}_2t\text{Bu})_3)$  complexes have afforded new, well-defined, tris-benzyl zirconium  $[(\equiv\text{SiO})_2\text{AlO-C}_6\text{H}_4-\text{OZr}(\text{CH}_2\text{Ph})_3.\text{Et}_2\text{O}]$  **H4** and bis-neopentyl neopentylidyne tungsten  $[(\equiv\text{SiO})_2\text{AlO-C}_6\text{H}_4-\text{OW}(\equiv\text{C}t\text{Bu}(\text{CH}_2t\text{Bu})_2.(\text{Et}_2\text{O})]$  **H6** surface species.

The new supported tungsten complex  $[(\equiv\text{SiO})_2\text{AlO-C}_6\text{H}_4-\text{OW}(\equiv\text{C}t\text{Bu}(\text{CH}_2t\text{Bu})_2.(\text{Et}_2\text{O})]$  **H6** is active in propylene metathesis, under mild conditions and without need of a co-catalyst. This system shows a higher activity than that displayed by its counterpart directly grafted onto silica  $[(\equiv\text{SiO})\text{W}(\equiv\text{C}t\text{Bu}(\text{CH}_2t\text{Bu})_2)]$  **H5**. This result proves the new concept of inserting an aryloxy linker between the surface and the tungsten center, increases the catalytic activity in olefin metathesis. This novel and unprecedented methodology will be applied to form calixarene-based tether onto SBA-15 LP<sub>(700)</sub> (see Chapter V). In this approach, the next chapter will present the preparation and the characterization of soluble zirconia- and titanacalix[4]arene models, that will be used to help the characterization of their supported counterparts.

## Experimental section

All manipulations were carried out under a dry argon atmosphere using standard Schlenk techniques. More specifically, the double Schlenk technique is described in Annex I. All solvents were dried by standard methods and freshly distilled before use. Gas-phase analyses were performed on a Hewlett-Packard 5890 series II gas chromatograph equipped with a flame ionization detector and a  $\text{Al}_2\text{O}_3/\text{KCl}$  on fused silica column (50 m x 0.32 mm). Elemental analyses were performed at the Central Analysis Service of Solaize (France) for hydrogen and carbon elements and at the Mikroanalytisches Labor Pascher of Remagen (Germany) for metals. DRIFT spectra were recorded on a Nicolet 6700 FT-IR by using DRIFT airtight cells. Solution NMR spectra were recorded on DRX400 and DRX300 Bruker instruments. Solid-state  $^1\text{H}$  MAS and  $^{13}\text{C}$  CP/MAS-NMR spectra were recorded on Bruker Avance-500 and 800 spectrometers with a conventional double-resonance 4 mm CP-MAS probe at the Laboratoire de Chimie in Ecole Normale Supérieure de Lyon, at the Laboratoire de Chimie Organométallique de Surface in Ecole Supérieure de Chimie Physique Electronique de Lyon or at the Unité de Catalyse et de Chimie du solide (Lille). The samples were introduced under Ar in a zirconia rotor, which was then tightly closed. In all experiments, the rotation frequency was set to 10 kHz unless otherwise specified. Chemical shifts were given with respect to TMS as external reference for  $^1\text{H}$  and  $^{13}\text{C}$ -NMR. The preparation of  $\text{Zr}(\text{CH}_2\text{Ph})_4$  was performed according to the reported procedure<sup>23</sup>, involving  $\text{PhCH}_2\text{MgCl}$  and  $\text{ZrCl}_4$ , but started with a 80:20 mixture of non-labeled and 100% labeled  $\text{Ph}^{13}\text{CH}_2\text{Cl}$  in the preparation of  $(\text{Ph}^{13}\text{CH}_2)\text{MgCl}$  (20%).

**Synthesis of benzylic alcohol  $\alpha$ - $^{13}\text{C}$  labeled at 100%:** A solution of benzoic acid  $\alpha$ - $^{13}\text{C}$  labeled at 100% (5.000 g, 40.940 mmol) in dry THF (100ml) was added dropwise to a solution of  $\text{BH}_3\cdot\text{Me}_2\text{S}$  (82 ml, 81.900 mmol, 1M in DCM) and  $\text{B}(\text{OEt})_3$  (14 ml, 81.900 mmol) in dry THF (300 ml). After  $\text{H}_2$  evolution, the resulting solution was stirred overnight at reflux. When cold, the mixture was quenched with 100 ml of MeOH at 0°C. After evaporation of the volatiles, the residue was dissolved again in 100 ml of MeOH and evaporated. Without further purification, benzylic alcohol was obtained in quantitative yield as a clear oil (4.430 g). NMR  $^1\text{H}$  ( $\text{C}_6\text{D}_6$ , 300MHz, 298K):  $\delta$  4.06 (d, 2H,  $\text{CH}_2$ ,  $^1\text{J}(\text{H,C}) = 150$  Hz), 7.00 (m, 5H, Ar-H).

**Synthesis of benzyl chloride  $\alpha$ - $^{13}\text{C}$  labeled at 100%:** Thionyl chloride (3.6 ml, 49.158 mmol) was added dropwise to a solution of benzylic alcohol (4.430 g, 40.94 mmol) in  $\text{Et}_2\text{O}$  (40 ml). Pyridine (0.15 ml) was then added and the resulting mixture stirred at reflux over 1h. The same quantity of thionyl chloride and pyridine was added again. After another 1h of stirring at reflux, the mixture was quenched with water, extracted with  $\text{Et}_2\text{O}$  (3 x 20 ml) and the resulting organic phases washed with brine and dried over  $\text{MgSO}_4$ . The resulting benzyl

chloride was obtained as clear oil in quantitative yield. NMR  $^1\text{H}$  ( $\text{C}_6\text{D}_6$ , 300MHz, 298K):  $\delta$  4.67 (d, 2H,  $\text{CH}_2$ ,  $^1\text{J}(\text{H,C}) = 144$  Hz), 7.40 (m, 5H, Ar-H).

**Synthesis of benzylmagnesium chloride  $\alpha$ - $^{13}\text{C}$  labeled at 20%:** A benzyl chloride solution in 80:20 ratio of non-labeled and  $\alpha$ - $^{13}\text{C}$  labeled at 100% (23.5 ml, 204.00 mmol) in 50 ml of  $\text{Et}_2\text{O}$  was added dropwise to 100 ml of  $\text{Et}_2\text{O}$  containing Mg turnings (30.000 g, 1235.000 mmol). The exothermicity of the reaction self-maintains the reflux of  $\text{Et}_2\text{O}$ . At the end of the adding, the resulting mixture was stirred at RT over 2h and filtrate to provide a yellowish clear solution. 1 ml of this solution was titrated with a solution of benzylic alcohol in dry xylene in presence of 2,2'-biquinoline as indicator (turns red to yellow), which indicates a solution of 1.05M in Grignard reagent.

**Synthesis of tetrabenzylzirconium  $\alpha$ - $^{13}\text{C}$  labeled at 20%:** In the dark and at -33°C, benzylmagnesium chloride  $\alpha$ - $^{13}\text{C}$  labeled at 20% (49 ml, 51.493 mmol, 1.05M in  $\text{Et}_2\text{O}$ ) was added dropwise to a suspension of  $\text{ZrCl}_4$  (3.000 g, 51.493 mmol) in 20 ml of toluene and 10 ml of  $\text{Et}_2\text{O}$ . After 1h of stirring at RT, 4.5 ml of 1,4-dioxane was added and the resulting mixture was stirred at RT over 1h. The salts were filtrate off and the resulting orange limpid solution reduced and crystallized at -30°C over 2 days.  $\text{Zr}({}^{13}\text{CH}_2\text{Ph})_4$  was collected as orange crystals (4.700 g, 80%). NMR  $^1\text{H}$  ( $\text{C}_6\text{D}_6$ , 300MHz, 298K):  $\delta$  1.53 (d (20%) + s (80%), 8H,  $\text{CH}_2$ ,  $^1\text{J}(\text{H,C}) = 136$  Hz), 6.37 (d, 8H, Ar-H), 6.98 (m, 12H, Ar-H).

## Notes and references

- (1) (a) Le Roux, E.; Taoufik, M.; Copéret, C.; de Mallmann, A.; Thivolle-Cazat, J.; Basset, J. M.; Maunders, B. M.; Sunley, G. J. *Angew. Chem., Int. Ed.* **2005**, *44*, 6755(b) Taoufik, M.; Roux, E.; Thivolle-Cazat, J.; Copéret, C.; Basset, J.-M.; Maunders, B.; Sunley, G. *Top. Catal.* **2006**, *40*, 65(c) Szeto, K. C.; Norsic, S.; Hardou, L.; Le Roux, E.; Chakka, S.; Thivolle-Cazat, J.; Baudouin, A.; Papaioannou, C.; Basset, J. M.; Taoufik, M. *Chem. Commun.* **2010**, *46*, 3985(d) Taoufik, M.; Le Roux, E.; Thivolle-Cazat, J.; Basset, J.-M. *Angew. Chem., Int. Ed.* **2007**, *46*, 7202.
- (2) Xiang, S.; Zhang, Y.; Xin, Q.; Li, C. *Chem. Commun.* **2002**, 2696.
- (3) Basset, J.-M.; Psaro, R.; Roberto, D.; Ugo, R. *Modern Surface Organometallic Chemistry*; Wiley ed.: Weinheim, 2009.
- (4) (a) Sinn, H.; Kaminsky, W. In *Adv. Organomet. Chem.*; Stone, F. G. A., Robert, W., Eds.; Academic Press, 1980; Vol. Volume 18(b) Chien, J. *Top. Catal.* **1999**, *7*, 23(c) Scott, S. L.; Church, T. L.; Nguyen, D. H.; Mader, E. A.; Moran, J. *Top. Catal.* **2005**, *34*, 109(d) Vansant, E. F.; Van Der Voort, P.; Vrancken, K. C. *Characterization and chemical modification of the silica surface*; Elsevier: New York, 1995.
- (5) Murray, J.; Sharp, M. J.; Hockey, J. A. *J. Catal.* **1970**, *18*, 52.
- (6) Yates, D. J. C.; Dembinski, G. W.; Kroll, W. R.; Elliott, J. J. *J. Phys. Chem.* **1969**, *73*, 911.
- (7) (a) Kinney, J. B.; Staley, R. H. *J. Phys. Chem.* **1983**, *87*, 3735(b) Puurunen, R. L.; Root, A.; Haukka, S.; Iiskola, E. I.; Lindblad, M.; Krause, A. O. I. *J. Phys. Chem. B* **2000**, *104*, 6599(c) Kratochvíla, J.; Kadlc, Z.; Kazda, A.; Salajka, Z. *J. Non-Cryst. Solids* **1992**, *143*, 14.
- (8) (a) Anwander, R.; Palm, C.; Groeger, O.; Engelhardt, G. *Organometallics* **1998**, *17*, 2027(b) Looveren, L. K. V.; Geysen, D. F.; Vercruyse, K. A.; Wouters, B. H.; Grobet, P. J.; Jacobs, P. A. *Angew. Chem., Int. Ed.* **1998**, *37*, 517.
- (9) Peglar, R. J.; Hambleton, F. H.; Hockey, J. A. *J. Catal.* **1971**, *20*, 309.
- (10) Bartram, M. E.; Michalske, T. A.; Rogers, J. W. *J. Phys. Chem.* **1991**, *95*, 4453.
- (11) Tao, T.; Maciel, G. E. *J. Am. Chem. Soc.* **2000**, *122*, 3118.
- (12) Müller, K. H. *Organic Aluminium Compounds*; Schering AG: Weinheim, 1977.
- (13) (a) Benn, R.; Janssen, E.; Lehmkuhl, H.; Rufinska, A. *J. Organomet. Chem.* **1987**, *333*, 155(b) Hoffmann, E. G. *Justus Liebigs Annalen der Chemie* **1960**, *629*, 104.
- (14) Oliver, J. P.; Kumar, R. *Polyhedron* **1990**, *9*, 409.
- (15) Li, J.; DiVerdi, J. A.; Maciel, G. E. *J. Am. Chem. Soc.* **2006**, *128*, 17093.
- (16) (a) Severn, J. R.; Chadwick, J. C.; Duchateau, R.; Friederichs, N. *Chem. Rev.* **2005**, *105*, 4073(b) George, S. M.; Yoon, B.; Dameron, A. A. *Acc. Chem. Res.* **2009**, *42*, 498.
- (17) Preishuber-Pflugl, P.; Brookhart, M. *Macromolecules* **2002**, *35*, 6074.
- (18) (a) Jacobsen, G. B.; Matsushita, F.; Spencer, L.; Wauteraerts, P. L.; Dow Global Technologies Inc., 2001(b) Van, D. J. J.; Miyamoto, A.; Jacobsen, G. B.; Matsushita,

F.; Schouterden, P. J.; Lee, S.; Chum, P.-W. S.; Meiske, L. A.; Peter, W. L.; Dow Chemical Co., 2003.

- (19) Holtcamp, M. W.; Univation Technologies, 2002.
- (20) Millot, N.; Santini, C. C.; Lefebvre, F.; Basset, J.-M. *C. R. Chim.* **2004**, *7*, 725.
- (21) Bassindale, A. R.; Liu, Z. H.; MacKinnon, I. A.; Taylor, P. G.; Yang, Y. X.; Light, M. E.; Horton, P. N.; Hursthouse, M. B. *Dalton Trans.* **2003**, 2945.
- (22) Le Roux, E.; Taoufik, M.; Chabanas, M.; Alcor, D.; Baudouin, A.; Copéret, C.; Thivolle-Cazat, J.; Basset, J.-M.; Lesage, A.; Hediger, S.; Emsley, L. *Organometallics* **2005**, *24*, 4274.
- (23) Rodriguez, G.; Cano, D. A.; McConville, D. H.; Rix, F. C.; (Univation Technologies, LLC, USA). Application: US, 2006.
- (24) (a) Tosin, G. r.; Delgado, M.; Baudouin, A.; Santini, C. C.; Bayard, F. o.; Basset, J.-M. *Organometallics* **2010**, *29*, 1312(b) Rosier, C.; Niccolai, G. P.; Basset, J.-M. *J. Am. Chem. Soc.* **1997**, *119*, 12408(c) Corker, J.; Lefebvre, F.; Evans, J.; Lécuyer, C.; Dufaud, V.; Quignard, F.; Choplín, A.; Basset, J.-M. *Science* **1996**, *271*, 966.
- (25) Gauvin, R. M.; Osborn, J. A.; Kress, J. *Organometallics* **2000**, *19*, 2944.
- (26) Stull, D. R.; Sinke, G. C. *The chemical thermodynamics of organic compounds*; Westrum Ed.; Malabar, Fla., 1987.
- (27) (a) Bilhou, J. L.; Basset, J. M.; Mutin, R.; Graydon, W. F. *J. Am. Chem. Soc.* **1977**, *99*, 4083(b) Leconte, M.; Basset, J. M. *J. Am. Chem. Soc.* **1979**, *101*, 7296.



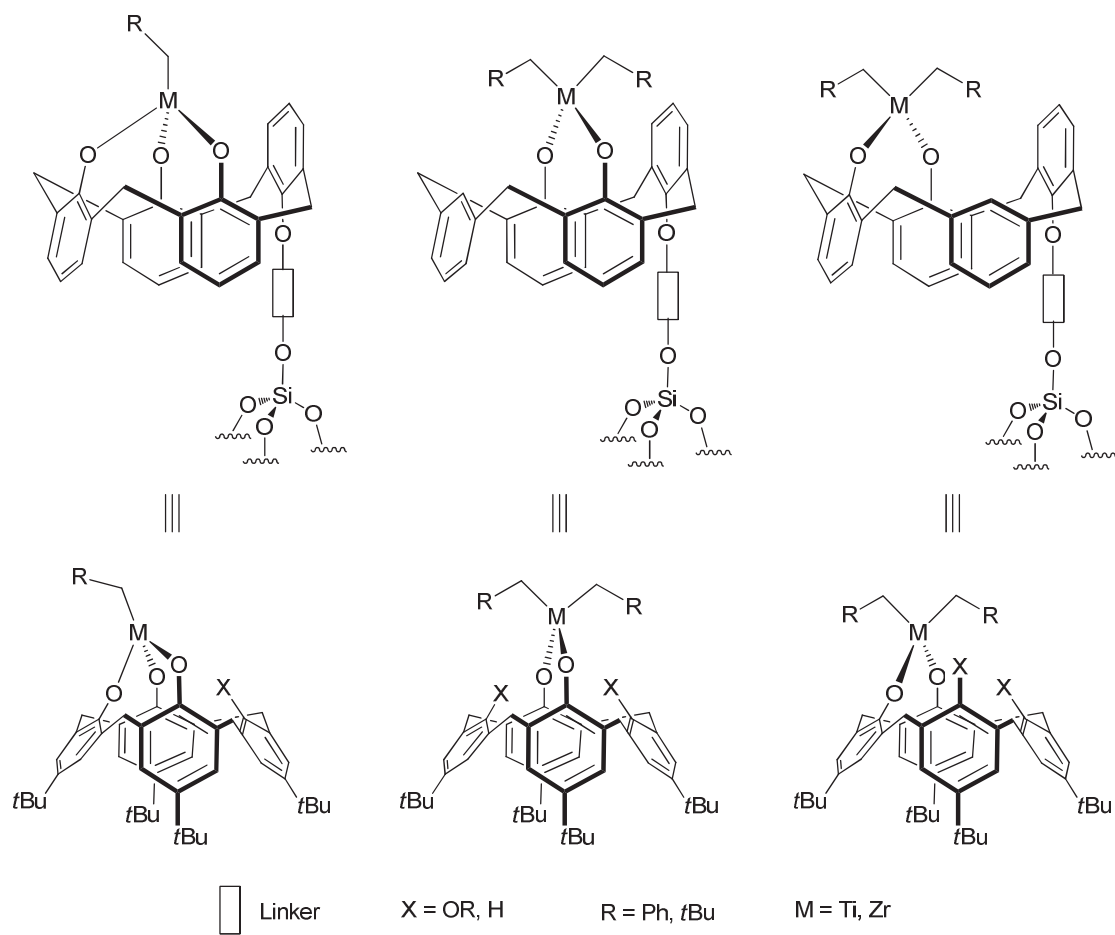
## **Chapter III**

**Synthesis of Titana- and Zirconacalix[4]arenes  
as soluble models of grafted species.  
(dichloro)metallacalix[4]arenes: application in  
homogeneous ethylene polymerization**



## 1. Introduction

In this chapter the preparation and the characterization of a series of novel titanium and zirconium complexes bearing alkyl fragments and grafted to calixarenic ligands are discussed. These compounds have been targeted to be included in our ongoing investigation of molecular models to mimic surface-organometallic species of metals of group IV in which at least one  $\sigma$ -bond is formed with surface oxygen (see Chapter I). Selected examples are given in **section 2** which illustrate the modeling approach using calix[4]arene-based derivatives; additional comparison using this time polysilsesquioxane as model ligands of surface organometallic complexes is also given. Specific metallacalix[4]arenes were targeted since they are judicious soluble counterparts of metallacalix[4]arenes grafted onto silica support (**Scheme 1**).



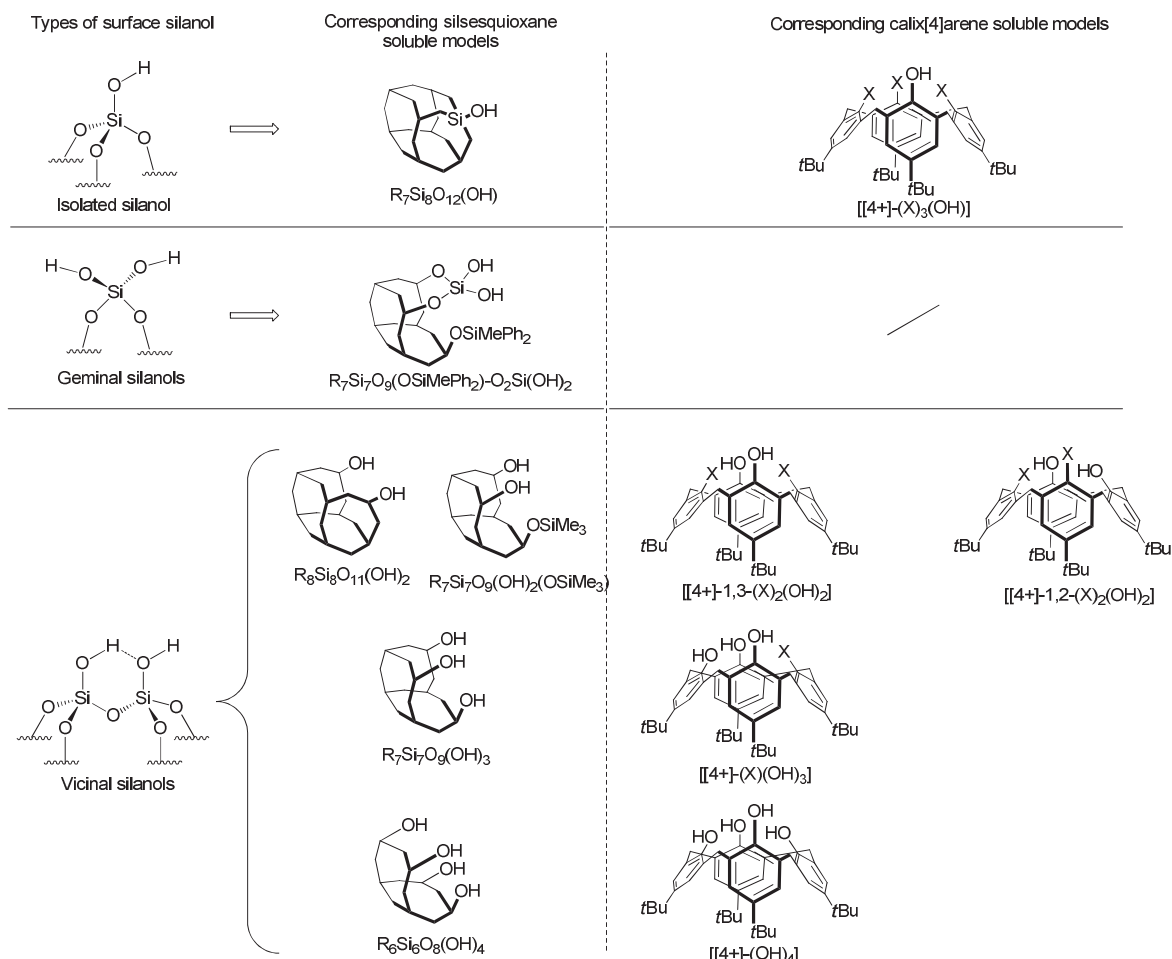
**Scheme 1:** Grafted metallacalix[4]arenes on a silica support and their corresponding soluble metallacalix[4]arene models

While most of the calix[4]arenic ligands employed were already reported, the corresponding complexes were, to our knowledge, not described. None the less, the syntheses

of the ligands were optimized; as a result, new routes were designed or existing ones were significantly improved (see **section 4**): Alkyl metallacalix[4]arenes were synthesized using two synthetic methodologies. Either chlorine metallacalix[4]arenes can be prepared (see **section 5**) prior to their alkylation (so called salt-elimination route, see **section 6**) or homoleptic metal alkyl can be directly reacted to calix[4]arene ligands (so called alkane-elimination route, see **section 6**).

## **2. Bibliographic study: Polysilsesquioxane and calix[4]arene-based complexes as molecular models of silica-grafted species of titanium and zirconium**

Silica surface organometallic complexes of titanium and zirconium can be modelized by means of ligands which mimic some of the silica support particularities and more especially, to some extent the different kinds of surface silanols (**Scheme 2**). Furthermore to emulate the silica surface environment, these ligands have to present: i) a well-defined number of hydroxyl groups as anchoring points and ii) the possibility of a total control of both electronic and geometric environments around the metal (presence of some strategic ancillary ligands, distance between the anchoring points...). In such an effort to mimic closely the surface structure by a molecular approach, polysilsesquioxane (POSS) and calix[4]arene-based ligands are outstanding candidates as they are soluble and offer a very large panel of derivatization to control the coordination mode of the metal. In this bibliographic paragraph, most of the reported titanium and zirconium POSS- and calix[4]arene-based models are described.

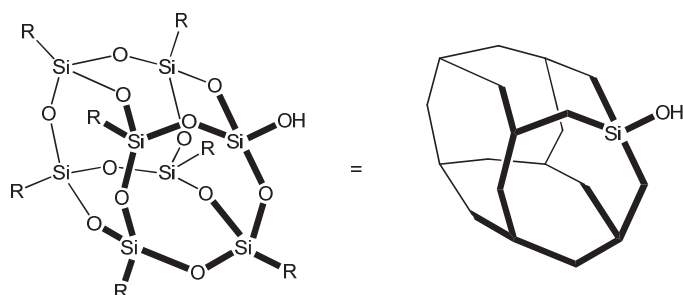


Scheme 2: Silsesquioxane and calix[4]arene derivatives as models for the different types of surface silanols (X = alkoxy, silane, H...)

## 2.1 Polyhedral Oligomeric Silsesquioxane-based complexes

### 2.1.1 Polyhedral oligomeric silsesquioxane ligands

The Polyhedral Oligomeric Silsesquioxanes (POSS) take part of the silsesquioxanes family, referring to the overall stoichiometry  $RSiO_{3/2}$  between silicon, oxygen and a generic organic group R. Those organo-silicates, interconnected *via* siloxane rings, exhibit a self-organized cage-like structure (**Scheme 3**).

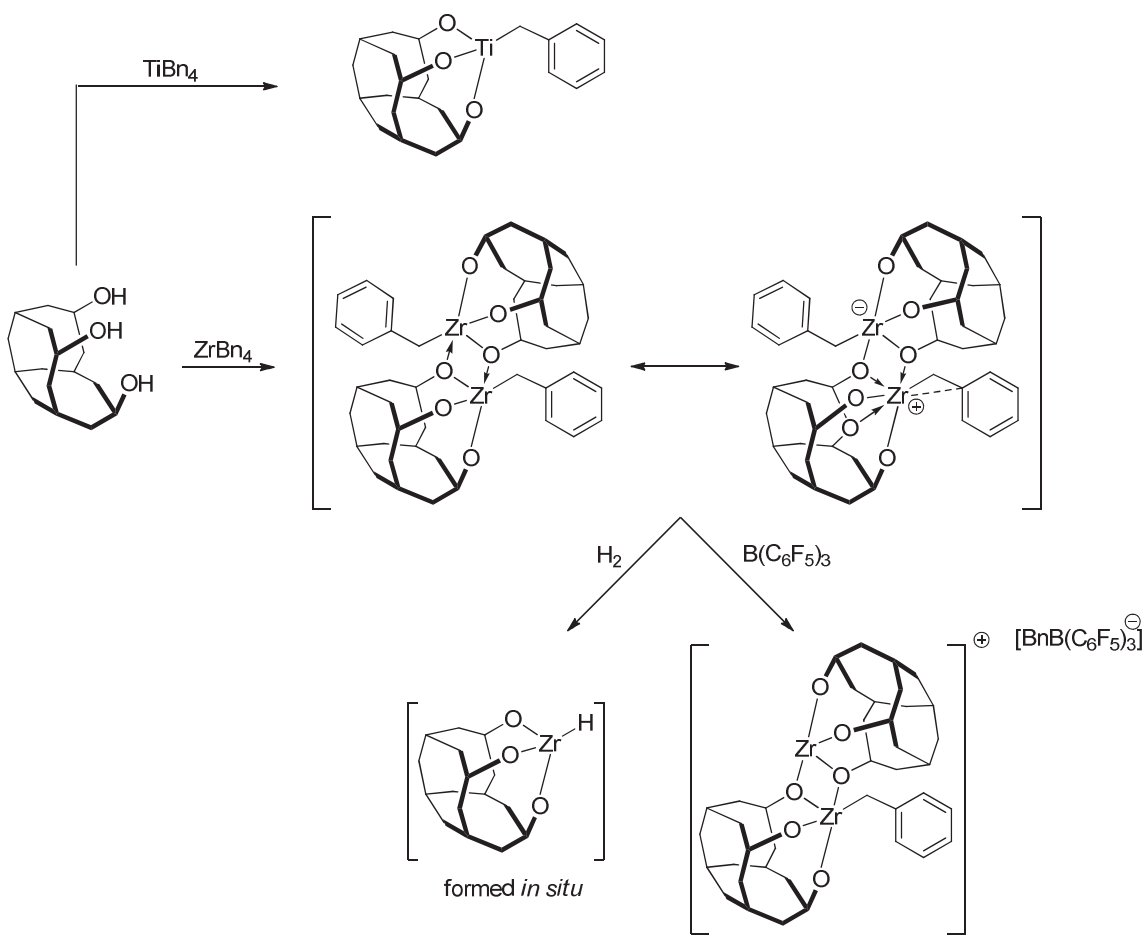


Scheme 3: Polyhedral Oligomeric Silsesquioxanes compounds (POSS) (R = organic group)

The cubic skeleton of the cage is constituted of silicon atoms bearing an organic group occupying the vertex position and oxygen atoms bridging the corners. When the polyhedron is not fully condensed, the dangling oxygen atoms belong to OH moieties, thus yielding bis-, tris- or tetrakis-silanols. By judicious silylation or cyclocondensation other silsesquioxanes have been used as molecular models for isolated, vicinal or germinal silanols (**Scheme 2**).<sup>1</sup>

### 2.1.2 Titanium and zirconium POSS-based models

Titanium-silsesquioxanes form the largest family of Metal-POSS models. As previously described in Chapter I, silica-supported titanium alkyls have been obtained by grafting TiNp<sub>4</sub> on SiO<sub>2-(500)</sub> and MCM-41-(500) yielding mostly [(≡SiO)Ti(Np)<sub>3</sub>] for the former and a mixture of monopodal [(≡SiO)Ti(Np)<sub>3</sub>] and bipodal [(≡SiO)<sub>2</sub>Ti(Np)<sub>2</sub>] for the latter. The proposed structures were based on IR-spectroscopy, solid-state NMR, EXAFS and elemental analysis.<sup>2</sup> Duchateau *et al.* have developed several routes to prepare homogeneous silsesquioxane based models of mono-, bi- and tripodal grafted titanium species.<sup>3</sup> As TiCl<sub>4</sub> reacts readily with R<sub>7</sub>Si<sub>8</sub>O<sub>12</sub>(OH) to provide the monopodal trichloro model R<sub>7</sub>Si<sub>8</sub>O<sub>13</sub>TiCl<sub>3</sub>, direct protolysis of TiBn<sub>4</sub> with R<sub>7</sub>Si<sub>8</sub>O<sub>12</sub>(OH) fails to provide the monopodal trialkyl model, since it yields a mixture of products including TiBn<sub>4</sub>. This low selectivity is due to the similar rate of protolysis by R<sub>7</sub>Si<sub>8</sub>O<sub>12</sub>(OH) for the intermediate silsesquioxane titanium tribenzyl and TiBn<sub>4</sub>. In a similar way, the reaction between equimolar amount of the bis-silanol R<sub>7</sub>Si<sub>7</sub>O<sub>9</sub>(OH)<sub>2</sub>(OSiMe<sub>3</sub>) and TiBn<sub>4</sub> resulted selectively in a 1:1 mixture of TiBn<sub>4</sub> and [R<sub>7</sub>Si<sub>7</sub>O<sub>11</sub>(OSiMe<sub>3</sub>)<sub>2</sub>Ti]. At the opposite, the tripodal models [R<sub>7</sub>Si<sub>7</sub>O<sub>12</sub>Ti(Bn)] (R = C<sub>6</sub>H<sub>11</sub><sup>4</sup> and C<sub>5</sub>H<sub>9</sub><sup>3</sup>) can be obtained in good yields (**Scheme 4**) in a monomeric form, as judged the NMR data.

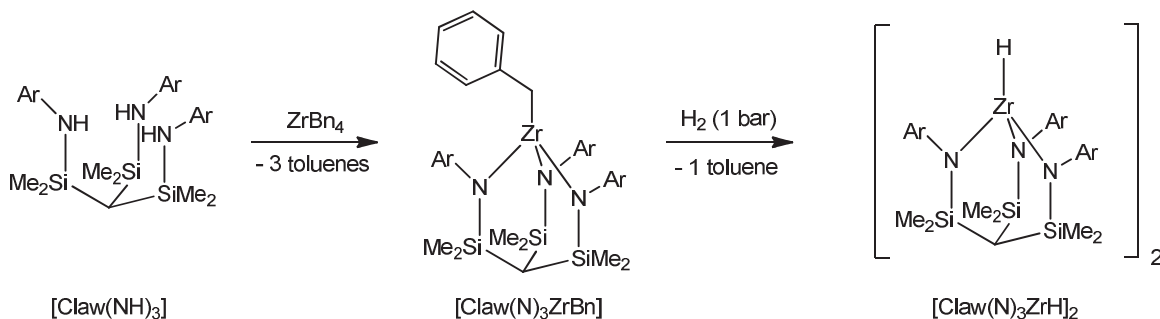


Scheme 4: Titanium and Zirconium silsesquioxane models

When  $ZrBn_4$  was reacted with 1 eq. of  $R_7Si_7O_9(OH)_2(OSiMe_3)$ , a 1:1 mixture of  $ZrBn_4$  and  $R_7Si_7O_{11}(OSiMe_3)]_2Zr$  was obtained. The reaction of the heteroleptic  $ZrCl_2Bn_2\cdot Et_2O$  with  $R_7Si_7O_9(OH)_2(OSiMe_3)$  provided the bipodal model  $R_7Si_7O_{11}(OSiMe_3)ZrCl_2\cdot 2THF$  in good yield (63%). The silsesquioxane model  $[R_7Si_7O_{12}Zr(Bn)]_2$  for the tripodal species of zirconium was obtained by reaction of  $ZrBn_4$  with the tris-silanol  $R_7Si_7O_9(OH)_3$  ( $R = C_5H_9$ ) and has been structurally characterized in the solid state as a dimeric structure (**Scheme 4**).<sup>3</sup> This latter is assumed to be in resonance with a zwitterionic entity in which the charges are distributed on both metallic centers of the dimeric structure, providing a propagation center for ethylene polymerization exhibiting a low activity; in contrast the monomeric titanium analogue is inactive. In the presence of  $B(C_6F_5)_3$ , the ethylene polymerization activity of  $[R_7Si_7O_{12}Zr(Bn)]_2$  increased considerably.

An attempt to isolate silsesquioxane  $M^{IV}$  hydrides by hydrogenation of  $R_7Si_7O_{12}MBn$  to obtain a close model for surface species  $[(\equiv SiO)_3MH]$  was partially successful. In the case of zirconium, the formation of the expected toluene suggests the *in situ* formation of the

titanium hydride. The indirect evidence of hydride formation was proven by the observation of catalytic hydrogenation of 1-hexene to *n*-hexane. By contrast, the monomeric titanium silsesquioxane [ $R_7Si_7O_{12}Ti(Bn)$ ] appears less prone to Ti-C bond hydrogenolysis, as both the benzyl complex and 1-hexene were recovered unchanged even under more drastic conditions. Isolation of hydride derivatives in solution is difficult because of the low steric hindrance of the POSS ligand, leading to dimerization by M-M formation and deactivation processes. However, the stabilization and isolating of the tripodal zirconium hydride requires a large sterically hindered ligand. For instance, the stability of tris-amido model  $[Claw(N)_3ZrH]_2$  prepared by Jia *et al.*<sup>5</sup> has been explained by the protecting wall of the three aromatic units toward the metal-hydride moiety (**Scheme 5**).



**Scheme 5:** Benzyl and hydride forms of the Zirconium “Claw” tris-amido models

In conclusion, POSS has proved to be relevant ligands for the modeling of organometallic grafted species onto silica but present some limits for mimicking supported metallacalix[4]arenes.

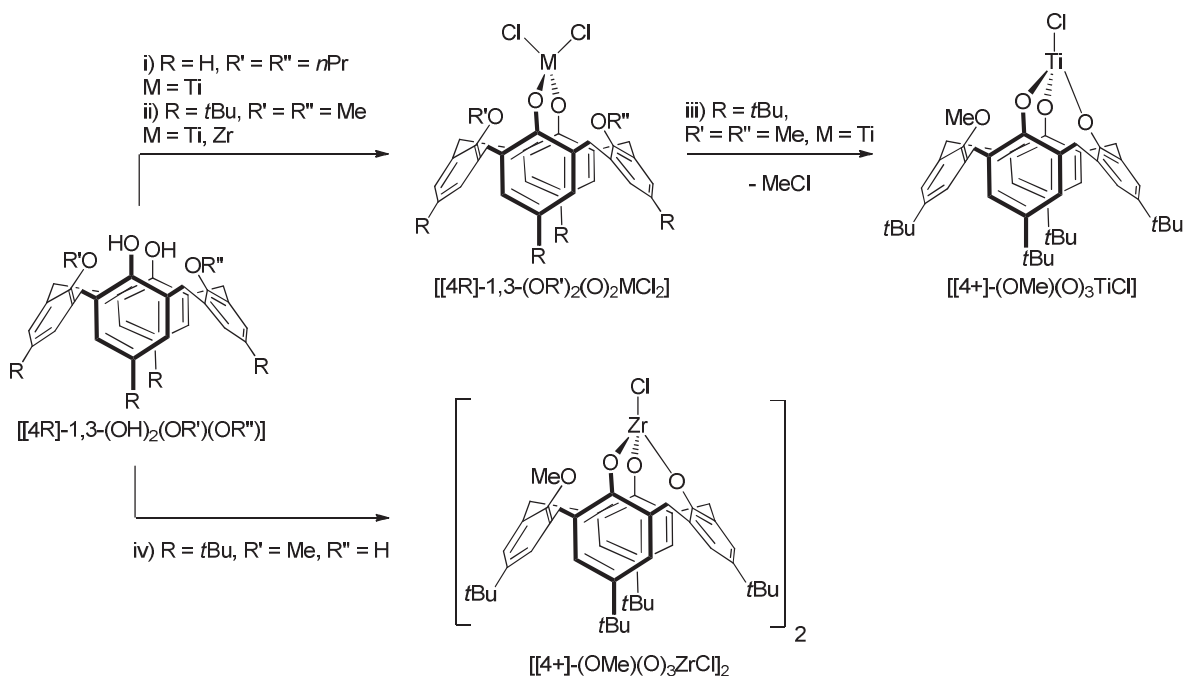
## 2.2 Calix[4]arene-based complexes: the metallacalix[4]arene models

### 2.2.1 Chlorine derivatives of the metallacalix[4]arenes

As mentioned in Chapter I, calix[4]arenes are the most employed type of calixarenes. The tetra-aryloxide closed scaffold had revealed structural and conformational properties that have been largely used in various areas (separation chemistry, selective ions complexation<sup>6</sup>, phase transfer agents, nanochemistry, medical diagnostics<sup>7</sup>...). Since the 1980’s, some elegant works on coordination chemistry have emerged. An exhaustive study was overall initiated by Floriani *et al.*<sup>8</sup> considering the calix[4]arenes as promising ligands for organometallic chemistry. The four anchoring or chelating oxygens of the lower-rim are organized in a “quasi-planar” geometry offering an ideal opportunity for modeling siloxy surfaces and

heterogeneous catalysts. In this paragraph, main calix[4]arene-based models of heterogeneous catalysts of the group IV will be discussed, as well as their catalytic applications.

Floriani principally focused on transition metals tetracoordinated to the four oxygens of the *p*-*tert*butylcalix[4]arene, considering them as X or L ligands. Models were obtained either *via* the HCl- or the salt-elimination route, by reacting  $MCl_4$  ( $M = Ti, Zr$ ) or a corresponding THF adduct, with neutral or deprotonated calix[4]arenes (**Scheme 6**). Reaction of  $MCl_4 \cdot 2THF$  ( $M = Ti^9, Zr^5$ ) with the 1,3-dimethoxy-*p*-*tert*butylcalix[4]arene  $[[4+]-1,3-(OMe)_2(OH)_2]$  provides the corresponding bipodal models  $[[4+]-1,3-(OMe)_2(O)_2M^{(IV)}Cl_2]$ , in which the metal-center is coordinated to two distal methoxy groups, thus leading to the free-THF compounds. As the zirconium model  $[[4+]-1,3-(OMe)_2(O)_2ZrCl_2]$  is thermally stable, its titanium analogue  $[[4+]-1,3-(OMe)_2(O)_2TiCl_2]$  shows total conversion to the tripodal model  $[[4+]-1,3-(OMe)(O)_3TiCl]$  when heated several hours at  $110^\circ C$ , by  $\sigma$ -bond metathesis of O-Me and Ti-Cl, with MeCl evolution. The corresponding tripodal zirconium model  $[[4+]-1,3-(OMe)(O)_3ZrCl]$  was obtained in a dimeric form by reaction of  $ZrCl_4 \cdot 2THF$  with previously deprotonated monomethoxy-*p*-*tert*-butylcalix[4]arene  $[[4+]-1,3-(OMe)(OLi)_3]$ .



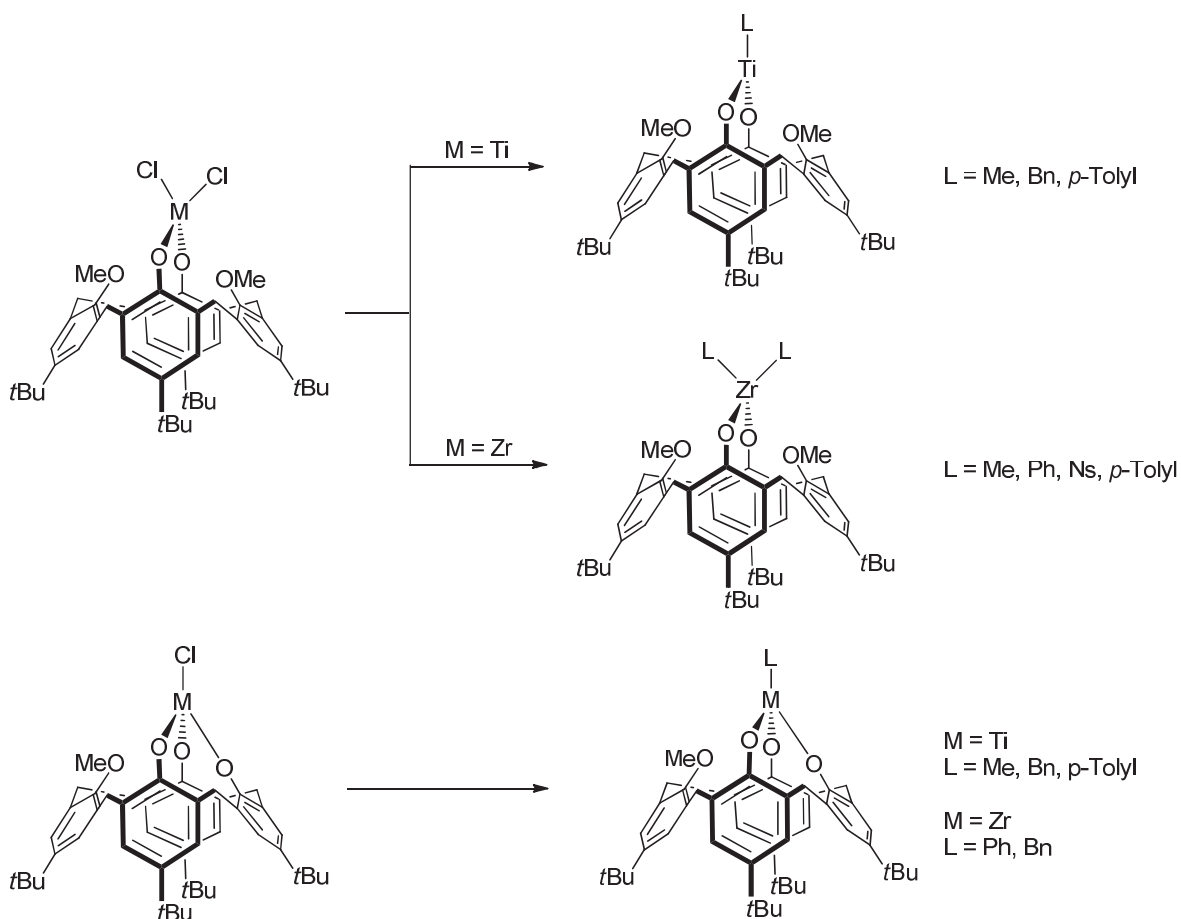
**Scheme 6: Synthetic pathways for the bipodal and tripodal chloro titana- and zirconacalix[4]arene models. Reagents and conditions: i)  $TiCl_4$ ,  $60^\circ C$ , toluene; ii)  $TiCl_4 \cdot 2THF$ ,  $60^\circ C$  or  $ZrCl_4 \cdot 2THF$ ,  $110^\circ C$ ; iii) toluene,  $110^\circ C$ ; iv)  $nBuLi$ ,  $ZrCl_4 \cdot 2THF$**

Upon activation of  $[[4+]-1,3-(OMe)_2(O)_2TiCl_2]$  with MAO, Proto *et al.* proved, by NMR spectroscopy, the existence of the titanium cationic species  $[[4+]-1,3-$

$(OMe)_2(O)_2TiMe]^+[MAOCl_2]^-$ , a catalyst active in ethylene polymerization.<sup>10</sup> This system has the particularity to produce very high molecular weights ( $M_w > 10^6$  g.mol<sup>-1</sup>) and linear polyethylene in moderate activities (*ca.* 0.1 kg<sub>PE</sub>.mol(Ti)<sup>-1</sup>.h<sup>-1</sup>.bar<sup>-1</sup>). Matt *et al.* developed more specifically the corresponding precursor  $[[4H]-1,3-(OPr)_2(O)_2TiCl_2]$  with propoxy ligands, from the calix[4]arene [4H], which was screened in different conditions (T°, P) in ethylene polymerization when activated with MAO.<sup>11</sup> It was found to be thermally stable as it shows activity up to 120°C (27.0 kg<sub>PE</sub>.mol(Ti)<sup>-1</sup>.h<sup>-1</sup>), which is maximal at 90°C (65.9 kg<sub>PE</sub>.mol(Ti)<sup>-1</sup>.h<sup>-1</sup>), providing a ultra-high molecular weight polyethylene ( $M_w = 1.1 \times 10^6$  g.mol<sup>-1</sup>), usually unexpected for such high temperatures. The *n*-propoxy groups help to stabilize and protect the active site from deactivation processes.

### 2.2.2 Alkyl derivatives of the metallacalix[4]arenes

The previously described bipodal  $[[4+]-1,3-(OMe)_2(O)_2MCl_2]$  and tripodal  $[[4+]-$   $(OMe)(O)_3MCl]$  complexes were readily alkylated with an appropriate Grignard or lithium reagent to lead to original models of heterogeneous catalysts (**Scheme 7**). Then  $[[4+]-1,3-$   $(OMe)_2(O)_2ZrR_2]$  ( $R = -CH_3, -CH_2Si(CH_3)_3, p$ -tosyl, Bn) were obtained in 33-78% yield, and the benzyl derivative, as an example, was found to be inactive in ethylene polymerization when treated with  $B(C_6F_5)_3$ .<sup>12</sup> Treatment of  $[[4+]-1,3-(OMe)_2(O)_2TiCl_2]$  with 2 eq. of MeLi, Bn<sub>2</sub>Mg or *p*-TolylMgCl provides the unexpected monoalkylated Ti<sup>(III)</sup> compounds  $[[4+]-1,3-$   $(OMe)_2(O)_2Ti^{(III)}R]$  in 48-74% yield,<sup>9a</sup> in which the Ti<sup>(III)</sup> center is stabilized by the distal methoxy groups. It is noteworthy that the alkane-elimination route has never been exploited to directly obtain the alkylated derivatives from organometallic complexes, like homoleptic compounds MR<sub>4</sub> (M = Ti, Zr; R = Np, Bn...). In addition, this route could avoid formation of Ti<sup>(III)</sup> species as the alkylating agent is suspected to act as a reducting entity.



**Scheme 7: Synthetic pathways for the bipodal and tripodal alkyl titana- and zirconacalix[4]arene models. Alkylating agents: MeLi, *p*-TolylLi, MgBn<sub>2</sub>, PhMgCl, LiCH<sub>2</sub>Si(CH<sub>3</sub>)<sub>3</sub>**

This bibliography reveals the importance of the molecular models for the understanding of elementary steps in surface organometallic chemistry on oxide and the characterizations of these species. POSS ligands offer silanols functions and a cage-like structure representative of the silica support. Calixarenic ligands have the advantages to present a well-defined number of anchoring points for the metal, with the remaining functions being functionalized with coordinative groups or not. In addition, the constrained structure of the calixarene imposes unprecedented behavior of the anchored metal. The metallacalix[4]arenes are then outgoing candidates for the modeling of their future grafted counterparts.

### 3. Strategy

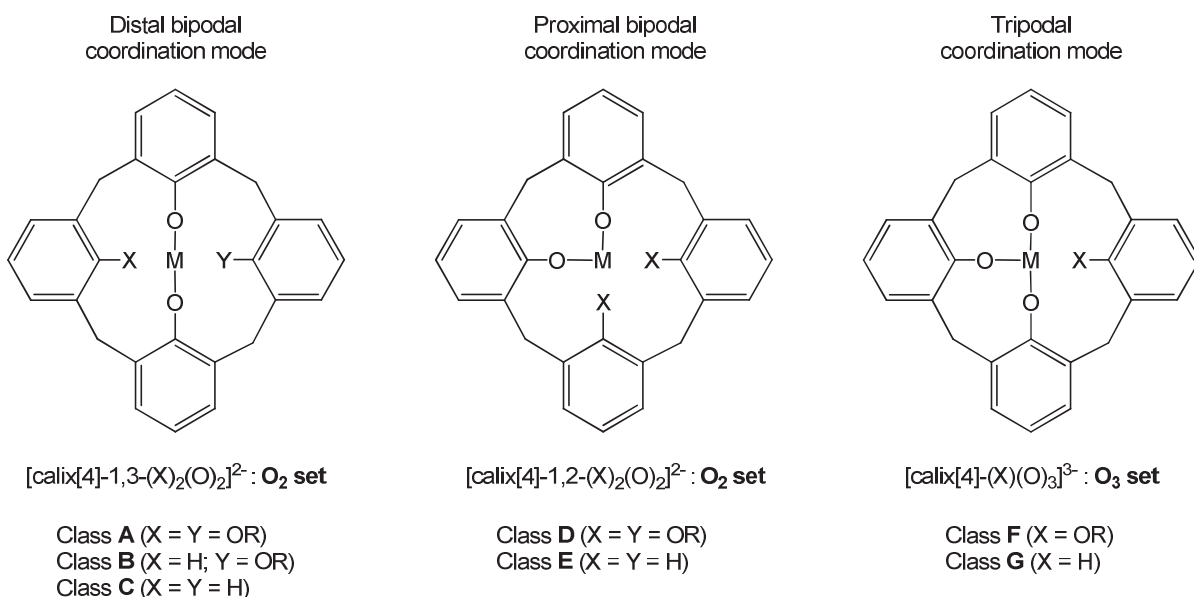
Generating of alkylated metallacalix[4]arenes by the direct reaction of homoleptic metal alkyl precursors on calix[4]arenes allows a general and straightforward access to many of the desired complexes. However, depending on the ligand and the metal combined, this

approach proved to be either unselective or unsuccessful. Alternatively, alkylation of the chlorine metallacalixarenes may potentially circumvent some of these problems. Yet, specific issues must then be addressed: additional steps are required to complete the reaction and the use of Grignard reagents, notably removing the byproducts, can be more synthetically demanding. The resulting series of complexes will be used as models not only to the well-known grafted species onto support oxide synthesized but also to the grafted metallacalixarenes developed in chapter V.

Another topic of interest is the podality of the metallacalix[4]arene complexes for they can significantly affect the reactivity of the metal. All ligands employed were selected so as to provide specific coordination modes to the metal:

- distal bipodal (Classes **A**, **B**, **C**)
- proximal bipodal (Classes **D**, **E**) and
- tripodal (Classes **F**, **G**) (**Scheme 8**)

For each configuration, the remaining phenolic oxygen atoms can potentially be selectively etherified or even dehydroxylated. This can be particularly relevant to command over the coordination of the metal center, hence generating desired alkyl-metal oxide models (**Scheme 8**).



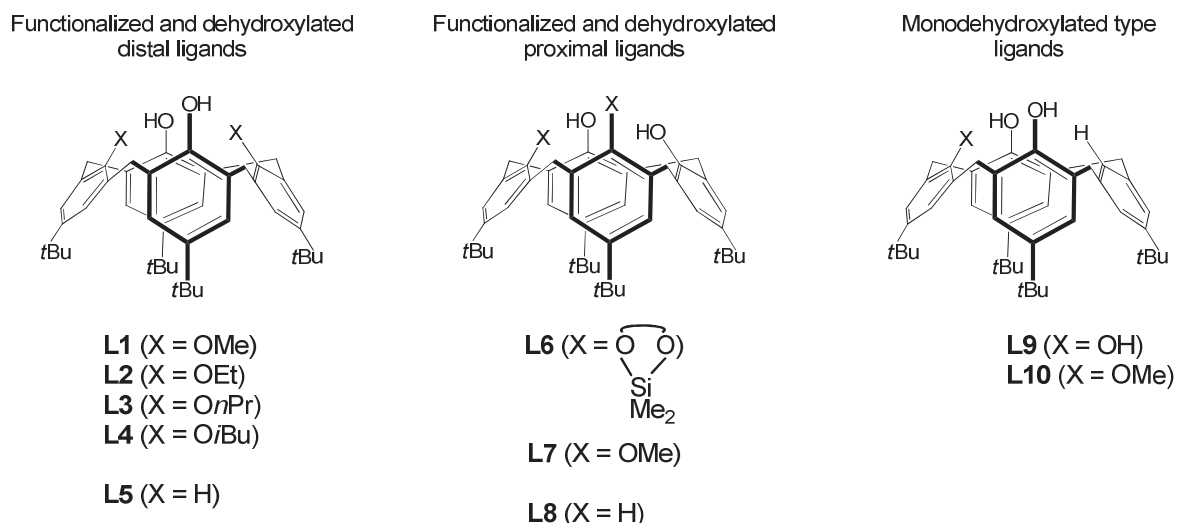
**Scheme 8:** Schematic representation of the potential coordination mode of metallacalix[4]arenes (classes *A-G*) (R = alkyl)

Some of these complexes can also have other applications. For instance, bipodal bis(chloro)titanacalixarenes (class **A-E**) can serve as precursors, upon cocatalyst addition, to the polymerization of ethylene. The effect of the variation of the geometric and electronic environments can be monitored and correlated with the metal performances. By characterization of the resulting polymers, the relationship between the structure and the activity is discussed when possible.

The preparation and the characterization of a series of both calix[4]arenic ligands and the corresponding titana- and zirconacalix[4]arene complexes belonging to the **A-G** classes are herein reported. The performance of all bis(chloro)titanium complexes belonging to the **A-E** classes was assessed as precursors for the polymerization of ethylene. All alkyl metallacalix[4]arenes obtained will be used as models of the grafted species counterparts (see chapter V).

#### 4. Preparation and conformational studies of the *p*-tertbutylcalix[4]arene derivatives ligands (**L1-L10**)

Syntheses, molecular and conformational studies of the ligands **L1-L10** (**Scheme 9**) will be discussed. Each of them was fully characterized by NMR and mass spectroscopies.



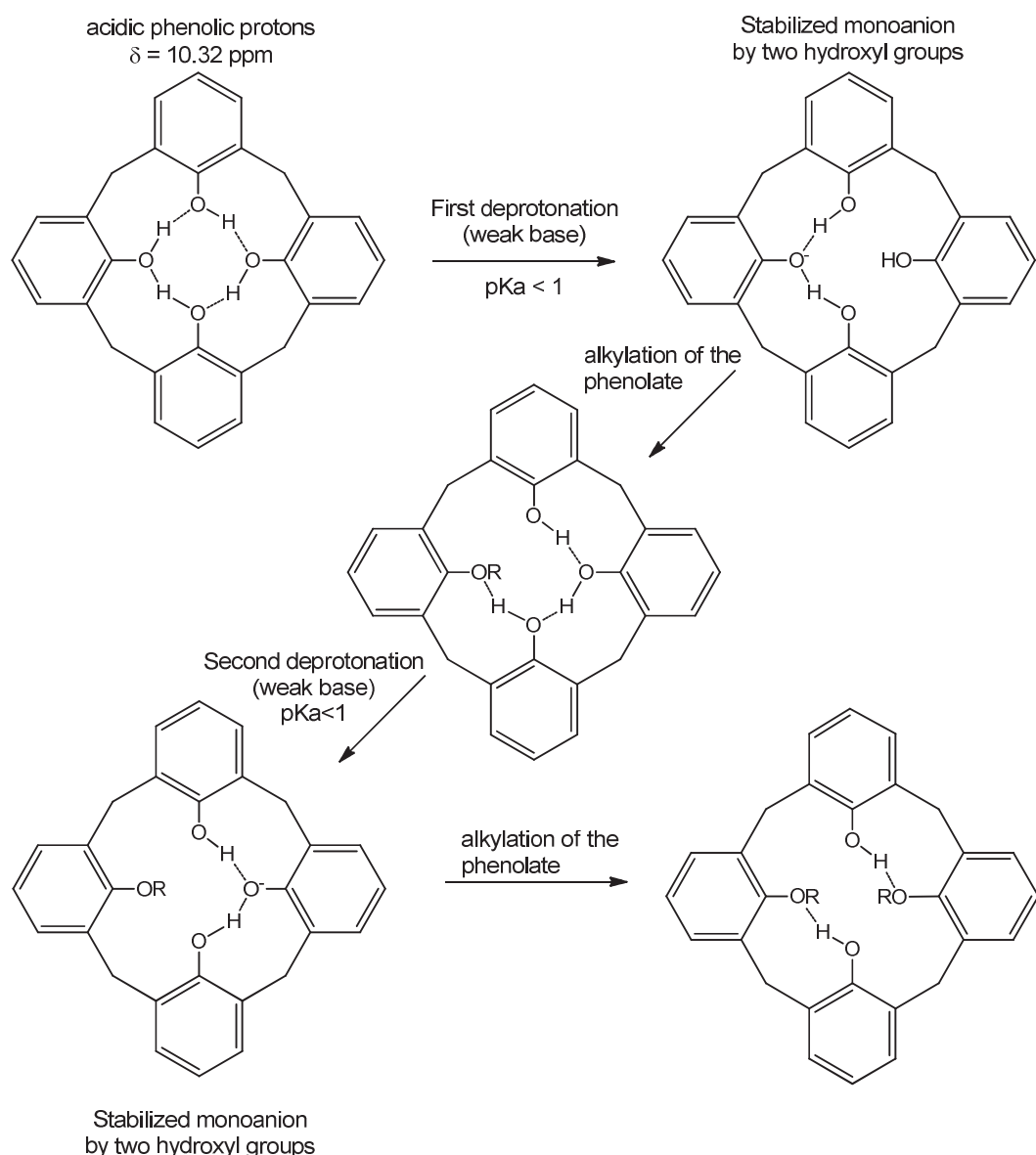
**Scheme 9:** Targeted *p*-tertbutylcalix[4]arene-based ligands

##### 4.1 Functionalized *p*-tertbutylcalix[4]arenes on distal positions (**L1-L4**)

Etherification of the *p*-tertbutylcalix[4]arene in distal positions has been successfully studied. Typically, the *p*-tertbutylcalix[4]arene is treated with an excess of an alkylating agent

(halogeno-alkane) in presence of a weak base, like  $M_2CO_3$  ( $M = K$  or  $Na$ ) in MeCN, or CsF in DMF, providing distal diethers in high yields.<sup>13</sup>

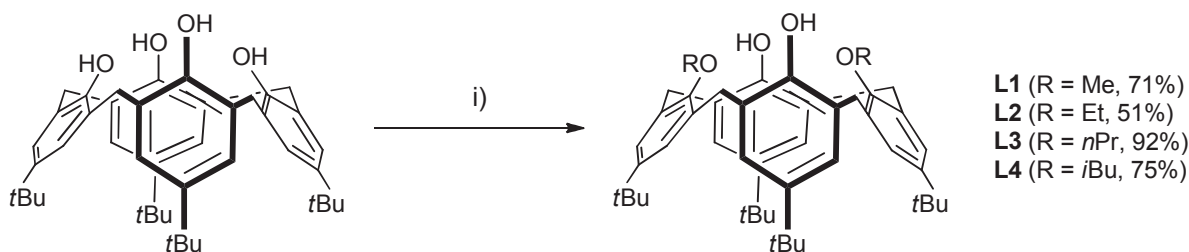
The remarkable selectivity of these reagents towards the distal positions can be explained by the difference of acidity of each of the hydroxyl groups. It appears that neutral *p*-*tert*butylcalix[4]arene has four equivalent acidic OH groups ( $\delta = 10.32$  ppm), due to the circular hydrogen bonding. However, each of the hydroxyl groups is known to exhibit a different consecutive constant of dissociation ( $pK_{a1} < 1$ ,  $pK_{a2} \approx 10$ ,  $pK_{a3} \approx 12$ ,  $pK_{a4} > 14$ , Scheme 10).<sup>14</sup>



**Scheme 10:** Mechanistic approach for the distal diether calix[4]arenes formation

The first deprotonation occurs in “super-acidic” pH region ( $\text{pK}_\text{a} < 1$ ) and is easily carried out with a weak base like  $\text{K}_2\text{CO}_3$ . The resulting monoanion is then stabilized by the two neighbouring phenol units. If not alkylated by an alkylating agent, the formation of the distal dianion is less obvious ( $\text{pK}_{\text{a}2} \approx 10$ ), because of the difficult stabilization of the dianion. When alkylated, the resulting monofunctionalized neutral calixarene has three remaining OH functions. The middle one, since its conjugate base is better stabilized by the two side hydroxyls, is deprotonated. The remaining hydroxyl functions (in distal positions) cannot be deprotonated with a weak base, because of their higher  $\text{pK}_\text{a}$ .

The diether compounds **L1**<sup>15</sup>, **L2**<sup>16</sup> and **L3**<sup>17</sup> (**Scheme 11**) have been synthesized according to this classic procedure. *p*-*tert*butylcalix[4]arene was treated with 1.1 eq of  $\text{K}_2\text{CO}_3$  as base in dry MeCN before addition of an excess of the corresponding halogeno-alkane and refluxing over 24h (**L1**, 71%; **L2**, 51%; **L3**, 92%). After optimisation of the same protocol, 1,3-diisobutoxy-*p*-*tert*butylcalix[4]arene compound **L4** was prepared and isolated in improved yield (75%) than reported<sup>18</sup> with the use of *i*BuI (**Scheme 11**).

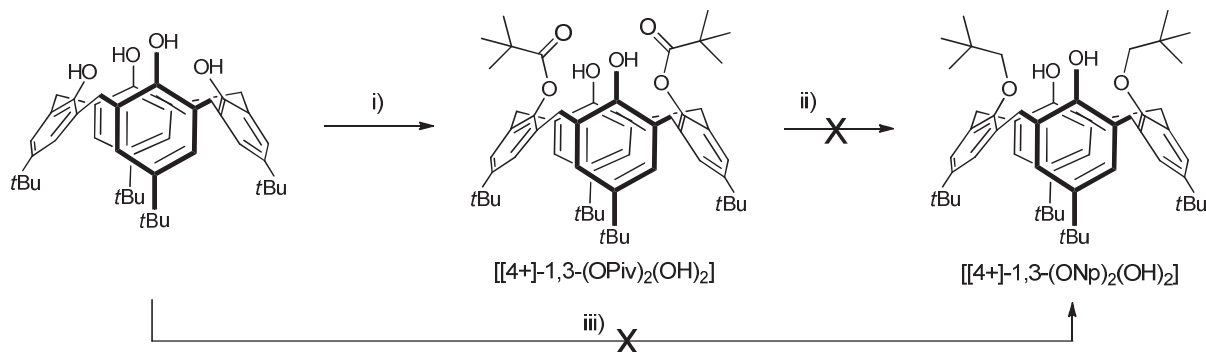


**Scheme 11:** Syntheses of the functionalised *p*-*tert*butylcalix[4]arenes on distal positions **L1-L4**. Reagents and conditions: i) xs. alkylating agent, 1.1 eq.  $\text{K}_2\text{CO}_3$ , MeCN, reflux, 24h

The methylene protons ( $\text{ArCH}_2\text{Ar}$ ) of **L1-L4** display a similar pattern of signals with two sets of doublet in  $^1\text{H}$  NMR and one signal around 31-32 ppm in  $^{13}\text{C}$  NMR consistent with the calixarene being in cone conformation.<sup>19</sup> The hydrogen bonds between the hydroxyl and the alkoxy groups maintain the four phenolic units in the same orientation. Moreover, the sets of two signals for  $\text{C}(\text{CH}_3)_3$  and for  $\text{ArH}$  and the signals for each proton of the alkoxy chain are characteristic of a  $C_{2v}$  symmetry.

Unlike the facile syntheses of **L1-L4**, reaction of *p*-*tert*butylcalix[4]arene with NpI over 60 h in presence of  $\text{K}_2\text{CO}_3$ , or directly with NpOTs at reflux over 5 days, surprisingly showed no conversion (**Scheme 12**). Assuming the methylenic proton of the neopentyl fragment cannot provide a primary cation, a  $\text{S}_{\text{N}}2$  mechanism should be proposed. Its occurrence is highly deterred by the steric hindrance of the three geminal methyls. Thus,

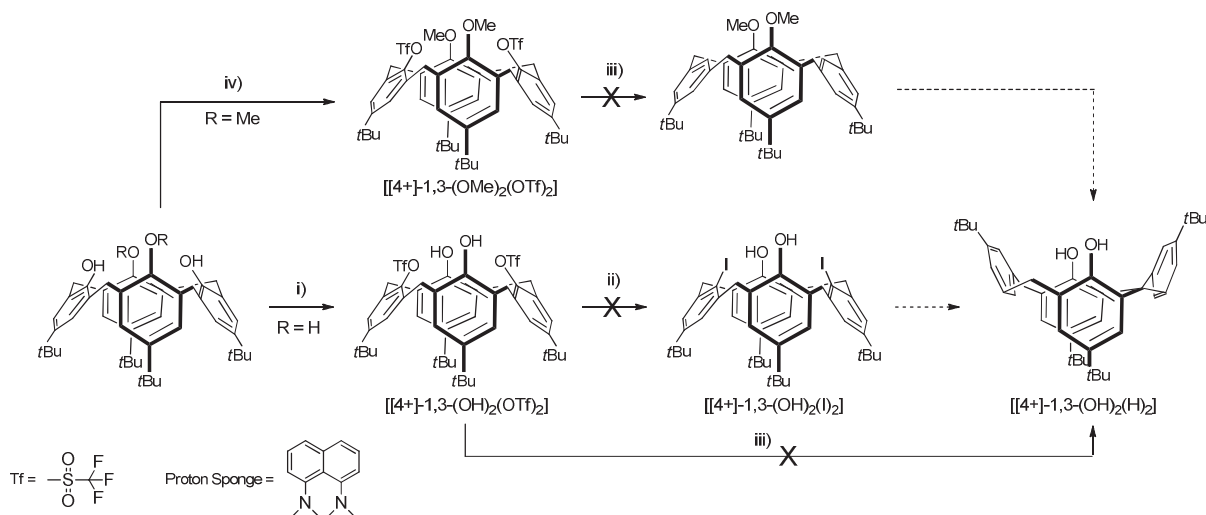
another approach was undertaken by first reacting pivaloyl chloride (Pivaloyl =  $(CH_3)_3CO-$ ) with *p*-*tert*butylcalix[4]arene in presence of  $NEt_3$  to get selectively  $[[4+]-1,3-(OPiv)_2(OH)_2]$  in 85% yield (**Scheme 12**). The acyl chloride, in spite of being highly reactive, provides the corresponding diester derivative that could not have been reduced, regardless the conditions operated, *i.e.*  $BH_4$  with  $BF_3\cdot(OEt)_2$ <sup>20</sup>,  $Et_3SiH$  with  $InBr_3$ <sup>21</sup>,  $Et_3SiH$  with  $InCl_3$ .



**Scheme 12:** Synthetic pathway proposed for the synthesis of  $[[4+]-1,3-(ONp)_2(OH)_2]$ . Reagents and conditions: i)  $x.s. PivCl$ ,  $x.s. NEt_3$ ,  $DCM$ ,  $RT$ ,  $1h$ ; ii)  $NaBH_4/BF_3\cdot(OEt)_2$  or  $Et_3SiH/InBr_3$  or  $Et_3SiH/InCl_3$ ; iii)  $x.s. NpI$ ,  $1.1\text{ eq. } K_2CO_3$ ,  $MeCN$ ,  $reflux$ ,  $60h$  or  $x.s. NpOTs$ ,  $2\text{ eq. } NaH$ ,  $MeCN$ ,  $reflux$ ,  $5\text{ days}$

## 4.2 Dehydroxylated *p*-*tert*butylcalix[4]arene on distal positions (L5)

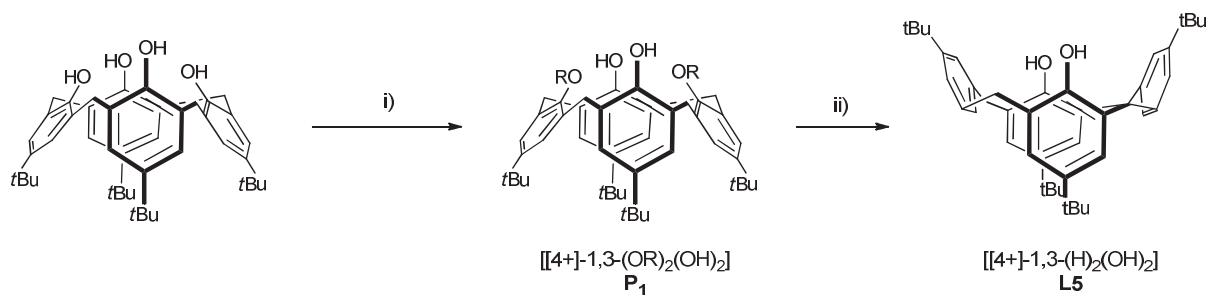
Synthesis of  $[[4+]-1,3-(OH)_2(H)_2]$  L5 involves selective OH-depletion of *p*-*tert*butylcalix[4]arene on distal positions. Different methods for the phenolic derivatives dehydroxylation have been reported, especially *via* the cleavage of triflate groups with palladium. In theory, it consists in the oxidative addition of  $Pd^0$  in the  $ArO-Tf$  bond, followed by the substitution of the OTf group by a hydride, provided by a reducing reagent. We first synthesized the 1,3-bis-triflate *p*-*tert*-butylcalix[4]arene according to a literature method<sup>22</sup>, by reaction of the *p*-*tert*butylcalix[4]arene with 4 eq. of triflic anhydride in presence of 5 eq. of Proton Sponge (1,8-bis-(dimethylamino)naphthalene) in 85 % yield, after purification by filtration of the reaction media through a pad of silica (**Scheme 13**). Treatment of  $[[4+]-1,3-(OTf)_2(OH)_2]$  with a catalytic amount of  $Pd(OAc)_2$  in presence of 1,3-bis-(diphenylphosphino)propane (dppp) and  $Et_3SiH$  in DMF was first attempted. No cleavage of the triflate groups was observed, but only a mixture of the starting material  $[[4+]-1,3-(OTf)_2(OH)_2]$  and some mono- and disilylated compounds, as judged by the mass spectrum electrospray.



**Scheme 13:** Synthetic pathway proposed for the synthesis of  $[[4+]\text{-}1,3\text{-(OH)}_2\text{(H)}_2]$ . Reagents and conditions: i) 4 eq.  $\text{Tf}_2\text{O}$ , 5.2 eq. Proton sponge, toluene, RT, 2.5h; ii) 6 eq. CuI, 1.8 eq. DBU, cat.  $\text{PdCl}_2(\text{PPh}_3)_2$ , toluene, RT, 3h; iii)  $\text{Pd}(\text{OAc})_2/\text{dppp/Et}_3\text{SiH}$  or  $\text{PdCl}_2(\text{PPh}_3)_2/\text{dppp/NBu}_3/\text{HOOCH}$  or  $\text{Pd/C/Mg/MeOH/NH}_4\text{OAc}$ ; iv) 4 eq.  $\text{Tf}_2\text{O}$ , 5.2 eq. Proton sponge, DCM, reflux, 4h

In order to avoid silylation of the free hydroxyl functions, **L1** was reacted with  $\text{Tf}_2\text{O}$  in presence of the Proton Sponge to lead  $[[4+]\text{-}1,3\text{-(OMe)}_2\text{(OTf)}_2]$  with 66% yield. Despite treatment with  $\text{Pd}(\text{OAc})_2/\text{dppp/Et}_3\text{SiH}$ ,  $\text{PdCl}_2(\text{PPh}_3)_2/\text{dppp/NBu}_3/\text{HOOCH}^{23}$  or  $\text{Pd/C/Mg/MeOH/NH}_4\text{OAc}^{24}$ , the dehydroxylated **L5** compound was not obtained (**Scheme 13**). As Georghiou *et al.* described from  $[[4+]\text{-}1,3\text{-(OH)}_2\text{(OTf)}_2]$  as starting material, the triflate groups can be substituted by iodine atoms with  $\text{PdCl}_2(\text{PPh}_3)_2/\text{CuI/DBU}$  in toluene to provide  $[[4+]\text{-}1,3\text{-(OH)}_2\text{(I)}_2]$ .<sup>25</sup> Then, transmetalation of the iodine groups by treatment with *n*BuLi, followed by hydrolysis, could lead to **L5**. Unfortunately, two attempts of iodation were not successful and  $[[4+]\text{-}1,3\text{-(OH)}_2\text{(I)}_2]$  was isolated only in very low yield (**Scheme 13**). In conclusion, all alternative methods using mild conditions to get **L5** failed. Biali *et al.* reported a methodology for the synthesis of a such ligand, but in more drastic conditions *via* distal phosphorylated calix[4]arenes.<sup>26</sup>

**L5** was synthesized by adapting this two-step method. The precursor **P1** was prepared by treatment of the *p*-*tert*butylcalix[4]arene with an excess of  $\text{ClPO(OEt)}_2$  instead of  $\text{HPO(OEt)}_2$  and  $\text{NEt}_3$  in toluene at room temperature with a good yield (76%). Secondly, the reductive cleavage of the phosphate groups in the presence of potassium metal in liquid ammonia at  $-78^\circ\text{C}$  leads to **L5**. The use of dichloromethane as an extraction solvent improved the yield from 15% to 58% (**Scheme 14**).



**Scheme 14:** Synthesis of  $[[4+]-1,3-(\text{H})_2(\text{OH})_2]$  **L5.** Reagents and conditions: i) 4 eq.  $\text{ClP}(\text{O})(\text{OEt})_2$ , 4 eq.  $\text{NEt}_3$ , toluene, RT, 2h; ii) xs.  $\text{K}/\text{NH}_3$ ,  $-78^\circ\text{C}$ , 1h ( $\text{R} = \text{P}(\text{O})(\text{OEt})_2$ )

On the  $^{13}\text{C}$  NMR spectrum of **L5**, a single signal at 37 ppm is assigned to  $\text{ArCH}_2$ . This value is typical of calixarenes having pairs of neighbor phenoxy groups *anti*-oriented.<sup>19</sup> The  $^1\text{H-NMR}$  spectrum (**Figure 1**) displays a unique singlet for the methylene, proving the fast interconversion rate at RT in a NMR acquisition time, by contrast with  $[[4+]-1,3-(\text{OH})_2(\text{OMe})_2]$ , for which the methoxy groups maintain the cone conformation *via* hydrogen bonding ( $\text{OH} = 8.5$  ppm in opposite to the free OH of **L5**), thus resulting in a slower interconversion rate (**Figure 1**). The *tBu* and ArH protons are of two sets of two singlets, indicating a plane of symmetry in the structure. These observations confirm that the ligand **L5** adopts an 1,3-alternated conformation.<sup>26-27</sup> In comparison to **L1-L4**, **L5** provides two distal anchoring points for the metal, but without extra coordination.

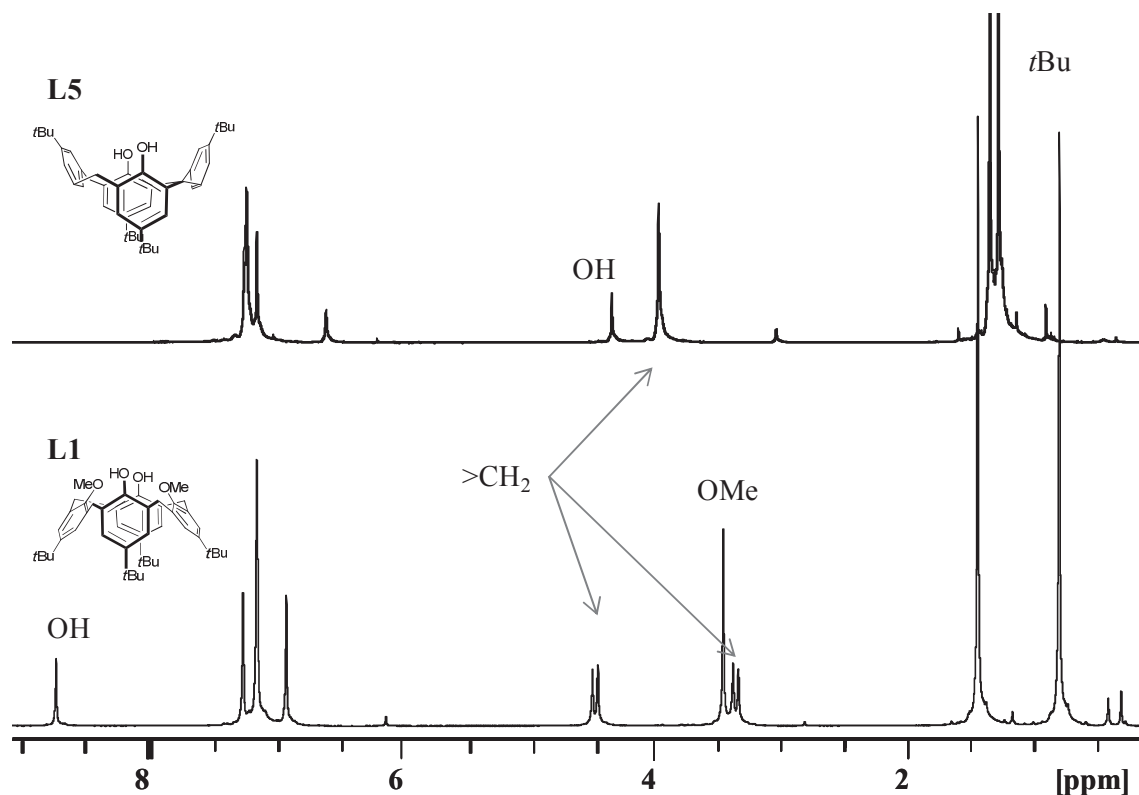
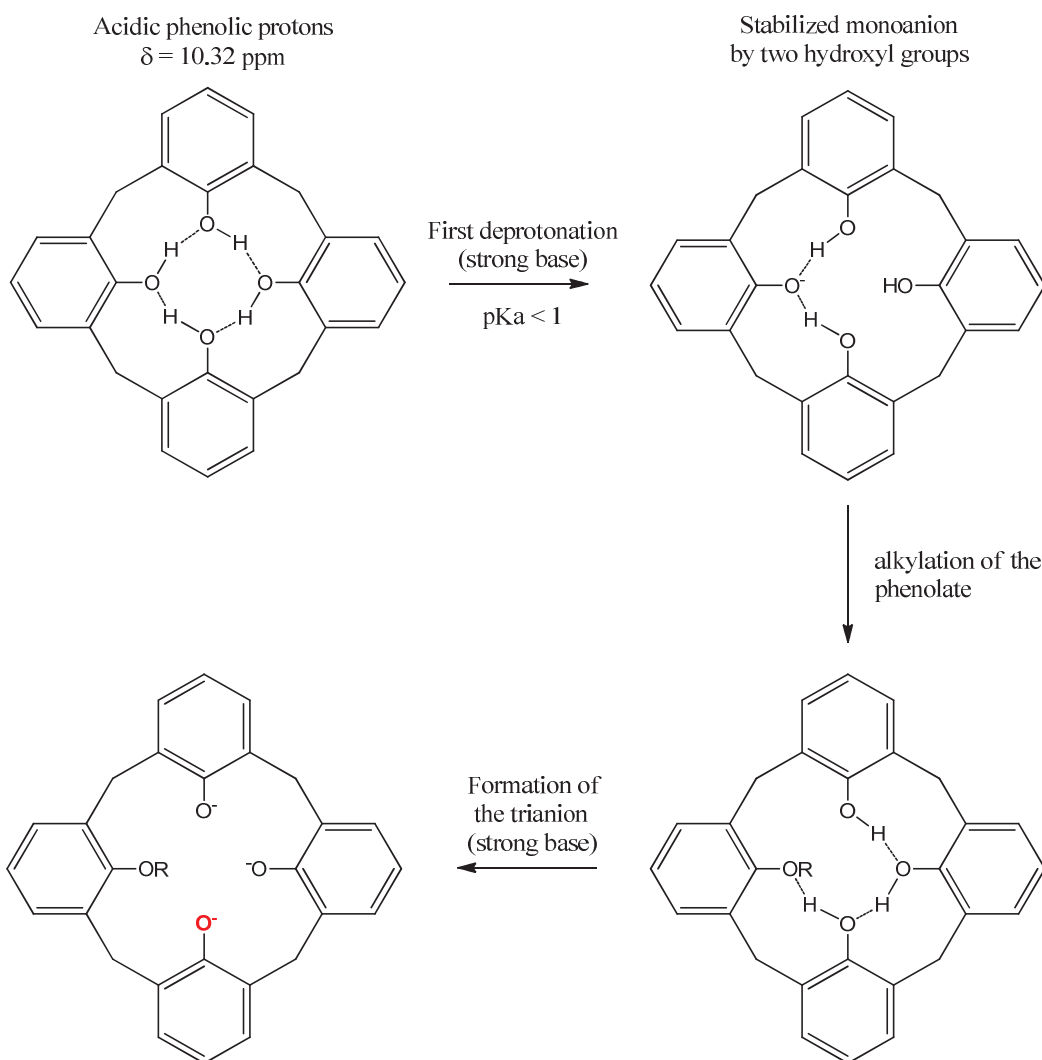


**Figure 1:**  $^1\text{H-NMR}$  of  $[[4+]-1,3-(\text{OMe})_2(\text{OH})_2]$  **L1** and  $[[4+]-1,3-(\text{H})_2(\text{OH})_2]$  **L5**

### 4.3 Functionalized *p*-*tert*butylcalix[4]arenes on proximal positions (L6-L7)

Several synthetic methodologies for the proximal functionalization are available: either by direct alkylation, by selective dealkylation of a tetra-etherified calix[4]arene, or by a series of protection-deprotection steps. In the particular case of direct alkylation, a strong base like NaH is used with a limiting amount of alkylating agent.<sup>28</sup> For example, *p*-*tert*butylcalix[4]arene treated with 2.2 eq. of benzylbromide and 5 eq. of NaH in acetonitrile provides 58% yield of the proximal diether  $[[4+]]\text{-}1,2\text{-(OH)}_2(\text{OBn})_2$  with 22% of tetra-ether  $[[4+]]\text{-(OBn)}_4$ , 1% of triether  $[[4+]]\text{-(OH)(OBn)}_3$ .<sup>29</sup> Shinkai *et al.* proposed a mechanistic approach to explain this selectivity (**Scheme 15**).



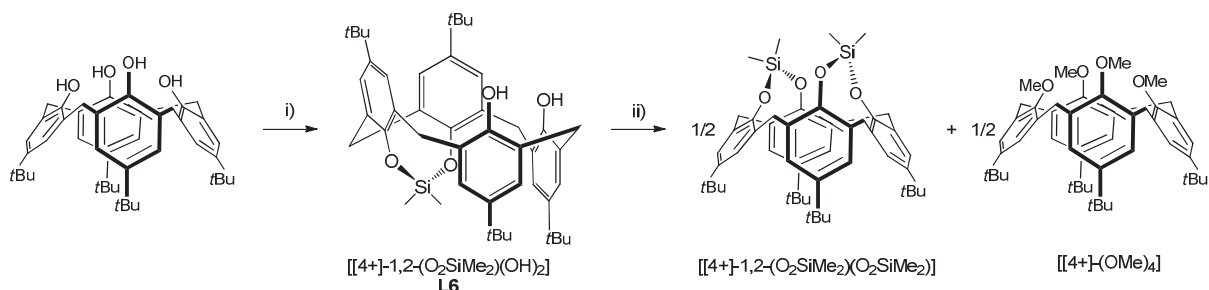
**Scheme 15:** Mechanistic approach for the proximal diether calix[4]arenes formation

After alkylation of the phenolate generated, easily obtained from the first deprotonation, the resulting mono-functionalized precursor is entirely deprotonated to provide a trianion, in

which the proximal anion (from the function) is a stronger nucleophile than the distal phenolate. Thus, the proximal functionalization is due to the selective reactivity of the proximal phenolate.

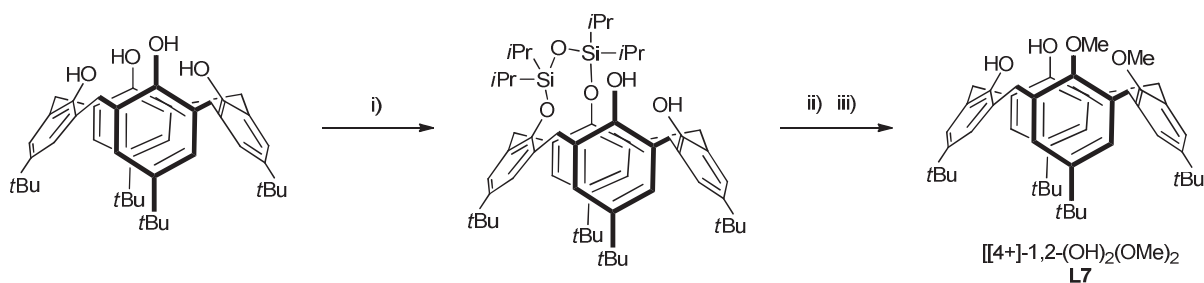
The selective dealkylation described by Pochini *et al.* is a less common method due to the increased number of steps.<sup>30</sup> The first one consists in the total alkylation of the *p*-*tert*butylcalix[4]arene with an excess of iodomethane to provide the  $[[4+]\text{-}(\text{OMe})_4]$ . When treated with 2 eq. of  $\text{TiBr}_4$  in  $\text{CHCl}_3$ , the distal  $[[4+]\text{-}1,2\text{-}(\text{OH})_2(\text{OMe})_2]$  is obtained in good yield.

A series of ligands displaying either silane bridge,  $[[4+]\text{-}1,2\text{-}(\text{OH})_2(\text{O})_2\text{SiMe}_2]$  **L6**, or methoxy groups,  $[[4+]\text{-}1,2\text{-}(\text{OH})_2(\text{OMe})_2]$  **L7**, on the proximal positions were targeted. In this way, another additional route *via* protection-deprotection steps with silane groups was retained since it allowed access to both targets in the same reaction pathway. Fan *et al.*<sup>31</sup> first developed the synthesis of the proximal protected compound  $[[4+]\text{-}1,2\text{-}(\text{O}_2\text{SiMe}_2)(\text{OH})_2]$  **L6** by reacting the *p*-*tert*butylcalix[4]arene with  $\text{Me}_2\text{SiCl}_2$  in presence of  $\text{NEt}_3$ , in 84% yield (**Scheme 16**). Etherification of the protected compound with *n*BuLi and MeOTf surprisingly lead to disproportionation, providing  $[[4+]\text{-}(\text{OMe})_4]$  and  $[[4+]\text{-}1,2\text{-}(\text{O}_2\text{SiMe}_2)(\text{O}_2\text{SiMe}_2)]$  in 1:1 ratio.



**Scheme 16:** Synthetic pathway proposed for the formation of  $[[4+]\text{-}1,2\text{-}(\text{OH})_2(\text{OMe})_2]$  **L7** *via* **L6**. Reagents and conditions: i) 1 eq.  $\text{Cl}_2\text{SiMe}_2$ , 2 eq  $\text{NET}_3$ ; ii) 2 eq. *n*BuLi, 2.1 eq. MeOTf

To avoid disproportionation, an alternative route was explored by Narumi *et al.*<sup>32</sup> As a result the use of bis-chlorotetra-isopropylsiloxane (TIPDS) as a less labile protecting agent was preferred to  $\text{Me}_2\text{SiCl}$ . *p*-*tert*butylcalix[4]arene was first reacted with 1 eq. of TIPDS in presence of imidazole as a base, to provide the proximal protected  $[[4+]\text{-}1,2\text{-}(\text{TIPDS})(\text{OH})_2]$  with a bridged siloxane function, in quantitative yield (**Scheme 17**).

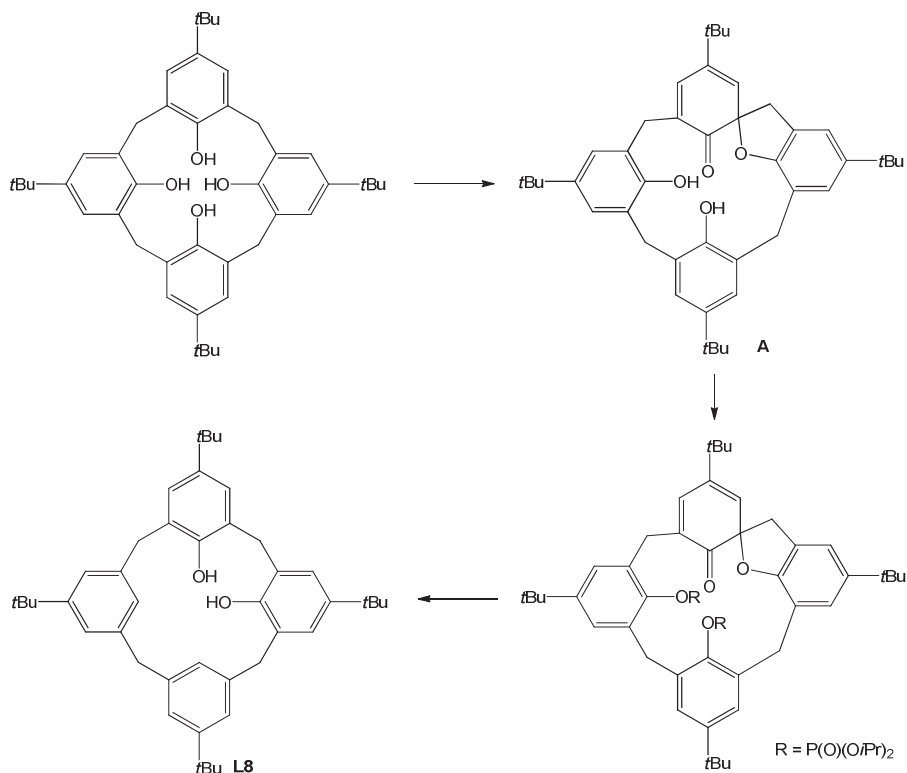


**Scheme 17:** Synthesis of  $[[4+]-1,2-(OH)_2(OMe)_2]$  **L7** via TIDPS protected *p*-*tert*-butylcalix[4]arene. Reagents and conditions: i) 1.2 eq. TIDPS, 3 eq. imidazole, DMF, RT, 4h; ii) 6 eq. MeI, 6 eq.  $Cs_2CO_3$ , THF, reflux, 18h; iii) 4 eq. TBAF, THF, RT, 30min

$[[4+]-1,2-(TIPDS)(OH)_2]$  was then reacted with MeI, and  $Cs_2CO_3$  as a base, to furnish, after deprotection of the siloxane bridge with TBAF, the proximal diether  $[[4+]-1,2-(OMe)_2(OH)_2]$  **L7** in 85% yield. Ligand **L7** shows complex  $^1H$ -NMR because it exists in both *syn* and *anti*-conformers in solution.<sup>30</sup>

#### 4.4 Dehydroxylated *p*-*tert*butylcalix[4]arene on proximal positions (**L8**)

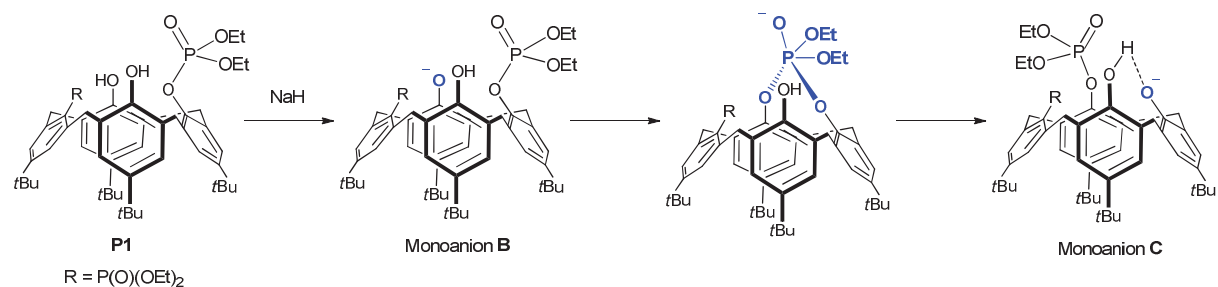
Only one example of synthesis of  $[[4+]-1,2-(H)_2(OH)_2]$  **L8** was reported by Biali *et al.* via the spirodienone route.<sup>33</sup> The first step consists in the formation of the monospirodienone **A** by mild oxidation of the *p*-*tert*butylcalix[4]arene in a biphasic solvent ( $CH_2Cl_2$ , aqueous  $NaHCO_3$ ) in modest yield (20%) (**Scheme 18**).



**Scheme 18:** Synthesis of  $[[4+]-1,2-(OH)_2(H)_2]$  **L8** via the monospirodienone route

This compound presents two intramolecular protected hydroxyls groups in the spirodienone moiety, and two free hydroxyls groups which are phosphorylated with  $\text{ClP(O)(OEt)}_2$  and finally cleaved with  $\text{K}/\text{NH}_3$  to provide  $[[4+]-1,2-(\text{H})_2(\text{OH})_2]$  **L8**.

With the aim to synthesize **L8** in a larger scale, we developed an original and more simple method. First, the proximal diethyl diphosphate ester precursor **P2** was obtained from the distal diethyl diphosphate ester precursor **P1** in quantitative yield by phosphorotropic rearrangement as described by Markovsky *et al.* (**Scheme 19**).<sup>34</sup> In a mechanistic approach, the monoanion **B** generated by the mono-deprotonation of **P1** with  $\text{NaH}$  readily attacks the phosphorylated group *via* an addition-elimination process. Migration of the latter from the distal position toward the proximal position allows the monoanion **C** to be stabilized by the remaining hydroxyl group by hydrogen bond (**Scheme 19**). Neutralization of **C** provides **P2** in quantitative yield. The compound **P2** was then used without further purification to obtain **L8** (80% yield) by reductive cleavage of the phosphate groups, in the same conditions as for **P1**.



**Scheme 19:** Mechanistic approach for the formation of **P2** from **P1** with the use of  $\text{NaH}$

**L8**, is in a fast conformational flipping equilibrium, at the NMR time scale, between the cone and the 1,2-alternate conformations.<sup>33</sup> This is reminiscent to the fluxionality processes observed with **L5**, as both compounds possess flexible scaffold.  $^1\text{H-NMR}$  spectrum of **L8** displays: three singlets in 2:1:1 ratio corresponding to the three different methylene bridges, one singlet for the identical *ipsoAr-H* and two singlets for the two types of *tBu* groups (**Figure 2**). As for **L5**, it presents a plane of symmetry ( $\text{Cs}$ ), including both singular types of methylene bridges. The OH signal of **L8** at 6.2 ppm is consistent with the hydroxyls interacting by hydrogen bonding in contrast to the free hydroxyls groups at 4.4 ppm of **L5**. Furthermore, whereas  $^{13}\text{C-NMR}$  of **L5** shows a unique singlet for the methylene bridges around 37 ppm, that of **L8** displays three singlets at 32, 38 and 43 ppm proving the supporting the 1,2-alternate conformation.

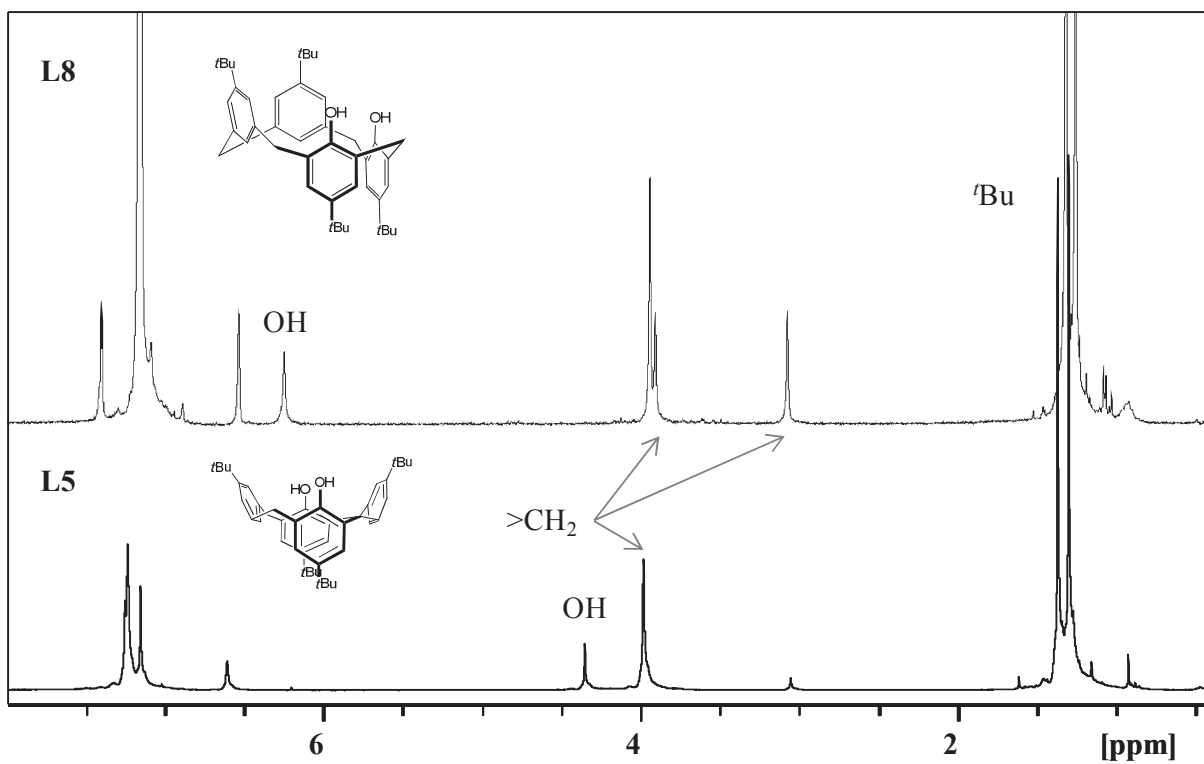
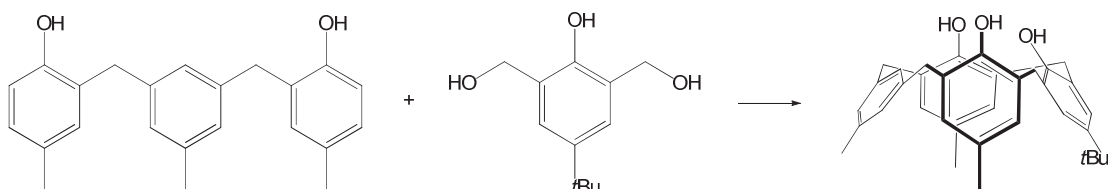


Figure 2:  $^1\text{H}$ -NMR of  $[[4+]\text{-}1,2\text{-(H)}_2(\text{OH})_2]$  L8 and  $[[4+]\text{-}1,3\text{-(H)}_2(\text{OH})_2]$  L5

#### 4.5 Mono-dehydroxylated *p*-*tert*butylcalix[4]arene (L9) and its mono-methoxy derivative (L10)

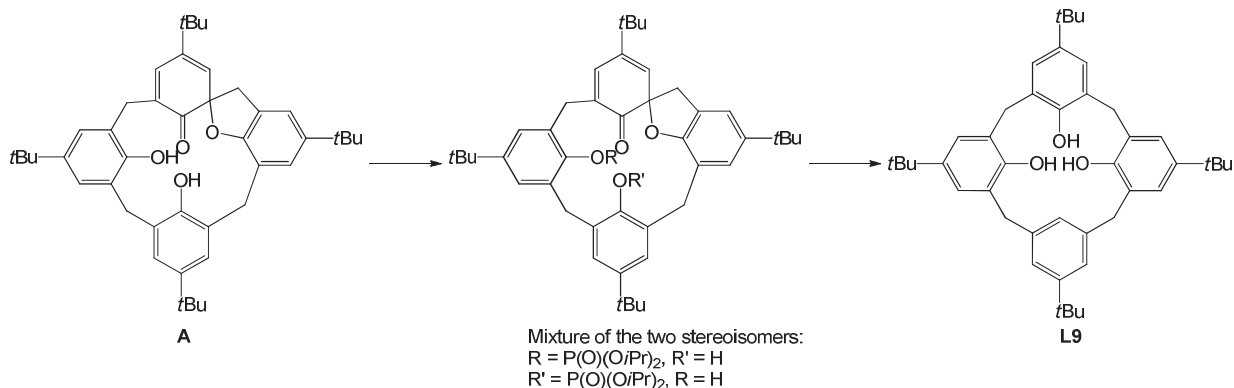
Several methods for the synthesis of  $[[4+]\text{-(OH)}_3(\text{H})]$  L9 derivatives are reported but in low yields. The first pathway consists in a  $[1 + 3]$  convergent synthesis of 3,5-bis-(2-hydroxy-5-methylbenzyl)toluene and 2,6-bis-(hydroxymethyl)-4-*tert*butylphenol *via* a modified Bohmer's route (**Scheme 20**).<sup>35</sup> Both syntheses of the linear trimeric and monomeric starting materials need too many steps, and the final condensation is not selective enough to get the  $[[4+]\text{-(OH)}_3(\text{H})]$  derivative in sufficient amount for further studies (< 10% yield).



Scheme 20: Synthesis of a  $[[4+]\text{-(H)(OH)}_3]$  derivative *via* a modified Bohmer's route

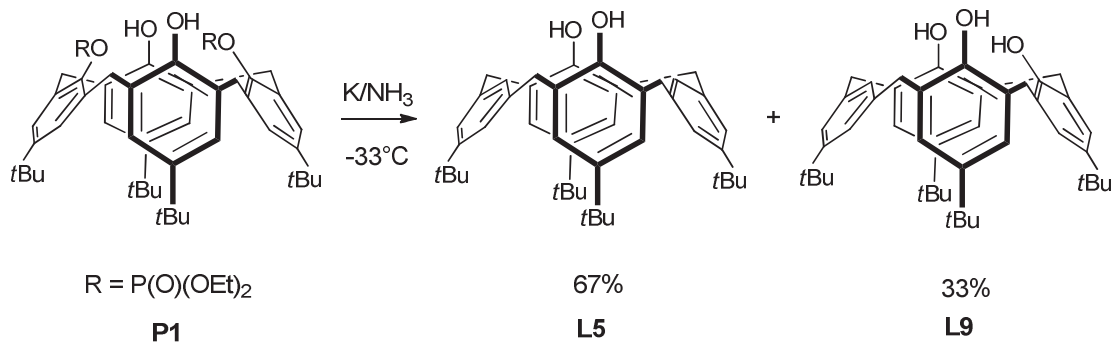
The monospirodiene route, was also described as a strategic tool to obtain  $[[4+]\text{-(OH)}_3(\text{H})]$  L9.<sup>36</sup> The monospirodiene A can be easily monophosphorylated with 1 eq. of LDA in dry THF at -78°C and ClP(O)(O*i*Pr)<sub>2</sub> in 47% yield. The resulting compound was

treated with K/NH<sub>3</sub> at -78°C to finally provide the [[4+]-OH)<sub>3</sub>(H)] **L9** in 57% yield (**Scheme 21**).



**Scheme 21:** Synthesis of [[4+]-OH)<sub>3</sub>(H)] **L9** via the monospirodiene route

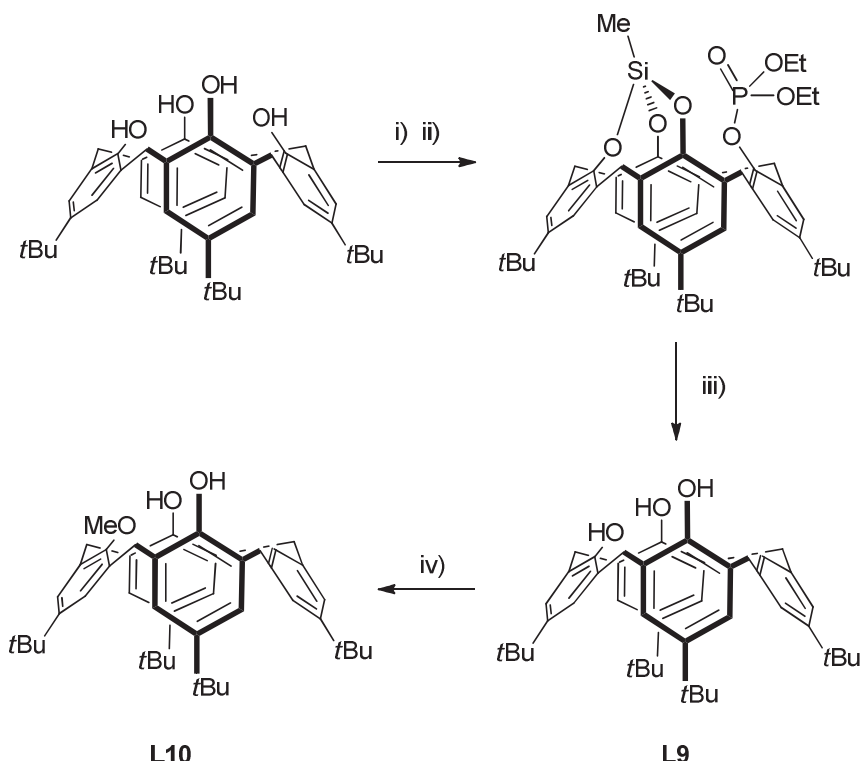
It is noteworthy that [[4+]-OH)<sub>3</sub>(H)] **L9** was first described by Biali *et al.* as a by-product of the reductive cleavage of **P1** with potassium in refluxing ammonia at -33°C, in low yield (**Scheme 22**).<sup>26</sup> The formation of [[4+]-1,3-(OH)<sub>2</sub>(H)<sub>2</sub>] **L5** and [[4+]-OH)<sub>3</sub>(H)] **L9** was based on the observation that under treatment of **P1** with K/NH<sub>3</sub>, as described in **section 4.2**, some Ar(O—P) bond cleavage takes place, in addition to the (Ar—O)P one. Increasing the reaction temperature to -33°C, instead of -78°C, the Ar(O—P) bond cleavage is slightly favored (**L9/L5**: 33/67).



**Scheme 22:** Synthesis of [[4+]-OH)<sub>3</sub>(H)] **L9** via the cleavage of **P1** at -33°C (Biali's route)

Even if the K/NH<sub>3</sub> conditions seem drastic, they provide very clean cleavage of the phosphorylated groups and require more attention to get **L9** in good yield. In an idealistic approach, [[4+]-OH)<sub>3</sub>(OP(O)(OEt)<sub>2</sub>)] could be the best precursor for the cleavage step to provide **L9**, but it has never been described because of its difficult synthesis. Indeed, the direct synthesis from [4+] with a substoechiometric quantity of the phosphorylating agent leads to a mixture of the starting material and several multisubstituted derivatives, certainly due to kinetics.<sup>26</sup>

In order to get selectively **L9** in larger scale (*ca.* 10 g), we herein report a new and selective three-step route, *via* the K/NH<sub>3</sub> cleavage. The first step consists in the protection of three of the four hydroxyl groups of [4+] with MeSiCl<sub>3</sub> as a selective protecting agent in presence of NEt<sub>3</sub>, according to the Lattman's method.<sup>37</sup> The unprotected OH-group is easily deprotonated with *n*BuLi and then reacted with ClP(O)(OEt)<sub>2</sub>, leaving the protected derivative in 65% yield. This latter was then treated with an excess of K/NH<sub>3</sub> at -78°C to finally provide **L9** in 44% yield (**Scheme 23**). The deprotection of the siloxane function occurs directly in the reductive K/NH<sub>3</sub> media.



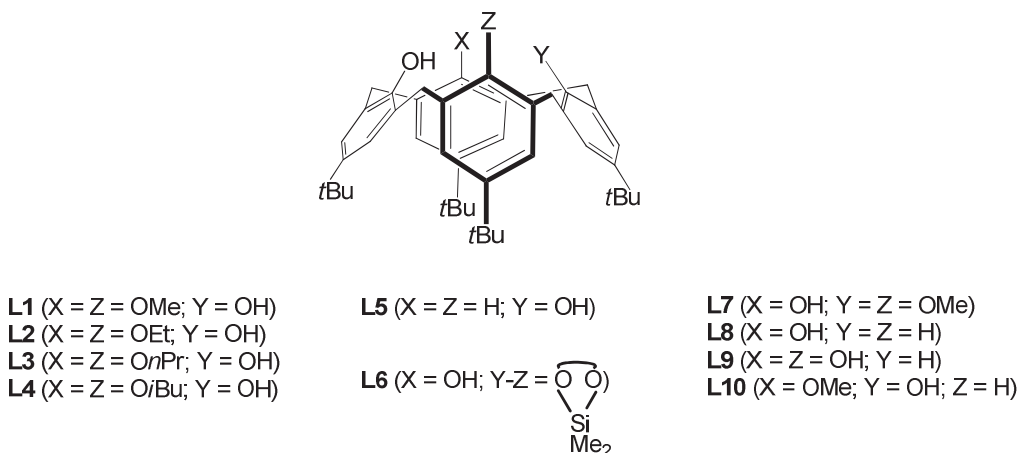
**Scheme 23:** Syntheses of [[4+]-H](OH)<sub>3</sub>] **L9** and [[4+]-1,3-(OH)<sub>2</sub>(OMe)(H)] **L10** *via* the cleavage of the protected monophosphorylated intermediate. Reagents and conditions: i) 1.1 eq. MeSiCl<sub>3</sub>, 5 eq. NEt<sub>3</sub>, toluene, RT, 2h; ii) 1.1 *n*BuLi, 1.1 eq. ClP(O)(OEt)<sub>2</sub>, toluene, RT, 2h; iii) xs. K/NH<sub>3</sub>, -78°C, 1h; iv) xs. MeI, 1.1eq K<sub>2</sub>CO<sub>3</sub>, MeCN, reflux, 24h

Reaction of **L9** with an excess of MeI in presence of K<sub>2</sub>CO<sub>3</sub> in refluxing MeCN provides **L10** in 63% yield in cone conformation, according to the method previously described by Fukazawa *et al.* (**Scheme 23**).<sup>38</sup> The mechanistic approach is similar of that of the diesters formation, since the middle hydroxyl proton is the more acidic.

#### 4.6 Conclusion

A series of functionalized *p*-*tert*-butylcalix[4]arenes **L1-L8** were synthesized either *via* etherification or dehydroxylation of the hydroxyl groups in 1,2- and the 1,3-positions, leaving

bis-anchoring ligands (**Scheme 24**). The tris-anchoring ligand **L9** was obtained from mono-dehydroxylation of *p*-*tert*butylcalix[4]arenes and easily derivated into its monomethoxy form **L10**. Each of those ligands has been prepared with a view to control both electronic and geometric environment of the metal center.



Scheme 24: *p*-*tert*butylcalix[4]arene derivative ligands (L1-L10)

## 5. Synthesis and characterization of bipodal (bis-chloro)titanacalix[4]arenes. Application in ethylene polymerization

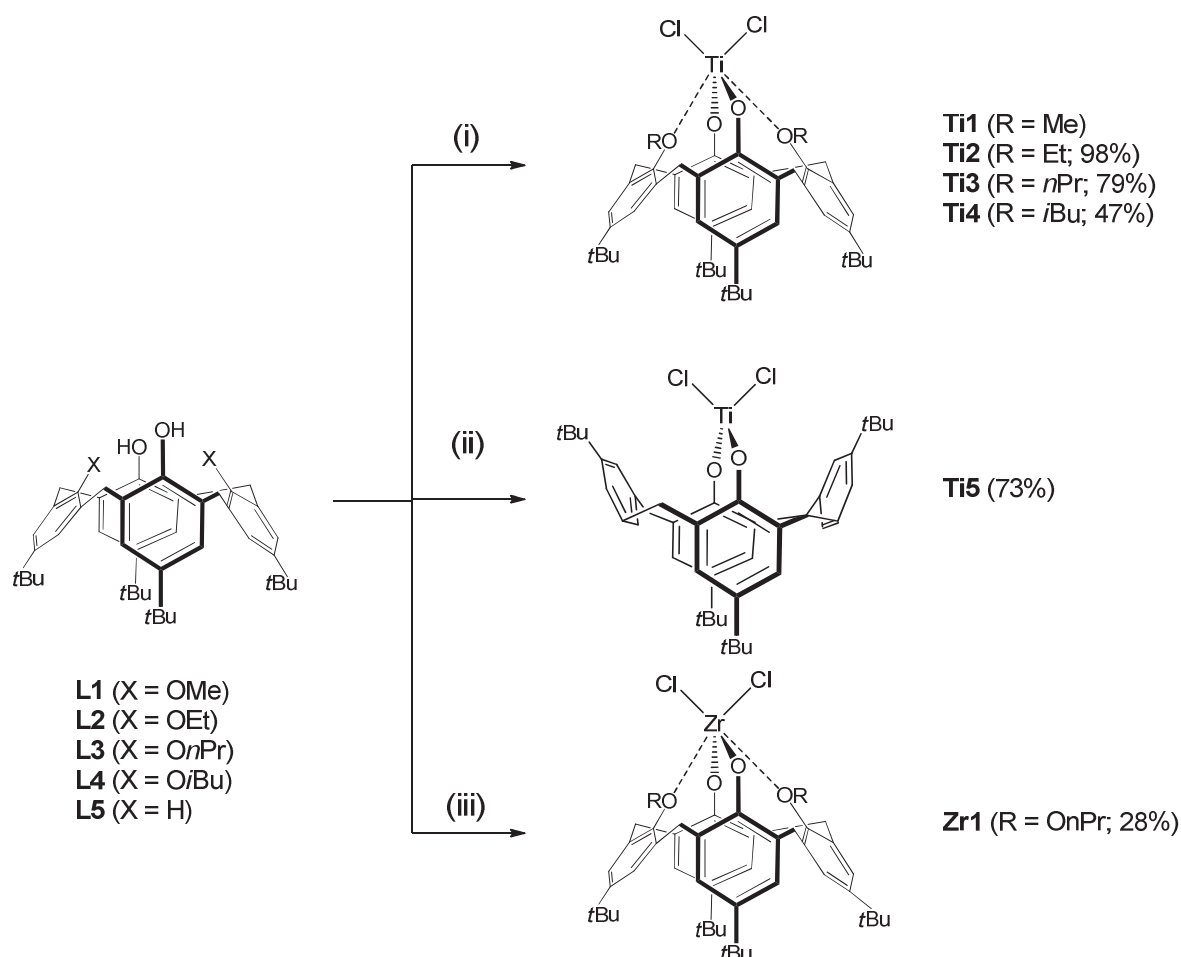
### 5.1 Syntheses of the bipodal (bis-chloro)titanacalix[4]arenes (Ti1-Ti9) and (bis-chloro)zirconacalix[4]arene (Zr1)

With the aim of understanding the role of steric hindrance, bite angle and coordination of titanium and zirconium towards polymerization of ethylene, we report the preparation and the characterization of a series of new titanacalix[4]arene and zirconacalix[4]arene systems belonging to classes **A–F**. The relationship structure-activity will be discussed based on the coordination modes of the metal and the conformation of the calixarene ligand using NMR and X-ray diffraction results.

#### 5.1.1 Preparation and conformational studies of the distal complexes presenting two alkoxy ligands (Ti1-Ti4 and Zr1):

The 1,3-(bis-alkoxy)bis-chlorotitanacalix[4]arene **Ti1-Ti4** have been synthesized by reacting the corresponding ligand **L1-L4** with  $\text{TiCl}_4 \cdot 2\text{THF}$  in toluene in moderate to good yield (47-98 %) (**Scheme 25**). According to Radius' observation<sup>9b</sup>, the reactions were carried out at 60°C over 24h to avoid the  $\sigma$ -bond metathesis between a Ti-Cl and an O-R bond with R-Cl evolution. Above this temperature (*i.e.* refluxing toluene), the  $\sigma$ -

bond metathesis occurs due to the proximity between the alkoxy groups and the titanium center imposed by the calixarene core (*vide infra*, Figures 3-5), providing tripodal titanacalix[4]arene. In contrast, the corresponding complex  $[[4+]-1,3-(\text{OMe})_2(\text{O})_2\text{ZrCl}_2]$  was selectively obtained from a refluxing toluene solution between  $\text{ZrCl}_4 \cdot 2\text{THF}$  and **L1**. Stability of the zirconium center toward  $\sigma$ -bond metathesis with its neighboring methoxy group is due to its less Lewis acidic character than Ti. Surprisingly, the complex  $[[4+]-1,3-(\text{OnPr})_2(\text{O})_2\text{ZrCl}_2]$  **Zr1** couldn't be synthesized directly from a refluxing toluene solution of  $\text{ZrCl}_4 \cdot \text{THF}$  and **L3** because of the very slow and non selective reaction. Then **L3** was first deprotonated with  $n\text{BuLi}$  in THF and then reacted with  $\text{ZrCl}_4 \cdot 2\text{THF}$  over 2h. Purification of the crude product with small amount of pentane only provided the wanted complex in 28% yield.



Scheme 25: Syntheses of the distal di(chloro)titana- Ti5-Ti6 and zirconacalix[4]arene Zr1

<sup>1</sup>H NMR spectra of **Ti1-Ti4** display a similar pattern of signals with two sets of doublets attributed to the methylene protons ( $\text{ArCH}_2\text{Ar}$ ), consistent with the calixarene being in cone conformation. Moreover, the sets of two signals for  $\text{C}(\text{CH}_3)_3$  and for  $\text{ArH}$  and the

signals for each proton of the alkoxy chain are characteristic of a  $C_{2v}$  symmetry. It is noteworthy for **Ti1** that in the  $^1\text{H}$  spectrum, the methoxy groups are equivalent as supported by a single singlet around 4.1 ppm. Finally, the significant  $\Delta\text{ppm}$  of the  $\alpha$ -protons of the alkoxy chains observed between the free ligands **L1-L4** and the corresponding complexes **Ti1-Ti4** indicates that the oxygens of the alkoxy chains participate as ancillary ligands to the coordination with the titanium atom.

Suitable crystals of **Ti2-Ti4** were obtained by cooling saturated toluene solutions to -30°C (see Annex III for crystallographic data). The molecular structures of **Ti2-Ti4** have not been documented but that of **Ti1** has previously been reported by Radius.<sup>9b</sup> The molecular structures of **Ti2-Ti4** have a similar arrangement (**Figures 3-5**): they consist of a monomeric compound in which the calixarene core is in an elliptic distorted cone conformation, coordinated to a single titanium atom. Both alkoxy groups are rejected out of the cone, in a  $C_{2v}$  symmetry, except the ethyl derivative which presents a  $C_s$  symmetry. Hexacoordinated titanium is bound to two phenoxy, two ethers and two terminal chlorines, mutually in *cis*-position. The resulting geometry is a distorted octahedron (relevant distances and angles are reported in **Table 1**). Each compound shows similar angles close to 180°C for the groups *trans* to each other ( $\text{Cl}_1\text{-Ti-O}_2$ ,  $\text{O}_3\text{-Ti-O}_4$ ). The ( $\text{O}\text{-Ti-O}$ ) bite angle alpha lies in the same range for all the complexes with values consistent with those of **Ti1** (*i.e.*,  $\alpha = 94.83^\circ$ ).

**Table 1:** Selected bonds length and angle for **Ti2**, **Ti3** and **Ti4**.

Distances (Å)	Ti2	Ti3	Ti4
Ti···O <sub>1</sub>	1.77(6)	1.78(6)	1.77(6)
Ti···O <sub>3</sub>	2.11(0)	2.12(2)	2.16(7)
Ti···Cl <sub>1</sub>	2.31(9)	2.34(0)	2.34(6)
Angle O <sub>1</sub> -Ti-O <sub>2</sub> (°)	95.3(2)	95.4(0)	97.0(7)
Angle O <sub>3</sub> -Ti-O <sub>4</sub> (°)	170.3(5)	171.7(6)	171.1(3)
Angle Cl <sub>1</sub> -Ti-O <sub>2</sub> (°)	178.3(4)	174.8(6)	173.4(3)
Angle Cl <sub>2</sub> -Ti-O <sub>1</sub> (°)	172.8(4)	174.7(6)	173.9(3)
Angle Cl <sub>1</sub> -Ti-Cl <sub>2</sub> (°)	86.6(2)	87.31(3)	87.11(12)

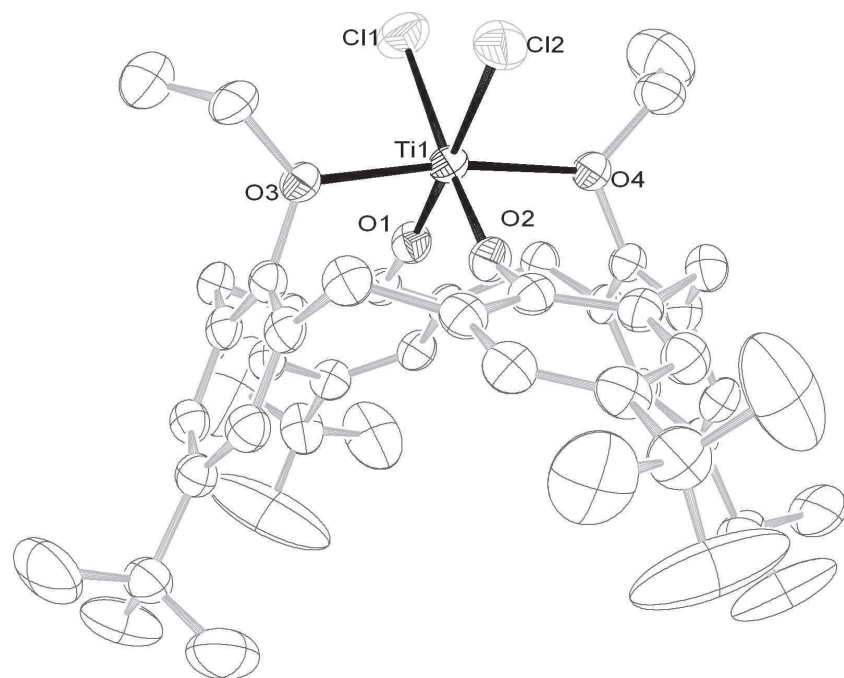


Figure 3: Molecular structure of  $\text{Ti}_2$  (only one of the two molecules of the unit cell is shown). For clarity H atoms and solvent molecules were omitted.

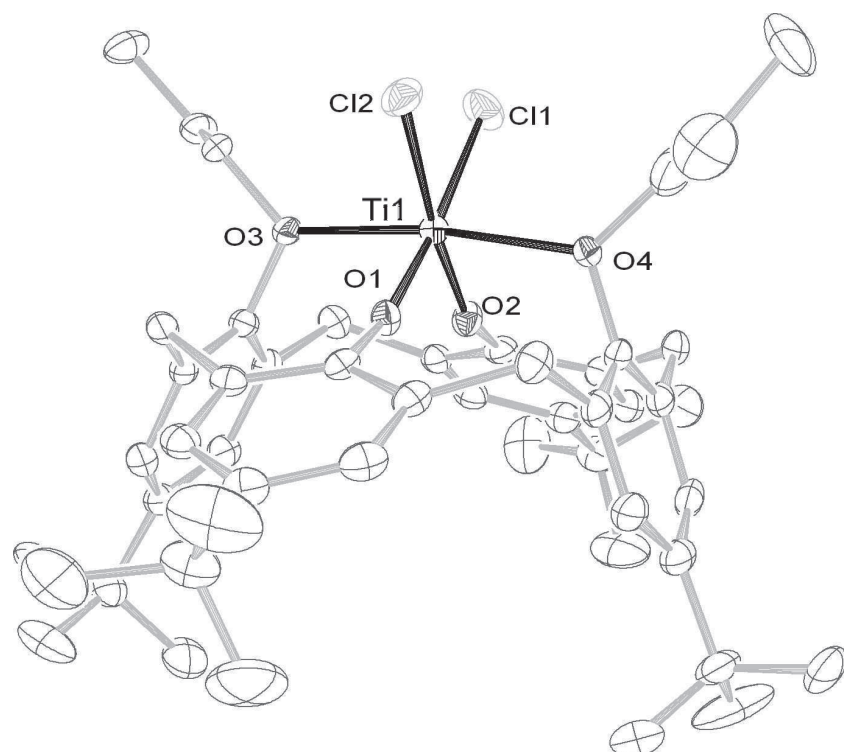
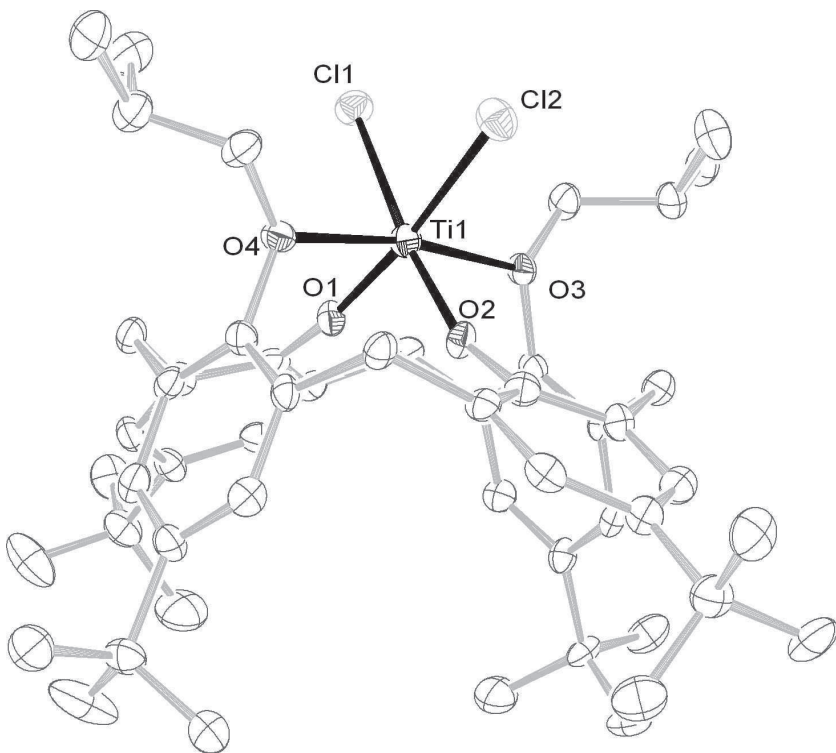


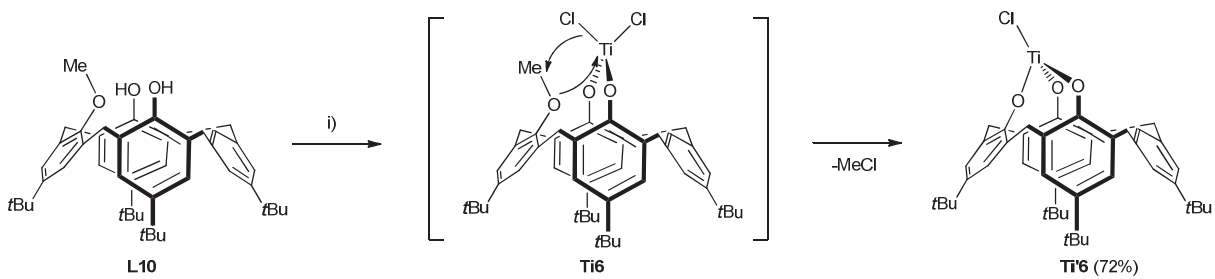
Figure 4: Molecular structure of  $\text{Ti}_3$  (only one of the two molecules of the unit cell is shown). For clarity H atoms and solvent molecules were omitted.



**Figure 5:** Molecular structure of **Ti4** (only one of the two molecules of the unit cell is shown). For clarity H atoms and solvent molecules were omitted.

### 5.1.2 Preparation and conformational studies of the distal complex presenting one methoxy ligand (**Ti6**)

Synthesis of the complex **Ti6** was attempted to study the influence of only one methoxy group, in comparison to its analogue **Ti1**, showing an extra coordinance. Surprisingly, reaction between  $\text{TiCl}_4$  and the ligand **L10** afforded the tripodal complex **T'6** (**Scheme 26**). We suppose the titanium close enough to the methoxy oxygen to substitute the methyl fragment and form an O-Ti  $\sigma$ -bond, thus leading to the complex **T'6**, even in mild conditions (RT). This unexpected reactivity can be explained by the lack of stability provided by tris-chelating **L10** compared to the tetra-chelating ligands counterparts (**L1-L4**).



**Scheme 26:** Synthetic pathway and mechanistic approach for  $[4+]-1,3-(\text{O})_3(\text{H})\text{TiCl}] \text{ T}'6$ . Reagents and conditions: i) 1 eq.  $\text{TiCl}_4$ , toluene, TA, 5 h

### 5.1.3 Preparation and conformational studies of the distal complex free of alkoxy ligand (**Ti5**)

Ligand free complex **Ti5** was synthesized from the bis-dehydroxylated calixarene **L5** and  $\text{TiCl}_4$  at RT in toluene in 73% yield (**Scheme 25**).  $\text{TiCl}_4$  was expected to be a better precursor for the synthesis of **Ti5** than its corresponding THF adduct  $\text{TiCl}_4\cdot 2\text{THF}$ , as it is assumed to afford the titanacalix[4]arenes uncoordinated to any spectator ligand. Many efforts were done to synthesize the zirconium analogue of **Ti5**, either from  $\text{ZrCl}_4$  or  $\text{ZrCl}_4\cdot 2\text{THF}$ , with **L5** or its deprotonated analogue, but leading to complex mixtures in each case. Kinetics could be highlighted in the way that  $\text{ZrCl}_4$  reacts slowly with aryloxide derivatives and the first and the second addition of the ligand **L5** onto  $\text{ZrCl}_4$  may occur in similar kinetic range.

On the  $^{13}\text{C}$  NMR spectrum, a single signal at 38 ppm is assigned to  $\text{ArCH}_2$ . This value is typical of calixarenes having pairs of neighbouring phenoxy groups *anti*-oriented. The  $^1\text{H}$  NMR spectrum displays three sets of two signals for the methylene, for the *tBu* and for the ArH protons, indicating a plane of symmetry in the structure (**Figure 6**). These observations led us to consider that the complex **Ti5** adopts an 1,3-alternated conformation. This receives further support from 2D experiments as the NOESY spectrum reveals a spatial interaction between the proton in *ipso* of one aryl and the *meta*-ArH of the neighbour's aryl unit, confirming the 1,3-alternated conformation (**Figure 6**).

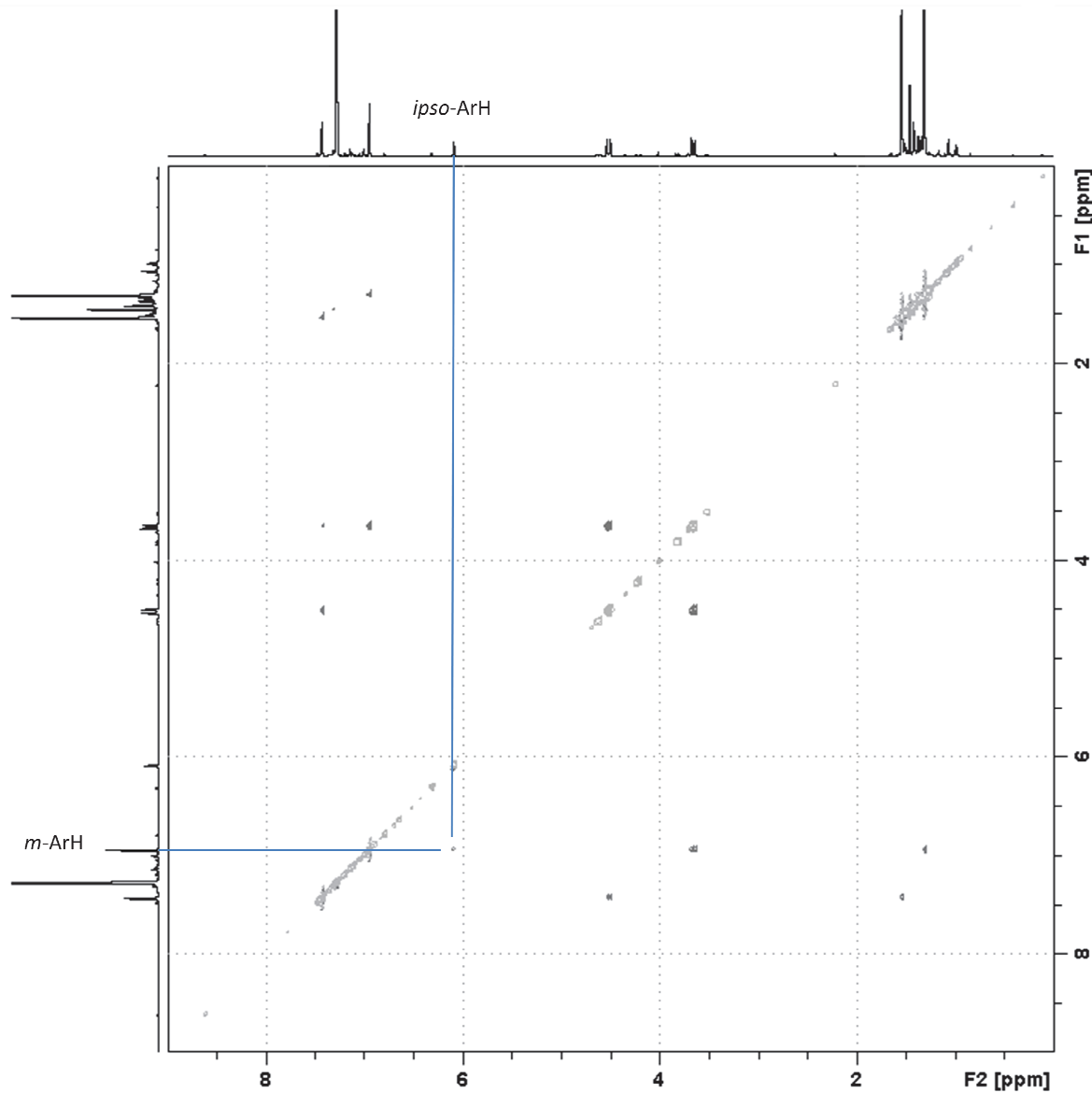
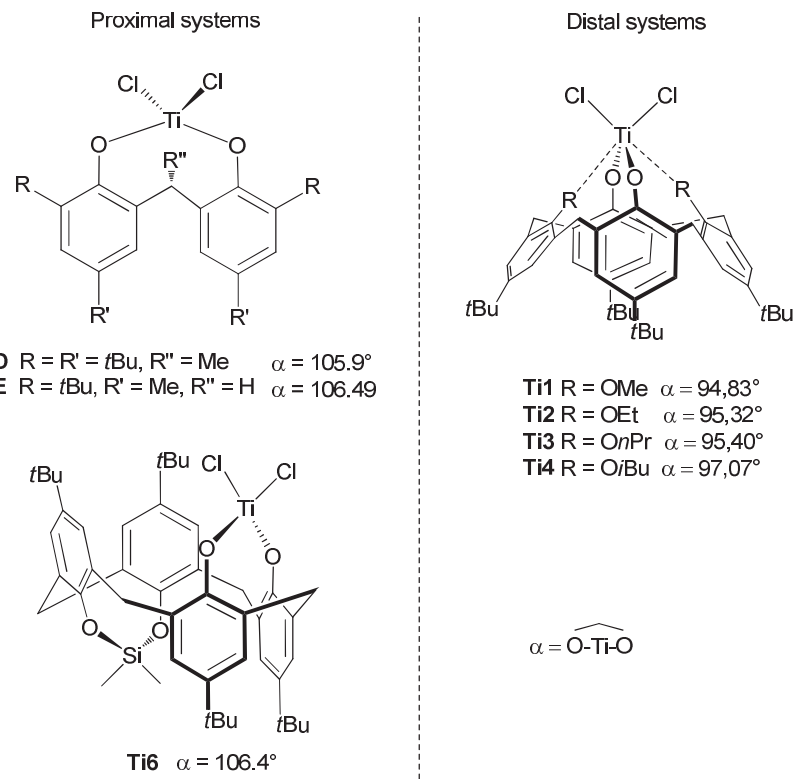


Figure 6: NOESY 2D-NMR experiment of Ti5

#### 5.1.4 Preparation and conformational studies of the proximal complexes (Ti6-Ti8): study of the bite-angle effect

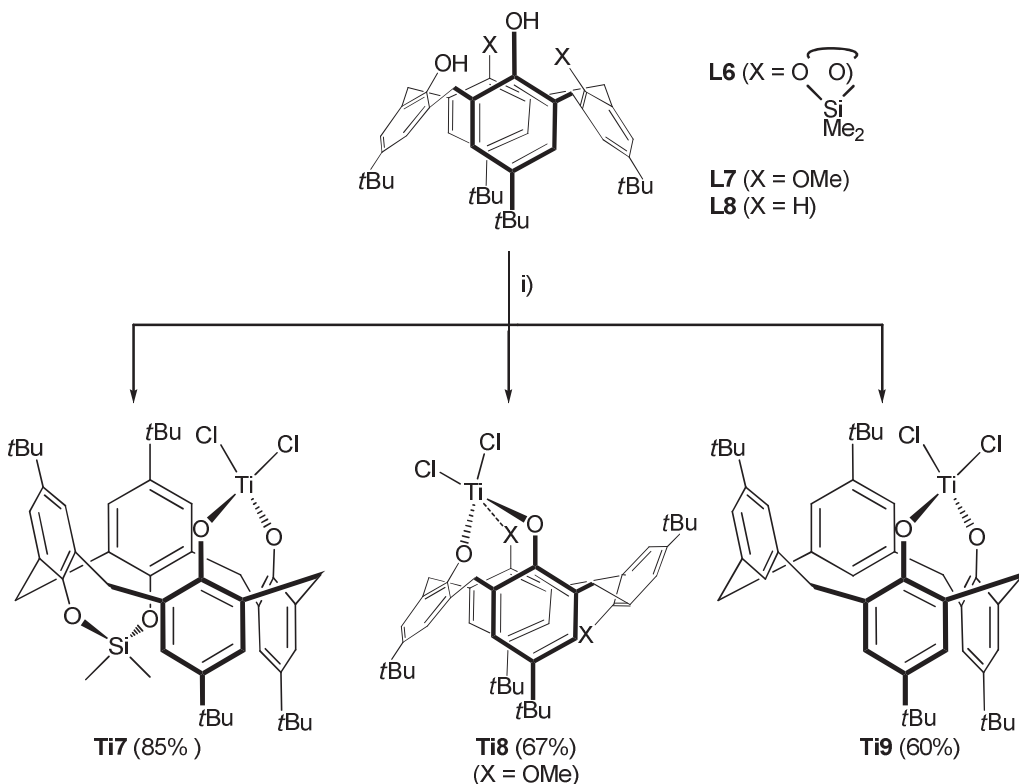
Proximal bipodal complexes will help to understand the real effect of the O-Ti-O bite-angle onto the catalytic properties of the metal center, by comparison of the corresponding distal analogues. Literature reports several bis-aryloxyde-based complexes of titanium with well-defined structural properties, considered as pseudo-calixarenic systems. For instance, reported X-Ray structures of the following compounds (**D**<sup>39</sup>, **E**, **Ti1**<sup>9b</sup>, **Ti2-Ti4**, **Ti6**<sup>40</sup>) permit to know the tendency of the O-Ti-O bite angles of (bis-chloro)-titanacalix[4]arenes and pseudo-calixarenic systems presenting distal and proximal anchoring points (**Scheme 27**).

There is evidence that proximal systems show more open bite-angles around  $106^\circ$ , whereas distal system bite angle are around  $95\text{-}97^\circ$ .



**Scheme 27: Reported (dichloro)-titanacalix[4]arenes and pseudo-calixarenic systems presenting distal and proximal anchoring points**

The proximal bis-(chloro)titanacalix[4]arenes **Ti7-Ti9** have been synthesized by reacting the corresponding ligand **L6-L8** with one equivalent of  $\text{TiCl}_4$ , at  $25^\circ\text{C}$  over 16h, in 60-85% yield (**Scheme 28**). As precised for the complex **Ti5**, the precursor  $\text{TiCl}_4$  was preferred to its THF adduct in order to avoid spectator ligand in the resulting complexes. The complexes **Ti8** and **Ti9** are new or unreported.



**Scheme 28:** Synthesis of the proximal chloro titanacalix[4]arenes **Ti7-Ti9**. Reagents and conditions: i) 1 eq.  $\text{TiCl}_4$ , toluene, RT, 16 h

Despite many attempts, proximal OH-depleted bipodal zirconium has never been obtained. Reactions of  $\text{ZrCl}_4$  and  $\text{ZrCl}_4 \cdot 2\text{THF}$ , with the neutral or the previously deprotonated ligand **L6** were totally no-selective.

The  $^1\text{H}$  NMR spectrum signature of **Ti8**, with a series of eight signals for the methylene protons, clearly indicates an asymmetrical species (**Figure 7**). Two singlets, at 1.67 and 4.09 ppm, can be assigned to the protons of the two methoxy groups bore by **L7**; the value of the latter is consistent with the oxygen of the methoxy coordinated to the titanium ( $\text{OMe}_{\text{out}}$ ). The drastic upfield shift observed for the other methoxy group ( $\Delta\text{ppm} = -2.2$ ) indicates that the corresponding aromatic ring remains uncoordinated and can undergo an inversion, thus orienting the  $\text{OMe}$  deeply inside the cavity ( $\text{OMe}_{\text{in}}$ ). 2D NMR investigations were undertaken to determine the conformation of **Ti8** (**Figure 7**) and confirm the spatial interactions between the methyl protons of  $\text{OMe}_{\text{in}}$  and the aromatic protons. Assuming the titanium atom is coordinated by the proximal alkoxy units, the calixarene **Ti8** can adopt a partial cone conformation. This is in contrast with the  $^1\text{H}$  NMR spectrum of the free ligand **L7** that adopts a classical cone conformation with only minor conformations being observed at NMR time scale.<sup>32</sup>

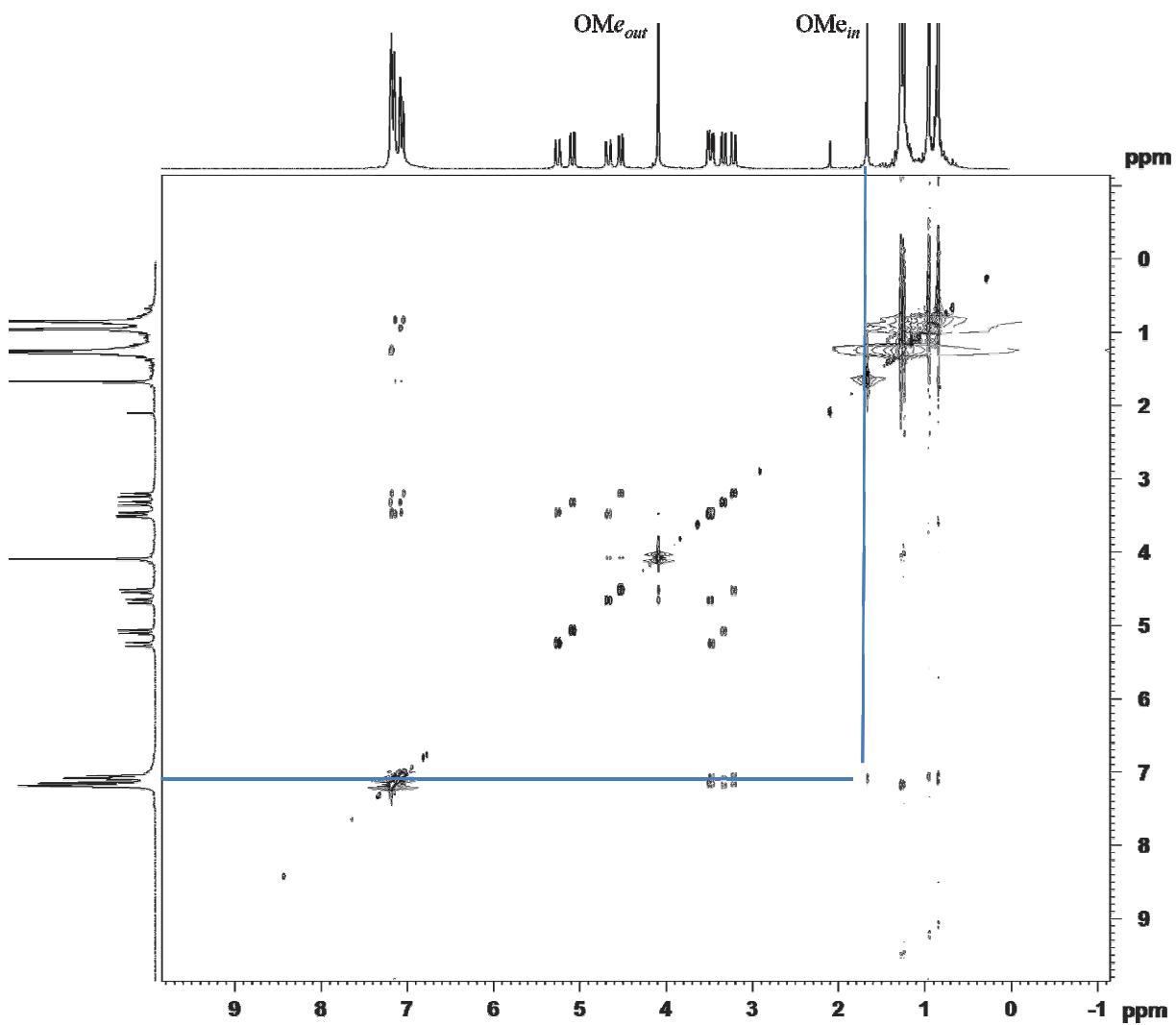


Figure 7: NOESY 2D-NMR experiment of Ti8

In the  $^1\text{H}$  NMR spectrum of complex **Ti9**, two sets of signals that can be assigned to *t*Bu protons indicate a plane of symmetry in the complex. Moreover, the six sets of signals for the methylene protons (1,2,2,1,1,1 integration) and the four sharp signals for ArH (2,2,2,2 *ortho*-ArH) confirm a frozen 1,2-alternate conformation (**Figure 8**). All the signals of **Ti9** have been attributed *via* H-C correlation in 2D NMR. Finally, NOESY spectrum of **Ti9** shows a correlation between the proximal  $\text{C}(\text{CH}_3)_3$  groups and is in full agreement with such an 1,2 alternated conformation (**Figure 8**). The conformational behavior of **Ti9** can be directly compared to the parent compound **Ti7<sup>40</sup>**, which was described in the same locked 1,2 alternated conformation.

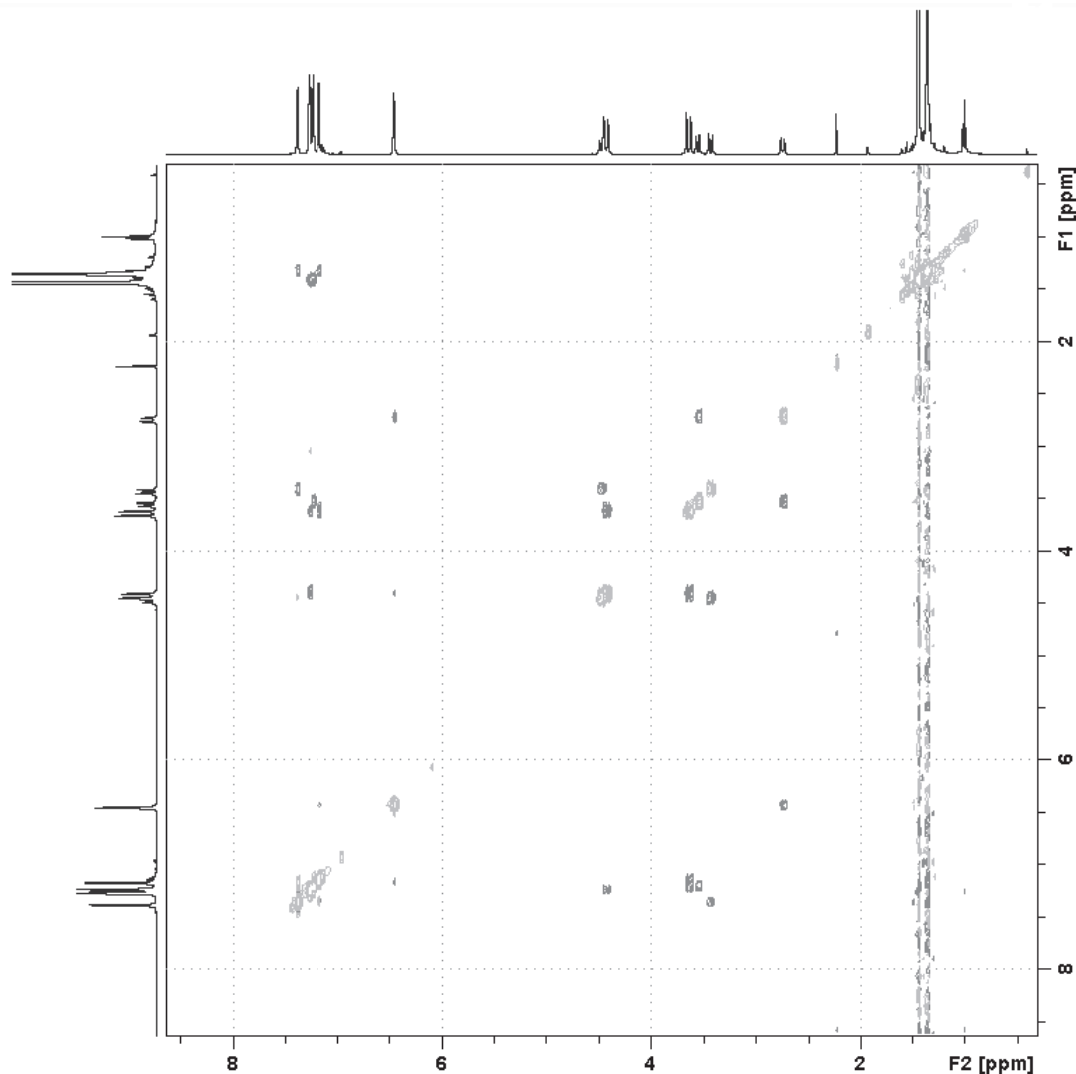


Figure 8: NOESY 2D-NMR experiment of Ti9

### 5.1.5 Conclusion

A series of titanacalix[4]arenes **Ti1–Ti9** and zirconacalix[4]arene derivatives **Zr1** has been synthesized and fully characterized by NMR spectroscopy and single-crystal X-ray diffraction studies (for **Ti2–Ti4**) to determine their conformation and their coordination mode. Distal titanacalix[4]arenes were identified as tetra-coordinate, class **A** (**Ti1–Ti4, Zr1**), or bis-coordinate, class **C** (**Ti5**). Proximal titanacalix[4]arenes were tris-chelating, class **D** (**Ti8**), and bis-chelating, class **E** (**Ti7 and Ti9**). To evaluate the influence of the coordination sphere of the titana-calix[4]arenes on their catalytic activity, **Ti1–Ti5** and **Ti7–Ti9** were screened for ethylene polymerization. In addition, a comparison between activities of **Ti3** and its zirconium analogue **Zr1** was done to evaluate the propensity of each metal to polymerize ethylene.

## 5.2 Catalytic properties of the bipodal (bis-chloro)titanacalix[4]arene and (bis-chloro)zirconacalix[4]arene complexes (Ti1-Ti5, Ti7-Ti9, Zr1)

### 5.2.1 Experimental conditions and results

The metallacalix[4]arenes **Ti1-Ti5**, **Ti7-Ti9** and **Zr1** were screened for ethylene polymerization under our standard conditions (see experimental part). **Table 2** summarizes the activities observed with the different complexes activated with 1400 eq. of MAO (**Ti1-Ti9/MAO** and **Zr1/MAO**) and keeping the experimental conditions constant ( $P = 30$  bar and  $T = 50^\circ\text{C}$ ). The performance of the different catalysts will be first discussed before moving on the optimization of the polymerization conditions.

**Table 2:** Ethylene polymerization results for **Ti1-Ti8/MAO** and **Zr1/MAO**.[a]

Entry	Catalyst	Yield	Activity <sup>[b]</sup>	$M_n^{[c]}$	$M_w/M_n$	$T_m^{[d]}$
1	<b>Ti1</b>	0.028	14	2.9	2.7	132.0
2	<b>Ti2</b>	0.034	16	2.7	2.5	132.4
3	<b>Ti3</b>	0.045	21	3.2	2.9	131.8
4	<b>Ti4</b>	0.033	16	2.3	3.0	131.4
5	<b>Ti5</b>	0.388	185	2.6	3.3	133.2
6	<b>Ti7</b>	0.238	113	1.7	4.4	137.4
7	<b>Ti8</b>	0.174	83	n/d	n/d	133.6
8	<b>Ti9</b>	0.735	350	1.4	5.4	134.6
9	<b>Zr1</b>	0.039	18	-	-	-

[a] All polymerization experiments were conducted at  $50^\circ\text{C}$  under 30 bar of ethylene for 120 min, using  $1.05\ \mu\text{mol}$  of catalyst precursor in 50 ml of toluene ( $[\text{Ti}] = 2.1 \times 10^{-5}\ \text{M}$ ) ; [b] Average activity in  $\text{kg}_{\text{PE}}.\text{mol}^{-1}(\text{Ti}).\text{h}^{-1}$  calculated over the whole polymerization time (120 min). [c] masses ( $\times 10^6\ \text{g}.\text{mol}^{-1}$ ) determined by HTSEC in 1,2,4-trichlorobenzene at  $150^\circ\text{C}$ , measured with a relative calibration based on standard polystyrene. [d] Determined by DSC (second heating).

For all runs (entries 1-9, **Table 2**), the melting temperatures ( $T_m$ ) of the polymers are similar (from 131.4 to 134.6°C, example of **Ti9**, **Figure 9**). All systems produced a similar type of polyethylene consistent with the range observed for high density polyethylene HDPE or UHMWPE.

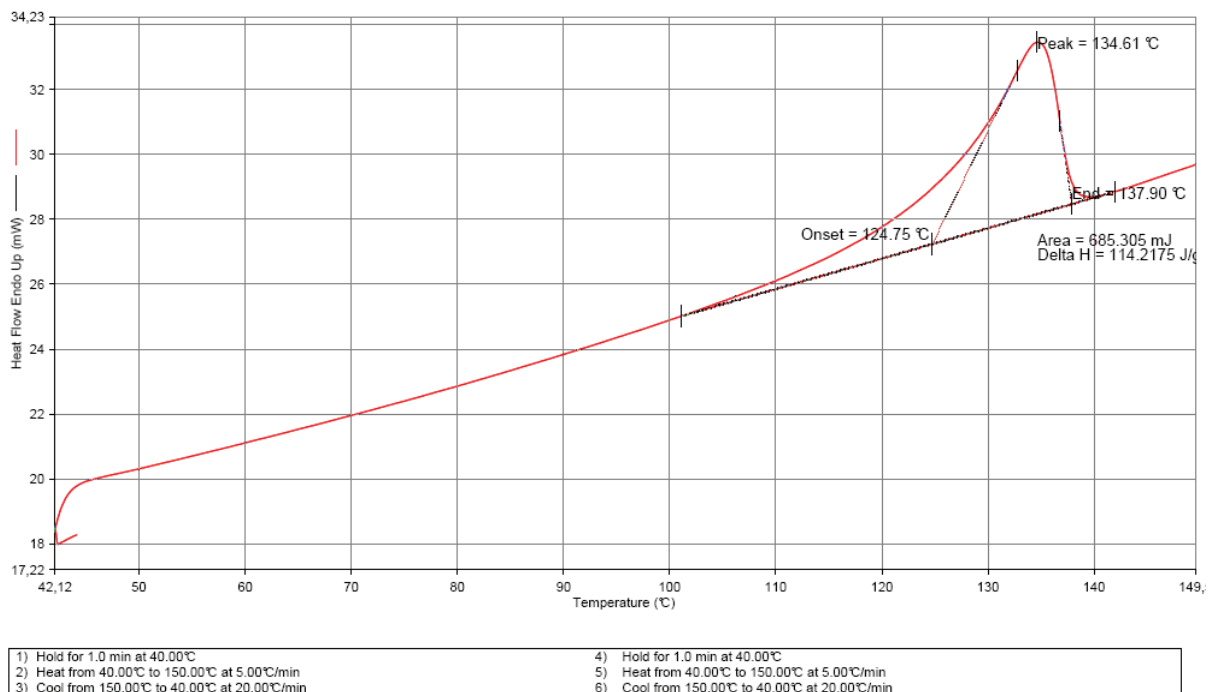


**Figure 9: DSC spectrum of polyethylene obtained at 50 °C in the presence of Ti9/MAO**

The average molar mass ( $M_n$ ) and the molar mass distribution ( $M_w/M_n$ ) of PE measured with high temperature size exclusion, suggest the occurrence of two different types of catalytic performance. For **Ti1-Ti5/MAO** (entries 1-5, **Table 2**),  $M_n$  are the highest, ranging from  $2.3$  to  $3.2 \times 10^6$  g.mol $^{-1}$ , which is typical of UHMWPE. In the case of **Ti7/MAO** and **Ti9/MAO**, the  $M_n$  values were significantly lower ( $1.7 \times 10^6$  g.mol $^{-1}$  and  $1.4 \times 10^6$  g.mol $^{-1}$ , respectively), consistent with HDPE. It is well established that increased protection around the catalytically active centre hinders the rate of chain transfer thus leading to the production of higher molecular weights.<sup>41</sup> The variation observed in the centre of the molecular weight distribution can be attributed to the difference of steric protection imparted by the calixarene backbone toward the titanium catalyst (**Ti1-Ti5/MAO** vs. **Ti7-Ti9/MAO**). In the same condition, the zirconium complex **Zr1/MAO** (entry 9, **Table 2**) gives similar activity compared to its titanium analogue **Ti3**. For **Ti7-Ti9/MAO** species, the titanium atom is supported in proximal position by *p*-*tert*butylcalix[4]arenes. In these cases, good catalytic activities for ethylene polymerization have been observed (entries 6-8, **Table 2**), **Ti9/MAO** exhibiting the highest and unprecedented activity for titanocalixarenes ( $350$  kg<sub>PE</sub>.mol $^{-1}$ (Ti).h $^{-1}$ ). **Ti5/MAO** ( $185$  kg<sub>PE</sub>.mol $^{-1}$ (Ti).h $^{-1}$ ), **Ti7/MAO** ( $113$  kg<sub>PE</sub>.mol $^{-1}$ (Ti).h $^{-1}$ ) and **Ti8/MAO** ( $83$  kg<sub>PE</sub>.mol $^{-1}$ (Ti).h $^{-1}$ ) show reduced activities, **Ti1-Ti4/MAO** displaying only moderate activities of  $21$  kg<sub>PE</sub>.mol $^{-1}$ (Ti).h $^{-1}$ .

### **5.2.2 Influence of the coordination mode on the catalytic performance of the metal center: effect of the electronic and geometric environment**

In term of the relative disposition of the titanacalix[4]arene, the direct comparison between **Ti5/MAO** and **Ti9/MAO** suggests that proximal geometry leads to better activity than distal counterparts. It is noteworthy that, when comparing the bond angle O-Ti-O of these titanium complexes, it is significantly larger in proximal titanacalix[4]arenes such as **Ti9**, with 106.4°, than for their distal counterpart (*i.e.*, **Ti1** (96.2°)).<sup>40</sup> This means that **Ti9** adopts a geometry closer to tetrahedron or distorted square plane in comparison with **Ti5** which seems to be close to an octahedron.

**Ti5/MAO** (class **C**), displays a much higher activity (185 kgPE.mol-1(Ti).h-1) and leads to higher molecular weight (entry 5, **Table 2**), compared to **Ti1-Ti4/MAO** (class **A**). This difference of behavior is probably due to the octahedral geometry of **Ti1-Ti4** which prevents olefin coordination after alkylation and Ti cation formation. In comparison, the coordinative unsaturations of **Ti5**, especially after alkylation and cationic formation due to the presence of MAO, could lead to highly unsaturated and very electrophilic titanium center. In other words the presence of two electron-donating oxygen atoms from the alkoxy groups coordinated to the metal increases both coordination number and electron density of the titanium center by  $\pi$ -donation to the active site. Accordingly, these geometric and electronic parameters make the coordination of ethylene to the metal centre more difficult which reduces the catalytic activity.

In proximal systems (**Ti7/MAO-Ti9/MAO**) as in distal system (**Ti1/MAO-Ti5/MAO**), increasing the number of the substituents on the proximal positions seems also to decrease the catalytic activity. In addition, **Ti1-Ti4/MAO** (entries 1-4, **Table 2**) revealed comparable low catalytic activities (up to *ca.* 21 kgPE.mol<sup>-1</sup>(Ti).h<sup>-1</sup>). These results suggest that a similar active species occurs in all four cases regardless of the nature of the alkoxy groups in distal positions. It appears that under these experimental conditions the steric effect of the various alkoxy ligands in distal positions affects neither the activities nor the polymer properties. Finally, the low activity of the dimethylsilyl-bridged titanium complex **Ti7/MAO** in comparison to the complex **Ti9/MAO** is probably attributed to the alkylation of the alkoxysilane part by MAO cocatalyst and the generation of a calixarene-aluminium alkyl species. The conformation of the latters might change in such a way to enhance the electron donors of the silicon to the titanium metal center.<sup>42</sup>

### 5.2.3 Influence of the pressure and the temperature parameters. Optimization of the catalysis

**Ti9/MAO**, due to its good performance, was retained as a favored candidate to optimize temperature and pressure conditions. Polymerization was performed firstly at constant pressure (30 bar) while increasing the temperature from 50 to 90°C (**Table 3, Figure 10**). In a second set of experiments, the temperature was maintained at 70°C with pressures ranging from 5 to 30 bar (**Table 3, Figure 11**). Finally, the initial activity was determined by shortening the length of the run to 15 min under the optimal condition of pressure and temperature.

**Table 3:** Ethylene polymerization results for Ti9/MAO

Entry	T [°C]	P [bar]	Yield [g]	Activity <sup>[b]</sup>	M <sub>n</sub> <sup>[c]</sup>	M <sub>w</sub> /M <sub>n</sub>	T <sub>m</sub> <sup>[d]</sup> [°C]
1	50	30	0.735	350	1.4	5.4	134.6
2	60	30	1.23	586	2.3	3.5	136.6
3	70	30	1.62	770	1	4.9	133.9
4	80	30	1.45	690	0.6	3	134.9
5	70	5	0.11	52	0.6	5.9	133.9
6	70	10	0.28	131	0.8	3.9	134.0
7	70	20	0.82	390	1.3	3.5	134.0
8	70	30	1.62	770	1	4.7	135.5
9 <sup>[e]</sup>	70	30	0.7	667	1.2	5.4	135.5

[a] All polymerization experiments were conducted for 120 min, using 1.05 µmol of catalyst precursor 6 in 50 ml of toluene ([Ti] = 2.1 × 10<sup>-5</sup> M); [b] Average activity in kg<sub>PE</sub>.mol<sup>-1</sup>(Ti).h<sup>-1</sup> calculated over the whole polymerization time (120 min); [c] masses (x 10<sup>6</sup> g.mol<sup>-1</sup>) determined by HTSEC in 1,2,4-trichlorobenzene at 150 °C, measured with a relative calibration based on standard polystyrene; [d] Determined by DSC (first heating); [e] run quenched after 15 mn

The activity of **Ti9/MAO** was found to be maximal at 70°C and 30 bar, giving an unprecedented value of 770 kg<sub>PE</sub>.mol<sup>-1</sup>(Ti).h<sup>-1</sup>. A significant decrease was observed at higher temperature, due probably to thermal decomposition. The PE produced seems to be largely unaffected by the change of temperature as T<sub>m</sub> for all runs were spanning from 133.9 to 136.6°C. However, M<sub>n</sub> showed significant variations with the higher molecular weight (2.3 x 10<sup>6</sup> g.mol<sup>-1</sup>) produced at 60°C and the lower at 80°C (**Table 3**). This suggests that the rate of chain termination or chain transfer increases much faster than the chain propagation by increasing the polymerization temperature.

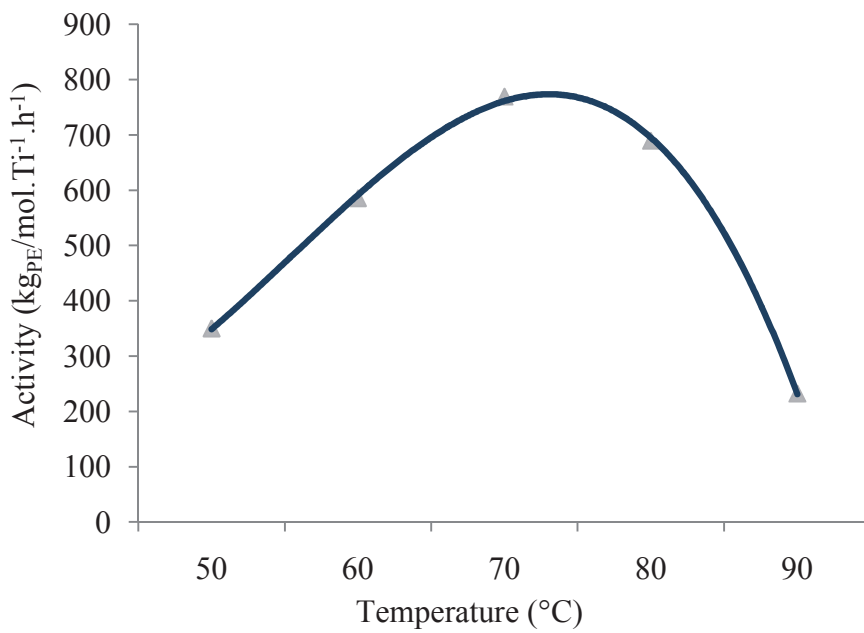


**Figure 10:** Ethylene polymerization with Ti9/MAO as catalyst at temperatures ranging from 50 to 90°C and constant pressure (30 bar)

The influence of the ethylene pressure on the activity was also studied at this optimum temperature of 70°C (**Figure 11**). As the ethylene pressure is raised from 5 to 30 bar, both the yield and catalyst activity increase as expected for such systems (entries 5-8, **Table 3**).

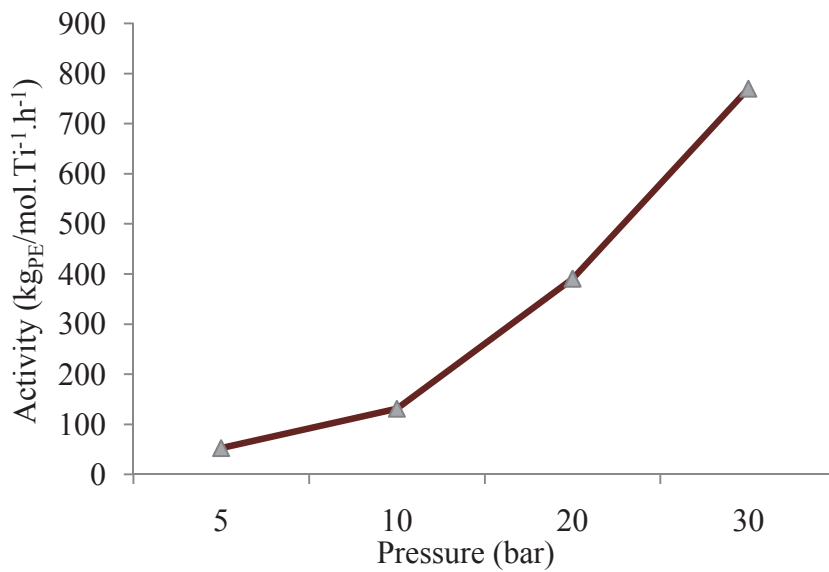


**Figure 11:** Ethylene polymerization with Ti9/MAO as catalyst at pressures ranging from 5 to 30 bars and constant temperature (70°C)

### 5.2.4 Conclusion

To evaluate the influence of the coordination sphere of the titanacalix[4]arene on its catalytic activity, **Ti1–Ti9** were screened for ethylene polymerization under our standard conditions (**Figure 12**). The difference in catalytic performance (*i.e.*, activity and molecular-weight distribution) between the distal and the proximal calixarene (classes **A** and **C** vs. classes **D** and **E**) derivatives suggests the formation of two different active species. This is probably due to the bite angle of O–Ti–O being wider. In both distal and proximal titanacalix[4]arenes, increasing the number of ether oxygen atoms coordinated to the titanacalix[4]arene decreases their productivity. In a similar coordination sphere, both titana-**Ti3** and zirconacalix[4]arene **Zr1** provides similar activities in ethylene polymerization.

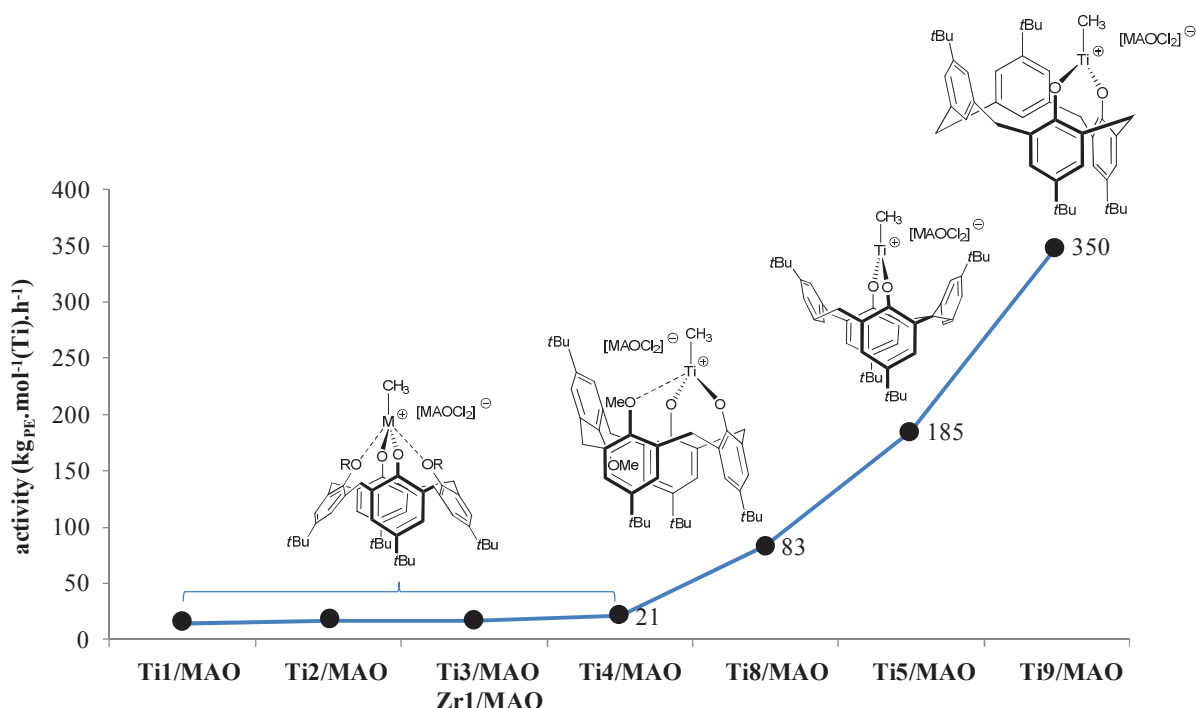


**Figure 12:** Relation structure-activity of the novel systems **Ti1–Ti5/MAO**, **Ti8–Ti9/MAO** and **Zr1/MAO**

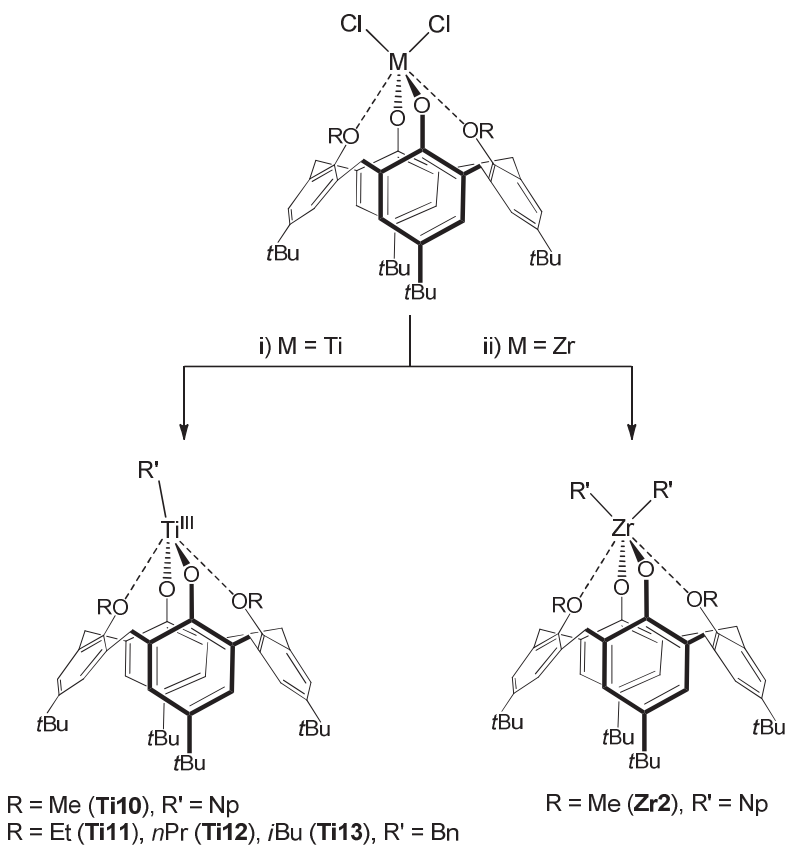
## 6. Synthesis and characterization of alkyl titana- and zirconacalix[4]arenes

We have been interested to create a set of soluble alkyl metallacalix[4]arenes with the objective to compare their characterizations in liquid state to their supported counterparts (**Scheme 1**). Two pathways are herein highlighted for the synthesis of such models: the salt-elimination route, by alkylation of the previously described chloro derivatives with a selected Grignard reagent, or the alkane-elimination route, by direct reaction of an organometallic

alkyl complex with the ligand calix[4]arene, when the first route is not proper. It is noteworthy that the second route has never been exploited with calix[4]arenes.

### 6.1 Syntheses of bipodal alkyl titana- and zirconacalix[4]arene models (T10-T13, Zr2)

Alkylation of **Ti1** with 2.1 eq of PhMgCl, *p*-TolylLi and MeLi was described by Floriani *et al.*<sup>9a</sup>. Surprisingly, a monoalkylated Ti<sup>III</sup> center was obtained and its structure confirmed by X-Ray. It was important to see the effect of the steric hindrance, of both the Ti-alkyl part and the two alkoxy groups of the calixarene ligand, on the stabilization of the Ti<sup>IV</sup> center. Therefore, first the alkylation of **Ti1** with 2 eq. of NpMgCl was carried out (**Scheme 29**).



**Scheme 29: Synthesis of the distal bipodal alkyl titana- T10-Ti13 and zirconacalix[4]arenes Zr2 models study of the influence of the ancillary ligands steric hindrance. Reagents and conditions: i) 2.1 eq. R'MgCl, toluene, 10°C, 16 h; ii) 2.1 eq. R'MgCl, toluene, RT, 3 h**

The Ti<sup>III</sup> complex **Ti10** was provided as green crystals in 80% yield, and characterized by elemental analyses. Complexes **Ti2-Ti4**, presenting alkoxy groups with different steric hindrances, were alkylated following the same procedure with BnMgCl, to provide the corresponding monoalkylated Ti<sup>III</sup> complexes in 60%-81% as more or less deep green solids

(R = Et, **Ti11**; R = nPr, **Ti12**, R = iBu, **Ti13**). These results show that, independently of the steric hindrance of both alkyl and alkoxy groups around the metal center, the formation of these paramagnetic species could be explained by the stabilization of the Ti<sup>III</sup> center by the two electron donating alkoxy groups.

In opposite, alkylation of the bis-(chloro)zirconacalix[4]arene **Zr1** with 2 eq. of NpMgCl at RT provides the corresponding bis-(neopentyl)zirconacalix[4]arene **Zr2**, in which the zirconium remains unchanged to the initial oxidation state (**Scheme 29**). Unfortunately, alkylation of the dehydroxylated chloro derivative **Ti5** was unsuccessful as a complex mixture was obtained, certainly due to concomitant formation of Ti<sup>IV</sup> and Ti<sup>III</sup> by-products.

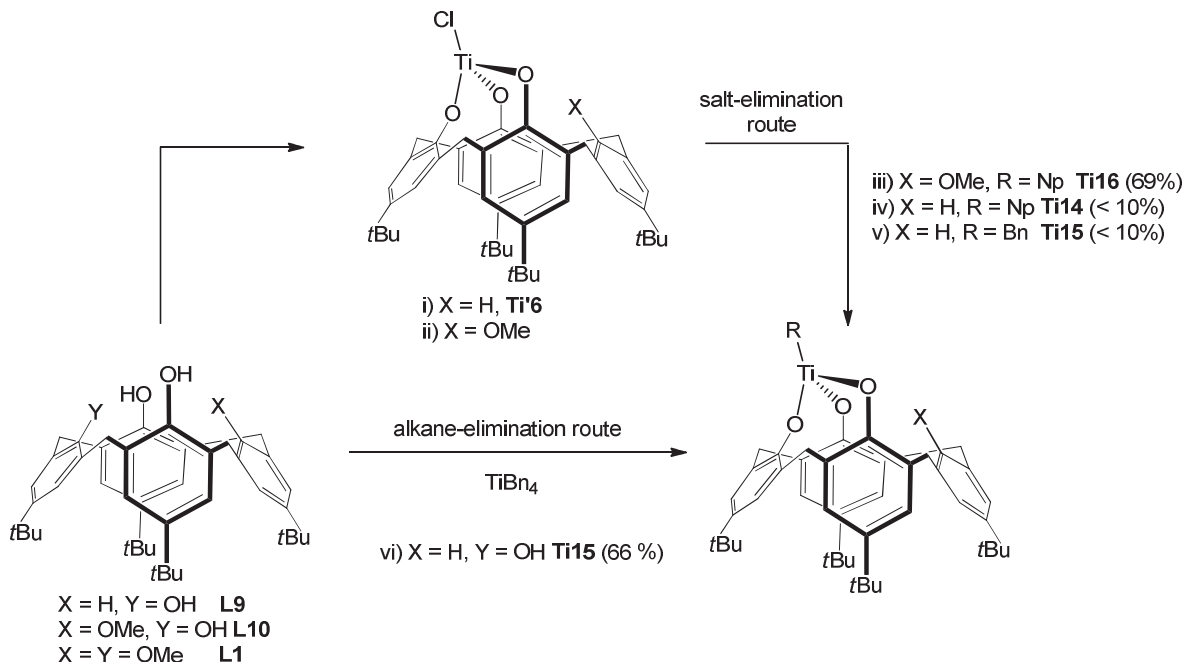
The paramagnetic feature of the titanium derivatives **Ti10-Ti13** did not give correct NMR spectra but each of them was characterized by elemental analysis. As observed by Floriani *et al.* by X-Ray diffraction, such compounds are in cone conformation, in which the Ti<sup>III</sup> center is stabilized by coordination of the two methoxy groups.<sup>9a</sup> The <sup>13</sup>C-NMR spectrum of the zirconium derivative **Zr2** displays a unique signal at 33.70 ppm for the four methylene bridges, confirming a cone conformation, and shows signals for the neopentyl group shifted to 1.57 ppm (-CH<sub>3</sub>), 1.66 ppm for (>CH<sub>2</sub>). Chemical shift of >CH<sub>2</sub> in <sup>13</sup>C-NMR is of 70.9 ppm.

Synthesize of the proximal bis-benzyl complex of zirconium [[4+]-1,2-(H)<sub>2</sub>(O)<sub>2</sub>ZrBn<sub>2</sub>] was attempted but without success. Indeed, when 1 eq. of ZrBn<sub>4</sub> was reacted with the proximal bis-dehydroxylated calix[4]arene [[4+]-1,2-(H)<sub>2</sub>(OH)<sub>2</sub>] **L8**, the <sup>1</sup>H-NMR of the crude product showed a calixarenic species with a complex symmetry in presence of unreacted ZrBn<sub>4</sub>. Kinetics could be highlighted, as already observed by Duchateau *et al.*<sup>3</sup> (see **section 2.1.2**) from the reaction of 1 eq. of ZrBn<sub>4</sub> and the bis-silanol POSS derivative R<sub>7</sub>Si<sub>7</sub>O<sub>9</sub>(OH)<sub>2</sub>(OSiMe<sub>3</sub>). In a similar way, the dimeric product [[4+]-1,2-(H)<sub>2</sub>(O)<sub>2</sub>]<sub>2</sub>Zr was probably generated.

## 6.2 Syntheses of the tripodal alkyl titana- and zirconacalix[4]arenes models

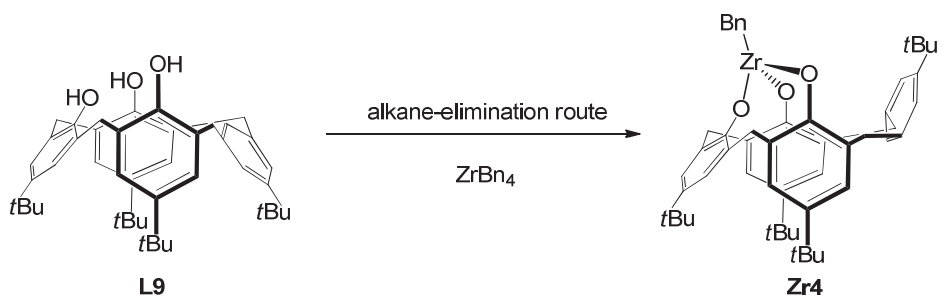
We herein report syntheses of tripodal alkyl titana- and zirconacalix[4]arene models either *via* the salt- or unprecedented alkane-elimination routes. The complex **Ti'6** was already obtained from the ligand **L10** as an unexpected product, as described in **section 5.1.2**. It must be stated that a more convenient approach to get **Ti'6** is to react the starting material [[4+]- (OH)<sub>3</sub>(H)] **L9** with TiCl<sub>4</sub>.2THF in toluene at 110°C in 59% yield. Alkylation of the latter with

NpMgCl and BnMgCl gave **Ti14** and **Ti15** respectively, but in low yields (*ca.* 10%) (**Scheme 30**). For the benzyl derivative, the relevant strategy was to react TiBn<sub>4</sub> with **L9** to give  $[[4+]\text{-}(\text{H})(\text{O})_3\text{TiBn}]$  **Ti15** in 66% yield. The analogue  $[[4+]\text{-}(\text{OMe})(\text{O})_3\text{TiNp}]$  **Ti16** of  $[[4+]\text{-}(\text{OMe})(\text{O})_3\text{TiBn}]$ , previously described by Floriani<sup>9a</sup>, was obtained by alkylation of  $[[4+]\text{-}(\text{OMe})(\text{O})_3\text{TiCl}]$ <sup>9a</sup> with NpMgCl in 69% yield.



**Scheme 30:** Synthesis of the tripodal alkyl titanacalix[4]arenes models

For the zirconium analogues, direct reactions of ZrCl<sub>4</sub> or ZrCl<sub>4</sub>.2THF onto **L9** were unsuccessful (low selectivity). Nevertheless, the alkane-elimination strategy was considered to get directly the tripodal alkyl zirconacalix[4]arenes  $[[4+]\text{-}(\text{H})(\text{O})_3\text{ZrR}]$  (R = Np, Bn). In a first attempt, **L9** was reacted with ZrNp<sub>4</sub> at -78°C in toluene or pentane to provide, unfortunately, a mixture of **L9** and many by-products and unclear NMR. However, when ZrBn<sub>4</sub> was used, the expected complex  $[[4+]\text{-}(\text{H})(\text{O})_3\text{ZrBn}]$  **Zr4** was obtained in 40% yield (a better selectivity was noticed when pentane was used as solvent) (**Scheme 31**). The different reactivity between ZrNp<sub>4</sub> and ZrBn<sub>4</sub> is probably due to the presence of the four Np groups causing a bulky sphere around the zirconium center, which could make the coordination of the ligand to the metal center more difficult than in the case of ZrBn<sub>4</sub>.



Scheme 31: Synthesis of the tripodal alkyl zirconacalix[4]arenes models

Complexes **Ti15** and **Zr4** display similar  $^1\text{H}$ -NMR patterns, with three singlets (18,9,9 integration) and two AB systems, corresponding to the methylenic protons of the calixarene moiety, relevant to a Cs symmetry (**Figure 13**). It is noteworthy that  $\text{CH}_2\text{Ph}$  signal of **Zr4** is slightly upfielded (2.90 ppm compared to 3.60 ppm for **Ti15**), probably due to a dimeric form in which two  $\text{Zr}\cdots\text{O}$  coordinations could result in this chemical shift. This is expected from the easier propensity of Zr to provide dimeric structures. Furthermore, NOESY experiment of **Zr4** shows spatial interaction between this *ipso*Ar-H and  $\text{CH}_2\text{Ph}$ . This spatial interaction is not observed in the case of **Ti15**, possibly due to the presence of second coordinated molecule. Signals of  $\text{CH}_2\text{Ph}$  are shifted to 85.13 ppm for **Ti15** and 66.19 ppm in the case of **Zr4**. *ipso*Ar-H signals are of 7.73 ppm in the case of **Zr4** and 6.76 ppm for **Ti15**. Both are in partial cone conformation as judged the two signals of the methylene bridge carbons at *ca.* 33 ppm and 39 ppm in  $^{13}\text{C}$ -NMR.

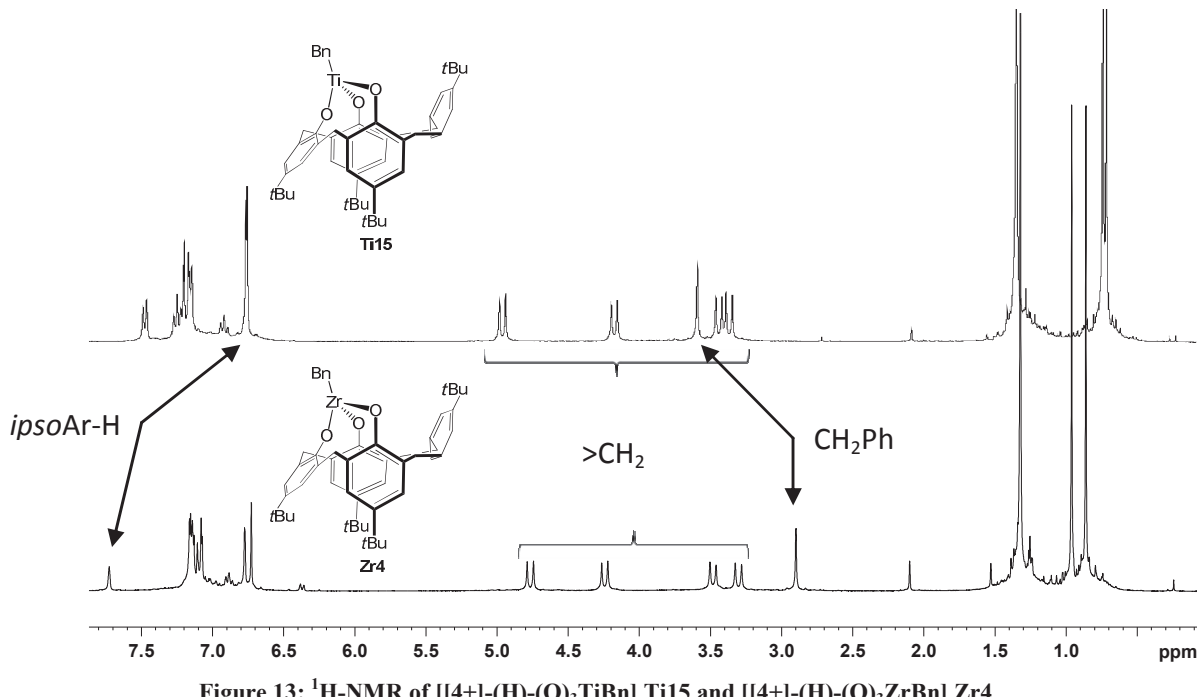


Figure 13:  $^1\text{H}$ -NMR of  $[4+](\text{H})-(\text{O})_3\text{TiBn}] \text{Ti15}$  and  $[4+](\text{H})-(\text{O})_3\text{ZrBn}] \text{Zr4}$

### 6.3 Conclusion

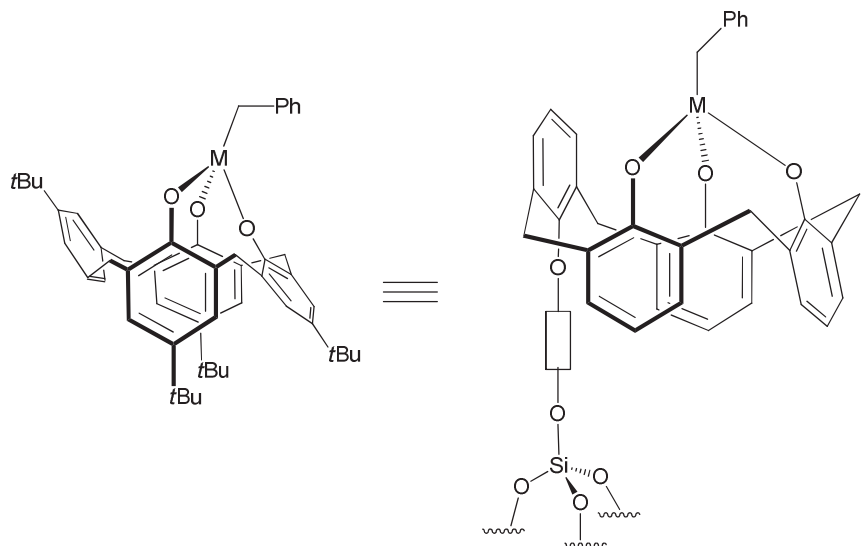
A set of alkyl titana- and zirconacalix[4]arenes were synthesized *via* the salt- and alkane-elimination routes. The latter was preferred for the synthesis of the tripodal compounds, bearing one methoxy group or one proton, as it provides two unprecedented ancillary ligand-free tripodal benzyl models of Ti and Zr, and presents interesting  $\sigma$ -bond metathesis for tripodal monomethoxy neopentyl and benzyl models. Those alkyl models will represent and provide analytical information for the further grafted metallacalix[4]arenes.

## 7. General conclusion

A number of strategic titana- and zirconacalix[4]arenes soluble models were synthesized and characterized. The first collection of those models consists in bipodal chloro derivatives, presenting different coordination modes. Judiciously modified calix[4]arene ligands, on the lower-rim, influence the geometric and electronic environment of the metal center, by the presence or not of diverse ancillary ligands: they exhibit various types of steric hindrance and are located in distal or proximal positions. Their behavior in ethylene polymerization as catalytic precursors permit to conclude that complexes free of ancillary ligand, as well as the ones presenting a more open O-Ti-O bite angle, show the best and unprecedented catalytic activities. Those crucial observations will lead us to the targeted preparation of supported metallacalix[4]arenes, in which the environment around the metal has to be optimized to obtain the most active single sites material.

The bipodal and tripodal alkyl derivatives of the titana- and zirconacalix[4]arenes, composing the alkyl models series, were synthesized either *via* the salt-elimination route (alkylation of the corresponding chlorine derivatives), or the alkane-elimination route, by direct reaction of a homoleptic complex with the ligands. It must be highlighted that many efforts were done to get systematically the models *via* the alkane-elimination route, as it represents the well-used method in COMS chemistry (**Scheme 32**). In this way, unprecedented tripodal benzyl and neopentyl titana- and zirconacalix[4]arenes were synthesized in good yields, by reduction of the number of steps, compared to the alkylation of the chlorine derivatives, often less selective. The titana- and zirconacalix[4]arenes bearing coordinative ancillary ligands are the less attractive as judged from the observations of the

ethylene polymerization but they are indispensable in the understanding of the behavior of the ligand-surface toward an approaching metal center.



Scheme 32: Grafted metallacalix[4]arenes and their corresponding soluble alkyl metallacalix[4]arenes ( $M = Ti, Zr$ )

## Experimental section

All manipulations were carried out under a dry argon atmosphere using standard Schlenk techniques. All solvents were dried by standard methods and freshly distilled before use. NMR spectra were recorded on DRX400 and DRX300 Bruker instruments. Elemental analyses were performed at the Central Analysis Service of Solaize (France). High purity ethylene was purchased from Air Liquide type and was dried over a deoxo catalyst (BASF R3-11 and 4 molecular sieves) prior to use.

### General procedure for ethylene polymerization

Solid methylaluminoxane was obtained by removing toluene and AlMe<sub>3</sub> under vacuum at 50°C overnight from a commercially available toluene solution (10 wt. %, Aldrich). A stock solution of MAO (100 mg.L<sup>-1</sup>) was prepared by dissolving the resulting white solid in toluene and used in the two weeks. All loading were realized into a glove box. To a 80 ml autoclave was charged 50 ml of toluene and 0.9 ml of the MAO solution (100 mg.L<sup>-1</sup>). After 10min, 1 ml of the precatalyst solution ( $1.05 \times 10^{-3}$  M) was injected and the reactor was heated to the wanted temperature. Under magnetic stirring, the wanted ethylene pressure was established and kept constant over 120min. The reaction was quenched by removing ethylene and pouring the mixture into a EtOH (40 mL), H<sub>2</sub>O (140 mL) and HCl (20 mL, 37%) solution. After 2h of stirring, the resulting solid polymer was filtered off and washed successively with water (80 mL) and EtOH (80 mL) and dried at 50°C under vacuum until constant mass. Differential scanning calorimetry measurements for determination of melting transition were performed on a Perkin Elmer Pyris 1 and a Mettler DSC1 apparatus. Samples were heated from 40°C to 150 °C at 5°C.min<sup>-1</sup>. In both cases, two successive heating and cooling of the samples were performed. We have considered data obtained during the second run. High temperature SEC analyses were performed using a Waters Alliance GPCV 2000 chromatograph equipped with three columns (PL gel Olexis 7x300 mm). Samples (1 mg.mL<sup>-1</sup>) were eluted with trichlorobenzene with a flow rate of 1 mL.min<sup>-1</sup> at 150°C. Online detection was performed by refractometry and viscosimetric measurements using Waters equipments. The system was calibrated with polystyrene standards in the range of 500 to 7 106 g.mol<sup>-1</sup>.

**Synthesis of 5,11,17,23-tetra-*tert*-butyl-25,27-dihydroxy-26,28-di((2-methylpropyl)oxy)calix[4]arene (L4):** *p*-*tert*butylcalix[4]arene (1.500 g, 2.311 mmol) and K<sub>2</sub>CO<sub>3</sub> (0.352 g, 2.543 mmol) were suspended in dry CH<sub>3</sub>CN (40 mL). iBuI (1.34 ml,

11.557 mmol) was then added and the mixture was stirred under reflux during 24 h. To complete the reaction, the same amounts of  $K_2CO_3$  and  $iBuI$  were added and the mixture was stirred under reflux during 24 h. After evaporation of the solvent, the residue was dissolved in  $CH_2Cl_2$  (30 mL), washed twice with HCl (1M), brine and dried ( $MgSO_4$ ). The solvent was removed under vacuum and the solid was washed with cold MeOH to give a white powder (1.317 g, 75%). NMR  $^1H$  ( $CDCl_3$ , 300MHz, 298K):  $\delta$  0.97 (s, 18H,  $tBu$ ), 1.22 (d, 12H,  $iBu$ ,  $^3J(H,H) = 6.9Hz$ ), 1.27 (s, 18H,  $CH_3-tBu$ ), 2.31 (m, 2H,  $CH-iBu$ ), 3.28 (d, 4H, calix- $CH_2$ ,  $^2J(H,H) = 12.9Hz$ ), 3.73 (d, 4H,  $CH_2-iBu$ ,  $^3J(H,H) = 6.0Hz$ ), 4.28 (d, 4H, calix- $CH_2$ ,  $^2J(H,H) = 12.9Hz$ ), 6.82 (s, 4H, Ar-H), 7.03 (s, 4H, Ar-H), 7.79 (s, 2H, OH). NMR  $^{13}C$ , DEPT, HSQC, HMBC ( $CDCl_3$ , 125 MHz):  $\delta$  19.47 ( $CH_3-tBu$ ), 29.39 ( $CH-tBu$ ), 31.02 ( $CH_3-tBu$ ), 31.70 ( $CH_3-tBu + CH_2$ -calix), 33.77 ( $tBu$ -quat), 33.92 ( $tBu$ -quat), 82.97 ( $CH_2-tBu$ ), 124.96 (Ar-*meta*), 125.44 (Ar-*meta*), 127.60 (Ar-*ortho*), 132.68 (Ar-*ortho*), 141.16 (Ar-*para*), 146.68 (Ar-*para*), 159.72 (Ar-O), 150.99 (Ar-O); LRMS (ES $^+$ ):  $[M+Na]^+ = 783.5$ . HRMS (ES $^+$ ) : Calcd. for  $C_{52}H_{72}O_4Na$  783.5328 found 783.5327.

**Synthesis of 5,11,17,23-tetra-*tert*-butyl-25,27-dihydroxy-26,28-di(ethyl 2,2-dimethylpropionate)calix[4]arene:** To a suspension of *p-tert*butylcalix[4]arene (3.000 g, 4.623 mmol) and  $NEt_3$  (5.15 ml, 36.985 mmol) in anhydrous  $CH_2Cl_2$  (60 ml) was added pivaloyl chloride (4.55 ml, 36.985 mmol) and the resulting mixture was stirred for 1h at RT under argon. The reaction was quenched with water and the organic phase separated, washed with water until neutrality, brine and dried over  $MgSO_4$ . The residue was triturated in cold MeOH and filtered to give a white powder (3.203 g, 85%). NMR  $^1H$  ( $CDCl_3$ , 300MHz, 298K):  $\delta$  0.85 (s, 18H,  $tBu$ ), 1.32 (s, 18H,  $tBu$ ), 1.53 (s, 18H, Piv), 3.32 (d, 2H,  $^3J(H,H) = 13.7Hz$ ), 3.87 3.32 (d, 2H,  $^3J(H,H) = 13.7Hz$ ), 5.58 (s, 2H, OH), 6.68 (s, 4H, Ar-H), 7.11 (s, 4H, Ar-H).  $^{13}C$  ( $CDCl_3$ , 75MHz, 298K):  $\delta$  27.42 ( $CH_3$ - Piv), 30.77 ( $CH_3-tBu$ ), 31.59 ( $CH_2$ -calix), 31.64 ( $CH_3-tBu$ ), 33.83 ( $tBu$ -quat), 33.91 ( $tBu$ -quat), 39.54 (Piv-quat), 125.29 ( $C_{Ar}$ ), 125.55 ( $C_{Ar}$ ), 127.96 ( $C_{Ar}$ ), 131.03 ( $C_{Ar}$ ), 141.96 ( $C_{Ar}$ ), 142.64 ( $C_{Ar}$ ) 148.38 ( $C_{Ar}$ ), 150.16 ( $C_{Ar}$ ), 176.69 (C=O). LRMS (ES $^+$ ):  $[M+Na]^+ = 839.4$ . HRMS (ES $^+$ ) : Calcd. for  $C_{54}H_{72}O_6Na$  839.5227 found 839.5228.

**Synthesis of 5,11,17,23-tetra-*tert*-butyl-25,27-dihydroxy-26,28-bis((diethoxyphosphinyl)oxy)calix[4]arene (P1) :** *p-tert*butylcalix[4]arene (5.000 g, 7.705 mmol) and  $NEt_3$  (4.3 mL, 30.821 mmol) were dissolved in toluene (125 mL).  $ClPO(OEt)_2$  (4.45 mL, 30.821 mmol) was added dropwise to the toluene solution and the

mixture was stirred over 60 h at room temperature. The resulting mixture was then successively washed with HCl (3N), NaOH 10%, brine and dried over MgSO<sub>4</sub>. After evaporation of the solvent, the residue was washed with cold MeOH to provide a white powder (5.393 g, 76%) ; NMR <sup>1</sup>H (CDCl<sub>3</sub>, 300MHz, 298K): δ 0.87 (s, 18H, <sup>t</sup>Bu), 1.33 (s, 18H, <sup>t</sup>Bu), 1.36 (m, 12H, OCH<sub>2</sub>CH<sub>3</sub>), 3.41 (d, 4H, CH<sub>2</sub>, <sup>2</sup>J(H,H) = 14.0 Hz), 4.28 (m, 8H, OCH<sub>2</sub>CH<sub>3</sub>), 4.40 (d, 4H, CH<sub>2</sub>, <sup>2</sup>J(H,H) = 14.0 Hz), 5.14 (s, 2H, OH), 6.71 (s, 4H, Ar-H), 7.13 (s, 4H, Ar-H). NMR <sup>13</sup>C (CDCl<sub>3</sub>, 75MHz, 298K): δ 15.97 (OCH<sub>2</sub>CH<sub>3</sub>), 30.61 (CH<sub>3</sub>-<sup>t</sup>Bu), 31.45 (CH<sub>3</sub>-<sup>t</sup>Bu), 32.09 (-CH<sub>2</sub>), 33.59 (<sup>t</sup>Bu-quat), 33.68 (<sup>t</sup>Bu-quat), 64.60 (OCH<sub>2</sub>CH<sub>3</sub>), 125.15 (Ar-*meta*), 125.79 (Ar-*meta*), 127.90 (Ar-*para*), 131.23 (Ar-*ortho*), 142.15 (Ar-*ortho*), 147.55 (Ar-O), 149.93 (Ar-O) ; ESI<sup>+</sup>: [M+H]<sup>+</sup> = 921.2

**Synthesis of 5,11,17,23-tetra-*tert*-butyl-25,27-dihydroxycalix[4]arene (L5):** Under argon, 100 ml of liquid ammonia was condensed onto potassium (1.220 g, 31.267 mmol) at -78°C to give a dark blue solution. A solution of **P1** (4.800 g, 5.211 mmol) in 30 ml of dry ether was added dropwise to the stirred blue solution. After 40 min, the reaction was slowly quenched with NH<sub>4</sub>Cl until the blue color was discharged and the ammonia solution became white. After evaporation of the ammonia, the residue was treated with CH<sub>2</sub>Cl<sub>2</sub> (200 ml). After filtration of the salts, the filtrate was washed twice with water and dried over MgSO<sub>4</sub>. After evaporation of the solvent, the residue was triturated and washed with cold MeOH to provide a white powder (1.852 g, 58%) ; NMR <sup>1</sup>H (CDCl<sub>3</sub>, 300MHz, 298K): δ 1.24 (s, 18H, <sup>t</sup>Bu), 1.34 (s, 18H, <sup>t</sup>Bu), 3.94 (s, 8H, CH<sub>2</sub>), 4.14 (s, 2H, OH), 6.11 (s, 2H, *ipso* Ar-H), 6.99 (s, 4H, Ar-H), 7.21 (s, 4H, Ar-H) ; NMR <sup>13</sup>C (CDCl<sub>3</sub>, 125 MHz, 298K): δ 31.41 (CH<sub>3</sub>-<sup>t</sup>Bu), 31.59 (CH<sub>3</sub>-<sup>t</sup>Bu), 33.85 (<sup>t</sup>Bu-quat), 34.54 (<sup>t</sup>Bu-quat), 37.37 (-CH<sub>2</sub>), 122.40 (Ar-*ipso*), 123.86 (Ar-*meta*), 125.34 (Ar-*ortho*), 127.02 (Ar-*meta*), 140.39 (Ar-*ortho*), 143.10 (Ar-*para*), 150.24 (Ar-*para*), 151.45 (Ar-O) ; ESI<sup>+</sup>: [M+H]<sup>+</sup> = 617.20

**Synthesis of 5,11,17,23-tetra-*tert*-butyl-25,26-dihydroxy-27,28-bis-((diethoxyphosphinyl)oxy)calix[4]arene (P2):** **P1** (1.005g, 1.091mmol) and NaH (0.053g, 1.309mmol, 60% in mineral oil) were dissolved in 10ml of dry THF and stirred at reflux over 1h. The mixture was then quenched with 10ml of HCl (3N) and the resulting solution was extracted with DCM (3x10ml). The organic phases were washed with 2x50ml of brine, dried over MgSO<sub>4</sub> and evaporated. The resulting residue was pure enough for the cleavage step. NMR <sup>1</sup>H (CDCl<sub>3</sub>, 300MHz, 298K): δ 1.04 (s, 18H, <sup>t</sup>Bu), 1.17 (s, 18H, <sup>t</sup>Bu), 1.34 (m, 12H,

OCH<sub>2</sub>CH<sub>3</sub>), 3.37 (m, 4H, calix-CH<sub>2</sub>), 4.25 (m, 9H, OCH<sub>2</sub>CH<sub>3</sub> + calix-CH<sub>2</sub>), 4.54 (d, 2H, CH<sub>2</sub>, <sup>2</sup>J(H,H) = 13.5 Hz), 4.87 (d, 1H, CH<sub>2</sub>, <sup>2</sup>J(H,H) = 13.5 Hz), 6.90 (m, 8H, Ar-H)

**Synthesis of 5,11,17,23-tetra-tert-butyl-25,26-dihydroxycalix[4]arene (L8):** NH<sub>3</sub> was condensed over K (2.300g, 58.626 mmol) at -78°C to give 75 ml of a dark blue solution. A solution of **P2** (0.540 g, 0.586 mmol) in 10 ml of dry diethyl ether was added dropwise to the blue solution and the mixture was stirred over 1h at -78°C. After quenching of the solution with NH<sub>4</sub>Cl until complete transformation of the blue solution into a white suspension, NH<sub>3</sub> was left to evaporation at RT. The resulting residue was extracted with CH<sub>2</sub>Cl<sub>2</sub> (3 x 30 mL) and the filtrate was washed with water (70 mL), brine, dried over MgSO<sub>4</sub> and evaporated. The solid was triturated with cold MeOH and filtered to provide a white solid (0.290 g, 80%). NMR <sup>1</sup>H (C<sub>6</sub>D<sub>6</sub>, 300MHz, 298K): δ 1.25 (s, 18H, <sup>t</sup>Bu), 1.31 (s, 18H, <sup>t</sup>Bu), 3.07 (s, 2H, CH<sub>2</sub>), 3.90 (s, 2H, CH<sub>2</sub>), 3.94 (s, 4H, CH<sub>2</sub>), 6.24 (s, 2H, OH), 6.53 (s, 2H, Ar-H), 7.08-7.15 (m, 6H, Ar-H), 7.40 (d, 2H, Ar-H, <sup>4</sup>J(H,H) = 2.4Hz). NMR <sup>13</sup>C, DEPT (C<sub>6</sub>D<sub>6</sub>, 75MHz, 298K): δ 31.48 (CH<sub>3</sub>-<sup>t</sup>Bu), 31.74 (CH<sub>3</sub>-<sup>t</sup>Bu), 32.18 (calix-CH<sub>2</sub>), 34.17 (<sup>t</sup>Bu-quat), 34.57 (<sup>t</sup>Bu-quat), 38.14 (calix-CH<sub>2</sub>), 42.69 (calix-CH<sub>2</sub>), 123.51 (C<sub>Ar</sub>), 124.03 (C<sub>Ar</sub>), 125.03 (C<sub>Ar</sub>), 126.61 (C<sub>Ar</sub>), 126.74 (C<sub>Ar</sub>), overlapped with C<sub>6</sub>H<sub>6</sub> 128.00 (C<sub>Ar</sub>), 128.84 (C<sub>Ar</sub>), 140.06 (C<sub>Ar</sub>), 142.92 (C<sub>Ar</sub>), 143.99 (C<sub>Ar</sub>), 149.63 (C<sub>Ar</sub>), 151.46 (C<sub>Ar</sub>). LRMS (ES<sup>-</sup>): [M-H]<sup>-</sup> = 615.6. HRMS (ES<sup>-</sup>) : Calcd. for C<sub>44</sub>H<sub>55</sub>O<sub>2</sub> 615.4202 found 615.4200.

**Synthesis of 5,11,17,23-tetra-tert-butyl-25-monohydroxy-26,27,28-trioxo(methylsilane)**  
To a suspension of *p*-tertbutylcalix[4]arene (11.000g, 16.952mmol) in 500ml of dry toluene, triethylamine (8.27ml, 59.331mmol) was added. Cl<sub>3</sub>SiMe (4.03ml, 33.904mmol) was then added dropwise and the resulting mixture was stirred overnight at RT. After filtration of the salts, the residue was washed with n-hexane (2x20ml) and dried to provide a white solid (8.900g, 76%). NMR <sup>1</sup>H (CDCl<sub>3</sub>, 300MHz): δ -0.34 (s, 3H, OSiMe), 1.25 (s, 9H, <sup>t</sup>Bu), 1.30 (s, 9H, <sup>t</sup>Bu), 1.32 (s, 18H, <sup>t</sup>Bu), 3.42 (d, 2H, calix-CH<sub>2</sub>, <sup>2</sup>J(H,H) = 13.8Hz), 3.77 (d, 2H, calix-CH<sub>2</sub>, <sup>2</sup>J(H,H) = 16.5Hz), 4.20 (d, 2H, calix-CH<sub>2</sub>, <sup>2</sup>J(H,H) = 16.5Hz), 4.41 (d, 4H, calix-CH<sub>2</sub>, <sup>2</sup>J(H,H) = 13.8Hz), 4.59 (s, 1H, OH), 7.07-7.13 (m, 8H, Ar-H).

**Synthesis of 5,11,17,23-tetra-tert-butyl-25-((diethoxyphosphinyl)oxy)-26,27,28-trioxo(methylsilane)calix[4]arene:** *n*BuLi (7.8 ml, 12.453 mmol, 1.6 M in hexanes) was added dropwise to a solution of 5,11,17,23-tetra-tert-butyl-25-monohydroxy-26,27,28-trioxo(methylsilane) (7.800 g, 11.321 mmol) in 300 ml of dry toluene and the resulting bright yellow mixture was stirred over 30min. ClP(O)(OEt)<sub>2</sub> (2.5 ml, 16.981 mmol) was then added

and the resulting mixture was stirred over 4h at RT. After filtration of the salts, the filtrate was evaporated and the residue washed with *n*-hexane (20 ml) to give a white solid (6.040 g, 65%). NMR  $^1\text{H}$  ( $\text{CDCl}_3$ , 300MHz):  $\delta$  -0.40 (s, 3H, OSiMe), 0.72 (t, 6H,  $\text{OCH}_2\text{CH}_3$ ,  $^3\text{J}(\text{H},\text{H}) = 7.2\text{Hz}$ ), 1.21 (s, 9H,  $^t\text{Bu}$ ), 1.28 (s, 9H,  $^t\text{Bu}$ ), 1.34 (s, 18H,  $^t\text{Bu}$ ), 3.48 (m, 2H + 4H, calix- $\text{CH}_2$  +  $\text{OCH}_2\text{CH}_3$ ), 3.67 (d, 2H, calix- $\text{CH}_2$ ,  $^3\text{J}(\text{H},\text{H}) = 13.8\text{Hz}$ ), 4.42 (d, 4H, calix- $\text{CH}_2$ ,  $^3\text{J}(\text{H},\text{H}) = 14.7\text{Hz}$ ), 7.08-7.13 (m, 8H, Ar-H). NMR  $^{13}\text{C}$ , DEPT ( $\text{CDCl}_3$ , 125 MHz):  $\delta$  -8.43 (OSiMe), 15.63 ( $\text{OCH}_2\text{CH}_3$ ), 15.70 ( $\text{OCH}_2\text{CH}_3$ ), 31.51 ( $\text{CH}_3\text{-}^t\text{Bu}$ ), 31.57 ( $\text{CH}_3\text{-}^t\text{Bu}$ ), 31.61 ( $\text{CH}_3\text{-}^t\text{Bu}$ ), 34.00 ( $^t\text{Bu}$ -quat), 34.26 ( $^t\text{Bu}$ -quat), 34.30 ( $^t\text{Bu}$ -quat), 35.19 (calix- $\text{CH}_2$ ), 37.20 (calix- $\text{CH}_2$ ), 63.95 ( $\text{OCH}_2\text{CH}_3$ ), 64.03 ( $\text{OCH}_2\text{CH}_3$ ), 124.65 ( $\text{C}_{\text{Ar}}$ ), 125.41 ( $\text{C}_{\text{Ar}}$ ), 126.47 ( $\text{C}_{\text{Ar}}$ ), 127.35 ( $\text{C}_{\text{Ar}}$ ), 129.94 ( $\text{C}_{\text{Ar}}$ ), 130.51 ( $\text{C}_{\text{Ar}}$ ), 130.66 ( $\text{C}_{\text{Ar}}$ ), 132.26 ( $\text{C}_{\text{Ar}}$ ), 132.30 ( $\text{C}_{\text{Ar}}$ ), 144.39 ( $\text{C}_{\text{Ar}}$ ), 145.93 ( $\text{C}_{\text{Ar}}$ ), 146.90 ( $\text{C}_{\text{Ar}}$ ), 147.37 ( $\text{C}_{\text{Ar}}$ ), 148.62 ( $\text{C}_{\text{Ar}}$ ). LRMS (ES $^+$ ):  $[\text{M}+\text{H}]^+ = 825.2$ . HRMS (ES $^+$ ): Calcd. for  $\text{C}_{49}\text{H}_{66}\text{O}_7\text{PSi}$  825.4315 found 825.4316.

**Synthesis of 5,11,17,23-tetra-*tert*-butyl-25,26,27-trihydroxycalix[4]arene (L9):**  $\text{NH}_3$  was condensed over K (14.000 g, 366.016 mmol) at -78°C to give 125 ml of a dark blue solution. A solution 5,11,17,23-tetra-*tert*-butyl-25-((diethoxyphosphinyl)oxy)-26,27,28-trioxo(methylsilane)calix[4]arene (6.040 g, 7.320 mmol) in 60 ml of dry diethylether was added dropwise to the blue solution and the mixture was stirred over 1h at -78°C. After quenching of the solution with  $\text{NH}_4\text{Cl}$  until complete transformation of the blue solution into a white suspension,  $\text{NH}_3$  was left to evaporation at RT. The resulting residue was extracted with  $\text{CH}_2\text{Cl}_2$  (3 x 50ml) and the filtrate washed with water until neutrality and dried over  $\text{MgSO}_4$ . After evaporation of the volatiles, the residue was triturated with MeOH to give a white solid (2.456g, 53%). NMR  $^1\text{H}$  ( $\text{CDCl}_3$ , 300MHz):  $\delta$  1.28 (s, 18H,  $^t\text{Bu}$ ), 1.29 (s, 9H,  $^t\text{Bu}$ ), 1.34 (s, 9H,  $^t\text{Bu}$ ), 3.92 (s, 4H,  $\text{CH}_2$ ), 3.97 (s, 4H,  $\text{CH}_2$ ), 7.08-7.28 (m, 9H, Ar-H).

**Synthesis of 5,11,17,23-tetra-*tert*-butyl-25,27-dioxo-26,28-diethyloxycalix[4]arene titanium (IV) dichloride (Ti2):** A slurry of **L2** (0.827 g, 1.173 mmol) and  $\text{TiCl}_4\cdot 2\text{THF}$  (0.392 g, 1.173 mmol) in 20 ml of toluene was stirred over 24h at 60°C. After evaporation of the volatiles, the residue was washed with pentane (10 mL) to provide a dark red solid (0.971 g, 98%).  $^1\text{H}$  NMR ( $\text{C}_6\text{D}_6$ , 300MHz, 298K):  $\delta$  0.69 (s, 18H,  $^t\text{Bu}$ ), 1.21 (t, 6H,  $\text{CH}_3\text{-CH}_2$ ,  $^3\text{J}(\text{H},\text{H}) = 6.9\text{Hz}$ ), 1.40 (s, 18H,  $^t\text{Bu}$ ), 3.16 (d, 4H, calix- $\text{CH}_2$ ,  $^2\text{J}(\text{H},\text{H}) = 13.2\text{Hz}$ ), 4.75 (d, 4H, calix- $\text{CH}_2$ ,  $^2\text{J}(\text{H},\text{H}) = 13.2\text{Hz}$ ), 4.95 (q, 4H,  $\text{CH}_3\text{-CH}_2$ ,  $^3\text{J}(\text{H},\text{H}) = 6.9\text{Hz}$ ), 6.83 (s, 4H, Ar-H), 7.16 (s, 4H, Ar-H).  $^{13}\text{C}$  NMR, DEPT ( $\text{C}_6\text{D}_6$ , 75MHz, 298K):  $\delta$  14.22 ( $\text{CH}_3\text{-Et}$ ), 30.58 ( $\text{CH}_3\text{-}^t\text{Bu}$ ), 31.88 ( $\text{CH}_3\text{-}^t\text{Bu}$ ), 33.76 ( $^t\text{Bu}$ -quat), 34.52 ( $^t\text{Bu}$ -quat), 35.20 (CH<sub>2</sub>-calix), 82.34 (CH<sub>2</sub>-Et),

124.55 (Ar-*meta*), 127.20 (Ar-*meta*), 130.98 (Ar-*ortho*), 132.50 (Ar-*ortho*), 144.36 (Ar-*para*), 149.31 (Ar-*para*), 155.53 (Ar-O), 165.64 (Ar-O) ; Suitable crystals for X-Ray analysis were obtained at -30°C from a saturated solution in toluene ; Anal. Calcd for C<sub>48</sub>H<sub>62</sub>Cl<sub>2</sub>O<sub>4</sub>Ti (821.18).(toluene)<sub>0.28</sub>: C, 70.80; H, 7.64; Found: C, 70.71;H, 7.49.

**Synthesis of 5,11,17,23-tetra-*tert*-butyl-25,27-dioxo-26,28-dipropoxycalix[4]arene titanium (IV) dichloride (Ti3):** A slurry of L3 (0.595 g, 0.812 mmol) and TiCl<sub>4</sub>.2THF (0.271 g, 0.812 mmol) in 10 ml of toluene was stirred over 20 h at 60°C. After evaporation of the volatiles, the residue was washed with pentane (2 x 5 mL) to provide a dark red solid (0.520 g, 79%). <sup>1</sup>H NMR (C<sub>6</sub>D<sub>6</sub>, 300MHz, 298K): δ 0.32 (t, 6H, CH<sub>3</sub>-CH<sub>2</sub>-CH<sub>2</sub>-O, <sup>3</sup>J(H,H) = 7.2Hz), 0.70 (s, 18H, <sup>t</sup>Bu), 1.41 (s, 18H, <sup>t</sup>Bu), 1.98 (m, 4H, CH<sub>3</sub>-CH<sub>2</sub>-CH<sub>2</sub>-O), 3.21 (d, 4H, calix-CH<sub>2</sub>, <sup>2</sup>J(H,H) = 13.2Hz), 4.83 (d, 4H, calix-CH<sub>2</sub>, <sup>2</sup>J(H,H) = 13.2Hz), 4.96 (m, 4H, CH<sub>3</sub>-CH<sub>2</sub>-CH<sub>2</sub>-O), 6.88 (s, 4H, Ar-H), 7.20 (s, 4H, Ar-H) ; <sup>13</sup>C NMR, DEPT (C<sub>6</sub>D<sub>6</sub>, 75MHz, 298K): δ 8.60 (CH<sub>3</sub>-CH<sub>2</sub>-CH<sub>2</sub>-O), 21.52 (CH<sub>3</sub>-CH<sub>2</sub>-CH<sub>2</sub>-O), 30.59 (CH<sub>3</sub>-<sup>t</sup>Bu), 31.89 (CH<sub>3</sub>-<sup>t</sup>Bu), 33.78 (<sup>t</sup>Bu-quat), 34.54 (<sup>t</sup>Bu-quat), 35.26 (CH<sub>2</sub>-calix), 87.50 (CH<sub>3</sub>-CH<sub>2</sub>-CH<sub>2</sub>-O), 124.59 (Ar-*meta*), 127.26 (Ar-*meta*), 130.98 (Ar-*ortho*), 132.45 (Ar-*ortho*), 144.45 (Ar-*para*), 149.40 (Ar-*para*), 156.22 (Ar-O), 165.68 (Ar-O) ; Suitable crystals for X-Ray analysis were obtained at - 30°C from a saturated solution in toluene ; Anal. Calcd for C<sub>50</sub>H<sub>66</sub>Cl<sub>2</sub>O<sub>4</sub>Ti (848.38).(toluene)<sub>0.5</sub> : C, 71.72; H, 7.88; Found: C, 71.72; H, 7.78.

**Synthesis of 5,11,17,23-tetra-*tert*-butyl-25,27-dioxo-26,28-di((2-methylpropyl)oxy)calix[4]arene titanium (IV) dichloride (Ti4):** A slurry of L4 (2.000 g, 2.628 mmol) and TiCl<sub>4</sub>.2THF (0.878 g, 2.628 mmol) in 40 ml of toluene was stirred over 24h at 60°C. The solution was reduced and left to crystallization at -30°C over two days. After filtration, a dark-red solid was obtained (1.090 g, 47%). <sup>1</sup>H NMR (C<sub>6</sub>D<sub>6</sub>, 300MHz, 298K): δ 0.68 (s, 18H, <sup>t</sup>Bu), 0.77 (d, 12H, (CH<sub>3</sub>)<sub>2</sub>-CH-CH<sub>2</sub>-O, <sup>3</sup>J(H,H) = 6.9Hz), 1.41 (s, 18H, <sup>t</sup>Bu), 2.52 (m, 2H, (CH<sub>3</sub>)<sub>2</sub>-CH-CH<sub>2</sub>-O), 3.22 (d, 4H, calix-CH<sub>2</sub>, <sup>2</sup>J(H,H) = 13.0Hz), 4.92 (d, 4H, calix-CH<sub>2</sub>, <sup>2</sup>J(H,H) = 13.2Hz), 4.99 (d, 4H, (CH<sub>3</sub>)<sub>2</sub>-CH-CH<sub>2</sub>-O, <sup>3</sup>J(H,H) = 6.0Hz), 6.85 (s, 4H, Ar-H), 7.19 (s, 4H, Ar-H) ; <sup>13</sup>C NMR, DEPT (C<sub>6</sub>D<sub>6</sub>, 75MHz, 298K): δ 20.56 ((CH<sub>3</sub>)<sub>2</sub>-CH-CH<sub>2</sub>-O), 28.10 ((CH<sub>3</sub>)<sub>2</sub>-CH-CH<sub>2</sub>-O), 30.56 (CH<sub>3</sub>-<sup>t</sup>Bu), 31.86 (CH<sub>3</sub>-<sup>t</sup>Bu), 33.73 (<sup>t</sup>Bu-quat), 34.52 (<sup>t</sup>Bu-quat), 35.33 (CH<sub>2</sub>-calix), 93.49 ((CH<sub>3</sub>)<sub>2</sub>-CH-CH<sub>2</sub>-O), 124.58 (Ar-*meta*), 127.26 (Ar-*meta*), 130.98 (Ar-*ortho*), 132.18 (Ar-*ortho*), 144.53 (Ar-*para*), 149.22 (Ar-*para*), 157.19 (Ar-O), 165.67 (Ar-O) ; Suitable crystals for X-Ray analysis were obtained at - 30°C from a saturated

solution in toluene; Anal. Calcd for C<sub>52</sub>H<sub>70</sub>Cl<sub>2</sub>O<sub>4</sub>Ti (876.41).(toluene)<sub>2</sub>: C, 74.63; H, 8.16; Found: C, 74.31; H, 7.78.

**Synthesis of 5,11,17,23-tetra-*tert*-butyl-25,27-dioxocalix[4]arene titanium (IV) dichloride (Ti5):** A solution of **L5** (0.800 g, 1.297 mmol) in 20 ml of toluene was added dropwise at 0°C to a solution of TiCl<sub>4</sub> (1.43 mL, 1M in toluene, added in 18 ml of toluene) and the resulting red solution was stirred over 72h at RT. After evaporation of the volatiles under vacuum, the red-brown residue was washed with pentane (15 ml + 10 mL) and dried to give an orange powder (0.690 g, 73%). NMR <sup>1</sup>H, NOESY, COSY, (C<sub>6</sub>D<sub>6</sub>, 300MHz, 298K): δ 1.19 (s, 18H, <sup>t</sup>Bu), 1.42 (s, 18H, <sup>t</sup>Bu), 3.54 (d, 4H, CH<sub>2</sub>, <sup>2</sup>J(H,H) = 16.7Hz), 4.40 (d, 4H, CH<sub>2</sub>, <sup>2</sup>J(H,H) = 16.7Hz), 5.96 (s, 2H, Ar-H), 6.82 (s, 4H, Ar-H), 7.31 (s, 4H, H<sub>Ar</sub>). NMR <sup>13</sup>C, DEPT (C<sub>6</sub>D<sub>6</sub>, 75MHz, 298K): δ 30.50 (CH<sub>3</sub>-<sup>t</sup>Bu), 30.57 (CH<sub>3</sub>-<sup>t</sup>Bu), 33.39 (<sup>t</sup>Bu-quat), 33.72 (<sup>t</sup>Bu-quat), 36.83 (CH<sub>2</sub>-calix), 120.18 (Ar-*Hipso*), 125.14 (Ar-*meta*), 126.18 (Ar-*meta*), 128.42 (Ar-*ortho*), 137.76 (Ar-*ortho*), 147.30 (Ar-*para*), 150.12 (Ar-*para*), 166.32 (Ar-OTi). Anal. Calcd for C<sub>44</sub>H<sub>54</sub>Cl<sub>2</sub>O<sub>2</sub>Ti (732.30): C, 72.03; H, 7.42; Found: C, 71.87; H, 7.50.

**Synthesis of 5,11,17,23-tetra-*tert*-butyl-25,26,27-trioxocalix[4]arene titanium (IV) monochloride (Ti6':)** (**Methode A**) **L9** (1.000g, 1.580mmol) and TiCl<sub>4</sub>.2THF (0.580g, 1.738mmol) were dissolved in 30 ml of toluene and the mixture was stirred at 110°C overnight. The clear solution was allowed to reach the room temperature and was crystallized at -30°C during 48h. The dark red solid was then collected (0.660g, 59%). (**Methode B**) TiCl<sub>4</sub> (0.99ml, 0.987mmol, 1M in toluene) was added dropwise at -40°C to a solution of **L10** (0.608g, 0.940mmol) in 15ml of toluene. The resulting dark red solution was allowed to reach RT overnight. After evaporation of the volatiles, the residue was washed with 3x4ml of pentane and dried in vacuum to provide a dark red solid (0.481, 72%). <sup>1</sup>H NMR (CDCl<sub>3</sub>, 300MHz): δ 0.93 (s, 9H, <sup>t</sup>Bu), 1.04 (s, 9H, <sup>t</sup>Bu), 1.31 (s, 18H, <sup>t</sup>Bu), 3.44 (d, 2H, CH<sub>2</sub>, <sup>2</sup>J(H,H) = 13.5Hz), 3.50 (d, 2H, CH<sub>2</sub>, <sup>2</sup>J(H,H) = 13.1Hz), 4.43 (d, 2H, CH<sub>2</sub>, <sup>2</sup>J(H,H) = 13.1Hz), 4.62 (d, 2H, CH<sub>2</sub>, <sup>2</sup>J(H,H) = 13.5Hz), 6.66 (s, 2H, Ar-H), 6.81 (s, 2H, Ar-H), 7.07 (s, 2H, Ar-H), 7.08 (s, 2H, Ar-H), 8.59 (s, 1H, Ar-H); <sup>13</sup>C NMR (CDCl<sub>3</sub>, 75MHz): δ 31.06 (2 x CH<sub>3</sub>-<sup>t</sup>Bu), 31.43 (CH<sub>3</sub>-<sup>t</sup>Bu), 33.58 (calix-CH<sub>2</sub>), 34.08 (<sup>t</sup>Bu-quat), 34.27 (<sup>t</sup>Bu-quat), 38.52 (calix-CH<sub>2</sub>), 122.41 (C<sub>Ar</sub>), 124.61 (C<sub>Ar</sub>), 124.90 (C<sub>Ar</sub>), 125.46 (C<sub>Ar</sub>), 127.55 (C<sub>Ar</sub>), 128.21 (C<sub>Ar</sub>), 130.57 (*ipso*-C<sub>Ar</sub>), 132.60 (C<sub>Ar</sub>), 139.49 (C<sub>Ar</sub>), 146.74 (C<sub>Ar</sub>), 147.76 (C<sub>Ar</sub>), 150.88 (C<sub>Ar</sub>), 157.79 (C<sub>Ar</sub>), 165.26 (C<sub>Ar</sub>). Anal. Calcd for C<sub>44</sub>H<sub>53</sub>ClO<sub>3</sub>Ti (712.32).(toluene)<sub>3</sub>: C, 78.89; H, 7.84; Found: C, 79.08 ; H, 7.54.

**Synthesis of 5,11,17,23-tetra-*tert*-butyl-25,26-dioxo-27,28-dimethyloxycalix[4]arene titanium (IV) dichloride] (Ti8):** TiCl<sub>4</sub> (0,38 mL, 0,377 mmol, 1M in toluene) was added dropwise to a solution of L7 (0.243 g, 0.359 mmol) in 20 ml of toluene at -40°C and the resulting mixture was allowed to reach RT overnight. After evaporation of the volatiles, the residue was triturated in hot pentane (10 mL), filtered and dried to provide a dark red solid (0,190 g, 67%). NMR <sup>1</sup>H (C<sub>6</sub>D<sub>6</sub>, 300MHz, 298K): δ 0.85 (s, 9H, <sup>t</sup>Bu), 0.96 (s, 9H, <sup>t</sup>Bu), 1.25 (s, 9H, <sup>t</sup>Bu), 1.28 (s, 9H, <sup>t</sup>Bu), 1.67 (s, 3H, OMe), 3.21 (d, 1H, CH<sub>2</sub>, <sup>2</sup>J(H,H) = 13.2Hz), 3.33 (d, 1H, CH<sub>2</sub>, <sup>2</sup>J(H,H) = 13.6Hz), 4.47 (d, 1H, CH<sub>2</sub>, <sup>2</sup>J(H,H) = 14.8Hz), 3.49 (d, 1H, CH<sub>2</sub>, <sup>2</sup>J(H,H) = 15.2Hz), 4.09 (s, 3H, OMe), 4.52 (d, 1H, CH<sub>2</sub>, <sup>2</sup>J(H,H) = 13.2Hz), 4.67 (d, 1H, CH<sub>2</sub>, <sup>2</sup>J(H,H) = 14.8Hz), 5.08 (d, 1H, CH<sub>2</sub>, <sup>2</sup>J(H,H) = 13.6Hz), 5.25 (d, 1H, CH<sub>2</sub>, <sup>2</sup>J(H,H) = 15.2Hz), 7.04-7.20 (m, 8H, Ar-H) ; NMR <sup>13</sup>C, DEPT, NOESY (C<sub>6</sub>D<sub>6</sub>, 125MHz, 298K): δ 30.97 (CH<sub>3</sub>-<sup>t</sup>Bu), 31.33 (CH<sub>3</sub>-<sup>t</sup>Bu), 31.55 (CH<sub>3</sub>-<sup>t</sup>Bu), 31.77 (CH<sub>3</sub>-<sup>t</sup>Bu), 34.07 (<sup>t</sup>Bu-quat), 34.08 (<sup>t</sup>Bu-quat), 34.19 (2 x calix-CH<sub>2</sub>), 34.52 (<sup>t</sup>Bu-quat), 34.73 (<sup>t</sup>Bu-quat), 36.76 (calix-CH<sub>2</sub>), 37.12 (calix-CH<sub>2</sub>), 67.23 (OMe), 68.51 (OMe), 124.44 (C<sub>Ar</sub>), 125.63 (C<sub>Ar</sub>), 126.25 (C<sub>Ar</sub>), 126.48 (C<sub>Ar</sub>), 126.52 (C<sub>Ar</sub>), 126.88 (C<sub>Ar</sub>), 127.44 (C<sub>Ar</sub>), 127.52 (C<sub>Ar</sub>), 128.53 (C<sub>Ar</sub>), 128.64 (C<sub>Ar</sub>), 131.83 (C<sub>Ar</sub>), 131.89 (C<sub>Ar</sub>), 133.28 (C<sub>Ar</sub>), 133.45 (C<sub>Ar</sub>), 134.14 (C<sub>Ar</sub>), 135.89 (C<sub>Ar</sub>), 146.32 (C<sub>Ar</sub>), 147.03 (C<sub>Ar</sub>), 149.33 (C<sub>Ar</sub>), 149.88 (C<sub>Ar</sub>), 155.52 (C<sub>Ar</sub>), 159.46 (C<sub>Ar</sub>), 165.42 (C<sub>Ar</sub>), 168.11 (C<sub>Ar</sub>) Anal. Calcd for C<sub>46</sub>H<sub>58</sub>Cl<sub>2</sub>O<sub>4</sub>Ti (792.32).(toluene)<sub>0.4</sub>: C, 70.57; H, 7.43; Found: C, 70.94 ; H, 7.15.

**Synthesis of 5,11,17,23-tetra-*tert*-butyl-25,26-dioxocalix[4]arene titanium (IV) dichloride (Ti9):** TiCl<sub>4</sub> (0,51 ml, 0,511 mmol, 1M in toluene) was added dropwise to a solution of L8 (0.300 g, 0.486 mmol) in 40 ml of toluene at -40°C and the resulting mixture was allowed to reach RT overnight. After evaporation of the volatiles, the residue was washed with pentane (2x5 mL) and dried to provide a dark red solid (0,215 g, 60%). NMR <sup>1</sup>H (C<sub>6</sub>D<sub>6</sub>, 300MHz, 298K): δ 1.22 (s, 18H, <sup>t</sup>Bu), 1.31 (s, 18H, <sup>t</sup>Bu), 2.61 (d, 1H, CH<sub>2</sub>, <sup>2</sup>J(H,H) = 13.0Hz), 3.28 (d, 1H, CH<sub>2</sub>, <sup>2</sup>J(H,H) = 14.0Hz), 3.42 (d, 1H, CH<sub>2</sub>, <sup>2</sup>J(H,H) = 13.0Hz), 3.50 (d, 2H, CH<sub>2</sub>, <sup>2</sup>J(H,H) = 15.6Hz), 4.29 (d, 2H, CH<sub>2</sub>) overlapped with 4.32 (d, 1H, CH<sub>2</sub>), 6.32 (s, 2H, Ar-H), 7.04 (d, 2, Ar-H, <sup>4</sup>J(H,H) = 1.6Hz), 7.11 (s, 2H, Ar-H), 7.15 (s, 2H, Ar-H), 7.24 (d, 2H, Ar-H, <sup>4</sup>J(H,H) = 1.6Hz) NMR <sup>13</sup>C, DEPT, NOESY, HSQC (C<sub>6</sub>D<sub>6</sub>, 125MHz, 298K): δ 31.40 (CH<sub>3</sub>-<sup>t</sup>Bu), 31.56 (CH<sub>3</sub>-<sup>t</sup>Bu), 34.53 (<sup>t</sup>Bu-quat), 34.61 (<sup>t</sup>Bu-quat), 34.73 (calix-CH<sub>2</sub>), 37.97 (calix-CH<sub>2</sub>), 42.88 (calix-CH<sub>2</sub>), 123.14 (C<sub>Ar</sub>), 123.40 (C<sub>Ar</sub>), 123.84 (C<sub>Ar</sub>), 125.72 (C<sub>Ar</sub>), 126.74 (C<sub>Ar</sub>),

127.10 (C<sub>Ar</sub>), 137.25 (C<sub>Ar</sub>), 139.87 (C<sub>Ar</sub>), 142.58 (C<sub>Ar</sub>), 148.49 (C<sub>Ar</sub>), 151.44 (C<sub>Ar</sub>), 163.22 (C<sub>Ar</sub>). Anal. Calcd for C<sub>44</sub>H<sub>54</sub>Cl<sub>2</sub>O<sub>2</sub>Ti (732.30): C, 72.03; H, 7.42; Found: C, 71.64; H, 7.07.

**Synthesis of 5,11,17,23-tetra-tert-butyl-25,27-dioxo-26,28-dimethoxycalix[4]arene titanium (III) mononeopentyl (Ti10):** NpMgCl (2.14 ml, 2.953 mmol, 1.38 M in diethyl ether) was added dropwise to a solution of **Ti1** (1.173 g, 1.477 mmol) in 75ml of toluene at -30°C. The reaction was then stirred over 20h at 10°C. After evaporation of the volatiles, the resulting residue was extracted with pentane and filtrated to remove the salts. Concentration and crystallisation of the filtrate at -30°C overnight provided a green solid (0.860g, 80%). Anal. Calcd for C<sub>51</sub>H<sub>69</sub>O<sub>4</sub>Ti: C, 77.15; H, 8.76; Found: C, 76.72; H, 9.48

**Synthesis of 5,11,17,23-tetra-tert-butyl-25,27-dioxo-26,28-diethoxycalix[4]arene titanium (III) monobenzyl (Ti11):** BnMgCl (0.37 ml, 0.743 mmol, 2 M in THF) was added dropwise to a solution of **Ti2** (0.300g, 0.354 mmol) in 15 ml of toluene at -30°C. The reaction was then stirred over 20h at 10°C. After evaporation of the volatiles, the resulting residue was extracted with pentane and filtrated to remove the salts. Concentration and crystallization of the filtrate at -30°C overnight provided a green solid (0.180g, 60%). Anal. Calcd for C<sub>55</sub>H<sub>69</sub>O<sub>4</sub>Ti.(toluene)2: C, 80.75; H, 8.35; Found: C, 80.75; H, 8.32.

**Synthesis of 5,11,17,23-tetra-tert-butyl-25,27-dioxo-26,28-dipropoxyxcalix[4]arene titanium (III) monobenzyl (Ti12):** BnMgCl (1.70ml, 1.675mmol, 1M in THF) was added dropwise to a solution of **Ti3** (0.679g, 0.798mmol) in 20ml of toluene at -30°C. The reaction was then stirred over 20h at 10°C. After filtration of the salts, the solution was concentrated and crystallised at -30°C overnight to provide a pale green solid (0.560g, 81%). Anal. Calcd for C<sub>57</sub>H<sub>73</sub>O<sub>4</sub>Ti: C, 78.69; H, 8.46; Found: C, 78.83; H, 8.52.

**Synthesis of 5,11,17,23-tetra-tert-butyl-25,27-dioxo-26,28-di(2-methylpropyl)oxy calix[4]arene titanium (III) monobenzyl (Ti13):** BnMgCl (0.74ml, 0.735mmol, 1M in THF) was added dropwise to a solution of **Ti4** (0.369g, 0.350mmol) in 15ml of toluene at -30°C. The reaction was then stirred over 20h at 10°C. After evaporation of the volatiles, the resulting residue was extracted with pentane and filtrated to remove the salts. Concentration and crystallisation of the filtrate at -30°C overnight provided a green solid (0.206g, 66%). Anal. Calcd for C<sub>59</sub>H<sub>77</sub>O<sub>4</sub>Ti.(toluene)2.5: C, 81.42; H, 8.66; Found: C, 81.49; H, 8.40.

**Synthesis of 5,11,17,23-tetra-tert-butyl-25,26,27-trioxocalix[4]arene titanium (IV) mononeopentyl (Ti14):** NpMgCl (0.38ml, 0.594mmol, 1.58M in diethyl ether) was added

dropwise to a stirred toluene (30ml) solution of **Ti6'** (0.400g, 0.540mmol) at -30°C. The reaction was stirred 1h at RT and the volatiles removed in vacuum. Pentane (30ml) was then added and the salts were filtered off through celite. The filtrate was concentrated and crystallized over three at -30°C to provide after filtration a brown solid (0.040g, 10%). NMR <sup>1</sup>H (C<sub>6</sub>D<sub>6</sub>, 300MHz): δ 0.74 (s, 9H, <sup>t</sup>Bu), 0.80 (s, 9H, <sup>t</sup>Bu), 1.38 (s, 18H, <sup>t</sup>Bu), 1.43 (s, 9H, Np), 2.69 (s, 2H, CH<sub>2</sub>-Np), 3.39 (d, 2H, CH<sub>2</sub>-calix, J = 13.2 Hz), 3.56 (d, 2H, CH<sub>2</sub>-calix, J = 12.4 Hz), 4.41 (d, 2H, CH<sub>2</sub>-calix, J = 12.4 Hz), 5.00 (d, 2H, CH<sub>2</sub>-calix, J = 13.2 Hz), 6.78 (s, 2H, Ar-H), 6.85 (s, 2H, Ar-H), 7.17 (d, 2H, Ar-H, J = 2.4 Hz), 7.23 (d, 2H, Ar-H, J = 2.4 Hz), 7.61 (s, 1H, Ar-H). NMR <sup>13</sup>C, DEPT, HSQC, ROESY (C<sub>6</sub>D<sub>6</sub>, 300MHz): δ 30.75 (CH<sub>3</sub>-<sup>t</sup>Bu), 30.87 (CH<sub>3</sub>-<sup>t</sup>Bu), 31.83 (CH<sub>3</sub>-<sup>t</sup>Bu), 33.03 (CH<sub>2</sub>-calix), 33.14 (CH<sub>3</sub>-Np), 33.77 (<sup>t</sup>Bu-quat), 34.04 (<sup>t</sup>Bu-quat), 34.35 (<sup>t</sup>Bu-quat), 36.35 (Np-quat), 39.76 (CH<sub>2</sub>-calix), 100.13 (CH<sub>2</sub>-Np), 123.61 (C<sub>Ar</sub>), 125.23 (C<sub>Ar</sub>), 125.56 (C<sub>Ar</sub>), 126.29 (C<sub>Ar</sub>), 126.49 (C<sub>Ar</sub>), 128.80 (C<sub>Ar</sub>), 130.44 (C<sub>Ar</sub>), 130.67 (C<sub>Ar</sub>), 139.04 (C<sub>Ar</sub>), 145.36 (C<sub>Ar</sub>), 146.99 (C<sub>Ar</sub>), 149.35 (C<sub>Ar</sub>), 151.19 (C<sub>Ar</sub>), 160.03 (C<sub>Ar</sub>). Anal. Calcd for C<sub>49</sub>H<sub>64</sub>O<sub>3</sub>Ti: C, 78.59; H, 8.61. Found: C, 77.65; H, 9.05.

**Synthesis of 5,11,17,23-tetra-tert-butyl-25,26,27-trioxocalix[4]arene titanium (IV) monobenzyl (Ti15):** A slurry of **L9** (0.600 g, 0.948 mmol) and TiBn4 (0.391g, 0.948 mmol) in 15 ml of pentane were stirred at -84°C (AE/N<sub>2</sub> bath) and the mixture was allowed to reach RT overnight. After evaporation of the volatiles, the residue was washed with 10ml of pentane and dried in vacuum to provide a salmon powder (0.484g, 66%). NMR <sup>1</sup>H (C<sub>6</sub>D<sub>6</sub>, 300MHz): δ 0.73 (s, 9H, <sup>t</sup>Bu), 0.76 (s, 9H, <sup>t</sup>Bu), 1.36 (s, 18H, <sup>t</sup>Bu), 3.37 (d, 2H, CH<sub>2</sub>-calix, J = 13.2 Hz), 3.45 (d, 2H, CH<sub>2</sub>-calix, J = 12.3 Hz), 3.60 (s, 2H, CH<sub>2</sub>-Bn), 4.18 (d, 2H, CH<sub>2</sub>-calix, J = 12.3 Hz), 4.96 (d, 2H, CH<sub>2</sub>-calix, J = 13.2 Hz), 6.76 (m, 5H, *m*-H<sub>Ar</sub>-calix + *ipso*-H<sub>Ar</sub>-calix), 6.92 (t, 1H, *p*-H<sub>Ar</sub>-Bn, J = 7.3 Hz), 7.17 (d, 2H, *m*-H<sub>Ar</sub>-calix, J = 2.4 Hz), 7.21 (d, 2H, *m*-H<sub>Ar</sub>-calix, J = 2.4 Hz), 7.25 (t, 2H, *m*-H<sub>Ar</sub>-Bn, J = 7.3 Hz), 7.48 (d, 2H, *o*-H<sub>Ar</sub>-Bn, J = 7.3 Hz). NMR <sup>13</sup>C (C<sub>6</sub>D<sub>6</sub>, 300MHz): δ 30.76 (CH<sub>3</sub>-<sup>t</sup>Bu), 30.84 (CH<sub>3</sub>-<sup>t</sup>Bu), 31.82 (CH<sub>3</sub>-<sup>t</sup>Bu), 32.96 (CH<sub>2</sub>-calix), 33.79 (<sup>t</sup>Bu-quat), 33.98 (<sup>t</sup>Bu-quat), 34.34 (<sup>t</sup>Bu-quat), 39.42 (CH<sub>2</sub>-calix), 85.13 (CH<sub>2</sub>-Bn), 123.38 (C<sub>Ar</sub>), 125.24 (C<sub>Ar</sub>), 125.24 (C<sub>Ar</sub>), 125.51 (C<sub>Ar</sub>), 126.07 (C<sub>Ar</sub>) 126.57 (C<sub>Ar</sub>), 127.74 (C<sub>Ar</sub>), 129.42 (C<sub>Ar</sub>), 130.04 (C<sub>Ar</sub>), 130.64 (C<sub>Ar</sub>), 130.78 (C<sub>Ar</sub>), 139.02 (C<sub>Ar</sub>), 143.02 (C<sub>Ar</sub>), 145.49 (C<sub>Ar</sub>), 147.06 (C<sub>Ar</sub>), 150.06 (C<sub>Ar</sub>), 150.78 (C<sub>Ar</sub>), 160.59 (C<sub>Ar</sub>) Anal. Calcd for C<sub>51</sub>H<sub>60</sub>O<sub>3</sub>Ti: C, 79.67; H, 7.87. Found: C, 79.22; H, 8.43

**Synthesis of 5,11,17,23-tetra-tert-butyl-25,26,27-trioxo-28-monomethoxycalix[4]arene titanium (IV) mononeopentyl (Ti16):** NpMgCl (0.17ml, 0.318mmol, 1.89M in diethyl ether)

was added dropwise to a stirred toluene (10ml) solution of  $[[4+]\text{-}(\text{OMe})(\text{O})_3\text{TiCl}]$  (0.243g, 0.318mmol) at -30°C. The reaction was stirred overnight and the volatiles removed in vacuum. Pentane (15ml) was then added and the salts were filtered off through celite. After evaporation of the solvent, a yellow-orange solid is obtained (0.170g, 69%). NMR  $^1\text{H}$  ( $\text{C}_6\text{D}_6$ , 300MHz):  $\delta$  0.69 (s, 9H, calix- $\text{CH}_3$ ), 0.79 (s, 9H, calix- $\text{CH}_3$ ), 1.42 (s, 18H, calix- $\text{CH}_3$ ), 2.63 (s, 2H, Np- $\text{CH}_2$ ), 3.30 (d, 2H, calix- $\text{CH}_2$ ,  $J = 12.0\text{Hz}$ ), 3.37 (d, 2H, calix- $\text{CH}_2$ ,  $J = 12.0\text{Hz}$ ), 3.59 (s, 3H,  $\text{OCH}_3$ ), 4.52 (d, 2H,  $\text{CH}_2$ -calix,  $J = 12.0\text{Hz}$ ), 5.24 (d, 2H,  $\text{CH}_2$ -calix,  $J = 12.0\text{Hz}$ ), 6.80 (s, 2H,  $\text{H}_{\text{Ar}}$ ), 6.87 (s, 2H,  $\text{H}_{\text{Ar}}$ ), 7.25 (s, 4H,  $\text{H}_{\text{Ar}}$ ). NMR  $^{13}\text{C}$ , DEPT ( $\text{C}_6\text{D}_6$ , 300MHz):  $\delta$  30.58 ( $\text{CH}_3$ - $t\text{-Bu}$ ), 31.00 ( $\text{CH}_3$ - $t\text{-Bu}$ ), 32.00 ( $\text{CH}_3$ - $t\text{-Bu}$ ), 33.37 ( $\text{CH}_3$ -Np), 33.62 ( $\text{CH}_2$ -calix), 33.63 ( $C$ - $t\text{-Bu}$ ) 33.67 ( $C$ - $t\text{-Bu}$ ), 33.90 ( $\text{CH}_2$ -calix), 34.41 ( $C$ - $t\text{-Bu}$ ), 36.67 (C-Np), 65.24 ( $\text{OCH}_3$ ), 100.29 (Np- $\text{CH}_2$ ), 123.98 ( $\text{C}_{\text{Ar}}$ ), 125.45 ( $\text{C}_{\text{Ar}}$ ), 125.72 ( $\text{C}_{\text{Ar}}$ ), 126.00 ( $\text{C}_{\text{Ar}}$ ), 127.07 ( $\text{C}_{\text{Ar}}$ ), 130.62 ( $\text{C}_{\text{Ar}}$ ), 131.44 ( $\text{C}_{\text{Ar}}$ ), 132.42 ( $\text{C}_{\text{Ar}}$ ), 144.54 ( $\text{C}_{\text{Ar}}$ ), 144.80 ( $\text{C}_{\text{Ar}}$ ), 148.40 ( $\text{C}_{\text{Ar}}$ ), 149.98 ( $\text{C}_{\text{Ar}}$ ), 155.05 ( $\text{C}_{\text{Ar}}$ ), 160.10 ( $\text{C}_{\text{Ar}}$ ). Anal. Calcd for  $\text{C}_{50}\text{H}_{66}\text{O}_4\text{Ti}$ : C, 77.10; H, 8.54. Found: C, 77.08; H, 8.64

**Synthesis of 5,11,17,23-tetra-tert-butyl-25,27-dioxo-26,28-dipropoxycalix[4]arene zirconium (IV) dichloride (Zr1):**  $n\text{BuLi}$  (0.86 ml, 1.364 mmol, 1.6 M in hexanes) was added dropwise to a stirred solution of **L3** (0.500 g, 0.682 mmol) in 10 ml of THF. The resulting orange solution was transferred to a dropping funnel and added dropwise to a suspension of  $\text{ZrCl}_4\cdot 2\text{THF}$  (0.257 g, 0.682 mmol) in 20 ml of THF, yielding a yellow solution. After 2h of stirring at RT, volatiles were removed in vacuum and the residue washed with pentane (2x7ml) to provide a white solid (0.170g, 28%). NMR  $^1\text{H}$  ( $\text{C}_6\text{D}_6$ , 300MHz):  $\delta$  0.38 (t, 6H,  $\text{OCH}_2\text{CH}_2\text{CH}_3$ ,  $J = 7.5\text{Hz}$ ), 0.69 (s, 18H,  $\text{CH}_3$ - $t\text{-Bu}$ ), 1.46 (s, 18H,  $\text{CH}_3$ - $t\text{-Bu}$ ), 2.04 (m, 4H,  $\text{OCH}_2\text{CH}_2\text{CH}_3$ ), 3.21 (d, 4H,  $\text{CH}_2$ ,  $J = 13.2\text{Hz}$ ), 4.59-4.65 (m, 4H + 4H,  $\text{CH}_2$  +  $\text{OCH}_2\text{CH}_2\text{CH}_3$ ), 6.85 (s, 4H, Ar-H), 7.23 (s, 4H, Ar-H). NMR  $^{13}\text{C}$ , DEPT ( $\text{C}_6\text{D}_6$ , 300MHz):  $\delta$  8.78 ( $\text{OCH}_2\text{CH}_2\text{CH}_3$ ), 21.92 ( $\text{OCH}_2\text{CH}_2\text{CH}_3$ ), 30.50 ( $\text{CH}_3$ - $t\text{-Bu}$ ), 32.07 ( $\text{CH}_3$ - $t\text{-Bu}$ ), 33.71 ( $t\text{-Bu}$ -quat), 34.41 ( $t\text{-Bu}$ -quat +  $\text{CH}_2$ -calix), 86.65 ( $\text{OCH}_2\text{CH}_2\text{CH}_3$ ), 124.71 (Ar-*meta*), 127.51 (Ar-*meta*), 130.20 (Ar-*ortho*), 132.28 (Ar-*ortho*), 142.89 (Ar-*para*), 149.44 (Ar-*para*), 153.24 (Ar-O), 158.64 (Ar-O). Anal. Calcd for  $\text{C}_{50}\text{H}_{66}\text{Cl}_2\text{O}_4\text{Zr}$ : C, 67.24; H, 7.45. Found: C, 66.95; H, 7.03

**Synthesis of 5,11,17,23-tetra-tert-butyl-25,27-dioxo-26,28-dipropoxycalix[4]arene zirconium (IV) bis-neopentyl (Zr2):**  $\text{ZrCl}_4\cdot 2\text{THF}$  (0.557 g, 1.477 mmol) and **L3** (1.000 g, 1.477 mmol) were suspended in 15 ml of toluene. The reaction mixture was refluxed for 2.5 h

and the volatiles were removed in vacuum. 15 ml of fresh toluene were then added again. After a further reflux (10 min), the solvent was removed and the residue dried in vacuum at 80°C. The flask was then charged with fresh toluene and to the stirred mixture, at -30°C, was added dropwise a solution of NpMgCl (2.14 ml, 2.954 mmol, 1.38 M in diethyl ether). The mixture, which became bright yellow in seconds, was allowed to reach RT. 1ml of 1,4-dioxane was added, and the mixture was stirred over 1h, filtered on celite and evaporated to give a bright yellow solid (1.0300g, 77%). NMR  $^1\text{H}$  ( $\text{C}_6\text{D}_6$ , 300MHz):  $\delta$  0.77 (s, 18H, calix-'Bu), 1.43 (s, 18H, calix-'Bu), 1.58 (s, 18H, 'Bu-CH<sub>2</sub>), 1.67 (s, 4H, 'Bu-CH<sub>2</sub>), 3.33 (d, 4H, CH<sub>2</sub>, J = 12.4Hz), 3.77 (s, 6H, OMe), 4.63 (d, 4H, CH<sub>2</sub>, J = 12.4Hz), 6.84 (s, 4H, Ar-H), 7.27 (s, 4H, Ar-H). NMR  $^{13}\text{C}$ , DEPT ( $\text{C}_6\text{D}_6$ , 300MHz):  $\delta$  30.65 (CH<sub>3</sub>-'Bu), 32.00 (CH<sub>3</sub>-'Bu), 33.69 (Np-quat), 33.70 (calix-CH<sub>2</sub>), 34.15 ('Bu-quat), 35.98 (CH<sub>3</sub>-Np), 36.22 ('Bu-quat), 67.84 (OMe), 70.89 (Np-CH<sub>2</sub>), 124.76 (Ar-meta), 126.74 (Ar-meta), 130.78 (Ar-ortho), 131.81 (Ar-ortho), 141.46 (Ar-para), 148.78 (Ar-para), 152.89 (Ar-O), 158.75 (Ar-O). Anal. Calcd for C<sub>56</sub>H<sub>80</sub>O<sub>4</sub>Zr: C, 74.04; H, 8.88. Found: C, 73.51; H, 8.64

**Synthesis of 5,11,17,23-tetra-tert-butyl-25,26,27-trioxocalix[4]arene zirconium (IV) monobenzyl (Zr4):** A slurry of **L9** (0.600 g, 0.948 mmol) and ZrBn<sub>4</sub> (0.432 g, 0.948 mmol) in 15 ml of pentane were stirred at -84°C (AE/N<sub>2</sub> bath) and the mixture was allowed to reach RT overnight. After evaporation of the volatiles, the residue was washed with 3 ml of pentane and dried in vacuum to provide a yellow powder (0.584 g, 40%). NMR  $^1\text{H}$  ( $\text{C}_6\text{D}_6$ , 300MHz):  $\delta$  0.86 (s, 9H, 'Bu), 0.96 (s, 9H, 'Bu), 1.32 (s, 18H, 'Bu), 2.90 (s, 2H, CH<sub>2</sub>-Bn), 3.30 (d, 2H, CH<sub>2</sub>-calix, J = 13.5 Hz), 3.48 (d, 2H, CH<sub>2</sub>-calix, J = 12.9 Hz), 4.24 (d, 2H, CH<sub>2</sub>-calix, J = 12.9 Hz), 4.76 (d, 2H, CH<sub>2</sub>-calix, J = 13.5 Hz), 6.73 (s, 2H, Ar-H), 6.78 (s, 2H, Ar-H), 7.07-7.16 (m, 9H, Ar-H), 7.73 (s, 1H, Ar-H). NMR  $^{13}\text{C}$  ( $\text{C}_6\text{D}_6$ , 300MHz):  $\delta$  30.6 (CH<sub>3</sub>-'Bu), 30.8 (CH<sub>3</sub>-'Bu), 31.4 (CH<sub>3</sub>-'Bu), 32.3 (CH<sub>2</sub>-calix), 33.6 ('Bu-quat), 33.8 ('Bu-quat), 33.9 ('Bu-quat), 38.3 (CH<sub>2</sub>-calix), 65.9 (CH<sub>2</sub>-Bn), 122.1 (C<sub>Ar</sub>), 123.0 (C<sub>Ar</sub>), 125.0 (C<sub>Ar</sub>), 125.2 (C<sub>Ar</sub>), 125.3 (C<sub>Ar</sub>) 125.7 (C<sub>Ar</sub>), 128.0 (C<sub>Ar</sub>), 128.9 (C<sub>Ar</sub>), 129.0 (C<sub>Ar</sub>), 131.1 (C<sub>Ar</sub>), 131.3 (C<sub>Ar</sub>), 139.6 (C<sub>Ar</sub>), 144.3 (C<sub>Ar</sub>), 146.6 (C<sub>Ar</sub>), 147.4 (C<sub>Ar</sub>), 148.0 (C<sub>Ar</sub>), 151.0 (C<sub>Ar</sub>), 156.5 (C<sub>Ar</sub>) Anal. Calcd for C<sub>51</sub>H<sub>60</sub>O<sub>3</sub>Zr: C, 75.41; H, 7.45. Found: C, 76.20; H, 8.31.

## Notes and references

- (1) (a) Feher, F. J.; Budzichowski, T. A. *Polyhedron* **1995**, *14*, 3239(b) Quadrelli, E. A.; Bassett, J. M. *Coord. Chem. Rev.* **2010**, *254*, 707.
- (2) Dijkstra, T. W.; Duchateau, R.; van Santen, R. A.; Meetsma, A.; Yap, G. P. A. *J. Am. Chem. Soc.* **2002**, *124*, 9856.
- (3) Duchateau, R.; Abbenhuis, H. C. L.; van Santen, R. A.; Meetsma, A.; Thiele, S. K. H.; van Tol, M. F. H. *Organometallics* **1998**, *17*, 5663.
- (4) Crocker, M.; Herold, R. H. M.; Orpen, A. G. *Chem. Commun.* **1997**, 2411.
- (5) Jia, L.; Ding, E.; Rheingold, A. L.; Rhatigan, B. *Organometallics* **2000**, *19*, 963.
- (6) (a) de Gaetano, Y.; Clarot, I.; Regnouf-de-Vains, J.-B. *Tetrahedron Lett.* **2009**, *50*, 5793(b) Psychogios, N.; Regnouf-de-Vains, J.-B.; Stoeckli-Evans, H. M. *Eur. J. Inorg. Chem.* **2004**, 2514(c) Engrand, P.; Regnouf-de-Vains, J.-B. *Tetrahedron Lett.* **2002**, *43*, 8863.
- (7) (a) Korchowiec, B.; Orlof, M.; Sautrey, G.; Ben Salem, A.; Korchowiec, J.; Regnouf-de-Vains, J.-B.; Rogalska, E. *J. Phys. Chem. B* **2010**, *114*, 10427(b) Mourer, M.; Psychogios, N.; Laumond, G.; Aubertin, A.-M.; Regnouf-de-Vains, J.-B. *Bioorg. Med. Chem.* **2010**, *18*, 36(c) Mourer, M.; Dibama Hugues, M.; Fontanay, S.; Grare, M.; Duval Raphael, E.; Finance, C.; Regnouf-de-Vains, J.-B. *Bioorg. Med. Chem.* **2009**, *17*, 5496.
- (8) Floriani, C.; Floriani-Moro, R. *Adv. Organomet. Chem.* **2001**, *47*, 167.
- (9) (a) Zanotti-Gerosa, A.; Solari, E.; Giannini, L.; Floriani, C.; Re, N.; Chiesi-Villa, A.; Rizzoli, C. *Inorg. Chim. Acta* **1998**, *270*, 298(b) Radius, U. *Inorg. Chem.* **2001**, *40*, 6637.
- (10) Capacchione, C.; Neri, P.; Proto, A. *Inorg. Chem. Commun.* **2003**, *6*, 339.
- (11) Frediani, M.; Sémeril, D.; Comucci, A.; Bettucci, L.; Frediani, P.; Rosi, L.; Matt, D.; Toupet, L.; Kaminsky, W. *Macromol. Chem. Phys.* **2007**, *208*, 938.
- (12) Giannini, L.; Caselli, A.; Solari, E.; Floriani, C.; Chiesi-Villa, A.; Rizzoli, C.; Re, N.; Sgambellotti, A. *J. Am. Chem. Soc.* **1997**, *119*, 9198.
- (13) (a) Cobben, P. L. H. M.; Egberink, R. J. M.; Bomer, J. G.; Bergveld, P.; Verboom, W.; Reinhoudt, D. N. *J. Am. Chem. Soc.* **1992**, *114*, 10573(b) Van Loon, J. D.; Arduini, A.; Coppi, L.; Verboom, W.; Pochini, A.; Ungaro, R.; Harkema, S.; Reinhoudt, D. N. *J. Org. Chem.* **1990**, *55*, 5639(c) No, K.; Hong, M. *J. Chem. Soc.-Chem. Commun.* **1990**, 572.
- (14) (a) Groenen, L. C.; Ruel, B. H. M.; Casnati, A.; Verboom, W.; Pochini, A.; Ungaro, R.; Reinhoudt, D. N. *Tetrahedron* **1991**, *47*, 8379(b) Shinkai, S.; Araki, K.; Koreishi, H.; Tsubaki, T.; Manabe, O. *Chem. Lett.* **1986**, 1351.
- (15) Casnati, A.; Arduini, A.; Ghidini, E.; Pochini, A.; Ungaro, R. *Tetrahedron* **1991**, *47*, 2221.
- (16) Ghidini, E.; Uguzzoli, F.; Ungaro, R.; Harkema, S.; Abu El-Fadl, A.; Reinhoudt, D. N. *J. Am. Chem. Soc.* **1990**, *112*, 6979.
- (17) Quintard, A.; Darbost, U.; Vocanson, F.; Pellet-Rostaing, S.; Lemaire, M. *Tetrahedron: Asymmetry* **2007**, *18*, 1926.

- (18) Kenis, P. J. A.; Noordman, O. F. J.; Schönherr, H.; Kerver, E. G.; Snellink-Ruël, B. H. M.; Hummel, G. J. v.; Harkema, S.; Vorst, C. P. J. M. v. d.; Hare, J.; Picken, S. J.; Engbersen, J. F. J.; Hulst, N. F. v.; Vancso, G. J.; Reinhoudt, D. N. *Chem. Eur. J.* **1998**, *4*, 1225.
- (19) Jaime, C.; De Mendoza, J.; Prados, P.; Nieto, P. M.; Sanchez, C. *J. Org. Chem.* **1991**, *56*, 3372.
- (20) Pettit, G. R.; Piatak, D. M. *J. Org. Chem.* **1962**, *27*, 2127.
- (21) Sakai, N.; Moriya, T.; Konakahara, T. *J. Org. Chem.* **2007**, *72*, 5920.
- (22) Gonzalez, J. J.; Nieto, P. M.; Prados, P.; Echavarren, A. M.; de Mendoza, J. *J. Org. Chem.* **1995**, *60*, 7419.
- (23) Behenna Douglas, C.; Stockdill Jennifer, L.; Stoltz Brian, M. *Angew. Chem., Int. Ed.* **2007**, *46*, 4077.
- (24) Sajiki, H.; Mori, A.; Mizusaki, T.; Ikawa, T.; Maegawa, T.; Hirota, K. *Org. Lett.* **2006**, *8*, 987.
- (25) Al-Saraierh, H.; Miller, D. O.; Georghiou, P. E. *J. Org. Chem.* **2005**, *70*, 8273.
- (26) Grynszpan, F.; Goren, Z.; Biali, S. E. *J. Org. Chem.* **1991**, *56*, 532.
- (27) Harada, T.; Ohseto, F.; Shinkai, S. *Tetrahedron* **1994**, *50*, 13377.
- (28) Brunink, J. A. J.; Verboom, W.; Engbersen, J. F. J.; Harkema, S.; Reinhoudt, D. N. *Recueil Des Travaux Chimiques Des Pays-Bas-Journal of the Royal Netherlands Chemical Society* **1992**, *111*, 511.
- (29) Araki, K.; Iwamoto, K.; Shigematsu, S.; Shinkai, S. *Chem. Lett.* **1992**, 1095.
- (30) Arduini, A.; Casnati, A.; Dodi, L.; Pochini, A.; Ungaro, R. *J. Chem. Soc.-Chem. Commun.* **1990**, 1597.
- (31) Fan, M.; Zhang, H. *Organometallics* **1996**, *15*, 5216.
- (32) Narumi, F.; Morohashi, N.; Matsumura, N.; Iki, N.; Kameyama, H.; Miyano, S. *Tetrahedron Lett.* **2002**, *43*, 621.
- (33) Aleksiuk, O.; Grynszpan, F.; Biali, S. E. *J. Chem. Soc.-Chem. Commun.* **1993**, 11.
- (34) Markovsky, L. N.; Visotsky, M. A.; Pirozhenko, V. V.; Kalchenko, V. I.; Lipkowski, J.; Simonov, Y. A. *Chem. Commun.* **1996**, 69.
- (35) Fukazawa, Y.; Deyama, K.; Usui, S. *Tetrahedron Lett.* **1992**, *33*, 5803.
- (36) Grynszpan, F.; Aleksiuk, O.; Biali, S. E. *J. Org. Chem.* **1994**, *59*, 2070.
- (37) Shang, S.; Khasnis, D. V.; Burton, J. M.; Santini, C. J.; Fan, M.; Small, A. C.; Lattman, M. *Organometallics* **1994**, *13*, 5157.
- (38) Haino, T.; Akii, H.; Fukazawa, Y. *Synlett* **1998**, *1998*, 1016.
- (39) Toscano, P. J.; Schermerhorn, E. J.; Barren, E.; Liu, S. C.; Zubietta, J. *J. Coord. Chem.* **1998**, *43*, 169.
- (40) Ozerov, O. V.; Ladipo, F. T.; Patrick, B. O. *J. Am. Chem. Soc.* **1999**, *121*, 7941.
- (41) Johnson, L. K.; Killian, C. M.; Brookhart, M. *J. Am. Chem. Soc.* **1995**, *117*, 6414.
- (42) Kemp, R. A.; Brown, D. S.; Lattman, M.; Li, J. *J. Mol. Catal. A: Chem.* **1999**, *149*, 125.

## **Chapter IV**

**Synthesis of Tantalacalix[4]arenes as soluble  
models of grafted species**

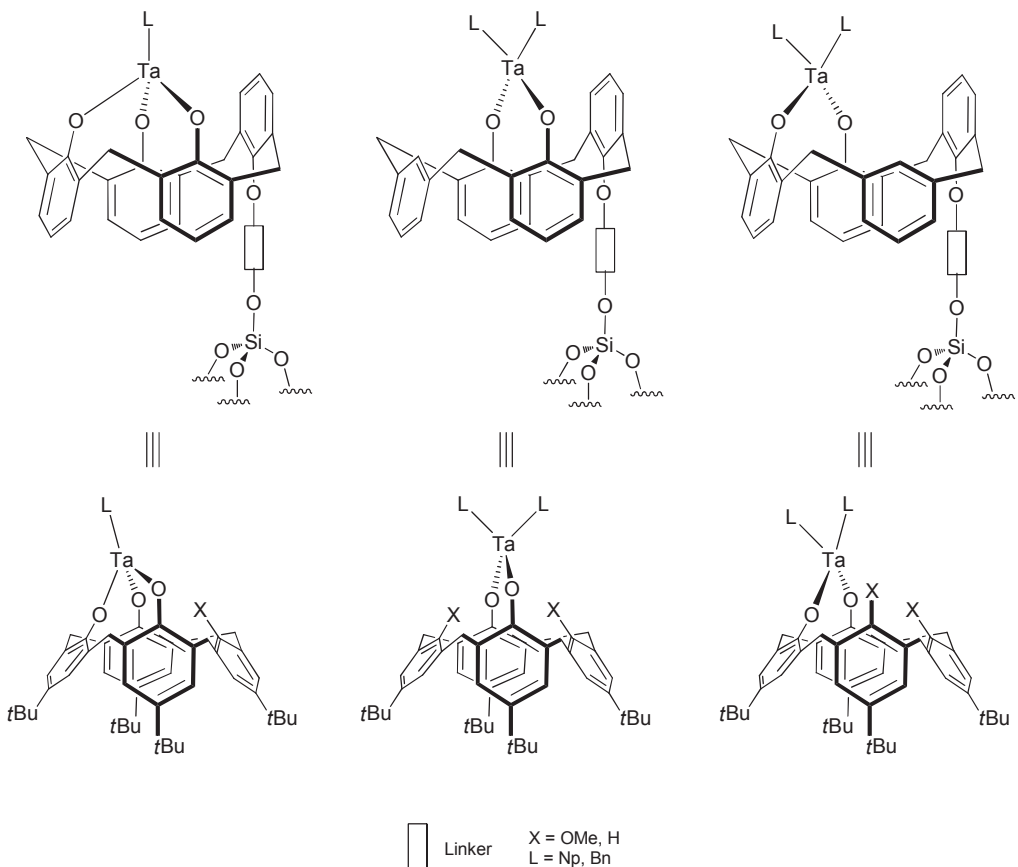


## 1. Introduction

In SOMC, tantalum has proven to be a metal with unexpected properties: totally new chemical transformations by single site silica surface tantalum hydrides, *e.g.* alkane metathesis, have never been observed using other homogeneous or heterogeneous catalysts. However, there are still some doubts about the single site character of surface tantalum species. EXAFS results indicate that with tantalum hydrides on the silica surface several species co-exist in which the metal may exhibit several types of coordination to the surface: bi- or tripodal<sup>1</sup>  $\sigma$ -bonded oxygen. Even for the bipodal Ta, it seems, according to EXAFS, that one or several  $\pi$ -bonded oxygens can coordinate to the metal center rendering it less electrophilic and limiting its accessibility due to the bulky nature of these surface oxygen ligands.

As already presented in chapter III, we have decided to pursue our investigation in modeling some of these surface organometallic species with the preparation and the characterization of a series of unprecedented tantalacalix[4]arenes complexes. A short literature survey will present selected soluble oxo systems relevant for their potential as models of surface organometallic catalysts. A series of tantalacalix[4]arenes were targeted in order to provide any models to help in the characterization of their grafted counterparts onto silica support modified by Al*i*Bu<sub>3</sub> (**Scheme 1**).

The syntheses of the tantalacalix[4]arene complexes are mostly based on the starting calix[4]arenic ligands described in chapter III except a new intermediate ligand, developed in **section 4.1**. Using the salt- or alkane-elimination route, the corresponding chloro and alkyl complexes obtained are new and unreported. In most cases the behavior of the tantalum center with its supporting ligand gives interesting results. The syntheses of the bipodal and the tripodal models are described in **sections 4.2** and **4.2.2**, respectively.

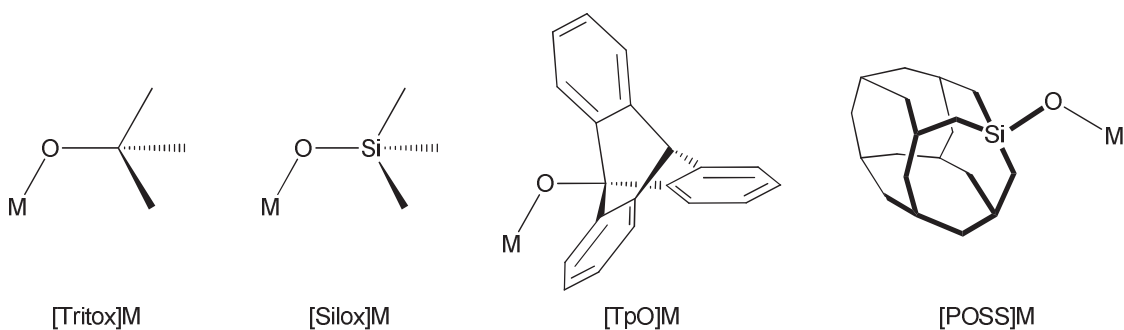


**Scheme 1: Grafted tantalacalix[4]arenes on a silica support and their corresponding soluble tantalacalix[4]arene models**

## 2. Bibliographic study: bulky oxo donor ligands, polysilsesquioxanes, aryloxy and calix[4,6,8]arenes-based complexes as molecular models of silica-grafted species of tantalum

### 2.1 Description of [Tritox], [Silox], 9-Oxytriptycene, as bulky oxo donor ligands, and POSS-based complexes of tantalum

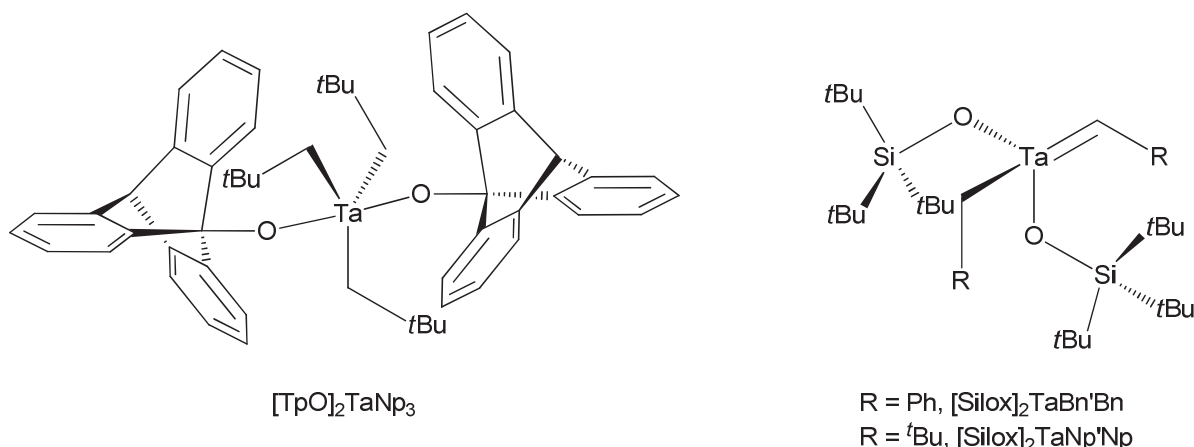
Different types of bulky oxo donor ligands have been reported in the literature not only for the understanding of elementary organometallic processes, but also to reinforce the characterization of supported tantalum complexes on oxides. These can be divided into two classes: i) ligands presenting C-O-M bonds ([Tritox] = -CtBu<sub>3</sub>, [TpO] = 9-oxotriptycene) and ii) ligands with Si-O-M bonds ([Silox] = -SitBu<sub>3</sub>, POSS) (**Scheme 2**).



Scheme 2: [Tritox], [Silox], [TpO] and POSS as bulky oxo donor ligands

Wolczanski<sup>2</sup> first introduced three types of bulky oxo donor ligands, namely [tritox], [TpO] and [silox], for the generation of electron-deficient and sterically saturated tantalum complexes.

All attempts to prepare [Tritox]-Ta derivatives *via* either salt- or alkane elimination routes were unsuccessful as degradable complexes were provided, due to the C-O bond heterolysis by the ease of triter*t*butylcarbonium formation. In contrast, [TpO] presenting a pyramidal structure of the quaternary bridgehead carbon not prone to carbonium formation, was then proposed as an alternative ligand. Subsequently, the complex  $[TpO]_2TaCl_3$  was obtained from  $TaCl_5$  and 2 eq. of  $TpOSiMe_3$ , as the starting material to avoid solubility problems. Alkylation of  $[TpO]_2TaCl_3$  with 3 eq. of  $NpLi$  provided a mixture containing the identifiable target compound  $[TpO]_2TaNp_3$ . The alkane-elimination route was however preferred, as reaction with 1 eq. of  $TaNp'Np_3$  provided  $[TpO]_2TaNp_3$  in 79% yield. Molecular structure of  $[TpO]_2TaNp_3$  shows a triangular-based bipyramidal structure in which both [TpO] groups are in *trans*-position along the axis. The three Np groups form the triangular base due to their bulkiness, thus avoiding any carbenic derivative formation (**Scheme 3**).

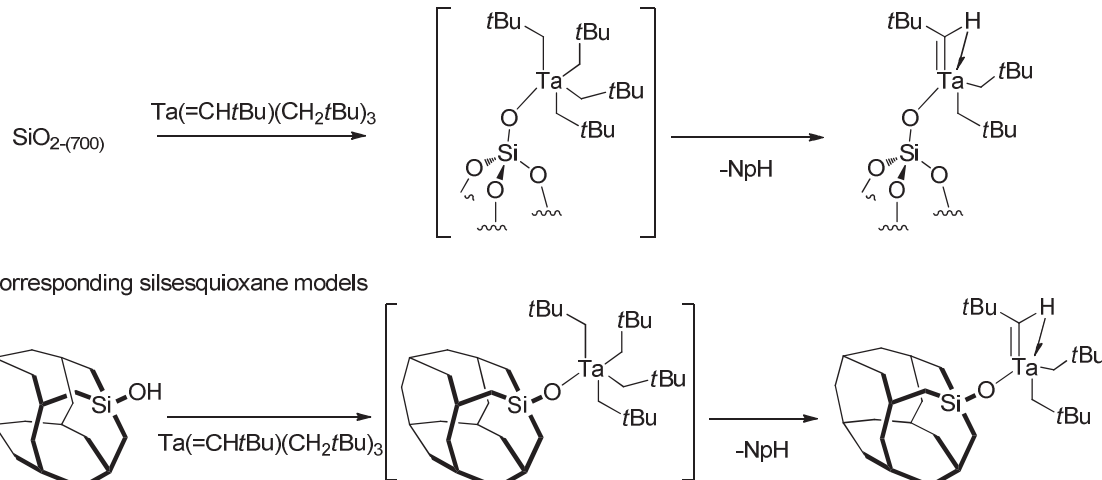


Scheme 3:  $[TpO]_2TaNp_3$ ,  $[Silox]_2TaBn'Bn$  and  $[Silox]_2TaNp'Np$  complexes<sup>2</sup>

Bulky ligands with more robust Si-O bonds ([Silox] and POSS) give more stable tantalum complexes either *via* alkane- or salt-elimination pathways. The derivative  $[\text{Silox}]_2\text{TaNp}'\text{Np}$  was isolated by alkylation of  $[\text{Silox}]_2\text{TaNp}_2\text{Cl}$  with 1 eq. of NpLi. The carbene formation suggests the relative *syn*-position of both [Silox] ligands in the starting material  $[\text{Silox}]_2\text{TaNp}_2\text{Cl}$ . These observations are also relevant for the benzyl benzylidene analogue  $[\text{Silox}]_2\text{TaBn}'\text{Bn}$ , obtained from thermal treatment of  $[\text{Silox}]_2\text{TaBn}_3$  (**Scheme 3**).

It has been reported in COMS laboratory the synthesis of the POSS model of the monografted tantalum complex ( $\equiv\text{SiO}\text{TaNp}_2\text{Np}'$ ), obtained on different supports such as  $\text{SiO}_{2(700)}^3$  and  $\text{MCM-41}_{(500)}^4$ . This was modeled with the monosilanol POSS compound  $(\text{C}_5\text{H}_9)_7\text{Si}_8\text{O}_{12}(\text{OH})$ , already described in Chapter III. Direct reaction of  $\text{TaNp}_3\text{Np}'$  with this POSS ligand affords the monopodal carbenic compound  $(\text{C}_5\text{H}_9)_7\text{Si}_8\text{O}_{13}\text{TaNp}_2\text{Np}'$ , which is isostructural and spectroscopically close to its grafted analogue (**Scheme 4**).<sup>5</sup> For instance, the NMR resonances of the two systems, both in solid-state and in solution in  $\text{C}_6\text{D}_6$ , are quite similar. It is noteworthy that the  ${}^1\text{J}(\text{C}-\text{H})$  coupling spectrum of the methylene moieties clearly indicates the presence of an agostic interaction of the methylene with the tantalum center in both grafted and soluble species ( ${}^1\text{J}(\text{C}-\text{H}) = 80 \pm 5$  Hz for the grafted species *vs.* 86 Hz for the homogenous model).<sup>5b</sup>

Grafted monopodal tantalum species

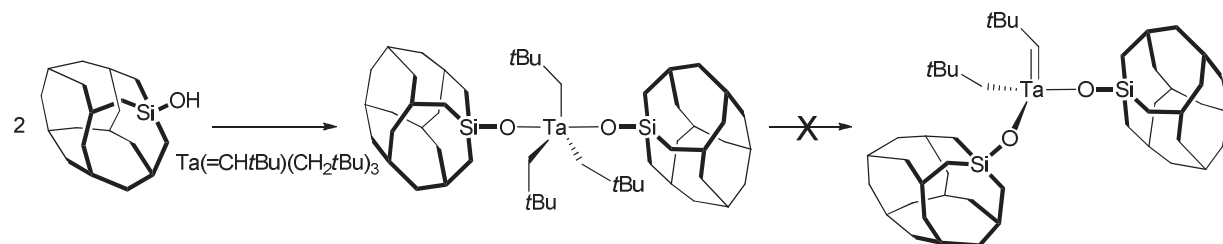


**Scheme 4: Tantalum silsesquioxanes models<sup>5</sup>**

Monitoring the synthesis of the model compound by NMR spectroscopy revealed the presence of a tetraneopentyl intermediate, with concomitant release of neopentane, indicative of a step-wise reaction mechanism. The first step consists of rapid addition of the carbene across the Si-OH bond followed by the slower  $\alpha$ -abstraction of neopentane. Spectroscopic

detection of the analogous surface tetraneopentyl intermediate complex for the silica-grafting reaction indicates the same mechanistic pathway.

In contrast, reaction between 2 eq. of  $(C_5H_9)_7Si_8O_{12}(OH)$  and  $TaNp'Np_3$  provides  $[(C_5H_9)_7Si_8O_{12}(O)]_2TaNp_3$ , which shows thermal stability (**Scheme 5**). This observation suggests, by analogy with  $[TpO]_2TaNp_3$ , the *trans* disposition of the two POSS ligands.<sup>6</sup>

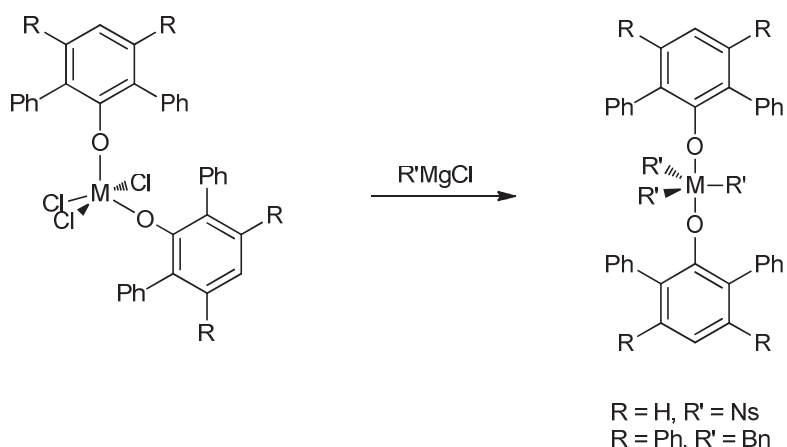


**Scheme 5:** Tantalum silsesquioxanes models<sup>7</sup>

The bulky oxo donor ligands [Silox] and [POSS] have proven to be fluxional and independent from another, hence position themselves in such a way to evenly distribute their steric bulk around the metal center. In opposite, the relative rigidity, the potential functionalization and the stability of the  $Csp^2$ -O bond rank the calix[4]arenes as the most relevant class of molecular models of grafted metallacalix[4]arenes species. The calix[4]arenic ligand offers a representative electronic environment and similar structural constrains for the metal center, imposed by the grafted calix[4]arenes. In addition to a brief overview on the preparation of some tantalum aryloxy complexes, tantalocalix[4]arenes models will be discussed in the next section.

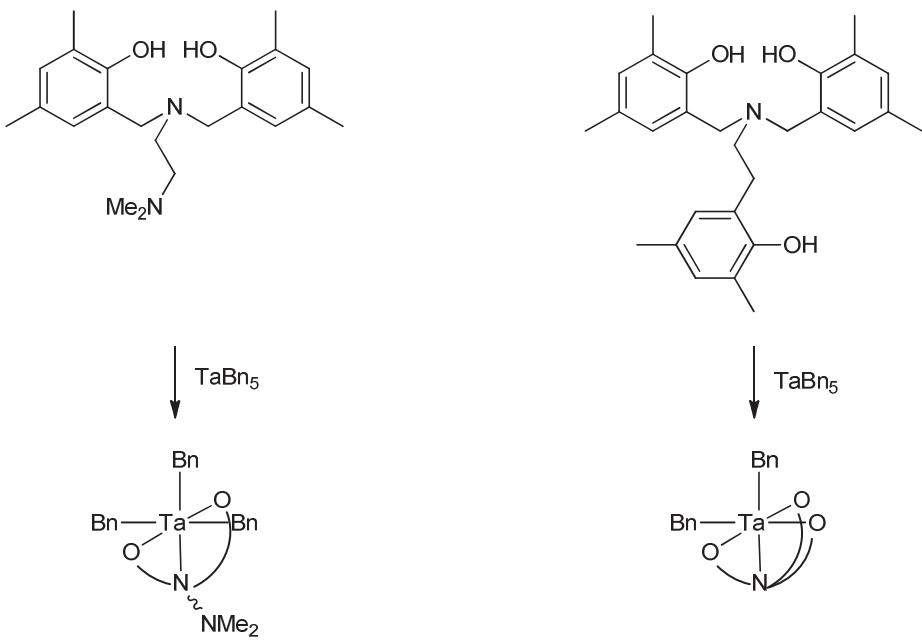
## 2.2 Aryloxy and calix[4,6,8]arenes-based complexes of tantalum

The preparation of different tantalum complexes presenting aryloxy ligands either *via* the salt- or the alkane-elimination pathways is referred. For instance, Rothwell *et al.* described the preparation of some bis-aryloxy tantalum trialkyl complexes by the salt-elimination pathway.<sup>8</sup> Typically, the bis-aryloxy compounds of tantalum  $[Ta(OAr)_2Cl_3]$  are isolated by simple addition of 2 eq. of the phenol to a solution of  $TaCl_5$ . By this method, different bis-aryloxy tantalum trichloride compounds have been isolated and characterized. The corresponding alkyls are obtained by alkylation of the corresponding chloride derivatives with  $BnMgX$  or  $NsMgX$  (**Scheme 6**).



Scheme 6: Alkylation of two bis-aryloxy tantalum trichloro complexes<sup>8</sup>

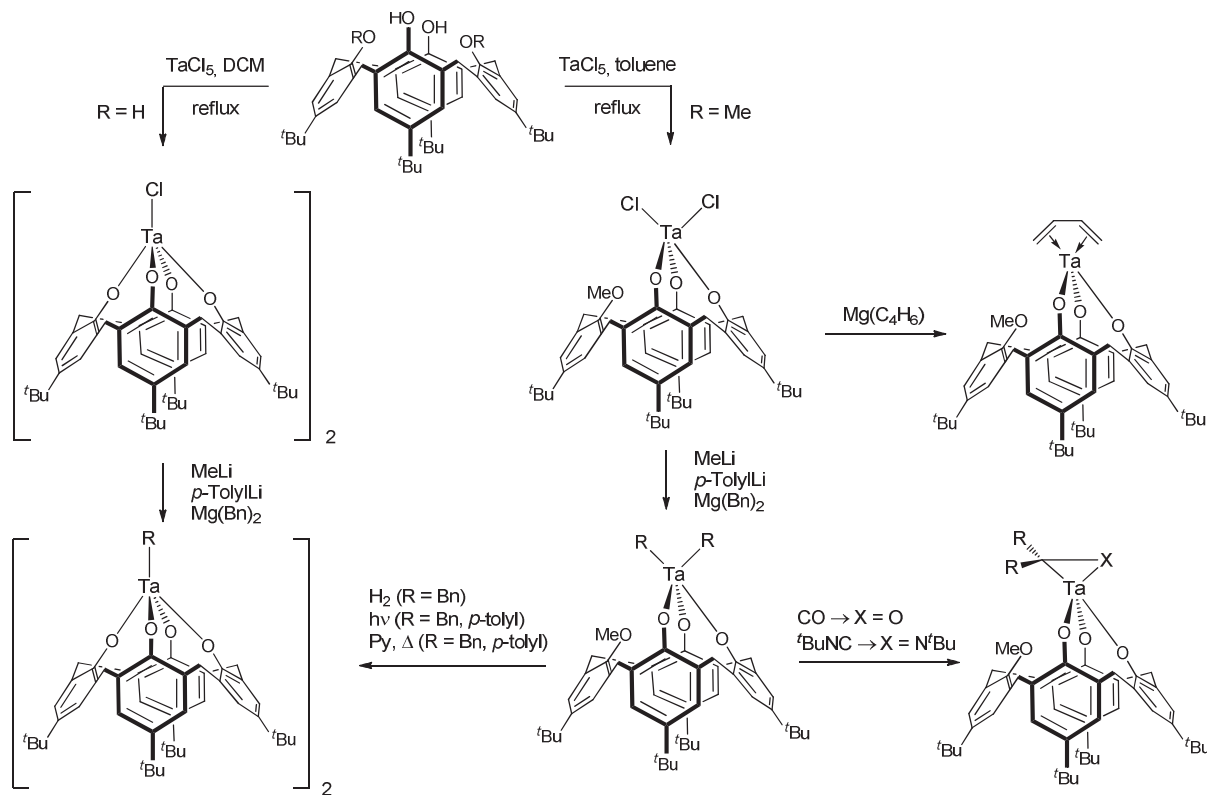
Kol *et al.* have also reported bis- or tris-aryloxy tantalum bis-benzyl systems by direct reaction between the corresponding ligand and  $TaBn_5$  (Scheme 7).<sup>9</sup> The generation of bis- or tris-aryloxy based tantalum complexes was more efficient when starting from  $TaBn_5$ . This may serve as a useful starting point for the synthesis of tantalum-alkyl complexes.



Scheme 7: Preparation of bis- and tris-aryloxy tantalum benzyl complexes from  $TaBn_5$ <sup>9</sup>

Calixarenes can be used in tantalum chemistry as a preorganized set of either distal O<sub>2</sub> (Classes **A**, **B**, **C**), proximal O<sub>2</sub> (Classes **D**, **E**), O<sub>3</sub> (Classes **F**, **G**) or O<sub>4</sub> (Class **H**) donor atoms, with a number of distinctive peculiarities, unlike the independent phenoxy groups (see Chapter III). Floriani *et al.* investigated organometallic chemistry of tantalum anchored to either the calix[4]arene O<sub>4</sub> or the monomethoxy calix[4]arene O<sub>3</sub>. The tantalacalix[4]arene [[4+]-O<sub>4</sub>TaCl]<sub>2</sub> was obtained in a dimeric form, by reaction of TaCl<sub>5</sub> with *p*-

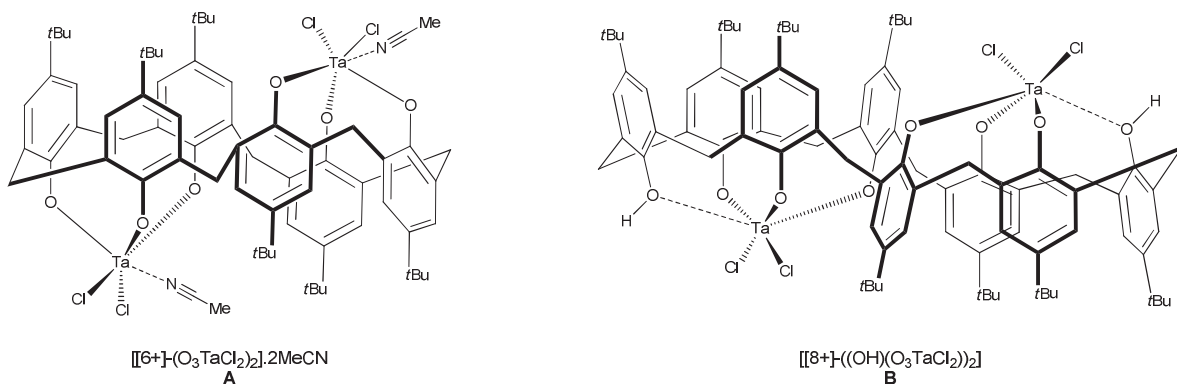
*tert*butylcalix[4]arene in DCM, which was easily alkylated into its methyl, benzyl and *p*-tolyl derivatives (**Scheme 8**).<sup>10</sup> Reaction with TaCl<sub>5</sub> and the ligand [[4+]-1,3-(OMe)<sub>2</sub>(OH)<sub>2</sub>] (Class A) in refluxing toluene provided the tripodal tantacalix[4]arene [[4+]-*(OMe)(O)*<sub>3</sub>TaCl<sub>2</sub>], with concomitant MeCl elimination, due to the σ-bond metathesis between O-Me and Ta-Cl. This was also alkylated into its methyl, benzyl and *p*-tolyl derivatives [[4+]-*(OMe)(O)*<sub>3</sub>TaR<sub>2</sub>], stable under usual storage conditions. On the other hand, when photochemically (in the case of R = Bn, *p*-tolyl) or thermally treated in presence of pyridine (R = Me, Bn, *p*-tolyl), demethylation of the remaining methoxy group is observed. In the case of R = Bn, the monobenzyl complex was also obtained by reacting the tripodal species with H<sub>2</sub>.<sup>11</sup> In addition, [[4+]-*(OMe)(O)*<sub>3</sub>TaR<sub>2</sub>] show CO and *t*BuNC insertion into the tantalum alkyl bond, resulting in the corresponding η<sup>2</sup>-acyl and η<sup>2</sup>-iminoacyl compounds. [[4+]-*(OMe)(O)*<sub>3</sub>TaCl<sub>2</sub>] was reduced into the Ta<sup>III</sup>-butadiene derivative [[4+]-*(OMe)(O)*<sub>3</sub>Ta-η<sup>4</sup>-(C<sub>4</sub>H<sub>6</sub>)] when treated with the reducing agent Mg(C<sub>4</sub>H<sub>6</sub>).<sup>10</sup>



**Scheme 8:** Synthetic pathways for the tripodal and tetrapodal chloro- and alkyl tantacalix[4]arenes models

Studies of the coordination of tantalum with larger calix[n]arenes (n > 4) are quite limited, but the few examples reported by Redshaw<sup>12</sup> are relevant for surface tantalum modeling, as they present new coordination modes for the metal. For instance, reaction of *p*-*tert*butylcalix[6]arene with 2 eq. of TaCl<sub>5</sub> in refluxing DCM affords, after extraction with

MeCN, the bimetallic acetonitrile adduct  $[[6+](O_3TaCl_2)_2].2\text{MeCN}$  **A** (**Scheme 9**). Despite the two coordinated acetonitriles, the tripodal tantalum center is not coordinated to any extra L ligands offered by the calixarene moiety, as the methoxy groups described hitherto. Reaction of 2 eq. of  $\text{TaCl}_5$  with *p*-*tert*butylcalix[8]arene provided the bimetallic tripodal complex  $[[8+]-((OH)(O_3TaCl_2))_2]$  **B**, in which the tantalum is unexpectedly coordinated to a hydroxyl group, without further protolysis (**Scheme 9**).  $[[4+](OMe)(O)_3TaCl_2]$ ,  $[[6+](O_3TaCl_2)_2].2\text{MeCN}$ ,  $[[8+]-((OH)(O_3TaCl_2))_2]$  and  $[[4+]-O_4TaCl]_2$  show low activity in ethylene polymerization when activated with  $\text{Me}_2\text{AlCl} (< 33 \text{ kg}_{\text{PE}}.\text{mol}(\text{Ta}).\text{h}^{-1}.\text{bar}^{-1})$ .



**Scheme 9: Tripodal dichloro tantalacalix[6,8]arenes models**

Bibliographic studies reveal that few groups have worked on tantalacalix[4]arene chemistry. Furthermore, the metal centers of the compounds reported show satisfactory electronic saturation by coordination with ancillary ligands from the calixarene moiety (methoxy, hydroxyl) or external (acetonitrile). Neither bipodal nor donor ligand-free tripodal tantalacalix[4]arenes from are reported. Thus, there is a need to develop these models with unprecedented coordination modes onto the calix[4]arene, which are the most representative models of the well-known bipodal and tripodal tantalum grafted species.

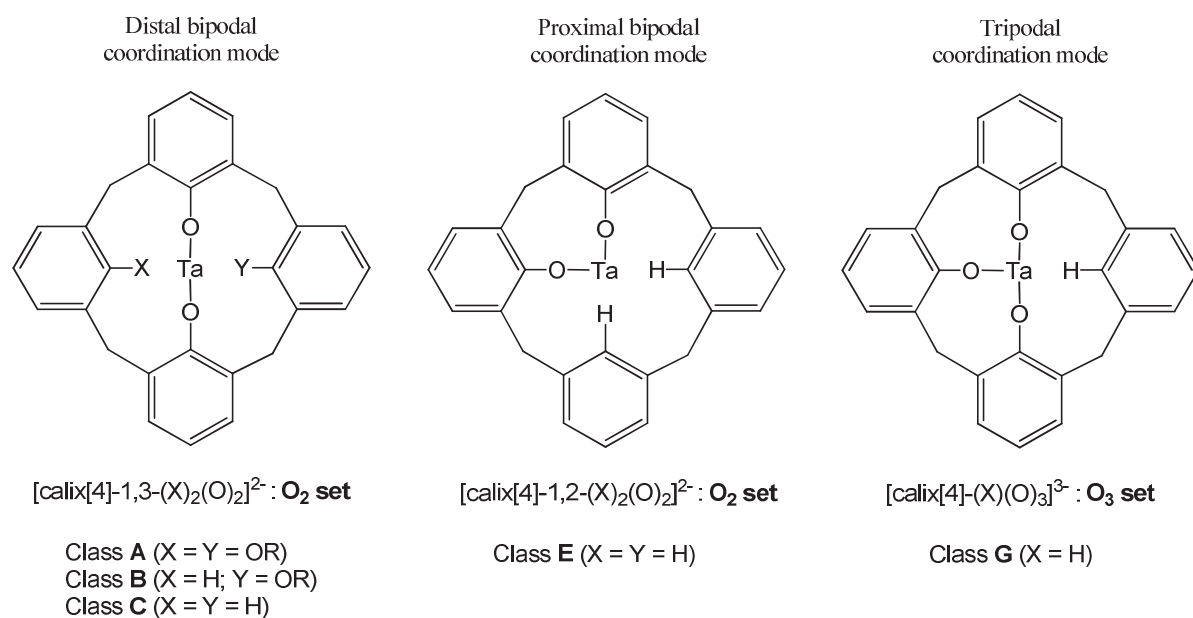
### 3. Strategy

From the few examples reported above, the syntheses of alkyl tantalacalix[4]arenes are commonly realized *via* the salt-elimination route. However, the alkane-elimination route is preferred in SOMC chemistry since it is a clean non-polluting process producing by-products that are easy to eliminate (small alkanes). In order to incorporate the metal alkyl fragment as will be subsequently realized on the grafted calix[4]arenes, our effort will be based on the generation of unreported alkyl tantalacalix[4]arenes *via* this method. Nevertheless, in the case

where direct reaction between metal alkyl complexes and calix[4]arenes proves unsuccessful, the salt-elimination route must be employed as an alternative method. Some of the complexes will be synthesized *via* both methods, if the alkane-elimination route is not efficient enough.

Differing by their podality, the two sets of tantalacalix[4]arenes are targeted:

- i. Distal and proximal bipodal complexes (Classes **A**, **B**, **C** vs **E**) (**Scheme 10**)
- ii. Ancillary ligand free tripodal complexes (Class **G**) (**Scheme 10**)



**Scheme 10:** Schematic representation of the potential coordination mode of tantalacalix[4]arenes (classes *A-F*) (R = alkyl, aryl, etc)

In addition, some complexes cannot be cleanly synthesized from the corresponding ligand but *via* one presenting particularities enhancing the global selectivity. Many phenomena, sometimes unreported, will be highlighted as elementary organometallic processes between the tantalum center and its ligand.

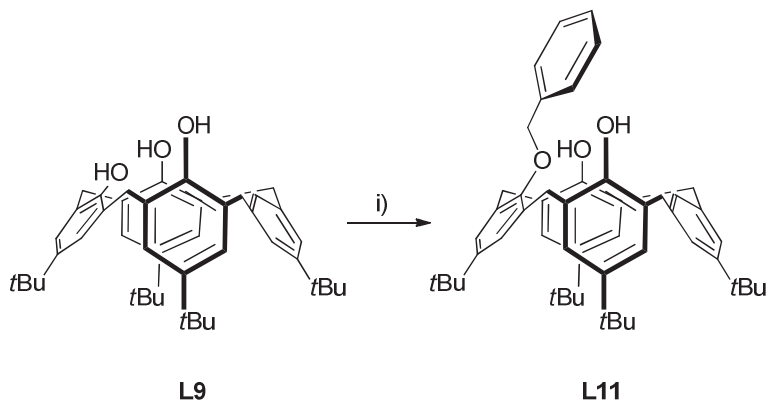
## 4. Results and discussions

### 4.1 Synthesis and characterization of the *p*-tertbutylcalix[4]arene derivative ligands

#### 4.1.1 Synthesis of [[4+]-1,3-(OH)<sub>2</sub>(OBn)(H)] (L11)

Syntheses and conformational studies of [[4+]-1,3-(OMe)<sub>2</sub>(OH)<sub>2</sub>] **L1**, [[4+]-<sub>3</sub>(H)] **L9** and [[4+]-1,3-(OH)<sub>2</sub>(OMe)(H)] **L10** are previously described in Chapter III. The

unreported mono-OH depleted mono-benzyloxy-*p*-*tert*butylcalix[4]arene [[4+]-1,3-(OH)<sub>2</sub>(OBn)(H)] **L11** was obtained by treatment of **L9** with half-equivalent of K<sub>2</sub>CO<sub>3</sub> and one equivalent of BnBr (**Scheme 11**). **L11** was characterized by NMR spectroscopy, mass spectrometry and X-Ray diffraction (**Figure 1**).



**Scheme 11:** Synthetic pathway for [[4+]-1,3-(OH)<sub>2</sub>(OBn)(H)] **L11**. Reagents and conditions: i) 0.5 eq. K<sub>2</sub>CO<sub>3</sub>, 1 eq. BnBr, CH<sub>3</sub>CN, 83°C, 2 h

#### 4.1.2 Structural and conformational studies of [[4+]-1,3-(OH)<sub>2</sub>(OBn)(H)] (**L11**)

<sup>1</sup>H-NMR of **L11** displays three singlets (9:9:18) for the *t*Bu groups and two AB systems corresponding to the two types of methylene bridges, consistent with the Cs symmetry of the system. The singlets at 5.22 ppm and 81.01 ppm in <sup>1</sup>H- and <sup>13</sup>C-NMR are attributed to the -CH<sub>2</sub>Ph carbon. The DEPT spectrum shows two >CH<sub>2</sub> signals at 32.92 and 38.16 ppm belonging to the methylene bridges consistent with the structure being in partial cone conformation.

A suitable crystal for X-ray studies was obtained from slow evaporation of a saturated DCM/MeOH solution at RT (**Figure 1**). Crystallographic data and details associated with data collection are given in Annex III. In contrast to its conformation in solution, **L11** presents a Cs symmetry in which the calixarene exhibits a cone conformation, which is stabilized by hydrogen bonding between hydroxyls and oxygen of the benzyloxy group, which lies along the vertical axis of the ligand.

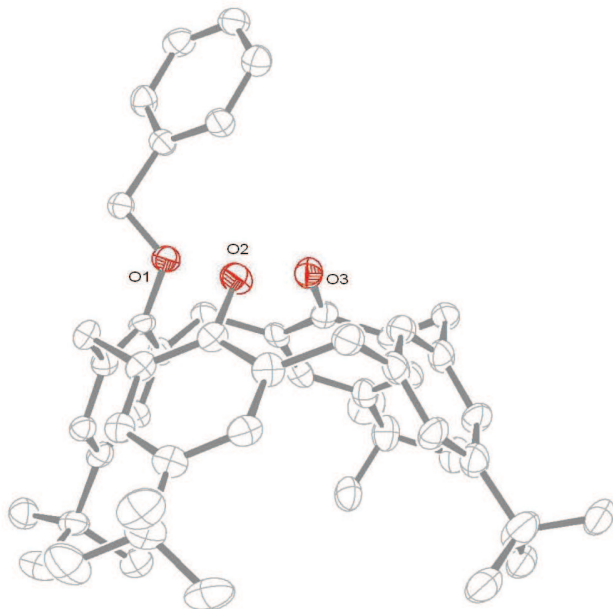


**Figure 1:** Molecular structure of **L11** (only one of the two molecules of the unit cell is shown). For clarity H atoms and solvent molecules were omitted.

## 4.2 Syntheses and characterization of bipodal and tripodal tantalacalix[4]arene complexes

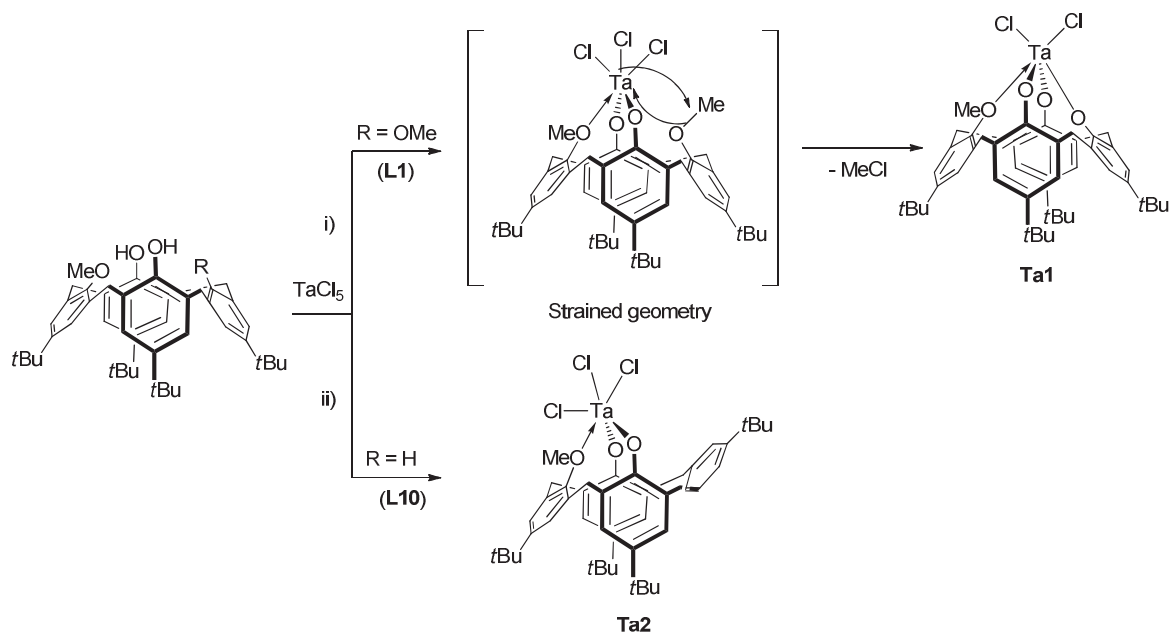
### 4.2.1 Synthesis and characterization of the bipodal tantalacalix[4]arenes

- **Chlorine derivatives of the bipodal tantalacalix[4]arenes**

The synthesis of the bis-chelating model  $[[4+]-1,3-(\text{OMe})_2(\text{O})_2\text{TaCl}_3]$  was attempted either by direct reaction of  $\text{TaCl}_5$  and **L1**, at RT to avoid monodemethylation of **L1** (see section 2.2), or *via* the previously deprotonated ligand  $[[4+]-1,3-(\text{OMe})_2(\text{OLi})_2]$ . In both cases, the desired complex has never been isolated probably due to geometry reasons. In contrast to the bipodal titanium complex  $[[4+]-1,3-(\text{OMe})_2(\text{O})_2\text{TiCl}_2]$  **Ti1**, in which the titanium presents an adaptable and satisfactory octahedral geometry, the corresponding bipodal tantalum intermediate  $[[4+]-1,3-(\text{OMe})_2(\text{O})_2\text{TaCl}_3]$  could not be observed due to a supposed high distortion of the metal center, strained by the calixarene ligand.<sup>10</sup> Therefore, the tantalum center will provoke a monodemethylation of **L1** to provide the tripodal compound  $[[4+]-(\text{OMe})(\text{O})_3\text{TaCl}_2]$  **Ta1** to accommodate a more stable octahedral geometry and coordination sphere (**Scheme 12**).

To support this hypothesis, the reaction with  $\text{TaCl}_5$  and **L10** as starting material was carried out in refluxing toluene over 2h (**Scheme 12**). The complex  $[[4+]-(\text{OMe})-1,3-(\text{O})_2\text{TaCl}_3]$  **Ta2** was readily isolated in a pure form by crystallization (60% yield). Heating of

a solution of **Ta2** at 110°C over 30h showed no conversion. Unlike its titanium analogue **Ti6** (see Chapter III), the tantalum center does not undergo demethylation.

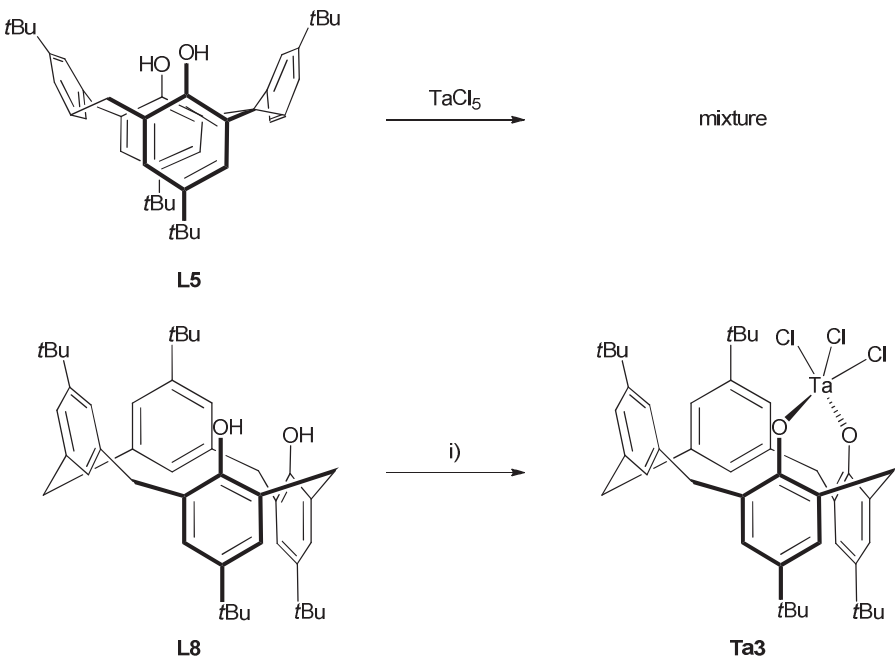


**Scheme 12: Synthetic pathway for the obtention of  $[4+](\text{OMe})(\text{O})_3\text{TaCl}_2]$  **Ta1** and  $[4+](\text{OMe})(\text{O})_2\text{TaCl}_3]$  **Ta2**.**

Reagents and conditions: i) 1 eq.  $\text{TaCl}_5$ , toluene, 110°C, 16 h; ii) 1 eq.  $\text{TaCl}_5$ , toluene, 110°C, 2h

The synthesis of the class C  $[4+]-1,3-(\text{H})_2(\text{O})_2\text{TaCl}_3]$  complex, free of ancillary ligands in the distal position, was also attempted. The reaction between  $\text{TaCl}_5$  and  $[4+]-1,3-(\text{H})_2(\text{OH})_2$  **L5** did not lead to the expected bipodal complex  $[4+]-1,3-(\text{H})_2(\text{O})_2\text{TaCl}_3$ ; only a mixture was observed. This may be because no coordinative alkoxy groups assist the approach of the metal center onto the distal OH groups, which are far enough apart to react independently on different metal centers.

However, direct reaction of  $\text{TaCl}_5$  with the OH-bis-depleted ligand in position 1,2  $[4+]-1,2-(\text{H})_2(\text{OH})_2$  **L8** provides, surprisingly, the targeted bipodal compound  $[4+]-1,2-(\text{H})_2(\text{O})_2\text{TaCl}_3$  **Ta3** in 79% yield (**Scheme 13**). Unlike its distal counterpart, both hydroxyl functions in **L8** are close enough together to react on the same tantalum center.



**Scheme 13:** Synthetic pathway for the bipodal chloro tantalacalix[4]arenes. Reagents and conditions: i) 1 eq.  $TaCl_5$ , toluene, 110°C, 16 h

The  $^1H$ -NMR spectrum of **Ta2** displays three singlets integrating 18:9:9 protons corresponding to the *tBu* groups and two AB systems for the methylenic protons in accordance a Cs symmetry (**Figure 2**). The signal of OMe is shifted drastically downfield from 3.18 ppm to 4.15 ppm. This is consistent with the OMe moiety coordinated to Ta.<sup>10</sup> The unexpected signal at 8.94 ppm, correlated to an aromatic carbon in the HSQC experiment, belongs to the *ipsoAr-H* (**Figure 2**). This chemical shift can be explained by the proximity of this proton with the tantalum center. Both CH<sub>2</sub> signals at 33.7 and 39.6 ppm in the  $^{13}C$ -NMR spectra confirm that **Ta2** is in a partial cone conformation.

The  $^1H$ -NMR spectrum of **Ta3** shows two singlets at 1.18 and 1.28 ppm (18:18 protons) corresponding to the *tBu* groups. In addition, three pairs of doublets belonging to the three different AB systems for the methylenic protons suggest a Cs symmetry. One singlet at 6.26 ppm, integrating for two protons, correlates to an aromatic carbon in the HSQC experiment and is assigned to the *ipsoAr-H*. In contrast with **Ta2**, this chemical shift suggests that these protons are not close to the metal. The DEPT experiment, displays three CH<sub>2</sub> signals at 34.6, 37.5 and 42.8 ppm: the molecule is in a 1,2-alternate conformation in which both OH-depleted units are *syn*-oriented.

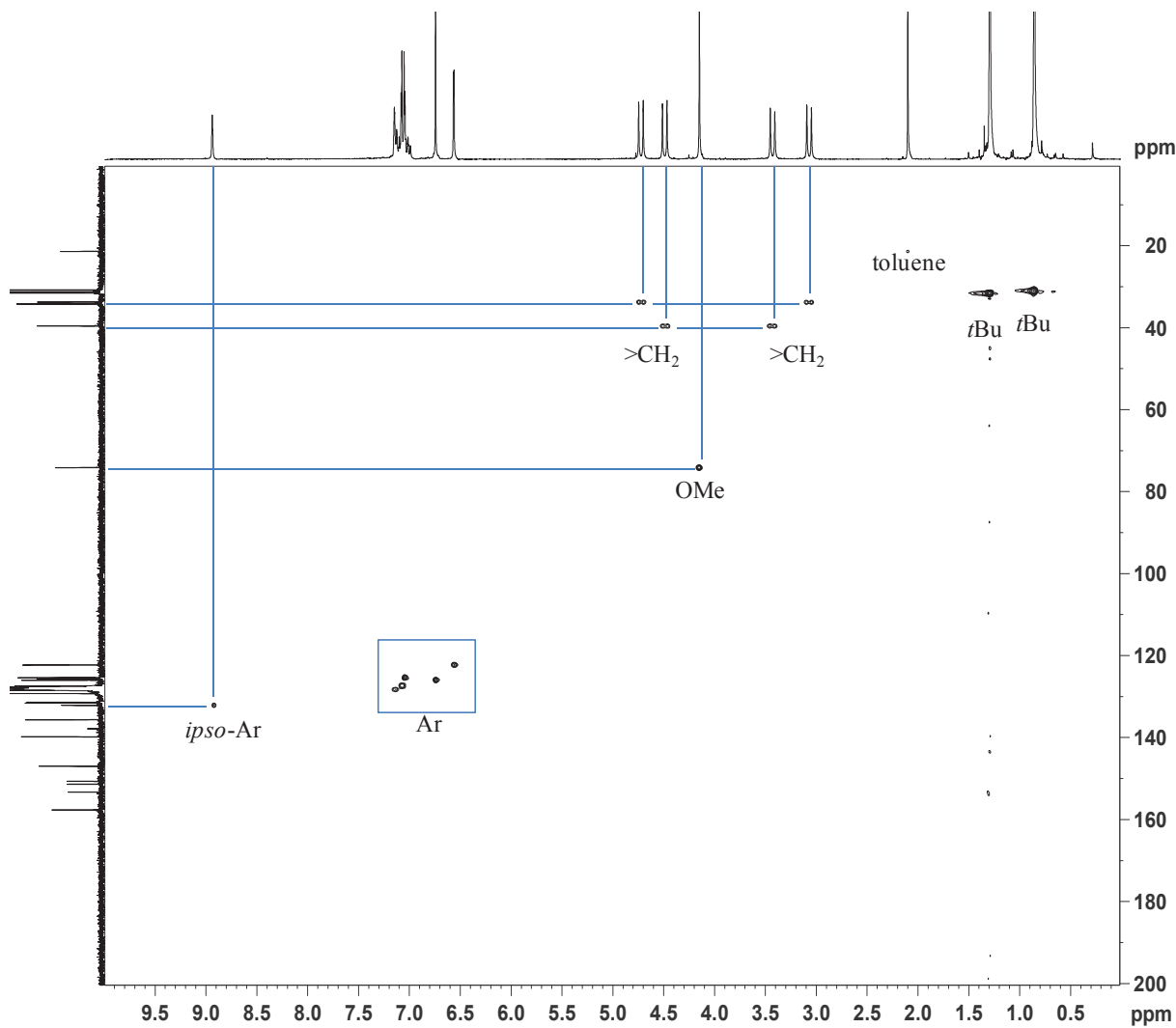
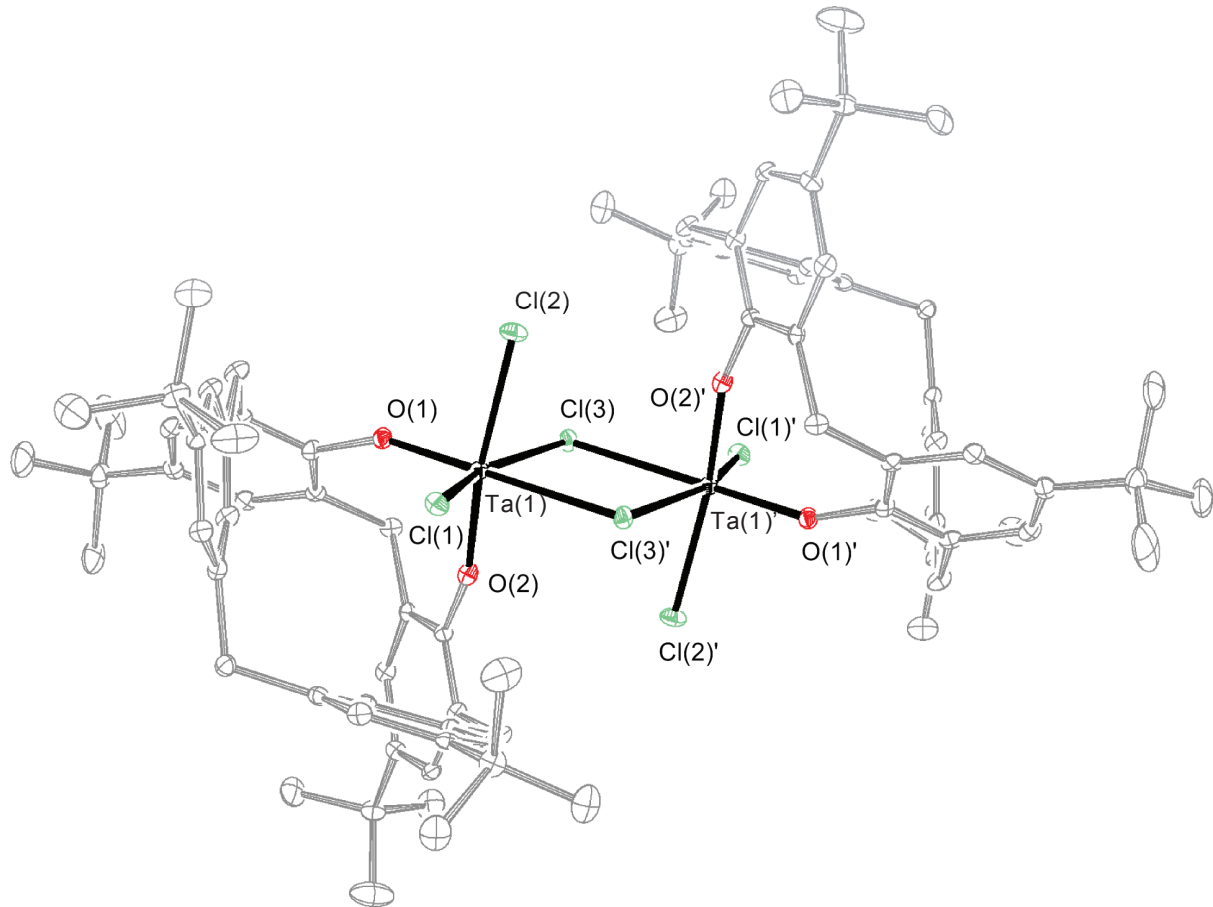


Figure 2: HSQC NMR spectrum of **Ta2** (300 MHz,  $C_6D_6$ )

Suitable crystals of **Ta3** for X-Ray diffraction were grown at RT from slow cooling of a hot saturated benzene solution. Crystallographic data and details associated with data collection are given in Annex III, while selected bonds angles and lengths for complexes **Ta3** are reported in Table 1. The X-ray structure of **Ta3** indicates a dimeric compound incorporating two tantalum atoms, bridged by two chlorines and both chelated by one calixarene ligand (**Figure 3**). This dimer is centrosymmetric with the centroid localized on the square formed by both tantalums  $Ta(1)$  and  $Ta(1)'$  and the bridging chlorine atoms  $Cl(3)$  and  $Cl(3)'$ . The calixarene ligand displays a 1,2-alternate conformation with the OH-depleted units *syn*-oriented.  $Ta(1)$  and  $Ta(1)'$  are equivalent and follow a distorted octahedral geometry in which  $Cl(3)'-Ta(1)-O(1)$  and  $Cl(3)-Ta(1)'-O(1)'$  show the more open angles of  $174.5^\circ$ , thus considered as the axis of the two octahedra. The two terminal chlorines  $Cl(1)$  and  $Cl(2)$ , and  $Cl(1)'$  and  $Cl(2)'$ , the two anchoring oxygens  $O(2)$  and  $O(2)'$  and the bridging chlorines  $Cl(3)$  and  $Cl(3)'$  constitute respectively the equatorial ligands of  $Ta(1)$  and  $Ta(1)'$ . The metals lie

out of the equatorial planes by 0.186 Å, confirming the distortion of the octahedral tantalum. A quasi plane passing through Ta(1) and Ta(1)' and containing all the axial ligands can also be drawn. The metal lies out of this plane by 0.023 Å.



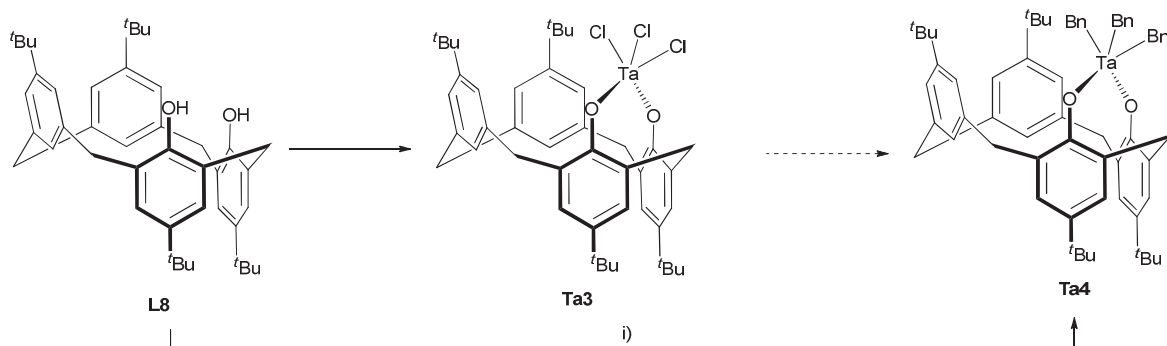
**Figure 3: Molecular structure of Ta3. For clarity H atoms and solvent molecules were omitted.**

**Table 1: Selected bond lengths [Å] and angles [°] for Ta3**

Bond lengths [Å] and angles [°]	Ta3	Bond lengths [Å] and angles [°]	Ta3
Ta(1)-Cl(1)	2.289(1)	Cl(2)-Ta(1)-Cl(3)	83.10(4)
Ta(1)-Cl(2)	2.355(2)	Cl(2)-Ta(1)-Cl(3)'	88.76(4)
Ta(1)-Cl(3)	2.538(1)	Cl(2)-Ta(1)-O(1)	92.50(1)
Ta(1)-Cl(3)'	2.571(1)	Cl(2)-Ta(1)-O(2)	168.50(1)
Ta(1)-O(1)	1.837(3)	Cl(3)-Ta(1)-Cl(3)'	77.37(4)
Ta(1)-O(2)	1.859(4)	Cl(3)-Ta(1)-O(1)	97.40(1)
Cl(1)-Ta(1)-Cl(2)	92.39(5)	Cl(3)-Ta(1)-O(2)	85.53(1)
Cl(1)-Ta(1)-Cl(3)	160.70(4)	Cl(3)''-Ta(1)-O(1)	174.50(1)
Cl(1)-Ta(1)-Cl(3)''	83.80(4)	Cl(3)''-Ta(1)-O(2)	87.30(1)
Cl(1)-Ta(1)-O(1)	101.5(1)	O(1)-Ta(1)-O(2)	90.50(2)
Cl(1)-Ta(1)-O(2)	97.90(1)	-	-

- Alkyl derivatives of the bipodal tantalacalix[4]arenes

Bipodal tris-benzyl and tris-neopentyl tantalacalix[4]arenes complexes from class C or E could be synthesized either *via* alkylation of their chlorine counterparts or by direct reaction between a tantalum complex ( $TaBn_5$  or  $TaNp'Np_3$ ) and the ligands. Even if alkylation of the chlorine compound **Ta3** was not attempted, the proximal tris-benzyl species  $[[4+]-1,2-(H)_2(O)_2TaBn_3]$  **Ta4** was obtained in 36% yield from direct reaction between  $TaBn_5$  and the ligand **L8** (**Scheme 14**). All reactions run from  $TaNp'Np_3$  were inconclusive as inseparable mixtures were observed. The non-selectivity of the reaction can be explained by the slow reactivity of the Schrock tantalum complex, in contrast to  $TaBn_5$ . In no case were the corresponding distal derivatives  $[[4+]-1,3-(H)_2(O)_2TaR_3]$  obtained.



**Scheme 14:** Synthetic pathways for the bipodal alkyl tantalacalix[4]arenes. Reagents and conditions: i) 1 eq.  $TaBn_5$ , toluene, RT, 16 h

The  $^1H$ -NMR spectrum of **Ta4** shows two singlets at 1.22 and 1.27 ppm (18:18 protons) corresponding to the *t*Bu groups (**Figure 4**). In addition, three pairs of doublets belonging to the three different AB systems for the methylenic protons suggest a Cs symmetry. A broad peak at 2.26 ppm correlating to the singlet at 88 ppm in  $^{13}C$  from the HSQC NMR experiment is undoubtedly assigned to the benzylic methylene moieties. This unprecedented observation is certainly due the geometry of the calixarene ligand imposing different environments on the three benzylic ligands. The methylene bridges of the calixarene core are displayed by three singlets at 39, 41 and 43 ppm.

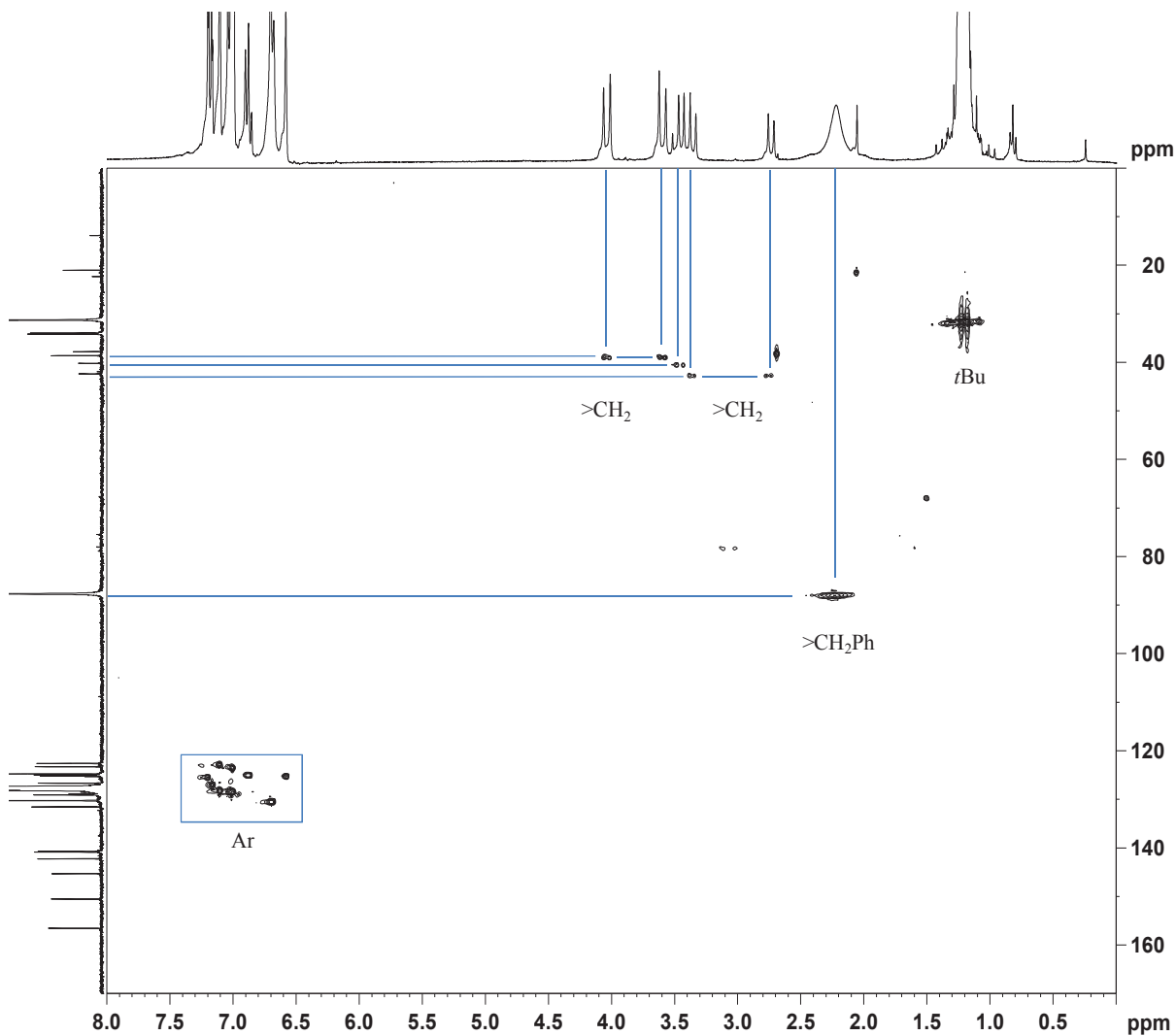


Figure 4: HSQC NMR spectrum of **Ta4** (300 MHz,  $\text{C}_6\text{D}_6$ )

#### 4.2.2 Synthesis and characterization of tripodal tantalacalix[4]arenes

Syntheses of the following tripodal models of classes **F** and **G** will be described here:

- $[[4+]\text{-}(\text{OMe})(\text{O})_3\text{TaR}_2]$  ( $\text{R} = \text{Cl}$ , alkyl) bearing one methoxy group as an ancillary ligand
- $[[4+]\text{-}(\text{H})(\text{O})_3\text{TaR}_2]$  free of any coordinative ligand.

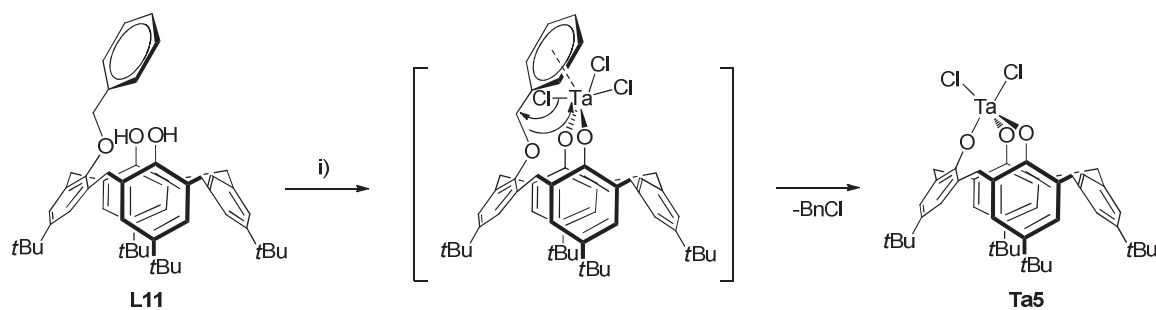
- **Chlorine derivatives**

The ligands **L1**, **L9-L11** were reacted with  $\text{TaCl}_5$  in toluene to obtain a series of complexes (**Ta1-Ta2**, **Ta5**) with **Ta2** and **Ta5**, to the best of our knowledge, previously unreported. **Ta1-Ta2**, **Ta5** were characterized by NMR studies and elemental analysis. A crystal of **Ta5** was obtained for X-ray diffraction studies.

The tripodal complex  $[[4+]\text{-}(\text{OMe})(\text{O})_3\text{TaCl}_2]$  **Ta1** was readily obtained with 85% yield in pure form following Floriani's classic procedure, by reaction of equimolar amounts of

**L1** and  $\text{TaCl}_5$  in refluxing toluene (**Scheme 8**, **Scheme 12**).<sup>10</sup> The corresponding ancillary ligand-free complex  $[[4+]\text{-}(\text{H})(\text{O})_3\text{TaCl}_2]$  **Ta5** has never before been described, hence is an interesting result. Firstly, direct reaction of 1 eq. of  $\text{TaCl}_5$  and the ligand  $[[4+]\text{-}(\text{H})(\text{OH})_3]$  **L9** in similar conditions as described for **Ta1**, leads to a mixture of products difficult both to identify and isolate. Mediating the complexation reaction with alternative solvents (toluene, ether) saw no improvement in the outcome of this reaction. In addition, deprotonation of **L9** with 3 eq. of  $n\text{BuLi}$  prior to the reaction with  $\text{TaCl}_5$  proved unsuccessful. In contrast with **L1**, **L10** does not present any ligand able to assist the approach of the tantalum center *via* prior coordination.

As described in **section 4.2.1**, introduction of an alkoxy group leads to a better selectivity. However, in this particular system, the methoxy group looks stable toward  $\sigma$ -bond metathesis (**Scheme 12**). Employment of an alkoxy function prone to cleavage, such as benzyloxy<sup>13</sup>, was therefore attempted. A limpid equimolar solution of  $\text{TaCl}_5$  and  $[[4+]\text{-}1,3\text{-}(\text{OH})(\text{OBn})(\text{H})]$  **L11** was stirred at RT to provide after 15 min a dense slurry. Filtration and washing of the solid phase with pentane permitted isolation of **Ta5** as a yellow solid in 82% yield (**Scheme 15**). It appears that the benzyloxy group is more readily cleaved than the methoxy group by  $\text{TaCl}_5$  even under milder conditions. The relative disposition of the aromatic ring over the hydroxyl functions in **L11** (**Figure 1**) may also explain the difference of reactivity observed with **L10**. The possible coordination of the aromatic ring to the tantalum atom allows a greater proximity of the metal and the ether group, hence favoring the cleavage of the O-CH<sub>2</sub>Ph bond (**Scheme 15**).



**Scheme 15:** Synthetic pathway and mechanistic approach for  $[[4+]\text{-}(\text{O})_3\text{(H)}\text{TaCl}_3]$  **Ta5**. Reagents and conditions: 1 eq.  $\text{TaCl}_5$ , toluene, TA, 5 h

Crystal of **Ta5** suitable for X-ray diffraction studies was obtained in pentane; its solid state structure can be compared with that of complex **Ta1**.<sup>10</sup> Crystallographic data and details associated with data collection are given in Annex III while selected bonds angles and lengths for complexes **Ta1** and **Ta5** are listed in **Table 2**. **Ta5** has a dimeric structure: two tantalum

atoms are bridged by two chlorines, each of them being chelated by one calixarene ligand (**Figure 5**). This dimer appears to be centrosymmetric with a centroid approximately localized on that of the square formed by the tantalum Ta(1) and Ta(2), and the bridging chlorine atoms Cl(2) and Cl(3). Ta(1) and Ta(2) are quasi equivalent and follow a distorted octahedral geometry, in which the equatorial ligands, can be identified as the bridging chlorines Cl(2) and Cl(3) and the oxygens of the phenols facing each other, O(1) and O(2), and O(4) and O(5), respectively. The remaining oxygen, O(3) and O(6), and the terminal chlorines, Cl(1) and Cl(4), occupy the axial positions for Ta(1) and Ta(2) respectively (**Table 2**). **Ta1** is monomeric with an octahedral geometry comprising two chlorines, three  $\sigma$ -bonded oxygens from the three phenols and the  $\pi$ -bonded methoxy group, which stabilizes the octahedral geometry and hence prevents the formation of a dimeric form of **Ta1**. A quasi plane passing through Ta(1) and Ta(2) and containing all the equatorial ligands [*viz.* Cl(2), Cl(3), O(2), O(3), O(4) and O(5)] can also be drawn. The metals lies out of this plane by 0.046 Å for Ta(1) and 0.040 Å for Ta(2). In contrast, the position of the tantalum centre in **Ta1** is significantly out of the equatorial plane with values of 0.146 Å. The octahedral geometry is more distorted in **Ta1** than in **Ta5**.

**Table 2: Comparison of selected bond lengths [Å] and angles [°] for Ta1 and Ta5**

Bond	Ta1	Ta5	Bond	Ta1	Ta5
Ta(1)-Cl(1)	2.364(4)	2.354(6)	Ta(2)-Cl(2)	-	2.580(5)
Ta(1)-Cl(2)	2.568(5)	2.384(5)	Ta(2)-Cl(3)	-	2.570(6)
Ta(1)-Cl(3)	-	2.583(5)	Ta(2)-Cl(4)	-	2.358(4)
Ta(1)-O(1)	1.82(2)	1.80(1)	Ta(2)-O(4)	-	1.81(1)
Ta(1)-O(2)	1.826(9)	1.83(1)	Ta(2)-O(5)	-	1.83(1)
Ta(1)-O(3)	1.87(1)	1.90(1)	Ta(2)-O(6)	-	1.89(1)
Ta(1)-O(4) (OMe)	2.27(1)	-			

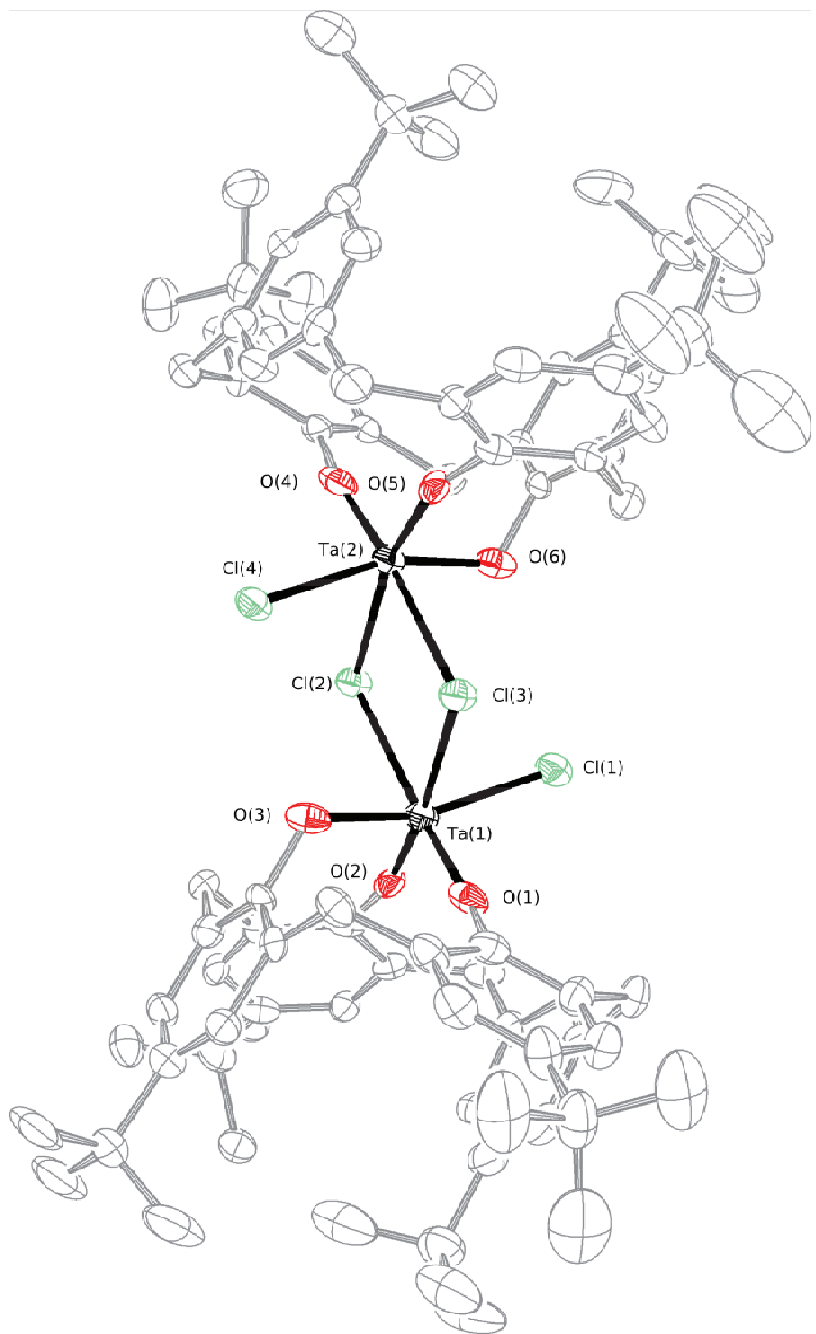


**Figure 5:** Molecular structure of  $[4+]-[O]_3(H)TaCl_3]_2Ta5$  (only one of the two molecules of the unit cell is shown). For clarity H atoms and solvent molecules were omitted.

Several attempts to characterize **Ta5** by NMR spectroscopy were unsuccessful due to its low solubility in most solvents; only resorting to acetonitrile permitted the solubilization of **Ta5**. This increase in solubility can be interpreted as the presence of a more soluble monomeric species, as for other complexes described by Redshaw *et al.*<sup>12</sup> The  $^1H$ -NMR spectrum of **Ta5** is typical of calixarene compounds with several series of peaks that can be easily assigned as follows: three large signals from the *t*Bu groups (1.0 to 2.0 ppm), eight main signals from the methylene protons (3.4-5.0 ppm), and large multiplets from the protons

on the meta position of the aromatic rings (7.0 to 7.5 ppm).<sup>14</sup> It is noteworthy that three signals are centered around 8.8 ppm with only one remaining when increasing the temperature from 263 to 343 K (**Figure 6**).

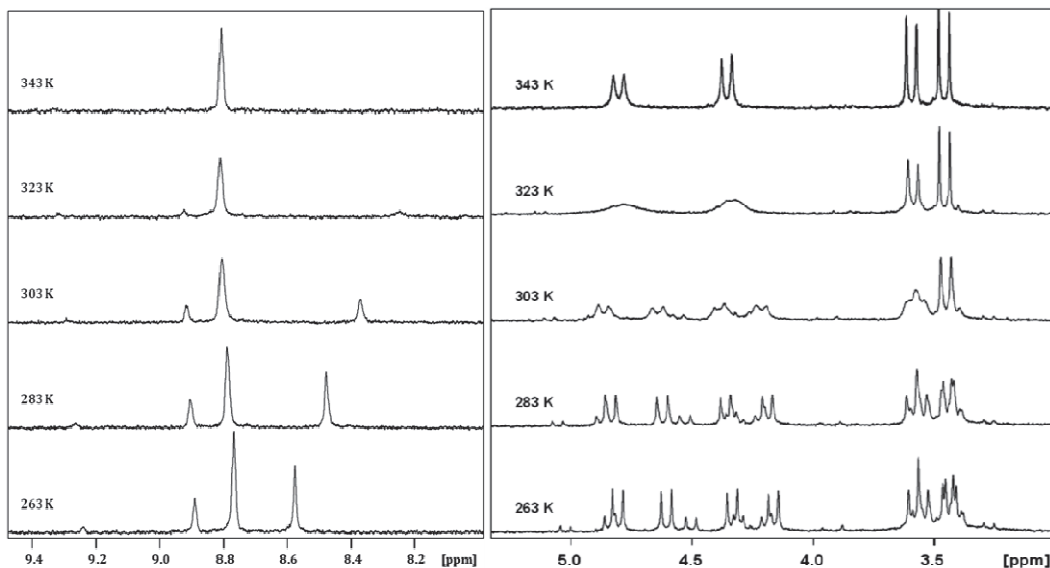


**Figure 6:** Temperature dependence from 263 to 343 K of the  $^1\text{H}$  NMR spectra for Ta5 (300 MHz,  $\text{CD}_3\text{CN}$ ). Left: Signal of *ipso*Ar-H; Right: Signal of the methylene protons

The corresponding proton is assumed to be located on the depleted site of the calixarene ligands (namely, the *ipso* position). HSQC experiments at that temperature impart a correlation between the signals at 8.8 ppm and that of an aromatic signal at 132 ppm (**Figure 7**), thus confirming without a doubt the *ipso* proton assignment.

At ambient temperature, eight stronger signals, each identified to one of the protons borne by the methylene bridges (**Figure 6**), indicate a highly unsymmetrical molecule. Nevertheless, increasing temperature simplifies the spectrum that only contains four averaged signals; this indicates the occurrence of a fluxional process with the coalescence temperature around 323 K. The HSQC experiments at 343 K shows that two types of carbon, (*i.e.*, 34 and 40 ppm) can be observed, each revealing correlations with two protons signals (*i.e.*, 3.4 and 4.8 ppm, and 3.6 and 4.4 ppm, respectively) (**Figure 8**).

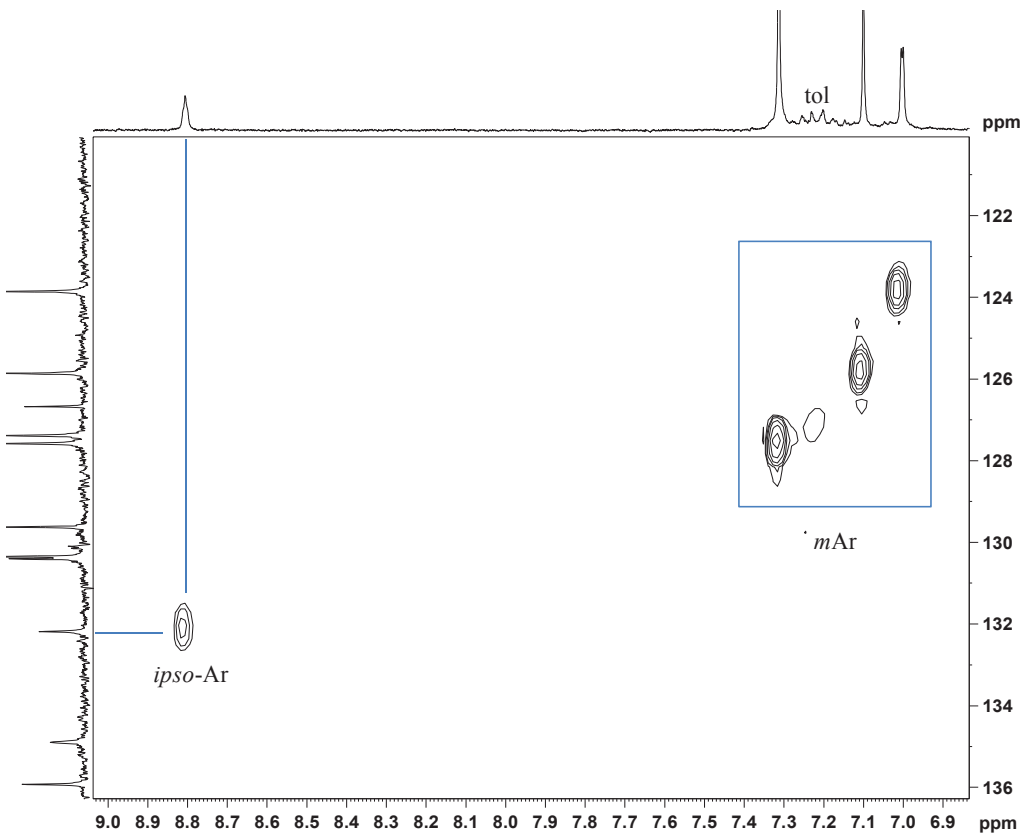


Figure 7: HSQC NMR spectra of Ta5 at 243K (300 MHz,  $\text{CD}_3\text{CN}$ ) ( $^1\text{H}$  aromatic zone)

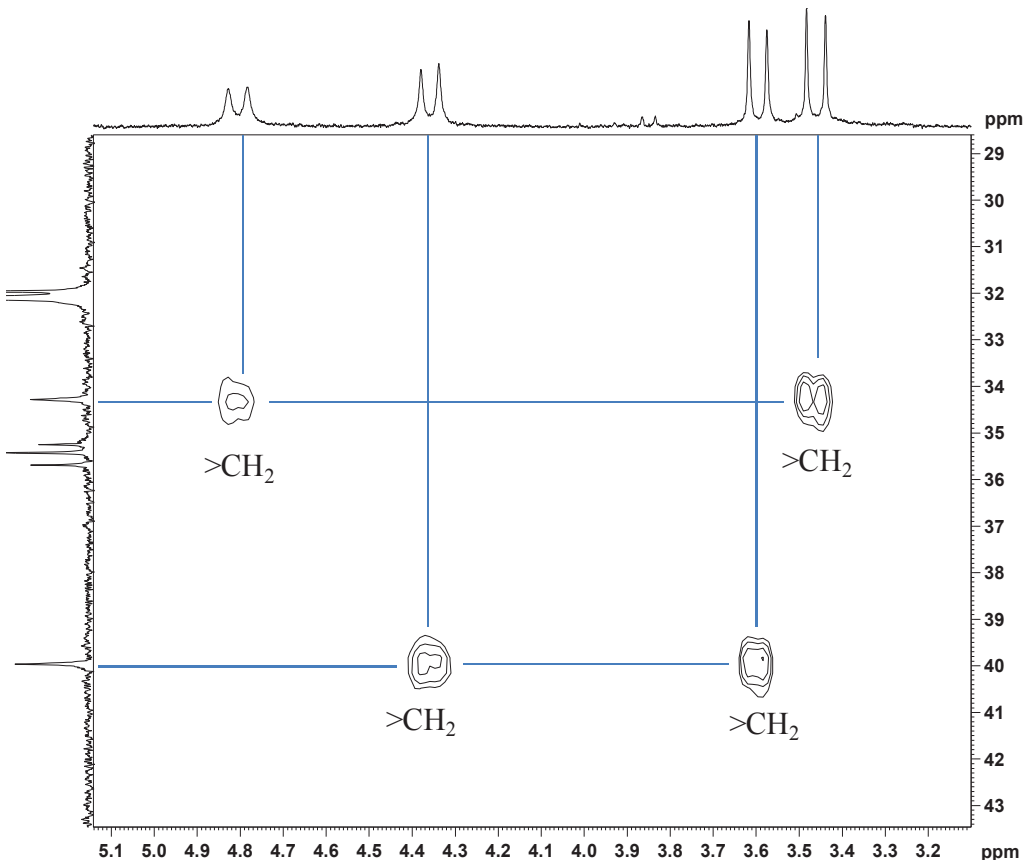
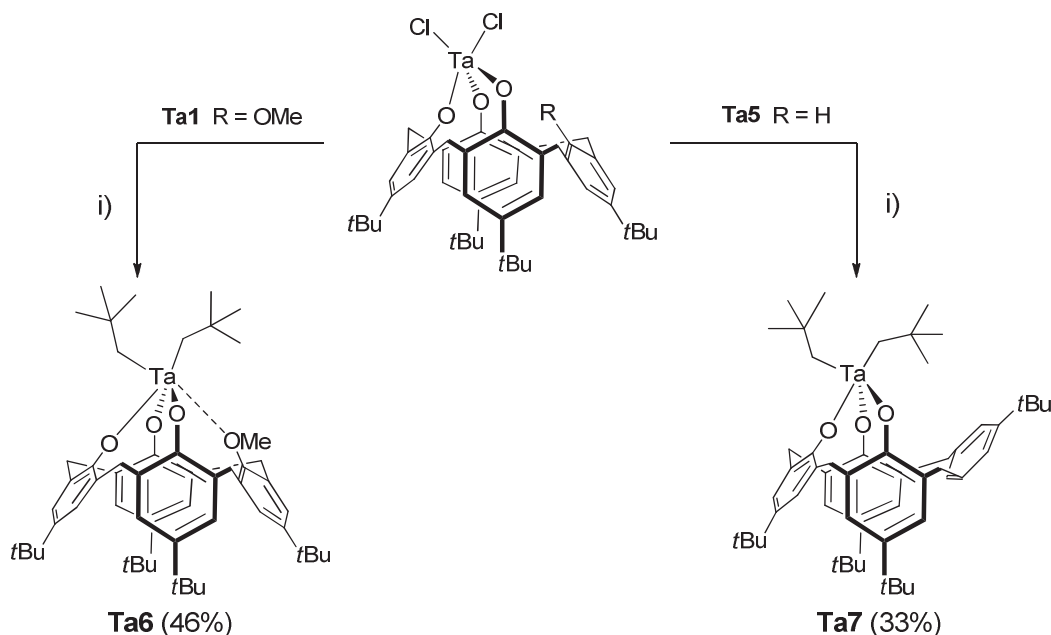


Figure 8: HSQC NMR spectra of Ta5 at 243K (300 MHz,  $\text{CD}_3\text{CN}$ ) ( $^1\text{H}$  methylene protons zone)

The chemical shift of the methylene carbons indicates a *syn* and an *anti* relative disposition of the attached phenyl groups; a partial cone conformation for **Ta5** can be concluded.

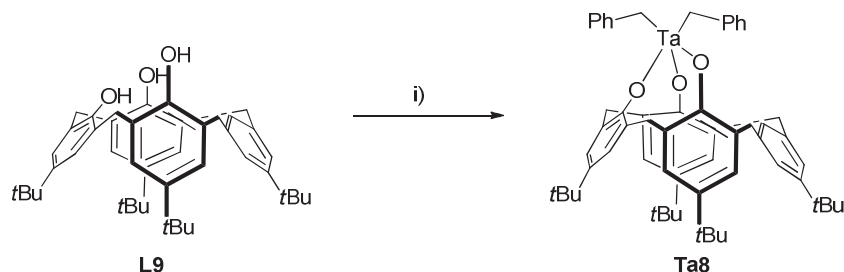
- **Alkyl derivatives**

As the alkane-elimination route was not convincing with the carbenic Schrock tantalum complex  $\text{TaNp}'\text{Np}_3$ , **Ta1** and **Ta5** were alkylated at  $-40^\circ\text{C}$  by two equivalents of  $\text{NpMgCl}$  to give the corresponding bis-neopentyl **Ta6** and **Ta7**, respectively (**Scheme 16**).



**Scheme 16:** Alkylation of **Ta1** and **Ta5**. Reagents and conditions: i) 2 eq.  $\text{NpMgCl}$ , toluene, RT, 1 h

In contrast to  $\text{TaNp}'\text{Np}_3$ ,  $[[4+]-(\text{H})(\text{O})_3\text{TaBn}_2]$  **Ta8** is obtained by the alkane elimination method from  $\text{TaBn}_5$  and **L9** at  $60^\circ\text{C}$  in 30% yield (**Scheme 17**).



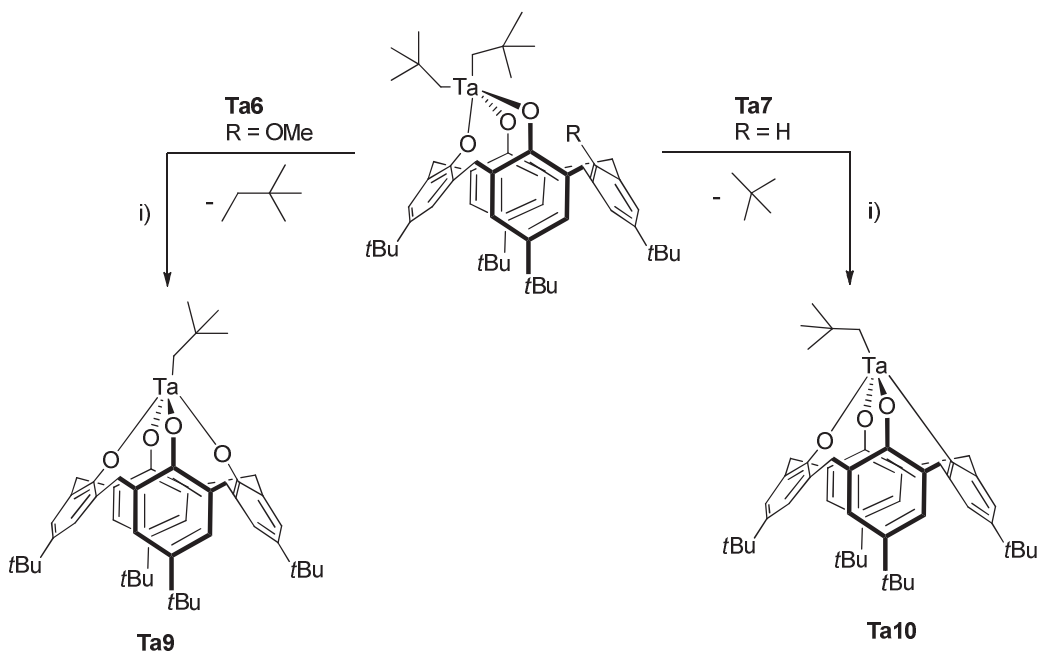
**Scheme 17:** Synthetic pathway for  $[[4+]-(\text{H})(\text{O})_3\text{TaBn}_2]$  **Ta8**. Reagents and conditions: i) 1 eq.  $\text{TaBn}_5$ , toluene,  $60^\circ\text{C}$ , 50h

The products were characterized by NMR spectroscopy ( $^1\text{H}$ ,  $^{13}\text{C}$ , DEPT, HMBC, HSQC) and elemental analysis. The  $^1\text{H-NMR}$  and  $^{13}\text{C-NMR}$  spectra of **Ta6-Ta8** are

consistent with the presence of only one  $C_s$  symmetric conformer in each case. The two benzyl groups of **Ta8** are identical and their  $^1\text{H}$ - and  $^{13}\text{C}$ -NMR display singlets at 3.47 ppm and 84.51 ppm respectively. The two neopentyl ligands of **Ta6** and **Ta7** are also equivalent and their methylenic groups show respectively one singlet at 2.50 and 2.55 ppm in  $^1\text{H}$ -NMR and one signal at 94.7 and 97.89 ppm in  $^{13}\text{C}$ -NMR. The signals formed by the *endo* and *exo* protons, coupling with each other, from the methylene units can be understood as two AB systems, one for each type of bridge. The conformation of **Ta6-Ta8** can be deduced from the chemical shift of the carbon atom of the methylene: with two signals at 34.19 and 34.59 ppm, a typical range of a methylenic bridge linked two *syn*-oriented phenolic units<sup>15</sup>, **Ta6** is a cone conformation. The spectra of **Ta7** and **Ta8** contain two peaks respectively at 34.3 ppm, 39.9 ppm, for the former and at 32.4, 39.7 ppm for the latter, with the most downfield consistent with the *anti*-oriented OH-depleted unit. Thus this indicates a partial-cone conformation. The presence of the OMe group coordinated to the tantalum center in **Ta6** could explain the slight up-field shift of the neopentyl signals. Furthermore, this coordination results in the cone conformation of **Ta6**.

- **Stability studies of the tripodal bis-alkyl tantalacalix[4]arenes **Ta6** and **Ta7****

The dibenzyl complex **Ta8** shows thermal stability up to 110°C, and is slowly degraded in many materials under prolonged heating. In contrast, both complexes **Ta6** and **Ta7** can be easily and cleanly converted at 80°C to **Ta9** and **Ta10**, respectively (**Scheme 18**).



**Scheme 18:** Thermal transformation of **Ta6** and **Ta7** to **Ta9** and **Ta10**, respectively. Conditions: i) toluene, 80°C, 16h

Comparing the  $^1\text{H}$  and  $^{13}\text{C}$  spectra of **Ta9** and its precursor **Ta6** revealed that the singlet at 3.65 ppm assigned to the methoxy disappears (**Figure 9**). The tantalum metal appears to be rearranging the calixarenic ligand by formation of new Ta-O and C-C bonds affording the elimination of neohexane, identified by  $^1\text{H}$  NMR spectroscopy.<sup>11</sup> Given that no carbene intermediate was observed, a mechanism in which the metal undergoes  $\sigma$ -bond metathesis can be judiciously proposed. The presence of a neopentyl group on the tantalum, compared to the analogue aryl complexes<sup>10</sup>, may favor the elimination reaction so as to form a monomeric **O<sub>4</sub>** complex that is rather stable, probably due to reduced steric hindrance. In contrast, the complexes reported by Floriani are less reactive towards demethylation and require, when necessary, activation, either photochemical, thermal or chemical using a base (*i.e.*, pyridine) (see section 2.2).

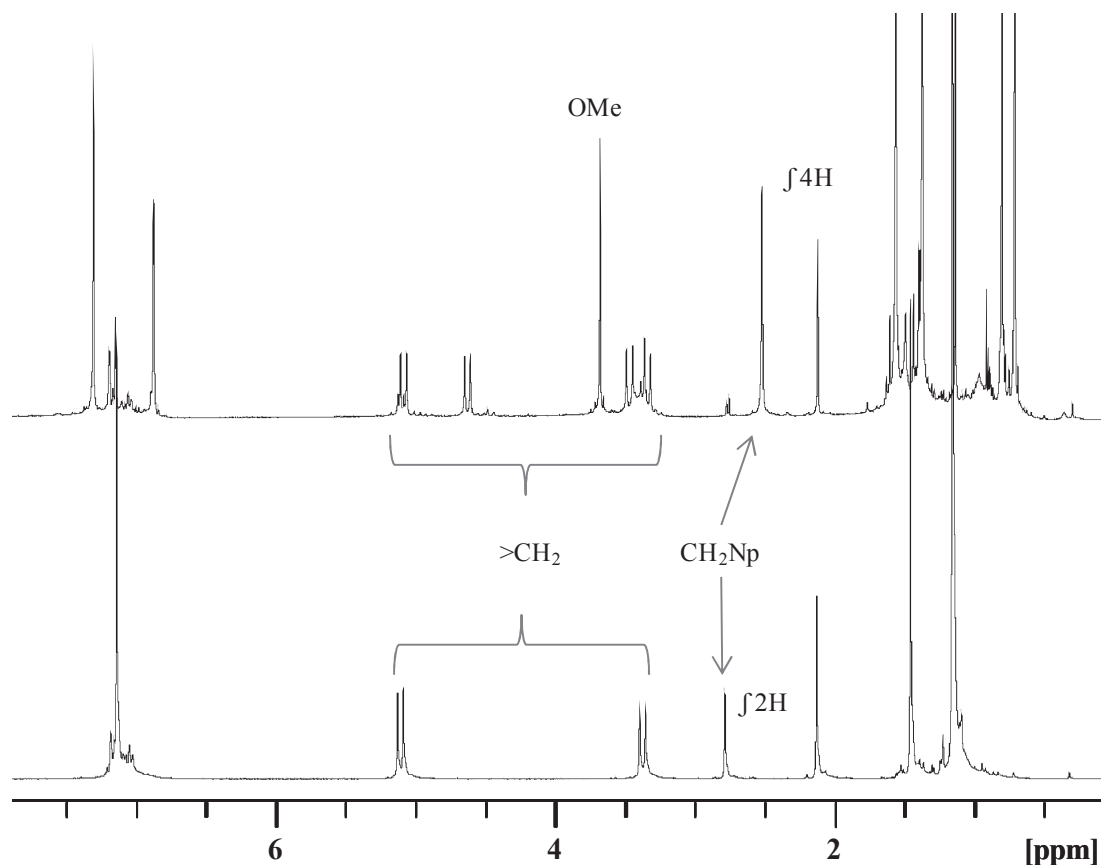


**Figure 9:**  $^1\text{H}$ -NMR spectra of **Ta6** and **Ta9** (300 MHz,  $\text{C}_6\text{D}_6$ , 293K)

A single crystal of **Ta9** suitable for X-ray diffraction studies was obtained from a saturated toluene solution at room temperature. The solid state structure of **Ta9** consists of a monomer displaying  $\text{C}_{4v}$  symmetry (**Figure 10**). The tantalum center follows a pyramidal coordination in which the square base is formed by the four oxygens of the  $\text{O}_4$  core and its summit by the methylenic carbon of the neopentyl group. The dihedral angles formed by  $\text{O}2-$

Ta-O4, O4-Ta-O3, O2-Ta-O5, O3-Ta-O5 are of similar values,  $86.31^\circ$ - $86.55^\circ$ , with the corresponding bond lengths also falling within a small range of  $1.904$ - $1.918$  Å.

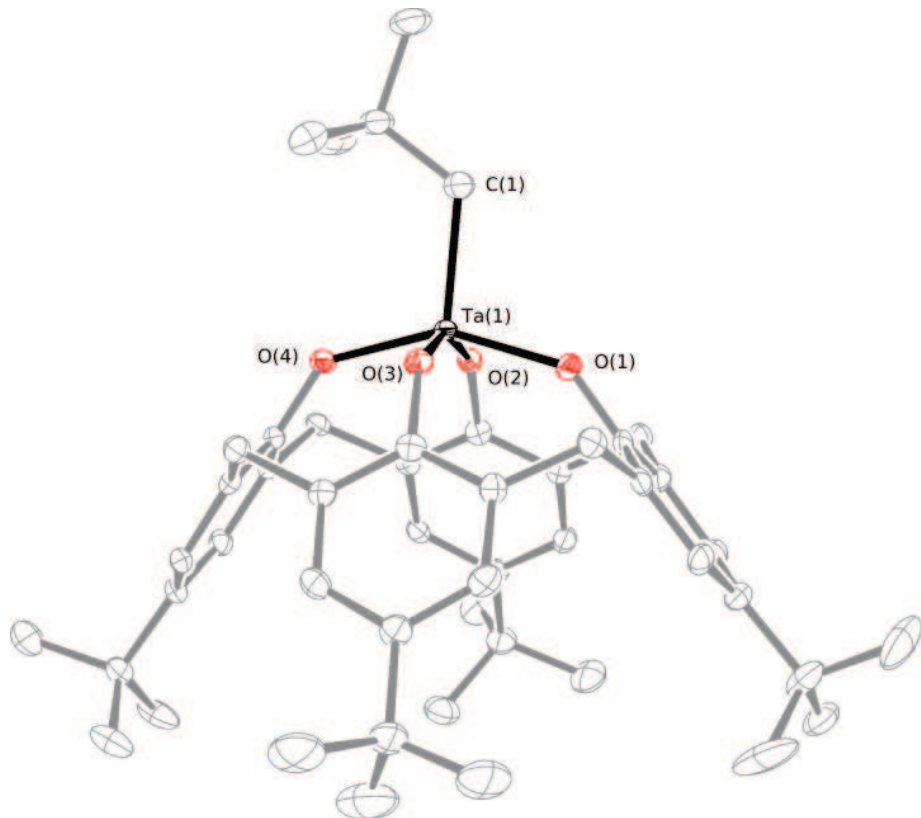


**Figure 10:** Molecular structure of **Ta9** (only one of the two molecules of the unit cell is shown). For clarity H atoms and solvent molecules were omitted.

In the NMR spectroscopic data of **Ta10**, the signal of the *ipso*Ar-H signal at 7.47 ppm in the  $^1\text{H}$  spectrum of **Ta7** is absent (**Figure 11**) while the  $^{13}\text{C}$  spectrum exhibits a new signal of quaternary carbon at 196 ppm that is consistent with a  $\text{Csp}^2$ -Ta (**Figure 13**). The gas evolved from the reaction is identified by  $^1\text{H-NMR}$  and GC as neopentane. All these characterizations support that the Ta center undergoes an intramolecular C-H activation on the depleted site of the calix[4]arene ligand *via* the  $\sigma$ -bond metathesis of  $[\text{Ta}-\text{CH}_2t\text{Bu}]$  with  $[\text{Cipso}-\text{H}]$ . Theoretical calculations are still pending for the determination of the most probable conformation of **Ta10** (in progress, collaboration with Pr. H. Chermette, IRCE Lyon).

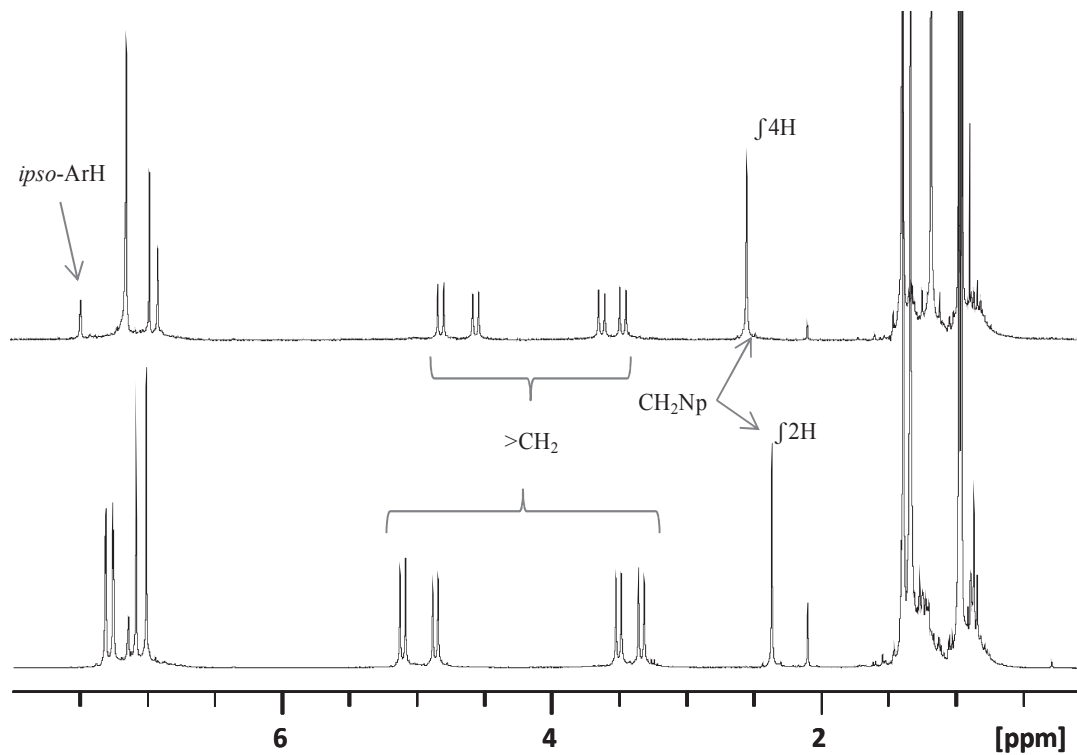
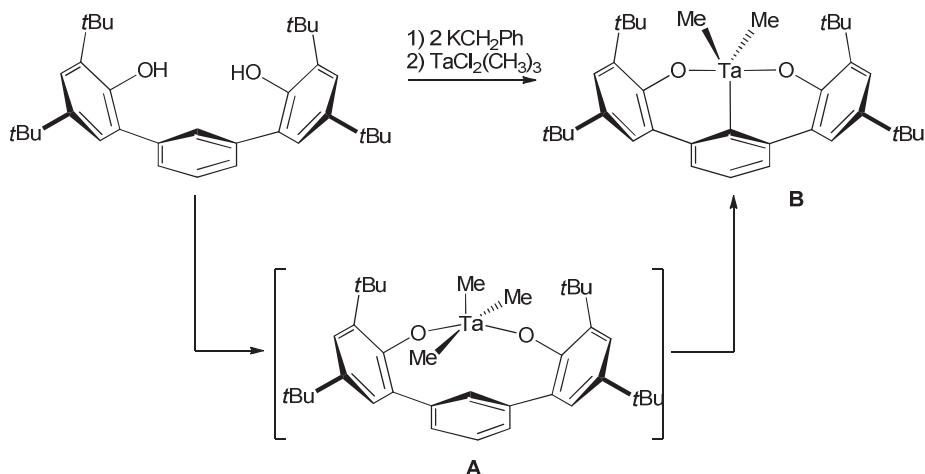


Figure 11:  $^1\text{H}$ -NMR spectra of Ta7 and Ta10 (300 MHz,  $\text{C}_6\text{D}_6$ , 293K)

This reactivity is reminiscent of cyclometalations *via*  $\sigma$ -bond metathesis observed for tantalum systems with phenolates ligands *ortho*-substituted with *t*Bu, *i*Pr or phenyl groups.<sup>16</sup> Bercaw *et al.*<sup>16</sup> reported similar activation with tantalum but on the *ipso*Ar-H of the middle aromatic part a pincer-like bis-phenoxy ligand. It is presumed that the *in situ* formation of the trialkyl intermediate **A**, evolves to give the activated complex **B** with methane elimination. The  $^{13}\text{C}$ -NMR spectrum of this compound also displays the corresponding signal of the *ipso*C<sub>Ar</sub>-Ta atom shifted to 196 ppm (**Scheme 19**).



Scheme 19: Intramolecular Ar-H activation on tantalum complexes supported by a benzene-linked bis-(phenolate) ligand (Bercaw's systems)

Similarly, with  $\text{W}(\text{OAr})(\text{OAr})(=\text{CHC}(\text{CH}_3)_3)\text{Cl}(\text{OEt}_2)$ <sup>17</sup> is reported the synthesis and crystal structure of a cyclometallated species (**Figure 12**), in which the formation of a  $\sigma$ -bond of the *ipso*Ar-H aromatic ring and a chloro atom in the tungsten is observed.

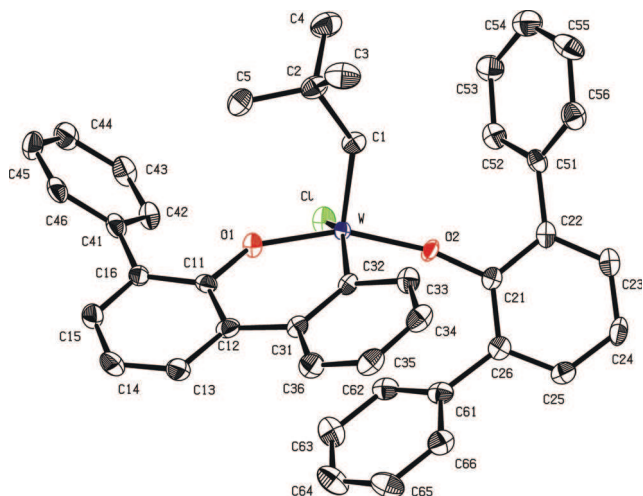
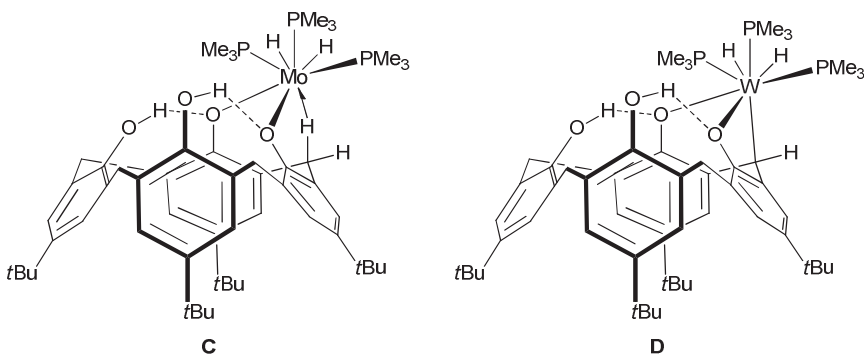


**Figure 12:** X-Ray structure of the cyclometallated  $\text{W}(\text{OAr})(\text{OAr})(=\text{CHC}(\text{CH}_3)_3)\text{Cl}$  ( $\text{W}=\text{C} = 1.887(4)$  Å for the neopentylidene group)<sup>17</sup>

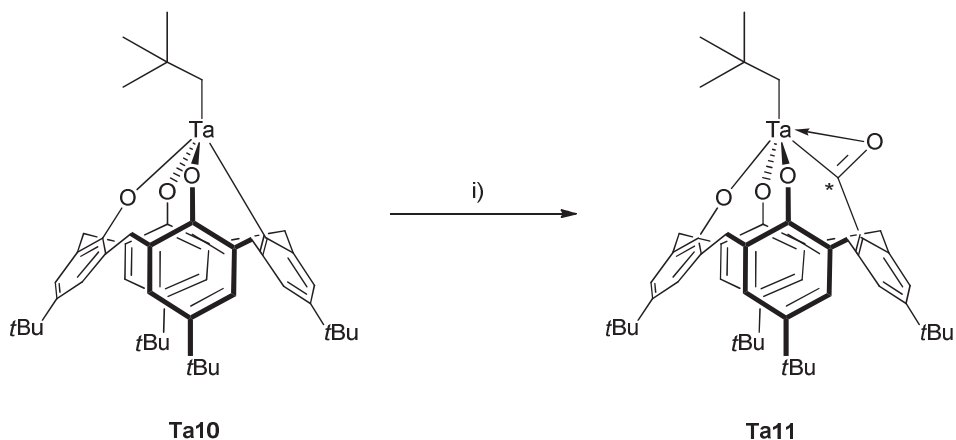
However, intramolecular C-H activation of the calix[4]arene moiety was only documented on the methylene bridges using tungsten complex. To our knowledge, this is the first example of a  $\text{Csp}^2$ -H bond activation by a transition metal occurring on the calix[4]arene framework. For example, Parkin compared the structures, both in the liquid and the solid state, of complexes formed by *p*-*tert*butylcalix[4]arene coordinated to various transition metals.<sup>18</sup> In all cases, the metal interacts only with a C-H bond from the methylene bridge. Nonetheless, the nature of this interaction is strongly affected by the metal to which the calixarene is coordinated. Early transition metals, such as those from group VI, appear to be prone to initiate agostic bonding (*i.e.*, 3-center-2-electron interactions), while those formed by late transition metals(*e.g.* Pt<sup>19</sup>, Rh<sup>20</sup>) such as a d<sup>8</sup> metal center seem to give weaker agostic bonds reminiscent of hydrogen bonding. Even early transition metals belonging to same group can exhibit distinct nuances towards CH bond activation process. Considering the molybdenum complex [[4+]-1,2-(OH)<sub>2</sub>(O)<sub>2</sub>Mo] **C** an agostic derivative that exhibits a Mo-H-C interaction with a d<sup>2</sup> metal, has been identified. In contrast, the tungsten analogue [[4+]-1,2(OH)<sub>2</sub>(O)<sub>2</sub>W] **B** is a d<sup>0</sup> trihydride formed by oxidative addition onto the CH bond (**Scheme 20**).



**Scheme 20:** Intramolecular methylene proton activation on  $[4+]-1,2-(OH)2(O)2Mo]$  A and  $[4+]-1,2-(OH)2(O)2W$  B (Parkin's systems)

- Reactivity of **Ta10** with CO

Comparing the reactivity and the structure of **Ta9** and **Ta10** suggests that the interaction between the tantalum and the calixarene scaffold promote the formation of bonds from tantalum (*i.e.*, Ta-O in **Ta9** and Ta-C in **Ta10**). This behavior can be seen as promising for functionalization of the *ispo* position of the calixarene backbone. Compound **Ta10**, which contains two types of Ta-C bonds (Ta-Csp<sup>3</sup> *vs.* Ta-Csp<sup>2</sup>) provides an interesting compound for reactivity. Direct reaction with <sup>13</sup>CO could result in the carbonylation of **Ta10** by migratory insertion either on the Csp<sup>2</sup>-Ta or the Csp<sup>3</sup>-Ta or both. The reaction of **Ta10** with an excess of 99% <sup>13</sup>C labeled carbon monoxide reaches completion within 15 min at room temperature to give **Ta11** (Scheme 21).



**Scheme 21:** \*CO insertion in the activated Ta-Ar bond of **Ta10**. Reagents and conditions: i) 500 Torr \*CO, benzene, RT, 15min

In the <sup>13</sup>C NMR spectrum, the peak (at 196 ppm) corresponding to the carbon bound to the tantalum is absent whereas a new peak appears at 314 ppm, a chemical shift consistent with a CO bridging between an aromatic ring and a tantalum metal (Figure 13).<sup>21</sup> Moreover,

the peak at 107.4 ppm in the  $^{13}\text{C}$  of **Ta10** assigned to the methylene group from the neopentyl ligand of the tantalum is shifted downfield to 84.1 ppm in **Ta11**.

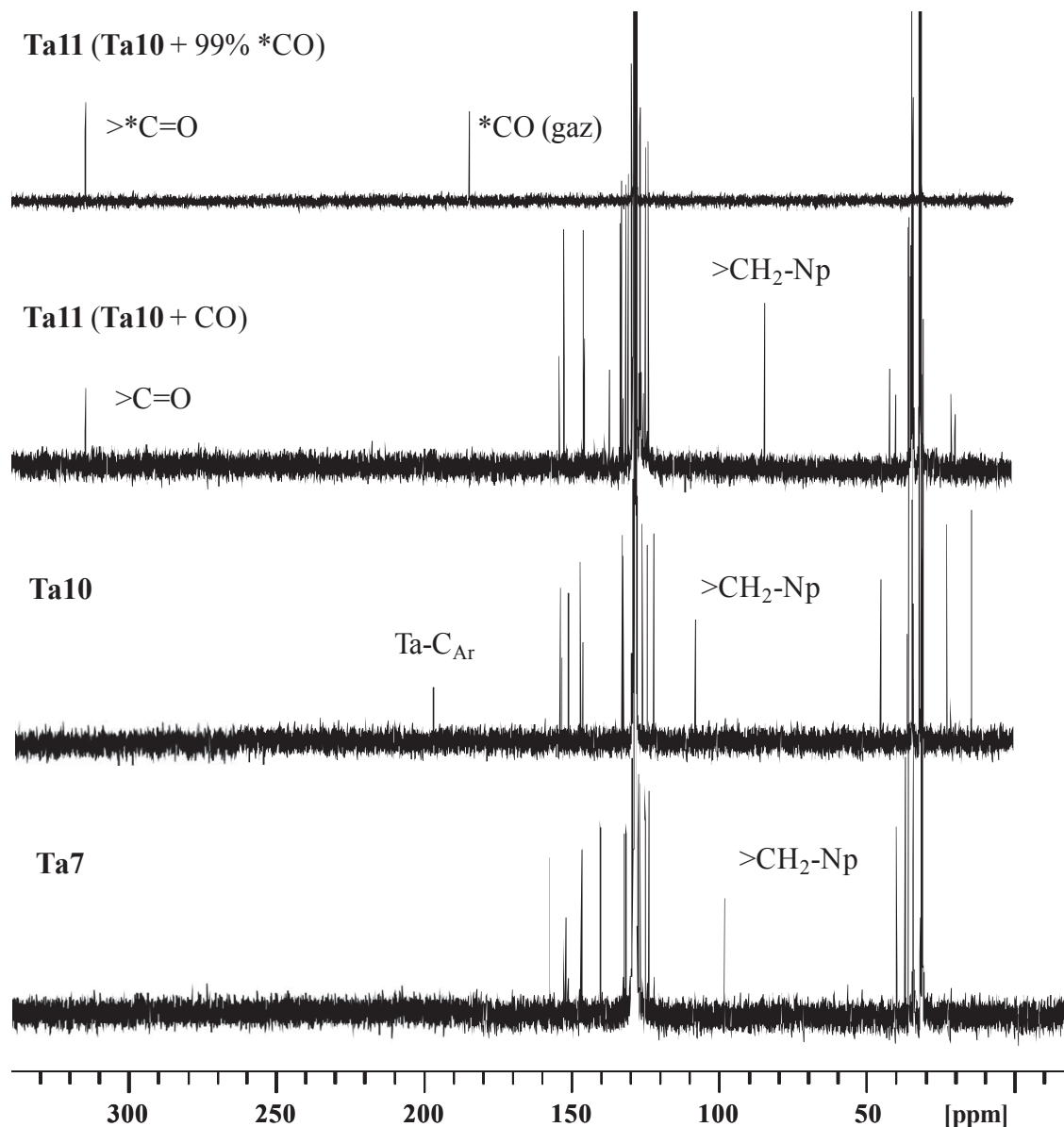
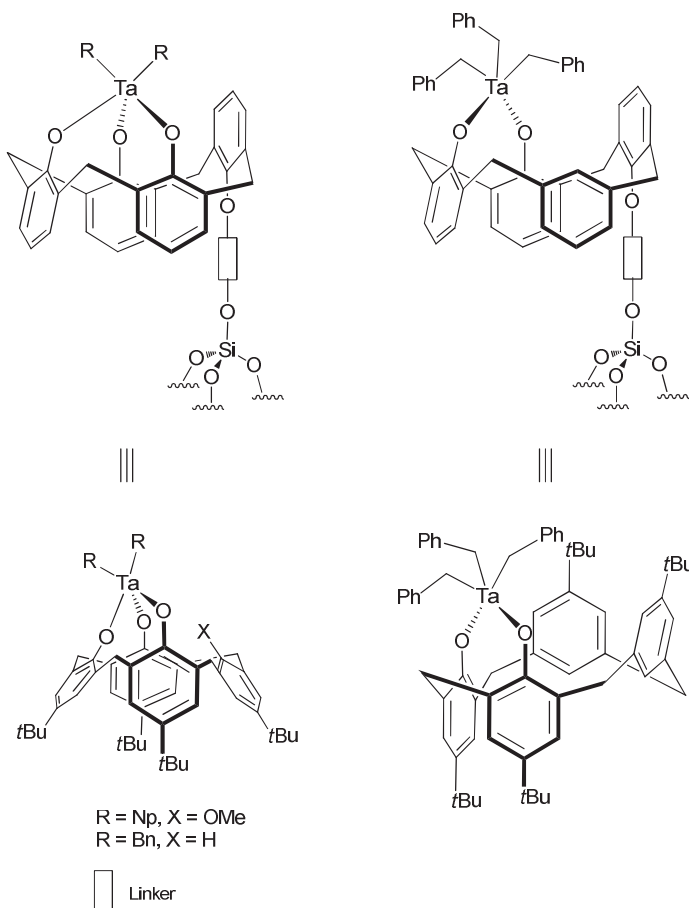


Figure 13:  $^{13}\text{C}$ -NMR spectra of **Ta7**, **Ta10** and **Ta11** (75 MHz,  $\text{C}_6\text{D}_6$ , 293K)

## 5. General conclusion

Throughout this chapter, a collection of soluble tantalacalix[4]arenes models have been synthesized and characterized (**Scheme 22**). These models are strategic in understanding surface organometallic complexes of tantalum. Bipodal tris-alkyl and tripodal bis-alkyl derivatives were prepared either *via* the salt- or the alkane-elimination routes. In the case of neopentyl derivatives, a C-O and C<sub>Ar</sub>-H activation of the calixarene moiety have been observed by thermal treatment of the tripodal bis-neopentyl homologues. It must be highlighted that many efforts were made to systematically obtain the models *via* the alkane-elimination route, as this represents the well-used method in SOMC chemistry.

In the next chapter, the generation of metallacalix[4]arene/silica materials will be developed using the alkane-elimination pathway. All of the novel systems will be characterized using the different surface techniques and supported by the analytical data collected from their soluble counterparts.



**Scheme 22:** Grafted tantalacalix[4]arenes and their corresponding soluble alkyl tantalacalix[4]arenes

## Experimental section

All manipulations were carried out under a dry argon atmosphere using standard Schlenk techniques. All solvents were dried by standard methods and were freshly distilled before use. NMR spectra were recorded on DRX400 and DRX300 Bruker instruments. Elemental analyses were performed at the Central Analysis Service of Solaize (France). 99 % <sup>13</sup>C labeled carbon monoxide was purchased from Aldrich and used as received.

**Synthesis of 5,11,17,23-tetra-*tert*-butyl-25,27-dihydroxy-26-benzyloxycalix[4]arene (L11):** **L9** (1.490 g, 2.354 mmol) and K<sub>2</sub>CO<sub>3</sub> (0.195 g, 1.413 mmol) were suspended in dry CH<sub>3</sub>CN (40 ml). BnBr (0.31 ml, 2.590 mmol) was then added and the mixture was stirred under reflux during 2 h. After evaporation of the solvent, the residue was dissolved in CH<sub>2</sub>Cl<sub>2</sub> (30 ml), washed successively with HCl (1 M), and by water until neutrality, brine and dried (MgSO<sub>4</sub>). The solvent was removed under vacuum and the brown resin was triturated with hot MeOH to precipitate a white powder which was filtrated when cold, and washed with cold MeOH (0.930 g, 55%). NMR <sup>1</sup>H (CD<sub>2</sub>Cl<sub>2</sub>, 300 MHz, 298K): δ 1.18 (s, 9H, <sup>1</sup>Bu), 1.19 (s, 9H, <sup>1</sup>Bu), 1.20 (s, 18H, <sup>1</sup>Bu), 3.29 (d, 2H, calix-CH<sub>2</sub>, <sup>2</sup>J(H,H) = 12.3 Hz), 3.55 (d, 2H, calix-CH<sub>2</sub>, <sup>2</sup>J(H,H) = 13.6 Hz), 4.05 (d, 2H, calix-CH<sub>2</sub>, <sup>2</sup>J(H,H) = 13.6 Hz), 4.18 (d, 2H, calix-CH<sub>2</sub>, <sup>2</sup>J(H,H) = 12.3 Hz), 5.22 (s, 2H, CH<sub>2</sub>Ph), 6.99-7.72 (m, 16H, Ar-H + OH); NMR <sup>13</sup>C, DEPT (CD<sub>2</sub>Cl<sub>2</sub>, 125 MHz): δ 31.3 (CH<sub>3</sub>-<sup>1</sup>Bu), 31.4 (CH<sub>3</sub>-<sup>1</sup>Bu), 31.7 (CH<sub>3</sub>-<sup>1</sup>Bu), 32.9 (CH<sub>2</sub>-calix), 34.1 (<sup>1</sup>Bu-quat), 34.7 (<sup>1</sup>Bu-quat), 34.7 (<sup>1</sup>Bu-quat), 38.2 (CH<sub>2</sub>-calix), 81.0 (CH<sub>2</sub>-Bn), 123.3 (C<sub>Ar</sub>), 125.2 (C<sub>Ar</sub>), 126.0 (C<sub>Ar</sub>), 126.2 (C<sub>Ar</sub>), 127.0 (C<sub>Ar</sub>), 128.3 (C<sub>Ar</sub>), 129.3 (C<sub>Ar</sub>), 129.7 (C<sub>Ar</sub>), 129.9 (C<sub>Ar</sub>), 130.1 (C<sub>Ar</sub>), 133.4 (C<sub>Ar</sub>), 134.9 (C<sub>Ar</sub>), 141.7 (C<sub>Ar</sub>), 143.6 (C<sub>Ar</sub>), 148.3 (C<sub>Ar</sub>), 149.8 (C<sub>Ar</sub>), 150.1 (C<sub>Ar</sub>), 151.0 (C<sub>Ar</sub>); LRMS (ES<sup>+</sup>): [M+Na]<sup>+</sup> = 745.3. HRMS (ES<sup>+</sup>) : Calcd. for C<sub>51</sub>H<sub>62</sub>O<sub>3</sub>Na 745.4597 found 745.4600; Crystals suitable for X-Ray analysis were obtained at room temperature from a saturated methanol/dichloromethane solution.

**Synthesis of 5,11,17,23-tetra-*tert*-butyl-25,27-dioxo-26-methyloxytantalum (V) trichloride (Ta2):** TaCl<sub>5</sub> (0.129 g, 0.360 mmol) and **L10** (0.233 g, 0.360 mmol) were dissolved in 10ml of toluene and the resulting solution was stirred over 2 h at reflux. The mixture was then cooled down, reduced and crystallized at -30°C over 3 days. The orange crystals were filtered and dried under vacuum (0.200 g, 60%). NMR <sup>1</sup>H (C<sub>6</sub>D<sub>6</sub>, 300 MHz): δ 0.85 (s, 9H, <sup>1</sup>Bu), 0.86 (s, 9H, <sup>1</sup>Bu), 1.30 (s, 18H, <sup>1</sup>Bu), 3.06 (d, 2H, calix-CH<sub>2</sub>, <sup>2</sup>J(H,H) = 13.5 Hz), 3.42 (d, 2H, calix-CH<sub>2</sub>, <sup>2</sup>J(H,H) = 13.5 Hz), 4.15 (s, 3H, OMe), 4.48 (d, 2H, calix-CH<sub>2</sub>, <sup>2</sup>J(H,H) = 13.5 Hz), 4.72 (d, 2H, calix-CH<sub>2</sub>, <sup>2</sup>J(H,H) = 13.5 Hz), 6.56 (s, 2H, Ar-H), 6.74 (s, 2H, Ar-H), 7.04 (d, 2H, Ar-H, <sup>4</sup>J(H,H) = 2.4 Hz), 7.07 (d, 2H, Ar-H, <sup>4</sup>J(H,H) = 2.4 Hz), 8.94 (s, 1H, *ipso*Ar-H); NMR <sup>13</sup>C, DEPT, COSY, HSQC (C<sub>6</sub>D<sub>6</sub>, 75 MHz): 30.8 (CH<sub>3</sub>-<sup>1</sup>Bu), 31.2 (CH<sub>3</sub>-<sup>1</sup>Bu), 31.5 (CH<sub>3</sub>-<sup>1</sup>Bu), 33.7 (CH<sub>2</sub>-calix), 34.2 (<sup>1</sup>Bu-quat), 39.6 (CH<sub>2</sub>-calix), 74.1 (OMe), 122.3 (C<sub>Ar</sub>), 125.4 (C<sub>Ar</sub>), 126.0 (C<sub>Ar</sub>), 127.4 (C<sub>Ar</sub>), 128.5 (C<sub>Ar</sub>), 131.4 (C<sub>Ar</sub>), 131.6 (C<sub>Ar</sub>), 132.2 (*ipso*CAr), 135.7 (C<sub>Ar</sub>), 139.8 (C<sub>Ar</sub>), 147.0 (C<sub>Ar</sub>), 150.7 (C<sub>Ar</sub>), 151.4 (C<sub>Ar</sub>), 153.3 (C<sub>Ar</sub>) (Elemental analysis in progress)

**Synthesis of 5,11,17,23-tetra-*tert*-butyl-25,26-dioxotantalum (V) trichloride (Ta3):** **L8** (0.400 g, 0.648 mmol) and TaCl<sub>5</sub> (0.232 g, 0.648 mmol) are dissolved in toluene (10 ml). The

resulting yellow solution was stirred over 16 h at 110°C. After evaporation of the volatiles, the residue was washed with pentane (2 x 5 ml) and dried under vacuum to provide a yellow solid (0.512 g, 79%). NMR  $^1\text{H}$  ( $\text{C}_6\text{D}_6$ , 300 MHz):  $\delta$  1.18 (s, 18H,  $^t\text{Bu}$ ), 1.28 (s, 18H,  $^t\text{Bu}$ ), 2.80 (d, 1H, calix- $\text{CH}_2$ ,  $^2\text{J}(\text{H},\text{H})$  = 15.0 Hz), 3.30 (d, 1H, calix- $\text{CH}_2$ ,  $^2\text{J}(\text{H},\text{H})$  = 15.0 Hz), 3.40 (d, 1H, calix- $\text{CH}_2$ ,  $^2\text{J}(\text{H},\text{H})$  = 15.0 Hz), 3.57 (d, 2H, calix- $\text{CH}_2$ ,  $^2\text{J}(\text{H},\text{H})$  = 15.0 Hz), 4.60 (d, 2H, calix- $\text{CH}_2$ ,  $^2\text{J}(\text{H},\text{H})$  = 15.0 Hz), 5.00 (d, 1H, calix- $\text{CH}_2$ ,  $^2\text{J}(\text{H},\text{H})$  = 15.0 Hz), 6.26 (s, 2H, *ipso*-Ar-H), 7.15 (m, 8H, Ar-H); NMR  $^{13}\text{C}$ , DEPT, HSQC ( $\text{C}_6\text{D}_6$ , 125 MHz):  $\delta$  31.4 ( $\text{CH}_3$ - $^t\text{Bu}$ ), 32.6 ( $\text{CH}_3$ - $^t\text{Bu}$ ), 34.4 ( $^t\text{Bu}$ -quat), 34.5 (CH<sub>2</sub>-calix), 34.6 ( $^t\text{Bu}$ -quat), 37.6 (CH<sub>2</sub>-calix), 123.6 ( $\text{C}_{\text{Ar}}$ ), 124.0 ( $\text{C}_{\text{Ar}}$ ), 124.9 ( $\text{C}_{\text{Ar}}$ ), 125.7 ( $\text{C}_{\text{Ar}}$ ), 129.3 ( $\text{C}_{\text{Ar}}$ ), 131.4 ( $\text{C}_{\text{Ar}}$ ), 137.2 ( $\text{C}_{\text{Ar}}$ ), 140.7 ( $\text{C}_{\text{Ar}}$ ), 142.1 ( $\text{C}_{\text{Ar}}$ ), 148.9 ( $\text{C}_{\text{Ar}}$ ), 151.6 ( $\text{C}_{\text{Ar}}$ ), 157.0 ( $\text{C}_{\text{Ar}}$ ). (Elemental analysis in progress). Crystals suitable for X-Ray analysis were obtained from a hot saturated benzene solution.

**Synthesis of 5,11,17,23-tetra-*tert*-butyl-25,26-dioxotantalum (V) tribenzyl (Ta4):**  $\text{TaBn}_5$  (0.310 g, 0.486 mmol) and **L8** (0.300 g, 0.486 mmol) were stirred in toluene (15 ml) over 24 h at 60°C. After evaporation of the volatiles, the residue was washed with pentane (2 x 3 ml) to provide **Ta4** (0.185 g, 36%). NMR  $^1\text{H}$  ( $\text{C}_6\text{D}_6$ , 300 MHz):  $\delta$  1.22 (s, 18H,  $^t\text{Bu}$ ), 1.27 (s, 18H,  $^t\text{Bu}$ ), 2.26 (bs, 6H, CH<sub>2</sub>Ph), 2.77 (d, 1H, calix- $\text{CH}_2$ ,  $^2\text{J}(\text{H},\text{H})$  = 13.5 Hz), 3.47 (m, 3H, calix- $\text{CH}_2$ ), 3.63 (d, 2H, calix- $\text{CH}_2$ ,  $^2\text{J}(\text{H},\text{H})$  = 15.8 Hz), 3.07 (d, 2H, calix- $\text{CH}_2$ ,  $^2\text{J}(\text{H},\text{H})$  = 15.8 Hz), 6.26 (s, 2H, *ipso*-Ar-H), 7.00 (m, 25H, Ar-H); NMR  $^{13}\text{C}$ , DEPT, HSQC ( $\text{C}_6\text{D}_6$ , 125 MHz):  $\delta$  31.2 ( $\text{CH}_3$ - $^t\text{Bu}$ ), 31.3 ( $\text{CH}_3$ - $^t\text{Bu}$ ), 34.0 ( $^t\text{Bu}$ -quat), 34.2 ( $^t\text{Bu}$ -quat), 38.6 (CH<sub>2</sub>-calix), 40.2 (CH<sub>2</sub>-calix), 42.4 (CH<sub>2</sub>-calix), 87.7 (CH<sub>2</sub>Ph), 122.6 ( $\text{C}_{\text{Ar}}$ ), 123.3 ( $\text{C}_{\text{Ar}}$ ), 124.8 ( $\text{C}_{\text{Ar}}$ ), 125.0 ( $\text{C}_{\text{Ar}}$ ), 125.1 ( $\text{C}_{\text{Ar}}$ ), 126.7 ( $\text{C}_{\text{Ar}}$ ), 128.0 ( $\text{C}_{\text{Ar}}$ ), 128.2 ( $\text{C}_{\text{Ar}}$ ), 128.9 ( $\text{C}_{\text{Ar}}$ ), 129.1 ( $\text{C}_{\text{Ar}}$ ), 130.2 ( $\text{C}_{\text{Ar}}$ ), 131.5 ( $\text{C}_{\text{Ar}}$ ), 140.7 ( $\text{C}_{\text{Ar}}$ ), 140.8 ( $\text{C}_{\text{Ar}}$ ), 142.2 ( $\text{C}_{\text{Ar}}$ ), 145.3 ( $\text{C}_{\text{Ar}}$ ), 150.5 ( $\text{C}_{\text{Ar}}$ ), 156.5 ( $\text{C}_{\text{Ar}}$ ). (Elemental analysis in progress).

**Synthesis of 5,11,17,23-tetra-*tert*-butyl-25,26,27-trioxotantalum (V) dichloride (Ta5):**  $\text{TaCl}_5$  (0.500 g, 0.692 mmol) and **L11** (0.248 g, 0.692 mmol) are dissolved in toluene (10 ml) to give immediately an orange-yellow clear solution. After 5 min, an orange solid precipitated and the resulting suspension was stirred over 5 h at room temperature. After evaporation of the volatiles, the residue was washed with pentane (2 x 5 ml) and dried under vacuum to provide a yellow solid (0.498 g, 82%). NMR  $^1\text{H}$  ( $\text{CD}_3\text{CN}$ , 300 MHz, 343K):  $\delta$  1.11 (s, 9H,  $^t\text{Bu}$ ), 1.13 (s, 9H,  $^t\text{Bu}$ ), 1.32 (s, 18H,  $^t\text{Bu}$ ), 3.46 (d, 2H, calix- $\text{CH}_2$ ,  $^2\text{J}(\text{H},\text{H})$  = 13.2 Hz), 3.59 (d, 2H, calix- $\text{CH}_2$ ,  $^2\text{J}(\text{H},\text{H})$  = 12.6 Hz), 4.36 (d, 2H, calix- $\text{CH}_2$ ,  $^2\text{J}(\text{H},\text{H})$  = 12.6 Hz), 4.80 (d, 2H, calix- $\text{CH}_2$ ,  $^2\text{J}(\text{H},\text{H})$  = 13.2 Hz), 6.99 (s, 2H, Ar-H), 7.00 (s, 2H, Ar-H), 7.31 (s, 4H, Ar-H), 8.80 (s, 1H, *ipso*-Ar-H); NMR  $^{13}\text{C}$ , DEPT ( $\text{CD}_3\text{CN}$ , 125 MHz, 343K):  $\delta$  31.9 ( $\text{CH}_3$ - $^t\text{Bu}$ ), 32.1 ( $\text{CH}_3$ - $^t\text{Bu}$ ), 32.1 ( $\text{CH}_3$ - $^t\text{Bu}$ ), 34.3 (CH<sub>2</sub>-calix), 35.3 ( $^t\text{Bu}$ -quat), 35.4 ( $^t\text{Bu}$ -quat), 35.7 ( $^t\text{Bu}$ -quat), 40.0 (CH<sub>2</sub>-calix), 123.9 ( $\text{C}_{\text{Ar}}$ ), 125.9 ( $\text{C}_{\text{Ar}}$ ), 127.4 ( $\text{C}_{\text{Ar}}$ ), 127.6 ( $\text{C}_{\text{Ar}}$ ), 130.4 ( $\text{C}_{\text{Ar}}$ ), 132.2 ( $\text{C}_{\text{Ar}}$ ), 134.9 ( $\text{C}_{\text{Ar}}$ ), 135.9 ( $\text{C}_{\text{Ar}}$ ), 141.5 ( $\text{C}_{\text{Ar}}$ ), 147.86 ( $\text{C}_{\text{Ar}}$ ), 149.4 ( $\text{C}_{\text{Ar}}$ ), 153.1 ( $\text{C}_{\text{Ar}}$ ), 157.3 ( $\text{C}_{\text{Ar}}$ ), 157.6 ( $\text{C}_{\text{Ar}}$ ). Anal. Calcd for  $\text{C}_{44}\text{H}_{53}\text{Cl}_2\text{O}_3\text{Ta}$ : C, 59.93; H, 6.06. Found: C, 60.02; H, 6.20. Crystals suitable for X-Ray analysis were obtained at RT from a saturated pentane solution.

**Synthesis of 5,11,17,23-tetra-*tert*-butyl-25,26,27-trioxo-28-methyloxycalix[4]arene tantalum (V) dineopentyl (Ta6):**  $\text{NpMgCl}$  (3.41 ml, 1.43M in  $\text{Et}_2\text{O}$ , 4.881 mmol) was added dropwise to a stirred toluene (100 ml) solution of 5,11,17,23-tetra-*tert*-butyl-25,26,27-trioxo-

28-methyloxycalix[4]arene tantalum (V) dichloride (2.450 g, 2.441 mmol) at room temperature. The reaction was stirred over 1 h and 5 ml of 1,4-dioxane was then added. After a further stirring of 1 h, the salts were filtered off and the volatiles evaporated to give a yellow solid (1.215 g, 46%). NMR  $^1\text{H}$  ( $\text{C}_6\text{D}_6$ , 300 MHz):  $\delta$  0.70 (s, 9H, calix- $^t\text{Bu}$ ), 0.79 (s, 9H, calix- $^t\text{Bu}$ ), 1.36 (s, 18H, calix- $^t\text{Bu}$ ), 1.55 (s, 18H, Np- $^t\text{Bu}$ ), 3.32 (d, 2H, calix- $\text{CH}_2$ ,  $^2\text{J}(\text{H},\text{H})$  = 12.4 Hz), 3.44 (d, 2H, calix- $\text{CH}_2$ ,  $^2\text{J}(\text{H},\text{H})$  = 13.2 Hz), 3.65 (s, 3H, OMe), 4.60 (d, 2H, calix- $\text{CH}_2$ ,  $^2\text{J}(\text{H},\text{H})$  = 12.4 Hz), 5.06 (d, 2H, calix- $\text{CH}_2$ ,  $^2\text{J}(\text{H},\text{H})$  = 13.2 Hz), 6.83 (s, 2H, Ar-H), 6.84 (s, 2H, Ar-H), 7.26 (s, 4H, Ar-H). NMR  $^{13}\text{C}$ , DEPT ( $\text{C}_6\text{D}_6$ , 75 MHz):  $\delta$  30.6 ( $\text{CH}_3$ - $^t\text{Bu}$ ), 30.9 ( $\text{CH}_3$ - $^t\text{Bu}$ ), 31.9 ( $\text{CH}_3$ - $^t\text{Bu}$ ), 33.5 ( $^t\text{Bu}$ -quat), 33.7 ( $^t\text{Bu}$ -quat), 34.2 (calix- $\text{CH}_2$ ), 34.4 ( $^t\text{Bu}$ -quat), 34.6 (calix- $\text{CH}_2$ ), 36.6 ( $\text{CH}_3$ -Np), 37.6 (Np-quat), 65.2 (OMe), 94.7 (Np- $\text{CH}_2$ ), 124.5 ( $\text{C}_{\text{Ar}}$ ), 125.7 ( $\text{C}_{\text{Ar}}$ ), 125.8 ( $\text{C}_{\text{Ar}}$ ), 126.9 ( $\text{C}_{\text{Ar}}$ ), 127.5 ( $\text{C}_{\text{Ar}}$ ), 132.5 ( $\text{C}_{\text{Ar}}$ ), 132.6 ( $\text{C}_{\text{Ar}}$ ), 133.1 ( $\text{C}_{\text{Ar}}$ ), 145.2 ( $\text{C}_{\text{Ar}}$ ), 145.6 ( $\text{C}_{\text{Ar}}$ ), 148.4 ( $\text{C}_{\text{Ar}}$ ), 152.8 ( $\text{C}_{\text{Ar}}$ ), 156.1 ( $\text{C}_{\text{Ar}}$ ), 157.6 ( $\text{C}_{\text{Ar}}$ ). Anal. Calcd for  $\text{C}_{55}\text{H}_{77}\text{O}_4\text{Ta}$ : C, 67.19; H, 7.89. Found: C, 66.89; H, 7.57

**Synthesis of 5,11,17,23-tetra-*tert*-butyl-25,26,27-trioxotantalum (V) dineopentyl (Ta7):**

**(Method A)** NpMgCl (0.54 ml, 0.644 mmol, 1.2M in diethyl ether) was added dropwise at -40°C to a solution of **Ta5** (0.300 g, 0.314 mmol) in 20ml of toluene. The resulting solution was allowed to reach RT and then stirred 30 min. 0.6 ml of 1,4-dioxane was added and after 30 min, the resulting mixture was filtered. The filtrate was evaporated until dryness, washed with  $\text{Et}_2\text{O}$  (5 ml) and dried under vacuum at RT to provide a pale yellow solid (0.096 g, 32%).

**(Method B)**  $\text{TaCl}_5$  (0.453 g, 1.264 mmol) and **L11** (0.914 g, 1.264 mmol) are dissolved in 15 ml of toluene to give immediately an orange-yellow clear solution. After 5 min, an orange solid precipitated and the resulting suspension was stirred over 5 h at room temperature. After evaporation of the volatiles, 15 ml of fresh toluene was added and NpMgCl (2.20 ml, 2.591 mmol, 1.2M in diethyl ether) was added dropwise at -40°C. The resulting solution was allowed to reach RT and then stirred 30min. 2.4 ml of 1,4-dioxane was added and after 30 min, the resulting mixture was filtered. The filtrate was evaporated until dryness, washed with  $\text{Et}_2\text{O}$  (2 x 5 ml) and dried under vacuum at RT to provide a pale yellow solid (0.640 g, 53%). NMR  $^1\text{H}$  ( $\text{C}_6\text{D}_6$ , 300 MHz):  $\delta$  0.95 (s, 9H, calix- $^t\text{Bu}$ ), 0.97 (s, 9H, calix- $^t\text{Bu}$ ), 1.18 (s, 18H, calix- $^t\text{Bu}$ ), 1.39 (s, 18H, Np- $^t\text{Bu}$ ), 2.55 (s, 4H, Np- $\text{CH}_2$ ), 3.46 (d, 2H, calix- $\text{CH}_2$ ,  $^2\text{J}(\text{H},\text{H})$  = 13.3 Hz), 3.62 (d, 2H, calix- $\text{CH}_2$ ,  $^2\text{J}(\text{H},\text{H})$  = 13.8 Hz), 4.55 (d, 2H, calix- $\text{CH}_2$ ,  $^2\text{J}(\text{H},\text{H})$  = 13.8 Hz), 4.80 (d, 2H, calix- $\text{CH}_2$ ,  $^2\text{J}(\text{H},\text{H})$  = 13.2 Hz), 6.90 (d, 2H, *meta*Ar-H), 6.97 (s, 2H, *meta*Ar-H), 7.14 (s, 4H, *meta*Ar-H), 7.48 (s, 1H, *ipso*Ar-H); NMR  $^{13}\text{C}$ , DEPT, HMBC, HSQC ( $\text{C}_6\text{D}_6$ , 75 MHz):  $\delta$  31.1 ( $\text{CH}_3$ - $^t\text{Bu}$ ), 31.2 ( $\text{CH}_3$ - $^t\text{Bu}$ ), 31.5 ( $\text{CH}_3$ - $^t\text{Bu}$ ), 31.9 ( $^t\text{Bu}$ -quat), 34.1 ( $^t\text{Bu}$ -quat), 34.2 (CH<sub>2</sub>-calix), 34.3 ( $^t\text{Bu}$ -quat), 35.7 ( $\text{CH}_3$ -Np), 37.0 (Np-quat), 39.9 (CH<sub>2</sub>-calix), 97.9 (CH<sub>2</sub>-Np), 123.5 ( $\text{C}_{\text{Ar}}$ ), 124.8 ( $\text{C}_{\text{Ar}}$ ), 126.4 ( $\text{C}_{\text{Ar}}$ ), 127.0 ( $\text{C}_{\text{Ar}}$ ), 127.1 ( $\text{C}_{\text{Ar}}$ ), 129.2 ( $\text{C}_{\text{Ar}}$ ), 131.2 ( $\text{C}_{\text{Ar}}$ ), 131.8 ( $\text{C}_{\text{Ar}}$ ), 139.9 ( $\text{C}_{\text{Ar}}$ ), 146.2 ( $\text{C}_{\text{Ar}}$ ), 146.4 ( $\text{C}_{\text{Ar}}$ ), 151.5 ( $\text{C}_{\text{Ar}}$ ), 152.3 ( $\text{C}_{\text{Ar}}$ ), 157.1 ( $\text{C}_{\text{Ar}}$ ). Anal. Calcd for  $\text{C}_{54}\text{H}_{75}\text{O}_3\text{Ta}$ : C, 68.05; H, 7.93. Found: C, 68.32; H, 8.03.

**Synthesis of 5,11,17,23-tetra-*tert*-butyl-25,26,27-trioxotantalum (V) bis-benzyl (Ta8):**

$\text{TaBn}_5$  (0.202 g, 0.316 mmol) and **L9** (0.200 g, 0.316 mmol) are dissolved in toluene (10 ml) and stirred over 50 h at 60°C. After evaporation of the volatiles, the residue was washed with pentane (5 ml) and dried under vacuum to provide a yellowish solid (0.094 g, 30%). NMR  $^1\text{H}$  ( $\text{C}_6\text{D}_6$ , 300MHz):  $\delta$  0.82 (s, 9H, calix- $^t\text{Bu}$ ), 0.90 (s, 9H, calix- $^t\text{Bu}$ ), 1.27 (s, 18H, calix- $^t\text{Bu}$ ),

3.08 (d, 2H, calix-CH<sub>2</sub>, <sup>2</sup>J(H,H) = 13.8Hz), 3.47 (s, 4H, CH<sub>2</sub>Ph), 3.51 (d, 2H, calix-CH<sub>2</sub>, <sup>2</sup>J(H,H) = 13.8Hz), 4.02 (d, 2H, calix-CH<sub>2</sub>, <sup>2</sup>J(H,H) = 13.8Hz), 4.38 (d, 2H, calix-CH<sub>2</sub>, <sup>2</sup>J(H,H) = 13.8Hz), 6.76-7.49 (m, 19H, Ar-H); NMR <sup>13</sup>C, DEPT (C<sub>6</sub>D<sub>6</sub>, 125 MHz): δ 30.9 (CH<sub>3</sub>-<sup>t</sup>Bu), 31.0 (CH<sub>3</sub>-<sup>t</sup>Bu), 31.6 (CH<sub>3</sub>-<sup>t</sup>Bu), 32.3 (CH<sub>2</sub>-calix), 33.8 (<sup>t</sup>Bu-quat), 34.2 (<sup>t</sup>Bu-quat), 38.1 (<sup>t</sup>Bu-quat), 39.8 (CH<sub>2</sub>-calix), 123.8 (C<sub>Ar</sub>), 124.0 (C<sub>Ar</sub>), 125.4 (C<sub>Ar</sub>), 126.0 (C<sub>Ar</sub>), 126.4 (C<sub>Ar</sub>), 128.0 (C<sub>Ar</sub>), 128.9 (C<sub>Ar</sub>), 129.1 (C<sub>Ar</sub>), 129.3 (C<sub>Ar</sub>), 131.5 (C<sub>Ar</sub>), 131.6 (C<sub>Ar</sub>), 139.8 (C<sub>Ar</sub>), 146.7 (C<sub>Ar</sub>), 146.8 (C<sub>Ar</sub>), 147.1 (C<sub>Ar</sub>), 150.6 (C<sub>Ar</sub>), 151.7 (C<sub>Ar</sub>), 156.7 (C<sub>Ar</sub>). (Elemental analysis in progress).

**Synthesis of 5,11,17,23-tetra-*tert*-butyl-tetraoxocalix[4]arene tantalum (V) mononeopentyl (Ta9):** A sample of **Ta6** heated in toluene at reflux for 16 h was fully converted into **Ta9**. NMR <sup>1</sup>H (C<sub>6</sub>D<sub>6</sub>, 300 MHz): δ 1.12 (s, 36H, calix-<sup>t</sup>Bu), 1.42 (s, 9H, Np-<sup>t</sup>Bu), 2.75 (s, 2H, CH<sub>2</sub>-Np), 3.34 (d, 2H, calix-CH<sub>2</sub>, <sup>2</sup>J(H,H) = 12.3 Hz), 5.07 (d, 2H, calix-CH<sub>2</sub>, <sup>2</sup>J(H,H) = 12.3 Hz), 7.11 (s, 8H, Ar-H); NMR <sup>13</sup>C, DEPT (C<sub>6</sub>D<sub>6</sub>, 75 MHz): δ 31.4 (CH<sub>3</sub>-<sup>t</sup>Bu), 33.6 (CH<sub>3</sub>-Np), 34.1 (<sup>t</sup>Bu-quat), 34.2 (calix-CH<sub>2</sub>), 34.8 (Np-quat), 90.4 (Np-CH<sub>2</sub>), 125.2 (Ar-*meta*), 132.1 (Ar-*ortho*), 146.1 (Ar-*para*), 152.1 (Ar-O); Anal. Calcd for C<sub>49</sub>H<sub>63</sub>O<sub>4</sub>Ta.(toluene)<sub>2</sub>: C, 69.98; H, 7.36; Found: C, 69.59; H, 7.59; Crystals suitable for X-ray analysis were grown from a saturated solution in toluene at RT.

**Synthesis of 5,11,17,23-tetra-*tert*-butyl-25,26,27-trioxotantalum (V) neopentyl (Ta10):** In a NMR tube, a sample of **Ta7** was totally converted into **Ta10** at 80°C overnight, with NpH evolution (NMR evidence, checked by GC injection of the gas phase). NMR <sup>1</sup>H (C<sub>6</sub>D<sub>6</sub>, 300 MHz): δ 0.96 (s, 9H, calix-<sup>t</sup>Bu), 0.98 (s, 9H, calix-<sup>t</sup>Bu), 1.34 (s, 18H, calix-<sup>t</sup>Bu), 1.39 (s, 9H, Np-<sup>t</sup>Bu), 2.37 (s, 2H, CH<sub>2</sub>-Np), 3.33 (d, 2H, calix-CH<sub>2</sub>, <sup>2</sup>J(H,H) = 12.3 Hz), 3.50 (d, 2H, calix-CH<sub>2</sub>, <sup>2</sup>J(H,H) = 12.0 Hz), 4.86 (d, 2H, calix-CH<sub>2</sub>, <sup>2</sup>J(H,H) = 12.0 Hz), 5.11 (d, 2H, calix-CH<sub>2</sub>, <sup>2</sup>J(H,H) = 12.3 Hz), 7.01 (s, 2H, Ar-H); 7.09 (s, 2H, Ar-H); 7.25 (d, 2H, Ar-H, <sup>2</sup>J(H,H) = 2.3 Hz), 7.31 (d, 2H, Ar-H, <sup>2</sup>J(H,H) = 2.3 Hz); NMR <sup>13</sup>C, DEPT (C<sub>6</sub>D<sub>6</sub>, 75 MHz): δ 30.7 (CH<sub>3</sub>-<sup>t</sup>Bu), 31.2 (CH<sub>3</sub>-<sup>t</sup>Bu), 31.9 (CH<sub>3</sub>-<sup>t</sup>Bu), 33.8 (<sup>t</sup>Bu-quat), 34.1 (CH<sub>3</sub>-Np), 34.2 (<sup>t</sup>Bu-quat), 34.4 (calix-CH<sub>2</sub>), 34.5 (<sup>t</sup>Bu-quat), 35.9 (Np-quat), 44.9 (calix-CH<sub>2</sub>), 107.8 (Np-CH<sub>2</sub>), 121.8 (C<sub>Ar</sub>), 124.0 (C<sub>Ar</sub>), 125.7 (C<sub>Ar</sub>), 127.4 (C<sub>Ar</sub>), 128.8 (C<sub>Ar</sub>), 132.1 (C<sub>Ar</sub>), 132.4 (C<sub>Ar</sub>), 145.8 (C<sub>Ar</sub>), 146.7 (C<sub>Ar</sub>), 150.7 (C<sub>Ar</sub>), 150.9 (C<sub>Ar</sub>), 152.8 (C<sub>Ar</sub>), 153.4 (C<sub>Ar</sub>), 196.4 (Ta-C<sub>Ar</sub>). Anal. Calcd for C<sub>49</sub>H<sub>63</sub>O<sub>3</sub>Ta: C, 66.80; H, 7.21. Found: C, 66.91; H, 7.52.

**Insertion of CO in Ta10:** 500 Torr of \*CO were established over a solution of **Ta10** in C<sub>6</sub>D<sub>6</sub> in a Young NMR tube. The tube was then shaken over 15min to provide **Ta11**. NMR <sup>1</sup>H (C<sub>6</sub>D<sub>6</sub>, 300 MHz): δ 0.92 (s, 18H, <sup>t</sup>Bu), 1.22 (s, 9H, <sup>t</sup>Bu), 1.28 (s, 9H, <sup>t</sup>Bu), 1.64 (s, 9H, CH<sub>3</sub>-Np), 3.15 (d, 2H, calix-CH<sub>2</sub>, <sup>2</sup>J(H,H) = 13.6 Hz), 3.22 (s, 2H, CH<sub>2</sub>-Np), 3.28 (d, 2H, calix-CH<sub>2</sub>, <sup>2</sup>J(H,H) = 12.3 Hz), 3.94 (d, 2H, calix-CH<sub>2</sub>, <sup>2</sup>J(H,H) = 13.6 Hz), 5.03 (d, 2H, calix-CH<sub>2</sub>, <sup>2</sup>J(H,H) = 12.3 Hz), 6.80 (d, 2H, Ar-H, <sup>4</sup>J(H,H) = 2.4 Hz), 6.94 (d, 2H, Ar-H, <sup>4</sup>J(H,H) = 2.4 Hz), 7.14 (s, 2H, Ar-H), 7.19 (s, 2H, Ar-H). NMR <sup>13</sup>C, DEPT (C<sub>6</sub>D<sub>6</sub>, 75 MHz): δ 31.1 (CH<sub>3</sub>-<sup>t</sup>Bu), 31.4 (CH<sub>3</sub>-<sup>t</sup>Bu), 31.8 (CH<sub>3</sub>-<sup>t</sup>Bu), 33.7 (<sup>t</sup>Bu-quat), 33.9 (CH<sub>2</sub>-calix), 34.3 (Np-CH<sub>3</sub>), 34.3 (Np-quat), 34.6 (<sup>t</sup>Bu-quat) 34.8 (<sup>t</sup>Bu-quat) 35.5 (CH<sub>2</sub>-calix), 84.1 (Np-CH<sub>2</sub>), 123.6 (C<sub>Ar</sub>), 124.5 (C<sub>Ar</sub>), 126.2 (C<sub>Ar</sub>), 126.5 (C<sub>Ar</sub>), 130.5 (C<sub>Ar</sub>), 131.1 (C<sub>Ar</sub>), 132.7 (C<sub>Ar</sub>), 133.1 (C<sub>Ar</sub>), 136.8 (C<sub>Ar</sub>), 145.2 (C<sub>Ar</sub>), 145.6 (C<sub>Ar</sub>), 152.2 (C<sub>Ar</sub>), 152.3 (C<sub>Ar</sub>), 153.8 (C<sub>Ar</sub>), 314.4 (Ar-CO-).

## Notes and references

- (1) Saggio, G.; de Mallmann, A.; Maunders, B.; Taoufik, M.; Thivolle-Cazat, J.; Basset, J.-M. *Organometallics* **2002**, *21*, 5167.
- (2) LaPointe, R. E.; Wolczanski, P. T.; Van Duyne, G. D. *Organometallics* **1985**, *4*, 1810.
- (3) (a) Dufaud, V.; Niccolai, G. P.; Thivolle-Cazat, J.; Basset, J.-M. *J. Am. Chem. Soc.* **1995**, *117*, 4288(b) Lefort, L.; Chabanas, M.; Maury, O.; Meunier, D.; Copéret, C.; Thivolle-Cazat, J.; Basset, J.-M. *J. Organomet. Chem.* **2000**, *593-594*, 96.
- (4) Soignier, S.; Taoufik, M.; Le Roux, E.; Saggio, G.; Dablemont, C.; Baudouin, A.; Lefebvre, F.; de Mallmann, A.; Thivolle-Cazat, J.; Basset, J.-M.; Sunley, G.; Maunders, B. M. *Organometallics* **2006**, *25*, 1569.
- (5) (a) Chabanas, M.; Quadrelli, E. A.; Fenet, B.; Copéret, C.; Thivolle-Cazat, J.; Basset, J. M.; Lesage, A.; Emsley, L. *Angew. Chem., Int. Ed.* **2001**, *40*, 4493(b) Le Roux, E.; Chabanas, M.; Baudouin, A.; de Mallmann, A.; Copéret, C.; Quadrelli, E. A.; Thivolle-Cazat, J.; Basset, J.-M.; Lukens, W.; Lesage, A.; Emsley, L.; Sunley, G. J. *J. Am. Chem. Soc.* **2004**, *126*, 13391.
- (6) Quadrelli, A; Private Communication, Laboratoire de Chimie Organométallique de Surface, Université Lyon 1 - CNRS
- (7) Quadrelli, A; Private Communication, Laboratoire de Chimie Organométallique de Surface, Université Lyon 1 - CNRS
- (8) Schweiger, S. W.; Salberg, M. M.; Pulvirenti, A. L.; Freeman, E. E.; Fanwick, P. E.; Rothwell, I. P. *J. Chem. Soc., Dalton Trans.* **2001**, 2020.
- (9) Groysman, S.; Goldberg, I.; Kol, M.; Goldschmidt, Z. *Organometallics* **2003**, *22*, 3793.
- (10) Castellano, B.; Solari, E.; Floriani, C.; Re, N.; Chiesi-Villa, A.; Rizzoli, C. *Chem.--Eur. J.* **1999**, *5*, 722.
- (11) Castellano, B.; Zanotti-Gerosa, A.; Solari, E.; Floriani, C.; Chiesi-Villa, A.; Rizzoli, C. *Organometallics* **1996**, *15*, 4894.
- (12) Carl, R.; Michael, R.; Damien , M. H.; Mark , R. J. E.; Takehiko, Y.; Carol, P.-C. *Chem.--Eur. J.* **2007**, *13*, 10129.
- (13) Bois, J.; Espinas, J.; Darbost, U.; Felix, C.; Taoufik, M.; Duchamp, C.; Bouchu, D.; Bonnamour, I. submitted
- (14) Gutsche, C. D.; Editor *Calixarenes: An Introduction, 2nd Edition*, 2008.
- (15) Jaime, C.; De Mendoza, J.; Prados, P.; Nieto, P. M.; Sanchez, C. *J. Org. Chem* **1991**, *56*, 3372.
- (16) Agapie, T.; Day, M. W.; Bercaw, J. E. *Organometallics* **2008**, *27*, 6123.
- (17) Rhers, B.; Grinerval, E.; Taoufik, M.; Fache, F.; Herdtweck, E.; Basset, J.-M.; Lefebvre, F. *Catal. Commun.* **2009**, *10*, 1111.
- (18) Buccella, D.; Parkin, G. *J. Am. Chem. Soc.* **2006**, *128*, 16358.
- (19) (a) Batsanov, S. S. *Russ. Chem. Bull.* **1995**, *44*, 2245(b) Kotzen, N.; Goldberg, I.; Lipstman, S.; Vigalok, A. *Inorg. Chem.* **2006**, *45*, 5266.

- (20) Ishii, Y.; Onaka, K.; Hirakawa, H.; Shiramizu, K. *Chem. Commun.* **2002**, 1150.  
(21) Durfee, L. D.; Rothwell, I. P. *Chem. Rev.* **1988**, 88, 1059.



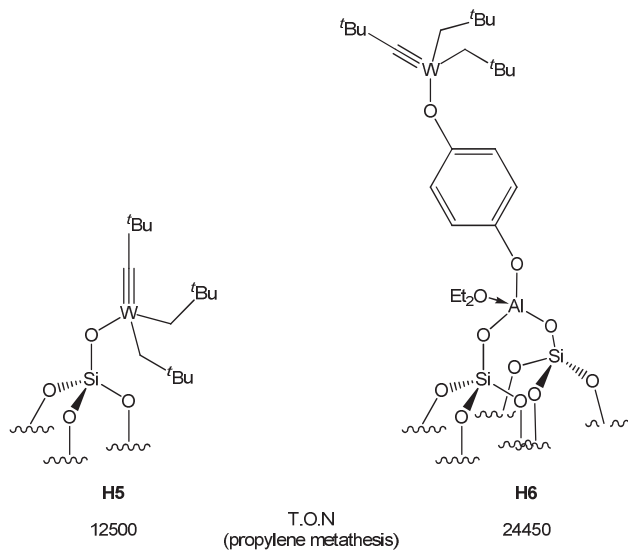
## **Chapter V**

**Preparation of supported  
metallacalix[4]arenes on SBA-15 LP-(700)**



## 1. Introduction

The development of new SOMC systems based on oxide supports that display aryloxy functions constitutes an unprecedented approach in the generation of new grafted catalysts. The insertion of an organic linker between the organometallic center and the surface has proven to be a good strategy to avoid undesired metal-support interactions resulting in the decrease of the activity of SOMC catalysts. Chapter II has defined a novel strategic method to provide an organic/inorganic silica-based support, in which the surface silanols have been substituted by monoaryloxy arms; each of them can act as anchoring hydroxyl points for grafting organometallic complexes. Applying this methodology permitted the generation of monopodal zirconium and tungsten complexes tethered through the hydroquinone linker. When comparing their catalytic performance in propylene metathesis, the new system **H6** revealed improved activity compared to its counterpart directly immobilized on the surface silanols (**H5**) (**Scheme 1**). In addition to the success of this new concept, the aryloxy spacer results, for instance, in the probable increase of the number of tungsten active sites and the electrophilicity of the metal (**H6**), compared to its monosiloxy analogue<sup>1</sup> (**H5**).

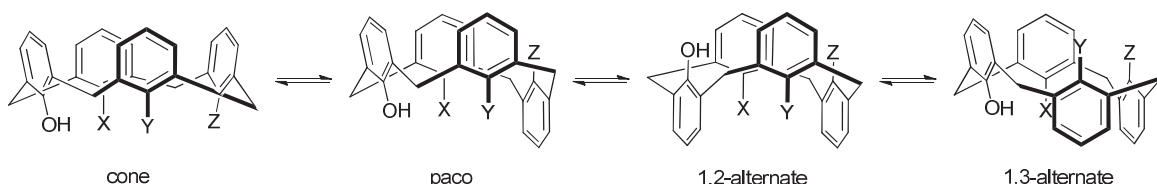


**Scheme 1:** Respective T.O.N. of  $[(\equiv \text{SiO})\text{W}(\equiv \text{C}t\text{Bu}(\text{CH}_2t\text{Bu})_2)]$  **H5** and  $[(\equiv \text{SiO})_2\text{AlO-C}_6\text{H}_4-\text{OW}(\equiv \text{C}t\text{Bu}(\text{CH}_2t\text{Bu})_2.\text{(Et}_2\text{O})]$  **H6** in propylene metathesis

Inserting hydroquinone type linker is only effective in producing monopodal supported species. With a view to extend this approach to species with higher podalities, calix[4]arenes derivatives, which present up to four linked functionalizable phenol groups, appear to be ideal candidates to replace the hydroquinone moiety. Similarly to the grafting of

hydroquinone, at least one of the phenols can be reacted with a surface alkyl aluminum site. The remaining hydroxyl groups, due to the flexible conformation of the calixarenes, can serve as anchoring points for any organometallic complexes. Selected functionalization of the calixarene may lead to improved catalysts by controlling the coordination mode of the metal center. To successfully incorporate calixarenes, several requirements have yet to be met:

- The type of silica selected has to allow well defined species to be generated, but also to facilitate its characterization. Considering that the average diameter of the calixarene is 0.5 nm, the silanols density has to be sufficiently low to reduce the interactions between the grafted calixarenes (e.g. Degussa type silica partially dehydroxylated at 700°C has a silanol density of 0.8 OH·nm<sup>-2</sup>). However, a mesoporous silica support will be preferred to increase the surface specific area and the concentration of grafted calixarenes. It should be emphasized that a mesostructure with large pores is required so as to permit molecular diffusion through the support (namely SBA-15 large pores, noted SBA-15 LP).
- The use of tertiobutylated calixarenes will make the *trans*-annular interconversion of the phenol units easier for both the anchoring on the support and the grafting of organometallic complexes (**Scheme 2**).



**Scheme 2: Different conformations observed for calix[4]arene derivatives (X, Y, Z = H, alkoxy...)**

- The tethered calixarenes have to offer two or three remaining hydroxyl functions for the subsequent incorporated organometallic complexes to obtain bi- and tripodal catalysts.

The first section of this chapter will be dedicated to the preparation and characterization of SBA-15 LP. Secondly, the synthetic methodology established in Chapter II will be applied to SBA-15 LP by grafting triisobutylaluminum etherate followed by tethering of selected calix[4]arene derivatives and then strategic incorporation of zirconium, tantalum and tungsten organometallic complexes. The characterization of these materials will be

directly supported with the spectroscopic data of their soluble models, synthesized in chapters III and IV. Once well-defined, they will be engaged in selected catalytic preliminary studies.

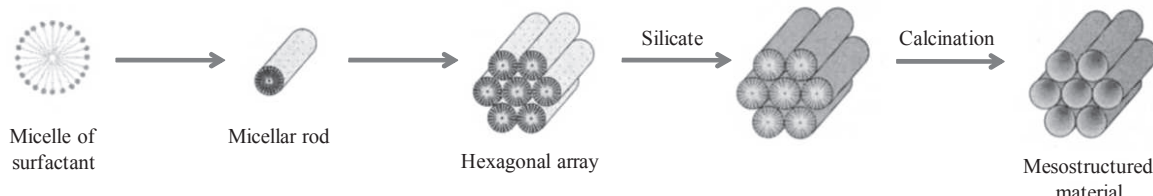
## 2. Choice of the support: SBA-15 LP

### 2.1 Bibliographic studies

Microporous and mesoporous inorganic solids (with pore diameters of  $\leq 20 \text{ \AA}$  and *ca*  $20\text{--}500 \text{ \AA}$  respectively) have found great utility as media for catalysts and sorption because of their large internal surface area. The concept of the molecular fingerprint has proved to be successful in the preparation of microporous materials such as zeolites<sup>2</sup> and was extended in the 1990s, to the generation of pure silica-based mesoporous material.<sup>3</sup> They present characteristic well-ordered, controlled and tunable mesostructures, high specific surfaces ( $> 700 \text{ m}^2\cdot\text{g}^{-1}$ ) and pore volumes ( $> 0.7 \text{ cm}^3\cdot\text{g}^{-1}$ ). In the extensive work reported these last decades<sup>4</sup>, two main families of mesoporous silica are highlighted:

- The X1S family (MCM-41, MCM-48, MCM-50)
- The SBA-15 family
- **Mesoporous silica X1S**

The preparation of X1S materials is directly related to the mesostructuration of the reaction media with the use of large surfactant molecules, able to form supramolecular systems (cationic, anionic, neutral or non ionic). In detail, molecules of surfactant will organize as micellar systems, themselves arranging as rods, to finally provide a hexagonal array (**Scheme 3**). The generation of such mesoporous material is in accordance to the “Liquid Crystal Templating” mechanism proposed by Beck,<sup>5</sup> for which the polycondensation of oxide precursors (*e.g.* tetraorthosilicate) occurs in the ordered array. Elimination of the surfactant molecules by washing with water and calcination leads to the required porosity.



**Scheme 3:** Possible mechanistic pathway for the formation of SBA-15 LP (Liquid Crystal Templating mechanism)

The preparation of such mesostructures is very sensitive to experimental conditions (*e.g.* pH, temperature, and surfactant) and a wide range of materials can then be obtained. Consequently, the MCM-41 material has been by far the most well-studied due to its easy synthetic access, variety and stability. Its mesophase shows a bidimensional structure with a hexagonal symmetry containing unidimensional channels (**Figure 1, (a)**). In contrast, MCM-48 displays a complex tridimensional organization (**Figure 1, (b)**) whereas MCM-50 presents a lamellar mesostructure (**Figure 1, (c)**).

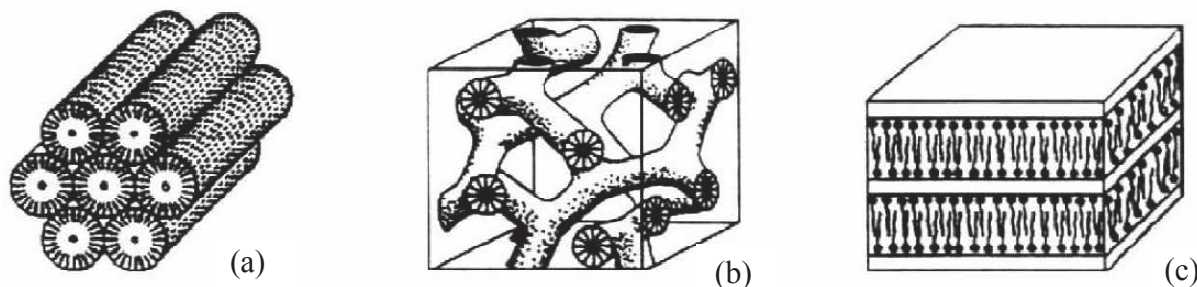


**Figure 1:** Schematic representation of different mesophases from the X1S family: MCM-41 (a), MCM-48 (b) and MCM-50 (c)

- **Mesoporous silica SBA-15**

In 1998, a new type of mesoporous silica, namely Santa Barbara Amorphous, or SBA-15, was developed by Stucky *et al.* at the University of California, Santa-Barbara.<sup>6</sup> These materials possessing a characteristic highly ordered hexagonal mesostructure, that contrasts with that of the MCM-41, are also thermally more stable. The general synthesis is based on the aggregation of amphiphilic molecules,<sup>6b</sup> namely neutral triblock copolymer of the type poly(ethylene oxide)<sub>n</sub>-poly(propylene oxide)<sub>m</sub>-poly(ethylene oxide)<sub>n</sub>, in which the propylene oxide functions constitute the more hydrophobic moieties. The polymer follows a self-organization process similar to that described above for the MCM-41 (**Scheme 3**). The inorganic phase is formed by polycondensation of the tetraorthosilicate molecules, as silicate

precursor, in acidic media.<sup>5</sup> Further washing and calcination of the material liberate the pores, for which the diameter could be considerably increased by using large tribloc copolymers. In this way, SBA-15 large pores, noted SBA-15 LP, are obtained with poly(ethylene oxide)<sub>20</sub>-poly(propylene oxide)<sub>70</sub>-poly(ethylene oxide)<sub>20</sub> (Pluronic 123) and present pore diameters up to 300 Å.<sup>6,7</sup> The use of neutral tribloc copolymers makes the mineral wall thickness and pore diameters larger than those observed for the MCM-41. This results in a better mechanical and thermal stability<sup>6a</sup>, making the SBA-15 LP more attractive in our study, requiring partial dehydroxylation before use.

In summary, a mesoporous structured silica was chosen as the starting support oxide for the creation of new silica/calix[4]arene materials because it offers a larger specific surface than its amorphous silica counterpart. More specifically, SBA-15 large pores (LP) was preferred to MCM-41 due to its higher thermal and mechanic stability, thus permitting the treatment of the support at 700°C without degradation of the mesostructure. Its large pores make the diffusion of calixarenes molecules possible, which present an average wingspan of 5 Å. The next section will present the synthesis and the characterization of the partially dehydroxylated SBA-15 LP<sub>-(700)</sub> at 700°C used throughout our studies.

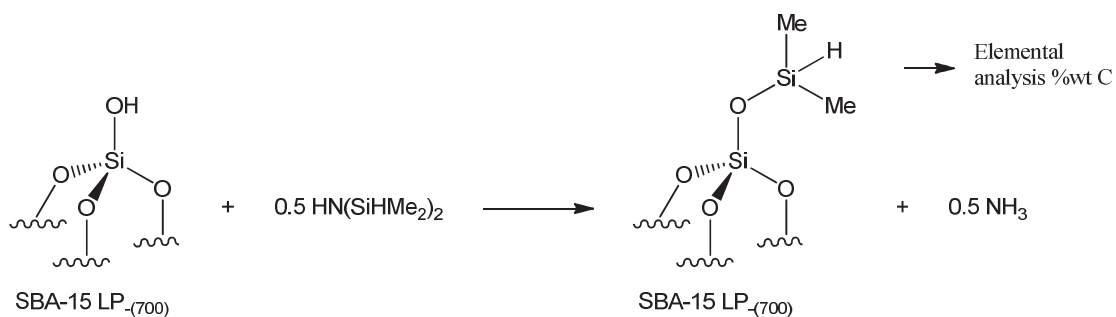
## 2.2 Preparation and characterization of SBA-15 LP<sub>-(700)</sub>

### 2.2.1 Synthesis of SBA-15 LP<sub>-(700)</sub>

SBA-15 LP was synthesized according to a procedure adapted from the literature<sup>7b</sup>, from tetraethyl orthosilicate reactant (TEOS) in presence of the surfactant Pluronic P123 (*vide supra*) in acidic media (see experimental part). SBA-15 LP is then obtained as a bidimensional hexagonal mesostructure, containing thin and uniform walls (31 to 64 Å), after removing of any organic compounds by calcination at 540°C. SBA-15 LP<sub>-(700)</sub> was obtained by careful dehydroxylation (973 K, 1 K·min<sup>-1</sup>, 16 h) to avoid collapse of the mesostructure.

### 2.2.2 Characterization and properties of SBA-15 LP<sub>-(700)</sub>

The concentration of the surface silanols is *ca.* 0.8 mmol<sub>OH</sub>·g<sup>-1</sup><sub>SBA</sub>, deduced by carbon elemental analysis of the support after reaction of silanols with tetramethyldisilazane HN(SiHMe<sub>2</sub>)<sub>2</sub> (**Scheme 4**).<sup>7a</sup>



Scheme 4: Titration of the surface silanols using TMDS and elemental analysis

SBA-15 LP<sub>(700)</sub> was characterized by several techniques including: nitrogen adsorption at 77 K (BET technique) for determination of the specific surface, size, volume and size distribution of the pores; X-Ray diffraction on powder, to reveal the structure of the mesoporous channels, supported by TEM microscopy, and IR spectroscopy.

- **BET technique**

Nitrogen physisorption (BET technique, see Annex IV) is an important tool for examination of the pores and surface properties of materials, giving isotherms which are the basis for the theoretical calculation of the specific BET surface  $a_s$  ( $\text{m}^2 \cdot \text{g}^{-1}$ ), the pore volume  $V_p$  ( $\text{cm}^3 \cdot \text{g}^{-1}$ ) and the pore diameter  $d_p$  (nm). Before any measure, the SBA-15 LP<sub>(700)</sub> sample was first degassed at 110°C overnight. Physisorption isotherm of the SBA-15 LP<sub>(700)</sub> used in our experiments is given in **Figure 2**. Its profile is characteristic of a mesoporous material in which the nitrogen adsorption proceeds *via* multilayer adsorption followed by capillary condensation. It must be specified that capillary condensation and evaporation often do not take place at the same pressure, leading to the appearance of a hysteresis loop, which give information about the cylindrical pore geometry. From **Figure 2** and **Table 1** the adsorption of the gas volume occurs between 0.7 and 0.9  $p/p^0$ , characteristic of high ordered mesoporous materials. The BJH pore size distribution is obtained from the isotherm of desorption (see Annex IV) and reveals a maximum at 8.8 nm. The BET surface is  $540 \text{ m}^2 \cdot \text{g}^{-1}$  whereas the total pore volume consists in  $1.19 \text{ cm}^3 \cdot \text{g}^{-1}$ .

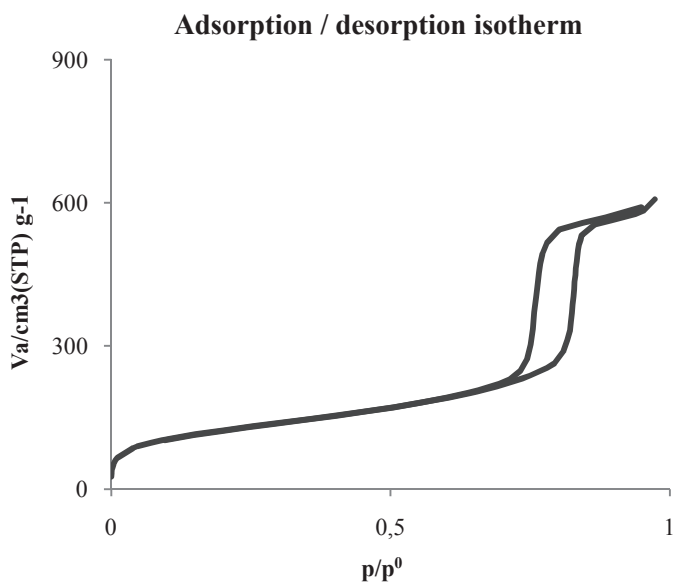


**Figure 2: Physisorption isotherm of the SBA-15 LP<sub>-(700)</sub>**

**Table 1: Structure parameters of the material SBA-15 LP<sub>-(700)</sub>**

	$a_{\text{S BET}} (\text{m}^2 \cdot \text{g}^{-1})$ [a]	$V_p (\text{cm}^3 \cdot \text{g}^{-1})$ [b]	$d_p (\text{nm})$ [c]
SBA-15 LP <sub>-(700)</sub>	540	1.19	8.8

[a] BET surface; [b] pore volume; [c] pore diameter

- **X-Ray powder diffraction**

The X-Ray powder diffraction method is a tool for determining the structure of the material. The diffraction pattern functions as a fingerprint for each material and gives information about the size of the unit cells and the pore system based on the absolute positions of the angles. The variety of the advanced diffraction patterns allows further determination of the hexagonal mesophase. **Figure 3** shows the X-ray diffraction pattern of the SBA-15 LP<sub>-(700)</sub> and reveals four well-resolved peaks in the  $2\theta$  domain at 92.9, 54.94, 47.98 and 31.63°. They can be respectively indexed as (100), (110), (200), and (210) diffraction peaks associated with  $p6mm$  hexagonal symmetry.<sup>7b</sup> This symmetry remains unchanged, even after dehydroxylation at 700°C, proving the great thermal stability of such a material.

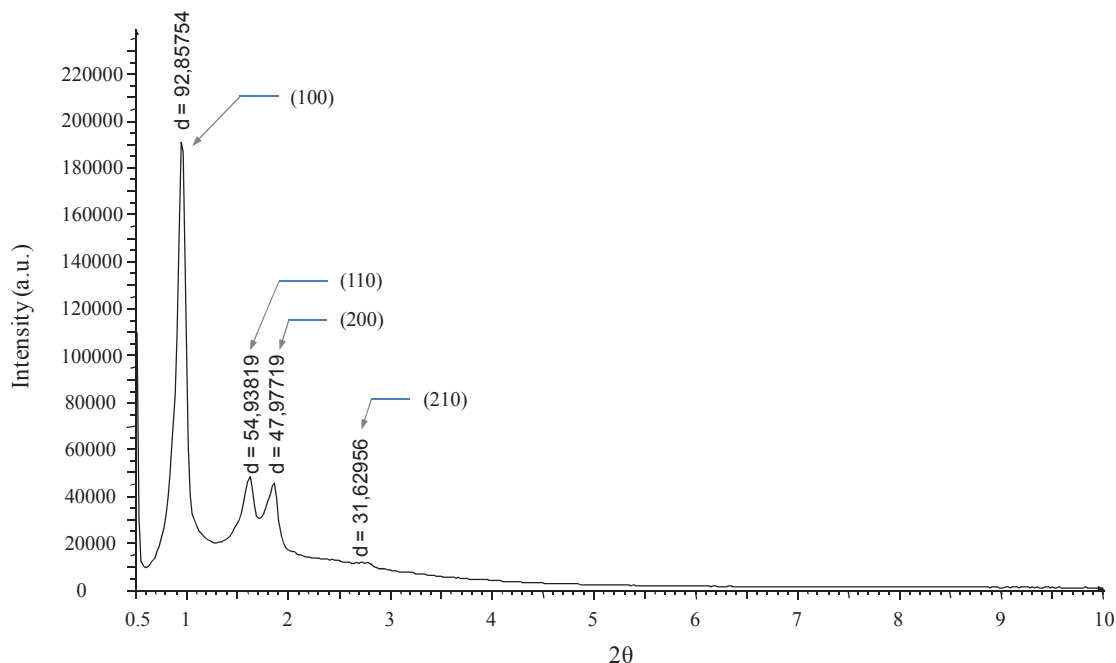


**Figure 3:** X-Ray pattern of SBA-15 LP<sub>(700)</sub>

- **Transmission electron microscopy (TEM)**

The transmission electron microscopy is based on the transmission of the electrons without diffusion through a very thin sample (5-100 nm). The contrast observed on the picture is related to the atomic mass of the elements observed. TEM data can be used to support the powder XRD data when it comes to the mesophase symmetry and pores size, because TEM pictures viewed from different angles can effectively reveal mesophase features of the materials. The TEM images of the SBA-15 LP used in our experiments clearly display cylindrical pores (**Figure 4**).

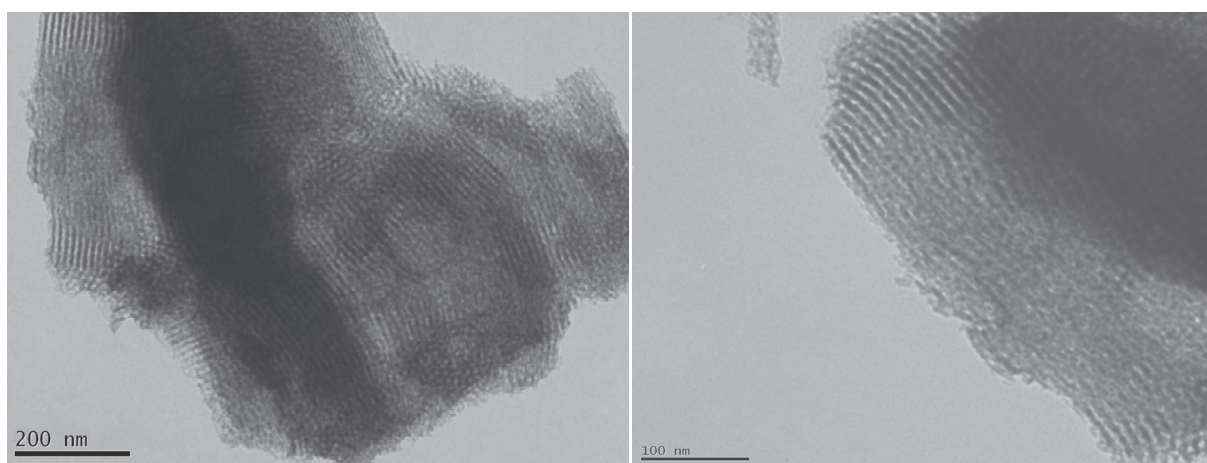


**Figure 4:** TEM images of the SBA-15 LP<sub>(700)</sub> used in our experiments (magnifying on the right)

- **Infra-red spectroscopy**

This support is also characterized by DRIFT, for which the spectrum displays a narrow peak at  $3747\text{ cm}^{-1}$  in the OH region corresponding to the sole isolated surface silanols after partial dehydroxylation at  $700^\circ\text{C}$  (**Figure 5**), similar to that observed for  $\text{SiO}_{2-(700)}$ .

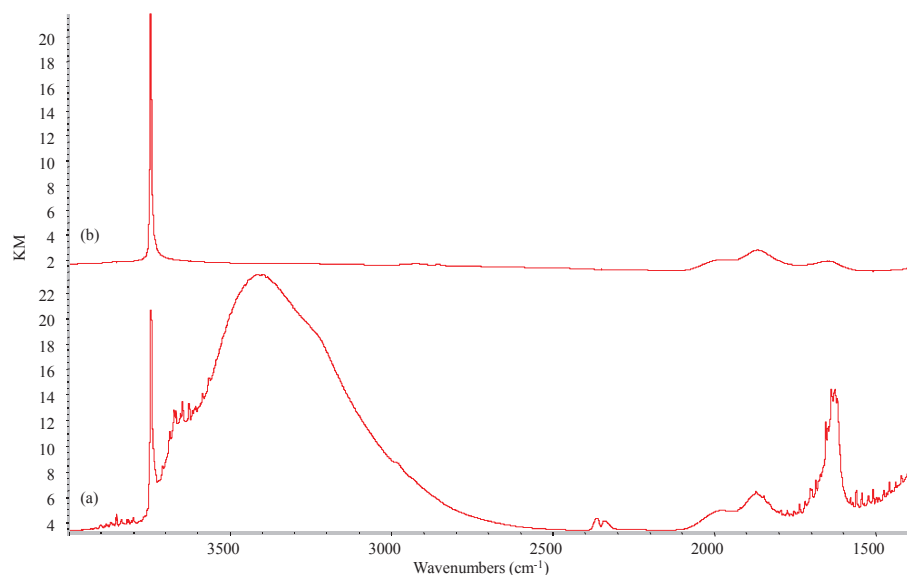


**Figure 5:** DRIFT spectrum of SBA-15 LP before (a) and after dehydroxylation at  $700^\circ\text{C}$  (b)

The starting support SBA-15 LP<sub>-(700)</sub> has been prepared by dehydroxylation of SBA-15 LP at  $700^\circ\text{C}$  to obtain only isolated silanols without any collapse of the mesostructure. This support was characterized using the common techniques for such materials (BET, XRD, TEM and IR). The next step consists in the grafting of  $\text{AliBu}_3\text{Et}_2\text{O}$  according the method developed in chapter II to check if similar species than observed with  $\text{SiO}_{2-(700)}$  is obtained.

### 3. Reactivity of $\text{AliBu}_3\text{Et}_2\text{O}$ with SBA-15 LP<sub>-(700)</sub>

Using the double Schlenk technique (see Annex I), SBA-15 LP<sub>-(700)</sub> was treated with 1.3 eq. of  $\text{AliBu}_3$  (based on the number of surface silanols: *ca.*  $0.8\text{ mmol}_{\text{OH}\cdot\text{g}^{-1}\text{SBA}}$ ) in diethylether (10 ml) for 2 h at room temperature. After repeated washings with diethylether (10 ml), followed by evacuation of the volatile, **M1** was afforded as a white powder and characterized employing DRIFT, solid-state NMR spectroscopy and mass balance analysis.

- **Infra-red spectroscopy**

After reaction with  $\text{Al}i\text{Bu}_3 \cdot \text{Et}_2\text{O}$ , the DRIFT spectrum of **M1** revealed that the band at  $3747 \text{ cm}^{-1}$ , corresponding to the isolated silanols displayed on the surface, is completely consumed (**Figure 6**). Simultaneously the appearance of two series of bands at  $2800\text{-}3000$  and at  $1300\text{-}1500 \text{ cm}^{-1}$  is consistent with the  $\nu_{(\text{Csp}^3\text{-H})}$  and  $\delta_{(\text{Csp}^3\text{-H})}$  vibrations of the alkyl moieties, respectively.

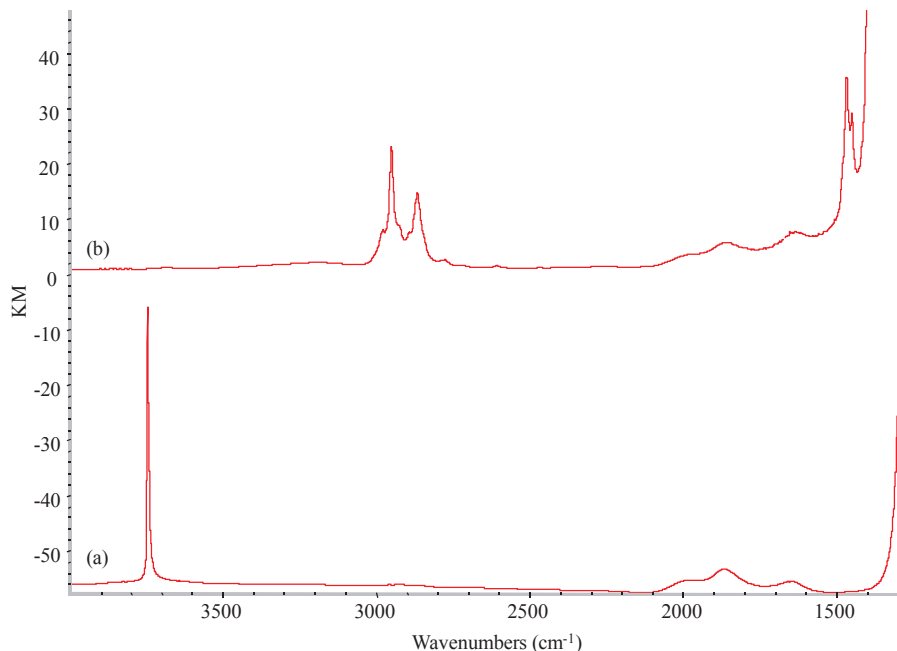


**Figure 6:** DRIFT spectra of SBA-15 LP<sub>-(700)</sub> before (a) and after treatment with  $\text{Al}i\text{Bu}_3$  in  $\text{Et}_2\text{O}$ , M1 (b)

- **Mass-balance analysis**

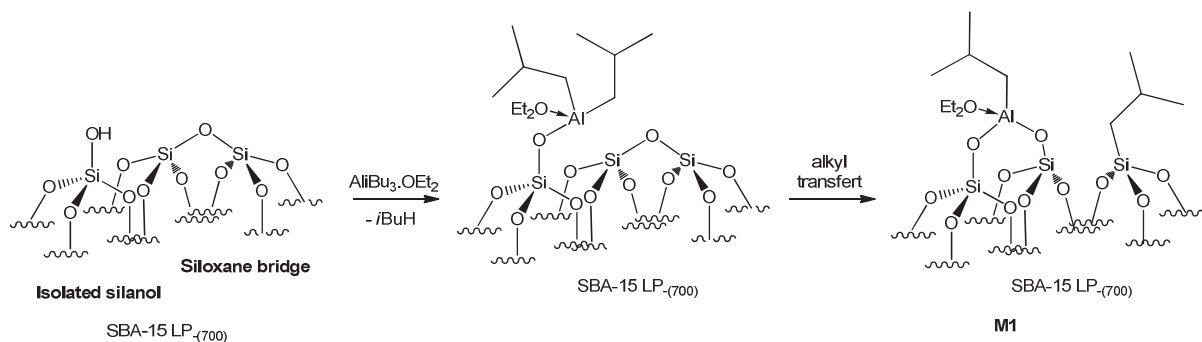
The gas evolved during the reaction was identified as isobutane and quantified as 1 eq. ( $0.711 \text{ mmol.g}^{-1}$  of silica) (**Table 2**) proving the total consumption of the surface silanols, in accordance to the DRIFT spectrum.

**Table 2: Mass balance analysis for M1**

	%wt Al <sup>[a]</sup>	<i>i</i> BuH/Al <sup>[b]</sup>	%wt C <sup>[a]</sup>	C/Al
Grafting	1.6	1.2	7.6	11 (th 12)
Hydrolysis <sup>[c]</sup>	-	0.9	-	-

<sup>[a]</sup> Percentage determined by elemental analysis. <sup>[b]</sup> Isobutane released during the grafting, quantified by GC. <sup>[c]</sup> Isobutane released after water vapor treatment.

Also 1 eq. of isobutane was evolved during the hydrolysis of the material **M1**, thus suggesting, as for  $\text{SiO}_{2-(700)}$ , a bipodal monoalkylaluminum etherate species with the concomitant transfer of one isobutyl group on the neighboring silicon, confirmed by the ratio of 12 carbons per aluminum from elemental analysis. The structure  $[(\equiv\text{SiO})_2\text{Al}i\text{Bu}.(\text{Et}_2\text{O})]_{\text{SBA}-15 \text{LP}_{-(700)}}$  can be rationally proposed for **M1** (**Scheme 5**).



**Scheme 5:** Grafting of  $\text{Al}i\text{Bu}_3$  onto  $\text{SBA-15 LP}_{-(700)}$  in diethyl ether

- **Solid-state NMR spectroscopy**

The  $^1\text{H}$  and  $^{13}\text{C}$  solid-state NMR spectra of  $[(\equiv\text{SiO})_2\text{Al}i\text{Bu}.(\text{Et}_2\text{O})]_{\text{SBA-15 LP}_{-(700)}} \textbf{M1}$  are quite similar to those obtained with  $\text{SiO}_{2-(700)}$  (**Figure 7**). In addition, due to the sufficient concentration of the alkyl species on SBA, a 2D  $^1\text{H}$ - $^{13}\text{C}$  HETCOR experiment was run to support the assignment (**Figure 7, (c)**). When using short contact time, correlations are usually observed only between the protons attached to a carbon. In the  $^1\text{H}$  MAS-NMR (**Figure 7, (a)**), the negative chemical shift at -0.1 ppm corresponds to the protons of  $\text{Al}(\text{CH}_2\text{CH}(\text{CH}_3)_2$  fragment correlating with the bonded carbon appearing at 22 ppm in  $^{13}\text{C}$  spectrum (**Figure 7, (b)**). The intense signal at 0.9 ppm is assigned to the protons of the  $\text{M}(\text{CH}_2\text{CH}(\text{CH}_3)_2$  ( $\text{M} = \text{Si, Al}$ ) and the  $\text{Si}(\text{CH}_2\text{CH}(\text{CH}_3)_2$  fragments in correlation with the signal centered at 26 ppm. The protons of  $\text{M}(\text{CH}_2\text{CH}(\text{CH}_3)_2$  ( $\text{M} = \text{Si, Al}$ ) moieties are displaced at 1.8 ppm which interacts undoubtedly with the large signal at 26-28 ppm in  $^{13}\text{C}$  spectrum. Protons of the diethylether molecule display two peaks at 1.2 and 3.8 ppm in correlation with the carbon signals at 14 and 65 ppm, respectively.

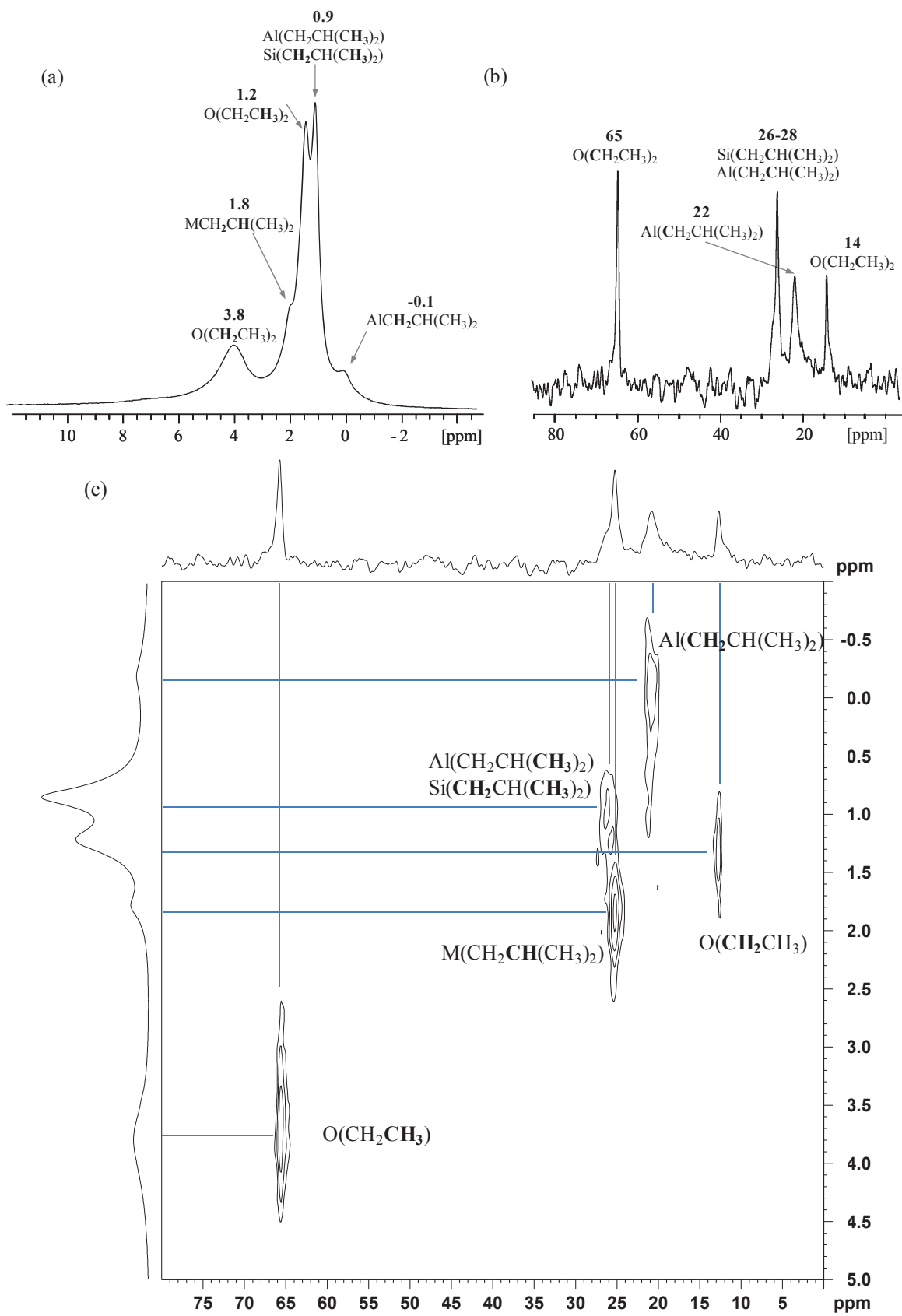
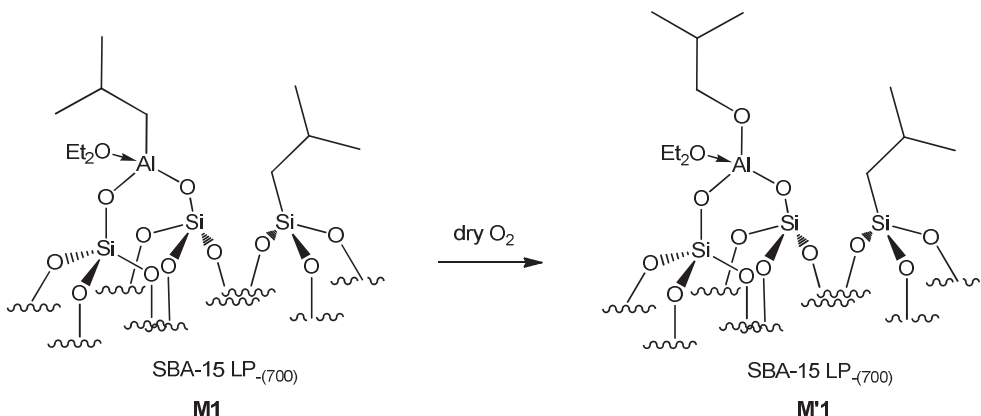


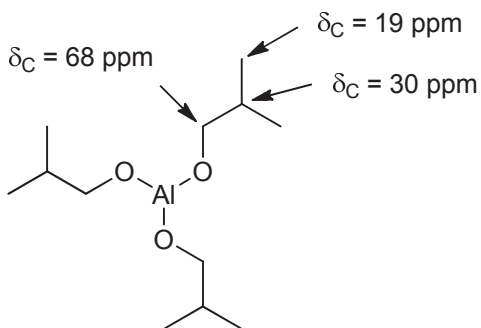
Figure 7:  $^1\text{H}$  MAS-NMR (a),  $^{13}\text{C}$  CP/MAS-NMR (b), HETCOR 2D NMR (c) of M1

In order to confirm the isobutyl transfer to silica, the material  $[(\equiv\text{SiO})_2\text{Al}i\text{Bu}(\text{Et}_2\text{O})]_{\text{SBA-15 LP-(700)}} \mathbf{M1}$  was exposed to dry  $\text{O}_2$  at RT over 2h. The selective oxidation of the alkyl aluminum fragments is expected to occur, thus providing aluminum isobutoxide species  $\mathbf{M}'\mathbf{1}$  alongside the  $\text{Si}-i\text{Bu}$  fragment, remaining intact (**Scheme 6**).



**Scheme 6:** Treatment of  $[(\equiv\text{SiO})_2\text{Al}i\text{Bu}(\text{Et}_2\text{O})]_{\text{SBA-15 LP-(700)}} \mathbf{M1}$  with dry  $\text{O}_2$

The peak assignment of the  $^{13}\text{C}$  CP/MAS spectrum of the resulting material **M'****1** will be supported with the  $^{13}\text{C}$ -NMR data collected from the available  $\text{Al}(\text{O}i\text{Bu})_3$  in DMSO (**Scheme 7**).



**Scheme 7:**  $^{13}\text{C}$  chemical shifts of  $\text{Al}(\text{O}i\text{Bu})_3$  in DMSO

The spectrum of **M'****1** exhibits a new profile in which the peak corresponding to the carbons of  $\text{Al}(\text{CH}_2\text{CH}(\text{CH}_3)_2)$  at 22 ppm has disappeared to give a signal at 69 ppm, corresponding the  $\text{CH}_2$  carbon of the aluminum isobutoxide in accordance to the NMR data of  $\text{Al}(\text{O}i\text{Bu})_3$ . Furthermore, the signal at 26-28 ppm has considerably decreased leaving a weak peak that can be judiciously attributed to the carbons of the  $\text{Si}(\text{CH}_2\text{CH}(\text{CH}_3)_2)$  moiety. New peaks have appeared at 17 and 30 ppm assigned respectively to the  $\text{CH}_3$  and  $\text{CH}$  carbons of

the aluminum isobutoxide (**Figure 8**), thus confirming the total oxidation of the Al-*i*Bu fragments.

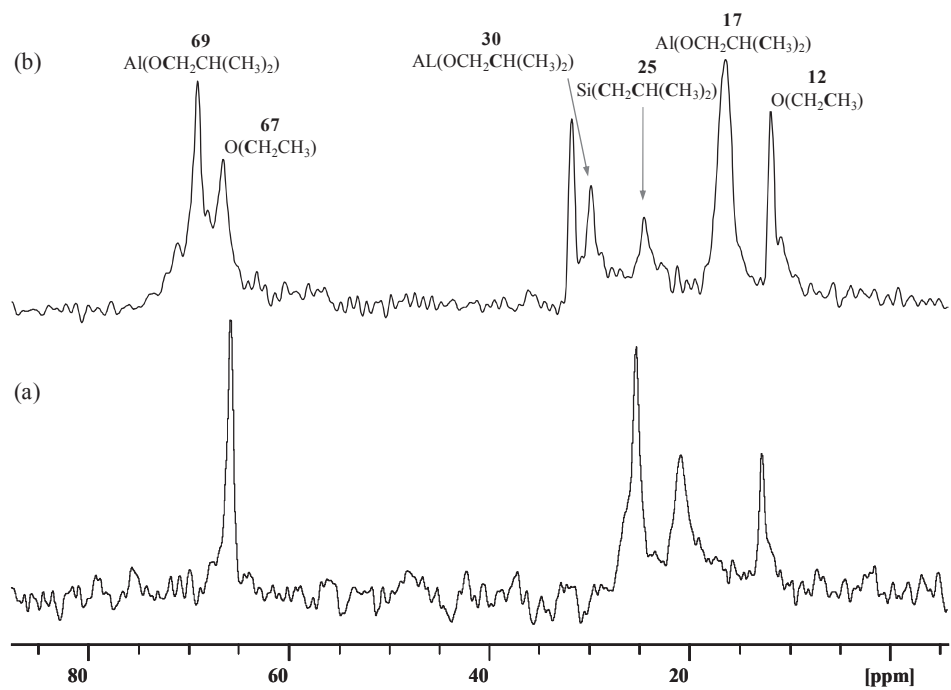
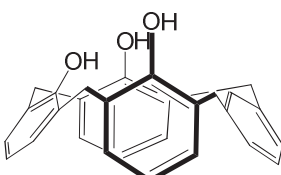


**Figure 8:**  $^{13}\text{C}$  CP/MAS spectra of **M1**, before (a) and after exposure to  $\text{O}_2$ , **M'1** (b)

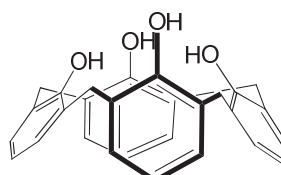
In summary, during the reaction of  $\text{Al}i\text{Bu}_3\text{Et}_2\text{O}$  with SBA-15 LP<sub>(700)</sub>, 1 eq. of isobutane per aluminum was evolved. Elemental analysis and chemical reactivity (hydrolysis) indicate that  $[(\equiv\text{SiO})_2\text{Al}i\text{Bu}(\text{Et}_2\text{O})]\text{SBA-15 LP}_{(700)}$  **M1** is the unique species. Further spectroscopic analyses (DRIFT, solid-state NMR) are consistent with the structure **M1** and particularly show that one isobutyl fragment is concomitantly transferred to the silica by siloxane bridge opening. The same result was obtained in the case of  $\text{SiO}_{2-(700)}$  (chapter II), this contradicts the intuitive thinking that alkyl transfer would be favored in the concave environment of the SBA 15 pores, as convex aerosil surface is also subjected to alkyl transfer. This demonstrates that the observed selectivity is not restricted to specific type of support, and further emphasizes that our method can be extended to other silica type materials independently of their structural features. This surface species, similar to that obtained in the case of  $\text{SiO}_{2-(700)}$ , will be engaged in the tethering of calixarene ligands bearing three or four hydroxyl functions.

## 4. Preparation of supported metallacalix[4]arenes: reaction of calix[4]arene derivatives with $[(\equiv \text{SiO})_2 \text{Al}i\text{Bu} \cdot (\text{Et}_2\text{O})]_{\text{SBA-15 LP-(700)}} \text{M1}$

Our approach to calixarene immobilization is the direct protolysis of an aluminum isobutyl fragment supported on SBA-15 LP<sub>(700)</sub> by one of its phenols. The grafting of the selected calixarenes  $[[4\text{H}]\text{-}(\text{H})(\text{OH})_3]$  **L12** and  $[[4\text{H}]\text{-}(\text{OH})_4]$  **L13** (**Scheme 8**) onto  $[(\equiv \text{SiO})_2 \text{Al}i\text{Bu} \cdot (\text{Et}_2\text{O})]_{\text{SBA-15 LP-(700)}} \text{M1}$  is driven by the interconversion of the aromatic units, the steric hindrance of both support and calixarene and the accessibility of the phenol, compared to the hydroquinone. Our choice was therefore focused on detertiobutylated calix[4]arenes in order to limit any steric hindrance and facilitate the *trans*-annular interconversion of the four aromatic units. In this way, the calixarenes present *anti*-oriented phenol functions for both their grafting onto the support and incorporation of organometallic complexes. The tethering of the calixarenes **L12** and **L13** leads to the novel materials **M2** and **M3**, which will serve as support for organometallic complexes of zirconium, tantalum and tungsten. They will finally be engaged in preliminary catalytic studies.



**L12**



**L13**

**Scheme 8:** Calixarene spacers  $[[4\text{H}]\text{-}(\text{H})(\text{OH})_3]$  **L12** and  $[[4\text{H}]\text{-}(\text{OH})_4]$  **L13**

### 4.1 Preparation and characterization of bipodal metallacalix[4]arenes supported on mesoporous SBA-15 LP<sub>(700)</sub>

#### 4.1.1 Grafting of the calixarene $[[4\text{H}]\text{-}(\text{OH})_3(\text{H})]$ onto $[(\equiv \text{SiO})_2 \text{Al}i\text{Bu} \cdot (\text{Et}_2\text{O})]_{\text{SBA-15 LP-(700)}} \text{ (M1)}$

$[[4\text{H}]\text{-}(\text{OH})_3(\text{H})]$  was prepared using the described derterbutylation method.<sup>8</sup> Typically,  $[[4+]\text{-}(\text{OH})_3(\text{H})]$  is treated with  $\text{AlCl}_3$  in presence of phenol to proceed to a *retro* Friedel-Craft reaction on the *tert*butyl groups.<sup>9</sup> Pure  $[[4\text{H}]\text{-}(\text{OH})_3(\text{H})]$  is obtained in 80% yield as a white powder, which was dried over 12h at 110°C before being used for the grafting.

Using the double Schlenk technique, 1.3 eq. of  $[[4\text{H}]\text{-}(\text{OH})_3(\text{H})]$  (based on 1 eq. per aluminum in 1.6%wt) in 10 ml of DCM was reacted with  $[(\equiv \text{SiO})_2 \text{Al}i\text{Bu} \cdot (\text{Et}_2\text{O})]_{\text{SBA-15 LP-(700)}}$

**M1** over 16h at room temperature. After repeated washings with DCM (10 ml), followed by evacuation of the volatiles, **M2** was afforded as a white powder and characterized by DRIFT, solid-state NMR spectroscopy, mass balance analysis and BET.

- **Mass-balance analysis**

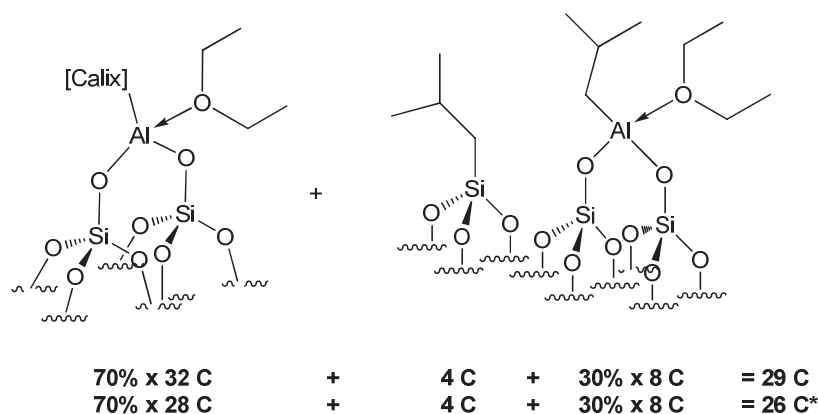
Elemental analysis shows the presence of aluminum to the extent of 1.1%wt. During the reaction of  $[[4\text{H}]\text{-}(\text{H})(\text{OH})_3]$  with  $[(\equiv\text{SiO})_2\text{Al}i\text{Bu}.\text{(Et}_2\text{O})]_{\text{SBA-15 LP-(700)}}$  **M1**, approximately 0.7 isobutane ( $0.285 \text{ mmol.g}^{-1}$  of SBA) was released per grafted aluminum (**Table 3**) consistent with the formation of  $[(\equiv\text{SiO})_2\text{Al-[O-[4H]}-\text{(OH)}_2\text{(H)}].\text{(Et}_2\text{O})]_{\text{SBA-15 LP-(700)}}$  **M2**.

**Table 3: Mass-balance analysis for M2**

	%wt Al <sup>[a]</sup>	iBuH/Al <sup>[b]</sup>	%wt C <sup>[a]</sup>	C/Al
Grafting	1.1	0.7	10.9	22 (th 26)
Hydrolysis <sup>[c]</sup>	1.1	0.3	-	-

<sup>[a]</sup> Percentage determined by elemental analysis. <sup>[b]</sup> Isobutane released during the grafting, quantified by GC. <sup>[c]</sup> Isobutane released after water vapor treatment.

Upon reaction of the solid **M2** with a water vapor pressure at RT, 0.3 iBuH/Al was evolved, thus confirming that  $[[4\text{H}]\text{-}(\text{OH})_3\text{(H)}]$  reacted on 70% of the isobutyl aluminum sites. This solid contains 10.9%wt of carbons, which corresponds to an average of 22 C/Al. In addition, due to similar analytical reasons discussed in chapter II, the count of 22 carbon atoms per aluminum is lower than the 26 expected (the diethyl ether molecule from the full oxidized aluminum is probably released during analysis). **Scheme 9** illustrates the correct expected count of carbons. This result suggests the anchoring of the calixarene on material **M1**.



**Scheme 9: Carbon atom count of M2 according the isobutane quantification. \*The second line is the corrected calculation by removing the diethyl ether molecule from the full oxydated aluminum center**

- **Infra-red spectroscopy**

The DRIFT spectrum of **M2** displays new bands at 1473-1590 and 3000-3100  $\text{cm}^{-1}$  assigned to the aromatic  $\nu_{(\text{Csp}2=\text{Csp}2)}$  and  $\nu_{\text{Csp}2-\text{H}}$  vibrations, respectively (**Figure 9**). The  $\nu_{\text{Csp}3-\text{H}}$  bands from 2888 to 2953  $\text{cm}^{-1}$  and the  $\delta_{\text{Csp}3-\text{H}}$  bands from 1320 to 1466  $\text{cm}^{-1}$  prove the presence of the transferred isobutyl groups on silicon atoms and some unreacted isobutyl aluminum etherate, also encapsulating the methylene bridges of the calixarene. The examination of the OH stretching region reveals a small band at 3490  $\text{cm}^{-1}$  due to the phenol functions of calixarene.

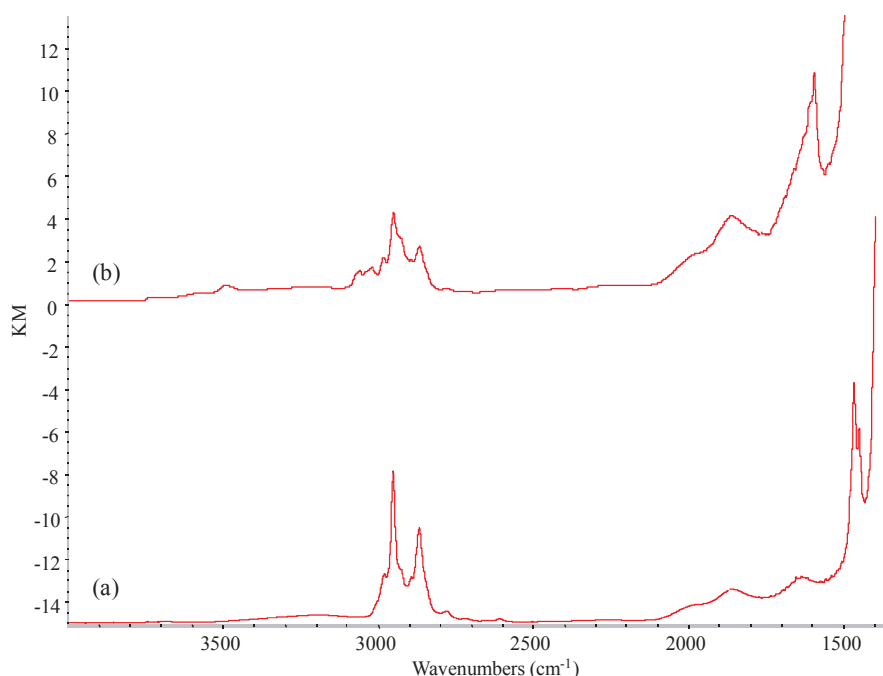


**Figure 9: DRIFT spectra of M1 (a) and after reaction with  $[4\text{H}]-(\text{OH})_3(\text{H})$ , M2 (b)**

- **Solid-state NMR spectroscopy**

$^1\text{H}$  MAS-NMR spectrum shows a new peak at 6.8 ppm corresponding to the aromatic protons (**Figure 10**). The signal at 0.9-1.8 ppm belongs to the protons of the isobutyl fragments and the methyl of diethylether group. The large signal at 3.6-5.3 ppm is supposed to contain both methylenic protons of the diethyl ether molecule and protons from the methylenic bridges of the calixarene ligand. It is noteworthy that the peak at -0.14 ppm, characteristic of the  $\text{Al}(\text{CH}_2\text{CH}(\text{CH}_3)_2$  protons, almost completely disappears. Unfortunately, the low resolution of the spectrum cannot permit to distinguish the different bridges  $\text{CH}_2$  of the calixarene.

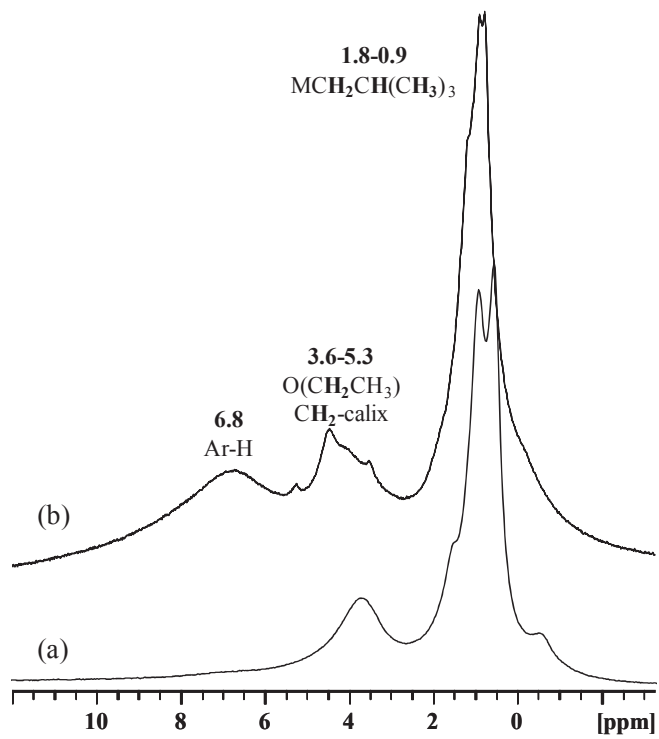


Figure 10:  $^1\text{H}$  MAS-NMR of M1 (a) and M2 (b)

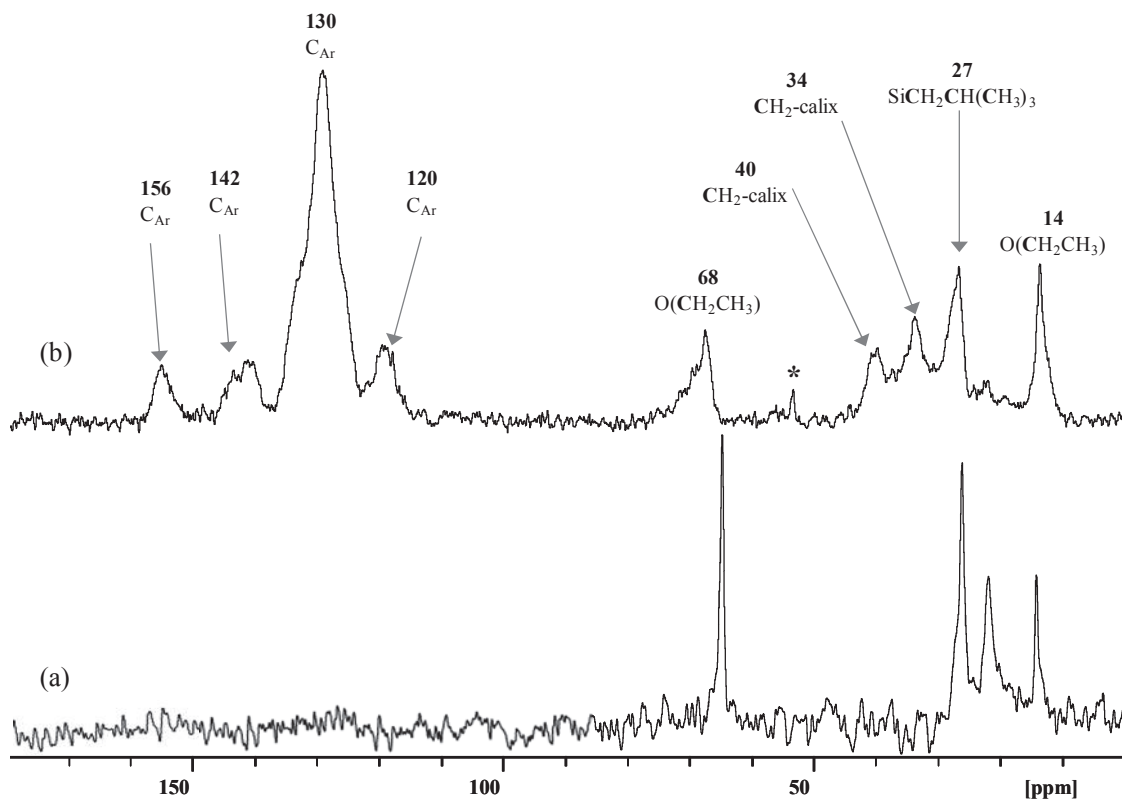


Figure 11:  $^{13}\text{C}$  CP/MAS-NMR of M1 (a) and M2 (b) (\* Spinning side band)

The solid state  $^{13}\text{C}$  CP/MAS spectrum of **M2** shows new peaks at 34 and 40 ppm as well as four signals at 120, 130, 142 and 156 ppm, in addition to the recurring diethyl ether and Si-*i*Bu fragment at 14, 68 and 27 ppm (**Figure 11**). The signals at 34 and 40 ppm probably correspond to two different methylenic bridges of the calixarene and those at lower field are assigned respectively to the carbons of the aromatic rings. As already observed from the  $^1\text{H}$  MAS spectrum, the Al(CH<sub>2</sub>CH(CH<sub>3</sub>)<sub>2</sub> peak at 22 ppm significantly decreases, consistent with the anchoring of the calixarene following by isobutane evolution.

- **BET analysis**

BET analysis of  $[(\equiv\text{SiO})_2\text{Al}-[\text{O}-[4\text{H}]-\text{(OH)}_2(\text{H})].(\text{Et}_2\text{O})]_{\text{SBA-15 LP-(700)}} \textbf{M2}$  was run in the same conditions as for the starting SBA-15 LP-(700). The profile of the resulting adsorption/desorption isotherm is characteristic of a mesoporous material in which the nitrogen adsorption proceeds *via* multilayer adsorption followed by capillary condensation, for which the major part of the volume of N<sub>2</sub> adsorbed occurs between 0.4 and 0.7 p/p<sup>0</sup> (**Figure 12**). In contrast to the cylindrical pore geometry of the starting SBA-15 LP-(700), the hysteresis loop of **M2** indicates an “inkbottle” pore geometry in which the pore present different shapes and sizes. The “coating” of the SBA surface leads to a decrease of its BET surface from 540 m<sup>2</sup>.g<sup>-1</sup> before any grafting to 406 m<sup>2</sup>.g<sup>-1</sup> for the material **M2** (**Table 4**). In parallel, the total pore volume and the average BJH pore diameter have considerably reduced from 1.19 to 0.38 cm<sup>3</sup>.g<sup>-1</sup> and from 8.8 to 4.6 nm, respectively. The decrease of both pore diameter and volume are in accordance with the presence of calixarene ligands, located on the internal surface of the pores of the mesoporous support.<sup>10</sup>

**Table 4: Structure parameters of the materials SBA-15 LP<sub>(700)</sub> and M2**

	a <sub>S</sub> BET (m <sup>2</sup> .g <sup>-1</sup> ) <sup>[a]</sup>	V <sub>p</sub> (cm <sup>3</sup> .g <sup>-1</sup> ) <sup>[b]</sup>	d <sub>p</sub> (nm) <sup>[c]</sup>
SBA-15 LP <sub>(700)</sub>	540	1.19	8.8
<b>M2</b>	406	0.38	4.6

<sup>[a]</sup> BET surface; <sup>[b]</sup> pore volume; <sup>[c]</sup> pore diameter

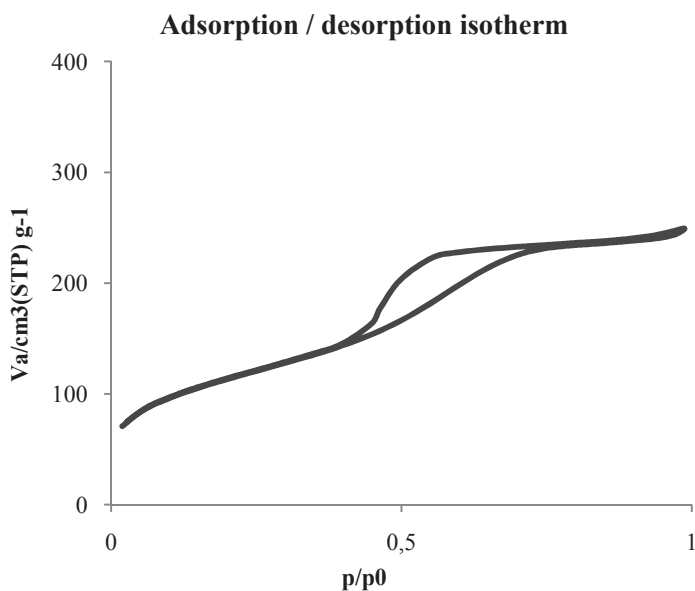
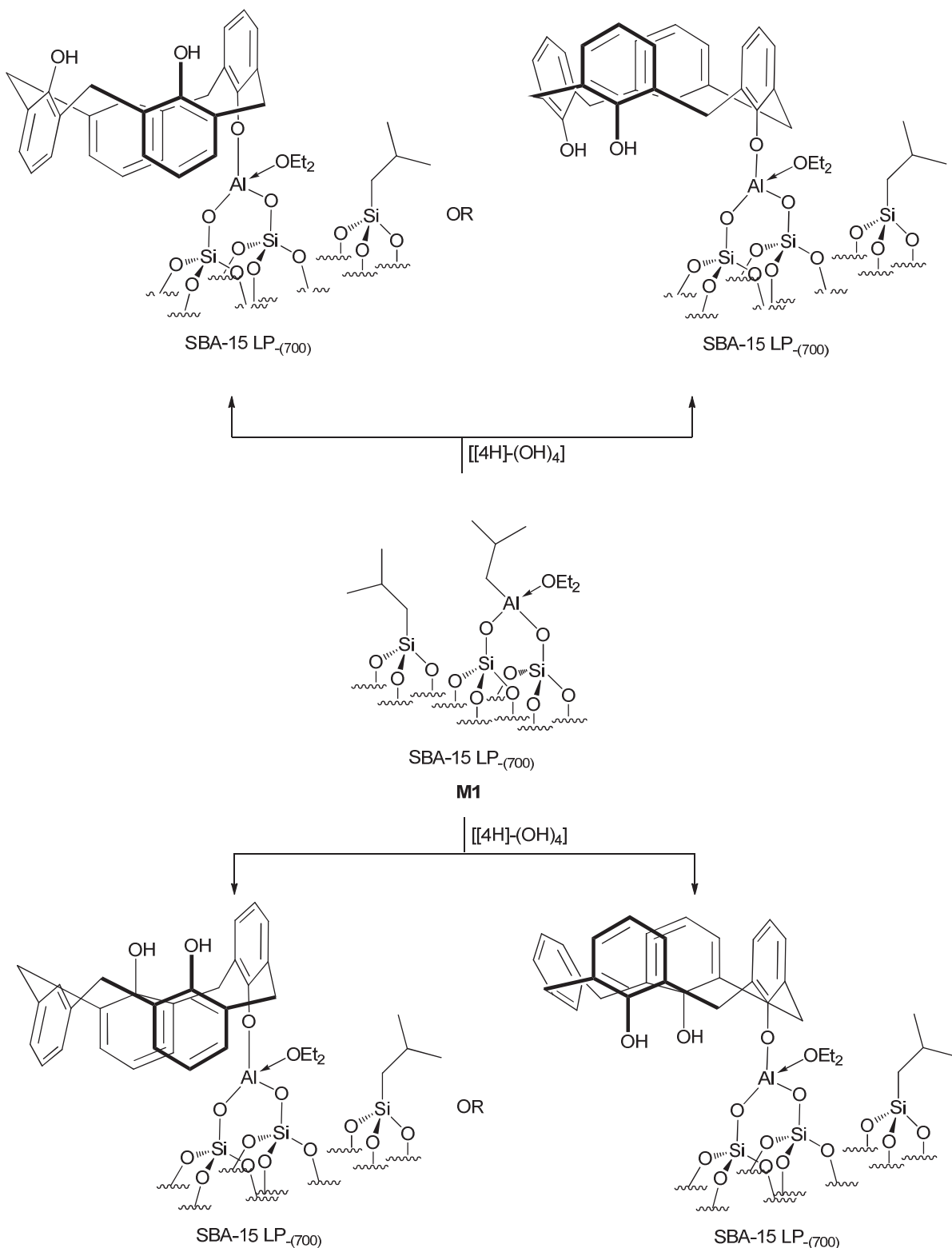


Figure 12: Physisorption isotherm of the M2

In regard of the collected spectroscopic data (DRIFT, solid-state NMR), mass balance analysis and BET, the concept of tethering calixarene ligands on SBA-15 LP previously modified with triisobutylaluminum etherate is successful. However, the steric hindrance of the calixarene leads to the grafting of  $[[4H]\text{-(H)(OH)}_3]$  **L12** onto only 70% of the isobutyl aluminum sites, to form a new species of the general formula  $[(\equiv\text{SiO})_2\text{Al-[O-}4\text{H}\text{-(OH)}_2\text{(H)}\text{].(Et}_2\text{O)}]_{\text{SBA-15 LP-(700)}}$  (**Scheme 10**). Unfortunately, the insufficient resolution of the solid-state NMR spectra collected is currently the limit in well-defining the conformation of this species and the selectivity of the grafting (**Scheme 10**). Thus, four main conformations can be proposed, according the position of the tethered phenoxo unit and the relative disposition of the three others. Further spectroscopic investigations using, for instance, Dynamic Nuclear Polarization for NMR spectroscopy, could provide a way to improve NMR signals.<sup>11</sup> An alternative method consisting in labeling the carbons of the methylene bridges of the calixarene can be proposed by condensation of  $^{13}\text{C}$  labeled formaldehyde with *p*-*tert*butylphenol (see Chapter I).



**Scheme 10 : Structures proposed for the material  $[(\equiv\text{SiO})_2\text{Al}-\text{O}-\text{[4H]}-\text{(OH}_2\text{H}\text{)}\cdot(\text{Et}_2\text{O})]_{\text{SBA-15 LP-(700)}} \text{M2}$**

In addition, deuteration of both phenolic hydrogens and study of the  $^2\text{H}$ -MAS NMR spectrum of the resulting adduct could help to overcome any doubt about the selectivity of the grafting,

in other words the relative position of the two remaining phenol functions. Indeed, as already mentioned in chapter III, the chemical shift of the hydrogen bonded protons of the proximal bis-dehydroxylated calixarene  $[4+]-1,2-(OH)_2(H)_2$  **L8** is 6.2 ppm, whereas that of the distal bis-dehydroxylated calixarene  $[4+]-1,3-(OH)_2(H)_2$  **L5**, is 4.4 ppm.

#### 4.1.2 Incorporation of $Zr(^{13}CH_2Ph)_4$ onto the material $[(\equiv SiO)_2Al-[O-[4H]-OH_2(H)].(Et_2O)]_{SBA-15\ LP-(700)}$ (**M2**)

The aim of this paragraph is to synthesize bipodal bis-benzyl zirconium anchored onto the calixarene ligand, compared to its analogous directly supported onto  $SiO_2-(200)$  **M'3**. These two materials are obtained by reaction of  $Zr(^{13}CH_2Ph)_4$  in pentane at RT.

Using the double Schlenk technique, 1.3 eq. (based on the quantity of grafted calixarenes: 0.285 mmol.g<sup>-1</sup> **M2**) of  $Zr(^{13}CH_2Ph)_4$   $\alpha-^{13}C$  randomly enriched at 20% (see preparation in chapter II) in pentane (10 ml) was reacted with  $[(\equiv SiO)_2Al-[O-[4H]-OH_2(H)].(Et_2O)]_{SBA-15\ LP-(700)}$  **M2** over 16 h at room temperature in the dark. After repeated washings with pentane (10 ml), followed by evacuation of the volatiles, **M3** was afforded as a yellow powder and characterized employing DRIFT, solid-state NMR spectroscopy, mass balance analysis and EXAFS. The solid-state NMR spectra of **M3** will be compared to those collected for the bis-siloxy counterpart **M'3** (see Annex V for the preparation and full characterization).

- **Infra-red spectroscopy**

After reaction with  $Zr(^{13}CH_2Ph)_4$ , the DRIFT spectrum of **M3** displays an increase of the bands at 1589 cm<sup>-1</sup> and 3000-3060 cm<sup>-1</sup> assigned to the  $\nu_{(Csp2=Csp2)}$  and  $\nu_{Csp2-H}$  aromatic vibrations, respectively (**Figure 13**). The bands from 2870 to 2990 cm<sup>-1</sup> are the result of the  $\nu_{Csp3-H}$  bond vibration corresponding to the Si-iBu groups plus the methylene bridges of the calixarene and methylene of  $ZrCH_2Ph$ . Examination of the OH stretching region reveals a weak band centered at 3589 cm<sup>-1</sup> revealing the presence of some unreacted phenol functions.

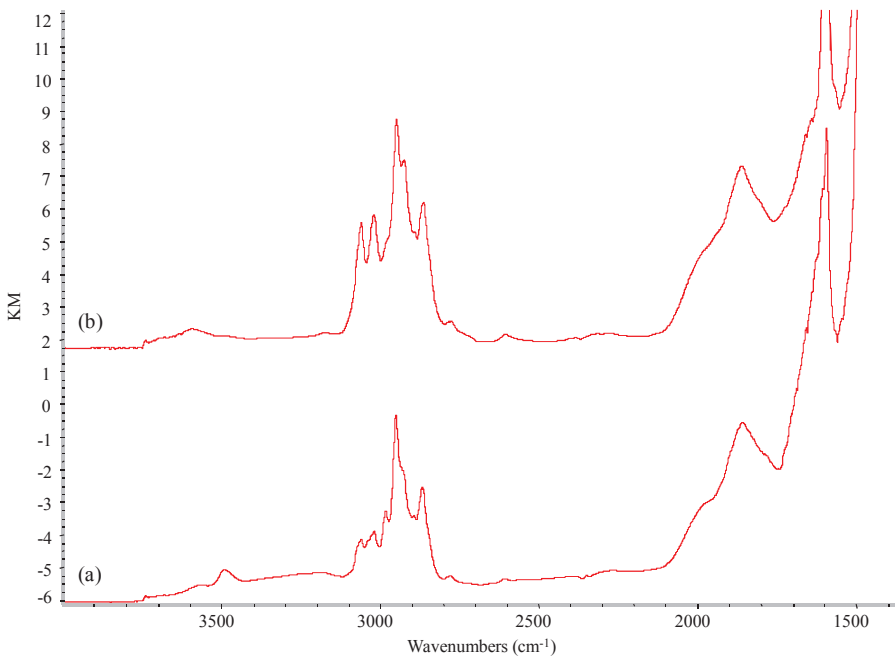


**Figure 13:** DRIFT spectra of M2 (a) and after reaction with  $\text{Zr}(\text{CH}_2\text{Ph})_4$ , M3 (b)

- **Mass-balance analysis**

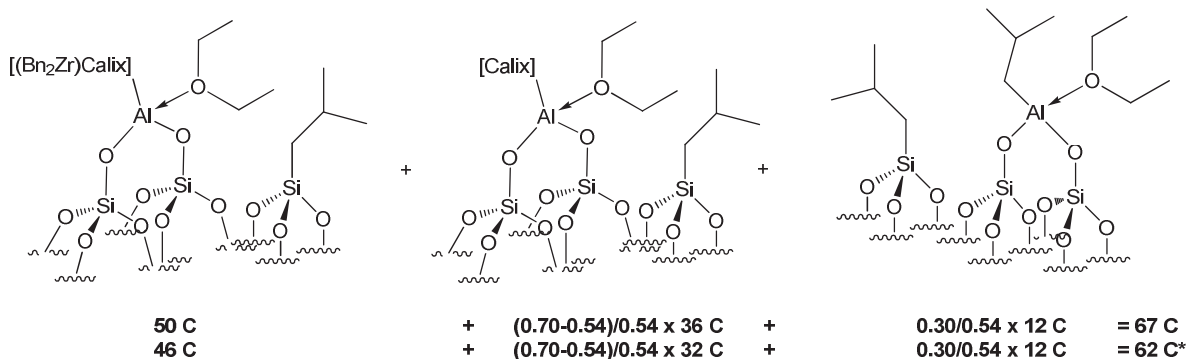
It must be mentioned that the quantification by GC of the toluene released was not conclusive due its low vapor pressure and physisorption on the support. Elemental analysis shows the presence of Zr and Al to the extent of 1.90%wt and 1.04%wt respectively (**Table 5**). This corresponds to 0.54 Zr/Al confirming the partial consumption of phenols from the supported calixarene (already present on 70% of the isobutyl aluminum sites) as observed by DRIFT spectroscopy. Carbon elemental analysis (15%wt) shows the presence of 60 C/Zr.

**Table 5:** Mass balance analysis for M3

	%wt Al <sup>[a]</sup>	%wt Zr <sup>[a]</sup>	Zr/Al	%wt C <sup>[a]</sup>	C/Zr
Grafting	1,04	1.90	0,54	15.00	60 (th 62 <sup>[b]</sup> )

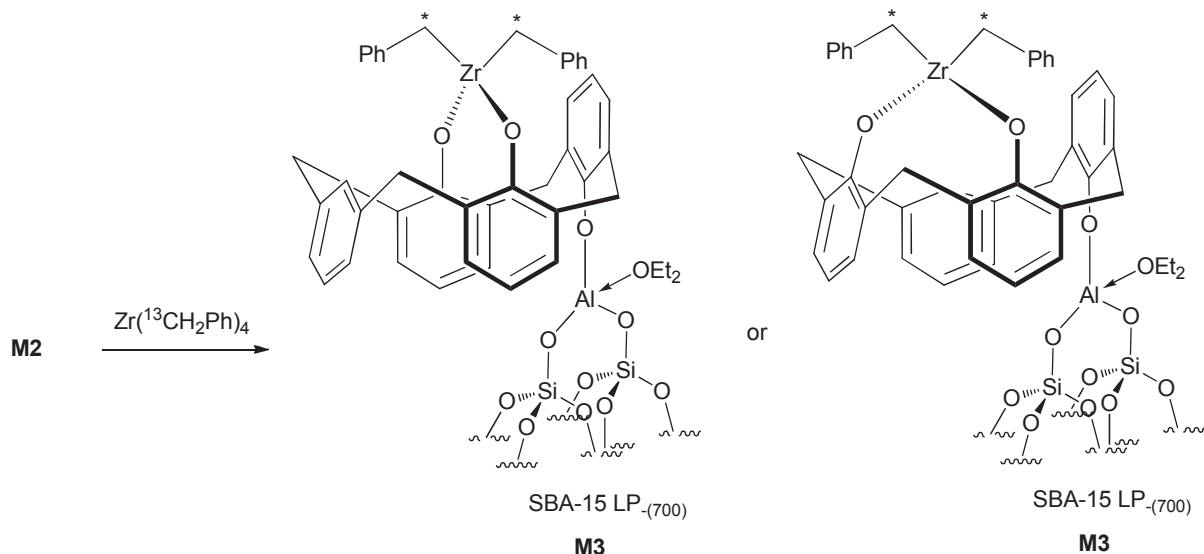
<sup>[a]</sup> Percentage determined by elemental analysis. <sup>[b]</sup> Considering partial release of diethyl ether

If  $54/70 = 77\%$  of the surface calixarene are considered to bear one  $\text{Zr}(\text{CH}_2\text{Ph})_2$  fragment, the correct expect count of carbons per zirconium atoms is 62 (considering the partial removal of diethyl ether during analysis), thus confirming the experimental one of 60 (**Scheme 11**).



**Scheme 11:** Carbon atom count of M3 reported to one zirconium atom. \*The second line is the corrected calculation by removing the two diethyl ether molecule from the two full oxydated aluminum centers

This result is consistent with the formation of  $[(\equiv \text{SiO})_2\text{Al}-\text{O}-[\text{H}]-(\text{H})(\text{O})_2\text{Zr}(\text{CH}_2\text{Ph})_2].(\text{Et}_2\text{O})]_{\text{SBA-15 LP-(700)}} \text{M3}$  where the zirconium is bipodal on the correspondent calixarene (**Scheme 12**), either in distal or proximal position.



**Scheme 12:** Structures proposed for the material  $[(\equiv \text{SiO})_2\text{Al}-\text{O}-[\text{H}]-(\text{H})(\text{O})_2\text{Zr}(\text{CH}_2\text{Ph})_2].(\text{Et}_2\text{O})]_{\text{SBA-15 LP-(700)}} \text{M3}$

- **Solid-state NMR spectroscopy**

Only one difference was noted between the  $^1\text{H}$  MAS-NMR spectra of  $[(\equiv \text{SiO})_2\text{Al}-\text{O}-[\text{H}]-(\text{H})(\text{O})_2\text{Zr}(\text{CH}_2\text{Ph})_2].(\text{Et}_2\text{O})]_{\text{SBA-15 LP-(700)}} \text{M2}$  (**Figure 14, (a)**) and **M3** (**Figure 14, (b)**); that of **M3** exhibits an intense signal at 6.9 ppm corresponding to the aromatic protons in accordance with the presence of the grafted benzyl groups. As already observed during the NMR analysis of **H4** (chapter II), the methyl of toluene from the decomposition of surface species inside the rotor is displayed at 2.0 ppm.

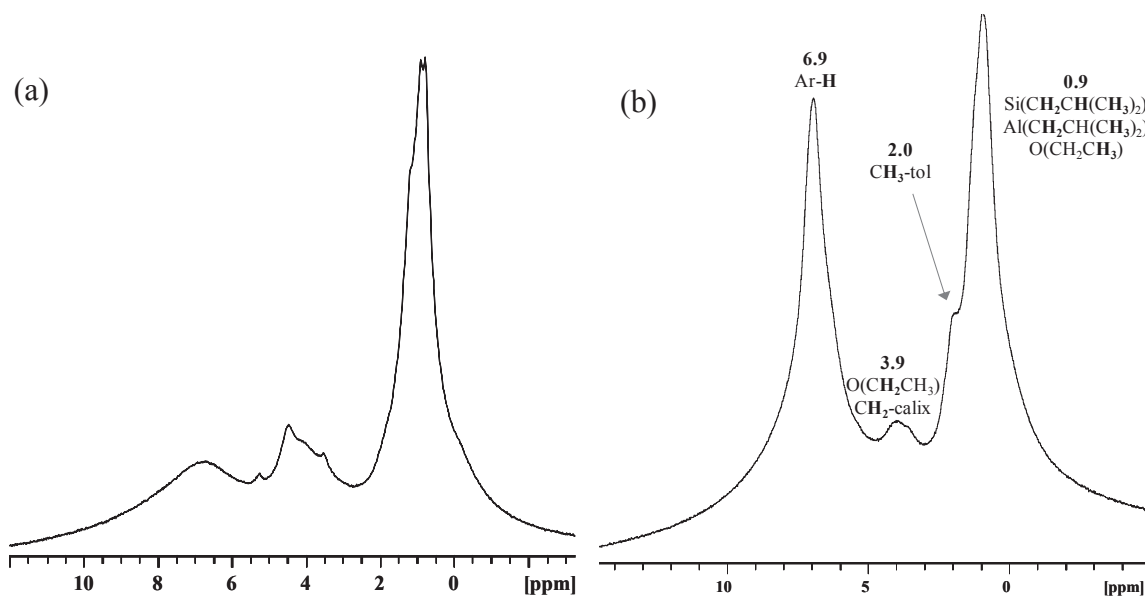


Figure 14:  $^1\text{H}$  MAS-NMR spectra of M2 (a) and M3 (b)

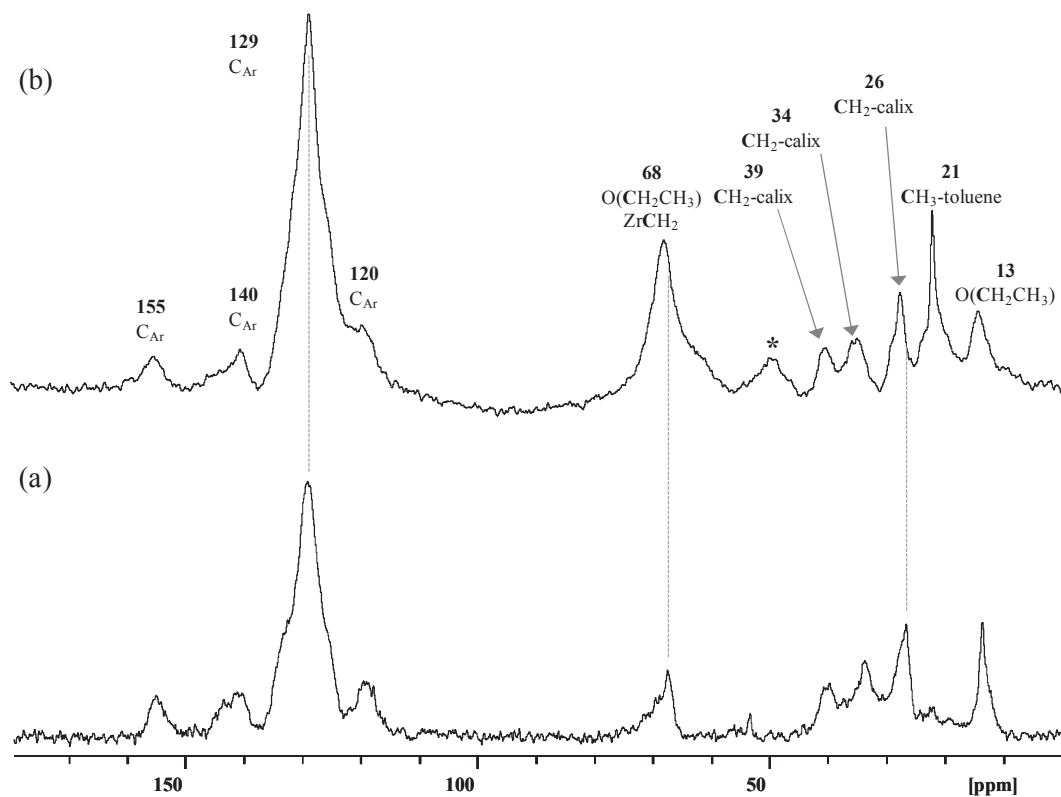
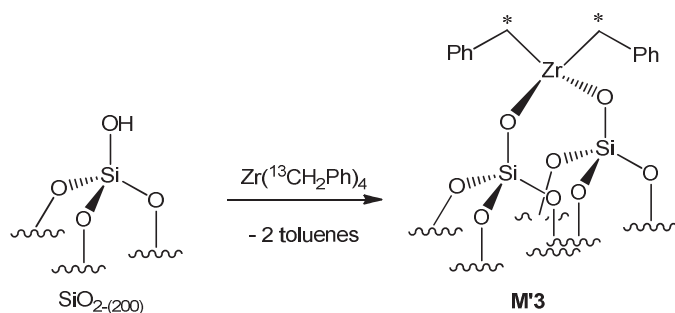


Figure 15:  $^{13}\text{C}$  CP/MAS-NMR of M2 (a) and M3 (b) (\* Spinning side band)

In comparison to the  $^{13}\text{C}$  CP/MAS spectrum of **M2** (Figure 15, (a)), that of **M3** (Figure 15, (b)) shows a significant peak at 129 ppm corresponding to the aromatic carbon from the calixarene and the benzyl groups. The signal at 68 ppm has considerably increased, which

could be attributed to the methylene of benzyl moieties also hiding the methylene carbons of diethylether. The signals at 32, 39 and 44 ppm have typical chemical shifts of the  $\text{CH}_2$  bridges of the calixarene ligand. The sharp signal at 21 ppm attributed to the methyl toluene confirms the decomposition of the surface species in the rotor. In order to reinforce the signal attribution of the  $^{13}\text{C}$  CP/MAS spectrum of **M3**, the analogue bis-siloxy bis-benzyl zirconium species  $[(\equiv\text{SiO})_2\text{Zr}(\text{CH}_2\text{Ph})_2]$  **M'3** was synthesized by reaction between  $\text{Zr}(\text{CH}_2\text{Ph})_4$  and  $\text{SiO}_{2-(200)}$ , and characterized by DRIFT, solid-state NMR (**Figure 16**) and mass balance analysis (see Annex V for the full preparation and characterization) (**Scheme 13**).



**Scheme 13:** Synthesis of  $[(\equiv\text{SiO})_2\text{Zr}(\text{CH}_2\text{Ph})_2]$  **M'3**. Reagents and conditions: 1.3 eq.  $\text{Zr}(\text{CH}_2\text{Ph})_4$ , pentane, 3 h, RT.

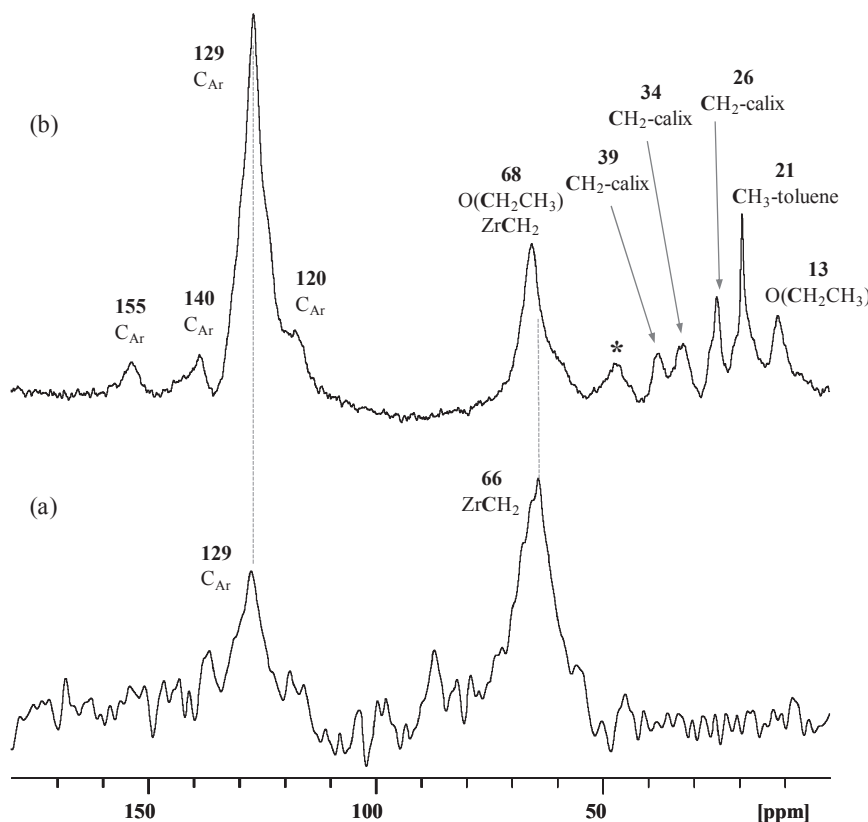


**Figure 16:**  $^{13}\text{C}$  CP/MAS-NMR of **M3'** (a) and **M3** (b) (\* Spinning side band)

Thus, the  $^{13}\text{C}$  CP/MAS spectrum of **M'3** (**Figure 16, (a)**) displays an intense signal at 129 ppm attributed to the aromatic carbons and one peak at 66 ppm for the methylene carbons of the benzyl groups, comparable to that observed for **M3** (**Figure 16, (b)**).

- **EXAFS**

The structure of the supported zirconium complex **M3** was further studied by the analysis of the Zr K-edge extended X-ray absorption fine structure (EXAFS) data (**Table 6** and **Figure 17**). The results are consistent with the following coordination sphere around Zr: more than one to two oxygen atoms at 1.95(1) Å, attributed to  $\sigma$ -bonded phenoxy type ligands and two to more than two carbon at 2.26(3) Å attributed to carbon of benzyl ligands, consistently with the bond distances found in the mixed aryl oxide  $\text{Zr}(\text{OAr}')(\text{OAr}'\text{-OMe})(\text{CH}_2\text{Ph})_2$ , where the Zr-O (1.899 - 1.940 Å), and Zr-C (2.234 - 2.280 Å) bond lengths are in the same range, as in [tris-(benzyl)(2,6-di-t-butylphenolato-O)Zr], for Zr-O (1.933 - 1.951 Å), and Zr-C (2.243 - 2.312 Å).<sup>12</sup>

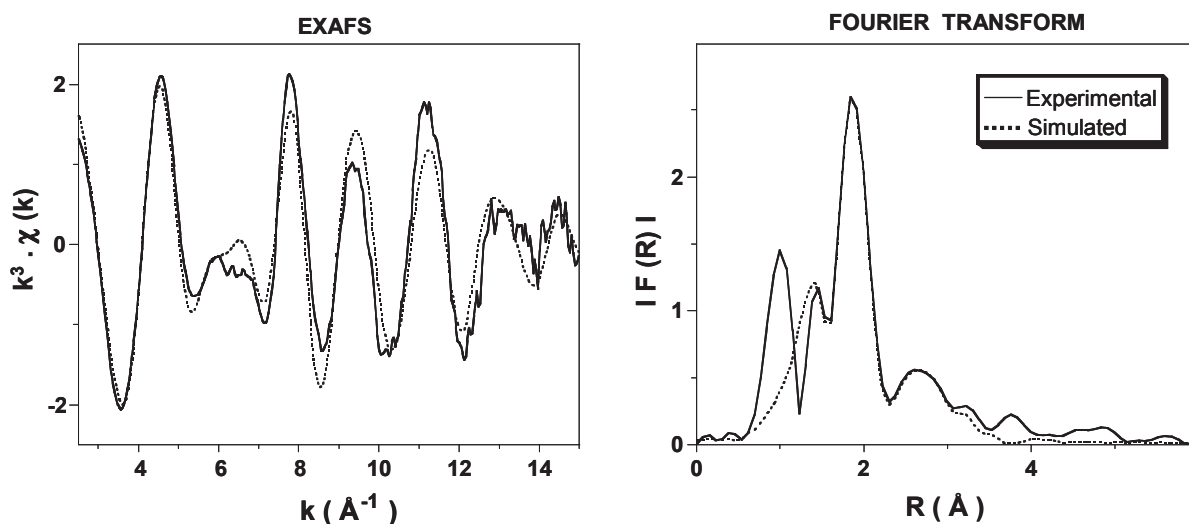


**Figure 17:** Zirconium K-edge  $k^3$ -weighted EXAFS (left) and corresponding Fourier transform (right) with comparison to simulated curves for the SBA<sub>700</sub> supported complex **M3**. Solid lines: experimental; dashed lines: spherical wave theory.

Furthermore, the fit was improved when considering further layers of backscatterers: (i) *ca.* one carbon at 2.66(5) Å, assigned to an *ipso* carbon of one of the benzyl ligand interacting with the Zr center, in agreement with the distance found by Latesky *et al.*, 2.591(17) Å in the  $\text{Zr}(\text{OAr}')(\text{CH}_2\text{Ph})_3$  complex cited above and by Gauvin *et al.*, 2.599(3) Å, for the complex [benzyl ( $\eta^2$ -benzylidene) bis(2,6-bis((1S,2S,5R)(-)menthoxo)pyridyl-N,O,O') zirconium];<sup>13</sup> (ii) one carbon at 3.03(4) Å, assigned to the *ipso* carbon of the other benzyl

ligand, also in agreement with the distance found by Gauvin *et al.* for the other *ipso* carbon at 3.054(4) Å, less or not interacting with Zr, in the complex mentioned above (2.85 - 3.25 Å for the Zr(OAr')(CH<sub>2</sub>Ph)<sub>3</sub> complex studied by Latesky *et al.*); (iii) *ca.* two other carbon atoms at 3.45(6) Å, which could be attributed to the aromatic carbons bonded to oxygen of a phenoxy part of the calixarene ligand (3.30 - 3.32 Å for the similar Zr-C<sub>Ar</sub> distances in the complexes with phenoxy ligands studied by Latesky *et al.* and mentioned above).

**Table 6: EXAFS parameters for the SBA supported complex M3.<sup>(a)</sup>** The errors generated by the EXAFS fitting program “RoundMidnight” are indicated between parentheses.

Type of Neighbor	Number of neighbors	Distance (Å)	$\sigma^2$ (Å <sup>2</sup> )
<b>Zr-Q-C<sub>Ar</sub></b>	1.3(6)	1.95(1)	0.0060(18)
<b>Zr-CH<sub>2</sub>C<sub>6</sub>H<sub>5</sub></b>	2.7(6)	2.26(1)	0.0048(12)
<b>Zr-CH<sub>2</sub>C<sub>ipso</sub></b>	1.4(7)	2.66(5)	0.009(3)
<b>Zr-CH<sub>2</sub>C<sub>ipso</sub></b>	1.2(6)	3.03(4)	0.007(5)
<b>Zr-O-C<sub>Ar</sub></b>	2.4(15)	3.45(6)	0.011(5)

<sup>(a)</sup>  $\Delta k$ : [2.5 - 15 Å<sup>-1</sup>] -  $\Delta R$ : [0.6-3.6 Å];  $S_0^2 = 1.0$ ;  $\Delta E_0 = 2.8 \pm 1.5$  eV (the same for all shells); Fit residue:  $\rho = 12$  %; Quality factor:  $(\Delta\chi)^2/v = 9$  ( $v = 10 / 25$ ).

In summary, the reaction of Zr(<sup>13</sup>CH<sub>2</sub>Ph)<sub>4</sub> with **M2** leads to the new zirconacalix[4]arene supported on SBA-15 LP-(700) [(≡SiO)<sub>2</sub>Al-[O-[4H]- (H)(O)<sub>2</sub>Zr(CH<sub>2</sub>Ph)<sub>2</sub>].(Et<sub>2</sub>O)]<sub>SBA-15</sub> LP-(700) **M3** as the major organometallic species. The reaction has been investigated using IR spectroscopy, elemental analysis, solid-state NMR spectroscopy and EXAFS. The data are fully consistent with the direct protolytic cleavage of the Zr-CH<sub>2</sub>Ph bond of Zr(<sup>13</sup>CH<sub>2</sub>Ph)<sub>4</sub> by the supported phenol groups. The preparation of grafted metallacalix[4]arenes proves to be successful and our investigation will be extended to the tantalum and tungsten metals.

#### 4.1.3 Incorporation of W(≡CtBu(CH<sub>2</sub>tBu)<sub>3</sub>) onto the material [(≡SiO)<sub>2</sub>Al-[O-[4H]- (OH)<sub>2</sub>(H)].(Et<sub>2</sub>O)]<sub>SBA-15</sub> LP-(700) (**M2**)

The aim of this paragraph is to synthesize tungsten-based surface complexes supported on the material calixarene **M2**. This surface species has been designed with a view to provide a catalytically active component in olefin metathesis, compared to its bis-siloxy counterpart

$[(\equiv \text{SiO})_2 \text{W}(\equiv \text{CtBu}(\text{CH}_2\text{tBu}))]$ .<sup>1</sup> Their screening will permit us to establish the effect over their catalytic performances in olefin metathesis of bis-aryloxy vs. a bis-siloxy linker to the metal.

The grafting of 1.3 eq. of  $\text{W}(\equiv \text{CtBu}(\text{CH}_2\text{tBu}))_3$  (based on the number of grafted calixarenes: 0.285 mmol.g<sup>-1</sup> M<sub>2</sub>) onto the material  $[(\equiv \text{SiO})_2 \text{Al}-[\text{O}-[\text{H}]-\text{O}(\text{H})_2-\text{H}].(\text{Et}_2\text{O})]_{\text{SBA-15 LP-(700)}} \textbf{M2}$  was realized by mechanical stirring at 65°C over 16h. The solid was then washed three times with freshly condensed pentane. After evacuation of the volatiles and drying under vacuum, the resulting light brown solid **M4** was characterized by DRIFT, solid-state NMR spectroscopy and mass balance analysis.

#### • Mass-balance analysis

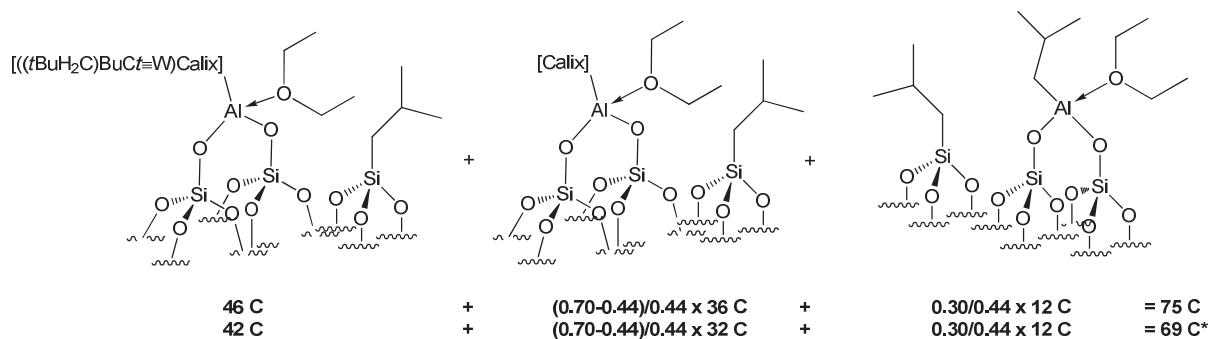
Elemental analysis reveals the presence of 1.04%wt in aluminum and 3.0%wt in tungsten, corresponding to 0.44 W/Al. The complex  $\text{W}(\equiv \text{CtBu}(\text{CH}_2\text{tBu}))_3$  was then grafted onto  $0.44/0.70 = 63\%$  of the supported calixarenes. Furthermore, the charge in carbon of **M4** is 12.2%wt thus proving the presence of 62 carbon atoms per tungsten.

**Table 7: Mass balance analysis for M4**

	%wt Al <sup>[a]</sup>	%wt W <sup>[a]</sup>	W/Al	%wt C <sup>[a]</sup>	C/W
Grafting	1.04	3.0	0.44	12.2	62 (th 64 <sup>[b]</sup> )

<sup>[a]</sup> Percentage determined by elemental analysis. <sup>[b]</sup> Considering partial release of diethyl ether

If 63% of the surface calixarene are considered to bear one  $\text{W}(\equiv \text{CtBu}(\text{CH}_2\text{tBu}))$  fragment, the correct expect count of carbons per tungsten atoms is 69 (considering the partial removal of diethyl ether during analysis) (**Scheme 14**).



**Scheme 14: Carbon atom count of M4 reported to one tungsten atom.** \* The second line is the corrected calculation by removing the two diethyl ether molecule from the two full oxydanted aluminum centers

However, the experimental ratio of 62 is far from this result and can only be explained by the absence of the neopentyl ligand. The release of one extra NpH molecule is probably due to a C<sub>Ar</sub>-H activation of one flexible aromatic unit from the calixarene, as already observed in the case of soluble tantalacalix[4]arene (Chapter IV). In order to confirm this hypothesis, **M4** was treated with an excess of dry HCl gas. Analysis of the gas phase gives 0.8 eq NpH/W proving the presence of only one neopentyl-like ligand on the metal center. Thus, by removing the neopentyl ligand, the theoretical count of carbon atoms per tungsten is 64.

- **Infra-red spectroscopy**

After reaction with W( $\equiv$ C*t*Bu(CH<sub>2</sub>*t*Bu)<sub>3</sub>), the DRIFT spectrum of **M4** displays an increase of the band from 2860 to 2950 cm<sup>-1</sup> assigned to the v<sub>(Csp<sup>3</sup>-H)</sub> vibrations of CH<sub>2</sub> and CH<sub>3</sub> of the neopentyl fragments (**Figure 18**). It is noteworthy a decrease of the OH-stretching band between 3200-3500 cm<sup>-1</sup> revealing the partial reaction of the tungsten complex with phenol functions, in accordance with the mass balance analysis.

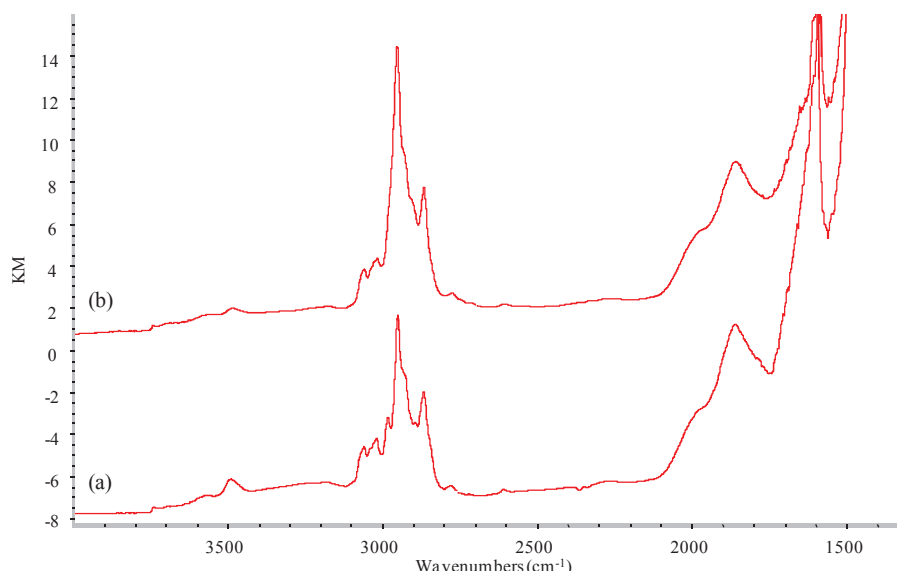


**Figure 18:** DRIFT spectra of M2 (a) and after reaction with W( $\equiv$ C*t*Bu(CH<sub>2</sub>*t*Bu)<sub>3</sub>), M4 (b)

- **Solid-state NMR spectroscopy**

In comparison to the <sup>1</sup>H MAS-NMR spectrum of **M2** (**Figure 19, (a)**), that of **M4** (**Figure 19, (b)**) shows a large peak centered around 0.9 ppm attributed to the protons of the CH<sub>3</sub> of W≡CC(CH<sub>3</sub>)<sub>3</sub> in addition to the recurrent signal for the aluminum and silicon fragments and the methyl protons of diethyl ether at 1.2 ppm. Both signals at 3.9 and 6.4 ppm

corresponding to the methylene of diethyl ether, the methylenic bridges of the calixarenic unit and the aromatic fragments, remain unchanged.

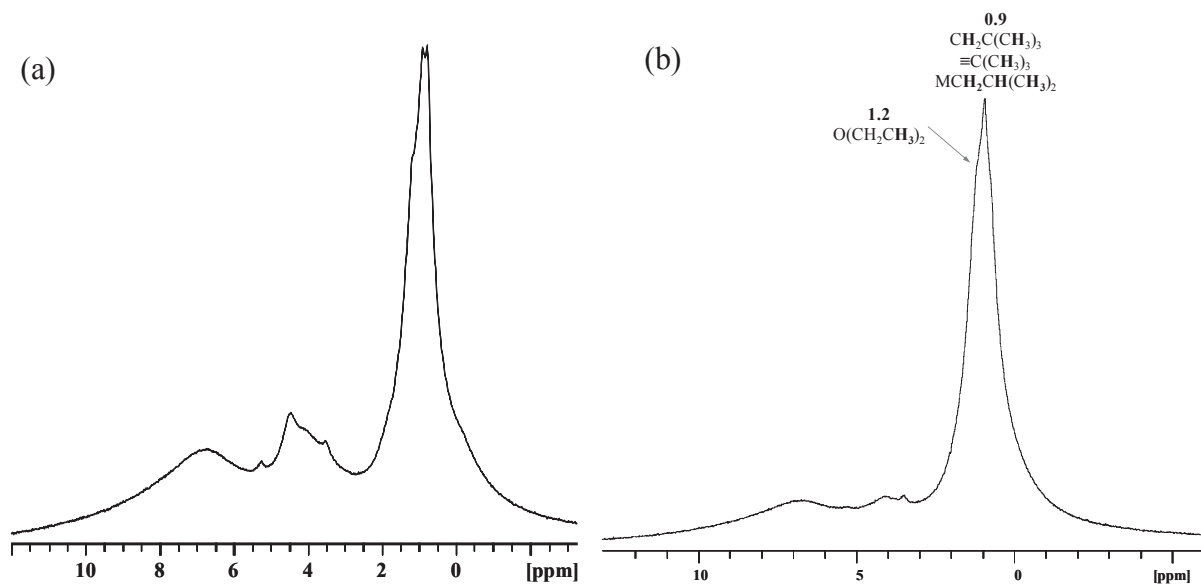


Figure 19: <sup>1</sup>H MAS-NMR of M2 (a) and M4 (b)

In addition to the signals observed from the <sup>13</sup>C CP/MAS-NMR spectrum of the starting material **M2** (Figure 20, (b)), that of **M4** (Figure 20, (a)) exhibits a new peak at 32 assigned to the CH<sub>3</sub> carbon of neopentylidyne W( $\equiv\text{C}(\text{CH}_3)_3$ ) moiety. The latter is thought to hide one signal from the methylenic bridge of the calixarene. The signal at 38 ppm is attributed to other methylenic bridge of the calixarene. No resonance at 95 ppm, characteristic of the methylene carbon<sup>1</sup> from WCH<sub>2</sub>C(CH<sub>3</sub>)<sub>3</sub>, was displayed, thus demonstrating the aromatic C<sub>Ar</sub>-H activation with concomitant elimination of neopentane. The signal attributed to the carbine W( $\equiv\text{C}(\text{CH}_3)_3$ ) is not observed, one reason being the poor signal-to-noise ratio, which is due to the low loading of W (3.0%wt) on the material **M4**. In order to increase the signal-to-noise ratio and demonstrate the aromatic C<sub>Ar</sub>-H activation, and also see the presence of the carbene fragment, <sup>13</sup>C labeling of the  $\alpha$ -carbon of the starting complex W( $\equiv\text{CtBu}(\text{CH}_2\text{tBu})_3$ ) should be prepared.

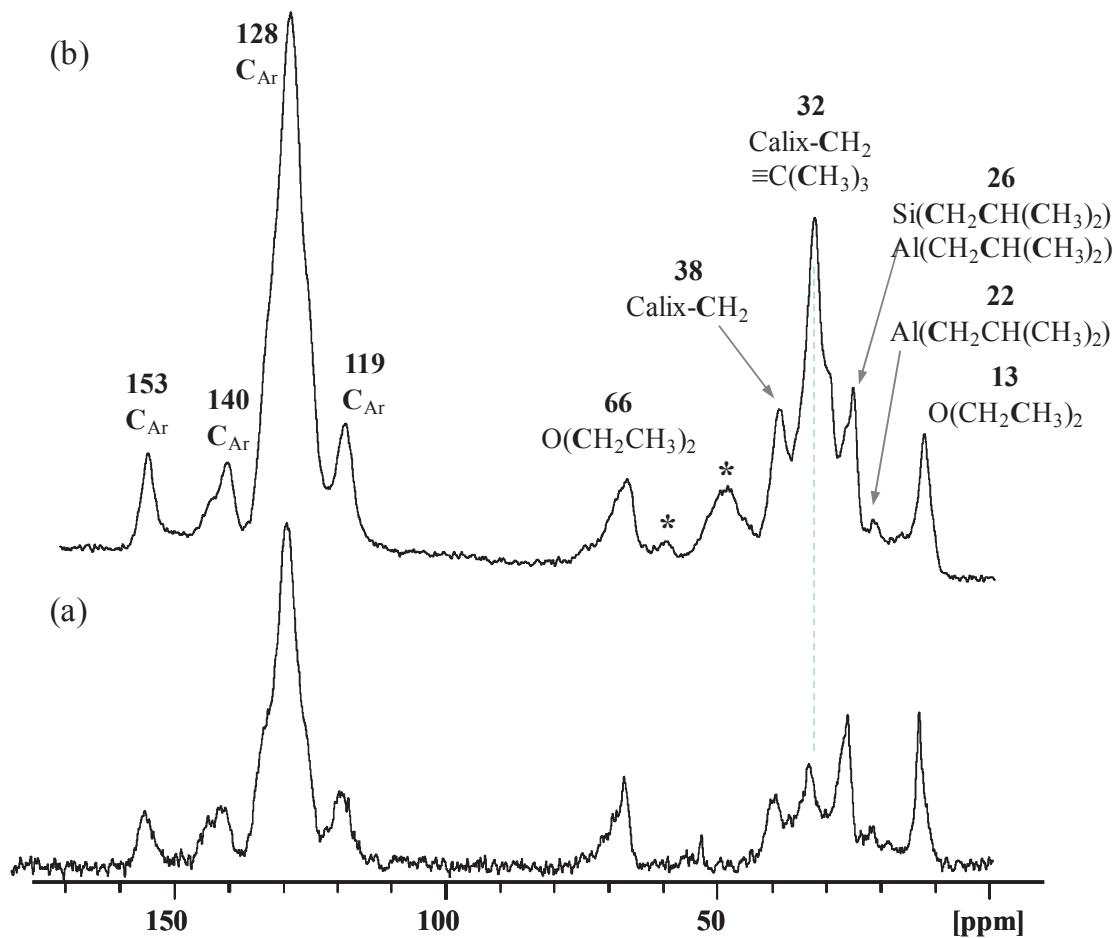
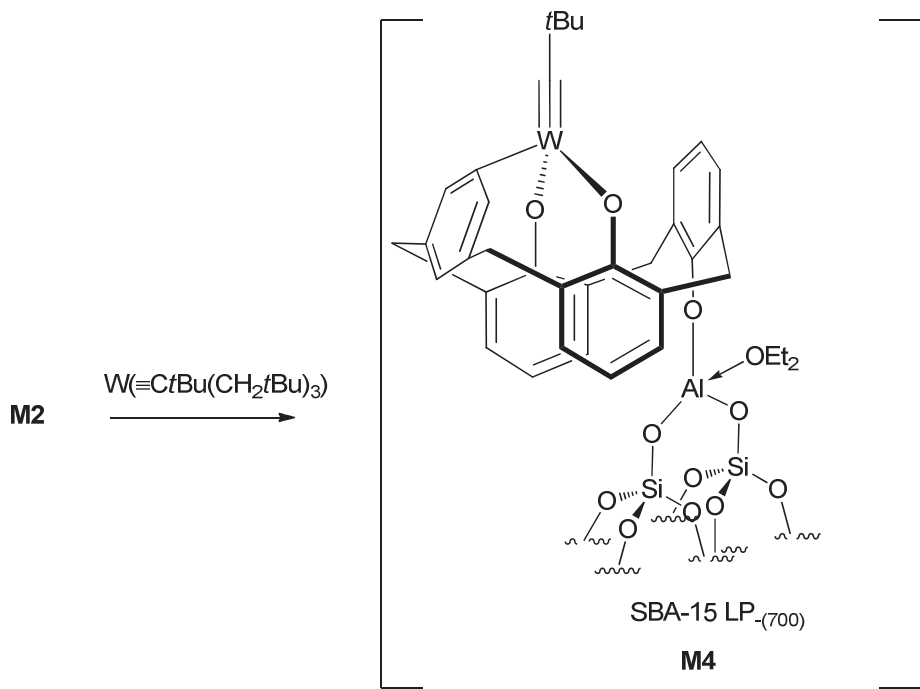


Figure 20:  $^{13}\text{C}$  CP/MAS-NMR of M2 (a) and M4 (b) (\* Spinning side band)

To conclude, the reaction of  $\text{W}(\equiv\text{CtBu}(\text{CH}_2\text{tBu})_3)$  with **M2** leads to the supposed tungstenacalix[4]arene supported on SBA-15 LP<sub>(700)</sub>  $[(\equiv\text{SiO})_2\text{Al}-[\text{O}-[\text{H}]-\text{(H})(\text{O})_2\text{W}(\equiv\text{CtBu})].(\text{Et}_2\text{O})]$ <sub>SBA-15 LP-(700)</sub> **M4** (Figure 15). The reaction has been investigated using IR spectroscopy, elemental analysis, solid-state NMR spectroscopy and stoichiometric reactivity with HCl. The data are consistent with the direct protolytic cleavage of the W-CH<sub>2</sub>tBu bond of the starting complex by the supported phenol groups. However, the absence of the signal of the methylene fragment WCH<sub>2</sub>tBu in NMR spectra and the release of 1 eq. of NpH during hydrolysis of **M4** are consistent to C<sub>Ar</sub>-H activation of an aromatic moiety. The further use of  $^{13}\text{C}$  labeled starting complex should help us to fully characterize the supported tungstenacalix[4]arene species. Additionally, the  $^{13}\text{C}$  labeling of the calixarenic methylene bridges should also provide more concise spectroscopic data for the structure determination of **M4**.



Scheme 15: Example of structure proposed for the material  $[(\equiv\text{SiO})_2\text{Al}-\text{O}-\text{[4H]}-\text{(H)(O)}_2\text{W}\equiv\text{CtBu}].(\text{Et}_2\text{O})]_{\text{SBA-15 LP-(700)}}$   
**M4**

#### 4.2 Preparation of tripodal metallacalix[4]arenes supported on mesoporous SBA-15 LP<sub>(700)</sub> by grafting of [[4H]-OH<sub>4</sub>] onto [(≡SiO)<sub>2</sub>Al<sub>i</sub>Bu.(Et<sub>2</sub>O)]<sub>SBA-15 LP-(700)</sub> (**M1**)

[[4H]-OH<sub>4</sub>] **L13** was prepared using the described derterbutylation method.<sup>8</sup> Pure [[4H]-OH<sub>4</sub>] is obtained in 83% yield as a white powder, which was dried over 12h at 110°C before used for the grafting. Using the double Schlenk technique, 1.3 eq. of [[4H]-OH<sub>4</sub>] in DCM (10 ml) were reacted with [(≡SiO)<sub>2</sub>Al<sub>i</sub>Bu.(Et<sub>2</sub>O)]<sub>SBA-15 LP-(700)</sub> **M1** over 16h at room temperature. After repeated washings with DCM (10 ml), followed by evacuation of the volatile, **M5** was afforded as a white powder and characterized by DRIFT, solid-state NMR spectroscopy and mass balance analysis.

- **Infra-red spectroscopy**

After reaction with [[4H]-OH<sub>4</sub>] **L13**, the DRIFT spectrum of **M5** displays new bands at 1473-1600 and 3000-3100 cm<sup>-1</sup> assigned to the aromatic  $\nu_{(\text{Csp}_2=\text{Csp}_2)}$  and  $\nu_{\text{Csp}_2-\text{H}}$  vibrations, respectively (Figure 21). The  $\nu_{\text{Csp}_3-\text{H}}$  bands from 2800 to 3000 cm<sup>-1</sup> and the  $\delta_{\text{Csp}_3-\text{H}}$  bands from 1320 to 1466 cm<sup>-1</sup> is attributed to the transferred isobutyl groups onto silicon atoms and some unreacted isobutyl aluminum etherate, also encapsulating the methylene bridges of the calixarene. The weak intensity of the bands characteristic of  $\nu_{(\text{Csp}_2=\text{Csp}_2)}$  and  $\nu_{\text{Csp}_2-\text{H}}$ , compared

to the DRIFT spectrum of supported  $[[4\text{H}]\text{-}(\text{H})(\text{OH})_3]$  **M2**, shows the low reactivity of **L13** with  $[(\equiv\text{SiO})_2\text{AliBu.}(\text{Et}_2\text{O})]_{\text{SBA-15 LP-(700)}} \text{M1}$ .

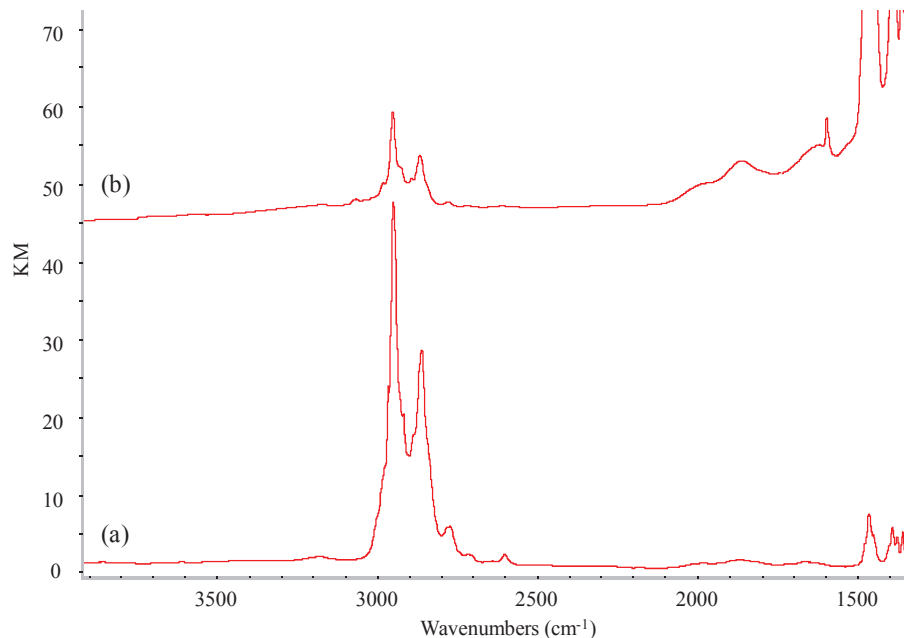


**Figure 21:** DRIFT spectra of **M2** (a) and after reaction with  $[[4\text{H}]\text{-}(\text{OH})_4]$ , **M5** (b)

- **Solid-state NMR spectroscopy**

$^1\text{H}$  MAS-NMR (800MHz) of **M5** displays a sufficient resolution to distinguish the unreacted isobutyl aluminum fragments for which the methylene protons clearly appear at -0.14 ppm (**Figure 22**). The signals at 0.9 and 1.8 ppm correspond respectively to the methyl and methine protons of both silicon and aluminum isobutyl ligands. The weak signal in the aromatic region at 6.8 ppm confirms the low reactivity of **L13** with the material **M2**. These results are supported by the mass balance analysis showing that only 10% of aluminum isobutyl fragments have reacted with the calixarenic ligand.

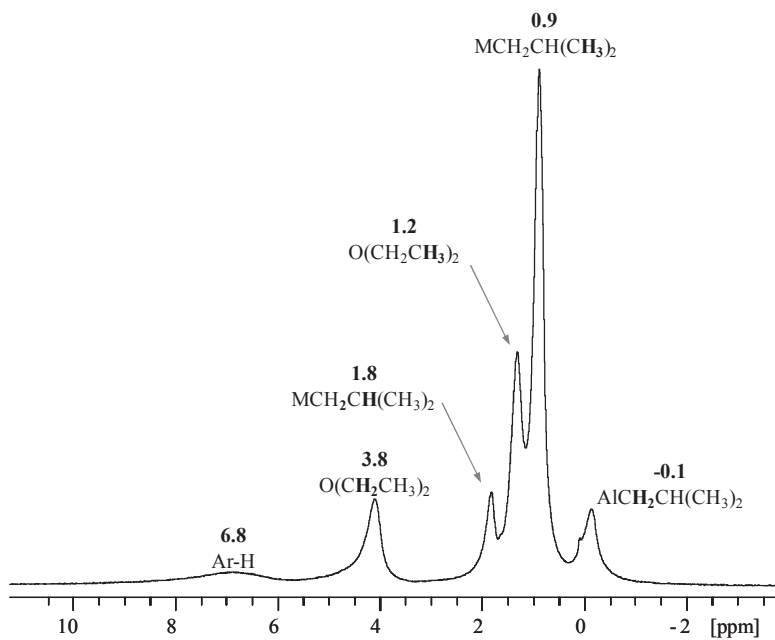


**Figure 22:** <sup>1</sup>H MAS-NMR of M5 (800 MHz)

The <sup>13</sup>C CP/MAS spectrum of **M5** shows clearly the signals of the unreacted CH<sub>2</sub> isobutyl aluminum at 22 ppm also containing the CH isobutyl silicon carbons (**Figure 23, (c)**). The large, sharp peak at 26 ppm corresponds to the methyl and methylene carbons of the isobutyl silicon fragments and the methine and methyl carbons of the isobutyl aluminum fragments. In contrast to the material **M2** (**Figure 23, (b)**), for which two signals were observed for the methylene bridges, the spectrum of **M5** exhibits only one weak peak at 32 ppm. The aromatic carbons are displayed between 120 and 160 ppm with a relative lower intensity compared to the <sup>13</sup>C CP/MAS of **M2**. From this observation, it could be postulated than the anchored calixarene could present a cone conformation, probably maintained by the strong circular hydrogen bonding between the three phenol functions and the anchored phenoxy one. This strong interaction, rendering the phenol less prone to reactivity toward the isobutyl aluminum moieties, can also explained the low concentration of calixarenes on the surface, in contrast to the ligand [[4H]-OH]<sub>3</sub>(H) **L12**, for which the reactivity is quite higher. Finally, studies concerning the solvent effect and the temperature of reaction, in order to improve the reactivity of [[4H]-OH]<sub>4</sub> **L13** with [(≡SiO)<sub>2</sub>AlBu.(Et<sub>2</sub>O)]<sub>SBA-15 LP-(700)</sub> **M1**, will constitute further work, not initiated during this thesis. Thus, the incorporation of organometallic complexes has not been investigated.

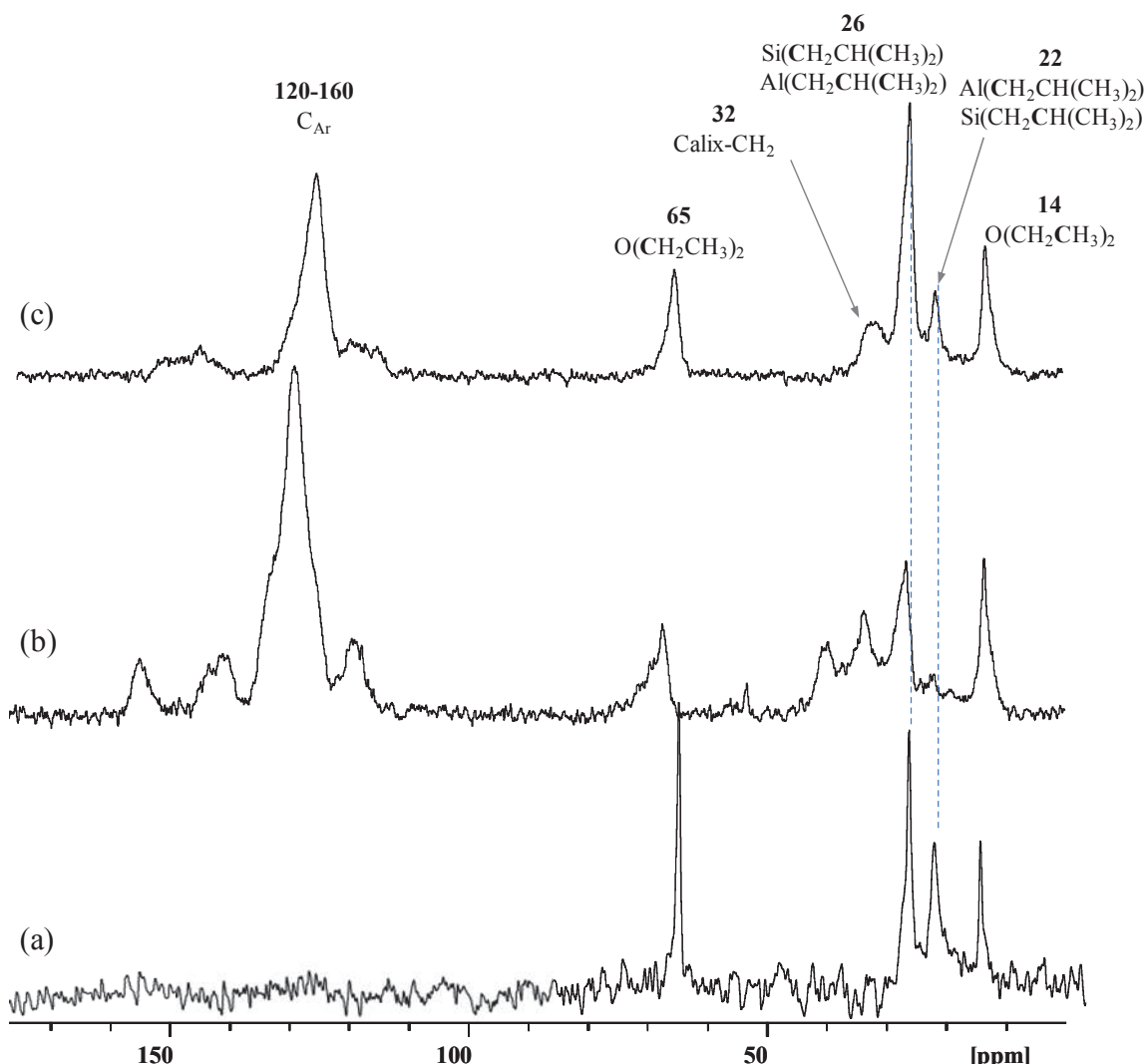


Figure 23:  $^{13}\text{C}$  CP/MAS-NMR of M1 (a), M2 (b), M5 (c)

## 5. Catalytic performance of $[(\equiv\text{SiO})_2\text{Al}-[\text{O}-[4\text{H}]-\text{(H})(\text{O})_2\text{W}\equiv\text{CtBu}(\text{CH}_2\text{tBu})].(\text{Et}_2\text{O})]_{\text{SBA-15 LP-(700)}}$ (M4) in propylene metathesis

In the same fashion as already performed with tungsten based catalysts directly bonded to silica,  $[(\equiv\text{SiO})\text{W}(\equiv\text{CtBu}(\text{CH}_2\text{tBu})_2]$  **H5**, and through the hydroquinone spacer,  $[(\equiv\text{SiO})_2\text{AlO-C}_6\text{H}_4-\text{OW}(\equiv\text{CtBu}(\text{CH}_2\text{tBu})_2.\text{(Et}_2\text{O})]$  **H6** (see Chapter II), the new supported tungsten calix[4]arene  $[(\equiv\text{SiO})_2\text{Al}-[\text{O}-[4\text{H}]-\text{(H})(\text{O})_2\text{W}\equiv\text{CtBu}(\text{CH}_2\text{tBu})].(\text{Et}_2\text{O})]_{\text{SBA-15 LP-(700)}}$  **M4** will be engaged in catalytic studies and compared to its analogue bis-siloxy species  $[(\equiv\text{SiO})_2\text{W}(\equiv\text{CtBu}(\text{CH}_2\text{tBu})]$ , noted **M7**, directly anchored on silica. In similar to its counterparts **H5** and **H6**, **M4** is potentially active in olefin metathesis but for which the

tungsten center is linked to two phenol functions. In order to compare their catalytic activity, stability and selectivity, the catalytic tests will also be based on the propylene metathesis. Any details concerning the practical terms in catalysis and the continuous flow reactor are related in Chapter II and Annex II.

The charge of catalyst of **M4** was calculated based on its tungsten content (**Table 8**). The propylene flow rate was maintained constant ( $25 \text{ ml} \cdot \text{min}^{-1}$ ,  $61 \text{ mol}_{\text{C}_3\text{H}_6} \cdot \text{mol}_W^{-1} \cdot \text{min}^{-1}$ ) at  $60^\circ\text{C}$  over 50h. A gas chromatograph analyzes the products generated at the outlet of the reactor.

**Table 8: Reaction conditions for the propylene metathesis catalyzed by M4 and M7**

	W %wt	Propylene flow rate (ml·min <sup>-1</sup> )	R <sup>[a]</sup> (mol <sub>C3=</sub> ·mol <sub>W</sub> <sup>-1</sup> ·min <sup>-1</sup> )	Temperature (°C)
Catalyst <b>M4</b>	3.0	25	61	60
Catalyst <b>M7</b>	6.4	25	61	60

[a] number of moles of propene which passes per tungsten atom per minute

The following graphs compare the conversions and the T.O.N of both catalysts **M4** and **M7** (**Figure 24**).

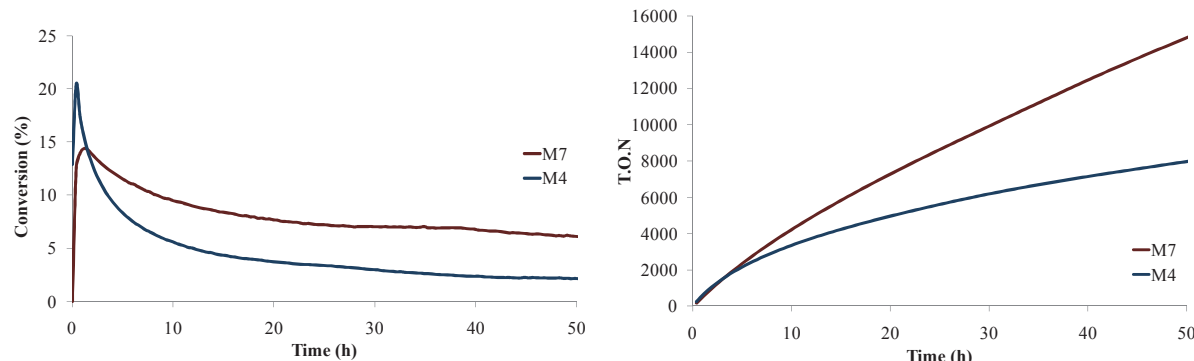


**Figure 24: Comparison of the conversions (a) and the TON (b) of both catalysts M4 and M7**

The reaction catalyzed by **M4** presents an initial step maximal conversion rate of  $22 \text{ mol}_{\text{C}_3=} \cdot \text{mol}_W^{-1} \cdot \text{min}^{-1}$  reaching  $2.7 \text{ mol}_{\text{C}_3=} \cdot \text{mol}_W^{-1} \cdot \text{min}^{-1}$  at 50 h with an overall TON of 7900 after 50h (**Figure 24**). The conversion profile of the reaction shows a fast deactivation during the 10 first hours of catalysis. In the case of the bis-siloxy catalyst  $[(\equiv\text{SiO})_2\text{W}(\equiv\text{C}t\text{Bu}(\text{CH}_2t\text{Bu})] \text{ M7}$ , the initial maximal conversion rate in propylene metathesis of  $11 \text{ mol}_{\text{C}_3=} \cdot \text{mol}_W^{-1} \cdot \text{min}^{-1}$  is twice weaker than that observed for **M4**, reaching  $5 \text{ mol}_{\text{C}_3=} \cdot \text{mol}_W^{-1} \cdot \text{min}^{-1}$  after 50h, with a cumulated TON of 14600.

The initial ratio *trans/cis* but-2-enes is 2.1 (therm. eq. = 2.3)<sup>14</sup> for the catalyst **M4** (**Figures 24-25**), which unexpectedly decreases on the time of stream to finally reach 0.9 at 50h. This inversion of selectivity to *cis*-but-2-ene can be explained by the presence of the supposed activated aromatic unit in the sphere coordination of the metal, compared to **M7** for which the ratio *trans/cis* but-2-enes is relatively constant around 1.5 (**Figures 24-25**). The fast deactivation and the inversion of selectivity *trans/cis* of the catalyst **M4** can be related to the change of the coordination sphere of the metal by the presence of aromatic units, rendering it more sterically hindered. It must be mentioned that the systems **M4** and **M7** are precursors for olefin metathesis, for which the carbene ligand is probably generated *in situ*, either by  $\alpha$ -H transfer from an alkyl ligand to generate a bis-alkylidene in the case **M7** (see Chapter II, Scheme 22, Route B), or by direct metathesis of the olefin with the alkylidyne, which generates in turn a propagating ligand in the case of **M4** (see Chapter II, Scheme 22, Route B).<sup>1</sup>

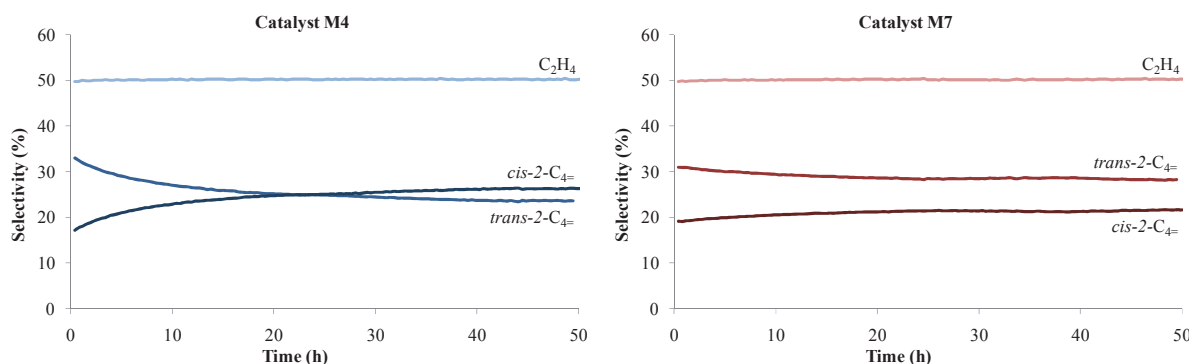


**Figure 25:** Selectivity in *trans*-but-2-ene (*trans*-2-C<sub>4</sub>=) and *cis*-but-2-ene (*cis*-2-C<sub>4</sub>=) for both catalysts **M4** and **M7**

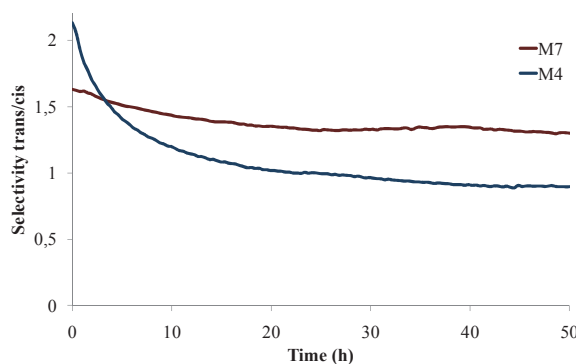


**Figure 26:** Selectivity in *trans*-2-C<sub>4</sub>=: *trans*-but-2-ene; *cis*-2-C<sub>4</sub>=: *cis*-but-2-ene for both catalysts **M4** and **M7**

In summary, the insertion of a calixarene spacer between the surface of silica (SBA-15-LP<sub>(700)</sub>) and the tungsten center increases the initial activity of [(≡SiO)<sub>2</sub>Al-[O-[4H]-

$(H)(O)_2W \equiv CtBu(CH_2tBu) \cdot (Et_2O)]_{SBA-15\ LP-(700)}$  **M4** in propene metathesis, compared to its bis-siloxy counterpart [ $\equiv SiO)_2W \equiv CtBu(CH_2tBu)$ ] **M7**. However, the presence of an aryl unit close to the metal center could result in the deactivation of the catalyst **M4**, probably due to a  $C_{Ar}-H$  activation, already observed in the case of soluble tantalacalix[4]arene (see chapter IV).

## 6. Conclusion

This last chapter was focused on the generation of grafted metallacalixarenes onto the mesoporous support SBA-15 LP partially dehydroxylated at 700°C. In accordance to the novel concept established in Chapter II, the calix[4]arene  $[[4H]-H(OH)_3]$  **L12**, presenting three phenol functions, was tethered on SBA-15 LP<sub>-(700)</sub>, previously treated with  $Al_iBu_3 \cdot Et_2O$ . For the new calixarene/SBA materials  $[(\equiv SiO)_2Al-[O-[4H]-H(OH)_2] \cdot (Et_2O)]_{SBA-15\ LP-(700)}$  **M2**, the conformations of the calixarene ligand remain undetermined, due to spectroscopic resolution limits. Further analytical solid-state NMR experiments of material **M2** presenting methylenic bridges and phenolic protons of the calixarene ligand isotopically enriched in  $^{13}C$  and  $^2H$ , respectively, could help to elucidate its structure (proximal or distal).

Nevertheless, the supported calixarene **M2** was reacted with  $Zr(^{13}CH_2Ph)_4$  and  $W(\equiv CtBu(CH_2tBu)_3)$  to provide totally new supported metallacalix[4]arenes. Thus, the bipodal zircon- and tungstenacalix[4]arenes  $[(\equiv SiO)_2Al-[O-[4H]-H(O)_2Zr(CH_2Ph)_2] \cdot (Et_2O)]_{SBA-15\ LP-(700)}$  **M3** and  $[(\equiv SiO)_2Al-[O-[4H]-H(O)_2W \equiv CtBu(CH_2tBu)] \cdot (Et_2O)]_{SBA-15\ LP-(700)}$  **M4** materials were obtained and characterized by IR, solid-state NMR spectroscopy, mass balance analysis and EXAFS (in the case of Zr), supported by analytical data of their analogues directly grafted onto silica. In propylene metathesis, the tungstenacalix[4]arene derivative presents an initial activity higher than its bis-siloxy counterpart  $[(\equiv SiO)_2W \equiv CtBu(CH_2tBu)]$  **M7** but deactivates rapidly by the probable presence of aromatic units bonded to the metal center by  $C_{Ar}-H$  activation.

## Experimental section

All experiments were carried out under a dry argon atmosphere using standard Schlenk techniques. More specifically, the double Schlenk technique is described in Annex I. All solvents were dried by standard methods and freshly distilled before use. Gas-phase analyses were performed on a Hewlett-Packard 5890 series II gas chromatograph equipped with a flame ionization detector and a  $\text{Al}_2\text{O}_3/\text{KCl}$  on fused silica column (50 m x 0.32 mm). Elemental analyses were performed at the Central Analysis Service of Solaize (France) for hydrogen and carbon elements and at the Mikroanalytisches Labor Pascher of Remagen (Germany) for metals. DRIFT spectra were recorded on a Nicolet 6700 FT-IR by using DRIFT airtight cells. Solution NMR spectra were recorded on DRX400 and DRX300 Bruker instruments.  $^1\text{H}$  MAS and  $^{13}\text{C}$  CP-MAS solid-state NMR spectra were recorded on Bruker Avance-500 and 800 spectrometers with a conventional double-resonance 4 mm CP-MAS probe at the Laboratoire de Chimie in Ecole Normale Supérieure de Lyon, at the Laboratoire de Chimie Organométallique de Surface in Ecole Supérieure de Chimie Physique Electronique de Lyon or at the Unité de Catalyse et de Chimie du solide (Lille). The samples were introduced under Ar in a zirconia rotor, which was then tightly closed. In all experiments, the rotation frequency was set to 10 kHz unless otherwise specified. Chemical shifts were given with respect to TMS as external reference for  $^1\text{H}$  and  $^{13}\text{C}$ -NMR. Conventional TEM micrographs were obtained at the Centre Technologique des Microstructures (Lyon) using a Philips 120 CX electron microscope operating at 120 kV. X-Ray diffraction on powder were run at the Centre de diffractométrie Henri Longchambon (Lyon) using a Bruker D8 Advance diffractometer. The preparation of  $\text{Ta}(\text{CH}_2\text{Ph})_5$  was performed according to the reported procedure<sup>15</sup>, involving  $\text{PhCH}_2\text{MgCl}$  and  $\text{TaCl}_5$ , but started with a 80:20 mixture of non-labeled and 100% labeled  $\text{Ph}^{13}\text{CH}_2\text{Cl}$  in the preparation of  $(\text{Ph}^{13}\text{CH}_2)\text{MgCl}$  (20%) (see experimental part Chapter II). The synthesis of mesoporous materials have been realized in collaboration with Dr. Erwan Leroux, University of Bergen (Norway). The catalytic studies were performed in a continuous flow reactor (see experimental part Chapter II).

## EXAFS studies

X-ray absorption spectra were acquired at ESRF (Grenoble, France), using beam-line BM01, at room temperature at the zirconium K edge, with a double crystal Si(111) monochromator detuned 70% to reduce the higher harmonics of the beam. The spectra were recorded in the transmission mode between 17.75 and 19.50 keV. The supported Zr sample was packaged within a nitrogen filled dry box in a double air-tight sample holder equipped with kapton windows. This type of cell has already been used and proved to be very efficient for air-sensitive compounds such as  $\equiv\text{SiO-HfNp}_3$  species supported onto aerosil silica<sub>(800)</sub> were the Hf-C contribution could be clearly distinguished from Hf-O by EXAFS.<sup>16</sup> The spectra analyzed were the results of four such acquisitions and no evolution could be observed between the first and last acquisition. The data analyses were performed by standard procedures using in particular the program “Athena”.<sup>17</sup> and the EXAFS fitting program “RoundMidnight” from the “MAX” package.

The program FEFF8 was used to calculate theoretical files for phases and amplitudes based on model clusters of atoms.<sup>18</sup> The value of the scale factor,  $S_0^2 = 1.0$ , was determined from the spectrum of the reference compound, a benzene solution of the molecular complex Zr(CH<sub>2</sub>-*t*Bu)<sub>4</sub> (four C at 2.226(7) Å, and four C at 3.50(5) Å). The refinements were performed by fitting the structural parameters N<sub>i</sub>, R<sub>i</sub>, σ<sub>i</sub> and the energy shift, ΔE<sub>0</sub> (the same for all shells). The fit residue, ρ (%), was calculated by the following formula:

$$\rho = \frac{\sum_k [k^3 \chi_{\text{exp}}(k) - k^3 \chi_{\text{cal}}(k)]^2}{\sum_k [k^3 \chi_{\text{exp}}(k)]^2} * 100$$

As recommended by the Standards and Criteria Committee of the International XAFS Society (Reports of the Standards and Criteria Committee of the International XAFS Society 2000: [http://ixs.iit.edu/subcommittee\\_reports/sc/](http://ixs.iit.edu/subcommittee_reports/sc/)), the quality factor,  $(\Delta\chi)^2/v$ , where v is the number of degrees of freedom in the signal, was also calculated and considered.

**Synthesis of SBA-15 large pores:** Pluronic P123 (2.400 g) was dissolved in a HCl solution (84 ml, 1.20 M), followed by the addition of NH<sub>4</sub>F (0.027 g). The mixture was then stirred at

15°C over 24 h. Hexane and TEOS were premixed and then introduced into the solution under mechanical stirring (300-360 rpm) (final P123/HCl/NH<sub>4</sub>F/H<sub>2</sub>O/TEOS/hexane molar ratios: 1/261/1.8/11278/110). The above mixture was stirred at 15°C for 20 h, and then transferred into an autoclave for further reaction at 110°C for 48 h. The products were collected by filtration, washed with distilled water, dried in air, and calcinated at 540°C for 5 h to remove the templates.

**Synthesis of pentabenzyltantalum  $\alpha$ -<sup>13</sup>C labeled at 20%:** At -33°C, benzylmagnesium chloride  $\alpha$ -<sup>13</sup>C labeled at 20% (30.7 ml, 33.500 mmol, 1.09M in Et<sub>2</sub>O) was added dropwise to a suspension of TaCl<sub>5</sub> (3.000 g, 8.375 mmol) in 15 ml of Et<sub>2</sub>O. After 2h of stirring at RT, 4.5 ml of 1,4-dioxane was added and the resulting mixture was stirred at RT over 1h. The salts were filtrate off and the resulting brown limpid solution was reduced and crystallized at -30°C over 2 days. Ta(<sup>13</sup>CH<sub>2</sub>Ph)<sub>5</sub> was collected as brown-orange crystals (3.199 g, 60%). NMR <sup>1</sup>H (C<sub>6</sub>D<sub>6</sub>, 300MHz, 298K):  $\delta$  2.62 (d (20%) + s (80%), 10H, CH<sub>2</sub>, <sup>1</sup>J(H,C) = 123 Hz), 6.72-7.13 (m, 25H, Ar-H).

**Synthesis of trihydroxycalix[4]arene [[4H]-OH<sub>3</sub>(H)]:** [[4+]-OH<sub>3</sub>(H)] (1.382 g, 2.184 mmol) and phenol (0.288 g, 3.058 mmol) were dissolved in dry toluene (20 mL). AlCl<sub>3</sub> (1.630 g, 12.230 mmol) was added to the toluene solution and the mixture was stirred over 2.5 h at room temperature. The resulting orange mixture was quenched with ice and evaporated. The residue was dissolved in DCM and successively washed with water until neutrality, brine and dried over MgSO<sub>4</sub>. After evaporation of the solvent, the residue was washed with cold MeOH to provide a white powder (0.650 g, 73%); NMR <sup>1</sup>H (CDCl<sub>3</sub>, 300MHz, 298K):  $\delta$  3.85 (s, 4H, CH<sub>2</sub>), 3.89 (s, 4H, CH<sub>2</sub>), 6.73-7.20 (m, 15H, Ar-H + OH), 8.05 (bs, 1H, OH). NMR <sup>13</sup>C (CDCl<sub>3</sub>, 75MHz, 298K):  $\delta$  31.8 (-CH<sub>2</sub>), 37.8 (-CH<sub>2</sub>), 121.5 (C<sub>Ar</sub>), 122.0 (C<sub>Ar</sub>), 127.17 (C<sub>Ar</sub>), 127.5 (C<sub>Ar</sub>), 127.8 (C<sub>Ar</sub>), 128.0 (C<sub>Ar</sub>), 128.4 (C<sub>Ar</sub>), 128.9 (C<sub>Ar</sub>), 129.0 (C<sub>Ar</sub>), 129.1 (C<sub>Ar</sub>), 129.3 (C<sub>Ar</sub>), 141.0 (C<sub>Ar</sub>), 149.4 (C<sub>Ar</sub>), 150.9 (C<sub>Ar</sub>). ). LRMS (CI): [M+H]<sup>+</sup> = 409.0. HRMS (ES<sup>+</sup>): Calcd. for C<sub>28</sub>H<sub>25</sub>O<sub>3</sub> 409.1804 found 409.1806.

## Notes and references

- (1) Le Roux, E.; Taoufik, M.; Chabanas, M.; Alcor, D.; Baudouin, A.; Copéret, C.; Thivolle-Cazat, J.; Basset, J.-M.; Lesage, A.; Hediger, S.; Emsley, L. *Organometallics* **2005**, *24*, 4274.
- (2) Barrett, E. P.; Joyner, L. G.; Halenda, P. P. *J. Am. Chem. Soc.* **1951**, *73*, 373.
- (3) (a) Beck, J. S.; Vartuli, J. C.; Roth, W. J.; Leonowicz, M. E.; Kresge, C. T.; Schmitt, K. D.; Chu, C. T. W.; Olson, D. H.; Sheppard, E. W. *J. Am. Chem. Soc.* **1992**, *114*, 10834(b) Beck, J. S.; Chu, C. T. W.; Johnson, I. D.; Kresge, C. T.; Leonowicz, M. E.; Roth, W. J.; Vartuli, J. C.; Corp, M. O., Ed. US, 1991; Vol. WO9111390.
- (4) (a) Beck, J. S.; Vartuli, J. C. *Current Opinion in Solid State and Materials Science* **1996**, *1*, 76(b) Morey, M. S.; Davidson, A.; Stucky, G. D. *J. Porous Mater.* **1998**, *5*, 195(c) Lindén, M.; Schacht, S.; Schüth, F.; Steel, A.; Unger, K. K. *J. Porous Mater.* **1998**, *5*, 177(d) Ying, J. Y.; Mehnert, C. P.; Wong, M. S. *Angew. Chem., Int. Ed.* **1999**, *38*, 56(e) Ciesla, U.; Schüth, F. *Microporous Mesoporous Mater.* **1999**, *27*, 131(f) Sayari, A.; Hamoudi, S. *Chem. Mater.* **2001**, *13*, 3151.
- (5) Kresge, C. T.; Leonowicz, M. E.; Roth, W. J.; Vartuli, J. C.; Beck, J. S. *Nature (London, U. K.)* **1992**, *359*, 710.
- (6) (a) Zhao, D.; Huo, Q.; Feng, J.; Chmelka, B. F.; Stucky, G. D. *J. Am. Chem. Soc.* **1998**, *120*, 6024(b) Zhao, D.; Feng, J.; Huo, Q.; Melosh, N.; Fredrickson, G. H.; Chmelka, B. F.; Stucky, G. D. *Science* **1998**, *279*, 548.
- (7) (a) Liang, Y.; Anwander, R. *J. Mater. Chem.* **2007**, *17*(b) Zhang, H.; Sun, J.; Ma, D.; Weinberg, G.; Su, D. S.; Bao, X. *J. Phys. Chem. B* **2006**, *110*, 25908.
- (8) Gutsche, C. D.; Lin, L.-G. *Tetrahedron* **1986**, *42*, 1633.
- (9) (a) Tashiro, M. *Synthesis* **1979**, *1979*, 921(b) Bohmer, V.; Rathay, D.; Kammerer, H. *Org. Prep. Proced. Int.* **1978**, *10*, 113(c) Kammerer, H.; Happel, G.; Bohmer, V.; Rathay, D. *Monatsh. Chem.* **1978**, *109*, 767.
- (10) Liu, C.; Lambert, J. B.; Fu, L. *J. Am. Chem. Soc.* **2003**, *125*, 6452.
- (11) Hall, D. A.; Maus, D. C.; Gerfen, G. J.; Inati, S. J.; Becerra, L. R.; Dahlquist, F. W.; Griffin, R. G. *Science* **1997**, *276*, 930.
- (12) Latesky, S. L.; McMullen, A. K.; Niccolai, G. P.; Rothwell, I. P.; Huffman, J. C. *Organometallics* **1985**, *4*, 902.
- (13) Gauvin, R. M.; Osborn, J. A.; Kress, J. *Organometallics* **2000**, *19*, 2944.
- (14) Stull, D. R.; Sinke, G. C. *The chemical thermodynamics of organic compounds*; Westrum Ed.; Malabar, Fla., 1987.
- (15) Groysman, S.; Goldberg, I.; Kol, M.; Goldschmidt, Z. *Organometallics* **2003**, *22*, 3793.
- (16) Tosin, G.; Santini, C. C.; Taoufik, M.; Mallmann, A. D.; Bassett, J.-M. *Organometallics* **2006**, *25*, 3324.
- (17) Ravel, B.; Newville, M. *Journal of Synchrotron Radiation* **2005**, *12*, 537.

- (18) Ankudinov, A. L.; Ravel, B.; Rehr, J. J.; Conradson, S. D. *Physical Review B* **1998**, *58*, 7565.

## **Conclusion générale**



La préparation et la caractérisation de matériaux métallacalix[4]arènes supportés sur silice mésoporeuse constitue un axe de recherche relativement nouveau de la chimie organométallique de surface. Jusqu'alors, cette méthode avait été appliquée avec succès à la préparation d'espèces organométalliques de surfaces liées directement aux supports oxydes, qui se sont avérées performantes dans de nombreuses réactions de valorisation d'hydrocarbures. La synthèse de ces catalyseurs est réalisée par réaction de complexes organométalliques avec les fonctions hydroxyles du support oxyde, qui par hydrogénolyse à basse température donne des catalyseurs hydrures correspondants. Une étude bibliographique détaillée sur ces phases actives a permis de mettre en évidence que seule une fraction des sites de surface est active dans certaines réactions. Ceci est la conséquence directe des interactions entre le centre métallique et les différentes fonctions du support.

L'idée innovante de ce projet a été d'utiliser des dérivés du calix[4]arène comme bras espaceurs entre le support et le centre métallique, macromolécules cycliques présentant plusieurs avantages, tels que :

- la stabilité thermique, permettant de réaliser des réactions catalytiques à haute température
- la multiplicité des fonctions phénols, permettant de synthétiser des systèmes monopodaux, bipodaux, tripodaux voire tétrapodaux
- leur flexibilité conformationnelle donnant accès à des complexes avec différentes géométries.

Après une étude bibliographique sur les différentes méthodes d'hétérogénéisation des calixarènes, il en ressort principalement que celles existantes, notamment par réaction entre des calixarènes portant des fonctions alkoxy silane, sur le lower ou l'upper-rim, sur un support activé, ne peuvent s'appliquer à la chimie organométallique de surface. En effet, ces matériaux calixarène/silice présentent, en plus des groupements phénols du calixarène, des fonctions silanols résiduelles pouvant ainsi donner un mélange important d'espèces de surface lors du greffage des complexes organométalliques. En plus, la fonctionnalisation des calixarènes à greffer nécessitent plusieurs étapes de synthèse.

Ainsi, dans un premier temps, nous nous sommes intéressés au développement d'une nouvelle stratégie de greffage d'espaceurs organiques du type phenoxy sur un support de silice préalablement fonctionnalisé par le triisobutylaluminium. Une fois ce nouveau concept prouvé, nous nous sommes penchés sur l'application de cette stratégie aux calixarènes. Nous avons donc étudié la préparation et la caractérisation de matériaux métallacalix[4]arènes en

utilisant une silice mésoporeuse portant des fragments aluminium-isobutyl. Ces différents matériaux ont ensuite été testés en métathèse du propène afin de comparer leurs propriétés catalytiques à leurs analogues directement liés au siloxy de surface.

- **Préparation et caractérisation d'espèces de zirconium et tungstène supportées sur le matériau hydroquinone /silice et application en métathèse du propène**

A notre connaissance, il s'agit de la première étude décrite dans la littérature mettant en jeu une méthode totalement nouvelle de greffage contrôlé de complexes organométalliques sur une surface présentant des fonctions phénols. Les conséquences d'une telle découverte sont importantes puisqu'elles débouchent sur un concept nouveau en chimie organométallique de surface : par un effet de ligand, une surface doit pouvoir être rendue plus active et plus sélective dans de nombreuses réactions catalytiques en diminuant les interactions métal-support, et par conséquence une augmentation des sites actifs. Cette nouvelle méthode de greffage de fragments phenoxy se divise en trois étapes.

La première consiste au greffage de  $\text{Al}i\text{Bu}_3$  sur une surface de silice partiellement déshydroxylée à  $700^\circ\text{C}$ . La grande réactivité de ce composé organométallique envers les fonctions hydroxyles -OH a permis d'obtenir une silice exempte de silanols. Cependant, une étude bibliographique préliminaire a permis de comprendre que les phénomènes de dimérisation, physisorption et restructuration de la surface étaient récurrents dans le greffage de tels dérivés aluminium, forts acides de Lewis. L'utilisation du diéthyléther comme solvant de greffage a permis de générer *in situ* l'adduit  $\text{Al}i\text{Bu}_3\text{Et}_2\text{O}$ , moins acide de Lewis, et ainsi rendu possible l'élimination complète de l'excès du réactif. Les analyses DRIFT, bilan de matière, RMN à l'état solide ont montré que seule l'espèce originale bipodale  $[(\equiv\text{SiO})_2\text{Al}i\text{Bu}(\text{Et}_2\text{O})]$  H1 était obtenue (**Schéma 1**).

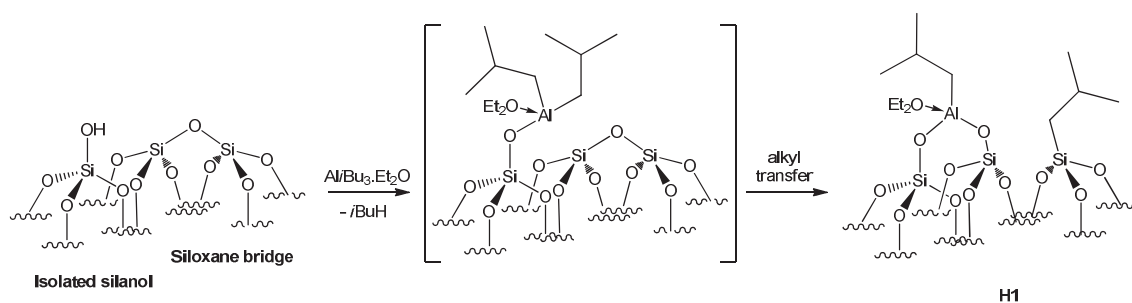


**Schéma 1:** Formation de l'espèce  $[(\equiv\text{SiO})_2\text{Al}i\text{Bu}(\text{Et}_2\text{O})]$  H1 par greffage de  $\text{Al}i\text{Bu}_3(\text{Et}_2\text{O})$  sur  $\text{SiO}_{2-(700)}$

Le caractère acide de Lewis de l'aluminium conduit parallèlement à l'ouverture d'un point siloxane voisin avec formation concomitante du fragment Si-*i*Bu. La réactivité de l'hydroquinone avec les sites aluminium alkyle générés a ensuite été étudiée.

La deuxième étape consiste à synthétiser le nouveau matériau  $[(\equiv \text{SiO})_2 \text{AlO-C}_6\text{H}_4-\text{OH} \cdot (\text{Et}_2\text{O})]$  **H2**, portant une fonction phénol, par réaction de l'espèce de surface **H1** avec l'hydroquinone qui s'accompagne d'un dégagement de 0,9 isobutane par aluminium de surface. Les caractérisations par spectroscopies infra-rouge, RMN à l'état solide et analyse élémentaire ont permis d'apporter une description précise de ce matériau (**Schéma 2**).

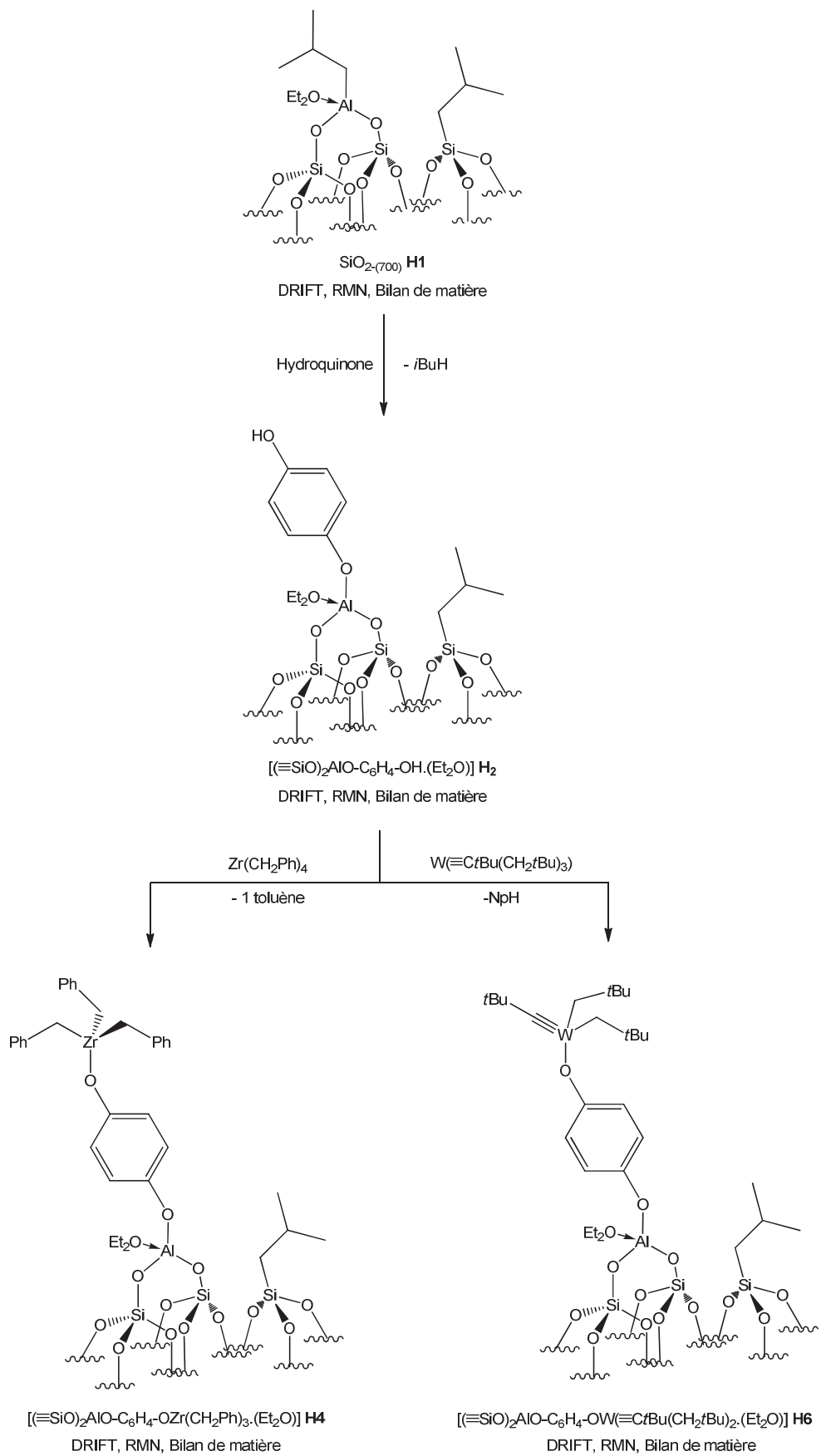


Schéma 2: Voie de synthèse des complexes de surface  $[(\equiv\text{SiO})_2\text{AlO-C}_6\text{H}_4\text{-OZr}(\text{CH}_2\text{Ph})_3\text{.(Et}_2\text{O)}]$  H4 et  $[(\equiv\text{SiO})_2\text{AlO-C}_6\text{H}_4\text{-OW}(\equiv\text{C}t\text{Bu}(\text{CH}_2t\text{Bu})_2\text{.(Et}_2\text{O)}]$  H6

La troisième étape consiste enfin à faire régir ce matériau  $[(\equiv\text{SiO})_2\text{AlO-C}_6\text{H}_4-\text{OH}(\text{Et}_2\text{O})]$  **H2** avec des complexes organométalliques de choix tels que  $\text{ZrBn}_4$  et  $\text{W}(\equiv\text{C}t\text{Bu}(\text{CH}_2t\text{Bu})_3)$  pour donner de nouveaux systèmes à sites uniques  $[(\equiv\text{SiO})_2\text{AlO-C}_6\text{H}_4-\text{OZr}(\text{CH}_2\text{Ph})_3.\text{Et}_2\text{O}]$  **H4** et  $[(\equiv\text{SiO})_2\text{AlO-C}_6\text{H}_4-\text{OW}(\equiv\text{C}t\text{Bu})(\text{CH}_2t\text{Bu})_2.\text{Et}_2\text{O}]$  **H6**. L'utilisation des spectroscopies infra-rouge, RMN à l'état solide ainsi que la comparaison avec leurs analogues directement greffés sur silice  $[(\equiv\text{SiO})\text{Zr}(\text{CH}_2\text{Ph})_3]$  **H3** et  $[(\equiv\text{SiO})\text{W}(\equiv\text{C}t\text{Bu}(\text{CH}_2t\text{Bu})_2]$  **H5** ont permis leur caractérisation. L'espèce de surface à base de tungstène **H6** s'est avérée beaucoup plus active en métathèse du propène que son analogue supporté sur silice  $[(\equiv\text{SiO})\text{W}(\equiv\text{C}t\text{Bu}(\text{CH}_2t\text{Bu})_2]$  (**Table 1**). Ces résultats montrent que le ligand aryloxy en surface a permis d'augmenter l'activité du tungstène, probablement due à la diminution des interactions métal-support et l'augmentation du nombre des sites actifs, ainsi qu'à l'effet électro-attracteur du couple aluminium et cycle aromatique.

**Table 1 : T.O.N cumulés et sélectivités en but-2-ène *trans/cis* observés à 50h lors de la métathèse du propène par les systèmes **H5**, **H6**, **M7** et **M4****

	<b>H5</b>	<b>H6</b>	<b>M7</b>	<b>M4</b>
T.O.N cumulé à 50 h	12500	24450	14600	7900
Sélectivité <i>trans/cis</i> à 50 h	1.1	1.1	1.5	0.9

Le concept de greffage de ligands phénols sur une silice exempt de silanols étant prouvé, nous nous sommes penchés sur la synthèse de métallacalix[4]arènes solubles afin de modéliser les métallacalix[4]arènes supportés et faciliter leur caractérisation. Les chapitres III et IV ont été consacrés à la synthèse ces complexes moléculaires. Si les modèles titana-, zirconia- and tantalacalix[4]arènes ont été préparés avec succès, les complexes tungstenacalix[4]arènes se sont malheureusement avérés plus difficiles à obtenir.

- **Synthèses de métallacalix[4]arènes solubles des groupe IV (Ti, Zr) et V (Ta)**

Tout comme les ligands POSS peuvent modéliser les complexes organométalliques supportés sur silice, des métallacalix[4]arènes ont été synthétisés dans le but de modéliser leurs analogues supportés et de choisir les calix[4]arènes espaceurs les plus pertinents, offrant le mode de coordination qui donne les meilleures propriétés catalytiques. Une collection de ligands **L1-L10** dérivés du *p-tertbutylcalix[4]arène*, présentant tous des modes de coordination différents pour le métal (bipodaux distaux et proximaux, tripodaux, bis, tris- ou tetra-coordinant suivant la fonctionnalisation du lower-rim) a été synthétisée (**Schéma 3**).

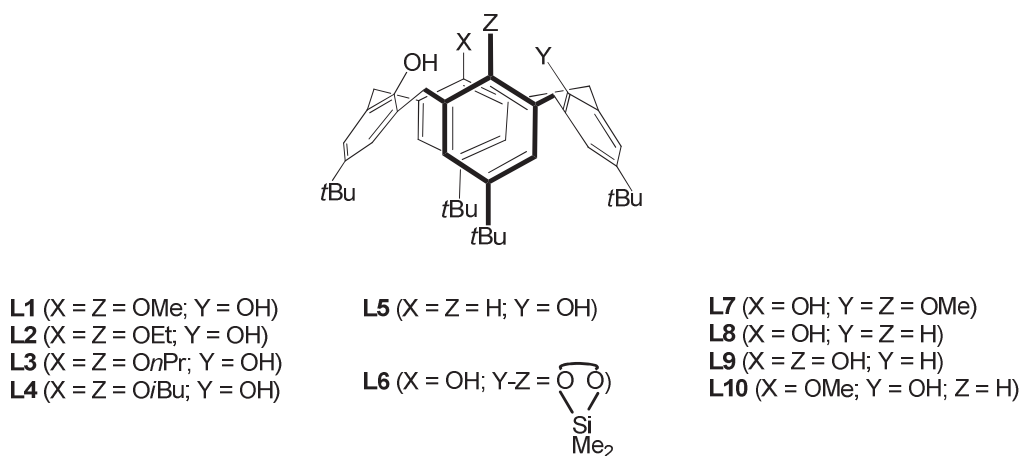


**Schéma 3:** Ligands L1-L10, dérivés du *p-tertbutylcalix[4]arène*, offrant divers modes de coordination pour le métal

Des complexes alkyles titana-, zircona- et tantalacalix[4]arenes bi- et tripodaux ont été synthétisés soit par alkylation des dérivés chlorés correspondants (voie « salt-elimination »), soit par réaction directe entre un complexe homoleptique et le ligand calixarene (voie « alkane-elimination »).

- **Métallacalix[4]arènes du groupe IV (Ti, Zr)**

Une série de complexes bis-chlorotitana- (**Ti1-Ti5, Ti8-Ti9**) et zirconacalix[4]arene (**Zr1**) solubles a été synthétisée et caractérisée (**Figure 1**). Tous présentent des modes de coordination variés, permettant d'étudier leurs propriétés catalytiques dans la polymérisation de l'éthylène selon les paramètres : i) positions proximale et distale des points d'ancrage du métal (étude de l'angle O-Ti-O), ii) encombrement stérique des ligands alkoxy présents dans la sphère de coordination du métal et iii) absence de ligands alkoxy dans la sphère de coordination du métal. L'étude comparative de ces complexes dans la polymérisation de l'éthylène, en présence de MAO, a permis de conclure que les complexes proximaux, présentant les angles O-Ti-O les plus ouverts, et sans ligand alkoxy dans leur sphère de

coordination, se sont montrés les plus actifs (**Figure 1**). Cette étude nous a permis de comprendre l'influence du mode de coordination offert par le calixarène sur le métal et d'exclure les calixarènes présentant des fragments coordinants de type éther. Elle nous a aussi orientés dans la préparation de métallacalix[4]arène supportés bipodaux, de préférence présentant des points d'ancrage proximaux.

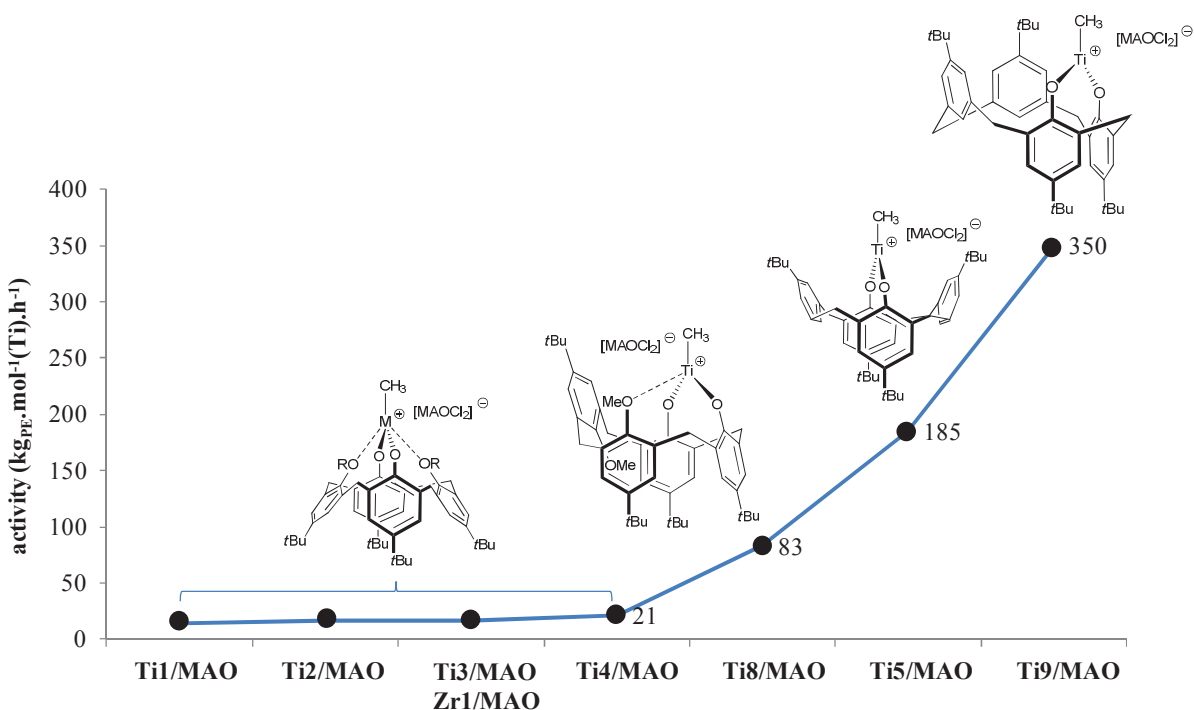


**Figure 1: Relation structure-activité des systèmes Ti1-Ti5/MAO, Ti8-Ti9/MAO et Zr1/MAO**

Des complexes mono-alkyles tripodaux et bis-alkyles bipodaux ziconacalix[4]arènes et titanacalix[4]arènes ont été synthétisés et caractérisés en utilisant les deux méthodes de synthèses, à savoir les voies « salt-elimination » et « alkane-elimination ».

#### - Métallacalix[4]arènes du groupe V (Ta)

Deux familles de complexes tris-alkyles bipodaux et bis-alkyles tripodaux (benzyl, neopentyl) ont été préparés selon les deux mêmes voies. Dans le cas des dérivés tripodaux, des activations C-O et C<sub>Ar</sub>-H ont été observées lors du traitement des complexes bis-neopentyl **Ta6** et **Ta7** à 80°C par élimination de neohexane ou neopentane (**Schéma 4**). Ceci constitue, à notre connaissance, un premier exemple d'activation intramoléculaire d'une liaison C-H

aromatique du calixarène. Alors que son analogue bis-benzyl ne présente aucune activation C-H lorsqu'il est chauffé à la même température.

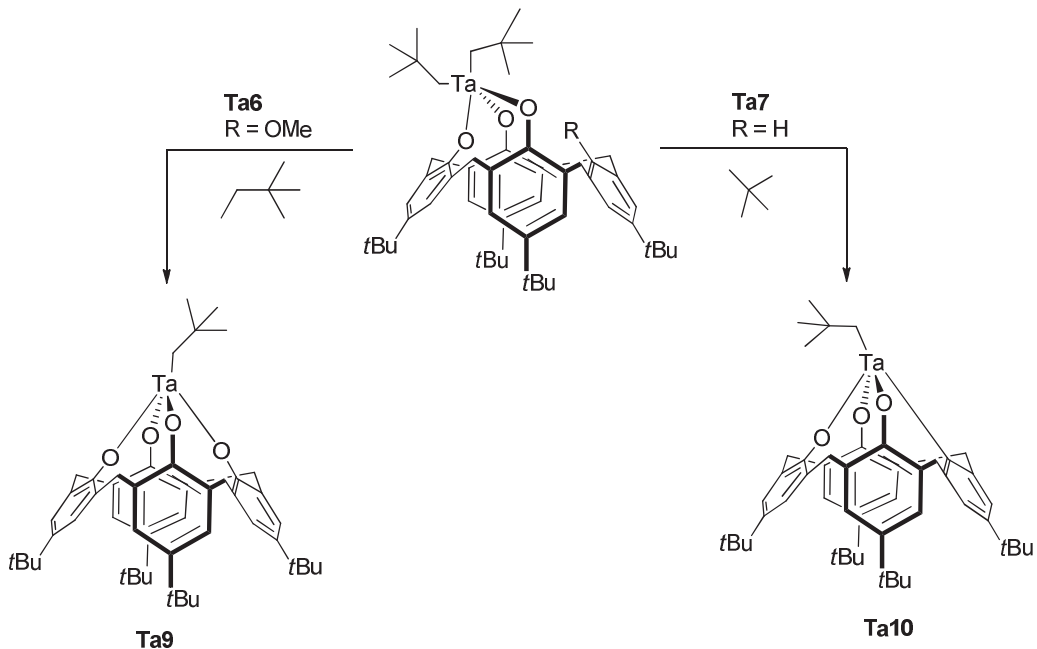


Schéma 4: Transformation thermique à 80°C de Ta6 et Ta7 en Ta9 and Ta10, respectivement

- Synthèse de métallacalix[4]arènes des groupe IV(Zr), V(Ta) et VI(W) supportés sur SBA-15 LP<sub>-(700)</sub>**

Dans cette partie du sujet la génération de matériaux métatallacalix[4]arene/SBA-15 LP<sub>-(700)</sub> de Zr et W a été réalisée selon le concept de greffage établi avec l'hydroquinone dans le chapitre II. Faute de temps, nous n'avons pas pu intégrer les tantalacalix[4]arènes supportés. Le choix du support a été porté sur la silice mésoporeuse SBA-15 LP (larges pores) partiellement déshydroxylée à 700°C, afin de fournir une surface spécifique plus grande que SiO<sub>2-(700)</sub> et des pores suffisamment larges pour le greffage des macromolécules calix[4]arènes. L'accès à l'espèce aluminium isobutyl de surface [(≡SiO)<sub>2</sub>Al*i*Bu.(Et<sub>2</sub>O)] n'est pas limité au support silice. En effet, la même réaction entre Al*i*Bu<sub>3</sub>.(Et<sub>2</sub>O) et la silice mésoporeuse SBA-15 LP<sub>-(700)</sub> a ainsi été réalisée et donne la même espèce de surface [(≡SiO)<sub>2</sub>Al*i*Bu.(Et<sub>2</sub>O)]<sub>SBA-15 LP-(700)</sub> (**M1**), caractérisée par DRIFT, RMN à l'état solide 1D et HETCOR, et microanalyse. La réactivité du calix[4]arène detertiobutylé [[4H]-(*H*)(OH)<sub>3</sub>] **L12** par une de ses fonctions phénols sur le fragment isobutyl aluminium présenté par **M1** conduit à la formation du nouveau matériau [(≡SiO)<sub>2</sub>Al-[O-[4H]-(*H*)(OH)<sub>2</sub>].(Et<sub>2</sub>O)]<sub>SBA-15 LP-(700)</sub> **M2** (**Schéma 5**) avec dégagement de 0,7 isobutane par aluminium (greffage sur 70% des sites alkyles aluminium).

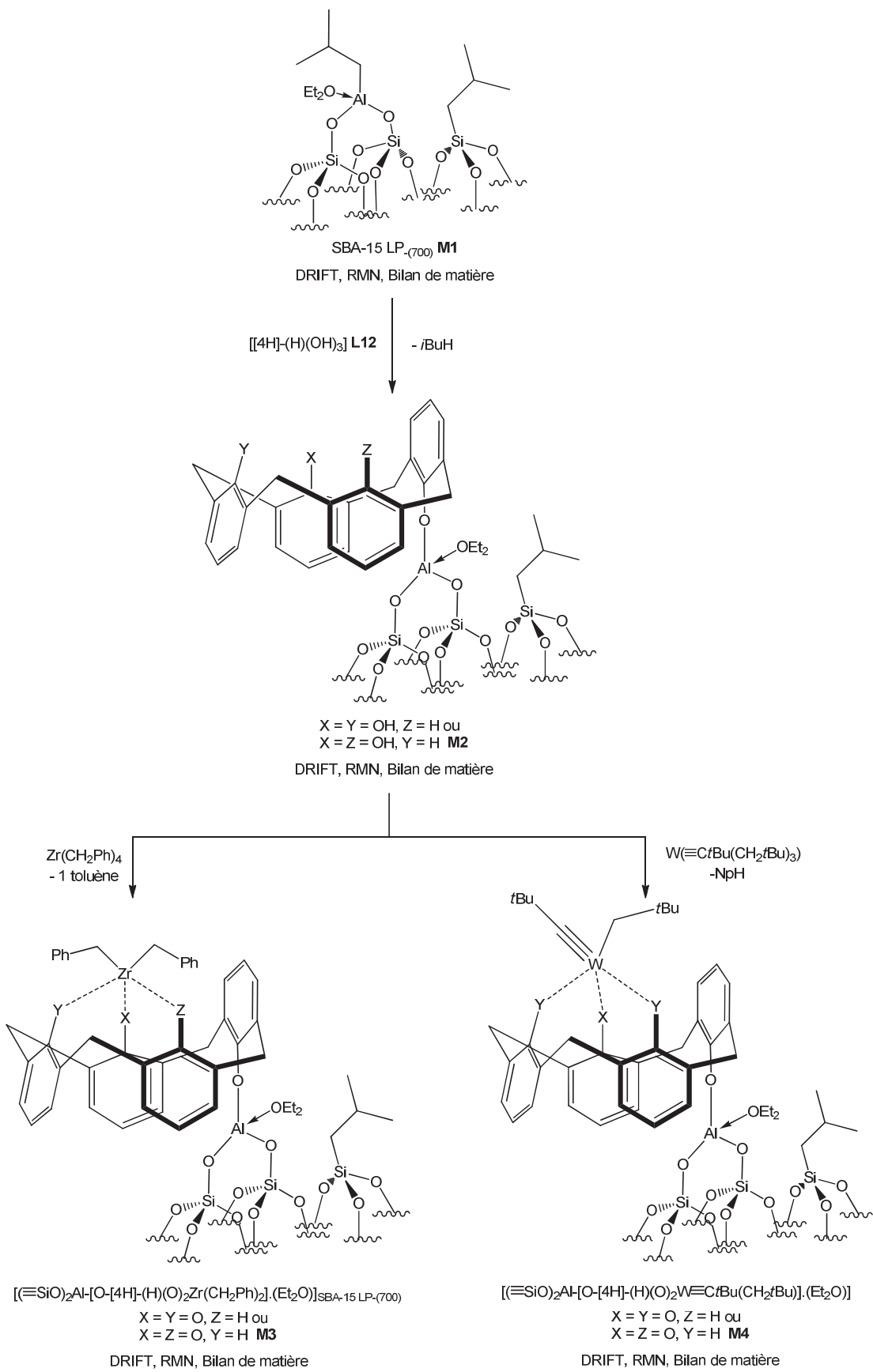


Schéma 5: Voie de synthèse des complexes de surface  $[(\equiv SiO)_2Al-[O-[4H]-(H)(O)_2Zr(CH_2Ph)_2].(Et_2O)]_{SBA-15 \text{ LP-(700)}} \quad \mathbf{M3}$  et  $[(\equiv SiO)_2Al-[O-[4H]-(H)(O)_2W\equiv C tBu(CH_2tBu)].(Et_2O)]_{SBA-15 \text{ LP-(700)}} \quad \mathbf{M4}$

Ce matériau calixarénique a été caractérisé par DRIFT, RMN à l'état solide et microanalyse. La sélectivité du greffage, laissant ainsi libres les deux autres fonctions phénols en position distal ou proximale, pourra être déterminée dans des travaux ultérieurs en utilisant la RMN  $^2\text{H}$  des phénols deutérés du calixarène supporté. La détermination de la conformation du calix[4]arène nécessitera aussi des études supplémentaires par RMN dynamique et RMN  $^{13}\text{C}$  du calixarène présentant des ponts méthyléniques isotopiquement enrichis, préparés en utilisant du formaldéhyde marqué en carbone  $^{13}\text{C}$ .

Ensuite, l'incorporation de complexes organométalliques tels que  $\text{Zr}(\text{CH}_2\text{Ph})_4$  et  $\text{W}(\text{CtBu}(\text{CH}_2\text{tBu})_3)$  mène à de nouveaux systèmes à sites uniques  $[(\equiv\text{SiO})_2\text{Al}-[\text{O}-[\text{H}](\text{H})(\text{O})_2\text{Zr}(\text{CH}_2\text{Ph})_2].(\text{Et}_2\text{O})]$ <sub>SBA-15</sub> LP-(700) **M3** et  $[(\equiv\text{SiO})_2\text{Al}-[\text{O}-[\text{H}](\text{H})(\text{O})_2\text{W}=\text{CtBu}(\text{CH}_2\text{tBu})].(\text{Et}_2\text{O})]$ <sub>SBA-15</sub> LP-(700) **M4**, dont les caractérisations ont été supportées à l'aide de leurs analogues directement greffés sur silice. L'espèce tungstène **M4** montre une activité initiale meilleure que son homologue bis-siloxy  $[(\equiv\text{SiO})_2\text{W}(\equiv\text{CtBu}(\text{CH}_2\text{tBu})]$  **M7** en métathèse du propène, mais se désactive beaucoup plus rapidement. Le rapport des sélectivités *trans/cis* but-2-ènes diminuent avec le temps pour favoriser en fin de réaction l'isomère *cis*, rarement observé en métathèse du propène. Ces données pourraient s'expliquer par l'encombrement stérique principalement dû aux noyaux aromatiques présents autour du métal s'accompagnant d'une activation C<sub>Ar</sub>-H intramoléculaire, comme observée en solution dans le cas du tantale (**Schéma 4**).

D'une manière générale, l'utilisation de ligands aryloxy en tant qu'espaces (hydroquinone ou calixarène suivant la podalité souhaitée pour le métal) s'avère très prometteuse. Les travaux de cette thèse vont ouvrir de nouvelles perspectives et de nouveaux axes de recherche dans l'élaboration de matériaux par voie COMS et en utilisant d'autres types de fonctions autres que les phénols, telles que les imidazoles et les phosphines. Malgré certaines faiblesses dans la caractérisation de ces nouveaux matériaux, qui nécessitent la synthèse de calixarènes et de complexes organométalliques marqués, l'objectif de préparer des matériaux métallacalix[4]arène supportés sur silice a été atteint dans le temps imparti.

## **Annexes**



## ANNEX I

### Grafting techniques using the double Schlenk apparatus

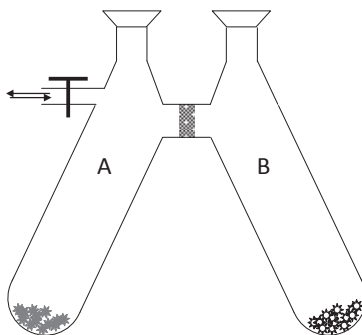


Figure: Double Schlenk apparatus (Compartments A and B)

- **Grafting by impregnation technique**

The double Schlenk apparatus is divided into two compartments connected *via* a frit. The first compartment A is charged with the organometallic complex under argon. The second one is charged with the desired support. When evacuated using the high vacuum line, the solvent is condensed onto the complex by a trap-to-trap process. The solution is then transferred to the compartment B. At the end of the reaction, the suspension is filtrated through the frit and the solvent condensed back to the compartment B. Washing cycle, namely filtration/condensation, is repeated until the excess of complex from B is totally removed to A. If desired, of the volatiles can be evacuated into a large flask of a known volume in order to analyze the phase gas by GC. Final removal of the trace of solvent is realized under high vacuum.

- **Grafting by mechanical stirring**

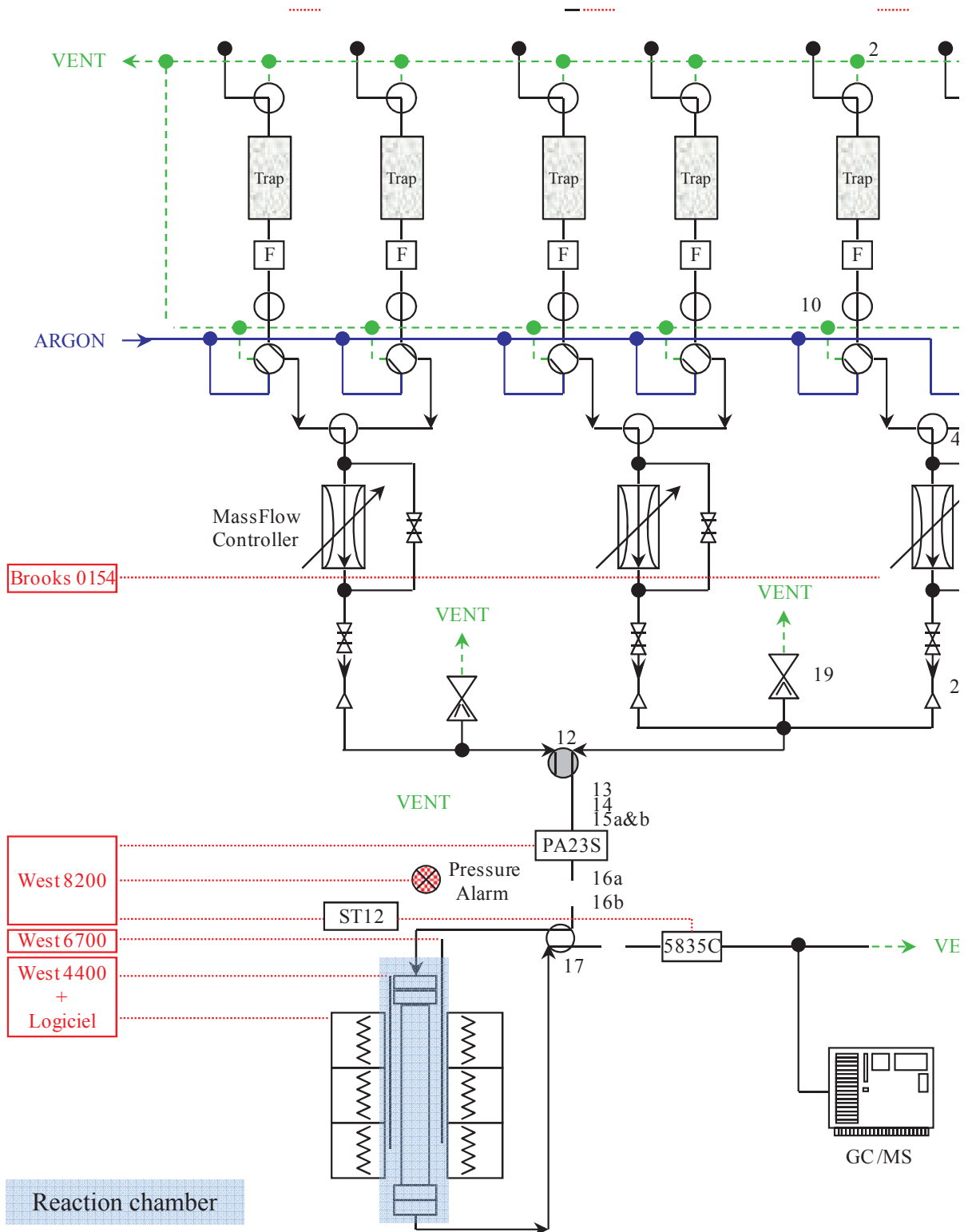
This alternative technique is useful when the organometallic complex sublimes easily at moderate temperature without degradation (*e.g.* 60°C for [W(≡CtBu(CH<sub>2</sub>tBu)<sub>3</sub>)]), in order to maximize the charge in complex on the support. In that approach, both solids are stirred in compartment B at the desired temperature under argon or vacuum. After completion of the reaction, the eventual volatiles from the reaction are collected in a large flask of a known volume. The apparatus is evacuated under high vacuum and the washing solvent is then condensed onto the solid by a trap-to-trap process. Washing cycles and final drying are realized as described above.



## ANNEX II

### Continuous flow reactor for the gas conversion

The catalytic studies (gas phase) were performed in a continuous flow reactor (**Scheme**). The reactor can be divided into three parts. The first one concerns the reaction chamber that can be filled in a glove box, and the system (furnace and temperature controller) which controls the temperature during catalytic test. The reactor is a stainless steel cylinder with a diameter of 1 cm and a length of 18 cm. Its volume can be adjusted by including inserts (by using 2 inserts,  $L = 4.5 \text{ cm}$ ,  $V = 2.9 \text{ cm}^3$ ; 1 insert,  $L = 11.6 \text{ cm}$ ,  $V = 7.4 \text{ cm}^3$ ; 0 insert,  $L = 18 \text{ cm}$ ,  $V = 11.4 \text{ cm}^3$ ). The second part is the peripheral system which contains the mass-flow controller (Brooks) allowing to monitor the flow rates during the reaction and a pressure regulator checking the inlet pressure. The last part concerns the analysis of products generated by the catalytic reaction, by a gas chromatograph (HP 8890 chromatograph fitted with an  $\text{Al}_2\text{O}_3/\text{KCl}$  50 m x 0.32 mm capillary column, FID detector for hydrocarbons and a 3 Å molecular sieve column, catharometer for hydrogen).



## ANNEX III

### Crystallographic data

- **Experimental and refinement**

Data collection, cell refinement and data reduction: CrysAlisPro,<sup>1</sup> program(s) used to solve structure: SIR97, program(s) used to refine structure: CRYSTALS,<sup>2</sup> molecular graphics: ORTEP3,<sup>3</sup> software used to prepare material for publication: CRYSTALS.<sup>2</sup> Cu- $K_{\alpha}$  radiation,  $\lambda = 1.54184 \text{ \AA}$ ,  $R_1 = \sum ||F_o| - |F_c|| / \sum |F_o|$ ,  $wR_2 = [\sum w(F_{o2} - F_{c2})^2 / \sum w(F_{o2})^2]^{1/2}$ ,  $w_{-1} = [\sigma_2(F_o) + (aP)]$ ,  $P = [\max(F_{o2}, 0) + 2(F_{c2})]/3$ , in which  $a$  is a constant adjusted by the program; goodness of fit =  $[\sum(F_{o2} - F_{c2})^2 / (n - p)]^{1/2}$ , in which  $n$  is the number of reflections and  $p$  the number of parameters.

The following crystal structures have been deposited at the Cambridge Crystallographic Data Centre and allocated a deposition number (**Table**).

- (1) CrysAlisPro, Oxford Diffraction Ltd., Version 1.171.33.52 (release 06-11-2009 CrysAlis171.NET) (compiled Nov 6 2009, 16:24:50).
- (2) Betteridge, P. W.; Carruthers, J. R.; Cooper, R. I.; Prout, K.; D.J., W. *J. Appl. Crystallogr.* **2003**, *36*, 1487.
- (3) Farrugia, L. J. *J. Appl. Crystallogr.* **1997**, *30*, 565.

**Table:** Crystallographic data

Compounds	Ti2	Ti3	Ti4	L11	Ta3	Ta6	Ta10
CCDC numbers	CCDC-748977	CCDC-748978	CCDC-748976	CCDC-778232		CCDC-778510	CCDC-778233
Color	Dark brown	Dark red	Dark brown	Colorless	Yellow	Yellow	Colorless
Formula	C <sub>48</sub> H <sub>62</sub> Cl <sub>2</sub> O <sub>4</sub> Ti.	C <sub>50</sub> H <sub>66</sub> Cl <sub>2</sub> O <sub>4</sub> Ti.	C <sub>52</sub> H <sub>70</sub> Cl <sub>2</sub> O <sub>4</sub> Ti.	C <sub>51</sub> H <sub>62</sub> O <sub>3</sub>	C <sub>62</sub> H <sub>72</sub> Cl <sub>2</sub> OTa	C <sub>88</sub> H <sub>106</sub> Cl <sub>4</sub> O <sub>6</sub> Ta <sub>2</sub>	C <sub>49</sub> H <sub>63</sub> O <sub>4</sub> Ta.
Formula weight	1006.05	1126.30	1062.21	723.01	1136.56	1763.51	1126.83
Crystal size (mm <sup>3</sup> )	0.39 × 0.18 × 0.16	0.48 × 0.29 × 0.18	0.22 × 0.17 × 0.15	0.35 × 0.08 × 0.03	0.62 × 0.16 × 0.04	0.19 × 0.04 × 0.03	0.33 × 0.25 × 0.18
Crystal system	Monoclinic	Monoclinic	Monoclinic	Monoclinic	Triclinic	Triclinic	Monoclinic
Space group	P2 <sub>1</sub> /n	P2 <sub>1</sub> /c	P2 <sub>1</sub> /c	Cc	P-1	P-1	P2 <sub>1</sub> /c
a (Å)	12.9019(6)	12.8768(6)	15.206 (2)	13.245(2)	11.973 (5)	16.359(1)	14.653(5)
b (Å)	19.0460(7)	25.2620(10)	18.120 (3)	22.608(3)	12.720 (5)	17.981(1)	19.076(5)
c (Å)	23.8319(14)	19.8828(9)	21.850 (4)	15.123(3)	19.507 (5)	19.781(1)	21.946(5)
α (°)	90	90	90	90	97.529 (5)	116.445(6)	90
β (°)	100.103(5)	92.164(4)	94.93(2)	102.710(10)	94.534 (5)	98.994(5)	105.975(5)
γ (°)	90	90	90	90	109.134 (5)	97.308(5)	90
V(Å <sup>3</sup> )	5765.4 (5)	6463.1(5)	5998.1 (17)	4417.5(13)	2758.8 (17)	5016.6(6)	5897(3)
Z	4	4	4	4	2	2	4
T (K)	200	150	180	150	100	150	150
ρ (g.cm <sup>-3</sup> )	1.159	1.157	1.176	1.087	1.368	1.167	1.269
F(000)	2152	2416	2280	1568	1168	1792	2346
μ(Mo-K <sub>α</sub> ) (mm <sup>-1</sup> )	2.44	0.261	0.277	0.50	2.18	5.25	1.91
Reflections collected	21858	43245	33503	7028	23269	14984	47482
Independent reflections	9745	15513	14226	4244	12796	13990	13666
R <sub>int</sub>	0.054	0.050	0.140	0.054	0.044	0.066	0.046
Restraints / parameters	66 / 622	18 / 731	98 / 658	86/544	6/ 614	172/982	24/676
Final R indices	0.093	0.0655	0.0711	0.078	0.040	0.076	0.033
[I>2σ(I)]							
All data	0.102	0.0898	0.2638	0.0971	0.054	0.0912	0.0890
Goodness-of-fit on F <sup>2</sup>	1.062	0.8039	1.1942	0.98	0.9617	1.08	1.13

## ANNEX IV

### Determination of specific surface by the BET method

The determination of specific surface by means of the BET theory, elaborated by Brunauer, Emmett and Teller,<sup>1</sup> is based upon the phenomenon of physical adsorption of gases on the external and internal surfaces of a porous material. Such a material which is surrounded by and in equilibrium with a certain gas which has a certain temperature  $T$ , and relative vapour pressure  $p/p_0$ , adsorbs physically a certain amount of gas. The amount of adsorbed gas is dependent on its relative vapour pressure and is proportional to the total external and internal surface of the material. The connection between relative vapour pressure and amount of adsorbed gas at a constant temperature is called an adsorption isotherm, which is the basis for the theoretical calculation of the specific BET surface as BET, the pore volume  $V_p$  and the pore diameter  $d_p$  of the material (BJH pore size distribution). **Figure 1** shows isotherms and the important areas for the different calculations. The quantitative data obtained from physisorption are depending on theoretical calculations and there is controversy about the credibility of the method, but it is the method of choice in most present publications.

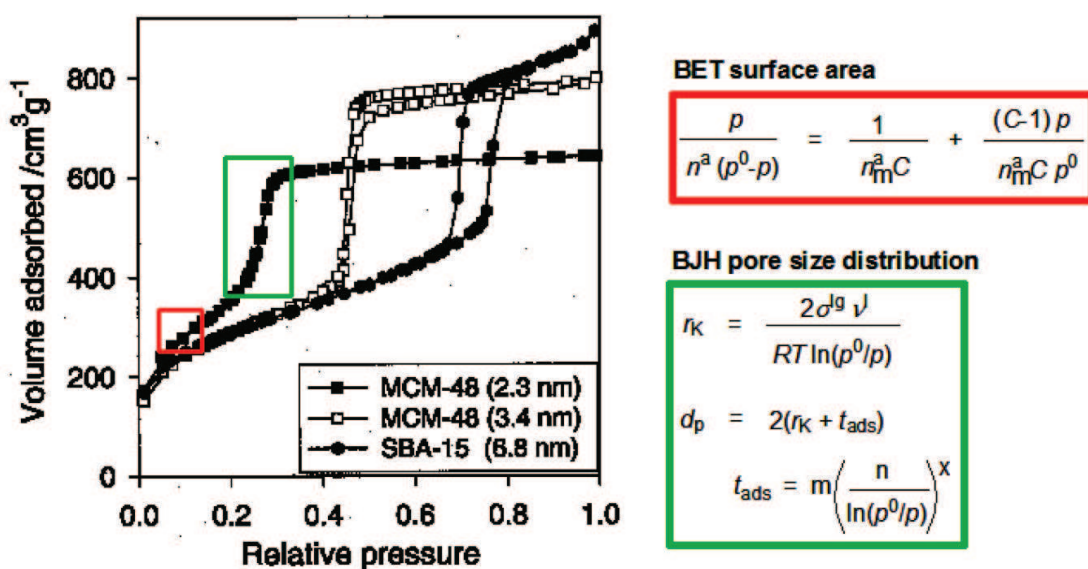


**Figure 1:** Mesostructured materials characterised by  $N_2$  physisorption (77.14 K). The isotherms have adsorption and desorption branch, and characteristic hysteresis loop can be observed.

Experimental gas adsorption isotherms usually fall into six categories, shown in **Figure 2, (a)**. Different properties in porosity (non-porous, microporous, mesoporous) give different types of isotherms.

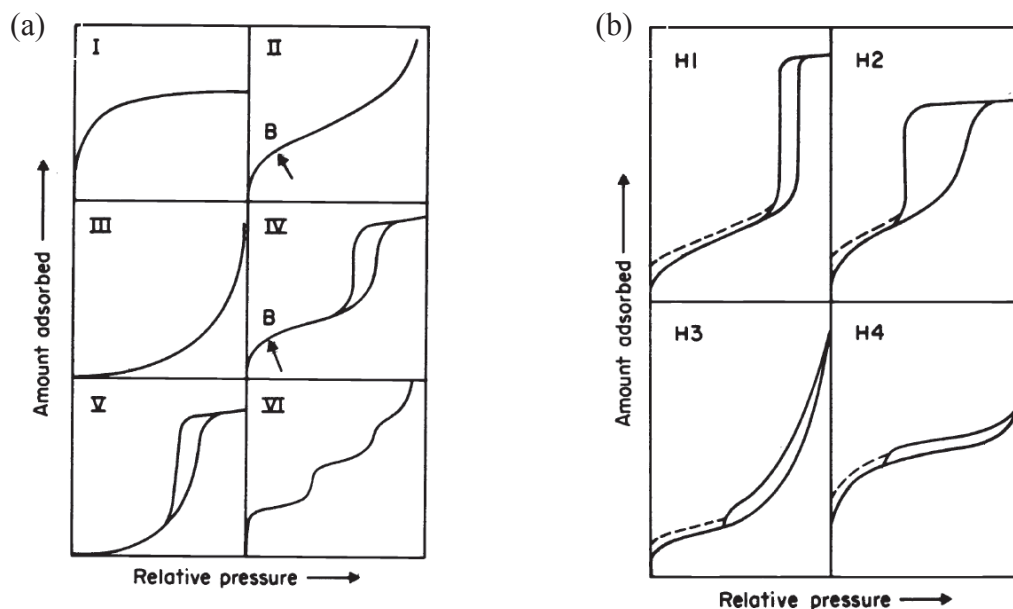


Figure 2: (a) Types of physisorption isotherms; (b) Types of hysteresis loops.

Type I isotherms are characteristic for microporous or mesoporous materials with pore sizes close to the micropore range. Type II and III isotherms do not show any adsorption/desorption hysteresis because the two branches coincide as an effect of multilayer formation and are typical for macroporous materials. Adsorption on mesoporous materials proceeds via multilayer adsorption followed by capillary condensation and gives us isotherms of type IV and V.

Capillary condensation and evaporation often do not take place at the same pressure, leading to the appearance of hysteresis loops, which give information about different pore geometries. There are four different types of hysteresis (Figure 2, (b)), giving indications of which type of pores the materials have, H1: Cylindrical pore geometry, H2: Ink bottle pores, H3: Slitlike pores and H4: Large mesopores embedded in a matrix with pores of much smaller size.

- (1) Brunauer, S.; Emmett, P. H.; Teller, E. *J. Am. Chem. Soc.* **1938**, *60*, 309.
- (2) Rodriguez, G.; Cano, D. A.; McConville, D. H.; Rix, F. C.; (Univation Technologies, LLC, USA). Application: US, 2006.
- (3) Millot, N.; Santini, C. C.; Lefebvre, F.; Basset, J.-M. *C. R. Chim.* **2004**, *7*, 725.

## ANNEX V

### Synthesis of $[(\equiv \text{SiO})_2 \text{Zr}(\text{CH}_2\text{Ph})_2] (\text{M}'3)$

The complex  $\text{Zr}(\text{CH}_2\text{Ph})_4$  was synthesized according an adapted reported method (see experimental section of Chapter II).<sup>1</sup> Using the double Schlenk technique, 1.3 eq. of  $\text{Zr}(\text{CH}_2\text{Ph})_4$  (based on the number of surface silanols<sup>2</sup>:  $0.778 \text{ mmol}_{\text{OH.g}^{-1}}$ ) in pentane (5 ml) were reacted with  $\text{SiO}_{2-(200)}$  over 3h at room temperature in the dark. After repeated washings with pentane (5 ml), followed by evacuation of the volatile, **M'3** was afforded as a yellow powder and characterized employing DRIFT, solid state NMR spectroscopy and mass balance analysis.

- **Infra-red spectroscopy**

After reaction with  $\text{Zr}(\text{CH}_2\text{Ph})_4$ , the DRIFT spectrum of **M'3** displays new bands at  $1485\text{-}1597 \text{ cm}^{-1}$  and  $3000\text{-}3100 \text{ cm}^{-1}$  assigned to the aromatic ring stretching  $\nu_{(\text{Csp}2=\text{Csp}2)}$  and  $\nu_{(\text{Csp}2-\text{H})}$ , respectively (**Figure 1**). The  $\nu_{\text{Csp}3-\text{H}}$  bands from 2800 to 3000  $\text{cm}^{-1}$  are the result of the  $\text{CH}_2$  bond vibration. The examination of the OH stretching region reveals a large band centered at  $3640 \text{ cm}^{-1}$  due to some benzyl-silica surface interaction. No signal from any free surface silanols is observed.

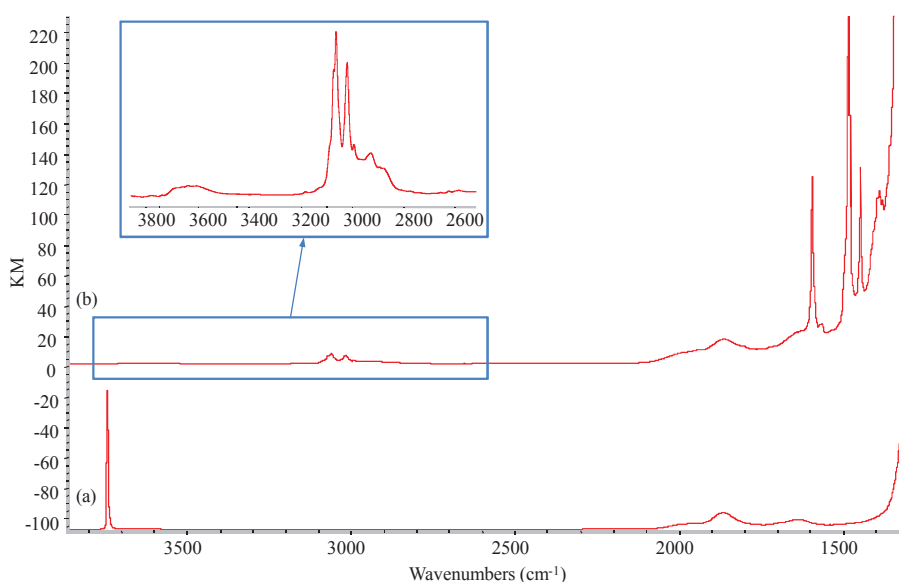


**Figure 1:** DRIFT spectra of  $\text{SiO}_{2-(700)}$  (a) and after grafting of  $\text{Zr}(\text{CH}_2\text{Ph})_4$ , **M'3** (b)

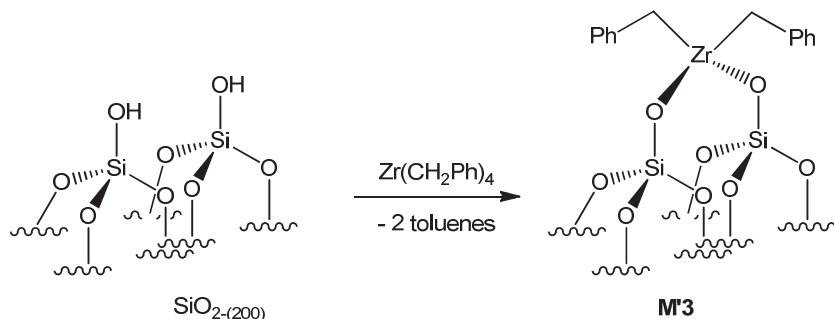
- **Mass-balance analysis**

It must be mentioned that the quantification by GC of the toluene released was not conclusive due its low vapor pressure and physisorption on the support. However, the percentages of zirconium and carbon after the grafting of  $\text{Zr}(\text{CH}_2\text{Ph})_4$  were found to 4.37 %wt and 7.46 %wt respectively, thus corresponding to 13 (th 14) carbons per metal (**Table**). The bis-siloxy tris-benzyl species  $[(\equiv\text{SiO})_2\text{Zr}(\text{CH}_2\text{Ph})_2]$  **M'3** (accounting 14 carbons) can reasonably be proposed, as drawn in **Scheme 1**.

**Table 1:** Mass balance analysis for **M'3**

	% wt Zr <sup>[a]</sup>	% wt C <sup>[a]</sup>	C/Zr
Grafting	4.37	7.46	13 (th 14)

<sup>[a]</sup> Percentage determined by elemental analysis.



**Scheme 1:** Grafting of  $\text{Zr}(\text{CH}_2\text{Ph})_4$  onto  $\text{SiO}_{2-(200)}$ . Synthesis of  $[(\equiv\text{SiO})_2\text{Zr}(\text{CH}_2\text{Ph})_2]$  **M'3**. Reagents and conditions: 1.3 eq.  $\text{Zr}(\text{CH}_2\text{Ph})_4$ , pentane, 3 h, RT

- **Solid-state NMR spectroscopy**

The  $^1\text{H}$  MAS-NMR spectrum of **M'3** exhibits a signal centered at 1.7 ppm assigned to the residual Si-OH in addition to the  $\text{ZrCH}_2$  protons (**Figure 2**). Signal at 6.5 ppm is assigned to the aromatic protons.

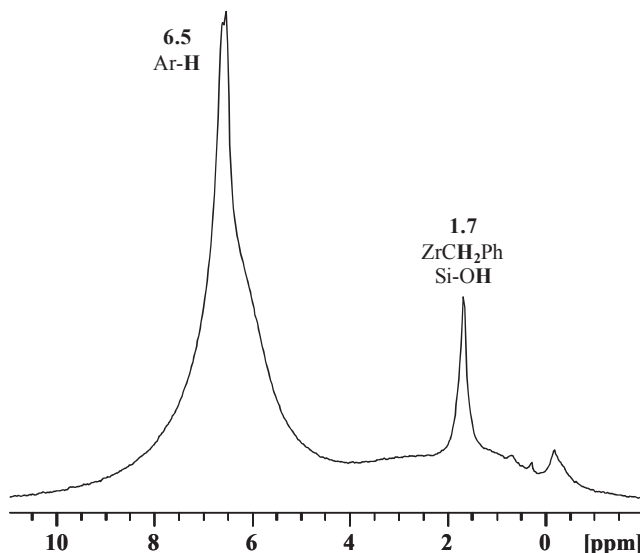


Figure 2:  $^1\text{H}$  MAS-NMR of M'3

The  $^{13}\text{C}$  CP/MAS NMR spectrum displays a significant peak at 66 ppm, belonging to the  $\text{Zr}^{13}\text{CH}_2$  carbons, and a broad peak at 129 ppm for the aromatic fragments (Figure 3).

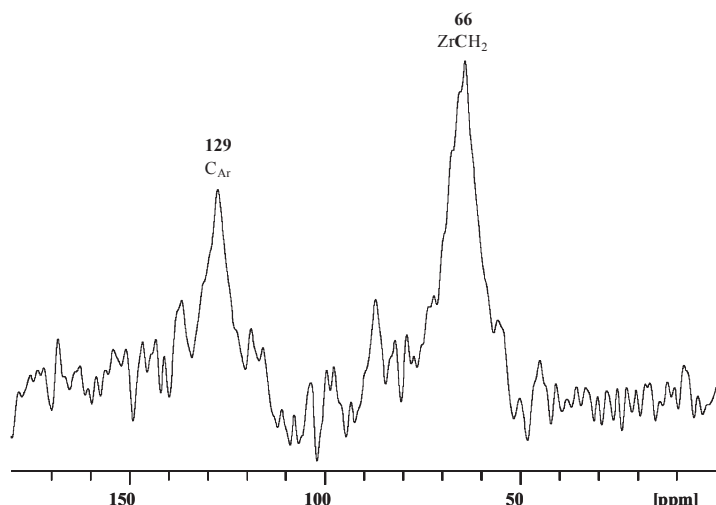


Figure 3 :  $^{13}\text{C}$  CP/MAS-NMR of M'3

In summary, reaction of  $\text{Zr}(^{13}\text{CH}_2\text{Ph})_4$  with  $\text{SiO}_{2-(200)}$  leads to the formation of the bis-siloxy bis-benzylzirconium species whose general structure can be formulated as  $[(\equiv\text{SiO})_2\text{Zr}(^{13}\text{CH}_2\text{Ph})_2]$  (**M'3**) in which the zirconium atom is grafted to the surface *via* two covalent bonds as evidenced by mass balance analysis and advanced NMR spectroscopy.

- (1) Rodriguez, G.; Cano, D. A.; McConville, D. H.; Rix, F. C.; (Univation Technologies, LLC, USA). Application: US, 2006.
- (2) Millot, N.; Santini, C. C.; Lefebvre, F.; Basset, J.-M. *C. R. Chim.* **2004**, 7, 725.